frontiers | Research Topics

Preclinical models and emerging technologies to study the effects of the tumor microenvironment on cancer heterogeneity and drug resistance

Edited by
Giulia Adriani, Paola Cappello and Sara Lovisa

Published in
Frontiers in Oncology

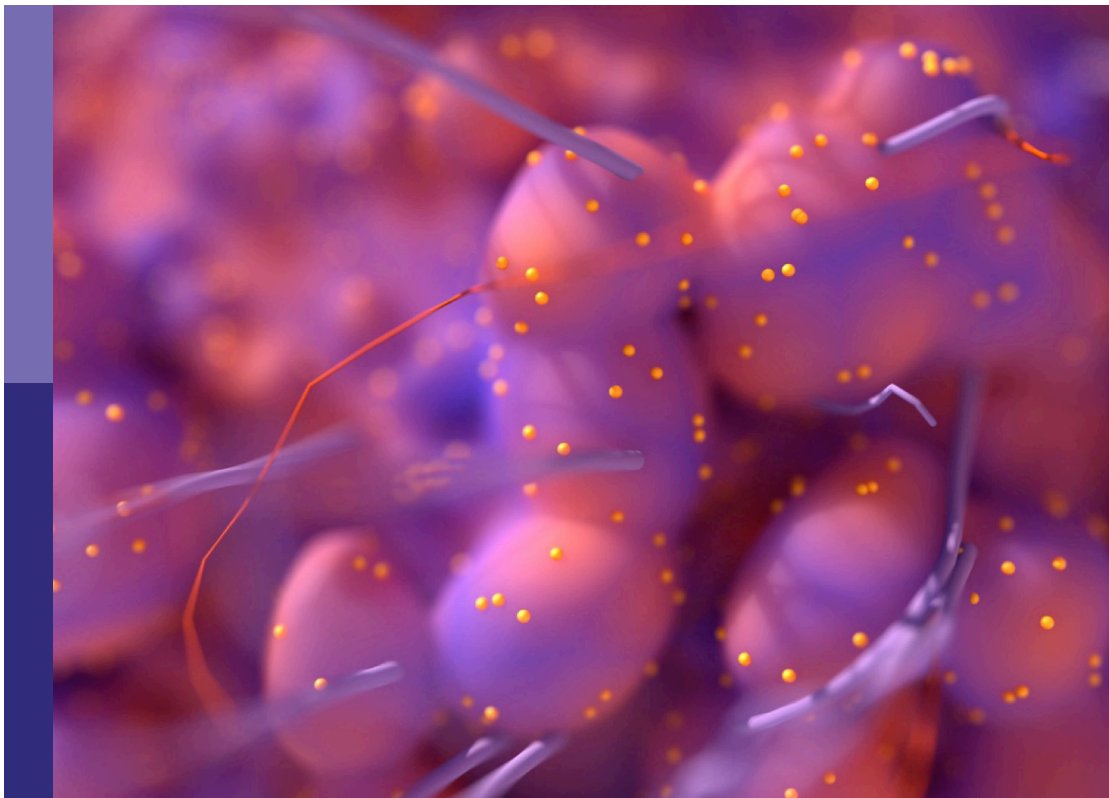

ISSN 1664-8714
ISBN 978-2-8325-3703-9
DOI 10.3389/978-2-8325-3703-9

About Frontiers

Frontiers is more than just an open access publisher of scholarly articles: it is a pioneering approach to the world of academia, radically improving the way scholarly research is managed. The grand vision of Frontiers is a world where all people have an equal opportunity to seek, share and generate knowledge. Frontiers provides immediate and permanent online open access to all its publications, but this alone is not enough to realize our grand goals.

Frontiers journal series

The Frontiers journal series is a multi-tier and interdisciplinary set of open-access, online journals, promising a paradigm shift from the current review, selection and dissemination processes in academic publishing. All Frontiers journals are driven by researchers for researchers; therefore, they constitute a service to the scholarly community. At the same time, the *Frontiers journal series* operates on a revolutionary invention, the tiered publishing system, initially addressing specific communities of scholars, and gradually climbing up to broader public understanding, thus serving the interests of the lay society, too.

Dedication to quality

Each Frontiers article is a landmark of the highest quality, thanks to genuinely collaborative interactions between authors and review editors, who include some of the world's best academicians. Research must be certified by peers before entering a stream of knowledge that may eventually reach the public - and shape society; therefore, Frontiers only applies the most rigorous and unbiased reviews. Frontiers revolutionizes research publishing by freely delivering the most outstanding research, evaluated with no bias from both the academic and social point of view. By applying the most advanced information technologies, Frontiers is catapulting scholarly publishing into a new generation.

What are Frontiers Research Topics?

Frontiers Research Topics are very popular trademarks of the *Frontiers journals series*: they are collections of at least ten articles, all centered on a particular subject. With their unique mix of varied contributions from Original Research to Review Articles, Frontiers Research Topics unify the most influential researchers, the latest key findings and historical advances in a hot research area.

Find out more on how to host your own Frontiers Research Topic or contribute to one as an author by contacting the Frontiers editorial office: frontiersin.org/about/contact

Preclinical models and emerging technologies to study the effects of the tumor microenvironment on cancer heterogeneity and drug resistance

Topic editors

Giulia Adriani — Singapore Immunology Network (A*STAR), Singapore

Paola Cappello — University of Turin, Italy

Sara Lovisa — Humanitas University, Italy

Citation

Adriani, G., Cappello, P., Lovisa, S., eds. (2023). *Preclinical models and emerging technologies to study the effects of the tumor microenvironment on cancer heterogeneity and drug resistance*. Lausanne: Frontiers Media SA.

doi: 10.3389/978-2-8325-3703-9

Table of contents

04 Editorial: Preclinical models and emerging technologies to study the effects of the tumor microenvironment on cancer heterogeneity and drug resistance
Giulia Adriani, Paola Cappello and Sara Lovisa

07 Patient-derived cancer models: Valuable platforms for anticancer drug testing
Sofia Genta, Bryan Coburn, David W. Cescon and Anna Spreafico

23 Modelling metastatic colonization of cholangiocarcinoma organoids in decellularized lung and lymph nodes
Gilles S. van Tienderen, Marije E. A. van Beek, Ivo J. Schurink, Oskar Rosmark, Henk P. Roest, Jantine Tieleman, Jeroen Demmers, Iain Muntz, James Conboy, Gunilla Westergren-Thorsson, Gijsje Koenderink, Luc JW van der Laan and Monique M. A. Verstegen

41 Recent advances in vascularized tumor-on-a-chip
Christina Bao Xian Huang and Ting-Yuan Tu

56 Optimizing culturing conditions in patient derived 3D primary slice cultures of head and neck cancer
Maria do Carmo Greier, Annette Runge, Jozsef Dudas, Lukas Carpentari, Volker Hans Schartinger, Avneet Randhawa, Melissa Mayr, Monika Petersson and Herbert Riechelmann

66 *In vitro* models of breast cancer bone metastasis: analyzing drug resistance through the lens of the microenvironment
Anaïs Lamouline, Simone Bersini and Matteo Moretti

84 Tumor heterogeneity: preclinical models, emerging technologies, and future applications
Marco Proietto, Martina Crippa, Chiara Damiani, Valentina Pasquale, Elena Sacco, Marco Vanoni and Mara Gilardi

108 The promise and challenge of spatial omics in dissecting tumour microenvironment and the role of AI
Ren Yuan Lee, Chan Way Ng, Menaka Priyadharsani Rajapakse, Nicholas Ang, Joe Poh Sheng Yeong and Mai Chan Lau

119 The role of tumor microenvironment in drug resistance: emerging technologies to unravel breast cancer heterogeneity
Vincenzo Salemme, Giorgia Centonze, Lidia Avalle, Dora Natalini, Alessio Piccolantonio, Pietro Arina, Alessandro Morellato, Ugo Ala, Daniela Taverna, Emilia Turco and Paola Defilippi

141 Three-dimensional heterotypic colorectal cancer spheroid models for evaluation of drug response
Jia Ning Nicolette Yau and Giulia Adriani

150 Characterization of 3D heterocellular spheroids of pancreatic ductal adenocarcinoma for the study of cell interactions in the tumor immune microenvironment
Giulio Giustarini, Germaine Teng, Andrea Pavesi and Giulia Adriani

frontiers | Frontiers in Oncology

TYPE Editorial
PUBLISHED 28 September 2023
DOI 10.3389/fonc.2023.1289756

OPEN ACCESS

EDITED AND REVIEWED BY
Tao Liu,
University of New South Wales, Australia

*CORRESPONDENCE
Giulia Adriani
Giulia_adriani@immunol.a-star.edu.sg

RECEIVED 06 September 2023
ACCEPTED 07 September 2023
PUBLISHED 28 September 2023

CITATION
Adriani G, Cappello P and Lovisa S (2023) Editorial: Preclinical models and emerging technologies to study the effects of the tumor microenvironment on cancer heterogeneity and drug resistance. *Front. Oncol.* 13:1289756. doi: 10.3389/fonc.2023.1289756

Editorial: Preclinical models and emerging technologies to study the effects of the tumor microenvironment on cancer heterogeneity and drug resistance

Giulia Adriani[1,2]*, Paola Cappello[3] and Sara Lovisa[4,5]

[1]Singapore Immunology Network (SIgN), Agency for Science, Technology and Research (A*STAR), Singapore, Singapore, [2]Department of Biomedical Engineering, National University of Singapore (NUS), Singapore, Singapore, [3]Department of Molecular Biotechnology and Health Sciences, University of Turin, Torino, Italy, [4]Department of Biomedical Sciences, Humanitas University, Milan, Italy, [5]Department of Gastroenterology, IRCCS Humanitas Research Hospital, Rozzano, Milan, Italy

KEYWORDS

tumor microenvironment, tumor heterogeneity, scRNA seq, spatial biology, preclinical tumor models, 3D tumor models, *in vivo* tumor models

Editorial on the Research Topic
Preclinical models and emerging technologies to study the effects of the tumor microenvironment on cancer heterogeneity and drug resistance

Cancer research has witnessed remarkable advancements in recent years, with molecularly targeted treatments and immunotherapy revolutionizing patient care. However, some cancer types, such as pancreatic ductal adenocarcinoma, continue to defy treatment, and the emergence of drug resistance remains a significant challenge, hampering efforts to achieve lasting remission, especially in metastatic disease. In the past, cancer development was solely attributed to the appearance of genomic alterations in cancer cells. In the last decades, a broad consensus arose about the necessity for cancer cells to cooperate with host cells, such as fibroblasts, vascular cells, lymphatic cells, and immune cells during carcinogenesis and cancer progression. Therefore, the focus shifted toward understanding the tumor microenvironment (TME) heterogeneity and its impact on cancer evolution and drug resistance. In this dynamic landscape, innovative preclinical models and cutting-edge technologies have emerged as indispensable tools in TME characterization and, in general, in the efforts against cancer (Figure 1).

Understanding the heterogeneous nature of tumors has presented significant challenges, but recent insights into the TME role have lightened up new paths for therapeutic exploration. This Research Topic examine various facets of the TME influence on cancer heterogeneity and drug resistance, encompassing diverse cancer types, including breast, colorectal, pancreatic, liver, and head and neck cancers. While each article offers a unique perspective, they collectively emphasize the role of the TME in shaping tumor behavior and response to treatment.

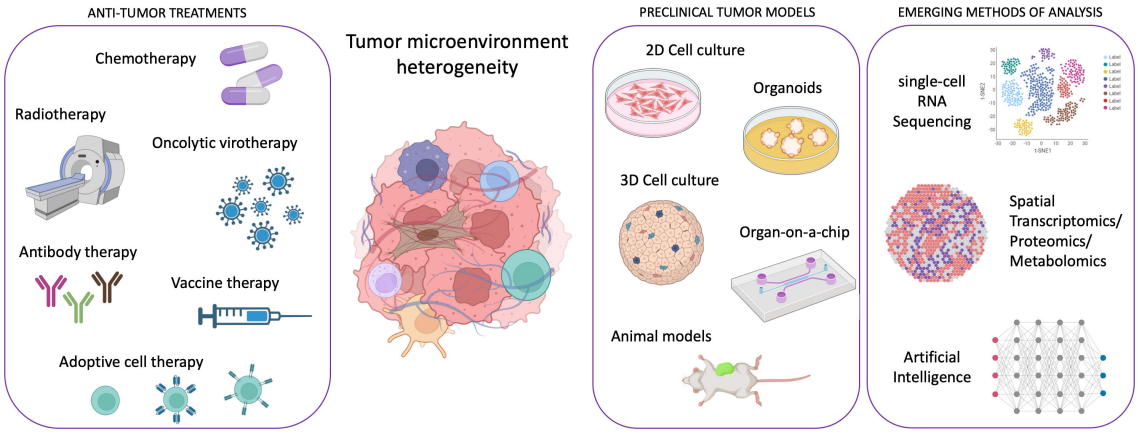

FIGURE 1
Scheme illustrating the framework of emergent technologies and preclinical tumor models for addressing the complexity of tumor microenvironment heterogeneity in order to enhance the efficacy of anti-tumor therapies. Created with Biorender.com.

Genta et al., Huang and Tu, and Proietto et al. highlight the advances of preclinical models in deciphering the complexities of the TME. Genetically engineered mouse models, patient-derived organoids and xenografts, and three-dimensional (3D) cell cultures have all emerged as essential tools to study cancer progression, acquired heterogeneity, and predict drug efficacy with an enhanced clinical relevance. Genta et al. encompass both *in vitro* and *in vivo* platforms for drug testing, stressing the relevance of patient-derived models to maintain the molecular affinity with the parental tumors and predict patient response. However, the authors also draw attention to the challenge that, despite their use in co-clinical trials and their value in understanding drug resistance, the data generated often arrive too late to modify the therapeutic plans effectively. Huang and Tu dive into the specific challenges posed by tumor heterogeneity and the microenvironment in vascularized tumor models, widely discussing the advantages and limitations of organ-on-a-chip models in replicating the vascularized tumor microenvironment. The addition of different types of supporting cells, namely pericytes, astrocytes, or lymphatic cells, makes those organ-on-a-chip models closely mimic the heterotypic cellular interactions within tumors. Further, the inclusion of organ-specific normal cells allows for assessing general drug toxicity. However, the authors also comment on some limitations, such as the accessibility to quantify cellular forces and cell stiffness. Proietto et al. extensively review the TME preclinical models and broaden the discussion to include the role of emerging single-cell, spatial genomic, and metabolomic technologies in understanding tumor complexity and evolution to design better targeted therapies. The authors highlight the need for multidisciplinary approaches to combat the challenges posed by tumor heterogeneity. Lee et al. remarkably contribute to further highlight the growing significance of cutting-edge spatial omics technologies in dissecting TME heterogeneity, also introducing the value added by artificial intelligence in unraveling the complex interactions within the TME.

The other articles in the Research Topic offer innovative insights on specific cancers, discussing advances in their modeling for preclinical studies and their organotypic TME role in drug resistance. Yau et al. look at the importance of incorporating diverse cell populations within colorectal cancer spheroid models to mimic the intricate signaling pathways and heterogeneity found *in vivo*. Salemme et al. extensively discuss the characteristics of breast cancer, a highly heterogeneous disease, that leads to drug resistance and encompass the advances in developing *in vivo* and *in vitro* models to recapitulate breast cancer complexity. Another work about breast cancer by Lamouline et al. focuses on *in vitro* models for breast cancer metastasis in bone, elegantly discussing the cellular heterogeneity of this specific microenvironment, shedding light on the critical need to account for the different microenvironments in *in vitro* models dedicated to the study of metastasis to accurately mimic tissue-specific cell-cell and cell-extracellular matrix (ECM) interactions when assessing drug sensitivity. Indeed, van Tienderen et al. present a novel *in vitro* model of cholangiocarcinoma metastasis by ingeniously combining patient-derived organoids with decellularized human tissues, confirming the intricate interplay between cancer cells and the ECM in driving dissemination to distant organs such as lung and lymph nodes. Dedicated to studying drug pharmacological effects and tissue physiology is the model proposed by Greier et al. in their paper, in which they demonstrate the promising potential of 3D primary slice cultures to provide preclinical models for studying head and neck cancer and obtain data in a week frame to guide clinicians in the choice of treatments. Giustarini et al. establish human 3D heterocellular tumor spheroids as models mirroring the complexity of the pancreatic ductal adenocarcinoma environment. Notably, these tissue-specific spheroids reveal immunosuppressive tendencies and mimic spatial and cytokine signatures observed in patients, confirming their value for better therapy testing. The more we advance our ability to reproduce complex high-throughput systems *in vitro*, particularly through the consistent and standardized utilization of patient-derived samples for drug library testing, the sooner we will have a time-saving and cost-effective alternative to *in vivo* mouse models. While very powerful and extensively used, these animal models present ethical and variance concerns in rigorously reflecting human tumor evolution and heterogeneity, delaying drug development processes.

This Research Topic presents a comprehensive picture of the recent advancements in understanding the TME influence on cancer heterogeneity and drug resistance. As these studies collectively suggest, it is clear that an accurate understanding of the TME role is pivotal for designing effective cancer therapies. This Research Topic highlights how the essential collaboration between clinicians, researchers, and technologists in developing advanced preclinical models and cutting-edge technologies is uncovering the subtle interactions between cancer cells, immune cells, and the surrounding microenvironment to develop effective therapeutics that will tackle drug resistance and improve patient outcomes worldwide.

Author contributions

GA: Writing – original draft. PC: Writing – review & editing. SL: Writing – review & editing.

Acknowledgments

We extend our sincere gratitude to the remarkable group of authors whose dedication and intellectual contributions have made this research topic a reality. We thank the institutions for providing resources to share advances and scientific knowledge in cancer research. This work was supported by the AIRC-IG grant (grant number 26341) and the Fondazione CRT grant (grant number CRT-2020.0719) to PC, by the 1st Italy-Singapore Science and Technology Cooperation grant (grant number R23I0IR036) to GA and PC, by the AIRC-Start-Up grant (grant number 24750), the European Union's Horizon 2020 research and innovation programme under Marie Sklodowska-Curie grant agreement (grant number 101029427) to SL.

Conflict of interest

The authors declare that the research was conducted in the absence of any commercial or financial relationships that could be construed as a potential conflict of interest.

Publisher's note

frontiers | Frontiers in Oncology

TYPE Review
PUBLISHED 12 August 2022
DOI 10.3389/fonc.2022.976065

OPEN ACCESS

EDITED BY
Sara Lovisa,
Humanitas University, Italy

REVIEWED BY
Julienne Leigh Carstens,
University of Alabama at Birmingham, United States
Alessandro De Vita,
Scientific Institute of Romagna for the Study and Treatment of Tumors (IRCCS), Italy

*CORRESPONDENCE
Anna Spreafico
anna.spreafico@uhn.ca

SPECIALTY SECTION
This article was submitted to Molecular and Cellular Oncology, a section of the journal Frontiers in Oncology

RECEIVED 23 June 2022
ACCEPTED 12 July 2022
PUBLISHED 12 August 2022

CITATION
Genta S, Coburn B, Cescon DW and Spreafico A (2022) Patient-derived cancer models: Valuable platforms for anticancer drug testing.
Front. Oncol. 12:976065.
doi: 10.3389/fonc.2022.976065

Patient-derived cancer models: Valuable platforms for anticancer drug testing

Sofia Genta[1], Bryan Coburn[2], David W. Cescon[1] and Anna Spreafico[1]*

[1]Division of Medical Oncology and Hematology, Princess Margaret Cancer Centre, University Health Network, University of Toronto, Toronto, ON, Canada, [2]Division of Infectious Diseases, Toronto General Hospital, University Health Network, Toronto, ON, Canada

Molecularly targeted treatments and immunotherapy are cornerstones in oncology, with demonstrated efficacy across different tumor types. Nevertheless, the overwhelming majority metastatic disease is incurable due to the onset of drug resistance. Preclinical models including genetically engineered mouse models, patient-derived xenografts and two- and three-dimensional cell cultures have emerged as a useful resource to study mechanisms of cancer progression and predict efficacy of anticancer drugs. However, variables including tumor heterogeneity and the complexities of the microenvironment can impair the faithfulness of these platforms. Here, we will discuss advantages and limitations of these preclinical models, their applicability for drug testing and in co-clinical trials and potential strategies to increase their reliability in predicting responsiveness to anticancer medications.

KEYWORDS

patient-derived model, PDO, drug-testing, co-clinical trial, PDX, cancer

Abbreviations: ADP, Acoustic droplet printing; BC, breast cancer; BRAF, B-rapidly accelerated fibro sarcoma; CAR-T, chimeric antigen receptor T-cell; CCN, CancerCellNet; CDX, cell line derived tumor xenograft; CRC, colorectal cancer; CRISPR-Cas9, clustered regularly interspaced short palindromic repeats/associated protein; CTC, circulating tumor cell; GEMM, Genetically engineered mouse model; ECM, extracellular matrix; EGFR, epidermal growth factor receptor; HER-2, epidermal growth factor receptor 2; HNSCC, head and neck squamous cell cancer; ICI, immune checkpoint inhibitors; IFN-γ, interferon gamma; MHC, major histocompatibility complex; NSCLC, non-small cell lung cancer; NK, natural killer; NOD/SCID, non-obese diabetic/severe combined immunodeficient; OS, overall survival; PD-1, protein death 1; PD-L1, protein death 1ligand; PDO, patient-derived organoid; PDX, patient derived xenograft; TCR, T cell receptor; TEC, tumour explant cultures; TIL, tumor infiltrating lymphocyte; TME, tumor microenvronment; TNBC, triple negative breast cancer; TSC, tumour slice cultures.

1 Introduction

Cancer is a genetic disease that results in cumulative alterations of molecular pathways involved in cell growth, survival and proliferation (1, 2). Until a few decades ago, chemotherapy and endocrine therapy represented the only treatment options for patients with advanced malignancies, and tumor histology was the only benchmark for drug selection (1). The identification of disrupted molecular pathways has notably broadened the therapeutic opportunities for cancer patients, allowing the development of small molecules and monoclonal antibodies exploiting oncogenic driver alterations as drug targets (3). The favorable therapeutic index demonstrated by several of these agents enabled their integration into clinical practice. A large number of such agents are now in clinical use, including epidermal growth factor receptor (*EGFR*) inhibitors in *EGFR* mutated non-small cell lung cancer (NSCLC) (4), anti-epidermal growth factor receptor 2 (*HER2*) agents in HER2-positive breast (5) and gastric cancer (6), B-rapidly accelerated fibro sarcoma (*BRAF*) inhibitors for the treatment of melanoma and other *BRAF* mutated tumors (7). The advent of immunotherapy has ushered in therapeutic strategies that promote immune response against neoplastic cells (8). Many different types of immune-therapeutics have now entered the clinic and some of them, such as immune checkpoint inhibitors (ICIs) and chimeric antigen receptor (CAR)-T cells, have improved patient outcomes (9, 10). In certain settings, including Hodgkin's lymphoma, melanoma, NSCLC, head and neck, urothelial and renal cell carcinoma, ICIs have replaced previous standard therapies due to overall survival (OS) benefits. Despite the achieved improvement in patient outcomes with the introduction of targeted drugs and immunotherapy, the majority of subjects do not respond to these treatments or experience only a temporary benefit (11, 12). Primary (or intrinsic) and secondary (or acquired) resistance, led by resistance-driving factors in neoplastic tissue before the exposure to an anticancer agent or as a consequence of the antitumor treatment respectively, represent the main reasons for treatment failure with these agents (12). To distinguish between primary and acquired resistance is not always straightforward. Different subpopulations of cancer cells, characterized by specific genomic profiles, usually coexist in the same patient. The phenomenon of intra-patient tumor heterogeneity can be spatial (e.g. in different locations) or temporal (e.g. between primary tumor versus metastasis) (13). Tumor heterogeneity adds complexity to the identification of pre-existing or exposure-induced resistant clones. Multiple mechanisms can be responsible for primary and acquired resistance to specific compounds in different tumor types and their identification is a crucial step in the identification of effective, individualized treatments (14) (Figure 1). Patient-derived human cancer models have the potential to retain their distinctive molecular hallmarks, representing a unique opportunity to study cancer cell survival and resistance mechanisms (15–17). If combined with clinical studies, these tools might increase the success of experimental treatments (18, 19). This review will discuss the available preclinical models and the reliability of such platforms to predict the responsiveness to anticancer agents, focusing on patient-derived models (Figure 2).

2 Two- and three-dimensional cell cultures modeling

2.1 Cancer cell lines

Human cancer cell lines represent the earliest and most widely used preclinical model for the investigation of tumor biology and antitumor drugs testing (20). Starting from the 1950s *in vitro* cultures of immortalized cancer cells have been developed from a wide variety of haematological and solid malignancies. These models have been used to assess the effectiveness of investigational anticancer compounds taking advantage of their ease of maintenance and propagation, relatively low cost, reproducibility and high-throughput evaluation (21). However, antitumor activity demonstrated with this approach is often not confirmed in clinical settings, mainly due to the low resemblance to human cancers *in vivo*, and lack of well-defined parameters to translate *in vitro* sensitivity into predicted clinical success (22). This divergence depends on several factors. Firstly, the *in vitro* growth process results in the selection of clones with specific features promoting their survival, outliving other subpopulations. Secondly, the progressive adaptation to culture conditions results in a loss of heterogeneity and differentiation (23). Thirdly, the absence of a natural tumor microenvironment (TME) impairs the evaluation of drugs whose mechanism of action is based on cell-cell interactions or is related to angiogenesis (24). To create platforms with a higher similarity to human cancers and to represent a broader range of tumor types, three-dimensional cultures and *in vivo* models have been developed.

2.2 Spheroids

Tumor-derived spheroids are self-assembled micro-aggregates of cancer cells grown in a culture medium, under low-adhesion conditions. They can be generated from cancer cell cultures, patient-derived tumor cells (tumor spheres) or from suspension of single cells from cancer cell lines (25, 26). Spheroid generation is characterized by an initial phase of exponential growth followed by a period of structural organization, which leads to the formation of an external coat of proliferating cells surrounding a necrotic core (27, 28). The cell population located in the inner, hypoxic layers displays a quiescent status. This results in resistance to anticancer drugs exploiting high proliferative rate as a target, mimicking tumor behavior *in vivo* (27). The source of cells used to establish the spheroids has a big impact on the model's characteristics: for

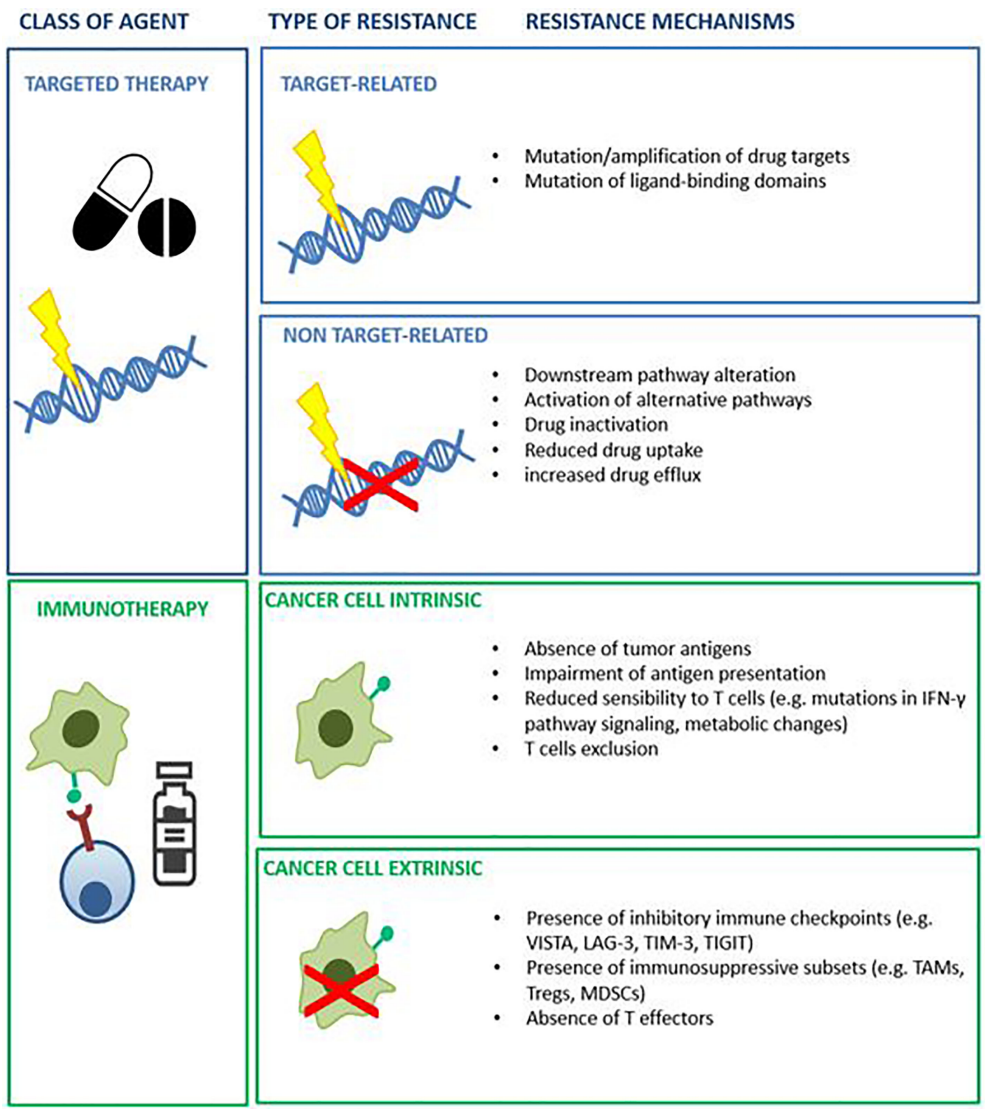

FIGURE 1
Example of known mechanism of resistance to targeted agents and immunotherapy.

example, spheroids derived from bi-dimensional cell lines will maintain cellular clonality while tumorspheres will display a higher heterogeneity (27, 29).

2.3 Organoids

Patient-derived organoids (PDOs) are preclinical models generated from cancer tissue, mechanically or enzymatically dissociated, and then embedded in an extracellular matrix. They differ from spheroids because they are self-organized in three-dimensional structures resembling the architecture and genomic features of the original tissue and retain the capability to regenerate (26, 30). The time required to generate organoids is variable and tumor dependant (31). PDOs of a wide range of malignancies have been established, with success rates up to 80% depending on tumor types (32–40). Mutagenesis technologies such as clustered, regularly interspaced, short palindromic repeats (CRISPR)/CRISPR-associated protein (Cas9) have been used to induce cancer-driving mutations to develop tumoral organoids starting from healthy human tissue (31, 41); an approach particularly useful to study carcinogenesis. Organoids derived from both neoplastic and healthy tissues can be established from the same patient to facilitate the identification of therapeutic agents with high antitumor activity and low impact on physiological tissues (42).

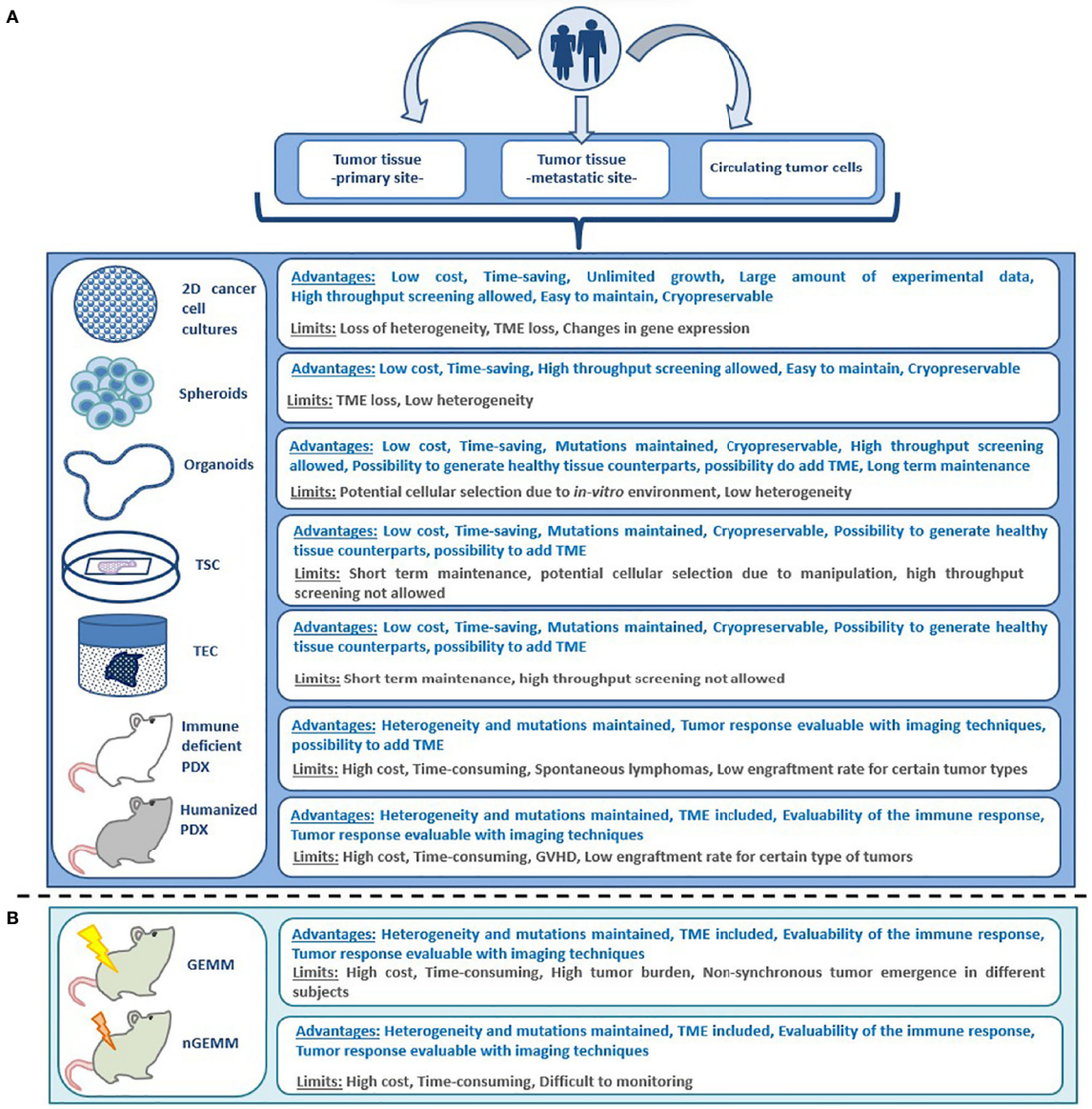

FIGURE 2
Advantages and limitations of different preclinical models for anticancer drug testing; **(A)** patient derived models, **(B)** non patient-derived animal models. GEMM, genetically engineered mouse model; GVHD, graft versus host disease; nGEMM, non-germinal genetically engineered mouse model; PDX, patient-derived xenograft; TEC, tumor explant culture; TME, tumor microenvironment; 2D, bi-dimensional; TSC, tumor slice culture.

2.4 *Ex-vivo* models: Organotypic tumor slice and tumor explant cultures

The term *ex-vivo* is referred to models generated by tissue samples collected from an individual and then preserved in an artificial environment, outside the original organism (43). Organotypic tumor slice cultures (TSCs) are obtained by incubation of thin slices of tissue in controlled conditions allowing oxygen and nutrient distribution (44). This approach has been used to develop models of different types of malignancies, including breast, gastric, head and neck and pancreatic cancer (45–51). When compared to other preclinical models, TSCs offer some advantages including the preservation of an intact tumour microenvironment and a quicker set up, allowing timely drug testing (47). TSCs however, have main limitations such as rapid deterioration of cell viability and tissue architecture as well as unfeasibility of culture propagation (52). Moreover, the resemblance of these

models to original tissue is highly influenced by procedural manipulation and sample processing (52). Tumour slice cultures represent only one of the multiple approaches attempted for the generation of *ex-vivo* models. Explanted cancer tissue can be preserved by submerging it in culture media or using a support to keep it in contact with the media such as gelatine sponges (53), grids or culture wells coated by a matrix (54, 55). One of the main advantages of these techniques as compared to tumor slice cultures is that they minimize tissue manipulation and assure higher tissue integrity. On the other hand, tissue slice models may allow a better distribution of anticancer drugs for testing. As for tumor slice cultures, short tissue viability is one of the main limitations for all tumor explant platforms (56). Several attempts have been made in order to delay models deterioration for example through the integration of microfluidic systems allowing prolonged tissue viablity (56).

3 *In vivo* models

3.1 Non-patient-derived *in vivo* models: The role of engineered mouse models

In vivo models enable the evaluation of cancer biology and treatment strategies in a complex organism. Genetically engineered mouse models (GEMMs) are transgenic mice harbouring alleles which lead to the spontaneous development of malignancies in immunocompetent animals (57). The development of GEMMs represented an important milestone in cancer research, as these models have been used to demonstrate that oncogene expression and tumor suppressor gene loss can induce neoplastic transformation of normal cells (58, 59). GEMMs have several limitations. The presence of pathogenic mutations affecting many target cells at an organism or tissue level can result in simultaneous development of multiple malignancies and consequently early death of the model. Furthermore, if present in germline cells, these mutations can affect embryonic viability, cause developmental abnormalities or impair normal tissue development (60). On the other hand, cancer onset in GEMMs can be delayed due to incomplete penetrance of the mutations, resulting in non-synchronous tumor occurrence in different mice and thus impairing the simultaneous evaluation of multiple anticancer agents. The development of non-germline GEMMs and conditional GEMMs, together with novel technologies for genome editing including CRISPR-Cas9 have helped overcome these limitations, enhancing the reliability of engineered mouse models in predicting drug responsiveness (59, 61, 62).

3.2 Patient-derived *in-vivo* models

Patient Derived Xenograft (PDXs) are preclinical models established from human neoplastic cells injection or tumor tissue implantation in immune-deficient animal hosts. PDXs are characterized by the maintenance of molecular and cellular heterogeneity of the primary tumor (63). The success rate of PDX establishment depends on multiple variables including the animal recipient, cancer type, and the technique used to implant the tumor (64). Metastatic tumors showing aggressive behaviour more frequently result in successful engraftment. Specific tumor types, such as colorectal or gastric cancer demonstrate a higher probability of engraftment compared with malignancies originating from other sites such as breast (particularly hormone dependent) or kidney (64–66). Many techniques have been used to optimize engraftment, including orthotopic transplant or, in the case of hormone-dependant cancers, the addition of human hormones (53, 67). Furthermore, the probability of obtaining successful engraftment increases with the degree of immunosuppression in the animal host. A greater rate of success can be achieved using animal models lacking functions of both B and T lymphocytes and of natural killer (NK) cells such as non-obese diabetic (NOD)/severe combined immunodeficient (SCID), in particular NOD/SCID/IL-2 receptor-γ deficient (NOG and NSG) and NOD/SCID/Janus kinase 3 deficient (NOJ) mouse models (64). Mice represent the most common type of host used for PDX generation however, other species can be used for this purpose (68–73). *In-vivo* models can also be generated in non-mammalian species, such as zebrafish (68). Both transgenic and xenograft models have been established for different tumor types including endocrine pancreatic cancer (69), multiple myeloma (74), head and neck squamous cell cancer (75), sarcoma (76)and melanoma (70–72), demonstrating some advantages in comparison with traditional mouse models. These include a higher rate of breeding, lower costs of maintenance and the possibility to track malignant cells with fluorescent labelling in the transparent casper zebrafish strain. Moreover, the process of engraftment for zebrafish PDXs is easier and faster compared to their murine counterparts (72, 73). To better recapitulate the original TME, humanized animal models have been developed (77, 78). These models can be obtained by xenotransplanting human immune cells or by engineering the host to express specific human genes. Humanized *in vivo* models, hosting not only human cancer cells but also a human-like TME are particularly suitable to test different anticancer strategies, including immunotherapy.

4 Key features of valuable platforms for antitumor drug testing

4.1 Genomic and transcriptomic fidelity

Faithful recapitulation of the molecular profile of the original tumor is one of the key characteristics to predict responsiveness to antitumor compounds. PDXs have been considered the most

reliable reproduction of human cancers for a long time, retaining more than 80% of the genomic alterations harboured by the engrafted neoplastic tissue (79–81). However, several potential discrepancies have been identified. PDXs often demonstrate a higher aggressiveness with increased proliferation rate -especially at later passages- than human tumors *in situ*. Moreover, some evidence suggests that these models may acquire or select for copy number alterations and single nucleotide variants, or exhibit transcriptional alterations, which can affect the anticancer drug sensitivity (82, 83). Organoids and spheroids have emerged as cost-effective alternatives to animal models, with high genomic concordance with primary tumors (81, 84–88). Multiple factors however, can reduce their resemblance to original cancer tissue or affect their long-term preservation. The purity and the viability of the cancer cells selected to initiate the culture are of crucial importance to ensure successful generation of the model (42). The composition of the culture medium is another key factor. Appropriate nutrient and growth factor modulation are needed to avoid overgrowth of normal cells that would counteract the development of the cancer models (41). The composition of the medium has also demonstrated to influence epigenomic modulation and gene expression (89, 90) and to affect the consumption of glutamine, alanine and other elements from cancer cells (89). *In vitro* culture itself can lead to significant transcriptomic changes, resulting in the upregulation of several growth and metabolism-related pathways such as PI3K, glycolysis and oxidative phosphorylation (90). Some attempts have been made to compare the transcriptional faithfulness of different types of models. As an example, Da Peng et al. have developed the CancerCellNet (CCN), a computational tool evaluating the transcriptomic fidelity of cancer cell lines, PDXs, GEMMs and 3D cultures, through comparison with The Cancer Genome Atlas dataset (91). This approach is burdened by significant limitations, including the small number of models for specific tumor types, the lack of proteomic and epigenomic information, and the fact that the transcriptomic profiles are compared with bulk RNA that includes also non-cancer cells. However, CCN provides some interesting insights indicating that the suitability of different models in proving a faithful reproduction of the original tissue may vary across tumors originating from different sites. This should be considered in studies where generating preclinical models across different tumor types is planned. The application of machine learning algorithms to large datasets collecting genomic and transcriptomic profiles from thousands of patient-derived models can partially overcome the discrepancy with original tumours and optimize drug testing in preclinical studies (92–95). This approach has indeed facilitated the identification of genomic signatures predicting drug sensitivity with a greater precision than single-gene biomarkers (96). Moreover, integrating tumor profiling with analysis of other components of TME, such as the T-cells deep learning models can identify multidimensional biomarker signatures and unveil mechanisms of resistance to anticancer drugs (97, 98).

4.2 Preserving tumor heterogeneity

The capability of a model to replicate the molecular features of the original tissue is not enough to ensure success in predicting treatment response. Tumor heterogeneity plays a crucial role in promoting the onset and selection of genomic alterations that lead to cancer cell survival from targeted and immunotherapeutic agents (90). Both PDXs and 3D cultures have been originated from different portions of a same tumor lesion or from different metastatic sites to investigate this phenomenon (99–101). As an example, Li et al. generated PDOs from the primary tumour and paired liver metastases in two patients with colorectal cancer (100). The organoids derived from the metastases demonstrated a more aggressive phenotype with a greater propensity for invasion and higher replication index. Despite providing useful information, this approach is expensive, complex and requires multiple invasive procedures. More importantly, the understanding of genomic aberrations is still limited to specific biopsy sites, hence not practical to predict drug responsiveness. Circulating tumor cells (CTCs), released into the bloodstream from the primary tumour and secondary lesions represent a unique opportunity for the development of complex models for broad evaluation of the genomic landscape of metastatic tumors. CTCs are challenging to isolate as they occur at low frequencies. Data regarding the generation of 3D cultures from CTCs are still limited, however, some successful attempts have been reported (33, 102, 103). In 2014 Gao et al. generated PDOs from CTCs in one patient with prostate cancer with extensive metastatic disease (33). Whole-exome sequencing of PDOs and of a metastatic lymph node resected from the same patient one year before were compared. Only 67% of the point mutations found in the PDOs were identified in the archival tissue. While some of the mutations might be acquired during the culturing process this can reflect tumor heterogeneity. CTCs have also been used to establish animal models, known as cell line derived tumour xenografts (CDXs). Hodgkinson et al. generated CDX models by injecting blood obtained from 4 patients with small cell lung cancer (SCLC), enriched with CTCs (104). Genomic analysis of CDXs shown preservation of original mutational profile, moreover these models mimicked patients responses to chemotherapy. Despite representing a possible strategy to overcome tumor heterogeneity, this approach has some limitations including technical challenges in isolation and expansion of CTCs, lack of stromal and immune components, uncertain representation of different metastatic sites and possible selection of specific clones (105). Despite using CTCs to initiate a patient-derived model the preservation of tumor heterogeneity might be challenged by the fact that cancer cells with particular molecular alterations are

more difficult to expand. As an example Li et al. reported a lower rate of success for organoids generation from colorectal cancer with microsatellite instability (MSI) or *BRAF* mutations (106). Interestingly when looking at the possible causes contributing to the failure of these models authors observed that cancer cells harbouring MSI or *BRAF* mutations were more dependant for their survivorship on other components of the tumor microenvironment such as immune cells. This indicate that the maintenance of a proficient TME aside from enabling the evaluation of anticancer therapies such as immunotherapy might be a key factor also for the maintenance of tumor heterogeneity.

4.3 Tumor Microenvironment Preservation

4.3.1 Tumor microenvironment preservation in 3D cultures

There has been much recent effort to develop preclinical models with an intact TME preserving functional immune effectors (25, 107). 3D models hosting competent immune cells can be obtained by co-culturing previously expanded immune cells (108). Both spheroid (109–111), and organoid (112, 113) cultures have been developed with this technique. T cells generated using this process were shown to efficiently kill cancer cells, while they did not show activity against organoids originated from healthy tissue, confirming the maintenance of self-tolerance (112). Courau et al. used this approach to generate immune-competent spheroids from colorectal cancer by co-culturing these models with immune cells obtained from healthy donors (111). They observed rapid infiltration from allogenic transferred T and NK cells, resulting in immune-related cell death. Moreover, they used this platform to test the activity of antibodies targeting natural killer group 2 member D (NKG2D) and its ligands. They observed an enhancement of spheroids immune-mediated killing, driven by an increase of NK infiltration, supporting the utility of this type of model to identify new therapeutic strategies. The co-culturing approach, however, does not fully recapitulate the complexity of the TME, as it lacks native infiltrating immune populations and other key factors, regulating the interaction between cancer and immune system. The extracellular matrix (ECM), the complex of proteins, polysaccharides and other elements surrounding the cells, give structure and sustain both normal and neoplastic tissues. Cancer-associated fibroblasts producing collagen as well as alterations of other elements of ECM, such as hyaluronic acid, metalloproteases and lysyl oxidases are known to promote cancer initiation and invasion through ECM remodeling (114) and have been related to resistance to multiple anticancer agents (115). Moreover, the recognition of the key role played by ECM in cancer resulted in the development of antitumor drugs directly targeting ECM molecules or the cell-matrix crosstalk (115). This led to an urgent need of preclinical models for drug testing retaining a functional ECM. Multiple synthetic and biological materials have been used to develop scaffolds to support the generation of 3D cultures, mimicking ECM. Examples include hydroxyapatite-graphene (116), polyethylene glycol oxide (117), chitosan alginate (118–120), collagen (76, 121) and matrigel (117, 122). Different materials present specific advantages but also limitations. As an example hydrogels are highly biocompatible and recapitulate the biochemical composition of original matrix but offer low mechanical resistance (122). To include original immune populations different 3D models have been developed (123). The feasibility of this approach has been initially demonstrated in healthy human epithelial breast tissue (124). Zumwalde et al. observed the presence of T cells in mammary ductal epithelial PDOs, producing interferon (IFN)-γ and proliferating in response to zoledronic acid. Interestingly, these lymphocytes showed cytotoxic activity towards a triple negative breast carcinoma cell line. The air-liquid interface technique allows to generate PDOs from both healthy and neoplastic tissue with preserved epithelial and mesenchymal components, retaining proficient immune effectors and ECM (123, 125, 126). This method enables organoids to be propagated as epithelial-mesenchymal hybrids using an inner collagen gel–containing transwell with direct air exposure (127). Using this approach Neal et al. generated PDOs from 28 distinct tumor types of human and murine malignancies including colorectal, kidney, lung and pancreatic cancer (123). Human PDO analysis demonstrated the presence of CD3+ tumor infiltrating lymphocytes (TILs), macrophages, B and NK cells. Single-cell gene expression profiling indicated that TILs present within PDOs maintained the original TCR repertoire observed in the tumor biopsy. Protein death 1 (PD-1) expression was observed on the surface of immune cells included in the cultures and the exposure to anti-PD/PD-ligand 1 (PD-L1) agents resulted in the expansion of TILs and in the promotion of neoplastic cells killing. The air-liquid interface technique is not the only possible approach to preserve original TME. Jacob et al. successfully generated PDOs from glioblastoma patients performing microdissection of original tissue into pieces of ≈1 mm diameter instead of dissociation, in order to preserve native cell-cell interactions (128). Single-cell transcriptome analysis shown similar cytokine expression in macrophage and microglia from original tissue and PDOs. Moreover, a similar distribution of cells in PDOs generated at later time points was observed, indicating the capability of this model to preserve and maintain at least in part the features of parental TME. Once established, these models have been used to test multiple antitumor compounds, including CAR-T cells. The resemblance of PDO models to the parental cancer can be further implemented by the organs-on-a-chip technology (129). Through the use of customized microfluidic cell culture devices, this approach allows the vascularization of 3D cultures, mimicking physiological delivery of drugs through the blood

vessels (130). Chemo- and biosensors can be integrated in this type of models to optimize the control of oxygen and metabolites levels (131). 3D bioprinting techniques can also be used to develop preclinical models fully recapitulating the architecture of parental tumors, including a functional vascular system and enabling a uniform distribution of different cellular components (132, 133). This approach consists in the controlled deposition of layers of patient-derived cancer and stromal cells, signalling molecules and other biomaterials to generate spheroids or organoids with a functional TME. The use of 3D bioprinting is rapidly expanding and different systems are currently available including extrusion-based bioprinting, laser-based bioprinting, and droplet-based bioprinting (134). 3D bioprinted PDOs and spheroids have already been successful established for multiple cancer types including glioblastoma, neuroblastoma, multiple myeloma, melanoma and cholangiocarcinoma and used to test novel anticancer treatments such as oncolytic viruses (135–141). TEC and TSC represent another possible approach to preserve TME and test immune-oncology strategies, despite the limited time frame for drug-testing. As an example, Sivakumar *et al.* successfully used TSC to test the effect of IFN-γ and PD L1 blockage (47).

4.3.2 Immune-competent *in-vivo* models

The reconstruction of a proficient TME can be applied to *in vivo* models. In GEMMs, spontaneous neoplastic transformation in immunocompetent animals leads to the onset of tumors retaining TME (61, 142). However, the cross-reactivity between the murine and the human targets, especially when the tested agents need antigen presentation by human MHC class I, limits the use of GEMMs to test immunotherapy (143). Humanized animal models are promising platforms for the evaluation of immunotherapeutic strategies. Knock-in mice expressing key human genes regulating the cross-talk between cancer and immune system have been generated, including PD-1 (144), PDL1 (145), LAG3 (145), CTLA4 (77) and IL-15 (146). These platforms could be useful to not only to test drug sensitivity but also to study immune related toxicities associated with monoclonal antibodies specifically binding human targets, such as human PD1 or CTLA4. As an example, Du et al. used CTLA4 humanized mice to test anti-CTLA4 antibodies including ipilimumab, alone and in combination with an anti-PD1 (77). They observed correlation between the development of immune related toxicity and systemic T cell activation with an increased percentage of effector T memory lymphocytes. Humanized PDX models obtained with the engraftment of human immune cells into immunocompromised animals represent another possible approach to obtain animal models suitable for immunotherapy testing (78). This strategy is however burdened by multiple limitations (147). Firstly, the efficacy of the model is limited by the severity of the immunosuppression of the PDX hosts; models with impaired T-cells function but maintained innate immunity will reject human cells. Secondly, since the hematopoietic cells cannot be propagated across multiple animals, this approach requires sequential blood draws from the patients. Finally, the infusion of human hematopoietic cells results in graft versus host disease of PDXs, limiting the timeframe for observation. The transfer of hematopoietic cells is not the only option attempted to generate humanized PDX models. The injection of patient-specific TILs has demonstrated to mimic antitumor responses observed in patients (148). This technique has contributed to identify a dysfunctional subset of CD8+ cells as possible mechanism of resistance to PD 1 inhibitors in NSCLC (149). *Ex-vivo* expansion and subsequent re-infusion of TILs is not the only approach attempted in order to elicit antitumor activity. Yin et al. injected nanoparticle incorporating immunostimulants molecules to induce antitumor activity in endogenous TILs in mouse models. This strategy resulted in CD8+ cells expansion and reduction of regulatory T cells as well as in a delay of tumour growth (150).

4.4 Evaluating the impact of microbiome

The human microbiota, the set microorganisms populating human epithelial surfaces, influences the development of several pathologic conditions, including cancer (151). For patient-derived models, this has important conceptual implications: First - for some patient-derived models, the microbial ecology of the model (e.g. the experimental animal's endogenous microbiota) may influence experimental outcomes and therefore must be accounted for in experimental design and analysis. For example, in murine models, vendor-specific microbiota (152), microbial metabolites (153) and microbiome-tumour neoantigen cross-reactivity (154) have all been implicated in immunotherapy responsiveness. Thus, ignorance of the composition or contribution of the microbiota to model outcomes may result in contradictory findings between investigators, or even within a research group based on variability in the composition of the microbiome between experimental replicates. Secondly - experimental manipulation of the microbiome in patient-derived models may identify novel (host or microbial) targets representing promising therapeutic avenues (155). Both 3D cultures and animal models have been used to mechanistically implicate the microbiome in cancer biology. Using intestinal PDOs, Kadosh et al. observed that the addition of the microbial metabolite gallic acid alters the effect of Trp53 gain of function mutations from tumor-suppressive to pro-oncogenic (156). In adenomatous polyposis coli (*APC*)-mutated mouse models, depletion of *Streptococcus thermophilus* plays a key role in colorectal cancer tumorigenesis (157). The impact of probiotic and high fiber diet on immunotherapy outcomes have been

evaluated in several studies showing controversial results (158, 159). Spencer et al. observed an association between higher dietary fiber content and prolonged progression-free survival in melanoma patients receiving ICI while the use of probiotic shown a detrimental effect in the same population (160). To validate these results, they tested the influence of fiber and probiotics on anti-PD1 responses in patient-derived mouse models, confirming that a diet with lower fiber content and addition of a probiotic reduced cytotoxic TILs (160). Finally, mice with microbiome transplanted from human donors (with cancer) represent a type of patient-derived model themselves (161). Routy et al. compared mice with fecal microbiomes transplanted from human patients who responded to anti-PD1 antibody and those receiving fecal transplant from non-responders and found a greater density of intratumoral CD8+ T cells, upregulation of PD L1 and a lower presence of myeloid suppressive cells was in mice transplanted with responders' stools, suggesting microbiota-induced "hot" TME (162). Critically, these observations have led to the development of novel, microbiome-targeting therapeutic strategies. Shi et al. evaluated the impact of combining a probiotic agent, *Escherichia coli* strain Nissle 1917, to an anti-Transforming Growth Factor, Beta (TGF-β) compound in mice transplanted with breast and hepatocellular carcinoma cells (163). They reported greater tumor growth inhibition and metastasis suppression in models receiving the probiotic. They also observed an increase in the proportion of intratumoral CD8+ T cells and greater numbers of mature dendritic cells in tumour-draining lymph nodes. Fecal transplants from treatment-responsive donors have been investigated in clinical trials assessing their potential to restore sensitivity to immunotherapy in refractory melanoma (164, 165). These data highlight the experimental importance and potential utility of microbiome-informed preclinical studies and the potential for patient-derived microbiome models for the investigation of cancer biology and therapeutic discovery (147).

5 Inclusion of patient-derived models in co-clinical trials

Patient-derived platforms have allowed investigators to perform drug testing in models originated from subjects simultaneously receiving therapy in clinical trials. These types of studies, known as co-clinical trials, use laboratory data to guide clinical development or treatment strategies, with the final goal of identifying predictive biomarkers and increasing the rate of success of experimental treatments (166). As an example, Kim et al. tested the fibroblast growth factor receptor (FGFR) inhibitor dovitinib in PDXs derived from squamous cell lung cancer patients treated with the same drug in a clinical study (167). They observed preservation of genomic and histologic profiles of parental tumours in PDXs. The responsiveness to dovitinib displayed by the models recapitulated the clinical outcomes observed in the patients. Gene expression profiling performed in the PDXs indicated upregulation of FGF3 and FGF19 in responders, representing a potential predictive biomarker. The Gustave Roussy MATCH-R project is another example of a co-clinical trial. This is a prospective study aimed at extensive characterization of tumours with acquired resistance to immunotherapeutic agents or targeted therapies. Generation of PDX models for 54 patients with a success rate of 33% and the highest probability of engraftment for urothelial bladder cancer (72.7%) was reported (168). Despite these models being helpful to provide further insights into the mechanism of drug resistance, the authors reported that the outcome data from drug testing were often not timely to guide clinical decision-making. Having a faster turnaround time and being easier to maintain, PDOs might be more suitable for co-clinical studies (169). Yao et al. used PDOs originated from patients with rectal cancer to test the efficacy of chemoradiation and compared it with clinical outcomes (170). The authors reported poor response to chemoradiation in 42/64 patients whose models were resistant, and a good response in 16/17 patients with matched responsive PDOs. They also tested the responsiveness to single components of the chemoradiation regiment (5-FU, irinotecan and radiation) and correlated it with clinical responses. Good clinical outcomes were observed in patients whose PDOs were sensitive to one, two or all the three agents. A good clinical response was reported in 3 patients with PDOs resistant to all three components of the chemoradiation regimen, tested separately. Interestingly, when these models were exposed to the combination, drug synergy was demonstrated in one of the PDOs indicating the potential utility of these models to explore combined treatments to overcome drug resistance. The reliability of PDOs in predicting responses to radiation and chemotherapy in patients with rectal cancer has been evaluated also by further co-clinical studies (171–173). Park et al. developed PDOs from 33 patients radiation for retal adenocarcinoma and confirmed the possibility to use these models to predict sensibility through a machine-learning algorithm (171). In another study, Ganesh et al. were able to generate 65 PDOs from 41 patients with newly diagnosed, metastatic or recurrent rectal cancer with a success rate of 77% (172). Interestingly, 43/65 PDOs were established from samples obtained after exposure to 1 or 2 lines of systemic therapy demonstrating the possibility to generate 3D cultures from pre-treated tumors. Hu et al. have shown that is possible to minimize the time for anticancer drug testing by using microwell arrays that enable to evaluate PDOs sensitivity to hundreds of different compounds at passage 0 (174). Aside from allowing a timely determination of anticancer activity the possibility to perform drug testing at an early stage might reduce the risk of phenotypic changes at later passages and the need of complex culture media

with growth factors enrichment. Acoustic droplet printing (ADP) is another approach attempted to decrease the time necessary for PDOs generation (134, 175, 176). This technique enables the development of PDOs in 2 weeks, with preservation of autologous immune cells and integration of a microfluidic system for drug delivery (134). These characteristics make ADP-generated PDOs a promising platform for anticancer drug testing including immunotherapeutic agents. Another critical step to implement co-clinical trial is the definition of fast and standardized methods for the interpretation of antitumor activity in the pre-clinical models. Usually drug sensitivity is estimated using cell viability assays such as ATP-dependent luminescence, tetrazolium-based colorimetric techniques, or fluoresce-based assays (90). These techniques however results PDOs death impairing sequential assessments (177). Emergent technologies such as label-free light microscopy and positron-emission microscopy have been tested to evaluate the antitumor activity of investigational agents in 3D cultures (90, 178, 179). Light microscopy might provide a more precise measurement of antitumor activity because it allows the evaluation of cell viability at single organoid level (90). Moreover, this technique demonstrated the potential to detect not only cytotoxic but also cytostatic activity (90). With the use of positron-emission microscopy was possible to establish that PDOs retain metabolic characteristics of parental tumours, indicating that this technique can be used to monitor responses in the organoid cultures (178). Even when the data obtained from preclinical models are not suitable to guide treatment decisions the information provided by these platforms might be precious to unveil mechanisms underlying drug resistances and develop strategies to restore or increase responsiveness to treatments (180, 181). Moreover, this approach can be used to support the

TABLE 1 Ongoing co-clinical trials using patient-derived models for drug testing.

Target population	Intervention	N of patients	Type of preclinical model	NCT number
Stage II-III TNBC	Neoadjuvant chemotherapy base clinical trial not guided by PDX	135	PDX	NCT02124902
Metastatic TNBC	Personalized treatament guided by miniPDX and RNA sequencing	100	miniPDX	NCT04745975
Operated GI cancers	Adjuvant chemotherapy not guided by PDX	120	PDX (zebrafish)	NCT03668418
Pancreatic cancer	Personalized treatment guided by miniPDX	100	miniPDX	NCT04373928
Lung and HNSCC	Standard or experimental systemic treatment not guided by PDX	30	PDX	NCT02597738
Metastatic NSCLC PD-L1+ who failed platinum based treatment	Pembrolizumab not guided by PDX	50	PDX	NCT03134456
Childhood cancers	Personalized treatment guided by molecular profiling and PDX	400	PDX	NCT03336931
Recurrent mantle cell lymphoma	Ibrutinib not guided by PDX	50	PDX	NCT03219047
Localized or metastatic kidney cancer	Personalised treatment guided by PDX	50	PDX	NCT04602702
Metastatic CRPC	Personalised treatment guided by miniPDX	15	miniPDX	NCT03786848
Metastatic CRC	Cetuximab not guided by PDO	80	PDO	NCT04906733
Metastatic pancreatic cancer	Chemotherapy guided by PDO	100	PDO	NCT04931381
Resected pancreatic cancer	Adjuvant chemotherapy guided by PDO	200	PDO	NCT04931394
HNSCC, CRC, breast or epithelial ovarian cancer	Chemotherapy guided by PDO	35	PDO	NCT04279509
Non muscle-invasive bladder cancer	Chemotherapy guided by PDO (instillation)	33	PDO	NCT05024734
Metastatic HER2 negative BC	Chemotherapy guided by PDO	15	PDO	NCT04450706
Operable HER2 positive BC	Chemotherapy + anti-HER2 agents not guided by PDO	94	PDO	NCT04281641
NSCLC	Treatment guided by PDO	100	PDO	NCT04826913
Localized and metastatic CRC	Standard chemotherapy not guided by PDO	120	3D bioprinted PDO	NCT04755907
Advanced BC	Standard therapy not guided by PDO	15	PDO	NCT04655573
Solid tumors	Engineering TCR-T cells	30	PDO	NCT03778814
Locally advanced resectable esophagogastric carcinoma	Standard chemotherapy not guided by PDO	40	PDO	NCT03429816
Locally advanced esophageal cancer	Chemoradiation not guided by PDO	140	PDO	NCT03081988

BC, breast cancer; CRC, colorectal cancer; CRPC, castration-resistant prostate cancer; GI, gastrointestinal; HNSCC, head and neck squamous cell cancer; NSCLC, non-small cell lung cancer; PDO, patient-derived organoids; PDX, patient-derived xenograft; TNBC, triple negative breast cancer.

development of non-invasive techniques for the prediction of disease response. As an example, Roy et al. used patient derived PDXs of TNBC to identify [(18)F] fluorodeoxyglucose with positron emission tomography radiomic signatures of response to neoadjuvant chemotherapy (182). A list of co-clinical trials currently ongoing is reported in Table 1.

6 Conclusion and future perspectives

Patient-derived models are powerful tools with multiple applications in oncology. Their molecular characterization and incorporation in multiomic biomarker-driven studies is crucial to identify mechanisms of resistance to anticancer treatments and guide the development of effective therapeutic strategies. The Immune Resistance Interrogation Study (IRIS, NCT04243720) currently ongoing at our institution, NEO-R (NCT04504747) and PITCHER (NCT04714957) are some examples of prospective trials using this approach. High genomic and transcriptomic fidelity, preservation of tumor heterogeneity and presence of a proficient TME are some of the key factors that should be implemented to obtain results that can be translated into clinic. The availability of large PDO and PDX repositories combined with the development of machine learning techniques can partially bridge the molecular gap with original tumors and optimize drug testing in preclinical studies (92–95). Until today, tumor heterogeneity represented a main pitfall, jeopardizing the reliability of preclinical models in predicting drug sensitivity. Although there is a big caveat on the success and expansion of CTCs, there is a question of whether they could help overcome this limitation by capturing inter- and intratumoral heterogeneity. The use of 3D bioprinting techniques might enable the development of complex 3D cultures starting from CTCs, comprising proficient autologous immune cells and vascular system. Aside from overcoming tumour heterogeneity, the use of CTCs as primary source for the development of cancer models may offer further advantages. Due to its relatively low invasiveness, a liquid biopsy-based approach might be particularly useful to investigate mechanisms of acquired resistance through the comparison of CDXs obtained by sequential blood draws. Finally multiple strategies have been implemented to preserve a functional TME leading to the development of complex *in-vivo*, *ex-vivo* and *in-vitro* models. These platforms may enable a deeper understanding of the factors regulating the networking between cancer cells and immune system, such as microbiome and ECM. Moreover humanized *in-vivo* models and 3D cultures retaining functional immune effectors and ECM are promising tools to test not only immunotherapy but also novel therapeutic strategies targeting critical processes underlying cancer initiation and progression such as matrix deposition and remodeling. Further elements should be taken into consideration if the patient derived model is intended to guide treatment selection in the context of a co-clinical trial. The models are highly time-sensitive. Despite the molecular affinity with the parental tumors, mouse PDXs need months to be established; therefore, limiting their applicability in treatment decision making, as demonstrated by the MATCH-R study (168). Alternative models including 3D cell cultures, along with innovative techniques such as 3D bioprinting and microwell arrays could overcome these limitations and have higher molecular fidelity thanks to the limited number of passages between tissue collection and drug-testing.

Author contributions

SG: conceptualization and original draft preparation; BC, DC, and AS: supervision and manuscript review/editing. All authors have read and agreed to the published version of the manuscript.

Conflict of interest

BC: Research funding: Nubiyota, Sanofi. DC: Consulting/Advisory: AstraZeneca, Extract Sciences, Eisai, Gilead, GlaxoSmithKline, Inivata, Merck, Novartis, Pfizer and Roche. Research funding to institution: AstraZeneca, Gilead, GlaxoSmithKline, Inivata, Merck, Pfizer and Roche. Patent (US62/675,228) for methods of treating cancers characterized by a high expression level of spindle and kinetochore associated complex subunit 3 (ska3) gene. AS: Consultant for (Advisory Board): Merck (compensated), Bristol-Myers Squibb (compensated), Novartis (compensated), Oncorus (compensated), Janssen (compensated). Grant/Research support from (Clinical Trials): Novartis, Bristol-Myers Squibb, Symphogen AstraZeneca/Medimmune, Merck, Surface Oncology, Northern Biologics, Janssen Oncology/Johnson & Johnson, Roche, Regeneron, Alkermes, Array Biopharma/Pfizer, GSK.

The remaining author declares that the research was conducted in the absence of any commercial or financial relationships that could be construed as a potential conflict of interest.

Publisher's note

References

1. Luo J, Solimini NL, Elledge SJ. Principles of cancer therapy: oncogene and non-oncogene addiction. *Cell* (2009) 136(5):823–37. doi: 10.1016/j.cell.2009.02.024

2. Hanahan D, Weinberg RA. Hallmarks of cancer: the next generation. *Cell* (2011) 144(5):646–74. doi: 10.1016/j.cell.2011.02.013

3. Dienstmann R, Rodon J, Barretina J, Tabernero J. Genomic medicine frontier in human solid tumors: prospects and challenges. *J Clin Oncol* (2013) 31(15):1874–84. doi: 10.1200/JCO.2012.45.2268

4. Li J, Kwok HF. Current Strategies for Treating NSCLC: From Biological Mechanisms to Clinical Treatment. *Cancers (Basel)* (2020). doi: 10.3390/cancers12061587

5. Loibl S, Gianni L. HER2-positive breast cancer. *Lancet* (2017) 389 (10087):2415–29. doi: 10.1016/S0140- 6736(16)32417-5

6. El Dika I, Ilson DH. Current and future therapies for targeting HER2 mutations in gastrointestinal cancer. *Expert Rev Anticancer Ther* (2018) 18 (11):1085–92. doi: 10.1080/14737140.2018.1510324

7. Subbiah V, Baik C, Kirkwood JM. . doi: 10.1016/j.trecan.2020.05.009

8. Velcheti V, Schalper K. Basic Overview of Current Immunotherapy Approaches in Cancer. *Am Soc Clin Oncol Educ Book* (2016) 35:298–308. doi: 10.14694/EDBK_15657210.1200/EDBK_156572

9. Feins S, Kong W, Williams EF, Milone MC, Fraietta JA. An introduction to chimeric antigen receptor (CAR) T-cell immunotherapy for human cancer. *Am J Hematol* (2019) 94(S1):S3–9. doi: 10.1002/ajh.25418

10. Gong J, Chehrazi-Raffle A, Reddi S, Salgia R. Development of PD-1 and PD-L1 inhibitors as a form of cancer immunotherapy: a comprehensive review of registration trials and future considerations. *J Immunother Cancer* (2018) 6(1):8. doi: 10.1186/s40425-018-0316-z

11. Sharma P, Hu-Lieskovan S, Wargo JA, Ribas A. Primary, Adaptive, and Acquired Resistance to Cancer Immunotherapy. *Cell* (2017) 168(4):707–23. doi: 10.1016/j.cell.2017.01.017

12. Hu X, Zhang Z. Understanding the Genetic Mechanisms of Cancer Drug Resistance Using Genomic Approaches. *Trends Genet* (2016) 32(2):127–37. doi: 10.1016/j.tig.2015.11.003

13. Bedard PL, AR H, MJ R, Siu LL. Tumour heterogeneity in the clinic. *Nature* (2013) 501(7467):355–64. doi: 10.1038/nature12627

14. Sarmento-Ribeiro AB, Scorilas A, Goncalves AC, Efferth T, Trougakos IP. The emergence of drug resistance to targeted cancer therapies: Clinical evidence. *Drug Resist Update* (2019) 47:100646. doi: 10.1016/j.drup.2019.100646

15. Tentler JJ, Tan AC, Weekes CD, Jimeno A, Leong S, Pitts TM, et al. Patient-derived tumour xenografts as models for oncology drug development. *Nat Rev Clin Oncol* (2012) 9(6):338–50. doi: 10.1038/nrclinonc.2012.61

16. Weeber F, Ooft SN, Dijkstra KK, Voest EE. Tumor Organoids as a Pre-clinical Cancer Model for Drug Discovery. *Cell Chem Biol* (2017) 24(9):1092–100. doi: 10.1016/j.chembiol.2017.06.012

17. Aparicio S, Hidalgo M, Kung AL. Examining the utility of patient-derived xenograft mouse models. *Nat Rev Cancer* (2015) 15(5):311–6. doi: 10.1038/nrc3944

18. Izumchenko E, Meir J, Bedi A, Wysocki PT, Hoque MO, Sidransky D. Patient-derived xenografts as tools in pharmaceutical development. *Clin Pharmacol Ther* (2016) 99(6):612–21. doi: 10.1002/cpt.354

19. Cescon D, Siu LL. Cancer Clinical Trials: The Rear-View Mirror and the Crystal Ball. *Cell* (2017) 168(4):575–78. doi: 10.1016/j.cell.2017.01.027

20. Gillet JP, Varma S, Gottesman MM. The clinical relevance of cancer cell lines. *J Natl Cancer Inst* (2013) 105(7):452–8. doi: 10.1093/jnci/djt007

21. Goodspeed A, Heiser LM, Gray JW, Costello JC. Tumor-Derived Cell Lines as Molecular Models of Cancer Pharmacogenomics. *Mol Cancer Res* (2016) 14 (1):3–13. doi: 10.1158/1541-7786.MCR-15- 0189

22. DiMasi JA, Reichert JM, Feldman L, Malins A. Clinical approval success rates for investigational cancer drugs. *Clin Pharmacol Ther* (2013) 94(3):329–35. doi: 10.1038/clpt.2013.117

23. Gao D, Chen Y. Organoid development in cancer genome discovery. *Curr Opin Genet Dev* (2015) 30:42– 8. doi: 10.1016/j.gde.2015.02.007

24. Sharma SV, Haber DA, Settleman J. Cell line-based platforms to evaluate the therapeutic efficacy of candidate anticancer agents. *Nat Rev Cancer* (2010) 10 (4):241–53. doi: 10.1038/nrc2820

25. Costa EC, Moreira AF, de Melo-Diogo D, Gaspar VM, Carvalho MP, Correia IJ. 3D tumor spheroids: an overview on the tools and techniques used for their analysis. *Biotechnol Adv* (2016) 34(8):1427– 41. doi: 10.1016/j.biotechadv.2016.11.002

26. Clevers H. Modeling Development and Disease with Organoids. *Cell* (2016) 165(7):1586–97. doi: 10.1016/j.cell.2016.05.082

27. Zanoni M, Cortesi M, Zamagni A, Arienti C, Pignatta S, Tesei A. Modeling neoplastic disease with spheroids and organoids. *J Hematol Oncol* (2020) 13(1):97. doi: 10.1186/s13045-020-00931-0

28. Minchinton AI, Tannock IF. Drug penetration in solid tumours. *Nat Rev Cancer* (2006) 6(8):583–92. doi: 10.1038/nrc1893

29. Carragher N, Piccinini F, Tesei A, Trask OJJr., Bickle M, Horvath P. Concerns, challenges and promises of high-content analysis of 3D cellular models. *Nat Rev Drug Discovery* (2018) 17(8):606. doi: 10.1038/nrd.2018.99

30. Gunti S, Hoke ATK, Vu KP, London NRJr.. Organoid and Spheroid Tumor Models: Techniques and Applications. *Cancers (Basel)* (2021). doi: 10.3390/cancers13040874

31. Tuveson D, Clevers H. Cancer modeling meets human organoid technology. *Science* (2019) 364(6444):952–55. doi: 10.1126/science.aaw6985

32. Boj SF, Hwang CI, Baker LA, Chio II, DD E, Corbo V, et al. Organoid models of human and mouse ductal pancreatic cancer. *Cell* (2015) 160(1-2):324–38. doi: 10.1016/j.cell.2014.12.021

33. Gao D, Vela I, Sboner A, Iaquinta PJ, Karthaus WR, Gopalan A, et al. Organoid cultures derived from patients with advanced prostate cancer. *Cell* (2014) 159(1):176–87. doi: 10.1016/j.cell.2014.08.016

34. Sachs N, de Ligt J, Kopper O, Gogola E, Bounova G, Weeber F, et al. A Living Biobank of Breast Cancer Organoids Captures Disease Heterogeneity. *Cell* (2018) 172(1-2):373–86 e10. doi: 10.1016/j.cell.2017.11.010

35. van de Wetering M, Francies HE, Francis JM, Bounova G, Iorio F, Pronk A, et al. Prospective derivation of a living organoid biobank of colorectal cancer patients. *Cell* (2015) 161(4):933–45. doi: 10.1016/j.cell.2015.03.053

36. Broutier L, Mastrogiovanni G, Verstegen MM, Francies HE, Gavarro LM, Bradshaw CR, et al. Human primary liver cancer-derived organoid cultures for disease modeling and drug screening. *Nat Med* (2017) 23(12):1424–35. doi: 10.1038/nm.4438

37. Lee SH, Hu W, Matulay JT, Silva MV, Owczarek TB, Kim K, et al. Tumor Evolution and Drug Response in Patient-Derived Organoid Models of Bladder Cancer. *Cell* (2018) 173(2):515–28.e17. doi: 10.1016/j.cell.2018.03.017

38. Nanki Y, Chiyoda T, Hirasawa A, Ookubo A, Itoh M, Ueno M, et al. Patient-derived ovarian cancer organoids capture the genomic profiles of primary tumours applicable for drug sensitivity and resistance testing. *Sci Rep* (2020) 10(1):12581. doi: 10.1038/s41598-020-69488-9

39. Wilson BE, Gorrini C, Cescon DW. Breast cancer immune microenvironment: from pre-clinical models to clinical therapies. *Breast Cancer Res Treat* (2021). doi: 10.1007/s10549-021-06431-0

40. Driehuis E, Kretzschmar K, Clevers H. Establishment of patient-derived cancer organoids for drug- screening applications. *Nat Protoc* (2020) 15(10):3380–409. doi: 10.1038/s41596-020-0379-4

41. Drost J, van Boxtel R, Blokzijl F, Mizutani T, Sasaki N, Sasselli V, et al. Use of CRISPR-modified human stem cell organoids to study the origin of mutational signatures in cancer. *Science* (2017) 358(6360):234–38. doi: 10.1126/science.aao3130

42. Drost J, Clevers H. Organoids in cancer research. *Nat Rev Cancer* (2018) 18 (7):407–18. doi: 10.1038/s41568-018-0007-6

43. Powley IR, Patel M, Miles G, Pringle H, Howells L, Thomas A, et al. Patient-derived explants (PDEs) as a powerful preclinical platform for anti-cancer drug and biomarker discovery. *Br J Cancer* (2020) 122(6):735–44. doi: 10.1038/s41416-019-0672-6

44. Vaira V, Fedele G, Pyne S, Fasoli E, Zadra G, Bailey D, et al. Preclinical model of organotypic culture for pharmacodynamic profiling of human tumors. *Proc Natl Acad Sci U.S.A.* (2010) 107(18):8352–6. doi: 10.1073/pnas.0907676107

45. Misra S, Moro CF, Del Chiaro M, Pouso S, Sebestyen A, Lohr M, et al. Ex vivo organotypic culture system of precision-cut slices of human pancreatic ductal adenocarcinoma. *Sci Rep* (2019) 9(1):2133. doi: 10.1038/s41598-019-38603-w

46. Salas A, Lopez J, Reyes R, Evora C, de Oca FM, Baez D, et al. Organotypic culture as a research and preclinical model to study uterine leiomyomas. *Sci Rep* (2020) 10(1):5212. doi: 10.1038/s41598- 020-62158-w

47. Sivakumar R, Chan M, Shin JS, Nishida-Aoki N, Kenerson HL, Elemento O, et al. Organotypic tumor slice cultures provide a versatile platform for immuno-oncology and drug discovery. *Oncoimmunology* (2019) 8(12):e1670019. doi: 10.1080/2162402X.2019.1670019

48. Kenerson HL, Sullivan KM, Seo YD, Stadeli KM, Ussakli C, Yan X, et al. Tumor slice culture as a biologic surrogate of human cancer. *Ann Transl Med* (2020) 8(4):114. doi: 10.21037/atm.2019.12.88

49. Weitz JR, Tiriac H, Hurtado de Mendoza T, Wascher A, Lowy AM. Using Organotypic Tissue Slices to Investigate the Microenvironment of Pancreatic

Cancer: Pharmacotyping and Beyond. *Cancers (Basel)* (2021). doi: 10.3390/cancers13194991

50. Gerlach MM, Merz F, Wichmann G, Kubick C, Wittekind C, Lordick F, et al. Slice cultures from head and neck squamous cell carcinoma: a novel test system for drug susceptibility and mechanisms of resistance. *Br J Cancer* (2014) 110 (2):479–88. doi: 10.1038/bjc.2013.700

51. Lim CY, Chang JH, Lee WS, Lee KM, Yoon YC, Kim J, et al. Organotypic slice cultures of pancreatic ductal adenocarcinoma preserve the tumor microenvironment and provide a platform for drug response. *Pancreatology* (2018) 18(8):913–27. doi: 10.1016/j.pan.2018.09.009

52. Klinghammer K, Walther W, Hoffmann J. Choosing wisely - Preclinical test models in the era of precision medicine. *Cancer Treat Rev* (2017) 55:36–45. doi: 10.1016/j.ctrv.2017.02.009

53. Centenera MM, Hickey TE, Jindal S, Ryan NK, Ravindranathan P, Mohammed H, et al. A patient- derived explant (PDE) model of hormone-dependent cancer. *Mol Oncol* (2018) 12(9):1608–22. doi: 10.1002/1878-0261.12354

54. Majumder B, Baraneedharan U, Thiyagarajan S, Radhakrishnan P, Narasimhan H, Dhandapani M, et al. Predicting clinical response to anticancer drugs using an ex vivo platform that captures tumour heterogeneity. *Nat Commun* (2015) 6:6169. doi: 10.1038/ncomms7169

55. Ghosh S, Prasad M, Kundu K, Cohen L, Yegodayev KM, Zorea J, et al. Tumor Tissue Explant Culture of Patient-Derived Xenograft as Potential Prioritization Tool for Targeted Therapy. *Front Oncol* (2019) 9:17. doi: 10.3389/fonc.2019.00017

56. Dorrigiv D, Simeone K, Communal L, Kendall-Dupont J, St-Georges-Robillard A, Peant B, et al. Microdissected Tissue vs Tissue Slices-A Comparative Study of Tumor Explant Models Cultured On-Chip and Off-Chip. *Cancers (Basel)* (2021). doi: 10.3390/cancers13164208

57. Kersten K, de Visser KE, van Miltenburg MH, Jonkers J. Genetically engineered mouse models in oncology research and cancer medicine. *EMBO Mol Med* (2017) 9(2):137–53. doi: 10.15252/emmm.201606857

58. Sinn E, Muller W, Pattengale P, Tepler I, Wallace R, Leder P. Coexpression of MMTV/v-Ha-ras and MMTV/c-myc genes in transgenic mice: synergistic action of oncogenes. *vivo. Cell* (1987) 49(4):465–75. doi: 10.1016/0092-8674(87)90449-1

59. Heyer J, Kwong LN, Lowe SW, Chin L. Non-germline genetically engineered mouse models for translational cancer research. *Nat Rev Cancer* (2010) 10(7):470–80. doi: 10.1038/nrc2877

60. Day CP, Merlino G, Van Dyke T. Preclinical mouse cancer models: a maze of opportunities and challenges. *Cell* (2015) 163(1):39–53. doi: 10.1016/j.cell.2015.08.068

61. Zitvogel L, Pitt JM, Daillere R, Smyth MJ, Kroemer G. Mouse models in oncoimmunology. *Nat Rev Cancer* (2016) 16(12):759–73. doi: 10.1038/nrc.2016.91

62. Gargiulo G. Next-Generation *in vivo* Modeling of Human Cancers. *Front Oncol* (2018) 8:429. doi: 10.3389/fonc.2018.00429

63. Hidalgo M, Amant F, Biankin AV, Budinska E, Byrne AT, Caldas C, et al. Patient-derived xenograft models: an emerging platform for translational cancer research. *Cancer Discovery* (2014) 4(9):998– 1013. doi: 10.1158/2159-8290.CD-14-0001

64. Okada S, Vaeteewoottacharn K, Kariya R. Application of Highly Immunocompromised Mice for the Establishment of Patient-Derived Xenograft (PDX) Models. *Cells* (2019). doi: 10.3390/cells8080889

65. Murayama T, Gotoh N. Patient-Derived Xenograft Models of Breast Cancer and Their Application. *Cells* (2019). doi: 10.3390/cells8060621

66. Namekawa T, Ikeda K, Horie-Inoue K, Inoue S. Application of Prostate Cancer Models for Preclinical Study: Advantages and Limitations of Cell Lines, Patient-Derived Xenografts, and Three- Dimensional Culture of Patient-Derived Cells. *Cells* (2019). doi: 10.3390/cells8010074

67. Hoffman RM. Patient-derived orthotopic xenografts: better mimic of metastasis than subcutaneous xenografts. *Nat Rev Cancer* (2015) 15(8):451–2. doi: 10.1038/nrc3972

68. Fazio M, Ablain J, Chuan Y, Langenau DM, Zon LI. Zebrafish patient avatars in cancer biology and precision cancer therapy. *Nat Rev Cancer* (2020) 20 (5):263–73. doi: 10.1038/s41568-020-0252-3

69. Yang HW, Kutok JL, Lee NH, Piao HY, Fletcher CD, Kanki JP, et al. Targeted expression of human MYCN selectively causes pancreatic neuroendocrine tumors in transgenic zebrafish. *Cancer Res* (2004) 64(20):7256–62. doi: 10.1158/0008-5472.CAN-04-0931

70. Patton EE, Widlund HR, Kutok JL, Kopani KR, Amatruda JF, Murphey RD, et al. BRAF mutations are sufficient to promote nevi formation and cooperate with p53 in the genesis of melanoma. *Curr Biol* (2005) 15(3):249–54. doi: 10.1016/j.cub.2005.01.031

71. Topczewska JM, Postovit LM, Margaryan NV, Sam A, Hess AR, Wheaton WW, et al. Embryonic and tumorigenic pathways converge *via* Nodal signaling: role in melanoma aggressiveness. *Nat Med* (2006) 12(8):925–32. doi: 10.1038/nm1448

72. Ablain J, Xu M, Rothschild H, Jordan RC, Mito JK, Daniels BH, et al. Human tumor genomics and zebrafish modeling identify SPRED1 loss as a driver of mucosal melanoma. *Science* (2018) 362(6418):1055–60. doi: 10.1126/science.aau6509

73. Yan C, Brunson DC, Tang Q, Do D, Iftimia NA, Moore JC, et al. Visualizing Engrafted Human Cancer and Therapy Responses in Immunodeficient Zebrafish. *Cell* (2019) 177(7):1903–14 e14. doi: 10.1016/j.cell.2019.04.004

74. Lin J, Zhang W, Zhao JJ, Kwart AH, Yang C, Ma D, et al. A clinically relevant *in vivo* zebrafish model of human multiple myeloma to study preclinical therapeutic efficacy. *Blood* (2016) 128(2):249–52. doi: 10.1182/blood-2016-03-704460

75. Miserocchi G, Spadazzi C, Calpona S, De Rosa F, Usai A, De Vita A, et al. Precision Medicine in Head and Neck Cancers: Genomic and Preclinical Approaches. *J Pers Med* (2022). doi: 10.3390/jpm12060854

76. De Vita A, Recine F, Miserocchi G, Pieri F, Spadazzi C, Cocchi C, et al. The potential role of the extracellular matrix in the activity of trabectedin in UPS and L-sarcoma: evidences from a patient-derived primary culture case series in tridimensional and zebrafish models. *J Exp Clin Cancer Res* (2021) 40(1):165. doi: 10.1186/s13046-021-01963-1

77. Du X, Liu M, Su J, Zhang P, Tang F, Ye P, et al. Uncoupling therapeutic from immunotherapy-related adverse effects for safer and effective anti-CTLA-4 antibodies in CTLA4 humanized mice. *Cell Res* (2018) 28(4):433–47. doi: 10.1038/s41422-018-0012-z

78. Mhaidly R, Verhoeyen E. Humanized Mice Are Precious Tools for Preclinical Evaluation of CAR T and CAR NK Cell Therapies. *Cancers (Basel)* (2020). doi: 10.3390/cancers12071915

79. deCarvalho AC, Kim H, Poisson LM, Winn ME, Mueller C, Cherba D, et al. Discordant inheritance of chromosomal and extrachromosomal DNA elements contributes to dynamic disease evolution in glioblastoma. *Nat Genet* (2018) 50 (5):708–17. doi: 10.1038/s41588-018-0105-0

80. Villafranca-Magdalena B, Masferrer-Ferragutcasas C, Lopez-Gil C, Coll-de la Rubia E, Rebull M, Parra G, et al. Genomic Validation of Endometrial Cancer Patient-Derived Xenograft Models as a Preclinical Tool. *Int J Mol Sci* (2022). doi: 10.3390/ijms23116266

81. Vanni S, De Vita A, Gurrieri L, Fausti V, Miserocchi G, Spadazzi C, et al. Myxofibrosarcoma landscape: diagnostic pitfalls, clinical management and future perspectives. *Ther Adv Med Oncol* (2022) 14:17588359221093973. doi: 10.1177/17588359221093973

82. Ben-David U, Ha G, Tseng YY, Greenwald NF, Oh C, Shih J, et al. Patient-derived xenografts undergo mouse-specific tumor evolution. *Nat Genet* (2017) 49 (11):1567–75. doi: 10.1038/ng.3967

83. Shi J, Li Y, Jia R, Fan X. The fidelity of cancer cells in PDX models: Characteristics, mechanism and clinical significance. *Int J Cancer* (2020) 146 (8):2078–88. doi: 10.1002/ijc.32662

84. Kim M, Mun H, Sung CO, Cho EJ, Jeon HJ, Chun SM, et al. Patient-derived lung cancer organoids as *in vitro* cancer models for therapeutic screening. *Nat Commun* (2019) 10(1):3991. doi: 10.1038/s41467-019-11867-6

85. Vlachogiannis G, Hedayat S, Vatsiou A, Jamin Y, Fernandez-Mateos J, Khan K, et al. Patient-derived organoids model treatment response of metastatic gastrointestinal cancers. *Science* (2018) 359(6378):920–26. doi: 10.1126/science.aao2774

86. Pasch CA, Favreau PF, Yueh AE, Babiarz CP, Gillette AA, Sharick JT, et al. Patient-Derived Cancer Organoid Cultures to Predict Sensitivity to Chemotherapy and Radiation. *Clin Cancer Res* (2019) 25(17):5376–87. doi: 10.1158/1078-0432.CCR-18-3590

87. de Witte CJ, Espejo Valle-Inclan J, Hami N, Lohmussaar K, Kopper O, Vreuls CPH, et al. Patient- Derived Ovarian Cancer Organoids Mimic Clinical Response and Exhibit Heterogeneous Inter- and Intrapatient Drug Responses. *Cell Rep* (2020) 31(11):107762. doi: 10.1016/j.celrep.2020.107762

88. Saito Y, Muramatsu T, Kanai Y, Ojima H, Sukeda A, Hiraoka N, et al. Establishment of Patient-Derived Organoids and Drug Screening for Biliary Tract Carcinoma. *Cell Rep* (2019) 27(4):1265–76 e4. doi: 10.1016/j.celrep.2019.03.088

89. Vande Voorde J, Ackermann T, Pfetzer N, Sumpton D, Mackay G, Kalna G, et al. Improving the metabolic fidelity of cancer models with a physiological cell culture medium. *Sci Adv* (2019). doi: 10.1126/sciadv.aau7314

90. Larsen BM, Kannan M, Langer LF, Leibowitz BD, Bentaieb A, Cancino A, et al. A pan-cancer organoid platform for precision medicine. *Cell Rep* (2021) 36 (4):109429. doi: 10.1016/j.celrep.2021.109429

91. Peng D, Gleyzer R, Tai WH, Kumar P, Bian Q, Isaacs B, et al. Evaluating the transcriptional fidelity of cancer models. *Genome Med* (2021) 13(1):73. doi: 10.1186/s13073-021-00888-w

92. Conte N, Mason JC, Halmagyi C, Neuhauser S, Mosaku A, Yordanova G, et al. PDX Finder: A portal for patient-derived tumor xenograft model discovery. *Nucleic Acids Res* (2019). doi: 10.1093/nar/gky984

93. Dudova Z, Conte N, Mason J, Stuchlik D, Pesa R, Halmagyi C, et al. The EurOPDX Data Portal: an open platform for patient-derived cancer xenograft data sharing and visualization. *BMC Genomics* (2022) 23(1):156. doi: 10.1186/s12864-022-08367-1

94. Adam G, Rampasek L, Safikhani Z, Smirnov P, Haibe-Kains B, Goldenberg A. Machine learning approaches to drug response prediction: challenges and recent progress. *NPJ Precis Oncol* (2020) 4:19. doi: 10.1038/s41698-020-0122-1

95. Mourragui SMC, Loog M, Vis DJ, Moore K, Manjon AG, van de Wiel MA, et al. Predicting patient response with models trained on cell lines and patient-derived xenografts by nonlinear transfer learning. *Proc Natl Acad Sci U.S.A.* (2021). doi: 10.1073/pnas.2106682118

96. Nguyen LC, Naulaerts S, Bruna A, Ghislat G, Ballester PJ. Predicting Cancer Drug Response In Vivo by Learning an Optimal Feature Selection of Tumour Molecular Profiles. *Biomedicines* (2021) 9(10). doi: 10.3390/biomedicines9101319

97. Gohil SH, Iorgulescu JB, Braun DA, Keskin DB, Livak KJ. Applying high-dimensional single-cell technologies to the analysis of cancer immunotherapy. *Nat Rev Clin Oncol* (2021) 18(4):244–56. doi: 10.1038/s41571-020-00449-x

98. Touat M, Li YY, Boynton AN, Spurr LF, Iorgulescu JB, Bohrson CL, et al. Mechanisms and therapeutic implications of hypermutation in gliomas. *Nature* (2020) 580(7804):517–23. doi: 10.1038/s41586- 020-2209-9

99. Cristobal A, van den Toorn HWP, van de Wetering M, Clevers H, Heck AJR, Mohammed S. Personalized Proteome Profiles of Healthy and Tumor Human Colon Organoids Reveal Both Individual Diversity and Basic Features of Colorectal Cancer. *Cell Rep* (2017) 18(1):263–74. doi: 10.1016/j.celrep.2016.12.016

100. Li H, Dai W, Xia X, Wang R, Zhao J, Han L, et al. Modeling tumor development and metastasis using paired organoids derived from patients with colorectal cancer liver metastases. *J Hematol Oncol* (2020) 13(1):119. doi: 10.1186/s13045-020-00957-4

101. Allaway RJ, Fischer DA, de Abreu FB, Gardner TB, Gordon SR, Barth RJ, et al. Genomic characterization of patient-derived xenograft models established from fine needle aspirate biopsies of a primary pancreatic ductal adenocarcinoma and from patient-matched metastatic sites. *Oncotarget* (2016) 7(13):17087–102. doi: 10.18632/oncotarget.7718

102. Zhang Z, Shiratsuchi H, Lin J, Chen G, Reddy RM, Azizi E, et al. Expansion of CTCs from early stage lung cancer patients using a microfluidic co-culture model. *Oncotarget* (2014) 5(23):12383–97. doi: 10.18632/oncotarget.2592

103. Mout L, van Dessel LF, Kraan J, de Jong AC, Neves RPL, Erkens-Schulze S, et al. Generating human prostate cancer organoids from leukapheresis enriched circulating tumour cells. *Eur J Cancer* (2021) 150:179–89. doi: 10.1016/j.ejca.2021.03.023

104. Hodgkinson CL, Morrow CJ, Li Y, Metcalf RL, Rothwell DG, Trapani F, et al. Tumorigenicity and genetic profiling of circulating tumor cells in small-cell lung cancer. *Nat Med* (2014) 20(8):897– 903. doi: 10.1038/nm.3600

105. Pantel K, Speicher MR. The biology of circulating tumor cells. *Oncogene* (2016) 35(10):1216–24. doi: 10.1038/onc.2015.192

106. Li X, Larsson P, Ljuslinder I, Ohlund D, Myte R, Lofgren-Burstrom A, et al. Ex Vivo Organoid Cultures Reveal the Importance of the Tumor Microenvironment for Maintenance of Colorectal Cancer Stem Cells. *Cancers (Basel)* (2020). doi: 10.3390/cancers12040923

107. Lamichhane SP, Arya N, Kohler E, Xiang S, Christensen J, Shastri VP. Recapitulating epithelial tumor microenvironment *in vitro* using three dimensional tri-culture of human epithelial, endothelial, and mesenchymal cells. *BMC Cancer* (2016) 16:581. doi: 10.1186/s12885-016-2634-1

108. Gronholm M, Feodoroff M, Antignani G, Martins B, Hamdan F, Cerullo V. Patient-derived organoids for precision cancer immunotherapy. *Cancer Res* (2021). doi: 10.1158/0008-5472.CAN-20-4026

109. Hirt C, Papadimitropoulos A, Mele V, Muraro MG, Mengus C, Iezzi G, et al. "*In vitro*" 3D models of tumor-immune system interaction. *Adv Drug Delivery Rev* (2014) 79-80:145–54. doi: 10.1016/j.addr.2014.05.003

110. Feder-Mengus C, Ghosh S, Reschner A, Martin I, Spagnoli GC. New dimensions in tumor immunology: what does 3D culture reveal? *Trends Mol Med* (2008) 14(8):333–40. doi: 10.1016/j.molmed.2008.06.001

111. Courau T, Bonnereau J, Chicoteau J, Bottois H, Remark R, Assante Miranda L, et al. Cocultures of human colorectal tumor spheroids with immune cells reveal the therapeutic potential of MICA/B and NKG2A targeting for cancer treatment. *J Immunother Cancer* (2019) 7(1):74. doi: 10.1186/s40425-019-0553-9

112. Dijkstra KK, Cattaneo CM, Weeber F, Chalabi M, van de Haar J, Fanchi LF, et al. Generation of Tumor-Reactive T Cells by Co-culture of Peripheral Blood Lymphocytes and Tumor Organoids. *Cell* (2018) 174(6):1586–98 e12. doi: 10.1016/j.cell.2018.07.009

113. Tsai S, McOlash L, Palen K, Johnson B, Duris C, Yang Q, et al. Development of primary human pancreatic cancer organoids, matched stromal and immune cells and 3D tumor microenvironment models. *BMC Cancer* (2018) 18(1):335. doi: 10.1186/s12885-018-4238-4

114. Walker C, Mojares E, Del Rio Hernandez A. Role of Extracellular Matrix in Development and Cancer Progression. *Int J Mol Sci* (2018). doi: 10.3390/ijms19103028

115. Cox TR. The matrix in cancer. *Nat Rev Cancer* (2021) 21(4):217–38. doi: 10.1038/s41568-020-00329-7

116. Li D, Nie W, Chen L, McCoul D, Liu D, Zhang X, et al. Self-Assembled Hydroxyapatite-Graphene Scaffold for Photothermal Cancer Therapy and Bone Regeneration. *J BioMed Nanotechnol* (2018) 14(12):2003–17. doi: 10.1166/jbn.2018.2646

117. Habanjar O, Diab-Assaf M, Caldefie-Chezet F, Delort L. 3D Cell Culture Systems: Tumor Application, Advantages, and Disadvantages. *Int J Mol Sci* (2021) 22(22). doi: 10.3390/ijms222212200

118. Le MN, Xu K, Wang Z, Beverung S, Steward RL, Florczyk SJ. Evaluation of the effect of 3D porous Chitosan-alginate scaffold stiffness on breast cancer proliferation and migration. *J BioMed Mater Res A* (2021) 109(10):1990–2000. doi: 10.1002/jbm.a.37191

119. Tan ML, Shao P, Friedhuber AM, van Moorst M, Elahy M, Indumathy S, et al. The potential role of free chitosan in bone trauma and bone cancer management. *Biomaterials* (2014) 35(27):7828–38. doi: 10.1016/j.biomaterials.2014.05.087

120. Shi X, Cheng Y, Wang J, Chen H, Wang X, Li X, et al. 3D printed intelligent scaffold prevents recurrence and distal metastasis of breast cancer. *Theranostics* (2020) 10(23):10652–64. doi: 10.7150/thno.47933

121. Hamdi DH, Barbieri S, Chevalier F, Groetz JE, Legendre F, Demoor M, et al. *In vitro* engineering of human 3D chondrosarcoma: a preclinical model relevant for investigations of radiation quality impact. *BMC Cancer* (2015) 15:579. doi: 10.1186/s12885-015-1590-5

122. Unnikrishnan K, Thomas LV, Ram Kumar RM. Advancement of Scaffold-Based 3D Cellular Models in Cancer Tissue Engineering: An Update. *Front Oncol* (2021) 11:733652. doi: 10.3389/fonc.2021.733652

123. Neal JT, Li X, Zhu J, Giangarra V, Grzeskowiak CL, Ju J, et al. Organoid Modeling of the Tumor Immune Microenvironment. *Cell* (2018) 175(7):1972–88 e16. doi: 10.1016/j.cell.2018.11.021

124. Zumwalde NA, Haag JD, Sharma D, Mirrielees JA, Wilke LG, Gould MN, et al. Analysis of Immune Cells from Human Mammary Ductal Epithelial Organoids Reveals Vdelta2+ T Cells That Efficiently Target Breast Carcinoma Cells in the Presence of Bisphosphonate. *Cancer Prev Res (Phila)* (2016) 9(4):305–16. doi: 10.1158/1940-6207.CAPR-15-0370-T

125. Li X, Nadauld L, Ootani A, Corney DC, Pai RK, Gevaert O, et al. Oncogenic transformation of diverse gastrointestinal tissues in primary organoid culture. *Nat Med* (2014) 20(7):769–77. doi: 10.1038/nm.3585

126. Wakamatsu T, Ogawa H, Yoshida K, Matsuoka Y, Shizuma K, Imura Y, et al. Establishment of Organoids From Human Epithelioid Sarcoma With the Air-Liquid Interface Organoid Cultures. *Front Oncol* (2022) 12:893592. doi: 10.3389/fonc.2022.893592

127. Ootani A, Li X, Sangiorgi E, Ho QT, Ueno H, Toda S, et al. Sustained *in vitro* intestinal epithelial culture within a Wnt-dependent stem cell niche. *Nat Med* (2009) 15(6):701–6. doi: 10.1038/nm.1951

128. Jacob F, Salinas RD, Zhang DY, Nguyen PTT, Schnoll JG, Wong SZH, et al. A Patient-Derived Glioblastoma Organoid Model and Biobank Recapitulates Inter- and Intra-tumoral Heterogeneity. *Cell* (2020) 180(1):188–204 e22. doi: 10.1016/j.cell.2019.11.036

129. Park SE, Georgescu A, Huh D. Organoids-on-a-chip. *Science* (2019) 364 (6444):960–65. doi: 10.1126/science.aaw7894

130. Shirure VS, Bi Y, Curtis MB, Lezia A, Goedegebuure MM, Goedegebuure SP, et al. Tumor-on-a-chip platform to investigate progression and drug sensitivity in cell lines and patient-derived organoids. *Lab Chip* (2018) 18(23):3687–702. doi: 10.1039/c8lc00596f

131. Dornhof J, Kieninger J, Muralidharan H, Maurer J, Urban GA, Weltin A. Microfluidic organ-on-chip system for multi-analyte monitoring of metabolites in 3D cell cultures. *Lab Chip* (2022) 22(2):225– 39. doi: 10.1039/d1lc00689d

132. Paolillo M, Comincini S, Schinelli S. *In Vitro* Glioblastoma Models: A Journey into the Third Dimension. *Cancers (Basel)* (2021). doi: 10.3390/cancers13102449

133. Augustine R, Kalva SN, Ahmad R, Zahid AA, Hasan S, Nayeem A, et al. 3D Bioprinted cancer models: Revolutionizing personalized cancer therapy. *Transl Oncol* (2021) 14(4):101015. doi: 10.1016/j.tranon.2021.101015

134. Gong Z, Huang L, Tang X, Chen K, Wu Z, Zhang L, et al. Acoustic Droplet Printing Tumor Organoids for Modeling Bladder Tumor Immune Microenvironment within a Week. *Adv Healthc Mater* (2021) 10(22):e2101312. doi: 10.1002/adhm.202101312

135. Quinn CH, Beierle AM, Hutchins SC, Marayati R, Bownes LV, Stewart JE, et al. Targeting High-Risk Neuroblastoma Patient-Derived Xenografts with Oncolytic Virotherapy. *Cancers (Basel)* (2022). doi: 10.3390/cancers14030762

136. Wu D, Wang Z, Li J, Song Y, Perez MEM, Wang Z, et al. A 3D-Bioprinted Multiple Myeloma Model. *Adv Healthc Mater* 2021:e2100884. doi: 10.1002/adhm.202100884

137. Jeong YM, Bang C, Park M, Shin S, Yun S, Kim CM, et al. 3D-Printed Collagen Scaffolds Promote Maintenance of Cryopreserved Patients-Derived Melanoma Explants. *Cells* (2021). doi: 10.3390/cells10030589

138. Tang M, Tiwari SK, Agrawal K, Tan M, Dang J, Tam T, et al. Rapid 3D Bioprinting of Glioblastoma Model Mimicking Native Biophysical Heterogeneity. *Small* (2021) 17(15):e2006050. doi: 10.1002/smll.202006050

139. Xie F, Sun L, Pang Y, Xu G, Jin B, Xu H, et al. Three-dimensional bio-printing of primary human hepatocellular carcinoma for personalized medicine. *Biomaterials* (2021) 265:120416. doi: 10.1016/j.biomaterials.2020.120416

140. Chadwick M, Yang C, Liu L, Gamboa CM, Jara K, Lee H, et al. Rapid Processing and Drug Evaluation in Glioblastoma Patient-Derived Organoid Models with 4D Bioprinted Arrays. *iScience* (2020) 23(8):101365. doi: 10.1016/j.isci.2020.101365

141. Mao S, He J, Zhao Y, Liu T, Xie F, Yang H, et al. Bioprinting of patient-derived *in vitro* intrahepatic cholangiocarcinoma tumor model: establishment, evaluation and anti-cancer drug testing. *Biofabrication* (2020) 12(4):045014. doi: 10.1088/1758-5090/aba0c3

142. Ireson CR, Alavijeh MS, Palmer AM, Fowler ER, Jones HJ. The role of mouse tumour models in the discovery and development of anticancer drugs. *Br J Cancer* (2019) 121(2):101–08. doi: 10.1038/s41416-019-0495-5

143. Pajot A, Michel ML, Fazilleau N, Pancre V, Auriault C, Ojcius DM, et al. A mouse model of human adaptive immune functions: HLA-A2.1-/HLA-DR1-transgenic H-2 class I-/class II-knockout mice. *Eur J Immunol* (2004) 34 (11):3060–9. doi: 10.1002/eji.200425463

144. DeAngelis N, Ferrante C, Powers G, Sendecki J, Mattson B, Pizutti D, et al. Discovery and pharmacological characterization of cetrelimab (JNJ-63723283), an anti-programmed cell death protein-1 (PD-1) antibody, in human cancer models. *Cancer Chemother Pharmacol* (2022) 89(4):515–27. doi: 10.1007/s00280-022-04415-5

145. Jiang H, Ni H, Zhang P, Guo X, Wu M, Shen H, et al. PD-L1/LAG-3 bispecific antibody enhances tumor-specific immunity. *Oncoimmunology* (2021) 10 (1):1943180. doi: 10.1080/2162402X.2021.1943180

146. Herndler-Brandstetter D, Shan L, Yao Y, Stecher C, Plajer V, Lietzenmayer M, et al. Humanized mouse model supports development, function, and tissue residency of human natural killer cells. *Proc Natl Acad Sci U.S.A.* (2017) 114(45): E9626–E34. doi: 10.1073/pnas.1705301114

147. Olson B, Li Y, Lin Y, Liu ET, Patnaik A. Mouse Models for Cancer Immunotherapy Research. *Cancer Discovery* (2018) 8(11):1358–65. doi: 10.1158/2159-8290.CD-18-0044

148. Jespersen H, Lindberg MF, Donia M, Soderberg EMV, Andersen R, Keller U, et al. Clinical responses to adoptive T-cell transfer can be modeled in an autologous immune-humanized mouse model. *Nat Commun* (2017) 8(1):707. doi: 10.1038/s41467-017-00786-z

149. Sanmamed MF, Nie X, Desai SS, Villaroel-Espindola F, Badri T, Zhao D, et al. . doi: 10.1158/2159-8290.CD-20-0962

150. Yin Q, Yu W, Grzeskowiak CL, Li J, Huang H, Guo J, et al. Nanoparticle-enabled innate immune stimulation activates endogenous tumor-infiltrating T cells with broad antigen specificities. *Proc Natl Acad Sci U.S.A.* (2021). doi: 10.1073/pnas.2016168118

151. Elinav E, Garrett WS, Trinchieri G, Wargo J. The cancer microbiome. *Nat Rev Cancer* (2019) 19(7):371– 76. doi: 10.1038/s41568-019-0155-3

152. Sivan A, Corrales L, Hubert N, Williams JB, Aquino-Michaels K, Earley ZM, et al. Commensal Bifidobacterium promotes antitumor immunity and facilitates anti-PD-L1 efficacy. *Science* (2015) 350(6264):1084–9. doi: 10.1126/science.aac4255

153. Mager LF, Burkhard R, Pett N, Cooke NCA, Brown K, Ramay H, et al. Microbiome-derived inosine modulates response to checkpoint inhibitor immunotherapy. *Science* (2020) 369(6510):1481–89. doi: 10.1126/science.abc3421

154. Fluckiger A, Daillere R, Sassi M, Sixt BS, Liu P, Loos F, et al. Cross-reactivity between tumor MHC class I-restricted antigens and an enterococcal bacteriophage. *Science* (2020) 369(6506):936–42. doi: 10.1126/science.aax0701

155. Bozzetti V, Senger S. . doi: 10.1016/j.molmed.2022.02.001

156. Kadosh E, Snir-Alkalay I, Venkatachalam A, May S, Lasry A, Elyada E, et al. The gut microbiome switches mutant p53 from tumour-suppressive to oncogenic. *Nature* (2020) 586(7827):133–38. doi: 10.1038/s41586-020-2541-0

157. Li Q, Hu W, Liu WX, Zhao LY, Huang D, Liu XD, et al. Streptococcus thermophilus Inhibits Colorectal Tumorigenesis Through Secreting beta-Galactosidase. *Gastroenterology* (2021) 160(4):1179–93 e14. doi: 10.1053/j.gastro.2020.09.003

158. Soldati L, Di Renzo L, Jirillo E, Ascierto PA, Marincola FM, De Lorenzo A. The influence of diet on anti-cancer immune responsiveness. *J Transl Med* (2018) 16(1):75. doi: 10.1186/s12967-018- 1448-0

159. Zhao S, Peralta RM, Avina-Ochoa N, Delgoffe GM, Kaech SM. Metabolic regulation of T cells in the tumor microenvironment by nutrient availability and diet. *Semin Immunol* (2021) 52:101485. doi: 10.1016/j.smim.2021.101485

160. Spencer CN, McQuade JL, Gopalakrishnan V, McCulloch JA, Vetizou M, Cogdill AP, et al. Dietary fiber and probiotics influence the gut microbiome and melanoma immunotherapy response. *Science* (2021) 374(6575):1632–40. doi: 10.1126/science.aaz7015

161. Singh RP, Bashir H, Kumar R. Emerging role of microbiota in immunomodulation and cancer immunotherapy. *Semin Cancer Biol* (2021) 70:37–52. doi: 10.1016/j.semcancer.2020.06.008

162. Routy B, Le Chatelier E, Derosa L, Duong CPM, Alou MT, Daillere R, et al. Gut microbiome influences efficacy of PD-1-based immunotherapy against epithelial tumors. *Science* (2018) 359(6371):91–7. doi: 10.1126/science.aan3706

163. Shi L, Sheng J, Wang M, Luo H, Zhu J, Zhang B, et al. Combination Therapy of TGF-beta Blockade and Commensal-derived Probiotics Provides Enhanced Antitumor Immune Response and Tumor Suppression. *Theranostics* (2019) 9(14):4115–29. doi: 10.7150/thno.35131

164. Baruch EN, Youngster I, Ben-Betzalel G, Ortenberg R, Lahat A, Katz L, et al. Fecal microbiota transplant promotes response in immunotherapy-refractory melanoma patients. *Science* (2021) 371(6529):602–09. doi: 10.1126/science.abb5920

165. Davar D, Dzutsev AK, McCulloch JA, Rodrigues RR, Chauvin JM, Morrison RM, et al. Fecal microbiota transplant overcomes resistance to anti-PD-1 therapy in melanoma patients. *Science* (2021) 371(6529):595–602. doi: 10.1126/science.abf3363

166. Clohessy JG, Pandolfi PP. Mouse hospital and co-clinical trial project–from bench to bedside. *Nat Rev Clin Oncol* (2015) 12(8):491–8. doi: 10.1038/nrclinonc.2015.62

167. Kim HR, Kang HN, Shim HS, Kim EY, Kim J, Kim DJ, et al. Co-clinical trials demonstrate predictive biomarkers for dovitinib, an FGFR inhibitor, in lung squamous cell carcinoma. *Ann Oncol* (2017) 28(6):1250–59. doi: 10.1093/annonc/mdx098

168. Recondo G, Mahjoubi L, Maillard A, Loriot Y, Bigot L, Facchinetti F, et al. Feasibility and first reports of the MATCH-R repeated biopsy trial at Gustave Roussy. *NPJ Precis Oncol* (2020) 4:27. doi: 10.1038/s41698-020-00130-7

169. Wensink GE, Elias SG, Mullenders J, Koopman M, Boj SF, Kranenburg OW, et al. Patient-derived organoids as a predictive biomarker for treatment response in cancer patients. *NPJ Precis Oncol* (2021) 5(1):30. doi: 10.1038/s41698-021-00168-1

170. Yao Y, Xu X, Yang L, Zhu J, Wan J, Shen L, et al. Patient-Derived Organoids Predict Chemoradiation Responses of Locally Advanced Rectal Cancer. *Cell Stem Cell* (2020) 26(1):17–26 e6. doi: 10.1016/j.stem.2019.10.010

171. Park M, Kwon J, Kong J, Moon SM, Cho S, Yang KY, et al. A Patient-Derived Organoid-Based Radiosensitivity Model for the Prediction of Radiation Responses in Patients with Rectal Cancer. *Cancers (Basel)* (2021). doi: 10.3390/cancers13153760

172. Ganesh K, Wu C, O'Rourke KP, Szeglin BC, Zheng Y, Sauve CG, et al. A rectal cancer organoid platform to study individual responses to chemoradiation. *Nat Med* (2019) 25(10):1607–14. doi: 10.1038/s41591-019-0584-2

173. Narasimhan V, Wright JA, Churchill M, Wang T, Rosati R, Lannagan TRM, et al. Medium-throughput Drug Screening of Patient-derived Organoids from Colorectal Peritoneal Metastases to Direct Personalized Therapy. *Clin Cancer Res* (2020) 26(14):3662–70. doi: 10.1158/1078-0432.CCR-20- 0073

174. Hu Y, Sui X, Song F, Li Y, Li K, Chen Z, et al. Lung cancer organoids analyzed on microwell arrays predict drug responses of patients within a week. *Nat Commun* (2021) 12(1):2581. doi: 10.1038/s41467-021-22676-1

175. Wood LD, Ewald AJ. Organoids in cancer research: a review for pathologist-scientists. *J Pathol* (2021) 254(4):395–404. doi: 10.1002/path.5684

176. Chen H, Du L, Li J, Wu Z, Gong Z, Xia Y, et al. Modeling cancer metastasis using acoustically bio- printed patient-derived 3D tumor microtissues. *J Mater Chem B* (2022). doi: 10.1039/d1tb02789a

177. Spiller ER, Ung N, Kim S, Patsch K, Lau R, Strelez C, et al. Imaging-Based Machine Learning Analysis of Patient-Derived Tumor Organoid Drug Response. *Front Oncol* (2021) 11:771173. doi: 10.3389/fonc.2021.771173

178. Khan S, Shin JH, Ferri V, Cheng N, Noel JE, Kuo C, et al. High-resolution positron emission microscopy of patient-derived tumor organoids. *Nat Commun* (2021) 12(1):5883. doi: 10.1038/s41467-021-26081-6

179. Liu Z, Zhang P, Ji H, Long Y, Jing B, Wan L, et al. A mini-panel PET scanner-based microfluidic radiobioassay system allowing high-throughput imaging of real-time cellular pharmacokinetics. *Lab Chip* (2020) 20(6):1110–23. doi: 10.1039/c9lc01066a

180. Echeverria GV, Ge Z, Seth S, Zhang X, Jeter-Jones S, Zhou X, et al. Resistance to neoadjuvant chemotherapy in triple-negative breast cancer mediated by a reversible drug-tolerant state. *Sci Transl Med* (2019) 11(488). doi: 10.1126/scitranslmed.aav0936

181. Kim HR, Kang HN, Yun MR, Ju KY, Choi JW, Jung DM, et al. Mouse-human co-clinical trials demonstrate superior anti-tumour effects of buparlisib (BKM120) and cetuximab combination in squamous cell carcinoma of head and neck. *Br J Cancer* (2020) 123(12):1720–29. doi: 10.1038/s41416-020-01074-2

182. Roy S, Whitehead TD, Li S, Ademuyiwa FO, Wahl RL, Dehdashti F, et al. Co-clinical FDG-PET radiomic signature in predicting response to neoadjuvant chemotherapy in triple-negative breast cancer. *Eur J Nucl Med Mol Imaging* (2022) 49(2):550–62. doi: 10.1007/s00259-021-05489-8

frontiers | Frontiers in Oncology

TYPE Original Research
PUBLISHED 18 January 2023
DOI 10.3389/fonc.2022.1101901

OPEN ACCESS

EDITED BY
Sara Lovisa,
Humanitas University, Italy

REVIEWED BY
Diletta Overi,
Department of Anatomical, Histological, Forensic Medicine and Orthopedic Sciences, Sapienza University of Rome, Italy
Ines Malenica,
Humanitas Research Hospital, Italy

*CORRESPONDENCE
Monique M.A. Verstegen
m.verstegen@erasmusmc.nl

SPECIALTY SECTION
This article was submitted to Molecular and Cellular Oncology, a section of the journal Frontiers in Oncology

RECEIVED 18 November 2022
ACCEPTED 23 December 2022
PUBLISHED 18 January 2023

CITATION
van Tienderen GS, van Beek MEA, Schurink IJ, Rosmark O, Roest HP, Tieleman J, Demmers J, Muntz I, Conboy J, Westergren-Thorsson G, Koenderink G, van der Laan LJW and Verstegen MMA (2023) Modelling metastatic colonization of cholangiocarcinoma organoids in decellularized lung and lymph nodes. *Front. Oncol.* 12:1101901. doi: 10.3389/fonc.2022.1101901

Modelling metastatic colonization of cholangiocarcinoma organoids in decellularized lung and lymph nodes

Gilles S. van Tienderen[1], Marije E. A. van Beek[1], Ivo J. Schurink[1], Oskar Rosmark[2], Henk P. Roest[1], Jantine Tieleman[3], Jeroen Demmers[3], Iain Muntz[4], James Conboy[4], Gunilla Westergren-Thorsson[2], Gijsje Koenderink[4], Luc JW van der Laan[1] and Monique M. A. Verstegen[1]*

[1]Department of Surgery, Erasmus MC Transplant Institute, University Medical Center Rotterdam, Rotterdam, Netherlands, [2]Lung Biology, Department of Experimental Medical Science, Lund University, Lund, Sweden, [3]Proteomics Center, Erasmus University Medical Center, Rotterdam, Netherlands, [4]Department of Bionanoscience, Kavli Institute of Nanoscience Delft, Delft University of Technology, Delft, Netherlands

Cholangiocarcinoma (CCA) is a type of liver cancer with an aggressive phenotype and dismal outcome in patients. The metastasis of CCA cancer cells to distant organs, commonly lung and lymph nodes, drastically reduces overall survival. However, mechanistic insight how CCA invades these metastatic sites is still lacking. This is partly because currently available models fail to mimic the complexity of tissue-specific environments for metastatic CCA. To create an *in vitro* model in which interactions between epithelial tumor cells and their surrounding extracellular matrix (ECM) can be studied in a metastatic setting, we combined patient-derived CCA organoids (CCAOs) (n=3) with decellularized human lung (n=3) and decellularized human lymph node (n=13). Decellularization resulted in removal of cells while preserving ECM structure and retaining important characteristics of the tissue origin. Proteomic analyses showed a tissue-specific ECM protein signature reflecting tissue functioning aspects. The macro and micro-scale mechanical properties, as determined by rheology and micro-indentation, revealed the local heterogeneity of the ECM. When growing CCAOs in decellularized lung and lymph nodes genes related to metastatic processes, including epithelial-to-mesenchymal transition and cancer stem cell plasticity, were significantly influenced by the ECM in an organ-specific manner. Furthermore, CCAOs exhibit significant differences in migration and proliferation dynamics

dependent on the original patient tumor and donor of the target organ. In conclusion, CCA metastatic outgrowth is dictated both by the tumor itself as well as by the ECM of the target organ. Convergence of CCAOs with the ECM of its metastatic organs provide a new platform for mechanistic study of cancer metastasis.

KEYWORDS

metastatic colonization, decellularization, Cholangiocarcinoma, tumor organoids, extracellular matrix

Introduction

Despite achievements in early detection and treatment of primary tumors, 90% of current cancer-related death occur after the disease has metastasized. In bile duct cancer (cholangiocarcinoma, CCA), the 5-year survival rate is approximately 7-20% (1), and drops to 2% when the cancer metastasizes (2–4). Distant metastasis occurs relatively frequently in CCA over the course of a patient's disease, ranging from 36.4-50.2% (5–7), with lung and lymph nodes the most common distant locations of metastasis (4, 6). Treatment options are surgical resection, liver transplantation, chemotherapeutics, intra-arterial treatments, and local ablative therapies, of which surgical intervention is the only potentially curative option (8). However, a large number of patients are not eligible, approximately 60-88%, including patients with distant metastatic loci (9). Understanding the micro-environmental cues of metastatic disease will aid in understanding the biology behind metastatic outgrowth and in developing novel therapeutic options for patients with unresectable CCA.

Tumor-derived organoids, consisting of primary epithelial cells grown as 3D structures, have emerged in recent years as highly promising biological disease models due to their self-renewal and self-organization capabilities, while maintaining the mutational landscape of the original tumor (10–12). CCA organoids (CCAOs) have been established as an attractive cellular source for various fundamental and translational biological applications, including identification of biomarkers, driver gene functionality testing, and drug screening (13–15). However, in a metastatic setting, micro-environmental cues at the target organ are crucial for cancer cell behavior, including colonization and proliferation of tumor cells (16, 17). These cues are not well recapitulated by current culture systems, as organoids are primarily cultured in basement membrane extracts (BME) derived from a mouse tumor (18). Particularly, the 'seed and soil' hypothesis, as posted by Paget in 1889, suggests that distant organs are different in their ability to provide a favorable environment (soil) for facilitating the growth of metastasized cancer cells (seeds) (19, 20). Progress in determining the role of the specific host organ, or 'soil', on the behavior of disseminated cancer cell, or 'seeds', aiming to colonize that organ is hindered by a lack of model systems that accurately recapitulate native organ structure.

As part of the micro-environment, the extracellular matrix (ECM) provides important biochemical and physical cues for tumor cell colonization (17). To isolate the ECM and study what the 'soil' comprises, decellularization methods can be applied. This technique uses enzymatic and/or chemical reagents to remove cells while preserving ECM characteristics, including architecture and protein composition (21–23). Decellularization has been established for many organs and tissues, including tumors. In previous work, we have shown that CCAO recellularization of decellularized liver and tumor scaffolds can unveil the influence of ECM on cancer-related processes, including growth, invasion, and chemo resistance. In CCA, location-specific metastases carry distinct prognostic values, with lymph node showing better prognostic outcomes compared to lung, however mechanistic insight into what is causing this is still unknown (4, 24). Therefore, modeling metastatic colonization in a tissue-mimicking structure that reflects *in vivo* micro-environmental cues is an outstanding challenge.

Here, we create an *in vitro* model encompassing patient-derived CCA organoids and decellularized human lung (dLu) and lymph node (dLN) to study metastatic cell-matrix interactions. The decellularized tissues were biochemically and biomechanically characterized, which revealed isolation of ECM components with an unique ECM protein signature for dLu and dLN and retention of tissue-specific function-related proteins. Recellularization of both decellularized tissues with CCAOs resulted in upregulation of different cancer stem cell populations, as determined by LGR5 and CD133, and an increased epithelial phenotype in dLN. Furthermore, CCAO grown in dLu and dLN had different proliferation patterns, influenced by both the original tumor and the ECM donor. These results illustrate the unique impact of the

patient-derived tumor and the ECM of the target organ on key metastasis-related pathways and associated growth patterns.

Materials and methods

Sample procurement and tissue collection

CCA (n=3, including n=2 intrahepatic CCA and n=1 perihilar CCA) tissue samples were obtained from patients who underwent a curative-intent surgical resection, performed at the Erasmus MC in Rotterdam (Table S1 for patient information). The Medical Ethical Council of the Erasmus MC approved the use of tissue for research purposes and patients provided written informed consent (MEC-2013-143). Samples were confirmed to be of tumor origin with histopathological assessment by a pathologist. CCA samples were stored at 4°C in Belzer UW cold storage solution (UW, Bridge to Life) and, if used for organoid initiation, processed within 24 hours after collection. Lung (n=3) tissue samples were obtained from donors for lung transplantation, performed at Sahlgrenska University hospital in Gothenburg, Sweden. Use of lung tissue was approved by the Swedish ethical review board in Lund (Dnr. 2008/413, 2011/581 and 2013/253). Lung tissue samples of peripheral lung was prepared by dissecting out cubes with a side length of approximately 10 mm with pleura remaining on one side and snap freezing them in isopentane chilled with liquid nitrogen. Lymph nodes (n=13) were obtained from donors who donated their liver for a liver transplantation procedure, performed at the Erasmus MC in Rotterdam (MEC-2014-060). The lymph nodes are hilar lymph nodes. Donor information for both lymph node and lung can be found in table S2. Lung and lymph node samples were initially stored at -80°C or -20°C and processed at a later stage for decellularization.

Initiation and propagation of human patient-derived cholangiocarcinoma organoids

Initiation of CCAOs was done as previously described (13). Organoids were passaged in a 1:3-1:6 ratio approximately every 7 days, depending on their proliferation rate. Expansion medium (EM, Table S3) was refreshed every 3 or 4 days. Passaging was done by removing the EM and collecting the organoids in a 15 mL tube by adding ice-cold Advanced DMEM/F12 (AdvDMEM, Gibco) supplemented with 1% v/v penicillin-streptomycin, 1% v/v hepes, 1% v/v ultraglutamine, 0.2% v/v primocin) to the wells and scraping/pipetting. Subsequently, ± 8 ml ice-cold AdvDMEM was added to the 15 ml tubes. After centrifugation (453g, 5 min, 4°C), the supernatant was removed and the pellet was re-suspended in ice-cold AdvDMEM while mechanically breaking the organoids by pipetting up and down. After another centrifugation step (453g, 5 min, 4°C), the supernatant was removed and the cell pellet was re-suspended in BME (Cultrex). The mixture of cells and BME was plated in droplets of 25 µl in 12-, 24- or 48-well suspension culture plates (Greiner or Sarstedt) and cultured for 7 days before passaging occurred again.

Decellularization procedure of human lymph nodes and lung tissue

Lung tissues were embedded in tissue-tek optical cutting temperature (OCT) compound, mounted on a metal holder and cut with a cryotome (Leica) at -15°C into 400 µm thick slices. 400 µm thick lung slices and entire lymph nodes were placed in a flask on a multi-position magnetic stirrer (Figure S1A). Lymph nodes were not cut into smaller slices before decellularization because of their relatively small surface area and disintegration of the lymph nodes during decellularization. Tissue samples were washed for 30 minutes with dH20, 1 hour with 9% hypertonic saline (NaCl) and again 30 minutes with dH20 to remove traces of blood, debris, and OCT compound by using osmotic effect. Thereafter, all tissue samples were decellularized with a solution consisting of 4% Triton-X-100 and 1% NH_3 (hereafter referred to as TX-100 solution). TX-100 solution was replaced every hour for a total of 10 cycles including two overnight (O/N) cycles of approximately 16 hours, which resulted in transparent tissues. Subsequently, the tissues were washed with PBS (Gibco, HyClone) for 1 hour to remove traces of TX-100. Thereafter, tissues were incubated with DNase solution (2 mg/l DNase type 1 (Sigma) in 0.9% NaCl + 100mM $CaCl_2$ + 100mM $MgCl_2$) for 3.5 hours at 37°C on the magnetic stirrer. Finally, tissues were washed twice with PBS. Biopsy samples were taken before and after decellularization for various analysis. To note, two lymph nodes contained >50ng/mg wet tissue after decellulariation and were not included in subsequent experiments and/or analyses.

Confirmation of decellularization procedure

Biopsies and decellularized tissue were fixed in 4% paraformaldehyde (PFA; Fresenius Kabi), solidified in 2% agarose in PBS, embedded in paraffin and sectioned at 4 µm using a microtome (HM 325). Slides of samples before and after decellularization were processed for routine histological stainings: hematoxylin and eosin (H&E), 4',6-diamidino-2-phenylindole (DAPI; Vectashield, Vectorlabs), Masson's Trichrome (TRI), Gomori's (GOM), and picrosirius red (PSR; Sigma). Collagen type 1 is stained according to standard protocol

by the pathology department (ErasmusMC, The Netherlands). Slides were imaged with a Zeiss Axioskop 20 microscope and captured with the Zeiss Axiocam 305 color or imaged and captured with Nanozoomer 2.0-HT (Hamamatsu). DAPI stained slides were analyzed using an EVOS microscope (Thermo Fisher Scientific). Additionally, DNA was isolated from lung and lymph nodes, before and after decellularization, using the QIAamp DNA Micro Kit (Qiagen) according to the manufacturer's protocol. Subsequently, the total DNA content was measured using a Nanodrop spectrophotometer (Thermo Fisher Scientific; LU n=3, LN n=13) and corrected for the corresponding wet weight of the measured sample (ng DNA/mg wet tissue). The wet weight of the samples was determined before performing analysis.

Collagen and sulfated glycosaminoglycan quantification

Total collagen content of lung and lymph nodes before and after decellularization (lung n=3 (T=0, T=decell); lymph node n=4 (T=0) and n=6 (T=decell)) was determined using a Total Collagen Kit (Quickzyme Biosciences) according to the manufacturer's protocol. The absorbance of the collagen-binding dye was measured in a clear 96-well plate at 570 nm using an infinite M nano plate reader (Tecan). Background absorbance was subtracted. The content was corrected for the wet weight of the corresponding samples (µg collagen/mg wet weight tissue).

Sulfated glycosaminoglycan (sGAG) content of lung and lymph nodes before and after decellularization (lung N=3 (T=0, T=decell), lymph nodes n=4 (T=0) and n=6 (T=decell)) was determined using a Blyscan Sulfated Glycosaminoglycan Assay (Biocolor) according to the manufacturer's protocol. Samples were digested in a Papain (Sigma) solution (10 mg/ml) at 65°C for 3 hours. The absorbance was measured in a clear 96-well plate at 656 nm using an infinite M nano plate reader (Tecan). The wet weight of the samples was weighted before performing analysis.

Nanoindentation

The effective Young's modulus (E) of decellularized tissue samples was measured using a Chiaro Nanoindenter (Optics11 Life) (Figure S1B). dLu (N=3) and dLN (N=3) were glued inside a 35 mm petri dish using NOA61 or NOA81 (Norland) and a UV torch (Walther Pro). The sample and probe were immersed in PBS before the measurement started. The stiffness of the probes used for dLu and dLN was respectively 0.027 N/m and 0.030 N/m. The probes had a tip radius of 3 µm and were ball shaped. First, the sample was indented to a depth of 2 µm in 4 seconds (0.5 µm/s). Then, the indentation was held at 2 µm for 1 second and finally the probe was retracted in 1 second. At least one matrix scan of 3x3 with a distance of 5 µm between indentation points was performed per decellularized extracellular matrix (dECM). The Hertzian contact model in the Optics 11 data viewer software (version V3.4.7) was used to calculate the effective Young's Modulus (E) (25). Measurements with an unreliable model fit (R^2<0.9) were considered as outliers and disregarded from further analysis.

Rheology

A rotational rheometer (KINEXUS PRO; Technex) with a flat parallel plate geometry with a diameter of 20 mm was used to determine the Young's modulus of the decellularized tissues (Figure S1C). All measurements were performed at 37°C and obtained by the rSpace software. dLu (n=3, 400 µm thick) and dLN (n=3) were placed on the bottom plate. Next, the top plate was lowered to a gap height of 2 mm (dLu1, dLu2), 3 mm (dLu3, dLN5) or 1.8 mm (dLN11, dLN10). First, the surface contact point was found by decreasing the gap at a rate of 0.01 mm/s with a measurement of the normal force every 0.01 second, which the software used to automatically determine the contact point. Subsequently, a shear oscillation frequency sweep (f: 10-0.01 Hz, slope: 10 points per decade) was performed to determine the viscoelastic properties of the samples. Subsequently, the dECM was compressed $4^{*}10^{-4}$ mm every second for 13.3 minutes. Then, another shear oscillation frequency sweep (f: 10-0.01 Hz, slope: 10 points per decade) was performed. An approximation of the Young's modulus (E) was determined over the whole range of compression. The strain was calculated by (h-h0/h0) where h is the gap while measuring and h0 is the initial gap when the surface contact point was found. The stress was calculated by (strain+1)*(Normal force/initial area) where the initial area was calculated by π^{*}(sample radius)^2, following the Cauchy stress calculations (26). In this way, the data was corrected for the size of each sample and increase in size after each compression step. The gradient slope over the whole range of compression resulted in an approximation of the Young's modulus (E).

Proteomic sample preparation

100 µL 50 mM Tris-HCl (pH 8.0) was added to the dECM scaffolds and the samples were snap frozen in liquid nitrogen, followed by homogenizing using a dismembrator. The sample was heated in a thermomixer for 5 min at 95°C. 90 µL 50 mM Tris-HCl and 5 µL 100 mM of 1,4-dithiothreitol were added and the sample was incubated at 50°C for 60 min. Subsequently, 5 µL 200 mM of 2-chloroacetamide was added and the sample was incubated at RT for 30 min. Then, 100 µL 50 mM Tris-HCl and 10 µL Peptide:N-glycosidase F (500 units/mL) was added and the

samples were further incubated at 37°C for 4 h, followed by 5 min at 95°C. Finally, 25 µL sodium deoxycholate and trypsin was added (1:100, trypsin:protein) and the sample was incubated in a thermomixer O/N at 30°C and 1100 RPM. The next day, 25 µL 10% trifluoroacetic acid (TFA) was added to the sample, followed by 2X washes with ethylacetate: 300 µL ethylacetate (H_2O saturated) was added, the mixture was mixed vigorously and then centrifuged for 2 min at 5,000 rpm. The upper layer was removed, followed by 45 min in the SpeedVac Vacuum Concentrator (Thermo Fisher Scientific) to evaporate the solvent and reduce the sample volume. The protein digest was desalted using C18 stage tips (Thermo Fisher Scientific). This was repeated for the flow through. The stage tip was then washed with 100 µL 0.1% TFA, centrifuged for 10 min at 2,000 rpm, followed by 2X elution of the peptides with 75 µL 50% acetonitrile (AcN) and centrifugation for 8 min at 2,000 rpm. Next, peptides were dried in the speedvac and reconstituted in 25 µL 2% AcN, 0.5% formic acid. Nanoflow liquid chromatography tandem mass spectrometry (nLC-MS/MS) was performed on an EASY-nLC coupled to an Orbitrap Fusion Lumos Tribrid mass spectrometer (Thermo), operating in positive mode. Peptides were separated on a ReproSil-C18 reversed-phase column (Dr Maisch; 15 cm × 50 µm) using a linear gradient of 0–80% acetonitrile (in 0.1% formic acid) during 90 min at a rate of 200 nl/min. The elution was directly sprayed into the electrospray ionization source of the mass spectrometer. Spectra were acquired in continuum mode; fragmentation of the peptides was performed in data-dependent mode by HCD.

Proteomic data processing

Raw mass spectrometry data were analyzed using the Proteome Discoverer 2.3 software suite (ThermoFisher Scientific). The Mascot search algorithm (version 2.3.2, MatrixScience) was used for searching against the Uniprot database (taxonomy: Homo sapiens). The peptide tolerance was typically set to 10 ppm and the fragment ion tolerance was set to 0.8 Da. A maximum number of 2 missed cleavages by trypsin were allowed and carbamido-methylated cysteine and oxidized methionine were set as fixed and variable modifications, respectively.

Proteomic data analysis

To identify and categorize the detected proteins that are related to the ECM, the dataset was compared to and filtered with the MatrisomeDB database (27). MatrisomeDB uses domain-based organization of matrisome-related proteins to obtain a complete collection of ECM proteomic data. Proteins identified are subdivided into ECM-affiliated proteins, secreted factors, collagens, ECM regulators, ECM glycoproteins, and proteoglycans. The identified matrisome proteins were further classified into 3 categories: a core ensemble of proteins, differentially expressed (DE) proteins, and exclusive proteins. The core ensemble of proteins consists of proteins that are present in all replicates of all conditions. Proteins are differentially expressed if the adjusted p-value is <0.05. Proteins are identified as 'exclusive' if they are present in samples of one condition, while absent in all replicates of another condition. To note, the difference between DE proteins and exclusive proteins is likely due to the sensitivity of mass spectrometry. Therefore, DE proteins and exclusive proteins were combined to apply enrichment analysis using the fgsea (version 1.16.0) R package.

Preparation of decellularized matrices for organoid culture

One day before recellularization, scaffolds were washed with sterile PBS three times, followed by washing with AdvDMEM three times. Subsequently, the scaffolds were incubated overnight at 37°C with AdvDMEM, supplemented with 10x the concentration of penicillin- streptomycin, primocin and antiobiotic-antimycotic (Gibco) to avoid infections in the recellularization experiments. Decellularized matrices were washed three times with AdvDMEM on the day of recellularization. The scaffolds were placed in the middle of a new suspension or culture well plate (Greiner or Sarstedt) and were folded out as much as possible using a needle or tweezer.

Recellularization

CCAOs (n=3) grown in BME droplets were harvested by removing the BME droplets from the wells using ice cold AdvDMEM as previously described. After removal of BME and AdvDMEM from the cell pellet, 1 ml trypsin (TrypLE, Thermo Fisher Scientific) was added. The suspension was incubated at 37°C for 15 minutes while applying mechanical disruption with a pipette every 5 minutes until organoid fragments were dissociated into small aggregates and single cells. Subsequently, 10 µl of the suspension was added to 10 µl Trypan Blue (Thermo Fisher Scientific) for cell counting using disposable cell counting chambers (Kova). After 15 minutes of incubation, trypsin was directly inactivated by the addition of cold AdvDMEM. The suspension was centrifuged for 5 minutes (453g, 4°C) and the resulting cell pellet was resuspended in EM to obtain the total amount of cells needed (approx. 200.000 cells/scaffold). Cells (5 µl) in EM were added to the dECM in a 12 or 24 suspension or culture well plate (Greiner or Sarstedt). The recellularized scaffolds were incubated for 3 hours at 37°C before adding 350-500 µl EM to the recellularized scaffolds. EM was refreshed every 3 or 4 days. Organoid cultures in BME were used as a control if appropriate.

RNA isolation, cDNA synthesis and RT-qPCR

For RNA isolation, 3 or 4 scaffolds were added to 700 µl Qiazol. Qiazol lysed samples (3-4 recellularized scaffolds per replicate) were homogenized with a TissueRuptor (Qiagen). Messenger RNA was isolated with a miRNeasy kit (Qiagen) according to the manufacturer's protocol. A Nanodrop spectrophotometer (Thermo Fisher Scientific) was used to measure RNA content. 500 ng complementary DNA (cDNA) was made by adding 5x PrimeScript RT Master Mix and dH2O to isolated RNA and inserted into a 2720 Thermal Cycler (Applied Biosystems) or SimpliAmp Thermal Cycler (Applied Biosystems). qPCR was performed according to standard procedures with 10 µl SYBR select master mix, 1 µl primers, 4 µl dH2O and 5 µl cDNA per reaction. All the tested primer sets are listed in (Table S4). The housekeeping genes Glyceraldehyde-3-Phosphate Dehydrogenase (GAPDH) and Hypoxanthine-guanine-phosphoribosyl-transferase (HPRT) were used as reference genes.

Live/dead staining

CCAOs cultured in dECM were incubated in EM supplemented with 100 µg/ml Hoechst (Hoechst 33342, Thermo Fisher Scientific), 50 µg/ml propidium iodide (PI, Sigma-Aldrich) and 0.5 µM calcein (Calcein AM, Thermo Fisher Scientific) at 37°C for 30 minutes protected from light. Images were made with an EVOS FL fluorescent microscope (Thermo Fisher Scientific).

Histological staining

PFA-fixed samples were solidified in 2% agarose in PBS. They were embedded in paraffin and sectioned at 4 µm using a microtome (HM325). Decellularized and recellularized scaffold slides were stained with H&E according to a standard protocol.

Cell metabolic activity assessment

PrestoBlue™ Cell Viability Reagent (Thermo Fisher Scientific) was used to assess metabolic activity of CCAOs in dLu and dLN for the same sample at day 1, 4, 8, 11, 14 after recellularization. Presto Blue compound was diluted 10-fold (1:10) in EM, filtered and pre-warmed in a 37°C water bath for 10 minutes. EM was removed from the recellularized scaffolds and 500 µl Presto Blue solution was added to each well. The recellularized scaffolds were incubated at 37°C for 3.5 hours protected from light. Subsequently, the medium was plated in a 96 well plate in triplicate. The absorbance was measured using an CytoFluor Multi-Well plate Reader series 4000 (Perseptive Biosystems) with excitation of 530nm and emission of 590nm. Background absorbance was measured using non-recellularized dLu and dLN (both n=3). Background measurements were subtracted and data was normalized to day 1.

Statistical analysis

Statistical analyses were performed using GraphPad Prism (version 9, GraphPad Software). Continuous unpaired variables between two groups were tested using a Mann-Whitney-U and presented graphically as means with standard deviation (SD). Kruskal-Wallis test was performed when more than two groups were compared. Two-way ANOVA test was performed for multi-variate analysis with multiple comparison testing for different time points or different donors (i.e. the sGAG/collagen contents). A description of the method and test results is noted if alternative statistical analysis was used. In all tests, a p value of <0.05 was considered significant.

Results

Decellularization of lymph node and lung tissue for isolation of a-cellular ECM scaffolds

To create tissue-specific *in vitro* metastatic colonization models for the lung and lymph node, we first decellularized lung (dLu) and hilar lymph nodes (dLN) (Table S2). An identical decellularization protocol was used for both tissue types. This is based on a previously described method for liver and liver tumor biopsy samples (28), so that recellularization would be minimally affected by the method of decellularization. Histological evaluation and DNA content quantification revealed successful decellularization (Figure 1). Lung sections show hollow structures of the alveoli and bronchiole before and after decellularization and preservation of ECM structure (Figures 1A, S2) (30). In lymph nodes, show the typical reticular meshwork architecture in T=0 conditions (Figures 1A, S3) (31). After decellularization, a relative dense structure lacking cellular material is observed, indicating preservation of overall tissue morphology. DAPI staining confirmed the removal of nuclear material from lung and lymph node (Figure 1B). Macroscopically, decellularization resulted in a white, translucent appearance for both lung and lymph node, as commonly seen for other decellularized organs as well (Figure 1C) (32, 33). Loss of nuclear material was confirmed by quantification of DNA. After decellularization, DNA content was significantly decreased in lung ($p<0.0001$) and lymph nodes ($p=0.0022$) (Figure 1D). Lymph node tissue has a

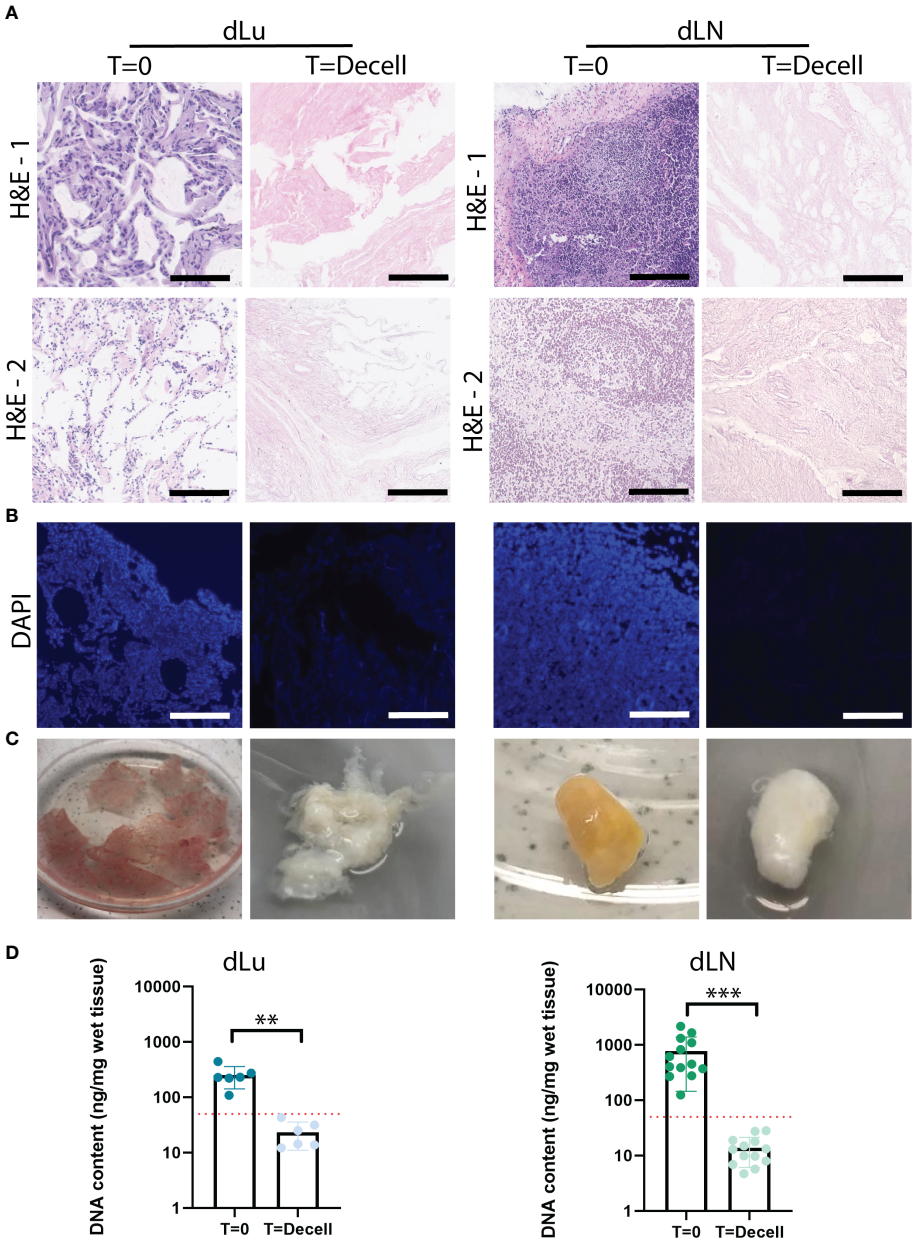

FIGURE 1
Extracellular matrix of lung and lymph nodes obtained by decellularization. **(A)** Representative H&E stainings of lung and lymph node before (T=0) and after (T=decell) decellularization show efficiently removal of cells from the scaffold and maintenance of ECM structure. Scale bars indicate 200 μm. 1 and 2 show different donors for dLU (dLu2, dLu3) and dLN (dLN2, dLN12). **(B)** Representative DAPI stainings of lung (dLu2) and lymph node (dLN6) before and after decellularization confirmed removal of nuclear material from the scaffold. Scale bars indicate 250 μm. **(C)** Lung slices of 400 μm thick and an entire lymph node of 0.75 cm thick before and after decellularization, show the transformation in color from brown/yellow to translucent white. **(D)** Quantitative DNA content analysis of lung (n=3 patients, with each patient measured in technical duplicate, p=0.003) and lymph node (n=13, p=0.0002) before and after decellularization confirms successful decellularization. Error bars indicate $\pm$ SD. ** = p-value < 0.005, *** = p-value < 0.001. Paired t-tests were used for determining significance in DNA content. The red dotted line indicates a threshold of 50 ng DNA/mg wet tissue, which is a common criteria for adequate cell removal (29). For the DNA content dLu1-3 and dLN1-13 were used. .

higher cell density compared to lung, which is reflected by an average DNA concentration before decellularization in lymph node of 720ng DNA/mg wet tissue (n=13, SD: ± 569.8ng) and of 250.2ng DNA/mg wet tissue (n=6, consisting of 3 patients and 2 technical replicates, SD: ± 98.7ng) in the lung. After decellularization, the DNA content is reduced to 19.9ng DNA/mg wet tissue (n=13, SD: ± 17.6ng) for dLN and 23.3ng DNA/mg wet tissue (n=6, SD: ± 11.2ng) for dLu, equaling a reduction

of 97.2% and 90.7%, respectively. Both absolute values and percentage reduction (i.e. <50 ng DNA/mg wet tissue and 90% reduction in DNA content) adhere to common criteria for complete cell removal (29). Thus, utilizing the same method, both lung and lymph node tissue was successfully decellularized.

Decellularized scaffolds show retention of ECM-related components

To further characterize the decellularized scaffolds, the level of retention of ECM-related components was assessed. Sulfated glycosaminoglycans (sGAG) are important regulators of various cancer-related processes, including angiogenesis, invasion, proliferation and metastasis (34, 35). For both lung and lymph nodes, sGAGs were preserved after decellularization. The total sGAG content for both lung and lymph node per mg wet tissue decreased slightly, with a 1.4-fold and 1.9-fold decrease for dLu and dLN, respectively (Figure 2A). The slight difference between the tissues could be related to the higher cell density in dLN, which means relatively more cell-associated sGAGs are lost during the process of decellularization. Subsequently, collagen content was assessed, as collagen is the primary structural component of the ECM. The collagen concentration increased for both lung (before decellularization: 3.36 μg/mg wet tissue, SD ± 0.54; after decellularization: 31.49 μg/mg wet tissue, SD± 5.94) and lymph node (before decellularization: 1.53 μg/mg wet tissue, SD± 0.58; after decellularization: 43.46 μg/mg wet tissue, SD± 15.63) (Figure 2B). Gomori's staining shows the presence of reticular fibers in lymph node tissue at T=0 and after decellularization (Figure 2C). The relatively high retention of collagen was confirmed by histological staining's (PicroSirius Red and Masson's Trichrome), with abundant positivity in both dLu and dLN (Figures 2D, E). In the lung, collagen type 1 is important for mechanics and confers primarily tensile properties, while in the lymph nodes it is part of the reticular fibers (30, 31). Figure 2F demonstrates diffuse abundance and presence of collagen type 1 after decellularization (black arrows). Overall, decellularization of human lung and lymph nodes resulted in preserved components of the ECM and in acellular scaffolds.

Divergent mechanical properties of decellularized lung and lymph node scaffolds

Collagens forms a three-dimensional network, and its architecture is central to tissue functioning through providing mechanical properties (36). Therefore, to determine both macro- and microscopic mechanical properties of dLu and dLN, rheology measurements and micro-indentation were performed, respectively. Macroscopic properties of dLu and dLN were determined by assessing rheological properties under compression. The approximation of the Young's Modulus (E), determined over the whole range of compression, for was 0.46 ± .18kPa for dLu and 0.53 ± .41kPa for dLN (Figure 3A). More heterogeneity in macroscopic stiffness is seen in dLN. On a micro-scale, by obtaining the effective Young's modulus by micro-indentation, the stiffness values ranged from 0.15-52.3 kPa for dLu and 0.05-40.9 kPa for dLN (Figure 3B). The effective Young's modulus is defined as the Young's modulus without making any assumptions regarding Poisson's ratio. This heterogeneity is also captured on a per donor basis, but did not show any significant differences between donors for dLu or dLN (Figure 3C). Thus, on a micro-scale a similar trends persists, with a large standard deviation indicating heterogeneity in the stiffness for both tissue types, and heterogeneity in macroscopic stiffness for dLN in particular.

Decellularized tissue scaffolds contain common and divergent ECM proteins

We next examined whether the heterogeneity in mechanical properties was also represented in the overall protein composition. For this, mass spectrometry was employed to find shared and divergent ECM proteins in dLu and dLN. ECM-related proteins were categorized following the matrisome classification standards: collagen, glycoproteins, ECM regulators, ECM-affiliated proteins, proteoglycans, and secreted factors (27). Analysis of the proteome identified proteins in all categories, highlighting the complexity of the dECM in both tissues (Figures 4A, B). The most abundant proteins in both dLN and dLU are largely overlapping, particularly collagens are present in both decellularized scaffolds (Figure S4). However, important differences in highly abundant proteins are also present, including elastin (ELN) in the lung, which is important for lung development and alveolar formation (37). Still, most differences are present in lower abundant ECM-related proteins, highlighting the complexity of the environments that are provided by decellularized scaffolds (Suppl. File 2). Filtering for proteins present in all biological replicates showed that dLu contained a larger variety of proteins in all categories compared to dLN (Figure 4A). This is similar when filtering for ECM proteins only present in one replicate, although the difference between dLu and dLN becomes less apparent, indicating a higher level of intra-dLN heterogeneity in protein composition (Figure 4B). The larger diversity in ECM glycoproteins and ECM regulators in dLu is translated to a significantly higher total abundance, based on summed tryptic peptide intensities (Figure 4C). However, dLN had a significantly higher total collagen abundance compared to dLu, congruent with the collagen quantification based on acid hydrolysis (Figures 4C, 2B). Surprisingly, dissecting the higher abundance per collagen subtype and subunit does not reveal

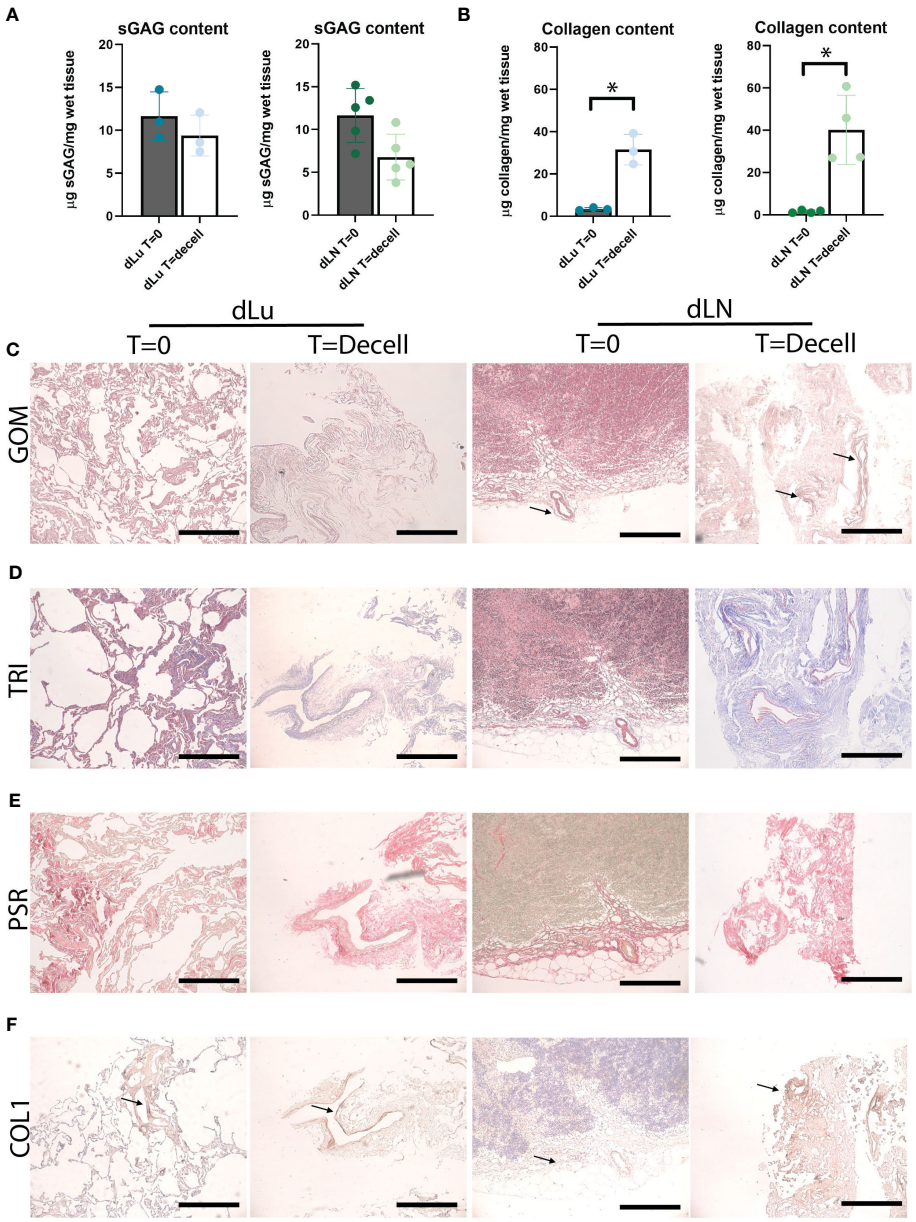

FIGURE 2
Preservation of ECM proteins after decellularization of human lung and lymph node. **(A)** Quantitative sGAG content analysis of lung (n=3, p=0.5) and lymph node (n=5, p=0.07) before and after decellularization showing retention of sGAG. dLu1, 2, 3 and dLN17, 27, 7, 10, 11 were used. **(B)** Quantitative collagen content analysis of lung (n=3, p=0.02) and lymph node (n=4, p=0.02) before and after decellularization, showing retention of collagen. dLu1, 2, 3 and dLN2, 4, 7, 15 were used. Paired t-tests were used for determining significance for determining significance in sGAG and collagen content. *= p-value <0.05. **(C–E)** Lung (dLu1) and lymph node (dLN12) before (T=0) and after (T=decell) decellularization stained with Gomori's (GOM, **C**), Masson's Trichrome (TRI, **D**) and PicroSirius Red (PSR, **E**) shows ECM architecture primarily consisting of collagen fibers. GOM shows reticulin (black), nuclei (red), and cytoplasm (pink). TRI shows muscle (red), collagen (blue), nuclei (brown/black), cytoplasm (brick red). **(F)** Representative images of collagen type 1 staining of lung (dLu1) and lymph node (dLN1) before and after decellularization. All scale bars indicate 200 µm.

major differences, with only COL6A6 (p=0.02) and COL28A1 (p=0.03) significantly upregulated in dLu compared to dLN (Figure 4D). Principal component analysis revealed tissue-specific signatures of ECM proteins by segregation of dLu and dLN clusters based on PC1 (Figure 4E). Furthermore, dLN showed a higher overall heterogeneity across donors, primarily displayed by PC2, which is in line with the higher heterogeneity in stiffness across donors (Figures 4E, 3A). The different signatures are also represented by exclusive expression of 42 proteins in dLu and 14 proteins in dLN (Figure 4F). Next, these uniquely identified proteins were used for enrichment analysis with the DAVID bioinformatics tool (38). The enriched terms

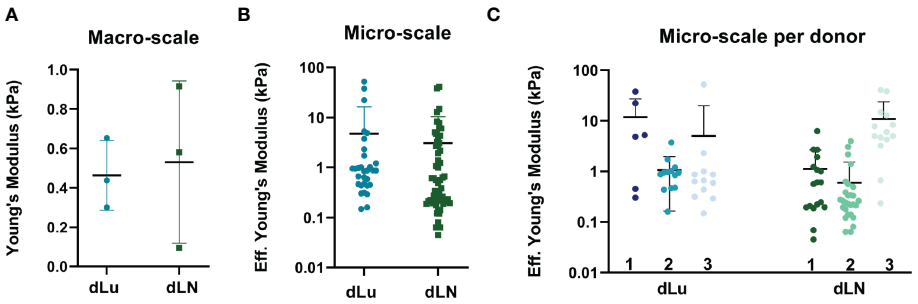

FIGURE 3
Macroscopic and microscopic mechanical characterization of dLu and dLN. **(A)** Macroscopic compression measurements showing the Young's Modulus of dLu (n=3, dLu1, dLu2, dLu3) and dLN (n=3, dLN11, dLN10, dLN5). **(B)** Effective Young's Modulus measured by micro-indentation (3x3 matrix scans, 5μm between indentations with a total measured area of 15x15 μm) of dLu (n=3 donors) and dLN (n=3 donors). **(C)** Effective Young's Modulus measured by micro-indentation split per donor for both dLu (dLu1, dLu2, and dLu3) and dLN (dLN11, dLN10, dLN5). Each data point is a different region of the sample obtained in a 3x3 matrix scan.

were divided into shared (Figure 4G) and distinct (Figures 4H, I). As expected, extracellular space (GO:0005615) and region (GO:0005576), similar enrichment terms both containing extracellular proteins, are enriched in both dLu and dLN, as ECM is isolated through decellularization (Figure 4G). The distinct enriched terms reveal retention of tissue-specific functions in the decellularized scaffolds, with enrichment of immune response in dLN, as it function is primary immune system-related, and basement membrane enrichment in dLu, which in native lung is crucial for functioning of gas exchange through binding endothelium and epithelium together (Figures 4H, I) (39). Altogether, dLu and dLN have distinct protein signatures, with high protein diversity and reflect tissue-specific functional aspects.

CCAOs grown in dLu and dLN scaffolds attain tissue-specific expression of cancer-related genes

Next, we assessed the effect of the decellularized ECM scaffolds on CCAOs, to mimic metastatic outgrowth in lung and lymph node. Patient-derived CCAOs (n=3) were cultured in BME, harvested, and seeded on dLu and dLN. CCAOs grown in BME were spherical in shape and proliferated over time as previously described (Figure S5) (40). In dLu and dLN, bright field microscopy images showed the adhesion of single cell and clumps of CCAOs to the ECM observed at day 1 of recellularization. Subsequently, organoid-like structures appeared around day 7, which transformed into a complete cellular layer surrounding the edge of the ECM scaffolds at day 14 (Figure 5A).

To identify the biological processes that are important for metastasis of CCA in the lung and lymph nodes, gene expression profiles of CCAOs cultured in dLu, dLN, and BME were compared. As expected, KRT7, a marker of cholangiocyte-lineage (41), was comparable between all conditions and showed high expression, indicating retention of CCA phenotype (Figure 5B). Integrin β1 (ITGB1) and integrin α5 (ITGA5), both ECM binding subunits of integrin receptors (42–44), were probed for their expression profiles (Figure 5C). ITGB1 was significantly upregulated in dLN (versus both dLu and BME p=0.03) revealing tissue-specific cell-ECM interactions. ITGA5 showed high heterogeneity in expression between different CCAOs, with a 13-fold increase of CCAO2 vs CCAO3 in dLN (p=0.1). This suggests that in lymph node metastasis upregulation could be patient-dependent. LGR5 and CD133, both markers of (different) cancer-stem cell subpopulations (45, 46), were significantly affected by the ECM (Figure 5D). LGR5 was significantly upregulated in dLN compared to dLu ($p<0.001$) and BME (p=0.005), while CD133 was significantly higher in BME compared to both decellularized scaffolds (both p=0.016). Thus, this indicates that there is a tissue-specific involvement of cancer-stem cell populations in metastatic outgrowth in CCA. Furthermore, significant higher expression of COL1A1 in dLN (vs BME p=0.0075, vs dLU p=0.013) and COL3A1 in BME (vs dLU p=0.007) indicates that the reciprocal production of ECM proteins by tumor cells is also affected by the ECM of the metastatic organ (Figure 5E). Additionally, epithelial-to-mesenchymal transition (EMT), and the reverse process of mesenchymal-to-epithelial transition (MET) are thought to play a role in metastatic dissemination and subsequent colonization, respectively (47, 48). ECAD was significantly upregulated in dLN (vs dLu $p<0.001$, vs BME p=0.002), indicating (re)expression induced by the extracellular microenvironment, possibly due to the tumor cells undergoing MET (Figure 5F). Classical EMT-markers VIM and SNAI1 showed heterogeneous expression (Figures S6A, B). The ECM also influences gene expression profiles of matrix modulating genes (Figures S6C, D). Tissue inhibitor of metalloproteinases 1 and 2 (TIMP1, TIMP2) are significantly upregulated in dLN compared to dLU (TIMP1 p=0.026, TIMP2 p=0.04 only for CCAO2), while metalloproteinases 2 and 9 (MMP2, MMP9) show varied expression profiles in the different decellularized scaffolds. Overall,

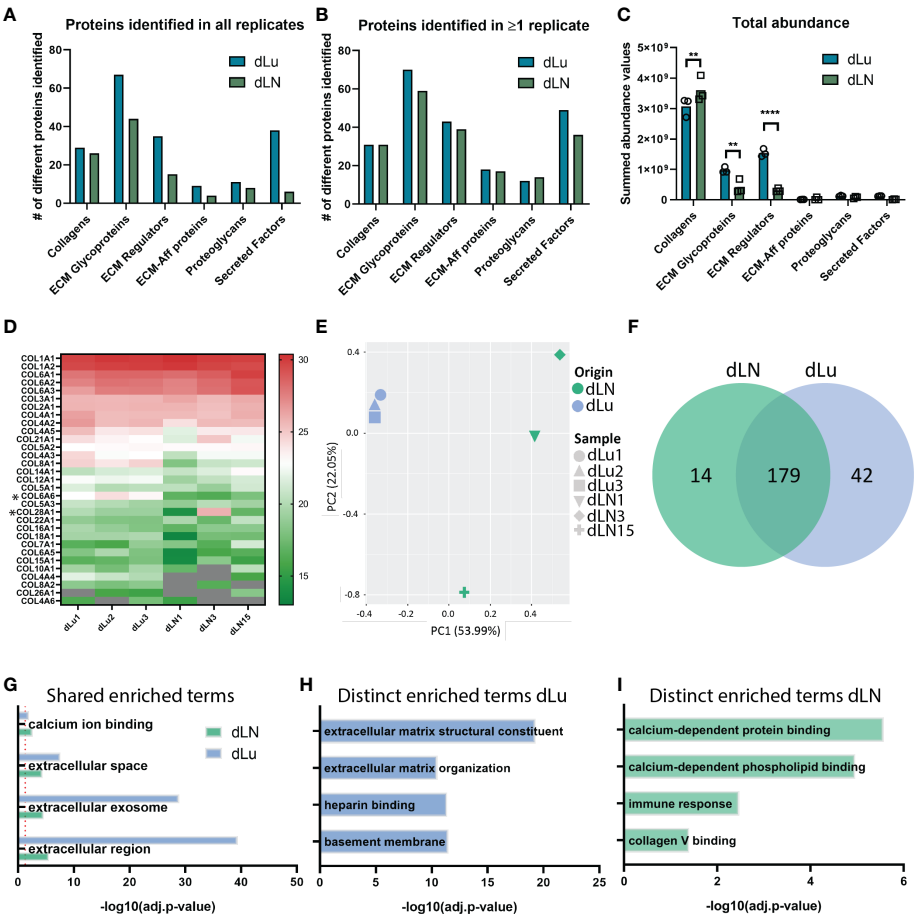

FIGURE 4
Analysis of global ECM proteome derived from decellularized lung and lymph node tissue. **(A, B)** Global matrisome protein composition identified by Mass Spectrometry displaying the total number of unique proteins identified in all biological replicates **(A)** or identified in at least 1 biological replicate **(B)**. Only proteins overlapping with MatrisomeDB classification for ECM-related proteins are included. **(C)** Total abundance values per ECM-related protein category. A two-way ANOVA with multiple comparisons per matrisome category statistical analysis was performed (Collagen p=0.006; ECM Glycoproteins p=004, ECM Regulators p<0.0001). **(D)** Heat map displaying the relative log_2(abundance) values for all identified collagen subunits. Grey color indicates that no abundance value was present. *p < 0.05. **(E)** Scatter plot based on principal component analysis (PCA) displays a global separation between ECM protein composition of dLN and dLu. **(F)** Exclusive and shared proteins identified in dLu and dLN. **(G–I)** Enrichment analysis of selected biological processes and pathways for protein abundance differences as displayed in **(E)** for dLu and dLN. Shared enriched processes are processes that are significantly enriched in both decellularized tissues, distinct enriched processes are processes that are exclusively enriched in either dLu or dLN. For all mass spectrometry analysis dLu1, dLu2, and dLu3 were used for lung, and dLN1, dLN3, and dLN13 were used for lymph node. **= p-value < 0.005; **** = p-value < 0.0001.

various cancer-related processes, including cancer stem cell plasticity, ECM production, cell-ECM binding, and EMT/MET, are influenced by the extracellular environment of the target metastatic organ in a tissue-specific pattern.

Metastatic outgrowth of CCAOs is ECM and patient dependent

In a metastatic setting, after reaching the microenvironment of the distant organ, cancer cells will colonize the niche and often display a state of dormancy before changing to a state of proliferation and outgrowth (49, 50). We therefore examined if the ECM plays a role in the change from dormancy to outgrowth, and the effect on the associated cell migration and proliferation dynamics. H&E staining of CCAOs cultured in dLN and dLu showed cell-ECM attachment, with the occurrence of different invasive patterns (Figures 6A, B). In dLu, CCAOs exhibited localized colonization, with extensive in-growth in the scaffold at these locations, reminiscent of the localized growth pattern *in vivo* (Figure 6A) (51). CCAOs in dLN colonized primarily the outer rim, either in single-cell or cellular clumps, with an epithelial-like phenotype and limited scaffold in-growth (Figure 6B). This is congruent with the upregulation of ECAD in CCAOs cultured in dLN compared to dLu (Figure 5F) and the upregulation of TIMPs in dLN compared to dLU suggesting that

10.3389/fonc.2022.1101901

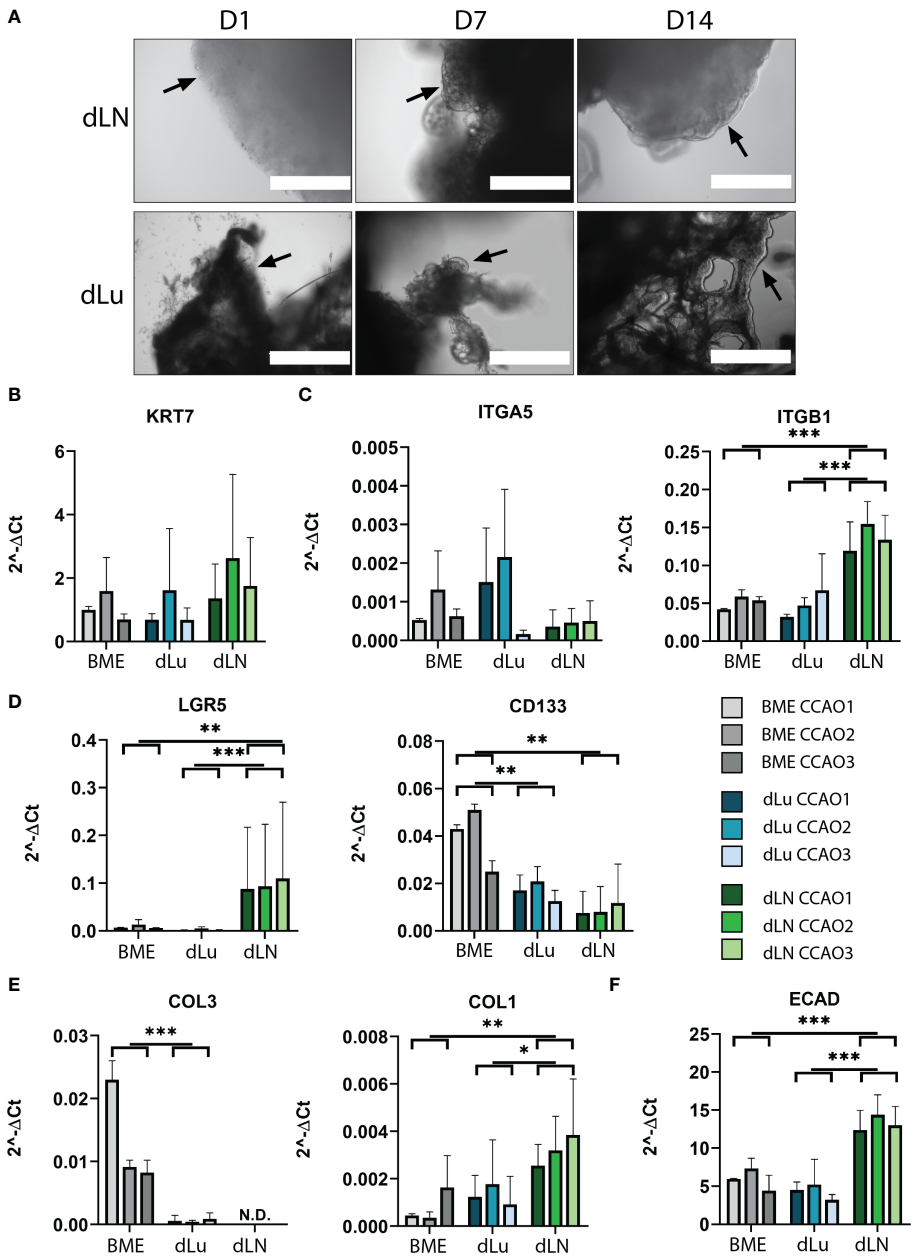

FIGURE 5
Recellularization of dLu and dLN with CCAOs reveals distinct gene expression profiles. **(A)** Representative bright field microscopy images of CCAOs cultured in dLu and dLN on day 1, 7 and 14 after recellularization. Day 1 scale bar indicates 1000 μm, day 7 and day 14 scale bars indicate 400 μm. Black arrows indicate the progression from single cells at day 1 to a complete cellular layer at day 14. **(B)** Gene expression of KRT7 in CCAOs for BME control and recellularized dLu and dLN. **(C)** Gene expression of ITGA5 and ITGB1 in CCAOs for BME control and recellularized dLu and dLN. **(D)** Gene expression of LGR5 and CD133 in CCAOs for BME control and recellularized dLu and dLN. **(E)** Gene expression of COL3A1 and COL1A1 in CCAOs for BME control and recellularized dLu and dLN. **(F)** Gene expression of ECAD in CCAOs for BME control and recellularized dLu and dLN. * = p-value < 0.05, ** = p-value < 0.005, *** = p-value < 0.0001. N.D. means that the values were not detectable. Mann-Whitney U statistical test was used for determining significance in gene expression profiles. All gene expression profiles were normalized to GAPDH. For recellularization experiments dLu1, dLu2, dLu3 were used for lung and dLN9, dLN8, and dLN1 were used for lymph node.

the inhibition of matrix degradation is associated with the limited invasion occurring (Figure S6C). In all, decellularized scaffolds of lung and lymph node can induce different migratory patterns.

Subsequently, a metabolic assay was used to probe the metabolic activity of the tumor organoids over time in each condition. As a control, BME-cultured CCAOs exhibited significant increase in metabolic activity over 14 days, as

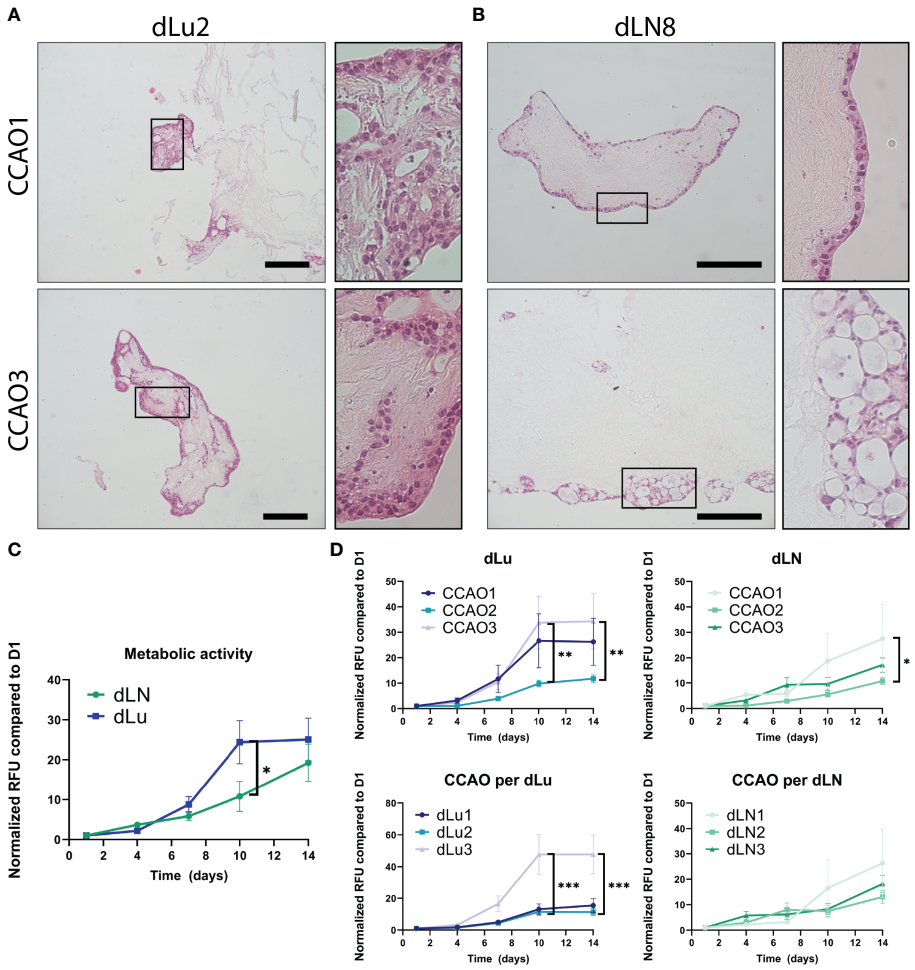

FIGURE 6
Proliferation and migration dynamics of metastasis in CCAOs. **(A, B)** Representative H&E stainings of CCAO1 (top) and CCAO3 (bottom) in dLu **(A)** and dLN **(B)**. The black rectangle shows a higher magnification image of the morphology of the CCAOs in the decellularized scaffolds. Scale bars indicate 250 μm. **(C)** Metabolic activity measurements of recellularized dLN (n=27, n=3 ECM donors with n=3 CCAO lines and n=3 technical replicates per combination) and dLu (n=27, n=3 ECM donors with n=3 CCAO lines and n=3 technical replicates per combination) consecutively measured on day 1, 4, 7, 10, and 14. All Relative Fluorescent Units (RFU) data is normalized to day 1. **(D)** Metabolic activity measurements for CCAOs in dLU split based on patient origin of CCAO (i.e. separated CCAO1, CCAO2, and CCAO3) and donor of decellularized scaffolds (i.e. separated dLu1, dLu2, and dLu3). **(E)** Metabolic activity measurements for CCAOs in dLU split based on patient origin of CCAO (i.e. separated CCAO1, CCAO2, and CCAO3) and donor of decellularized scaffolds (i.e. separated dLN1, dLN2, and dLN3). * = p-value<0.05, ** = p-value<0.005, *** = p-value<0.0001. Multiple t-test were used together with Holm-Sidak correction method to correct for multiple comparisons. For recellularization experiments dLu1, dLu2, dLu3 were used for lung and dLN9, dLN8, and dLN1 were used for lymph node.

expected and reported in literature (Figure S7A, (13)). CCAOs in dLN (n=27, n=3 ECM donors with n=3 CCAO lines and n=3 technical replicates per combination) and dLu (n=27, n=3 ECM donors with n=3 CCAO lines and n=3 technical replicates per combination) also showed an increase in metabolic activity over time (Figure 6C). However, a different growth pattern was observed in both metastatic locations, with a significant delay in metabolic activity increase after 10 days in dLN compared to dLu (10.8x increase in dLU vs 24.4x increase in dLN, p=0.014). After 14 days, no significant difference was observed (p=0.97), indicating that it was a delay in growth, rather than a consistently lower growth rate. Dissecting the role of seed (i.e. the CCAO) and soil (i.e. the ECM) reveals that in lung metastasis, both seed and soil have a significant influence on metastatic outgrowth (Figure 6D). This is exhibited by CCAO3 and Lu3 showing significantly higher metabolic activity after 10 and 14 days when comparing tumor and donor scaffold, respectively. For lymph node metastasis, this effect was less evident, with CCAO3 having a significantly larger increase in metabolic activity after 7 days, suggesting an earlier switch from dormancy to outgrowth in this case (Figure 6E). No ECM-dependent differences were found in dLN (Figure 6E). To note, no difference in initial seeding efficiency was observed between dLN and dLu, as represented by absolute metabolic activity

values at day 1 (Figure S7B). In summary, these data suggest that the dynamics of outgrowth after colonization are multi-factorial, both patient and ECM related. In this model, metaphorically both the "seed" and "soil" influence metastatic growth of cancer cells in the lung, while in the lymph node the growth is dictated primarily by the seed (cancer cell).

Discussion

The process of cancer metastasis consists of a multi-step cascade during which tumor cells disseminate from the primary tumor, survive in the lymphatic or blood circulation, and colonize distant organs. The tumor cells are heavily influenced by the various microenvironments that they encounter during this cascade, including, but not limited to, the ECM of the target organ for metastasis (52–54). Particularly, the interaction of seed (i.e. cancer cells) and soil (i.e. ECM) that is encountered in the metastatic organ plays a role in the dynamics of metastatic colonization (20, 55). Herein, we show the possibility to obtain a tissue-specific metastatic model by converging decellularized human lung and lymph nodes with patient-derived CCAOs to investigate the role of the ECM in metastatic outgrowth. We demonstrated the capability to decellularize human derived tissue of distant metastatic locations for CCA and reveal the biomechanical and biochemical characteristics of dLu and dLN, which recapitulate the tissue of origin. Furthermore, dLu and dLN scaffolds support adhesion and culture of CCAOs while stimulating distinct, tissue-specific gene expression profiles. The associated growth patterns further delineate the role of both seed and soil in the outgrowth of colonized metastatic CCA, with dLu inducing a significantly higher proliferation rate compared to dLN.

The decellularization method employed in this study, utilizing Triton X-100, was able to successfully eliminate cellular material from both human lung and lymph node tissue. The resulting decellularized scaffolds recapitulated the composition of native ECM, with enrichment of basement membrane-related proteins in dLu and immune system-related proteins in dLN. Decellularization of human lymph nodes has not been reported yet in literature, but employing an identical decellularization method as lung provided comparative scaffolds for studying cell-ECM interactions in these respective organs.

The mechanical role of ECM in cancer metastasis is highly diverse, affecting matrix remodeling, cell spreading, migration and metastasis (53, 56, 57). Therefore, biomechanical characterizations of the decellularized tissue were obtained, which indicated similar stiffness for dLu and dLN, with a notable variability in macro-scale stiffness for dLN. Although the obtained mechanical properties (Young's Modulus) of dLu are comparable to literature, these properties are only known for animal-derived decellularized ECM, non-decellularized human ECM or engineered hydrogels (58–62), extending the relevance of this study. Mechanical characterization of human lymph node ECM is absent in literature. The heterogeneity in mechanical properties in dLN is mimicked by a diversity in ECM proteins, showing the correlation between mechanical and chemical properties of the extracellular environment. To note, causation is not inferred, as not only molecular composition, but also cross-linking, spatial heterogeneity, and alignment of ECM architecture can contribute to the heterogeneity observed in mechanical properties.

Cell adhesion to ECM is crucial for the process of metastasis, and integrins are the main cell adhesion receptors that facilitate these functions. In multiple cancer types, integrin β1 signaling plays a crucial role in metastatic colonization and outgrowth (63). In dLN, CCAOs upregulate integrin β1, indicating that the role of integrin β1 in CCA metastasis is organ-dependent. Furthermore, the production of ECM-proteins, and their associated proteases, by tumor cells in a metastatic environment can remodel the environment (64, 65). COL1A1 is upregulated in a lymph node environment, which coincides with findings in breast cancer, where collagen 1 fiber density was increased in lymph node metastasis, and lung cancer, where COL1A1 expression highly correlated with lymph node metastasis (66, 67). E-cadherin, an epithelial marker, is also upregulated in dLN. This is corroborated by the epithelial-phenotype present in dLN, as well as the observed limited invasion. In other tumors, an epithelial phenotype is often associated with formation of secondary tumors, with E-cadherin-positive metastatic foci (68, 69). The associated lack of invasion in dLN could be due to the absence of cellular interactions normally present in the lymph node during the process of metastasis, including interactions between resident immune cells and recruited bone marrow-derived cells (70, 71). Incorporation of these cell types in this system would allow for even deeper understanding of metastatic colonization by modelling the interactions between primary tumor, immune cells, and secondary target sites.

Combining multiple decellularized scaffold donors with patient-specific organoids allows for delineating the role of both seed and soil in cancer metastasis. Importantly, after arrival at a distant metastatic organ, cancer cells will colonize the niche and often initiate a dormant phenotype (49). Dormancy licenses the cancer cells to survive this novel environment through chemotherapeutic resistance (i.e. less cellular division means less susceptibility to conventional chemotherapy) and immune cell avoidance, mediated by downregulation of MHC-1 expression (72). Here we show that the ECM can dictate the timing and duration of this dormancy phase, whereby dLN (2.9-fold increase from day 4 to 10) resulted in a slower increase in metabolic activity compared to dLu (11-fold increase from day 4 to 10). The cause of the switch from dormancy to proliferation is complex, and this study shows that the ECM in isolation can influence this process.

Lymph node colonization might not be a final destination for metastasis, and could contribute to further distant metastases

including lung. The frequency of cells metastasizing from the lymph node to different distant organs is dependent on the cancer-type, and still a topic of debate (73, 74). Mechanistically, cancer cells are able to colonize lymph nodes, invade lymph node blood vessels and subsequently colonize the lung (75). In our study, CCAOs cultured in dLN exhibited a significant upregulation of LGR5, a well-recognized stem cell marker (76, 77), compared to both dLu and BME. LGR5 marks tumor-initiating cells with a cancer stem cell-phenotype in liver cancer (77) and these cancer stem cells are thought to be responsible for tumor progression, including metastasis (78). Thus, the high level of LGR5 in CCAOs that colonize the lymph node suggests that there is a pool of cancer stem cell-like cells present which could be responsible for migration from the lymph node to the lungs. This is congruent with the clinical observation that lymph node metastasis often precedes lung metastasis in CCA patients (24), and the association of LGR5 expression with lymph node metastases in other tumor types (76, 79).

For the lung, donor-dependent proliferation differences were observed, with dLu3 favoring proliferation compared to dLu1 and dLu2. To note, this lung was obtained from a current smoker, which is in contrast with the other two donors (former smoker <10 years and never smoker). Although the relationship between smoking and metastasis of CCA has not been studied, it is known that smoking affects the initiation and progression of multiple other cancers such as soft tissue sarcoma, esophageal cancer, breast cancer colorectal cancer, and lung cancer (80–82). Further research is necessary to establish a direct relationship between smoking and metastasis of CCA to the lungs, given the dependence on multiple variables.

In summary, acellular scaffolds of human lung and lymph nodes were successfully obtained *via* decellularization. Biochemical and biomechanical characterization revealed the retention of tissue-specific characteristics, as well as expanded our understanding of the mechanical properties of the ECM. Subsequent recellularization revealed differences in CCA metastatic colonization in the lung and lymph nodes through gene expression profiles and proliferation dynamics. Converging organoids with organ-specific decellularized ECM provides a valuable tool for probing cell-matrix interactions in a metastatic setting.

Data availability statement

The datasets presented in this study can be found in the PRIDE database (https://www.ebi.ac.uk/pride/ - accession number: PXD038191) or in the Supplementary Material.

Ethics statement

The studies involving human participants were reviewed and approved by Medical Ethical Council of the Erasmus MC and the Swedish ethical review board in Lund. The patients/participants provided their written informed consent to participate in this study.

Author contributions

GT, LL, MV designed the study. MV, LL and GK obtained funding. HR, IS, GW-T, OR aided in the collection of tissues. IS collected patient information. GT, MB performed experiments. GT, JT, JD aided in the conception and implementation of mass spectrometry experiments, and JT and GT performed the analysis. GT, MB, JC, IM, GK set-up mechanical characterization of decellularized scaffolds, with MB and IM conducting rheological measurements and MB and JC conducting nanoindentation measurements. GT, MB, IS, JC performed data analysis of mechanical measurements. GT, MB collected all data and drafted the figures. GT, MB, LL, MV wrote the manuscript. All authors critically reviewed and revised the manuscript.

Funding

This project was partly funded by the Erasmus MC Human Disease Model Award 2018 (HDMA-380801), ENW-XS (Project OCENW.XS21.2.003), Dutch Cancer Society (KWF: COCOON Study, project number 14364) and the Dutch Society of Gastroenterology and Hepatology (NVGE, Gastrostart Vervolgsubsidie project number 01-2022). GK gratefully acknowledges funding from the VICI project 'How cytoskeletal teamwork makes cells strong' (project number VI.C.182.004) which is financed by the Dutch Research Council (NWO) and from the Convergence program Syn-Cells for Health(care) of the Erasmus MC and TU Delft under the theme of Health and Technology.

Acknowledgments

We would like to thank Kübra Köten for assistance with organoid culture and tumorigenicity confirmation.

Conflict of interest

The authors declare that the research was conducted in the absence of any commercial or financial relationships that could be construed as a potential conflict of interest.

Publisher's note

All claims expressed in this article are solely those of the authors and do not necessarily represent those of their affiliated organizations, or those of the publisher, the editors and the reviewers. Any product that may be evaluated in this article, or claim that may be made by its manufacturer, is not guaranteed or endorsed by the publisher.

Supplementary material

The Supplementary Material for this article can be found online at: https://www.frontiersin.org/articles/10.3389/fonc.2022.1101901/full#supplementary-material

References

1. Bertuccio P, Malvezzi M, Carioli G, Hashim D, Boffetta P, El-Serag HB, et al. Global trends in mortality from intrahepatic and extrahepatic cholangiocarcinoma. *J Hepatol* (2019) 71:104–14. doi: 10.1016/j.jhep.2019.03.013

2. Nakagawa T, Kamiyama T, Kurauchi N, Matsushita M, Nakanishi K, Kamachi H, et al. Number of lymph node metastases is a significant prognostic factor in intrahepatic cholangiocarcinoma. *World J Surg* (2005) 29:728–33. doi: 10.1007/s00268-005-7761-9

3. Ghouri YA, Mian I, Blechacz B. Cancer review: cholangiocarcinoma. *J carcinog* (2015) 14:1. doi: 10.4103/1477-3163.151940

4. Yan X, Wang P, Zhu Z, Ning Z, Xu L, Zhuang L, et al. Site-specific metastases of intrahepatic cholangiocarcinoma and its impact on survival: a population-based study. *Future Oncol* (2019) 15:2125–37. doi: 10.2217/fon-2018-0846

5. Wu W, He X, Andayani D, Yang L, Ye J, Li Y, et al. Pattern of distant extrahepatic metastases in primary liver cancer: a SEER based study. *J Cancer* (2017) 8:2312. doi: 10.7150/jca.19056

6. Wang X, Yu GY, Chen M, Wei R, Chen J, Wang Z. Pattern of distant metastases in primary extrahepatic bile-duct cancer: A SEER-based study. *Cancer Med* (2018) 7:5006–14. doi: 10.1002/cam4.1772

7. Hahn F, Müller L, Mähringer-Kunz A, Tanyildizi Y, Santos DPD, Düber C, et al. Distant metastases in patients with intrahepatic cholangiocarcinoma: does location matter? a retrospective analysis of 370 patients. *J Oncol* (2020) 2020. doi: 10.1155/2020/7195373

8. Brindley PJ, Bachini M, Ilyas SI, Khan SA, Loukas A, Sirica AE, et al. Cholangiocarcinoma. *Nat Rev Dis Primers* (2021) 7:1–17. doi: 10.1038/s41572-021-00300-2

9. Gravely AK, Vibert E, Sapisochin G. Surgical treatment of intrahepatic cholangiocarcinoma. *J Hepatol* (2022) 77(3):865–7. doi: 10.1016/j.jhep.2022.01.004

10. Nagle PW, Plukker JTM, Muijs CT, Van Luijk P, Coppes RP. Patient-derived tumor organoids for prediction of cancer treatment response. *Semin Cancer Biol* (2018) 53:258–64. doi: 10.1016/j.semcancer.2018.06.005

11. Veninga V, Voest EE. Tumor organoids: Opportunities and challenges to guide precision medicine. *Cancer Cell* (2021) 39(9):1190–201. doi: 10.1016/j.ccell.2021.07.020

12. Van Tienderen GS, Li L, Broutier L, Saito Y, Inacio P, Huch M, et al. Hepatobiliary tumor organoids for personalized medicine: a multicenter view on establishment, limitations, and future directions. *Cancer Cell* (2022) 40(3):226–30. doi: 10.1016/j.ccell.2022.02.001

13. Broutier L, Mastrogiovanni G, Verstegen MMA, Francies HE, Gavarró LM, Bradshaw CR, et al. Human primary liver cancer–derived organoid cultures for disease modeling and drug screening. *Nat Med* (2017) 23:1424. doi: 10.1038/nm.4438

14. Saito Y, Muramatsu T, Kanai Y, Ojima H, Sukeda A, Hiraoka N, et al. Establishment of patient-derived organoids and drug screening for biliary tract carcinoma. *Cell Rep* (2019) 27:1265–1276.e1264. doi: 10.1016/j.celrep.2019.03.088

15. Cristinziano G, Porru M, Lamberti D, Buglioni S, Rollo F, Amoreo CA, et al. FGFR2 fusion proteins drive oncogenic transformation of mouse liver organoids towards cholangiocarcinoma. *J hepatol* (2021) 75(2):351–62. doi: 10.1016/j.jhep.2021.02.032

16. Chaudhuri O, Koshy ST, Branco Da Cunha C, Shin J-W, Verbeke CS, Allison KH, et al. Extracellular matrix stiffness and composition jointly regulate the induction of malignant phenotypes in mammary epithelium. *Nat mat* (2014) 13:970–8. doi: 10.1038/nmat4009

17. Eble JA, Niland S. The extracellular matrix in tumor progression and metastasis. *Clin Exp metastasis* (2019) 36:171–98. doi: 10.1007/s10585-019-09966-1

18. Broguiere N, Isenmann L, Hirt C, Ringel T, Placzek S, Cavalli E, et al. Growth of epithelial organoids in a defined hydrogel. *Advanced Materials* (2018) 30:1801621. doi: 10.1002/adma.201801621

19. Paget S. The distribution of secondary growths in cancer of the breast. *Lancet* (1889) 133:571–3. doi: 10.1016/S0140-6736(00)49915-0

20. Fidler IJ, Poste G. The "seed and soil" hypothesis revisited. *Lancet Oncol* (2008) 9:808. doi: 10.1016/S1470-2045(08)70201-8

21. Gilbert TW, Sellaro TL, Badylak SF. Decellularization of tissues and organs. *Biomaterials* (2006) 27:3675–83. doi: 10.1016/j.biomaterials.2006.02.014

22. Verstegen MMA, Willemse J, Van Den Hoek S, Kremers G-J, Luider TM, Van Huizen NA, et al. Decellularization of whole human liver grafts using controlled perfusion for transplantable organ bioscaffolds. *Stem Cells Dev* (2017) 26:1304–15. doi: 10.1089/scd.2017.0095

23. Willemse J, Verstegen MMA, Vermeulen A, Schurink IJ, Roest HP, van der Laan LJW, et al. Fast, robust and effective decellularization of whole human livers using mild detergents and pressure controlled perfusion. *Materials Sci Engineering: C* (2020) 108:110200. doi: 10.1016/j.msec.2019.110200

24. Cheng R, Du Q, Ye J, Wang B, Chen Y. Prognostic value of site-specific metastases for patients with advanced intrahepatic cholangiocarcinoma: A SEER database analysis. *Medicine* (2019) 98. doi: 10.1097/MD.0000000000018191

25. Kontomaris S-V. The hertz model in AFM nanoindentation experiments: applications in biological samples and biomaterials. *Micro Nanosyst* (2018) 10:11–22. doi: 10.2174/1876402910666180426114700

26. Khanafer K, Schlicht MS, Berguer R. How should we measure and report elasticity in aortic tissue? *Eur J Vasc Endovas Surg* (2013) 45:332–9. doi: 10.1016/j.ejvs.2012.12.015

27. Shao X, Taha IN, Clauser KR, Gao Y, Naba A. MatrisomeDB: the ECM-protein knowledge database. *Nucleic Acids Res* (2020) 48:D1136–44. doi: 10.1093/nar/gkz849

28. Van Tienderen GS, Rosmark O, Lieshout R, Willemse J, De Weijer F, Rendin LE, et al. Extracellular matrix drives tumor organoids toward desmoplastic matrix deposition and mesenchymal transition. *Acta Biomat* (2022), 27. doi: 10.1016/j.actbio.2022.11.038

29. Crapo PM, Gilbert TW, Badylak SF. An overview of tissue and whole organ decellularization processes. *Biomaterials* (2011) 32:3233–43. doi: 10.1016/j.biomaterials.2011.01.057

30. Itoh H, Nishino M, Hatabu H. Architecture of the lung: morphology and function. *J Thorac Imaging* (2004) 19:221–7. doi: 10.1097/01.rti.0000142835.06988.b0

31. Willard-Mack CL. Normal structure, function, and histology of lymph nodes. *Toxicol Pathol* (2006) 34:409–24. doi: 10.1080/01926230600867727

32. Mayorca-Guiliani AE, Madsen CD, Cox TR, Horton ER, Venning FA, Erler JT. ISDoT: *in situ* decellularization of tissues for high-resolution imaging and proteomic analysis of native extracellular matrix. *Nat Med* (2017) 23:890–8. doi: 10.1038/nm.4352

33. Mazza G, Al-Akkad W, Telese A, Longato L, Urbani L, Robinson B, et al. Rapid production of human liver scaffolds for functional tissue engineering by high shear stress oscillation-decellularization. *Sci Rep* (2017) 7:5534. doi: 10.1038/s41598-017-05134-1

34. Vitale D, Kumar Katakam S, Greve B, Jang B, Oh ES, Alaniz L, et al. Proteoglycans and glycosaminoglycans as regulators of cancer stem cell function and therapeutic resistance. *FEBS J* (2019) 286:2870–82. doi: 10.1111/febs.14967

35. Wei J, Hu M, Huang K, Lin S, Du H. Roles of proteoglycans and glycosaminoglycans in cancer development and progression. *Int J Mol Sci* (2020) 21:5983. doi: 10.3390/ijms21175983

36. Fratzl P. Collagen: structure and mechanics, an introduction. In: *Collagen*. Springer (2008). p. 1–13. doi: 10.1007/978-0-387-73906-9_1

37. Mecham RP. Elastin in lung development and disease pathogenesis. *Matrix Biol* (2018) 73:6–20. doi: 10.1016/j.matbio.2018.01.005

38. Jiao X, Sherman BT, Huang DW, Stephens R, Baseler MW, Lane HC, et al. DAVID-WS: a stateful web service to facilitate gene/protein list analysis. *Bioinformatics* (2012) 28:1805–6. doi: 10.1093/bioinformatics/bts251

39. Jandl K, Mutgan AC, Eller K, Schaefer L, Kwapiszewska G. The basement membrane in the cross-roads between the lung and kidney. *Matrix Biol* (2021) 105:31–52. doi: 10.1016/j.matbio.2021.11.003

40. Saito Y, Muramatsu T, Saito H. Establishment and long-term culture of organoids derived from human biliary tract carcinoma. *STAR Protoc* (2020) 1:100009. doi: 10.1016/j.xpro.2019.100009

41. Rullier A, Le Bail B, Fawaz R, Blanc JF, Saric J, Bioulac-Sage P. Cytokeratin 7 and 20 expression in cholangiocarcinomas varies along the biliary tract but still differs from that in colorectal carcinoma metastasis. *Am J Surg Pathol* (2000) 24:870–6. doi: 10.1097/00000478-200006000-00014

42. Ruoslahti E, Reed JC. Anchorage dependence, integrins, and apoptosis. *Cell (Cambridge)* (1994) 77:477–8. doi: 10.1016/0092-8674(94)90209-7

43. Hamidi H, Ivaska J. Every step of the way: integrins in cancer progression and metastasis. *Nat Rev Cancer* (2018) 18:533–48. doi: 10.1038/s41568-018-0038-z

44. Kechagia JZ, Ivaska J, Roca-Cusachs P. Integrins as biomechanical sensors of the microenvironment. *Nat Rev Mol Cell Biol* (2019) 20:457–73. doi: 10.1038/s41580-019-0134-2

45. Reya T, Morrison SJ, Clarke MF, Weissman IL. Stem cells, cancer, and cancer stem cells. *nature* (2001) 414:105–11. doi: 10.1038/35102167

46. Bocci F, Gearhart-Serna L, Boareto M, Ribeiro M, Ben-Jacob E, Devi GR, et al. Toward understanding cancer stem cell heterogeneity in the tumor microenvironment. *Proc Natl Acad Sci* (2019) 116:148–57. doi: 10.1073/pnas.1815345116

47. Aiello NM, Maddipati R, Norgard RJ, Balli D, Li J, Yuan S, et al. EMT subtype influences epithelial plasticity and mode of cell migration. *Dev Cell* (2018) 45:681–695.e684. doi: 10.1016/j.devcel.2018.05.027

48. Usman S, Waseem NH, Nguyen TKN, Mohsin S, Jamal A, Teh M-T, et al. Vimentin is at the heart of epithelial mesenchymal transition (EMT) mediated metastasis. *Cancers* (2021) 13:4985. doi: 10.3390/cancers13194985

49. Hedley BD, Chambers AF. Tumor dormancy and metastasis. *Adv Cancer Res* (2009) 102:67–101. doi: 10.1016/S0065-230X(09)02003-X

50. Di Martino JS, Nobre AR, Mondal C, Taha I, Farias EF, Fertig EJ, et al. A tumor-derived type III collagen-rich ECM niche regulates tumor cell dormancy. *Nat Cancer* (2022) 3:90–107. doi: 10.1038/s43018-021-00291-9

51. Zhai N, Liu J, Xu P, Liu B, Fan Y, Lv C. Pulmonary metastasis of distal cholangiocarcinoma with multiple cavities in bilateral lungs: A case report. *Thorac Cancer* (2020) 11:2998–3000. doi: 10.1111/1759-7714.13584

52. Leyva-Illades D, Mcmillin M, Quinn M, Demorrow S. Cholangiocarcinoma pathogenesis: Role of the tumor microenvironment. *Trans gastrointestinal Cancer* (2012) 1:71. doi: 10.3978/j.issn.2224-4778

53. Spill F, Reynolds DS, Kamm RD, Zaman MH. Impact of the physical microenvironment on tumor progression and metastasis. *Curr Opin Biotechnol* (2016) 40:41–8. doi: 10.1016/j.copbio.2016.02.007

54. Amos SE, Choi YS. The cancer microenvironment: mechanical challenges of the metastatic cascade. *Front Bioengineering Biotechnol* (2021) 9:625859. doi: 10.3389/fbioe.2021.625859

55. Gillot L, Lebeau A, Baudin L, Pottier C, Louis T, Durré T, et al. Periostin in lymph node pre-metastatic niches governs lymphatic endothelial cell functions and metastatic colonization. *Cell Mol Life Sci* (2022) 79:1–18. doi: 10.1007/s00018-022-04262-w

56. Emon B, Bauer J, Jain Y, Jung B, Saif T. Biophysics of tumor microenvironment and cancer metastasis-a mini review. *Comput Struct Biotechnol J* (2018) 16:279–87. doi: 10.1016/j.csbj.2018.07.003

57. Winkler J, Abisoye-Ogunniyan A, Metcalf KJ, Werb Z. Concepts of extracellular matrix remodelling in tumour progression and metastasis. *Nat Commun* (2020) 11:1–19. doi: 10.1038/s41467-020-18794-x

58. Petersen TH, Calle EA, Colehour MB, Niklason LE. Matrix composition and mechanics of decellularized lung scaffolds. *Cells Tissues Organs* (2012) 195:222–31. doi: 10.1159/000324896

59. Melo E, Garreta E, Luque T, Cortiella J, Nichols J, Navajas D, et al. Effects of the decellularization method on the local stiffness of acellular lungs. *Tissue Eng Part C: Methods* (2014) 20:412–22. doi: 10.1089/ten.tec.2013.0325

60. Pouliot RA, Link PA, Mikhaiel NS, Schneck MB, Valentine MS, Kamga Gninzeko FJ, et al. Development and characterization of a naturally derived lung extracellular matrix hydrogel. *J Biomed mat Res Part A* (2016) 104:1922–35. doi: 10.1002/jbm.a.35726

61. Jorba I, Beltrán G, Falcones B, Suki B, Farré R, García-Aznar JM, et al. Nonlinear elasticity of the lung extracellular microenvironment is regulated by macroscale tissue strain. *Acta biomaterialia* (2019) 92:265–76. doi: 10.1016/j.actbio.2019.05.023

62. Júnior C, Narciso M, Marhuenda E, Almendros I, Farré R, Navajas D, et al. Baseline stiffness modulates the non-linear response to stretch of the extracellular matrix in pulmonary fibrosis. *Int J Mol Sci* (2021) 22:12928. doi: 10.3390/ijms222312928

63. Shibue T, Weinberg RA. Integrin β1-focal adhesion kinase signaling directs the proliferation of metastatic cancer cells disseminated in the lungs. *Proc Natl Acad Sci* (2009) 106:10290–5. doi: 10.1073/pnas.0904227106

64. Sevenich L, Bowman RL, Mason SD, Quail DF, Rapaport F, Elie BT, et al. Analysis of tumour-and stroma-supplied proteolytic networks reveals a brain-metastasis-promoting role for cathepsin s. *Nat Cell Biol* (2014) 16:876–88. doi: 10.1038/ncb3011

65. Hebert JD, Myers SA, Naba A, Abbruzzese G, Lamar JM, Carr SA, et al. Proteomic profiling of the ECM of xenograft breast cancer metastases in different organs reveals distinct metastatic NichesECM proteomics of breast cancer metastases in diverse organs. *Cancer Res* (2020) 80:1475–85. doi: 10.1158/0008-5472.CAN-19-2961

66. Kakkad SM, Solaiyappan M, Argani P, Sukumar S, Jacobs LK, Leibfritz D, et al. Collagen I fiber density increases in lymph node positive breast cancers: pilot study. *J Biomed optics* (2012) 17:116017. doi: 10.1117/1.JBO.17.11.116017

67. Dong S, Zhu P, Zhang S. Expression of collagen type 1 alpha 1 indicates lymph node metastasis and poor outcomes in squamous cell carcinomas of the lung. *PeerJ* (2020) 8:e10089. doi: 10.7717/peerj.10089

68. Chaffer CL, Brennan JP, Slavin JL, Blick T, Thompson EW, Williams ED. Mesenchymal-to-epithelial transition facilitates bladder cancer metastasis: role of fibroblast growth factor receptor-2. *Cancer Res* (2006) 66:11271–8. doi: 10.1158/0008-5472.CAN-06-2044

69. Chao YL, Shepard CR, Wells A. Breast carcinoma cells re-express e-cadherin during mesenchymal to epithelial reverting transition. *Mol Cancer* (2010) 9:1–18. doi: 10.1186/1476-4598-9-179

70. Lee JW, Stone ML, Porrett PM, Thomas SK, Komar CA, Li JH, et al. Hepatocytes direct the formation of a pro-metastatic niche in the liver. *Nature* (2019) 567:249–52. doi: 10.1038/s41586-019-1004-y

71. Wang M, Zhao X, Qiu R, Gong Z, Huang F, Yu W, et al. Lymph node metastasis-derived gastric cancer cells educate bone marrow-derived mesenchymal stem cells *via* YAP signaling activation by exosomal Wnt5a. *Oncogene* (2021) 40:2296–308. doi: 10.1038/s41388-021-01722-8

72. Pommier A, Anaparthy N, Memos N, Kelley ZL, Gouronnec A, Yan R, et al. Unresolved endoplasmic reticulum stress engenders immune-resistant, latent pancreatic cancer metastases. *Science* (2018) 360:eaao4908. doi: 10.1126/science.aao4908

73. Siegel MB, He X, Hoadley KA, Hoyle A, Pearce JB, Garrett AL, et al. Integrated RNA and DNA sequencing reveals early drivers of metastatic breast cancer. *J Clin Invest* (2018) 128:1371–83. doi: 10.1172/JCI96153

74. Zhang C, Zhang L, Xu T, Xue R, Yu L, Zhu Y, et al. Mapping the spreading routes of lymphatic metastases in human colorectal cancer. *Nat Commun* (2020) 11:1–11. doi: 10.1038/s41467-020-15886-6

75. Pereira ER, Kedrin D, Seano G, Gautier O, Meijer EFJ, Jones D, et al. Lymph node metastases can invade local blood vessels, exit the node, and colonize distant organs in mice. *Science* (2018) 359:1403–7. doi: 10.1126/science.aal3622

76. Michelotti G, Jiang X, Sosa JA, Diehl AM, Henderson BB. LGR5 is associated with tumor aggressiveness in papillary thyroid cancer. *Oncotarget* (2015) 6:34549. doi: 10.18632/oncotarget.5330

77. Cao W, Li M, Liu J, Zhang S, Noordam L, Verstegen M, et al. LGR5 marks targetable tumor-initiating cells in mouse liver cancer. *Nat Commun* (2020) 11:1–16. doi: 10.1038/s41467-020-15846-0

78. Clevers H. The cancer stem cell: premises, promises and challenges. *Nat Med* (2011) 17:313–9. doi: 10.1038/nm.2304

79. Wang XF, Zhang XL, Xu LP, Shi GG, Zheng HY, Sun BC. Expression of stem cell markers CD44 and Lgr5 in colorectal cancer and its relationship with lymph node and liver metastasis. *Zhonghua yi xue za zhi* (2018) 98:2899–904. doi: 10.3760/cma.j.issn.0376-2491.2018.36.005

80. Holschneider CH, Baldwin RL, Tumber K, Aoyama C, Karlan BY. The fragile histidine triad gene: a molecular link between cigarette smoking and cervical cancer. *Clin Cancer Res* (2005) 11:5756–63. doi: 10.1158/1078-0432.CCR-05-0234

81. Kenfield SA, Wei EK, Stampfer MJ, Rosner BA, Colditz GA. Comparison of aspects of smoking among the four histological types of lung cancer. *Tobacco control* (2008) 17:198–204. doi: 10.1136/tc.2007.022582

82. Warner ET, Park ER, Luberto CM, Rabin J, Perez GK, Ostroff JS. Internalized stigma among cancer patients enrolled in a smoking cessation trial: The role of cancer type and associations with psychological distress. *Psycho-Oncology* (2022) 31:753–60. doi: 10.1002/pon.5859

frontiers | Frontiers in Oncology

TYPE Review
PUBLISHED 30 March 2023
DOI 10.3389/fonc.2023.1150332

OPEN ACCESS

EDITED BY
Giulia Adriani,
Singapore Immunology Network (A*STAR), Singapore

REVIEWED BY
Maxine Lam,
Institute of Molecular and Cell Biology (A*STAR), Singapore
Bingmei M. Fu,
City College of New York (CUNY), United States

*CORRESPONDENCE
Ting-Yuan Tu
tingyuan@mail.ncku.edu.tw

SPECIALTY SECTION
This article was submitted to Molecular and Cellular Oncology, a section of the journal Frontiers in Oncology

RECEIVED 24 January 2023
ACCEPTED 13 March 2023
PUBLISHED 30 March 2023

CITATION
Huang CBX and Tu T-Y (2023) Recent advances in vascularized tumor-on-a-chip. *Front. Oncol.* 13:1150332. doi: 10.3389/fonc.2023.1150332

Recent advances in vascularized tumor-on-a-chip

Christina Bao Xian Huang[1] and Ting-Yuan Tu[1,2,3]*

[1]Department of Biomedical Engineering, National Cheng Kung University, Tainan, Taiwan, [2]Medical Device Innovation Center, National Cheng Kung University, Tainan, Taiwan, [3]International Center for Wound Repair and Regeneration, National Cheng Kung University, Tainan, Taiwan

The vasculature plays a critical role in cancer progression and metastasis, representing a pivotal aspect in the creation of cancer models. In recent years, the emergence of organ-on-a-chip technology has proven to be a robust tool, capable of replicating *in vivo* conditions with exceptional spatiotemporal resolution, making it a significant asset in cancer research. This review delves into the latest developments in 3D microfluidic vascularized tumor models and their applications *in vitro*, focusing on heterotypic cellular interactions, the mechanisms of metastasis, and therapeutic screening. Additionally, the review examines the benefits and drawbacks of these models, as well as the future prospects for their advancement.

KEYWORDS

organ-on-a-chip, tumor-on-a-chip, vascularized tumor-on-a-chip, microfluidics, vasculogenesis

1 Introduction

Despite substantial efforts and advancements in cancer research, many of the mechanisms that drive cancer progression remain to be elucidated. There is currently no model that can perfectly recapitulate all of the components of the tumor microenvironment (TME). The most widely used tools for cancer research are currently animal models and 2D cell cultures. Although 2D cell culture offers simplicity and high throughput, it does not recapitulate the complex interaction between cells in the TME. Although animal models, which are the current gold standard, can provide a complex TME, it is not uncommon for the results to have a poor correlation to biological response in humans, leading to a high failure rate of drugs in clinical trials (1). This phenomenon might be due to various factors, such as species differences, which are becoming more important as an increasing number of biologics and cell-based therapies are being developed, and the use of immunocompromised models, which are different from cancer patients who still have a functional immune system. Furthermore, animal experiments usually have a longer testing period, are costly, and are subject to tighter regulations in terms of subject numbers due to ethical concerns.

It is well established now that the tumor has a complex and dynamic microenvironment comprising cancer cells, stroma cells, and other abiotic components. Vasculature is one of the key components affecting tumor progression and treatment response (2, 3). Over the past decade, microfluidic models have emerged to bridge the gap between traditional *in vitro* models and *in vivo* models. It is a robust tool that better mimics human physiological and pathological conditions *in vitro*, including cancer (4, 5). The modular nature of microfluidic systems offers the ease of incorporating different cell types and controlling biochemical and biophysical factors such as concentration gradients and flow. This allows researchers to delineate the role of different players and to elucidate emerging behaviors more conveniently. In addition, it offers higher throughput, spatiotemporal control, and resolution compared to traditional *in vivo* models.

In addition to delivering oxygen, nutrients, and drugs, as well as removing metabolic wastes, the vasculature also serves as an important route for tumor metastasis, which accounts for approximately 90% of cancer-associated deaths (6). After invading the surrounding tissue, cancer cells reach the vasculature and intravasate, becoming circulating tumor cells (CTCs). CTCs circulate throughout the body either as single cells or as clusters and may associate with other cells circulating in the bloodstream. Upon arrest, they may extravasate from the vessel and potentially form a secondary tumor. The design of vascularized tumor-on-a-chip models can be customized to elucidate the mechanisms of the various steps of cancer metastasis.

With the abovementioned advantages, microfluidic vascularized tumor-on-a-chip models also hold great potential for therapeutic screening applications. The presence of vasculature has been shown to improve drug or engineered immune cell trafficking to the tumor (3). Moreover, the minute working volume of microfluidic devices is excellent for handling valuable samples. Vascularized tumor-on-a-chip can be designed to match the 96- or 384-well format compatible with high-throughput machinery, making it an attractive tool for drug screening. It is also convenient for assessing the dynamic TME continuously or periodically.

In this review, we first introduce the state-of-the-art strategies for vascularizing tumors-on-a-chip and then elaborate on the recent advances using vascularized tumors-on-a-chip for different applications including heterotypic cellular interactions in the TME, unveiling the mechanisms of the metastatic cascade, and therapeutic screening. Finally, we conclude this review by discussing the advantages, limitations, and future directions for vascularized tumor-on-a-chip development.

2 Vascularization strategies

To establish vascularized tumor models in microfluidic devices, vasculature can be generated separately or together with the tumor (single cells or spheroids). To generate the vasculature itself, three different methods can be used—endothelial cell (EC) lining, vasculogenesis, and angiogenesis. EC lining usually generates vasculature at the mesoscale (approximately a few hundred micrometers in diameter), while vasculogenesis and angiogenesis produce a narrower vessel lumen, which better resembles capillaries *in vivo*.

2.1 Endothelial cell lining

Usually, ECs can be lined on the outer side of a gel channel, on a membrane in a vertically stacked model (7), or on the inner side of a prepatterned lumen (Figure 1A). EC seeding density from 1 million cells/ml (8) to 20 million cells/ml (9) has been reported, usually ranging about a few million cells per ml, possibly due to the differences in geometry of the surface to be lined and other conditions. The vessel will be ready to use for experiments as soon as 24 h postseeding, depending on the seeding density, and can be sustained for a few more days before the ECs overgrow. A past application showed that the vessel had been maintained for up to 16 days to investigate the angiogenic potential of inflammatory breast cancer (IBC) cells (10). Another advantage of this method is the more consistent and reproducible geometry. However, the vessel diameter of a few hundred micrometers is much larger than that of the capillaries *in vivo*. It is also convenient that several different types of ECs can be used for this method.

In the lumen prepatterning method, a microneedle or rod of various diameters can be inserted into the pregel and is carefully removed after the gel has polymerized. Alternatively, lumen formation in microfluidic channels can be achieved with the viscous finger patterning method (11, 12), where the gel is first injected into the microfluidic channel and subsequently displaced with less viscous fluid, creating a hollow lumen upon gel polymerization (Figure 1B). This step is performed to prevent heterogeneity in the EC monolayer between the part attached to the gel interface and the microfluidic post if directly seeded.

2.2 Self-assembling methods

To obtain a more natural vessel morphology, self-assembling methods can be utilized. These methods usually achieve vascularization around the tumor and even into the tumor interior.

2.2.1 Vasculogenesis

Vasculogenesis is the process of *de novo* formation of vessels in the presence of endothelial (progenitor) cells at high density. For *in vitro* vasculature formation, generally seeded at a density between 5 to 10 million cells/mL, together with supporting cells. Fibroblasts are the most widely used cell stromal cells, although other cell types have also been used depending on the microenvironment to be mimicked (13–18). The main reason for incorporating stromal cells is to support the formed microvasculature, which will otherwise regress after initial formation in the EC monoculture (19).

In vasculogenesis, using a high EC density tends to result in more opening to the lateral channel. Using high EC density,

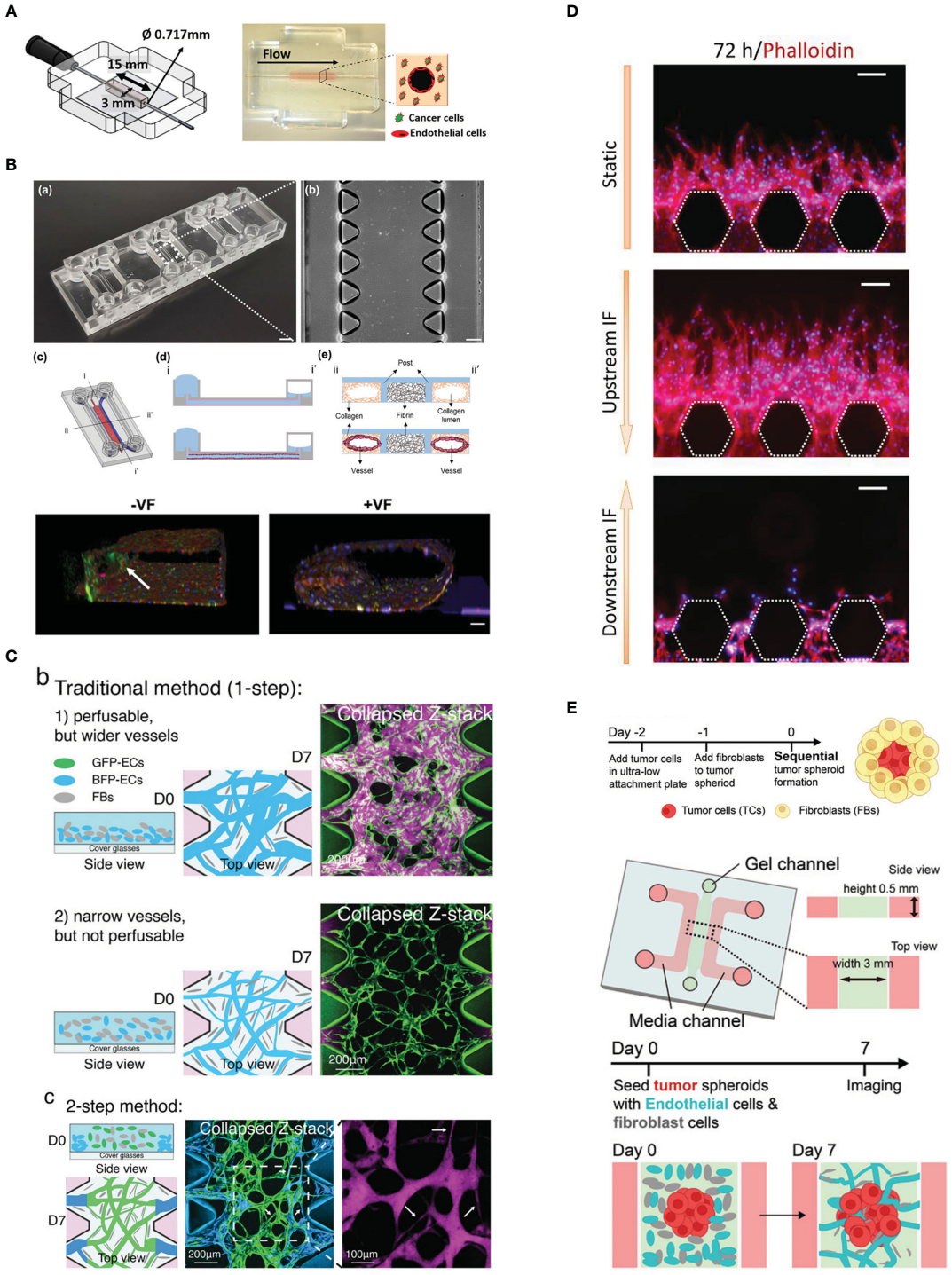

FIGURE 1
Vascularization strategies. **(A)** Endothelial cell lining on a gel channel pre-patterned using needle. Adapted with permission. Copyright 2020 Wiley Periodicals LLC. **(B)** The viscous fingerprinting method is used to line the microfluidic channels, ensuring a more even endothelial cell coverage. Adapted under the terms of the Creative Commons Attribution License (CC BY). Copyright 2022 Tu et al. **(C)** The two-step vasculogenesis method allows the formation of a narrower vessel in the middle and good opening to the lateral channels. The top part and middle part show the vessel formed under the traditional method with high and low density of EC, respectively. Adapted with permission. Copyright 2022 Wan, Zhong, et al. Small Methods published by Wiley-VCH GmbH. **(D)** Sprouting angiogenesis is enhanced by interstitial flow from upstream. Adapted under the terms of the Creative Commons Attribution License (CC BY). Copyright 2022 Liu et al. **(E)** The sequential seeding of fibroblast on tumor spheroid enhances tumor vascularization. The vascularized tumor model is used for evaluating CAR T performance. Adapted with permission. Copyright 2022 Wan, Floryan, et al. Advanced Healthcare Materials published by Wiley-VCH GmbH.

however, will result in larger vessel diameter, which is different from the small capillaries (under 10 μm) *in vivo*. Recently, a two-step seeding method (20) was established to address this problem (Figure 1C). In this method, the first step involves coating the gel channel with fibrin gel containing a high density of EC (10 million cells/ml). This is done by injecting the gel and cell mixture and quickly aspirating it. The mixture of EC and normal human lung fibroblasts (NHLFs) of lower cell density is immediately injected in the gel. Subsequently, the device is flipped every 30 s for a few times to distribute the cells more evenly in the vertical direction. This method results in the middle region of the gel having a smaller diameter vessel network and perfusable openings at the sides. It has been demonstrated that CTC clusters consisting of a few cells are more easily trapped in the microvascular network (MVN) generated with two-step seeding.

One of the most attractive features of this method is the microvasculature architecture, which is similar to *in vivo* capillaries in terms of having complex branches and anastomoses, although the lumen diameter is usually still larger than capillaries. Perfusability is also one of the desired parameters to be evaluated when characterizing the MVN. This feature makes it a suitable tool for studying tumor extravasation. However, there is also a drawback: the vasculature architecture cannot be precisely controlled, which may, for example, make image analysis and fluid dynamics simulations more challenging.

Moreover, vasculogenesis usually requires 4–5 days for the vasculature to develop into a perfusable vasculature. This method is relatively time-consuming compared to the EC lining method, which generally only takes 1 day for the seeded ECs to form a confluent monolayer on the patterned lumen. Despite the longer time needed for establishment, the microvasculature network can be maintained for up to a few weeks, making it compatible with experiments requiring a longer time frame. To date, almost all works on vasculogenesis require early passage (up to P7) primary cells, which is more costly and may have batch-to-batch variation. Recent exploration of the use of hTert-immortalized human umbilical vein endothelial cells (HUVECs) and normal human lung fibroblasts (NHLFs) shows that immortalized HUVECs can form a perfusable vasculature network in the presence of Thy1+ immortalized NHLF as a substitute for low-passage primary NHLF (21).

Fibrinogen is a glycoprotein highly abundant in plasma. Thrombin cleavage of fibrinogen into fibrin exposes the interaction site that allows fibrin monomers to self-polymerize and form fibrillar structure (22). Fibrin gel is the most commonly used ECM material for forming microvasculature networks-on-a-chip *via* vasculogenesis. The final concentrations for fibrinogen and thrombin typically range from 2 to 3 mg/ml and from 0.5 to 2.0 U/ml, respectively. Other ECM components, such as collagen I or the mixture of fibrin and collagen I, have also been tested. However, the vessel network formed is not as complex and connected as that formed in fibrin gel only. Moreover, the incorporation of collagen I leads to gel contraction and detachment from the microfluidic channel (23). Perhaps pretreatment of the channel with adhesive such as glutaraldehyde might help resolve this issue. The following questions remain: Can fibrin be used as a representative ECM in the TME, which is well known for its collagen ECM? Can the relatively soft fibrin gel simulate the relatively stiff tumor ECM? Recently, there have been some reports on the application of other hydrogels on vasculogenesis, such as PEG-based hydrogel (24) and agarose supplementation to collagen or Matrigel (25). The hydrogels are able to support vessel network formation but further characterization of the vessel (e.g., perfusability, junctional integrity, and barrier function) is warranted.

2.2.2 Angiogenesis

Angiogenesis is the formation of new vessels from an existing vessel under angiogenic stimulation. The two main mechanisms of angiogenesis *in vivo* are sprouting angiogenesis and intussusception or vessel splitting (26). Vascularizing tumor-on-a-chip using an angiogenesis method usually refers to sprouting angiogenesis as the vessel needs to grow into and reach the previously non-perfused region. This is more challenging to achieve with intussusception, which mainly gives rise to a new vessel in the area with some existing vessel.

The first step in this method is to create an endothelial monolayer through the EC lining method, by lining either the whole channel or only the side of the gel. Alternatively, the vessel can also sprout from an adjacent vascular bed formed by vasculogenesis (27). Under the stimulation of interstitial flow or certain growth factor gradients, such as the VEGF gradient (Figure 1D), which can be introduced by supplementing exogenous growth factors or coculture with stromal cells or certain types of cancer cells, ECs are activated and start to proliferate and sprout vessels toward the direction of the stimulus (28, 29). The direction of interstitial flow can also greatly affect angiogenic sprouting where interstitial flow in the direction opposite to vessel sprouting enhances angiogenesis while flow in the same direction suppresses vessel sprouting (27). However, it should be noted that angiogenic sprouts can sometimes be difficult to perfuse if the sprouts do not anastomose.

2.3 Heterotypic spheroid to improve intratumoral vascularization

Recently, quite a few groups have proposed introducing fibroblast and/or ECs to the tumor spheroid to improve vascularization, especially in the internal part of the tumor (17, 30–32).

To better vascularize tumor spheroid, Ahn et al. (17) use a heterotypic spheroid that comprises HepG2 liver cancer cells and blood ECs. In the presence of intratumoral vessels, the tumor is found to have higher expression of genes associated with aggressive behavior in cancer, such as EMT, cell migration, cell proliferation, and vessel development. To further vascularize the tumor, blood and lymphatic ECs are embedded together with the heterotypic spheroid in fibrin gel in the microfluidic channel. Interstitial flow is established to promote vessel network formation.

Besides forming spheroids from tumor cells and ECs, co-culturing cancer cells and fibroblasts can also improve vascularization. Wan et al. (30) tried two co-culture methods (1):

mixing cancer cells and fibroblasts prior to seeding and (2) sequentially layering tumor spheroids with fibroblasts. They found that the latter method significantly improves vascularization in the internal part and the vicinity of the tumor (Figure 1E).

Park et al. (31) demonstrate the use of tri-culture spheroid comprising tumor cells, ECs, and fibroblasts. The tri-culture spheroid has a more robust intratumoral vasculature and connects better with the external microvasculature network. They observed the sprouting of ECs from the spheroid and the anastomosis with the external vessel. The improved vascularization results in higher tumor growth and more efficient delivery of drugs to the tumor core.

To form perfusable vessel lumen connected to the interior of tumor, Nashimoto et al. (32) tri-cultured HUVECs, fibroblasts, and MCF-7 as a spheroid in 96-well ULA, which was then embedded in collagen-fibronectin hydrogel at the middle channel of a three-channel microfluidic device. The sides of the lateral channels were lined with HUVECs. Both HUVECs from the sides and in the spheroid sprouted and anastomosed, forming vessels capable of perfusing the interior of the spheroid.

3 Heterotypic cellular interactions in the vascularized tumor microenvironment

3.1 Tumor–vessel interactions

Tumor-on-a-chip technology has recapitulated various phenomena of tumor–vessel interaction such as tumor angiogenesis, vessel destruction in pancreatic cancer, and mosaic vessel, where the vessel is composed of both ECs and cancer cells. Furthermore, it has also been used to study the importance of organ-specific EC.

Kim et al. (33) designed an alternative vascularized tumor-on-a-chip model where ECs and fibroblasts are seeded in two adjacent prepatterned channels. Mimicking the high interstitial fluid pressure of tumors, interstitial flow is introduced in a direction that can aid the transfer of fibroblast-secreted molecules toward the EC channel, which promotes angiogenic sprouting toward the fibroblast channel. It is interesting that the device allows spheroid introduction to the fibroblast channel after the main vasculature has matured, as early introduction of tumor cells might potentially have an adverse effect on vessel formation (34). In this study, they showed that tumor vascularization enhances therapeutic delivery, whether drugs, CAR T cells, or nanoparticles (Figure 2A).

Miller et al. (35) cocultured patient-derived renal carcinoma cells with HUVECs lining the hollow lumen created with rods. Under perfusion, the blood vessel structure was well preserved over time near the inlet while the vessel regressed near the outlet. In contrast, in the coculture, more prominent angiogenic sprouts were observed near the outlet. They hypothesized that the tumor secreted pro-angiogenic that concentrate near the outlet. The results of computational fluid dynamics (CFD) simulation also support their hypthesis.

A recent work by Nguyen et al. (36) investigated the interaction between a biomimetic pancreatic cancer duct and a blood vessel positioned 500 μm apart. Intriguingly, pancreatic ductal adenocarcinoma (PDAC) cells collectively migrated toward blood vessels and induced contact-dependent EC apoptosis. This phenomenon was mediated by activin and the receptor ALK7 expressed by PDAC cells. Their observation of this cancer hallmark was validated in a mouse ectopic tumor model and genetically engineered mouse models (GEMMs). Their results provide an explanation for the mechanism underlying PDAC hypovascularization despite high vascular invasiveness and explain the high CTC load in PDAC patients. Another study using MMTV-PyMT mouse tumor organoids (37) also described the formation of mosaic vessels as one of results of the interaction. Cancer cells were observed detaching from the fused organoids to the vascular lumen. In addition, the tumor organoid constricted or pulled the vessel.

Different cancer subtypes may have different interactions with the vasculature. As demonstrated by Gadde et al. (10), inflammatory breast cancer (IBC) cells did not disrupt ECs through anoikis as severely as non-IBC cells. Instead, IBC cells induced more angiogenic sprouting. VEGF expression levels were also found to be higher in IBC cells. During the course of the 16-day experiment, tumor clusters were found in the sprouted vessel. In terms of matrix degradation, the IBC microenvironment had increased porosity, supposedly due to degradation.

Usually, numerous spheroids or single cells are seeded in the ECM material to mimic cancer. However, in early-stage cancer, the tumor burden might not be that high. Thus, Li et al. (38) only added a single, small spheroid (30, 60, or 90 μm) into the ECM, together with ECs and fibroblasts, which formed a network through vasculogenesis; the tumor exhibited increased migration and spreading when ECs were present. They also observed chains of migrating cells and vasculogenic mimicry, which refers to the ability of cancer cells to organize themselves into vessel-like structures (39). (Figure 2B).

The importance of using the biologically relevant EC source is also demonstrated in the work by Gerigk et al. (40) Cultured in their glioblastoma (GBM) microfluidic-based model, ECs derived from the brain are shown to have lower permeability compared to HUVEC and lung HMVEC (human microvascular ECs) as a result of higher ZO-1 expression. Interestingly, the GBM cells migrate further when co-cultured with brain EC.

3.2 Interactions with immune cells

In addition to vasculature formation, the other significant advantage of the tumor-on-a-chip model is the incorporation of immune cells. This feature of immune cell incorporation can provide insights that are more relevant to the phenomena

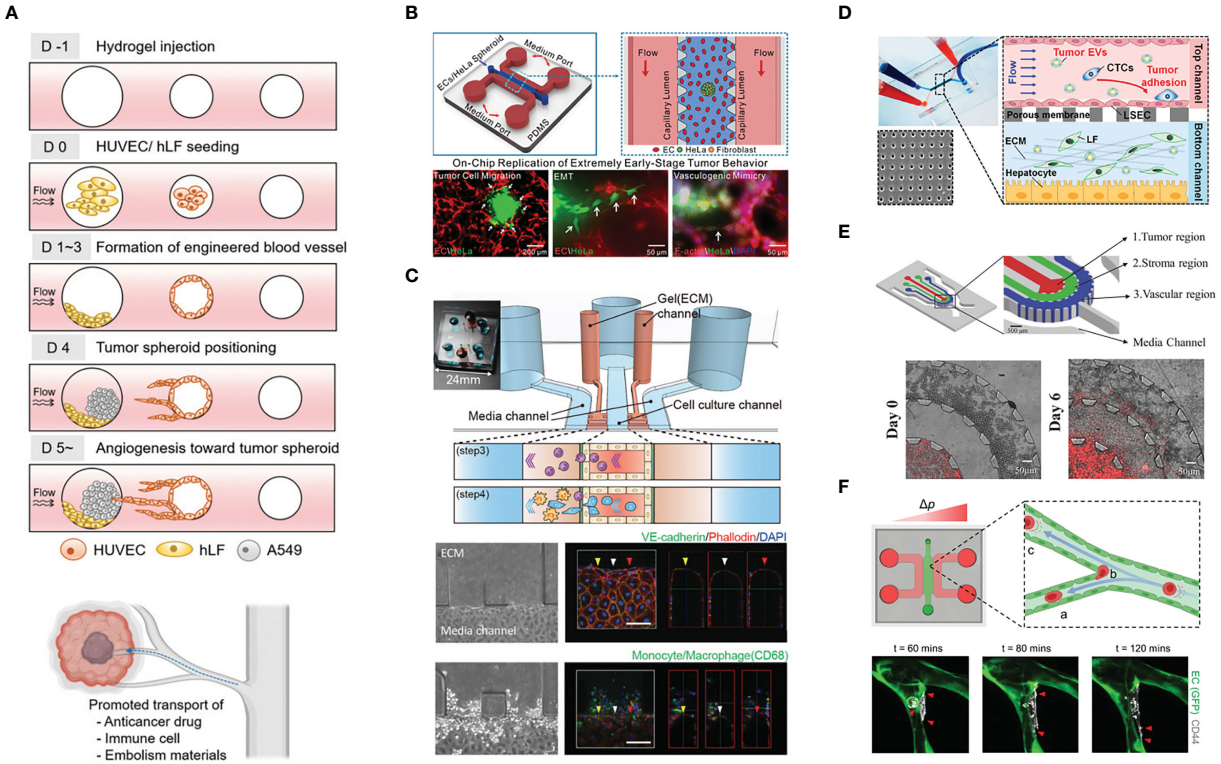

FIGURE 2
Example of the application of vascularized tumor-on-a-chip for mechanistic studies. **(A)** The study of tumor vascularization by angiogenesis and the promotion of therapeutic transport. Adapted with permission. Copyright 2022 **(D)** Kim et al. Advanced Healthcare Materials published by Wiley-VCH GmbH. **(B)** The recapitulation of extremely early-stage tumor dynamics and interaction with blood vessel. Adapted with permission. Copyright 2021, American Chemical Society. **(C)** Elucidating the role of monocyte/macrophage in forming pre-metastatic niche. Adapted with permission. Copyright 2019 **(H)** Kim et al. Published by WILEY-VCH Verlag GmbH & Co. KGaA, Weinheim. **(D)** Investigating the effect of tumor-derived extracellular vesicles in priming the pre-metastatic niche. Adapted with permission. Copyright 2020, American Chemical Society. **(E)** The concentric three-layer channels to study breast cancer cell migration and intravasation. Adapted with permission. Copyright 2018 WILEY-VCH Verlag GmbH & Co. KGaA, Weinheim. **(F)** Investigation of tumor extravasation mechanism in a microvascular network enabled by the good live imaging resolution. Adapted under the terms of the Creative Commons Attribution License (CC BY). Copyright 2021 Offeddu et al.

happening in the human body. The presence of vessel can better mimic the *in vivo* conditions during immune cell extravasation. Vascularized tumor-on-a-chip platforms have also been utilized to study immune cell polarization and exhaustion in the hostile TME. Finally, it has also been used to study the role of immune cells in cancer extravasation.

STING (STimulator of INterferon Genes) expression and cytokine secretion by tumors can induce T-cell chemotaxis. Using a vasculogenic approach, Campisi et al. (41) cocultured KRAS/LKB1 mutant lung cancer spheroids with HUVECs and observed a synergistic effect on cytokine production. Strikingly, the re-expression of LKB1 (upstream negative regulator of STING) in tumors did not show a significant increase in cytokine production in the coculture, suggesting a greater contribution from ECs. Apparently, the paracrine effect of cGAMP from tumor spheroids regulates STING expression in ECs. Consequently, vessel permeability increased, and ECs upregulate adhesion molecules for T-cell adhesion. Thus this work demonstrated an indirect mechanism of immune escape via vasculature priming.

Mollica et al. (42) investigated T-cell infiltration into the pancreatic cancer TME comprising Panc-1 cells, pancreatic stellate cells, and HUVECs, each seeded in different microfluidic channels. The model mimicked the increased vessel permeability in the presence of T cells. There was also increased infiltration of activated (through CD3/CD28 stimulation) T cells toward the PDAC compartment. Cytokine analysis revealed that the T cells in coculture of pancreatic cancer cells and stellate cells exhibited stronger activation, as indicated by higher IL-2 and IFNγ levels measured by a multiplex immunoassay. Upregulation of granzyme B, perforin, and Fas suggested that activated T cells were more cytotoxic than nonactivated T cells in the presence of HUVECs and Panc-1 cells. The tri-culture group showed lower levels of these genes, suggesting that pancreatic stellate cells diminished the inflammatory response and supported tumor growth.

By stacking tumor cell-seeded collagen gel with a porous membrane for culturing ECs in a microfluidic channel, Lee et al. (43) observed reduced T-cell transendothelial migration (TEM) and extravasation in the presence of tumor cells. ECs downregulated

ICAM-1 and E-selectin due to tumor VEGF production, while the chemokines secreted from tumor cells still attracted T cells.

Humayun et al. (44) designed a microfluidic device to have a vessel channel that is close to one side of the gel to mimic the characteristic oxygen and nutrient tension in a large, necrotic tumor. The device was able to show a viability gradient across the gel. When used for NK cell TEM study, most of the extravasated cells migrated only up to 200 μm from the vessel. Thus, NK cells needed to be homogeneously resuspended in the gel for subsequent NK cell exhaustion experiments. Interestingly, they observed a lower NK cell proliferation rate and less responsiveness to chemokines on the distant side. Immune checkpoint inhibitor treatment alleviated exhaustion, but cytotoxicity was only partially restored at the distal side. In their previous work using a similar method (9), they observed poor antibody penetration into tumor spheroids, in part due to endocytosis.

Recently, the recapitulation of indirect signaling of tumor and T cells was confirmed *in vitro* (45). The researchers observed that the microvascular network cocultured with HepG2 cells (hepatocellular carcinoma cells) exhibited higher expression levels of FasL, which then induced the apoptosis of T cells. In vessel monoculture, hypoxia alone also induced the upregulation of FasL in ECs. Moreover, the MVN perfused with conditioned medium from HepG2 cells grown under hypoxic conditions also showed increased FasL expression. Subsequently, they interfered with this pathway by anti-Fas, anti-FasL, or pan-Caspase inhibitors and observed a significant reduction in the percentage of apoptotic T cells.

Kim et al. (46) used a basement membrane and EC-lined microfluidic channel flanked by collagen I gel on the lateral sides to study the role of monocytes/macrophages in establishing the premetastatic niche. Strikingly, monocytes increased vessel permeability by disrupting EC junctions and secreted MMP9 to disrupt the vascular barrier, promoting tumor extravasation. As monocytes/macrophages migrated in the lateral ECM, they left behind microtracks, which were then utilized by the tumor cells to more easily invade the ECM (Figure 2C).

Macrophage polarization toward the M2 (anti-inflammatory) phenotype has been implicated in promoting cancer progression. By culturing the microvascular network and tumor cells—in fibrin and Matrigel growth factor reduced (GFR) basement membrane matrix, respectively—in different microfluidic compartments, the work by Bi et al. (47) reproduced the angiogenic potential of the cancer, by comparing CD31 staining from the parental tumor. They also showed how the introduction of different macrophage lineages (nonpolarized, M1, and M2) can differentially affect the three parameters mentioned above. Moreover, they demonstrated how the device could be used for antibody-based drug studies. Finally, the uniform manifold approximation and projection (UMAP) from scRNA-seq revealed two EC populations, and immunostaining confirmed the different locations of the populations in the microfluidic device—the population related to tumor development and progression was located at the center of the vessel compartment, while the population related to the immune pathway and cell functions was located at the periphery of the vessel compartment and beyond. In addition, the introduction of M2 macrophages significantly increased the population related to the immune pathway and cell functions.

With their signature microvascular network, Boussommier-Calleja et al. (48) investigated the influence of monocytes on cancer extravasation. First, to elucidate whether TEM is necessary for monocytes to mature into macrophages, they compared CD68 (macrophage marker) expression between monocytes that exited to the stroma during perfusion and monocytes that were directly embedded in the gel with ECs and fibroblasts. They found that TEM was not necessary for monocyte maturation. Interestingly, they found that the same group of tumor cells in circulation differed in extravasation fate, suggesting that the inherent difference between cells, not merely their position, contribute to extravasation potential. The presence of circulating monocytes reduced the tumor extravasation rate, while the presence of macrophages in the stroma caused different changes in the extravasation rate in two different cell lines.

Using a microvasculature network-on-a-chip, Chen et al. (49) explored the role of inflamed neutrophils in tumor extravasation. In the inflamed state, endothelial ICAM-1 and neutrophil CD11b were upregulated to better support neutrophil and tumor cell aggregation. This heterotypic clustering prevented tumor cell loss due to fluid flow. In addition, the presence of an inflamed neutrophil cluster produced IL-8, and tumor cells produced CXCL-1. This chemotactic gradient caused neutrophils to undergo confined migration. In addition, IL-8 caused endothelial activation and barrier function disruption. Furthermore, the microfluidic device design, which included two large media reservoirs on top, allowed a steadier flow to be generated passively to continuously perfuse the microvascular network with neutrophils and tumor cells.

In another study on the role of neutrophils in tumor extravasation, an MVN chip model was used to complement mouse *in vivo* observations. The MVN model revealed that neutrophils increased tumor extravasation in a paracrine manner, facilitating cancer cell protrusion formation in the early phase of TEM (50).

In a microvasculature network-based extravasation assay, the introduction of platelets and neutrophils increased the tumor extravasation rate (51). Treatment with eptifibatide, an integrin β3 antagonist, not only prevented platelet aggregation but also reduced tumor PAI-1 and MMP-9 expression and interfered with tumor-EC adhesion. By blocking EC integrin β3, FAK and Src activation were reduced, which subsequently decreased VE-Cad phosphorylation and internalization, thus restoring the junctional barrier. Interestingly, the researchers retrieved and sorted the cells to perform Western blot analysis, but they did not mention the number of devices each sample was pooled from.

3.3 Interactions with other components

Thrombocytosis, the condition where blood platelet is elevated, is associated with adverse prognosis in various types of cancer (52–

55). Platelets can contribute to tumor progression through a few mechanisms. In the circulation, platelet interaction with CTCs and ECs promotes tumor extravasation. In addition, platelet can directly affect primary or metastatic tumor, and this requires platelet extravasation to the tumor site (56). In microfluidic device, the platelet–tumor interaction has been recreated for both intravascular and extravascular context.

Using their OvCa-Chip device, which has vertically stacked microfluidic channels with the vessel in the lower compartment and ovarian cancer cells in the upper compartment separated by a porous membrane, Saha et al. (57) confirmed the role of tumor cytokines in activating the Src/ERK/FAK pathway, which led to VE-Cad and β-catenin downregulation in ECs, compromised EC junction integrity, and increased platelet extravasation. Statin, a class of cholesterol-lowering drug, can be repurposed to improve clinical outcome in cancer patients (58), although the exact mechanism is not fully understood yet. In the context of blood vessel, statin treatment has been shown to preserve endothelium junctional integrity (59, 60) and to have antiangiogenic effect (58). In this study, atorvastatin treatment "rescued" vessel integrity and reduced the number of extravasated platelets. Their findings were validated with patient biopsy samples.

An upgrade from their previous OvCa-Chip, the new OTME-Chip (61) has an additional gel channel on each lateral side of the tumor compartment separated by a micropillar, which allows the investigation of matrix invasion. Interestingly, the tumor only migrated to the ECM when extravasated platelets were bound to it. The interaction involved tumor galectin-3, which binds to platelet GPVI—a glycoprotein upregulated by shear stress. As tumor platelet interactions have been reported to promote chemoresistance, they utilized this platform to study the effect of cisplatin only versus cisplatin and antiplatelet drug combinations. Compared to cisplatin monotherapy, dual therapy showed reduced tumor invasion and proliferation. RNA-seq was performed, with the different cell types sorted prior to sequencing, revealing the upregulated pathways that can potentially be targeted, such as those regulating cell cycle.

Cancer cell-derived extracellular vesicles carry cargos such as oncoproteins and miRNA that may aid tumor progression by shaping the TME and establishing pre-metastatic niche (62). Recently, Kim et al. (63) investigated the effect of breast cancer cell-derived extracellular vesicles (cancer EVs) on priming in the liver premetastatic niche (Figure 2D). Utilizing two-layered microfluidics primed by cancer EVs, ECs underwent endothelial-to-mesenchymal transition (EMT), as shown by decreased ZO-1 intensity and increased vimentin and FAPa (fibroblast activating protein) intensity. Furthermore, priming enabled more cancer cells to adhere to ECs.

Mechanical cues such as stiffness is well known to affect cell function and behavior. Moreover, it has also been shown that cells can have mechanical memory; i.e., cell behavior can be regulated by its past mechanical environment (64, 65). Azadi et al. (66) showed that breast cancer cells previously cultured on stiffer substrates were associated with higher extravasation rates and migration distances in malignant breast cancer models. This trend was found to be correlated with increased MMP9 expression levels.

4 Unveiling the mechanisms of metastatic cascade using the vascularized tumor microenvironment

4.1 Invasion and intravasation

Nagaraju et al. (67) created a microfluidic model with concentric layers comprising, from inner to outer sides, breast cancer cells, collagen gel, and ECs that form a microvasculature network over a few days in culture. The incorporation of ECs enhanced the outward migration of invasive cancer cells, likely in a paracrine manner, as suggested by cytokine profiling. The presence of invasive cancer cells decreased vessel diameter and increased vessel permeability through VEGF secretion (Figure 2E).

Using the same microfluidic device setup, Truong et al. (68) cultured glioma stem cells (GSCs) and ECs to study invasion and extravasation. On-chip vasculogenesis requires serum, but serum exposure can induce GSC differentiation, so the authors first formed the microvascular network for 3 days and subsequently introduced the GSCs into the chip. The tumor cell chain migration was observed in both the GSC-on-a-chip model and their animal model. In the presence of vasculature, phosphorylated CXCR4 staining in GSCs showed a punctate pattern, suggesting its activation under the stimulation of CXCL12 secreted by ECs. When treated with AMD3100, a CXCR4 inhibitor, GSCs migrated over a shorter distance.

Using the vessel formed by lining ECs on rod-patterned channels, Wong & Searson (69) observed how the location of breast cancer cells with regard to the vessel wall and the mitosis of cancer cells can affect the intravasation rate. The rounding of tumor cells was proposed to exert mechanical stress on the EC junction, causing junctional adhesion to fail when cancer cells transmigrated successfully. Moreover, the fluid flow in the luminal side helped to detach the cancer cells into circulation.

4.2 Extravasation

Integrin signaling plays important roles in cell migration (70). Using an *in vitro* microvascular network, Gilardi et al. (71) investigated the Cdk5/Talin-1/FAK pathway in cancer cell TEM (transendothelial migration). Cdk5 controlled the phosphorylation of Talin-1, which regulates FAK phosphorylation. Silencing Talin-1 was associated with compromised vascular adhesion, while inhibiting FAK phosphorylation at S732 rendered the cells unable to perform TEM. The lower rate of extravasation observed *in vitro* was validated using an *in vivo* model.

Another study highlights the importance of tumor integrin β1 in extravasation (72). The depletion of integrin β1 did not affect TEM but arrested the tumor cell in the compartment between ECs and the basement membrane (BM) due to the impaired integrin β1-mediated interaction with laminin in the BM, which is crucial for the formation of actin-rich protrusions that breach the BM. In a mouse model, integrin β1 knockdown reduced metastatic colony formation, corresponding with the *in vitro* experimental conclusions.

In transformed breast ECs, activation of the EMT (epithelial-to-mesenchymal transition) program upregulated the expression of podocalyxin, which facilitated ezrin-mediated cortical actin polarization and initial TEM (73). The use of the MVN chip here allowed the imaging and quantification of tumor extravasation.

Extravasation requires cell–cell contact. Traditionally, the glycocalyx is seen as a protective barrier to prevent adhesion due to its dense and charged molecular nature (74). However, it can also be a ligand for cellular receptors (75). Using the MVN-on-a-chip model (Figure 2F), it was revealed that tumor cells shed hyaluronic acid, which accumulates on ECs, thus priming their adhesion with tumor cell CD44 and promoting extravasation (76).

Cells circulating in the vasculature is subjected to mechanical forces arising from fluid flow that can affect cellular response (77, 78). *In vivo*, the fluid flow is not limited to luminal flow (fluid flow in the vessel lumen). There are also transendothelial and interstitial flows, which are the flow of fluid entering or exiting the vessel and the flow of fluid in the matrix, respectively. A recent study examined the individual roles of transendothelial and luminal flow in tumor extravasation (79). Luminal flow was found to increase the tumor extravasation rate, while transendothelial flow accelerated the transendothelial migration process as well as migration in the surrounding matrix.

4.3 Other metastasis models

In ovarian cancer, tumor cells can shed into the peritoneal fluid and adhere to and invade the mesothelium to form peritoneal metastasis, which is common (80). To mimic the peritoneal metastatic site, the MVN-on-a-chip model can be modified to have an adipocyte coculture in the gel with mesothelial cells layered on one end. Then, ovarian cancer cells can be introduced from the reservoir on that end, mimicking the peritoneal cavity (81). In this tri-culture platform consisting of ECs, adipocytes, and mesothelium, vascular and mesothelial permeability were in a range similar to that observed *in vivo*. Using modular combination, it was observed that the mesothelium acted as a protective barrier, while the presence of ECs and adipocytes increased tumor attachment to the mesothelium. When cancer cell density was high, they clustered and invaded the mesothelium, while low-density cancer cells attached the mesothelium but were not capable of invading it, suggesting the importance of cancer cell density. Adipocytes are thought to support metastatic tumor growth by providing lipid as an energy source (82). Interestingly, lipid droplets were also present in cancer cells that had successfully invaded in the device.

5 Therapeutic screening

5.1 Chemotherapeutics

To study both drug-sensitive and drug-resistant clones of tumor cell lines in the same device, Wang et al. (83) designed two-layer vertical microfluidic channels, with the bottom layer lined with ECs and separated from the top by membrane. The top layer consisted of two narrower channels for the two tumor clones. This platform enabled simultaneous assessment of both clones while keeping them in different compartments. However, the interpretation of the results should be done with caution as another study has shown that the paracrine effect from one cell type (senescent MCF10A due to centrosome amplification) can affect the behavior of the other cell type (MDA-MB-468 breast cancer cells) (84). This is especially important for senescent cells, which is common in cancer drug treatment (85).

Jing et al. (86) demonstrated the use of a vertically stacked microfluidic device to study metastasis and drug sensitivity in MDA-MB-231 and HepG2 cell lines. Interestingly, the tumor clusters migrated along the flow direction of "blood vessel" fluid, and different mechanisms of TEM were observed—paracellular in MDA-MB-231 cells and transcellular in HepG2 cells. They also performed a tumor adhesion assay and drug sensitivity test for 5-fluorouracil (5-FU). There was a more pronounced decrease in the cancer progression parameters in vascularized tumor-on-a-chip compared to coculture in transwell inserts, suggesting the importance of ECs and fluid flow in modulating 5-FU efficacy. A similar setup was also used to evaluate the anti-tumor potency of partially acetylated chitosan oligosaccharide (87).

An open microfluidic device with a 96-well plate format was used to coculture the MVN and CRC cell lines (34). They found that primary endothelial progenitor cell (EPC) and HUVEC source and passage number affected their ability to form MVNs in their rhomboidal gel chamber. EPCs or HUVECs from all sources were able to form a network by day 6, but only ECs from three out of seven sources tested had a perfusable network. They also observed different network formation dynamics for different cell sources. Among the cell sources tested, one of the two HUVEC lines showed the most consistent network formation dynamics in the presence and absence of HCT 116 colorectal cancer cells (which might be important for drug screening control). The system was used to assess drug safety by assessing tumor growth, vessel length, and cell viability. Although some cell sources resulted in nonperfusable MVN, the chemotherapeutic 5-FU still reached the tumor through diffusion despite the drop in efficiency indicated by higher IC_{50} compared to the cell lines capable of forming a perfusable network. Thus, vessel network perfusability should also be considered when assessing drug safety and sensitivity.

By reproducing GBM cells in vertically stacked microfluidic channels, Lin et al. (88) identified that the presence of ECs maintained the stem-cell like nature of GBM cells and weakened the response to DNA alkylating agents, as shown by reduced 7-mG and 6-O-mG levels assessed *via* LC–MS.

5.2 Antiangiogenic therapy

To better vascularize tumor spheroids, Ahn et al. (17) used heterotypic spheroids comprising HepG2 liver cancer cells and blood ECs. They demonstrated that in the presence of intratumoral vessels, the tumor cells exhibited more aggressive metastasis. To further vascularize the tumor, blood and lymphatic ECs were embedded together with the heterotypic spheroid in fibrin

gel in the microfluidic channel. Interstitial flow was established to promote vessel network formation. Then, the researchers tested the tumor response to axitinib, an antiangiogenic drug. Outside of the chip, the heterotypic spheroids showed a dose-dependent response to axitinib treatment. When vascularized on-chip, the tumor shows no significant dose-dependent decrease in area in response to treatment at the earlier time point, when the vessel network was not properly developed yet. However, the vasculature still regresses in a dose-dependent manner. When drug treatment is started by the time the vasculature has already been well established (day 5 postseeding on-chip), the tumor responded to axitinib treatment, suggesting the importance of intratumoral vascularization for drug delivery.

5.3 Targeted therapy

Hassell et al. (7) modeled lung cancer in an orthotropic manner where a low density of non-small cell lung cancer (NSCLC) cells was mixed with normal alveolar ECs and added into the top chamber and the EC-lined bottom chamber. Interestingly, NSCLC cells in the coculture exhibited a 12-day dormancy period, and proliferation resumed at a lower rate than that in the monoculture. In the presence of cyclic stretch mimicking breathing motion, the tumor exhibited higher resistance to tyrosine kinase inhibitors (TKIs). Additionally, EGFR expression and phosphorylation levels were decreased under cyclic stretch. This observation might explain the reduced growth rate of tumors under breathing motion. The IL-8 and VEGF levels were increased in the effluent flow from the coculture, while the IL-6 level was decreased.

5.4 Combination therapy

Kim et al. (18) recently developed an all-in-one IMPACT device, where spheroid formation and vascularization can be performed in the same device (Figure 3A). By injecting a small volume of cell suspension, the droplet was maintained by surface

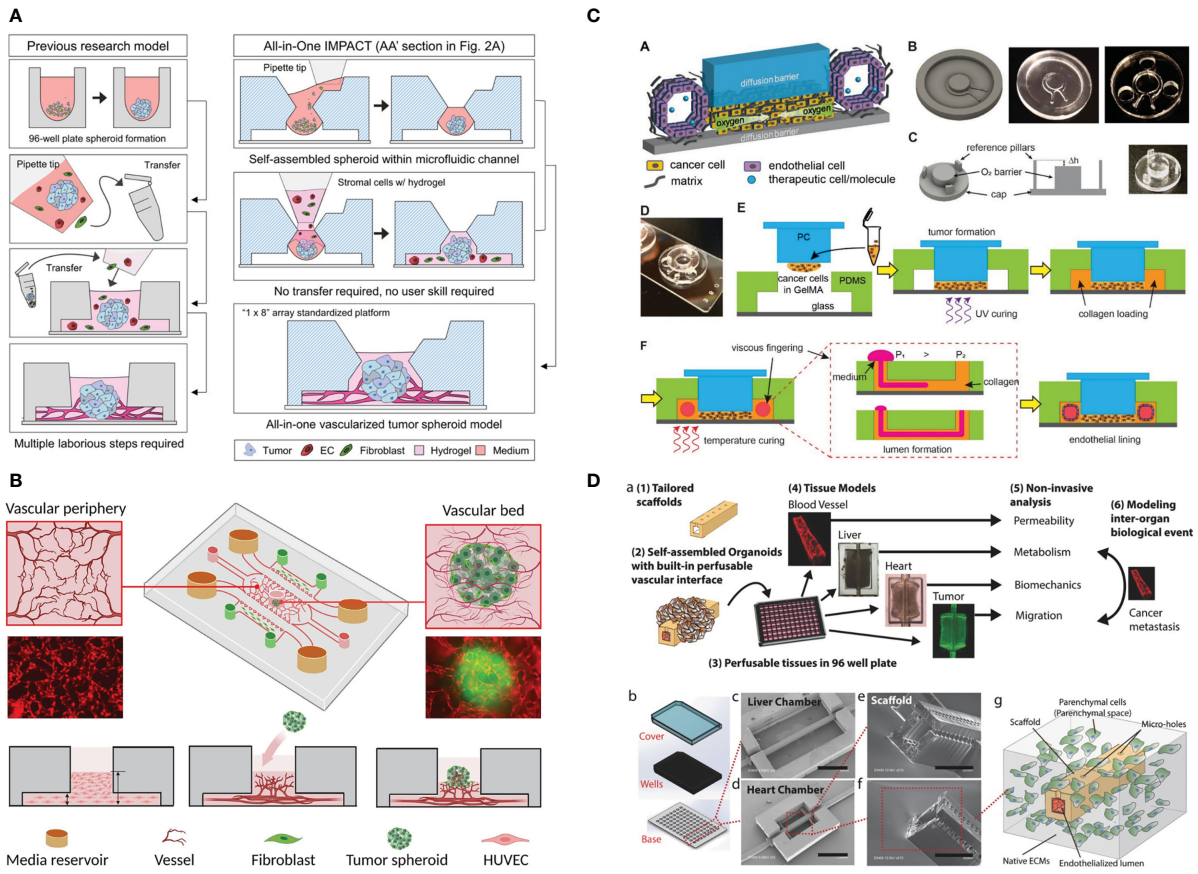

FIGURE 3
Example of the application of vascularized tumor-on-a-chip for therapeutics screening. **(A)** The all-in-one IMPACT device allows spheroid formation and vascularization on the same device, making it more user-friendly. Adapted with permission. Copyright 2022 Wiley Periodicals LLC. **(B)** The device design with a small hole on top of the device enabled spheroid introduction after microvascular network formation. Adapted with permission. Copyright 2022, American Chemical Society. **(C)** Device design allowing oxygen gradient generation with the gas-impermeable PC cap. Endothelial cells are seeded on lumen created by viscous finger patterning. Adapted under the terms of the Creative Commons Attribution License (CC BY). Copyright 2021 Ando et al. **(D)** The multi-organ InVADE platform that enables drug sensitivity and other organs' toxicity test in one chip. Adapted with permission. Copyright 2017 WILEY-VCH Verlag GmbH & Co. KGaA, Weinheim.

tension. After 24 h of spheroid formation, stromal cells and hydrogel were injected into the same space to vascularize the spheroid. The device was subsequently used to evaluate the effect of Taxol (chemotherapeutic) and Avastin (antiangiogenic drug) and the combination towards patient-derived cancer spheroid and vessel growth. After drug treatment from day 3 to day 5, all drug-treated groups experienced significant decrease in vessel area. Interestingly, Taxol monotherapy resulted in the highest decrease in tumor size change. Furthermore, the bottom of the device was detached, and the hydrogel was sectioned for high-resolution imaging. This was done to obtain clearer confocal images of vascularized mono- or heterotypic spheroids (cancer cells, fibroblasts, and ECs).

The vasculogenic-formed vasculature network mimics physiological size and architecture. However, in the commonly used microfluidic device, tumor cells can only be seeded together with ECs to form MVNs within tumors and are thus the size of tumor clusters cannot be finely controlled. In the work by Hu et al. (89), a small hole was punched on the central channel to introduce tumor spheroids after MVN formation (Figure 3B). However, the higher position of the spheroid in this design might potentially reduce the imaging quality. The platform was utilized to study the effect of HIF1a stabilization by inhibiting prolyl hydroxylase (PHD) on improving traditional chemotherapeutic outcomes. PHD inhibitor treatment reduced the EC apoptosis rate and vessel permeability (vessel normalization), leading to the more effective delivery of chemotherapeutics to the tumor.

5.5 Nanoparticles

Nanoparticles has recently emerged as a potential approach to treat cancer that can be engineered to have advantageous effect such as targeted-delivery and optimized drug release pattern (90), vascularized tumors-on-chips have been utilized to study how the presence of the endothelial barrier affects the delivery of micelle-based nanoparticles. As expected, the delivery rate of nanoparticles was the highest in 2D culture, followed by 3D spheroids and vascularized tumor-on-a-chip models (91). Separately, Wang et al. (92) investigated the effect of different mophologies of Gd2O3 NPs, namely sphere, scroll, and oblate, towards the tumor-killing efficacy. Scroll and oblate shape NPs had similarly good adhesion on the ECs but the oblate shape NPs was superior in supressing the growth of lung tumor due to the larger NP surface area (92).

5.6 Cell therapy

In addition to forming spheroids from tumor cells and ECs, sequentially layering tumor spheroids with fibroblasts can also improve vascularization within the tumor and its surrounding areas (30). Experiments with CAR T cells showed higher CAR T-cell recruitment, IFNg production, and apoptotic cell number in the tumor formed with fibroblast layering.

To perform drug screening under hypoxia, a steep oxygen gradient was created with a polydimethylsiloxane (PDMS) device and polycarbonate (PC) cap (11). Tumor cells were embedded in GelMA in the chamber underneath the PC cap, while the vessel was created by viscous fingering of the hollow space surrounding the tumor chamber (Figure 3C). Strikingly, no angiogenic response was observed, but the ECs directly invaded the tumor chamber by day 7. The vessel was found to be leaky as assessed by dextran perfusion. Most of the CAR T cells that flowed to the vascular channel did not attach, but when they did attach, they migrated against the flow, suggesting active migration.

5.7 Vascularized multi organs-on-a-chip

Recently, tumor-on-a-chip has been coupled with cells derived from other organs, such as the liver (8, 93) and heart (93, 94), to assess toxicity to other vital organs. This investigation can be achieved by coupling of various organ cell types in different compartments, such as growing cancer cells in one lateral channel and cardiomyocytes in the other lateral channel. The InVADE platform (Figure 3D) enables this arrangement by separating the tumor cells and organ-derived cells into different but interconnected 96-well plates. Alternatively, Ozkan et al. (8) created a PDMS chip with two lumenized hydrogel compartments, one seeded with tumor cells and the other had liver cells in it. ECs were seeded on the lumen and the two compartments were connected with tubing.

6 Discussion and conclusions

The introduction of vasculature into the tumor-on-a-chip method has allowed more accurate reproduction of the TME. It is highly important for the study of tumor–vessel interactions as well as being the platform for therapeutic evaluation, as drugs and immune cells circulate through the vasculature. The modular nature of microfluidic models makes them a robust tool to delineate the contribution of each factor and to study their interactions. In addition, compared to animal models, microfluidic models offer better control and reproducibility while simultaneously being rapid and cost-effective.

Perfusable vessels were successfully generated by coculturing ECs and stromal cells. However, there are limited examples of *in vitro* models where pericytes are present. Pericyte crosstalk with ECs is important for vessel maturation and endothelial barrier function (95, 96). HUVECs are the primary cell lines most commonly used in vasculature-on-a-chip formation. Nevertheless, it is known that vessel characteristics differ from organ to organ. For example, the liver has sinusoid capillaries, the kidney has fenestrated capillaries, and the brain has dense capillaries. For the blood–brain-barrier (BBB) in particular, a complex vessel model where pericytes and astrocytes are cultured together with ECs has been generated (13). ECs form the MVN, and pericytes and

astrocytes obtain perivascular localization. To date, most of the studies on vascularized tumor-on-a-chip only incorporate blood vessels. However, in an *in vivo* context, lymphatic vessels are also an important route for metastasis in various types of cancer (97). Thus, lymphatic vessels have currently been introduced together with blood vessels for a tumor-on-a-chip model (17). These factors might lead to discrepant or even contradictory findings when compared to *in vivo* results.

Currently, microfluidic devices for organs-on-a-chip are usually PDMS-based with coverslip bottoms. PDMS is gas-permeable, nontoxic, and transparent, making it suitable for cell culture and imaging applications. However, the manufacturing of this device requires personnel skilled in microfabrication and special instruments that are not commonly found in biomedical laboratories. Furthermore, the fabrication process is somewhat time-consuming, and there is also concern about the nature of PDMS, which can absorb small-molecule drugs (98), making it not the most ideal material for use in drug screening. To enable a wider adoption of vascularized tumors-on-a-chip and organs-on-a-chip methods in general, a more standardized microfluidic device is needed. It is also preferred, especially in drug screening applications, that the device format is compatible with high-throughput systems. Currently, devices suitable for vascularized tumors-on-a-chip can also be made from plastic materials and have been made commercially available in various designs. Devices such as OrganoPlate® Graft (Mimetas) (https://www.mimetas.com/en/organoplate-sup-sup-product-overview/ last accessed 2023-01-10) and OrganiX (AIM Biotech) (https://aimbiotech.com/ last accessed 2023-01-10) enable the grafting of single tumor spheroids or organoids on/in a vascular bed. For more general applications, devices such as IdenTX (AIM Biotech) are a more versatile option.

Another hurdle is that the workflow of cell isolation for downstream analysis is tedious and has a higher chance of contamination. Usually, the whole gel slab needs to be extracted from the device, and the ECM is digested. Subsequently, the cells are collected and sorted for further analysis. Although the small volume allows more replicates to be produced, it prevents the ability to perform conventional analyses, such as Western blotting, due to an insufficient cell number. It is still possible to perform them, but cells need to be pooled from several devices.

Tumor-on-a-chip analysis relies heavily on imaging tools and is currently incompatible with many conventional *in situ* assays. For example, in the 3D culture of cells embedded in gel, traction force microscopy analysis remains challenging and computationally expensive, and the potential alternative for quantifying cellular forces is fluorescence resonance energy transfer (FRET) tension sensors (99). To study calcium release in vascular smooth muscle cells surrounding the MVN, Cuenca et al. (100) transduced the cells with an ultrasensitive calcium sensor, GCaMP6f. Similar molecular tools can be exploited for other molecules of interest. Atomic force microscopy, a common tool to investigate tissue or cell stiffness, is also not compatible with the geometry of most microfluidic devices. Alternatively, Brillouin has recently been proposed to potentially solve this problem (101, 102). However, the instrument is not very common yet.

In conclusion, the development of *in vitro* vascularized tumor models has significantly advanced our ability to recreate a more biologically realistic cancer microenvironment in the laboratory. This has provided researchers with a more precise and accurate way to study the mechanisms of cancer and evaluate therapeutic response. With further refinement, standardization, and simplification of the technology, we are optimistic that *in vitro* microvasculature will gain wider adoption as a replacement for animal experimentation and play a crucial role in advancing personalized cancer therapy.

Author contributions

CBXH wrote and reviewed the manuscript under supervision by T-YT. All authors contributed to the article and approved the submitted version.

Funding

This work was funded by the National Science and Technology Council (NSTC), Taiwan, and the Young Scholar Program (MOST 111- 2740-B-006-002-, MOST 111-2636-B-006-010-, and NSTC 112-2636-B-006-001- to T-YT). This work was also supported in part by the Higher Education Sprout Project, Ministry of Education to the Headquarters of University Advancement at National Cheng Kung University.

Acknowledgments

The authors are grateful for the support from the Core Research Laboratory, College of Medicine, and the Center for Micro/Nano Science and Technology, NCKU. The authors also thank the service provided by the "Bioimaging Core Facility of the National Core Facility for Biopharmaceuticals, Ministry of Science and Technology, Taiwan".

Conflict of interest

The authors declare that the research was conducted in the absence of any commercial or financial relationships that could be construed as a potential conflict of interest.

Publisher's note

References

1. van Norman GA. Limitations of animal studies for predicting toxicity in clinical trials: Part 2: Potential alternatives to the use of animals in preclinical trials. *JACC Basic Transl Sci* (2020) 5(4):387–97. doi: 10.1016/j.jacbts.2020.03.010

2. Lamplugh Z, Fan Y. Vascular microenvironment, tumor immunity and immunotherapy. *Front Immunol* (2021) 12:5414. doi: 10.3389/fimmu.2021.811485

3. Hendry SA, Farnsworth RH, Solomon B, Achen MG, Stacker SA, Fox SB. The role of the tumor vasculature in the host immune response: Implications for therapeutic strategies targeting the tumor microenvironment. *Front Immunol* (2016) 7(DEC):621. doi: 10.3389/fimmu.2016.00621

4. Ngan Ngo TK, Kuo CH, Tu TY. Recent advances in microfluidic-based cancer immunotherapy-on-a-chip strategies. *Biomicrofluidics* (2023) 17(1):011501. doi: 10.1063/5.0108792

5. Zhang X, Karim M, Hasan MM, Hooper J, Wahab R, Roy S, et al. Cancer-on-a-Chip: Models for studying metastasis. *Cancers* (2022) 14(3):648. doi: 10.3390/cancers14030648

6. Lambert AW, Pattabiraman DR, Weinberg RA. Emerging biological principles of metastasis. *Cell* (2017) 168:670–91. doi: 10.1016/j.cell.2016.11.037

7. Hassell BA, Goyal G, Lee E, Sontheimer-Phelps A, Levy O, Chen CS, et al. Human organ chip models recapitulate orthotopic lung cancer growth, therapeutic responses, and tumor dormancy *In vitro*. *Cell Rep* (2017) 21(2):508–16. doi: 10.1016/j.celrep.2017.09.043

8. Ozkan A, Ghousifam N, Hoopes PJ, Yankeelov TE, Rylander MN. *In vitro* vascularized liver and tumor tissue microenvironments on a chip for dynamic determination of nanoparticle transport and toxicity. *Biotechnol Bioeng* (2019) 116 (5):1201–19. doi: 10.1002/bit.26919

9. Ayuso JM, Truttschel R, Gong MM, Humayun M, Virumbrales-Munoz M, Vitek R, et al. Evaluating natural killer cell cytotoxicity against solid tumors using a microfluidic model. *Oncoimmunology* (2019) 8(3). doi: 10.1080/2162402X.2018.1553477

10. Gadde M, Phillips C, Ghousifam N, Sorace AG, Wong E, Krishnamurthy S, et al. *In vitro* vascularized tumor platform for modeling tumor-vasculature interactions of inflammatory breast cancer. *Biotechnol Bioeng* (2020) 117(11):3572–90. doi: 10.1002/bit.27487

11. Ando Y, Oh JM, Zhao W, Tran M, Shen K. Engineering a vascularized hypoxic tumor model for therapeutic assessment. *Cells* (2021) 10(9). doi: 10.3390/cells10092201

12. Tu TY, Shen YP, Lim SH, Wang YK. A facile method for generating a smooth and tubular vessel lumen using a viscous fingering pattern in a microfluidic device. *Front Bioeng Biotechnol* (2022) 10:634. doi: 10.3389/fbioe.2022.877480

13. Hajal C, Offeddu GS, Shin Y, Zhang S, Morozova O, Hickman D, et al. Engineered human blood–brain barrier microfluidic model for vascular permeability analyses. *Nat Protoc* (2021) 17(1):95–128. doi: 10.1038/s41596-021-00635-w

14. Sontheimer-Phelps A, Hassell BA, Ingber DE. Modelling cancer in microfluidic human organs-on-chips. *Nat Rev Cancer* (2019) 19(2):65–81. doi: 10.1038/s41568-018-0104-6

15. Chen MB, Whisler JA, Fröse J, Yu C, Shin Y, Kamm RD. On-chip human microvasculature assay for visualization and quantification of tumor cell extravasation dynamics. *Nat Protoc* (2017) 12(5):865–80. doi: 10.1038/nprot.2017.018

16. Haase K, Gillrie MR, Hajal C, Kamm RD. Pericytes contribute to dysfunction in a human 3D model of placental microvasculature through VEGF-Ang-Tie2 signaling. *Adv Sci* (2019) 6(23). doi: 10.1002/advs.201900878

17. Ahn J, Kim DH, Koo DJ, Lim J, Park TE, Lee J, et al. 3D microengineered vascularized tumor spheroids for drug delivery and efficacy testing. *Acta Biomater* (2022) 13. doi: 10.1016/j.actbio.2022.10.009

18. Kim Y, Ko J, Shin N, Park S, Lee SR, Kim S, et al. All-in-one microfluidic design to integrate vascularized tumor spheroid into high-throughput platform. *Biotechnol Bioeng* (2022) 119(12):3678–93. doi: 10.1002/bit.28221

19. Whisler JA, Chen MB, Kamm RD. Control of perfusable microvascular network morphology using a multiculture microfluidic system. *Tissue Eng Part C Methods* (2014) 20(7):543–52. doi: 10.1089/ten.tec.2013.0370

20. Wan Z, Zhong AX, Zhang S, Pavlou G, Coughlin MF, Shelton SE, et al. A robust method for perfusable microvascular network formation in vitro. *Small Methods* (2022) 6(6):2200143. doi: 10.1002/smtd.202200143

21. Wan Z, Zhang S, Zhong AX, Shelton SE, Campisi M, Sundararaman SK, et al. A robust vasculogenic microfluidic model using human immortalized endothelial cells and Thy1 positive fibroblasts. *Biomaterials* (2021) 1:276. doi: 10.1016/j.biomaterials.2021.121032

22. Weisel JW. Fibrinogen and fibrin. *Adv Protein Chem* (2005) 70:247–99. doi: 10.1016/S0065-3233(05)70008-5

23. Park YK, Tu TY, Lim SH, Clement IJM, Yang SY, Kamm RD. *In vitro* microvessel growth and remodeling within a three-dimensional microfluidic environment. *Cell Mol Bioeng* (2014) 7(1):15–25. doi: 10.1007/s12195-013-0315-6

24. Brown A, He H, Trumper E, Valdez J, Hammond P, Griffith LG. Engineering PEG-based hydrogels to foster efficient endothelial network formation in free-swelling and confined microenvironments. *Biomaterials* (2020) 243:119921. doi: 10.1016/j.biomaterials.2020.119921

25. Ichanti H, Sladic S, Kalies S, Haverich A, Andrée B, Hilfiker A. Characterization of tissue engineered endothelial cell networks in composite collagen-agarose hydrogels. *Gels* (2020) 6(3):27. doi: 10.3390/gels6030027

26. Adair TH, Montani JP. Chapter 1, overview of angiogenesis. In: *Angiogenesis*. San Rafael (CA: Morgan & Claypool Life Sciences (2010).

27. Kim S, Chung M, Ahn J, Lee S, Jeon NL. Interstitial flow regulates the angiogenic response and phenotype of endothelial cells in a 3D culture model. *Lab Chip* (2016) 16 (21):4189–99. doi: 10.1039/C6LC00910G

28. Liu Y, Li J, Zhou J, Liu X, Li H, Lu Y, et al. Angiogenesis and functional vessel formation induced by interstitial flow and vascular endothelial growth factor using a microfluidic chip. *Micromachines (Basel)* (2022) 13(2):225. doi: 10.3390/mi13020225

29. Nashimoto Y, Hayashi T, Kunita I, Nakamasu A, Torisawa YS, Nakayama M, et al. Integrating perfusable vascular networks with a three-dimensional tissue in a microfluidic device. *Integr Biol* (2017) 9(6):506–18. doi: 10.1039/C7IB00024C

30. Wan Z, Floryan MA, Coughlin MF, Zhang S, Zhong AX, Shelton SE, et al. New strategy for promoting vascularization in tumor spheroids in a microfluidic assay. *Adv Healthc Mater* (2022) 15:2201784. doi: 10.1002/adhm.202201784

31. Park J, Kim S, Hong J, Jeon JS. Enabling perfusion through multicellular tumor spheroids promoting lumenization in a vascularized cancer model. *Lab Chip* (2022) 22 (22):4335–48. doi: 10.1039/D2LC00597B

32. Nashimoto Y, Okada R, Hanada S, Arima Y, Nishiyama K, Miura T, et al. Vascularized cancer on a chip: The effect of perfusion on growth and drug delivery of tumor spheroid. *Biomaterials* (2020) 1:229. doi: 10.1016/j.biomaterials.2019.119547

33. Kim D, Seob Hwang K, Seo EU, Seo S, Chul Lee B, Choi N, et al. Vascularized lung cancer model for evaluating the promoted transport of anticancer drugs and immune cells in an engineered tumor microenvironment. *Adv Healthc Mater* (2022) 11 (12):2102581. doi: 10.1002/adhm.202102581

34. Liu Y, Sakolish C, Chen Z, Phan DTT, Bender RHF, Hughes CCW, et al. Human in vitro vascularized micro-organ and micro-tumor models are reproducible organ-on-a-chip platforms for studies of anticancer drugs. *Toxicology* (2020) 1:445. doi: 10.1016/j.tox.2020.152601

35. Miller CP, Tsuchida C, Zheng Y, Himmelfarb J, Akilesh S. A 3D human renal cell carcinoma-on-a-Chip for the study of tumor angiogenesis. *Neoplasia (United States)* (2018) 20(6):610–20. doi: 10.1016/j.neo.2018.02.011

36. Nguyen DHT, Lee E, Alimperti S, Norgard RJ, Wong A, June-Koo Lee J, et al. A biomimetic pancreatic cancer on-chip reveals endothelial ablation *via* ALK7 signaling. *Sci Adv* (2019) 5. doi: 10.1126/sciadv.aav6789

37. Silvestri VL, Henriet E, Linville RM, Wong AD, Searson PC, Ewald AJ. A tissue-engineered 3d microvessel model reveals the dynamics of mosaic vessel formation in breast cancer. *Cancer Res* (2020) 80(19):4288–301. doi: 10.1158/0008-5472.CAN-19-1564

38. Li C, Li S, Du K, Li P, Qiu B, Ding W. On-chip replication of extremely early-stage tumor behavior. *ACS Appl Mater Interfaces* (2021) 13(17):19768–77. doi: 10.1021/acsami.1c03740

39. Fernández-Cortés M, Delgado-Bellido D, Javier Oliver F. Vasculogenic mimicry: Become an endothelial cell "But not so much". *Front Oncol* (2019) 9(AUG):803. doi: 10.3389/fonc.2019.00803

40. Gerigk M, Bulstrode H, Shi HTH, Tönisen F, Cerutti C, Morrison G, et al. On-chip perivascularnichesupporting stemness of patient-derived glioma cells in a serum-free, flowable culture. *Lab Chip* (2021) 21(12):2343–58. doi: 10.1039/D1LC00271F

41. Campisi M, Sundararaman SK, Shelton SE, Knelson EH, Mahadevan NR, Yoshida R, et al. Tumor-derived cGAMP regulates activation of the vasculature. *Front Immunol* (2020) 4:11. doi: 10.3389/fimmu.2020.02090

42. Mollica H, Teo YJ, Tan ASM, Tan DZM, Decuzzi P, Pavesi A, et al. A 3D pancreatic tumor model to study T cell infiltration. *Biomater Sci* (2021) 9(22):7420–31. doi: 10.1039/D1BM00210D

43. Lee J, Kim SE, Moon D, Doh J. A multilayered blood vessel/tumor tissue chip to investigate T cell infiltration into solid tumor tissues. *Lab Chip* (2021) 21(11):2142–52. doi: 10.1039/D1LC00182E

44. Humayun M, Ayuso JM, Brenneke RA, Virumbrales-Muñoz M, Lugo-Cintrón K, Kerr S, et al. Elucidating cancer-vascular paracrine signaling using a human organotypic breast cancer cell extravasation model. *Biomaterials* (2021) 1:270. doi: 10.1016/j.biomaterials.2020.120640

45. Kim S, Park J, Kim J, Jeon JS. Microfluidic tumor vasculature model to recapitulate an endothelial immune barrier expressing FasL. *ACS Biomater Sci Eng* (2021) 7(3):1230–41. doi: 10.1021/acsbiomaterials.0c01542

46. Kim H, Chung H, Kim J, Choi DH, Shin Y, Guk Kang Y, et al. Macrophages-triggered sequential remodeling of endothelium-interstitial matrix to form pre-metastatic niche in microfluidic tumor microenvironment. *Adv Science* (2019) 6 (11):1900195. doi: 10.1002/advs.201900195

47. Bi Y, Shirure VS, Liu R, Cunningham C, Ding L, Meacham JM, et al. Tumor-on-a-chip platform to interrogate the role of macrophages in tumor progression. *Integr Biol (Camb)* (2020) 12(9):221–32. doi: 10.1093/intbio/zyaa017

48. Boussommier-Calleja A, Atiyas Y, Haase K, Headley M, Lewis C, Kamm RD. The effects of monocytes on tumor cell extravasation in a 3D vascularized microfluidic model. *Biomaterials* (2019) 198:180–93. doi: 10.1016/j.biomaterials.2018.03.005

49. Chen MB, Hajal C, Benjamin DC, Yu C, Azizgolshani H, Hynes RO, et al. Inflamed neutrophils sequestered at entrapped tumor cells *via* chemotactic confinement promote tumor cell extravasation. *Proc Natl Acad Sci U S A.* (2018) 115 (27):7022–7. doi: 10.1073/pnas.1715932115

50. Spiegel A, Brooks MW, Houshyar S, Reinhardt F, Ardolino M, Fessler E, et al. Neutrophils suppress intraluminal NK cell-mediated tumor cell clearance and enhance extravasation of disseminated carcinoma cells. *Cancer Discovery* (2016) 6(6):630–49. doi: 10.1158/2159-8290.CD-15-1157

51. Crippa M, Bersini S, Gilardi M, Arrigoni C, Gamba S, Falanga A, et al. A microphysiological early metastatic niche on a chip reveals how heterotypic cell interactions and inhibition of integrin subunit β3 impact breast cancer cell extravasation. *Lab Chip* (2021) 21(6):1061–72. doi: 10.1039/D0LC01011A

52. Ma Y, Li G, Yu M, Sun X, Nian J, Gao Y, et al. Prognostic significance of thrombocytosis in lung cancer: a systematic review and meta-analysis. *Platelets* (2020) 32(7):919–27. doi: 10.1080/09537104.2020.1810653

53. Nie D, Yang E, Li Z. Pretreatment thrombocytosis predict poor prognosis in patients with endometrial carcinoma: A systematic review and meta-analysis. *BMC Cancer* (2019) 19(1):1–8. doi: 10.1186/s12885-018-5264-y

54. Hufnagel DH, Cozzi GD, Crispens MA, Beeghly-Fadiel A. Platelets, thrombocytosis, and ovarian cancer prognosis: Surveying the landscape of the literature. *Int J Mol Sci* (2020) 21(21):8169. doi: 10.3390/ijms21218169

55. Ramjeesingh R, Jones A, Orr C, Bricks CS, Hopman WM, Hammad N. Thrombocytosis as a predictor of poor prognosis in colorectal cancer patients. *Journ of Clin Oncol* 34(4). doi: 10.4251/wjgo.v6.i2.34

56. Braun A, Anders HJ, Gudermann T, Mammadova-Bach E. Platelet-cancer interplay: Molecular mechanisms and new therapeutic avenues. *Front Oncol* (2021) 11:2576. doi: 10.3389/fonc.2021.665534

57. Saha B, Mathur T, Handley KF, Hu W, Afshar-Kharghan V, Sood AK, et al. OvCa-chip microsystem recreates vascular endothelium-mediated platelet extravasation in ovarian cancer. *Blood Adv* (2020) 4(14):3329–42. doi: 10.1182/bloodadvances.2020001632

58. Jiang W, Hu JW, He XR, Jin WL, He XY. Statins: a repurposed drug to fight cancer. *J Exp Clin Cancer Res* (2021) 40(1):1–33. doi: 10.1186/s13046-021-02041-2

59. Wilkinson EL, Sidaway JE, Cross MJ. Statin regulated ERK5 stimulates tight junction formation and reduces permeability in human cardiac endothelial cells. *J Cell Physiol* (2018) 233(1):186–200. doi: 10.1002/jcp.26064

60. Lampi MC, Faber CJ, Huynh J, Bordeleau F, Zanotelli MR, Reinhart-King CA. Simvastatin ameliorates matrix stiffness-mediated endothelial monolayer disruption. *PloS One* (2016) 11(1):e0147033. doi: 10.1371/journal.pone.0147033

61. Saha B, Mathur T, Tronolone JJ, Chokshi M, Lokhande GK, Selahi A, et al. Human tumor microenvironment chip evaluates the consequences of platelet extravasation and combinatorial antitumor-antiplatelet therapy in ovarian cancer. *Sci Adv* (2020) 7. doi: 10.1126/sciadv.abg5283

62. Xu R, Rai A, Chen M, Suwakulsiri W, Greening DW, Simpson RJ. Extracellular vesicles in cancer — implications for future improvements in cancer care. *Nat Rev Clin Oncol* (2018) 15(10):617–38. doi: 10.1038/s41571-018-0036-9

63. Kim J, Lee C, Kim I, Ro J, Kim J, Min Y, et al. Three-dimensional human liver-chip emulating premetastatic niche formation by breast cancer-derived extracellular vesicles. *ACS Nano* (2020) 14(11):14971–88. doi: 10.1021/acsnano.0c04778

64. Nasrollahi S, Walter C, Loza AJ, Schimizzi GV, Longmore GD, Pathak A. Past matrix stiffness primes epithelial cells and regulates their future collective migration through a mechanical memory. *Biomaterials* (2017) 146:146–55. doi: 10.1016/j.biomaterials.2017.09.012

65. Yang C, Tibbitt MW, Basta L, Anseth KS. Mechanical memory and dosing influence stem cell fate. *Nat Materials* (2014) 13(6):645–52. doi: 10.1038/nmat3889

66. Azadi S, Tafazzoli Shadpour M, Warkiani ME. Characterizing the effect of substrate stiffness on the extravasation potential of breast cancer cells using a 3D microfluidic model. *Biotechnol Bioeng* (2021) 118(2):823–35. doi: 10.1002/bit.27612

67. Nagaraju S, Truong D, Mouneimne G, Nikkhah M. Microfluidic tumor–vascular model to study breast cancer cell invasion and intravasation. *Adv Healthc Mater* (2018) 7(9):1701257. doi: 10.1002/adhm.201701257

68. Truong D, Fiorelli R, Barrientos ES, Melendez EL, Sanai N, Mehta S, et al. A three-dimensional (3D) organotypic microfluidic model for glioma stem cells – vascular interactions. *Biomaterials* (2019) 198:63–77. doi: 10.1016/j.biomaterials.2018.07.048

69. Wong AD, Searson PC. Mitosis-mediated intravasation in a tissue-engineered tumor–microvessel platform. *Cancer Res* (2017) 77(22):6453–61. doi: 10.1158/0008-5472.CAN-16-3279

70. Huttenlocher A, Horwitz AR. Integrins in cell migration. *Cold Spring Harb Perspect Biol* (2011) 3(9):a005074. doi: 10.1101/cshperspect.a005074

71. Gilardi M, Bersini S, Valtorta S, Proietto M, Crippa M, Boussommier-Calleja A, et al. The driving role of the Cdk5/Tln1/FAKS732 axis in cancer cell extravasation dissected by human vascularized microfluidic models. *Biomaterials* (2021) 1:276. doi: 10.1016/j.biomaterials.2021.120975

72. Chen MB, Lamar JM, Li R, Hynes RO, Kamm RD. Elucidation of the roles of tumor integrin β1 in the extravasation stage of the metastasis cascade. *Cancer Res* (2016) 76(9):2513–24. doi: 10.1158/0008-5472.CAN-15-1325

73. Fröse J, Chen MB, Hebron KE, Reinhardt F, Hajal C, Zijlstra A, et al. Epithelial-mesenchymal transition induces podocalyxin to promote extravasation *via* ezrin signaling. *Cell Rep* (2018) 24(4):962–72. doi: 10.1016/j.celrep.2018.06.092

74. van den Berg BM, Nieuwdorp M, Vink H, Stroes E. Endothelial luminal glycocalyx: Protective barrier between endothelial cells and flowing blood. *Endothelial Biomed* (2007) 1:689–95. doi: 10.1017/CBO9780511546198.076

75. Moore KH, Murphy HA, George EM. The glycocalyx: A central regulator of vascular function. *Am J Physiol Regul Integr Comp Physiol* (2021) 320(4):R508–18. doi: 10.1152/ajpregu.00340.2020

76. Offeddu GS, Hajal C, Foley CR, Wan Z, Ibrahim L, Coughlin MF, et al. The cancer glycocalyx mediates intravascular adhesion and extravasation during metastatic dissemination. *Commun Biol* (2021) 4(1):1–10. doi: 10.1038/s42003-021-01774-2

77. Follain G, Herrmann D, Harlepp S, Hyenne V, Osmani N, Warren SC, et al. Fluids and their mechanics in tumour transit: shaping metastasis. *Nat Rev Cancer* (2019) 20(2):107–24. doi: 10.1038/s41568-019-0221-x

78. Mitchell MJ, King MR. Computational and experimental models of cancer cell response to fluid shear stress. *Front Oncol* (2013). 3. doi: 10.3389/fonc.2013.00044

79. Hajal C, Ibrahim L, Serrano JC, Offeddu GS, Kamm RD. The effects of luminal and trans-endothelial fluid flows on the extravasation and tissue invasion of tumor cells in a 3D in vitro microvascular platform. *Biomaterials* (2021) 1:265. doi: 10.1016/j.biomaterials.2020.120470

80. Kenny HA, Nieman KM, Mitra AK, Lengyel E. The first line of intra-abdominal metastatic attack: Breaching the mesothelial cell layer. *Cancer Discovery* (2011) 1 (2):100–2. doi: 10.1158/2159-8290.CD-11-0117

81. Ibrahim LI, Hajal C, Offeddu GS, Gillrie MR, Kamm RD. Omentum-on-a-chip: A multicellular, vascularized microfluidic model of the human peritoneum for the study of ovarian cancer metastases. *Biomaterials* (2022) 288:121728. doi: 10.1016/j.biomaterials.2022.121728

82. Chaudhry S, Thomas SN, Chaudhry S, Thomas SN, Simmons GEJr. Targeting lipid metabolism in the treatment of ovarian cancer. *Oncotarget* (2022) 13(1):768–83. doi: 10.18632/oncotarget.28241

83. Wang S, Mao S, Li M, Li HF, Lin JM. Near-physiological microenvironment simulation on chip to evaluate drug resistance of different loci in tumour mass. *Talanta* (2019) 191:67–73. doi: 10.1016/j.talanta.2018.08.016

84. Wu SK, Ariffin J, Tay SC, Picone R. The variant senescence-associated secretory phenotype induced by centrosome amplification constitutes a pathway that activates hypoxia-inducible factor-1α. *Aging Cell* (2023) 20:e13766. doi: 10.1111/acel.13766

85. Wang L, Lankhorst L, Bernards R. Exploiting senescence for the treatment of cancer. *Nat Rev Cancer* (2022) 22(6):340–55. doi: 10.1038/s41568-022-00450-9

86. Jing B, Luo Y, Lin B, Li J, Wang ZA, Du Y. Establishment and application of a dynamic tumor-vessel microsystem for studying different stages of tumor metastasis and evaluating anti-tumor drugs. *RSC Adv* (2019) 9(30):17137–47. doi: 10.1039/C9RA02069A

87. Jing B, Cheng G, Li J, Wang ZA, Du Y. Inhibition of liver tumor cell metastasis by partially acetylated chitosan oligosaccharide on a tumor-vessel microsystem. *Mar Drugs* (2019) 17(7). doi: 10.3390/md17070415

88. Lin C, Lin L, Mao S, Yang L, Yi L, Lin X, et al. Reconstituting glioma perivascular niches on a chip for insights into chemoresistance of glioma. *Anal Chem* (2018) 90 (17):10326–33. doi: 10.1021/acs.analchem.8b02133

89. Hu Z, Cao Y, Galan EA, Hao L, Zhao H, Tang J, et al. Vascularized tumor spheroid-on-a-Chip model verifies synergistic vasoprotective and chemotherapeutic effects. *ACS Biomater Sci Eng* (2022) 8(3):1215–25. doi: 10.1021/acsbiomaterials.1c01099

90. Cheng Z, Li M, Dey R, et al. Nanomaterials for cancer therapy: current progress and perspectives. *J Hematol Oncol* (2021) 14:85. doi: 10.1186/s13045-021-01096-0

91. Feiner-Gracia N, Glinkowska Mares A, Buzhor M, Rodriguez-Trujillo R, Samitier Marti J, Amir RJ, et al. Real-time ratiometric imaging of micelles assembly state in a microfluidic cancer-on-a-Chip. *ACS Appl Bio Mater* (2021) 4(1):669–81. doi: 10.1021/acsabm.0c01209

92. Wang LC, Chang LC, Su GL, Chang PY, Hsu HF, Lee CL, et al. Chemical structure and shape enhance MR imaging-guided X-ray therapy following marginative delivery. *ACS Appl materials interfaces* (2022) 14(11):13056–69. doi: 10.1021/acsami.1c24991

93. Lai BFL, Huyer LD, Lu RXZ, Drecun S, Radisic M, Zhang B. InVADE: Integrated vasculature for assessing dynamic events. *Adv Funct Mater* (2017) 27(46). doi: 10.1002/adfm.201703524

94. Weng KC, Kurokawa YK, Hajek BS, Paladin JA, Shirure VS, George SC. Human induced pluripotent stem-Cardiac-Endothelial-Tumor-on-a-Chip to assess anticancer

efficacy and cardiotoxicity. *Tissue Eng Part C Methods* (2020) 26(1):44–55. doi: 10.1089/ten.tec.2019.0248

95. van Dijk CGM, Brandt MM, Poulis N, Anten J, van der Moolen M, Kramer L, et al. A new microfluidic model that allows monitoring of complex vascular structures and cell interactions in a 3D biological matrix. *Lab Chip* (2020) 20(10):1827–44. doi: 10.1039/D0LC00059K

96. Kim J, Chung M, Kim S, Jo DH, Kim JH, Jeon NL. Engineering of a biomimetic pericyte-covered 3D microvascular network. *PloS One* (2015) 10(7):e0133880. doi: 10.1371/journal.pone.0133880

97. Karaman S, Detmar M. Mechanisms of lymphatic metastasis. *J Clin Invest* (2014) 124(3):922. doi: 10.1172/JCI71606

98. Toepke MW, Beebe DJ. PDMS absorption of small molecules and consequences in microfluidic applications. *Lab Chip* (2006) 6(12):1484–6. doi: 10.1039/b612140c

99. LaCroix AS, Rothenberg KE, Berginski ME, Urs AN, Hoffman BD. Construction, imaging, and analysis of FRET-based tension sensors in living cells. *Methods Cell Biol* (2015) 125:161–86. doi: 10.1016/bs.mcb.2014.10.033

100. Vila Cuenca M, Cochrane A, van den Hil FE, de Vries AAF, Lesnik Oberstein SAJ, Mummery CL, et al. Engineered 3D vessel-on-chip using hiPSC-derived endothelial- and vascular smooth muscle cells. *Stem Cell Rep* (2021) 16(9):2159–68. doi: 10.1016/j.stemcr.2021.08.003

101. Roberts AB, Zhang J, Raj Singh V, Nikolić M, Moeendarbary E, Kamm RD, et al. Tumor cell nuclei soften during transendothelial migration. *J Biomech* (2021) 24:121. doi: 10.1016/j.jbiomech.2021.110400

102. Zhang J, Nikolic M, Tanner K, et al. Rapid biomechanical imaging at low irradiation level *via* dual line-scanning brillouin microscopy. *Nat Methods* (2023). doi: 10.1038/s41592-023-01816-z

frontiers | Frontiers in Oncology

TYPE Original Research
PUBLISHED 30 March 2023
DOI 10.3389/fonc.2023.1145817

OPEN ACCESS

EDITED BY
Paola Cappello,
University of Turin, Italy

REVIEWED BY
Stephen B. Keysar,
University of Colorado Anschutz Medical Campus, United States
Michele Zanoni,
Scientific Institute of Romagna for the Study and Treatment of Tumors (IRCCS), Italy

*CORRESPONDENCE
Annette Runge
annette.runge@tirol-kliniken.at

SPECIALTY SECTION
This article was submitted to Molecular and Cellular Oncology, a section of the journal Frontiers in Oncology

RECEIVED 16 January 2023
ACCEPTED 27 February 2023
PUBLISHED 30 March 2023

CITATION
Greier MC, Runge A, Dudas J, Carpentari L, Schartinger VH, Randhawa A, Mayr M, Petersson M and Riechelmann H (2023) Optimizing culturing conditions in patient derived 3D primary slice cultures of head and neck cancer. *Front. Oncol.* 13:1145817. doi: 10.3389/fonc.2023.1145817

Optimizing culturing conditions in patient derived 3D primary slice cultures of head and neck cancer

Maria do Carmo Greier[1], Annette Runge[1]*, Jozsef Dudas[1], Lukas Carpentari[1], Volker Hans Schartinger[1], Avneet Randhawa[2], Melissa Mayr[3], Monika Petersson[3] and Herbert Riechelmann[1]

[1]Department of Otorhinolaryngology, Head and Neck Surgery, Medical University of Innsbruck, Innsbruck, Austria, [2]Department of Otolaryngology, Head and Neck Surgery, Rutgers New Jersey Medical School, Newark, NJ, United States, [3]ViraTherapeutics GmbH, Rum, Austria

Background: Three-dimensional primary slice cultures (SC) of head and neck squamous cell carcinomas (HNC) are realistic preclinical models. Until now, preserving structure and viability *ex vivo* for several days has been difficult. The aim of this study was to optimize cultivation conditions for HNC SC and analyze the added effects of platelet rich fibrin (PRF) on these conditions.

Methods: SC were prepared from the tumor biopsies of 9 HNC patients. Cultures were incubated for 1 and 7 days in three different media- Keratinocyte serum-free medium (SFM), RPMI-1640i, and 1:1 mix of both, with and without addition of PRF. After culturing, SC were fixated, embedded, and stained with Hematoxylin-Eosin (HE) and cleaved caspase-3. In addition, triple immune fluorescence staining for cytokeratin, vimentin and CD45 was performed. Outcome parameters were cell count and cell density, viability and apoptosis, SC total area and proportions of keratinocytes, mesenchymal and immune cells. The effects of culture time, medium, and addition of PRF were calculated in an SPSS generalized linear model and using the Wald Chi-Squared test.

Results: Ninety-four slice cultures were analyzed. Viability remained stable for 7 days in culture. After addition of PRF, cell viability increased (p=0.05). SC total area decreased (0.44 $\pm$ 0.04 mm^2 on day 1 (95% CI: 0.35 to 0.56) to 0.29 $\pm$ 0.03 mm^2 on day 7 (95% CI: 0.22 to 0.36), but cell density and cell proportions remained stable. Differences in cultivation media had no significant impact on outcome parameters.

Conclusion: HNC SC can be preserved for up to 7 days using the tested cultivation media. Cell viability was best preserved with addition of PRF. HNC SC are a versatile experimental tool to study physiology and drug actions. Autologous PRF can help simulate realistic conditions *in vitro*.

KEYWORDS

head and neck cancer, tumor microenvironment, cultured neoplastic cells, platelet rich fibrin, culture media

1 Introduction

Head and neck squamous cell carcinomas (HNC) are heterogeneous tumors with highly variable cellular composition, invasion patterns, and therapy response (1). Realistic preclinical models for personalized therapy strategies are lacking. Cell cultures are currently the standard models (2) of basic tumor mechanisms (3). However, without the tumor microenvironment (TME), cell cultures are limited in their translational applicability (4, 5). Tumor architecture, physiological state, and interactions among different cell types (6) can play important roles in cancer progression and invasion (7, 8). Recently, patient-derived HNC models with the TME have been used to study tumor-specific characteristics and develop individualized therapies (8–11). Such TME models can be *in-vivo*, two- and three-dimensional co-cultures (11, 12), patient derived xenograft models (13, 14), organoids (14, 15), microfluidic designs (16–18), organ-on-a-chip models (19, 20), spheroids (21), 3D bio prints (22, 23), 3D collagen-based scaffolds (24) and advanced three-dimensional spheroid models from dissected whole tumor tissues. However, in all of the above-mentioned models, the *in situ* spatial arrangement of the TME is dissolved and interactions with neighboring tissue may be altered (24–26). Primary slice cultures (SC) are 250 to 400 µm thick slices of tumor tissue samples in which the original 3D structures and organization of the TMEs are preserved (4). As SC are open systems, substances can easily be added and therapeutic efficacy and resistance mechanisms may be directly studied (27). The impact of the HNC cell- microenvironment interaction on invasion patterns and response to antitumoral treatment has become more apparent during the last few years. Different 3D preclinical models of HNC have thus been established recently to study tumor cell characteristics in a "close to real life environment" over the course of several days in a laboratory setting. 3D cultures of oropharyngeal squamous cell carcinoma cell lines were mounted on a collagen – based scaffold to study expression of markers of epithelial- mesenchymal transition as well as matrix interactions and migration behavior and drug resistance pathways both *in vitro* and as xenografts (28). Gerlach and coauthors first described cultivation of HNC SC and observed the effect of cytotoxic drugs for up to 7 days (29). Three-dimensional organotypic co-culture models mounted on a dermal equivalent of fibroblasts and viscose fibers were successfully cultured for 7- 21 days to study proliferation, infiltrative growth patterns and distribution of cancer associated fibroblasts and leukocytes depending on HPV status (30). Furthermore, the applicability of HNC 3D SC as a platform to study novel therapeutic approaches such an oncolytic virus was recently described by Runge and Mayr et al. (31). However, viability and cell proportions may vary due to heterogeneity of HNC tumor tissue samples, effects of culture media, and SC incubation times. Furthermore, *ex vivo* viability of HNC SC might be compromised due to a lack of several autologous growth factors. Platelet rich fibrin (PRF), a completely autologous substance obtained by centrifugation of peripheral venous blood, contains platelets, leukocytes and several biologically active proteins including platelet alpha granules, platelet–derived growth factor (PGDF), transforming growth factors–β (TGF–β), vascular endothelial growth factors (VEGF), and epidermal growth factors (32, 33) in a fibrin matrix. PRF has been suggested to have beneficial effects on viability of tumor explants (32, 34).

The main objective of this study was to optimize HNC SC culturing conditions over a period of seven days. Quality of SC of different media were compared after 1 and 7 days. The effects of autologous PRF on cell viability in HNC SC and selective effects of different culturing media and PRF on epithelial cells, fibroblasts and immune cells were studied.

2 Methods

2.1 Study design

In this study in HNC SC, effects of 3 experimental parameters were examined: cultivation time of 1 day and 7 days, three cultivation media (Keratinocyte SFM, RPMI1640, 1:1 mix of both), and addition of autologous patient derived PRF. The outcome parameters included SC total area (mm2), the total number of cells in relation to the area (the "cell density", cells/mm2), viability (%), number of tumor cells, fibroblasts, and leukocytes per mm2, and their relative proportions.

2.2 Patients

Tumor tissue samples from nine patients with suspected incident, locally advanced head and neck squamous cell carcinomas were collected, who underwent endoscopy under anesthesia as part of their initial staging between October 2020 and June 2021 at the Department of Otorhinolaryngology, Head and Neck Surgery, Medical University of Innsbruck (Table 1). The samples were always collected from the primary tumor. Approval for this study was obtained from the Ethics Committee of the Medical University of Innsbruck (EK-number: 1199/2019, date of approval: 19/05/2019). Written informed consent was obtained from all patients. Inclusion criteria comprised of patient age over 18 years, endoscopy under anesthesia, and locally advanced primary tumor (T3-T4). Patients were excluded if there was a contraindication for endoscopy under anesthesia or if they had received prior treatment for HNC.

2.3 Explant collection and cutting

Samples with a diameter of > 4 mm^3 were collected with biopsy forceps from a non-necrotic tumor area during endoscopy under anesthesia (13). After submersion in Medium 199 (#31150022, Thermo Fischer Scientific, Rochester, NY, USA), the samples were immediately transferred to the laboratory for installation of SC. Afterwards, 12 slices with a thickness of 300 µm were cut from each sample with the vibratome (VT1200S Leica, Wetzlar, Germany; Figure 1A).

TABLE 1 Patient characteristics and tumor locations.

Patient	Sex	Age	Location of primary tumor	TNM	p16 status
1	male	61	Oropharynx	cT4 cN1 cM0	positive
2	female	52	Oropharynx	cT4a cN2c cM1	negative
3	male	73	Larynx	cT4a cN1 cM0	negative
4	male	72	Larynx	cT3 cN2c cM0	negative
5	male	54	Oropharynx	cT3 cN2c cM0	negative
6	male	64	Hypopharynx	cT4a cN3b cM0	negative
7	male	59	Hypopharynx	cT3 cN3b cM0	negative
8	female	87	Oropharynx	cT3 cN1 cM0	negative
9	female	31	Nasopharynx	cT1 cN0 cM0	negative

2.4 Autologous platelet rich fibrin

To prepare PRF, one S-PRF tube (#S-PRF, Mectron, Köln, Germany) of 4.9 ml of peripheral venous blood was obtained by cubital venipuncture from the same HNC patients. The blood sample was centrifuged immediately (Choukroun - PRF Duo Quattro System centrifuge, Cologne, Germany) at 44g for 8 min without addition of any substances. After centrifugation, 50µl of PRF were taken from the tube and added to the corresponding well with a syringe.

2.5 Cultivation media

For optimization of culturing conditions, separate examination of HNC SC in three different media with and without serum, growth factors, and PRF was performed (35). SC were submerged in hanging membrane inserts of a 24-well plate (Corning Incorporated-Life sciences, Durham, USA; Figures 1B, C). 50 µL of patient derived autologous PRF were added to 12/24 inserts. Afterwards, 150 µL of the respective medium were added. The media used were Keratinocyte SFM enriched with human recombinant epidermal growth factor (rEGF), bovine pituitary extract (BPE) (serum free medium; #10724-011, Gibco, Grand Island, NY, USA), RPMI-1640 (#31150022 Thermo Fisher Scientific, Rochester, NY, USA) with additional 10% fetal bovine serum (FBS), and a 1:1 mix of Keratinocyte SFM and RPMI-1640 in a 50 ml Falcon tube (#10788561, Szabo Scandic, Vienna, Austria). All media were supplemented with Gibco Antibiotic-Antimitotic (100x) (#15240062, Thermo Fischer Scientific, Rochester, NY, USA), a mix of three antibiotics (10.000 µg/mL streptomycin, 25 µg/mL amphotericin B and 10.000 units/mL penicillin). SC were then incubated in a 37°C incubator (5% CO2) over 1 and 7 days.

2.6 Fixation and embedding

After cultivation periods of 1 and 7 days, SC were fixed in 4% paraformaldehyde (#FN-10000-4-1, SAV Liquid Production GMBH, Flintsbach am Inn, Germany) overnight (4° C) and washed with phosphate-buffered saline (PBS) (Fresenius Kabi GmbH, Bad Homburg vor der Höhe, Germany) the next day. Fixed SC were embedded in HistoGel (#HG-4000-012, Thermo Scientific, Massachusetts, USA) and prepared for paraffin

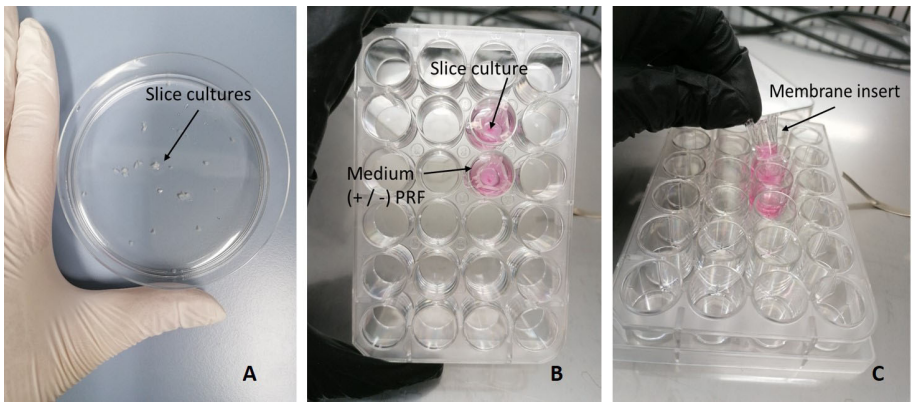

FIGURE 1
Culture setup of SC. **(A)** SC after being cut with the Vibratome. **(B)** SC cultivated in a 24-well plate, submerged in medium with or without PRF. **(C)** Hanging membrane insert.

embedding *via* dehydration and paraffin impregnation with the Histos 5 microwave system (Milestone, Bergamo, Italy). All steps were performed as described by Lechner M et al. (36). Afterwards, hardened paraffin blocks were cut into 5µm slices with the HM 355S microtome (Microm, Walldorf, Germany) and transferred onto Superfrost Plus slides (Menzel, Braunschweig, Germany).

2.7 Staining procedures

Prior to staining, slides were dewaxed following the protocol of Giotakis et al. (37). Hematoxylin-Eosin (HE) staining was done following the manufacturers´ protocol (#1.05174.0500, Merck KGaA, Darmstadt, Germany). Following the protocol of Fischer N et al., cleaved caspase-3 (CC3) staining was performed using the fully automated immunostaining system (Ventana Roche Discovery Classic, Tucson, AZ, USA) and the CC3 antibody (1:400x, polyclonal rabbit, #9661, Cell Signaling Technology, MA, USA) (36). Epithelial, mesenchymal and immune cells were analyzed with triple immunofluorescence staining, containing conjugated vimentin (eFluor 570 conjugated) (#14-9897-82, eBioscience™, ThermoFischer, Waltham, MA United States), cytokeratin (CK) (Alexa Fluor 488 conjugated) (#628601, BioLegend, San Diego, United States), and CD45 (Alex Fluor 594 conjugated (#304060, BioLegend, San Diego, United States) as described by Giotakis et al. (37). Per slide, 8 µL of CD45 and 4 µL CK and vimentin, respectively, were used and mixed with 100 µL of antibody diluent (Roche, Ventana, Tucson, AZ, USA). The mix was then pipetted manually on the slides in the Ventana Discovery Slide Autoimmunostainer. For nuclear counterstain, 4′,6-diamidin-2-phenylindolethen (DAPI, 1:46.000, Thermo Fisher Scientific, Darmstadt, Germany) was pipetted onto the slides manually. To reduce auto fluorescence, the Vector TrueVIEW Auto Fluorescence Quenching Kit (#VEC-SP-8400, Vector Laboratories, Burlingame, California, USA) was used (37). After staining procedures, the slides were mounted with Vectashield Vibrance (Vector Laboratories) and dried overnight (38).

2.8 SC quality rating

Gross quality of SC was rated microscopically after 1 and 7 days of cultivation on HE staining. Texture and compactness of the tissue, viability, and necrotic areas were rated from 0 to 3, with 0 as the lowest and 3 as the highest quality score (Table 2).

TABLE 2 Scoring system (0-3) for SC quality in HE stained slices.

Score	Description
0	≤20% viable cells
1	21-40% viable cells
2	41-60% viable cells
3	≥60% viable cells

2.9 Image acquisition and analysis

TissueFAXS (TissueGnostics GmbH, Vienna, Austria) was used for image acquisition. Viability score, SC total area, total cell count, and total count of CC3 positive and-negative cells were analyzed in HE and CC3 stainings with HistoQuest according to Ingruber et al. (37) and Steinbichler et al. (39). In IF stained images, proportions and distributions of epithelial tumor cells, fibroblasts, and leukocytes were analyzed with TissueQuest according to Giotakis et al. (35). Tumor cells were defined in fluorescence-stained slices as cytokeratin or combined cytokeratin-vimentin-stained cells. Fibroblasts were defined as single vimentin-stained cells and leucocytes as single CD45 or CD45- vimentin combined stained cells.

2.10 Data analysis

Given the right-skewed distributions of the outcome parameters, a generalized linear model was used, assuming a gamma distribution and a logistic link function. All main effects and interactions were included. Parameters were estimated using the maximum likelihood method, and p values and confidence intervals were calculated according to Wald. Calculations were performed with SPPS Statistics Ver. 27 (IBM, Armonk, NY). Estimated marginal means (EMM) and their standard errors (SEM) were graphically presented using GraphPad Prism 9 (GraphPad Software, San Diego, CA, USA).

3 Results

Ninety-four out of 108 SC from 9 patients were evaluable. Four primary tumors were in the oropharynx, 2 in the larynx, 2 in the hypopharynx, and one in the nasopharynx. The patients were between 31 and 87 years old (average 61.4 years). All patients but one were diagnosed with UICC stage III or IV HNC by clinical and radiologic evaluation. The cervical lymph nodes were involded in 8/9 cases, distant metastasis was found in one patient. All but one oropharyngeal carcinoma were p16 negative. Treatment after initial staging involved surgery with curative intent in 5 cases, adjuvant radiation or chemoradiation in 4 cases and primary Chemoradiation in 3 cases. SC were generated from each of the tumor explants (Table 1).

3.1 Gross slice quality

Microscopic evaluation of gross SC quality in HE stainings revealed differences in quality and tissue composition depending on incubation time. After 24h, the tissue was mostly compact with almost nonnecrotic areas (Figure 2). After 7 days, the tissue structure and quality were still compact, but there were slightly more necrotic and dissembled areas visible (Figure 2).

Both in parametric and non-parametric tests, there was a significant correlation of HE quality score grade with SC total

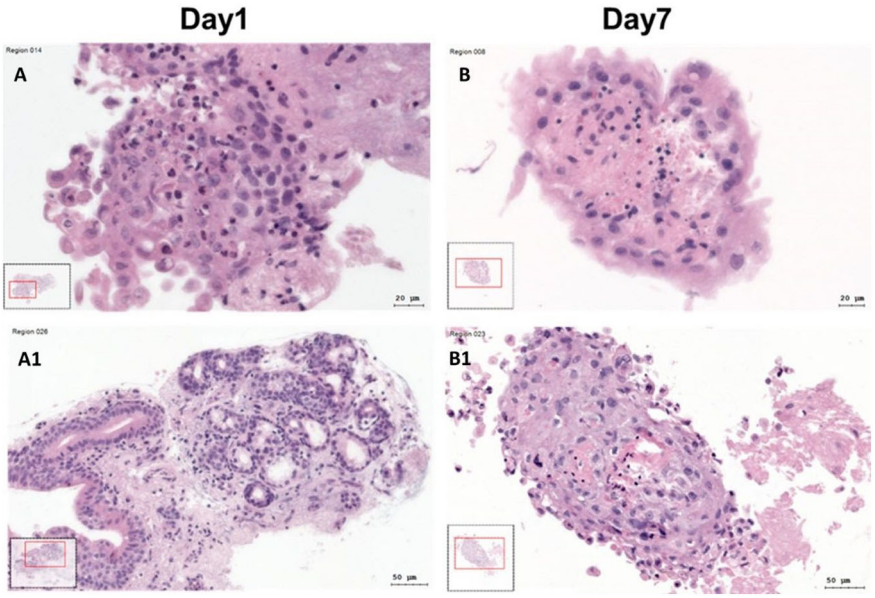

FIGURE 2
Hematoxylin–Eosin (HE) stained SC at day 1 and day 7. **(A, A1)** HE stained SC at day 1. **(B, B1)** HE stained SC at day 7.

area. (Spearman´s rho=0.39; n=94; p<0.001). These tests also revealed a statistically significant correlation of HE quality scoring grades with the cell density (Spearman´s rho=0.6; n=94; p<0.001).

3.2 Effects of cultivation time, cultivation medium, and PRF on SC total area and cell density

3.2.1 SC total area

Both cultivation time and addition of PRF had significant effects on the SC total area. Total area decreased from 0.44 ± 0.04 mm2 on day 1 (95% CI: 0.35 to 0.56) to 0.29 ± 0.03 mm2 on day 7 (95% CI: 0.22 to 0.36; p=0.007), (Figure 3B). SC total area was larger when cultivated with PRF (0.43 ± 0.05 mm2; 95% CI: 0.34 to 0.55; p=0.009) than without PRF (0.29 ± 0.03 mm2; 95% CI: 0.22 to 0.37; Figure 3A). This effect was independent of cultivation time. No significant effect of cultivation medium on SC total area and cell count was observed (p=0.205). Detailed patient specific data, in correspondence to Figures 3A, B, can be found in Supplementary Table S1.

3.2.2 SC cell density

Cell density was calculated by relating absolute cell count and SC total area. In all 94 slices, the mean cell density was 3544 ± 334 cells/mm2. PRF reduced cell density (p=0.003). Without PRF, 4669 ± 584 cells/mm2 (95% CI: 3654 to 5965) were counted in the slice cultures; whereas with PRF, 2690 ± 377 cells/mm2 (95% CI: 2045 to 3538) were observed (Figure 3C; Supplementary Table S2). Comparative visualization of SC after 1 and 7 days suggested increased cell counts in some of the PRF free, but barely in PRF containing SC (Figures 4A, B).

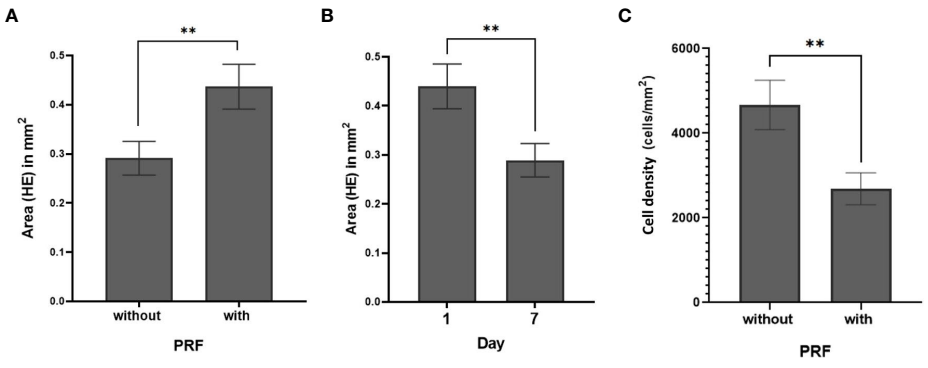

FIGURE 3
SC total area (mm2) (HE) **(A)** with and without PRF (p=0.009). **(B)** at day 1 and day 7 (p=0.007) **(C)** Cell density with and without PRF (p=0.003). (**significant at the 0.05 level; Bars: SEM).

3.3 Effects of cultivation medium, cultivation time and PRF and on cell viability

CC3 negative cells were considered viable and viability was calculated as the proportion of CC3 negative cells. Seventy-six SC were included in the viability analysis. Overall cell viability was 64.3 ± 2.1% (95% CI: 60.1 to 68.5). PRF increased cell viability (p=0.05). Cell viability was 60.1 ± 3% (95% CI: 54.2 to 66) without PRF vs. 68.48 ± 3.06% (95% CI: 62.5 to 75.5) with PRF (Figure 5A). There was no significant effect of cultivation media and cultivation time on cell viability (p=0.546 and p=0.834, respectively). Cell viability remained stable between 1 day (63.8 ± 2.8%; 95% CI: 58.2 to 69.5) and 7 days (64.7 ± 3.1%; 95% CI: 58.6 to 70.8; Figure 5B). Detailed patient specific data, in correspondence to Figures 5A, B, can be found in Supplementary Table S3.

3.4 Effects of cultivation time, cultivation medium, and PRF on different cell types

Effects of the three media, addition of PRF, and cultivation period on proportions of epithelial cells, mesenchymal cells and immune cells were also studied. There was a significant effect of the cultivation medium on leukocytes density (p=0.02). Highest leukocyte density were detected when SC were cultivated in combined medium (2686 ± 432 leukocytes/mm2; 95% CI: 1839 to 3534), compared to cultivation in Keratinocyte (1154 ± 367; 95% CI: 434 to 1873) and RPMI-1640 (1449 ± 445; 95% CI: 575 to 2322) media, respectively. Culture time and addition of PRF did not influence leukocyte density (p=0.61 and 0.498 respectively). No significant effect of cultivation medium, time, or PRF on tumor cells and fibroblast density were observed (p-values 0.105-0.835 and 0.485-0.901 for tumor cells and fibroblasts, respectively).

Proportions of tumor cells, leukocytes, and fibroblasts were investigated in the context of cultivation time, medium, and addition of PRF. Culture time decreased the relative amount of tumor cells (p=0.046). After 1 day and 7 days, tumor cells presented 33% ± 3.02 (95% CI: 27.4 to 39.2) and 25% ± 3.19 (95% CI: 18.3 to 30.8) of all DAPI-positive cells. There was no significant effect of cultivation time, media, or PRF on the relative amounts of fibroblasts and leukocytes (Figure 6).

4 Discussion

Due to their preserved tissue architecture, native stroma, and heterogeneity, patient derived slice cultures may be suitable for testing patient specific treatments. HNC SC have been established previously as a platform to study HNC and its microenvironment and novel therapeutic approaches. Cytotoxic effects of high doses of Cisplatin, Docetxel and Cetuximab were studied by Gerlach et al. in HNC SC. According to their observations, they detected fragmentation of nuclei, pygnotic alterations and cellular polymorphisms as hallmarks of apoptosis. Recently, Runge, Mayr et al. reported on HNC SC as a platform to evaluate oncolytic virus action. In this study, it was possible to observe both tumor cell killing effects of the virus and lymphocytic tumor infiltration over the course of several days (29, 31). The goal of this study was to optimize HNC SC cultivation conditions and observe the effect of autologous PRF and different cultivation media on gross quality, viability, and composition of cell types in SC over a period of 7 days. This study was intended to set the ground works for stable culturing conditions over a course of several days, when effects of cytotoxic drugs and check point inhibitors are to be studied in close to real life *in vitro* conditions.

4.1 SC area and cell density, viability and proportions on day 1 and day 7

Gross slice quality, as estimated by HE stainings, remained stable for 7 days with intact structure, discernible cell types, and only a few necrotic areas. An earlier cultivation cut-off due to reduced SC quality, as described by Gerlach and coauthors, was not

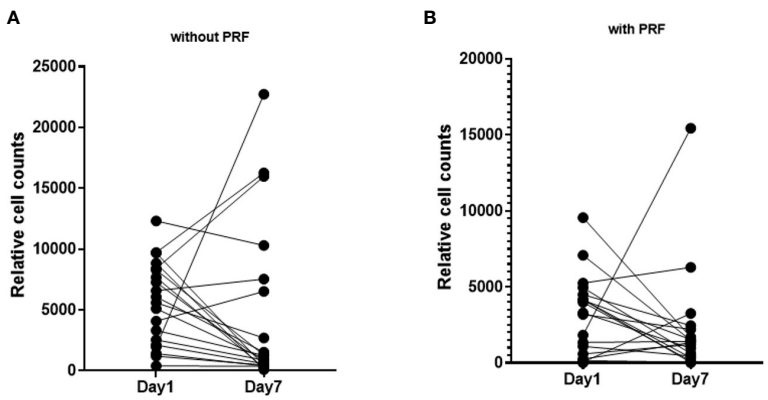

FIGURE 4
Pairwise visualization of slice cultures after 1 day and on day 7 without and with PRF. **(A)** Cell density of slice cultures without PRF on day 1 and day 7. **(B)** Cell density of slice cultures with PRF on day 1 and day 7.

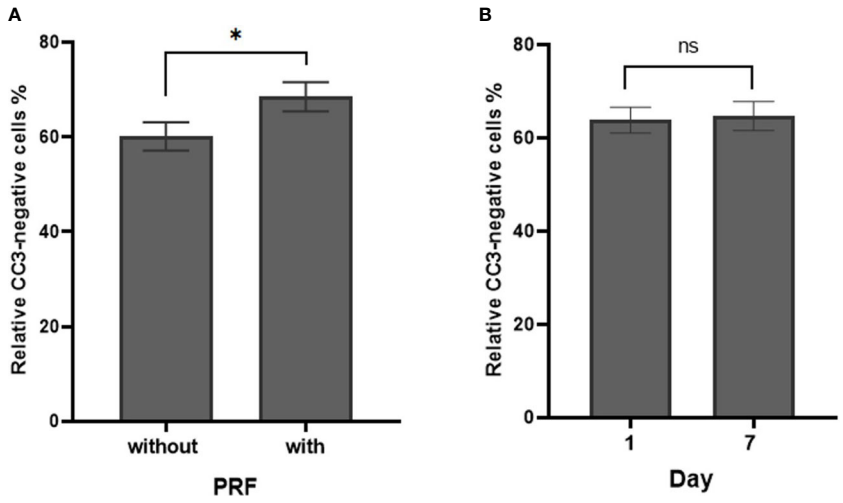

FIGURE 5
Cell density of CC3-negative stained cells in percentage in dependence of PRF and culture time. **(A)** Percentage of relative CC3-negative stained cells without and with PRF in percent (p=0.05). **(B)** Percentage of relative CC3-negative stained cells on day 1 and day 7 (p=0.834). (*significant at the 0.1 level, ns, not significant; Bars: SEM).

necessary (29). However, culturing time influenced SC total area and SC cell density. The initial cutting process may trigger inflammatory immune responses in SC, and modify cell growth and/or survival. While the TME can remain intact, SC total area may decrease over the course of 7 days, as observed in this and previous studies (29, 37, 40). However, viability and cell proportions, including the tumor cells as primary therapeutic targets, did not vary greatly between day 1 and day 7. As a result, future preclinical targeted therapeutic trials using HNC SC may be less biased by *in vitro* cell death or shifts in cell proportions. Still, according to our observations and similar earlier studies, SC quality is best preserved after 24-48 hours. Thus experiments need to be performed at early time points in the culturing period for optimal results (31). Finally, the impact of decreased SC size should be

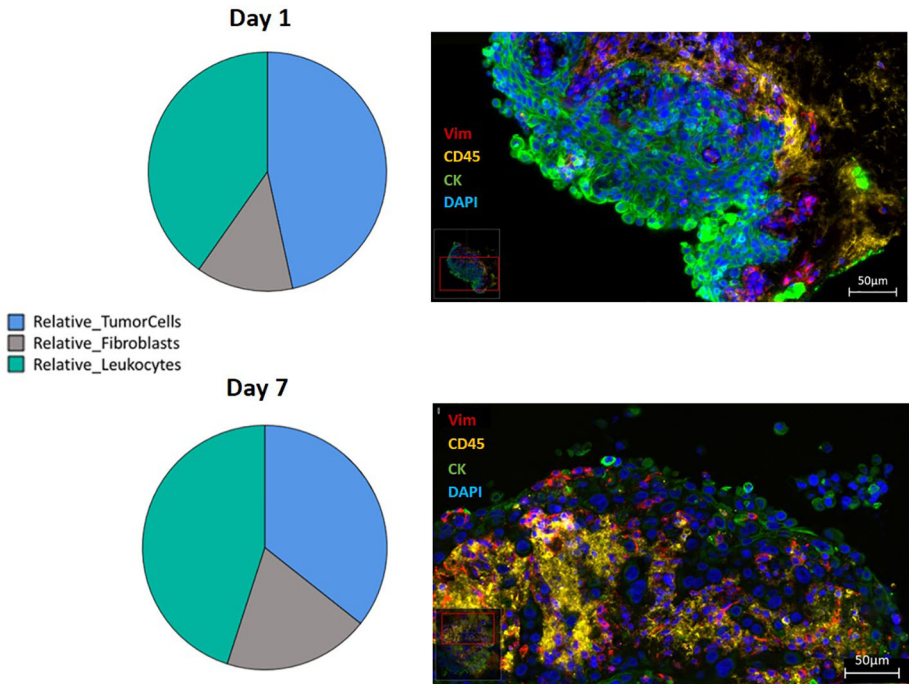

FIGURE 6
Relative distribution of the three different cell types, presented in a pie-diagram and IF triple staining using direct conjugated antibodies (CD45 conjugated with Alexa Fluor 594 presented in yellow, vimentin conjugated with eFluor 570 presented in red, pan-cytokeratin conjugated with Alexa Fluor 488 presented in green and counterstained with DAPI presented in blue) of SC from HNSCC at day 1 and day 7 (400 times magnification; Scale bars: 50µm).

considered when calculating the effect of cytotoxic or immune modulating therapies in HNC SC.

4.2 SC area, cell viability, density and proportions with and without PRF

However, the addition of PRF was beneficial for preserving the SC total areas (p=0.023) and cell viability over several days. Similar effects have been observed in SC with fetal bovine serum (FBS) in other studies (41). FBS is a widely used cultivation medium rich in growth factors, but its use is not encouraged due to ethical concerns and the presence of highly variable amounts of xenogeneic components which may cause adverse immunological effects. Autologous growth factors, like those contained in PRF, may contribute to conservation of the original tumor size and cell viability by stimulating a biologically active "in situ" environment.

After 7 days and addition of PRF, an overall lower cell density was observed (Figure 4). Still, cell density increased in some SC, regardless of PRF. Standardization of growth factors and cell counts both in PRF and in HNC SC is hardly feasible, considering the means of material collection. As a result, cell counts may vary during longer cultivation periods.

According to our findings, PRF may have a stabilizing effect on cell proportions in HNC SC, even during longer cultivation periods. This finding contradicts observations of cell proliferation of osteoblasts and fibroblasts (42, 43). However, remodeling may occur after time frames longer than 7 days, which was beyond the scope of this study.

4.3 SC area and cell density, viability and proportions in different cultivation media

Cultivation media on the other hand had no such impact on the SC total area, cell density or viability. Keratinocyte SFM supposedly supports the growth of anchorage independent cancer stem cells and epithelial cells in cell cultures and spheroids. This medium contains all essential nutrients and supplements for culturing. Addition of FBS is not necessary, rendering cultivation conditions consistent throughout the whole experiment. RPMI on the other hand was supplemented with additional FBS. This medium is known to promote the growth of many different cell types, esp. fibroblasts and leukocytes in culture (44). In our study, Keratinocyte SFM, RPMI +FBS and the 1:1 mix of both did not promote any specific cell type in HNSCC SC. However, this may be different for primary cell culture. Robust cell viability regardless of cultivation media may be attributed to preservation of intercellular signaling and contacts as well as protective structures such as extracellular matrix in the tumor microenvironment of the HNSCC SC. Our results reveal that out of the three media, Keratinocyte SFM would be beneficial for SC culturing, due to its neutral effects and FBS-free conditions.

For future experiments, frequent SC movement during the culturing period should be considered. Kishan et al. observed facilitated nutrient exchange between the medium and SC and increased cell proliferation in floating SC installed in a shaker (45). These results may be applicable to tumors that are subject to passive nutrient distribution by constant muscle action, such as those in the head and neck region.

4.4 Strengths

HNC is characterized by heterogeneity in terms of patient and tissue characteristics, which can be fully represented in HNC SC. A cultivation period of up to 7 days allows for sufficient observation of treatment effects. Cultivation media seem to be interchangeable without generating major changes in the SC. A standard biopsy of > 4 mm^3, taken during routine endoscopy under anesthesia, procures up to 12 slices with 300 µm. Out of these slices it was possible to generate 94 SC with good quality.

4.5 Limitations

The majority (94) of the planned 108 slices were applicable for cultivation. However, some slices were lost due to squashing or disintegration during initial cutting and staining or after cultivation for 7 days. Therefore, despite the already good quality slice cultures the application of the Compresstome® vibrating microtome (Precisionary, MA, USA) yielded a high number of slices for further processing and statistically significant results (unpublished additional information). The consistency of tumor tissue was highly variable, and some samples were harder to cut than others. Consequently, an individual quality scoring had to be established to estimate SC quality, which was subject to observational bias and may have led to exclusion of further samples to achieve comparability. Additional input parameters, such as movement, longer incubation time, and additional media may be necessary to further optimize HNC SC conditions.

5 Conclusions

Despite high inter-individual variations in texture and cellular proportions, cultivation of HNSCC slice cultures up to 7 days with a useful number of viable cells is possible. As cultivation media did not impact SC quality, HNC SC may be highly versatile tools for studying physiology and drug effects in HNC. The addition of PRF provides an environment comparable to *in situ* conditions of the tumor and further stabilizes SC size and cell proportions. These results may aid in future experiments on patient-based therapy planning.

Data availability statement

The raw data supporting the conclusions of this article will be made available by the authors, without undue reservation.

Ethics statement

The studies involving human participants were reviewed and approved by Ethics committee of the Medical University of Innsbruck. The patients/participants provided their written informed consent to participate in this study.

Author contributions

MG - methodology, investigation, data curation, writing- original draft, review and editing, visualization, project administration, formal analysis. AnR – methodology, investigation, writing- original draft, writing- review and editing, project administration, project administration, formal analysis. JD - methodology, investigation, data curation, resources, writing- editing, project administration. LC - investigation, data curation, formal analysis, writing- original draft. AvR - interpretation of data, formal analysis, writing-review and editing. MM - conceptualization, methodology, formal analysis, writing- review and editing. MP - methodology, investigation, resources, writing- review and editing. HR - Conceptualization, methodology, formal analysis, data curation, supervision, validation, writing-review and editing. VS - conzeptualization, material acquisition, writing- review and editing. All authors contributed to the article and approved the submitted version.

Funding

This research project was financially funded by ViraTherapeutics GmbH. Acquisition, Production and laboratory culturing set up of Head and Neck Cancer Slice Cultures as described in this paper was establised in cooperation with ViraTherapeutics GmbH. The funder was not involved in the study design, collection, analysis, interpretation of data, the writing of this article or the decision to submit it for publication.

Conflict of interest

Authors MM and MP were employed by ViraTherapeutics GmbH.

The remaining authors declare that the research was conducted in the absence of any commercial or financial relationships that could be construed as a potential conflict of interest.

Publisher's note

Supplementary material

The Supplementary Material for this article can be found online at: https://www.frontiersin.org/articles/10.3389/fonc.2023.1145817/full#supplementary-material

References

1. Johnson DE, Burtness B, Leemans CR, Lui VWY, Bauman JE, Grandis JR. Head and neck squamous cell carcinoma. *Nat Rev Dis Primers* (2020) 6(1). doi: 10.1038/s41572-020-00224-3

2. Lin C. J., Grandis J. R., Carey T. E., Gollin S. M., Whiteside T. L., Koch W. M., et al. Head and neck squamous cell carcinoma cell lines: Established models and rationale for selection. *Head & neck* (2007) 29(2):163–188. doi: 10.1002/hed.20478

3. Fontana F, Marzagalli M, Sommariva M, Gagliano N, Limonta P. *In vitro* 3D cultures to model the tumor microenvironment. *Cancers (Basel)* (2021) 13(12). doi: 10.3390/cancers13122970

4. Duval K, Grover H, Han LH, Mou Y, Pegoraro AF, Fredberg J, et al. Modeling physiological events in 2D vs. 3D cell culture. *Physiol (Bethesda)* (2017) 32(4):266–77. doi: 10.3390/cancers13122970

5. Franchi-Mendes T, Eduardo R, Domenici G, Brito C. 3D cancer models: Depicting cellular crosstalk within the tumour microenvironment. *Cancers (Basel)* (2021) 13(18):1–49. doi: 10.3390/cancers13184610

6. Palechor-Ceron N, Krawczyk E, Dakic A, Simic V, Yuan H, Blancato J, et al. Conditional reprogramming for patient-derived cancer models and next-generation living biobanks. *Cells* (2019) 8(11). doi: 10.3390/cells8111327

7. Roma-Rodrigues C, Mendes R, Baptista PV, Fernandes AR. Targeting tumor microenvironment for cancer therapy. *Int J Mol Sci* (2019) 20(4). doi: 10.3390/ijms20040840

8. Carter EP, Roozitalab R, Gibson SV, Grose RP. Tumour microenvironment 3D-modelling: Simplicity to complexity and back again. *Trends Cancer* (2021) 7(11):1033–46. doi: 10.1016/j.trecan.2021.06.009

9. Majumder B, Baraneedharan U, Thiyagarajan S, Radhakrishnan P, Narasimhan H, Dhandapani M, et al. Predicting clinical response to anticancer drugs using an *ex vivo* platform that captures tumour heterogeneity. *Nat Commun* (2015) 6(1):1–14. doi: 10.1038/ncomms7169

10. Giraldo NA, Sanchez-Salas R, Peske JD, Vano Y, Becht E, Petitprez F, et al. The clinical role of the TME in solid cancer. *Br J Cancer* (2019) 120(1):45–53. doi: 10.1038/s41416-018-0327-z

11. Demers I, Donkers J, Kremer B, Speel EJ. *Ex vivo* culture models to indicate therapy response in head and neck squamous cell carcinoma. *Cells* (2020) 9(11):1–27. doi: 10.3390/cells9112527

12. Dudás J, Bitsche M, Schartinger V, Falkeis C, Sprinzl GM, Riechelmann H. Fibroblasts produce brain-derived neurotrophic factor and induce mesenchymal transition of oral tumor cells. *Oral Oncol* (2011) 47(2):98–103. doi: 10.1016/j.oraloncology.2010.11.002

13. Yamaguchi R, Perkins G. Animal models for studying tumor microenvironment (TME) and resistance to lymphocytic infiltration. *Cancer Biol Ther* (2018) 19(9):745–54. doi: 10.1080/15384047.2018.1470722

14. Lee TW, Lai A, Harms JK, Singleton DC, Dickson BD, Macann AMJ, et al. Patient-derived xenograft and organoid models for precision medicine targeting of the tumour microenvironment in head and neck cancer. *Cancers* (2020) 12(12):1–20. doi: 10.3390/cancers12123743

15. Drost J, Clevers H. Organoids in cancer research. *Nat Rev Cancer* (2018) 18(7):407–18. doi: 10.1038/s41568-018-0007-6

16. Sontheimer-Phelps A, Hassell BA, Ingber DE. Modelling cancer in microfluidic human organs-on-chips. *Nat Rev Cancer* (2019) 19(2):65–81. doi: 10.1038/s41568-018-0104-6

17. Xie H, Appelt JW, Jenkins RW. Going with the flow: Modeling the tumor microenvironment using microfluidic technology. *Cancers (Basel)* (2021) 13(23):1–26. doi: 10.3390/cancers13236052

18. Li XJ, Valadez AV, Zuo P, Nie Z. Microfluidic 3D cell culture: potential application for tissue-based bioassays. *Bioanalysis* (2012) 4(12):1509–25. doi: 10.4155/bio.12.133

19. Liu X, Fang J, Huang S, Wu X, Xie X, Wang J, et al. Tumor-on-a-chip: from bioinspired design to biomedical application. *Microsyst Nanoeng* (2021) 7:50. doi: 10.1038/s41378-021-00277-8

20. Sun W, Luo Z, Lee J, Kim HJ, Lee K, Tebon P, et al. Organ-on-a-Chip for cancer and immune organs modeling. *Advanced healthcare materials* (2019) 8(4):e1801363. doi: 10.1002/adhm.201801363

21. Breslin S, O'Driscoll L. Three-dimensional cell culture: the missing link in drug discovery. *Drug Discovery Today* (2013) 18(5):240–9. doi: 10.1016/j.drudis.2012.10.003

22. Samavedi S, Joy N. 3D printing for the development of *in vitro* cancer models. *Curr Opin Biomed Eng* (2017) 2:35–42. doi: 10.1016/j.cobme.2017.06.003

23. Tinhofer I, Braunholz D, Klinghammer K. Preclinical models of head and neck squamous cell carcinoma for a basic understanding of cancer biology and its translation into efficient therapies. *Cancers Head Neck* (2020) 5:9. doi: 10.1186/s41199-020-00056-4

24. Hagemann J, Jacobi C, Gstoettner S, Welz C, Schwenk-Zieger S, Stauber R, et al. Therapy testing in a spheroid-based 3D cell culture model for head and neck squamous cell carcinoma. *J visualized experiments JoVE* (2018) 134). doi: 10.3791/57012

25. Katt ME, Placone AL, Wong AD, Xu ZS, Searson PC. *In vitro* tumor models: Advantages, disadvantages, variables, and selecting the right platform. *Front Bioeng Biotechnol* (2016) 4:12. doi: 10.3389/fbioe.2016.00012

26. Kenerson HL, Sullivan KM, Seo YD, Stadeli KM, Ussakli C, Yan X, et al. Tumor slice culture as a biologic surrogate of human cancer. *Ann Trans Med* (2020) 8:114. doi: 10.21037/atm.2019.12.88

27. Cavaliere F, Benito-Muñoz M, Matute C. Organotypic cultures as a model to study adult neurogenesis in CNS disorders. *Stem Cells Int* (2016) 2016:3540568. doi: 10.1155/2016/3540568

28. Miserocchi G, Cocchi C, De Vita A, Liverani C, Spadazzi C, Calpona S, et al. Three-dimensional collagen-based scaffold model to study the microenvironment and drug-resistance mechanisms of oropharyngeal squamous cell carcinomas. *Cancer Biol Med* (2021) 18(2):502–16. doi: 10.20892/j.issn.2095-3941.2020.0482

29. Gerlach MM, Merz F, Wichmann G, Kubick C, Wittekind C, Lordick F, et al. Slice cultures from head and neck squamous cell carcinoma: A novel test system for drug susceptibility and mechanisms of resistance. *Br J Cancer* (2014) 110:479–88. doi: 10.1038/bjc.2013.700

30. Engelmann L, Thierauf J, Koerich Laureano N, Stark HJ, Prigge ES, Horn D, et al. Organotypic Co-cultures as a novel 3D model for head and neck squamous cell carcinoma. *Cancers (Basel)* (2020) 12(8):1–20. doi: 10.3390/cancers12082330

31. Runge A, Mayr M, Schwaiger T, Sprung S, Chetta P, Gottfried T, et al. Patient-derived head and neck tumor slice cultures: A versatile tool to study oncolytic virus action. *Sci Rep* (2022) 12(1):15334. doi: 10.1038/s41598-022-19555-0

32. Dohle E, El Bagdadi K, Sader R, Choukroun J, James Kirkpatrick C, Ghanaati S. Platelet-rich fibrin-based matrices to improve angiogenesis in an *in vitro* co-culture model for bone tissue engineering. *J Tissue Eng regenerative Med* (2018) 12:598–610. doi: 10.1002/term.2475

33. Giannini S, Cielo A, Bonanome L, Rastelli C, Derla C, Corpaci F, et al. Comparison between PRP, PRGF and PRF: Lights and shadows in three similar but different protocols. *Eur Rev Med Pharmacol Sci* (2015) 19:927–30.

34. Dereli Can G, Akdere ÖE, Can ME, Gümüşderelioğlu M. A simple and efficient method for cultivation of limbal explant stem cells with clinically safe potential. *Cytotherapy* (2019) 21:83–95. doi: 10.1016/j.jcyt.2018.11.005

35. Humpel C. Organotypic brain slice cultures: A review. *Neuroscience* (2015) 305:86–98. doi: 10.1016/j.neuroscience.2015.07.086

36. Lechner M, Schartinger VH, Steele CD, Nei WL, Ooft ML, Schreiber L-M, et al. Somatostatin receptor 2 expression in nasopharyngeal cancer is induced by Epstein Barr virus infection: Impact on prognosis, imaging and therapy. *Nat Commun* (2021) 12(1):117. doi: 10.1038/s41467-020-20308-8

37. Giotakis AI, Dudas J, Glueckert R, Dejaco D, Ingruber J, Fleischer F, et al. Characterization of epithelial cells, connective tissue cells and immune cells in human upper airway mucosa by immunofluorescence multichannel image cytometry: A pilot study. *Histochem Cell Biol* (2021) 155(3):405–21. doi: 10.1007/s00418-020-01945-y

38. Fischer N., Mathonia N. M., Hoellerich G., Veser J., Pinggera L., Dejaco D., et al. Surviving murine experimental sepsis affects the function and morphology of the inner ear. *Biol open* (2017) 6(6):732–40. doi: 10.1242/bio.024588

39. Steinbichler TB, Dudas JA-O, Ingruber J, Glueckert R, Sprung S, Fleischer F, et al. Slug is a surrogate marker of epithelial to mesenchymal transition (EMT) in head and neck cancer. *J Clin Med* (2020) 9(7):2061. doi: 10.3390/jcm9072061

40. Jiang X, Seo YD, Sullivan KM, Pillarisetty VG. López-Soto A, Folgueras AR, editors. *Cancer immunosurveillance: Methods and protocols*. New York, NY: Springer New York (2019). p. 283–95.

41. Nußbaum SM, Krabbe J, Böll S, Babendreyer A, Martin C. Functional changes in long-term incubated rat precision-cut lung slices. *Respir Res* (2022) 23(1):261. doi: 10.1186/s12931-022-02169-5

42. Dohan Ehrenfest DM, Doglioli P, Fau - de Peppo GM, de Peppo Gm, Fau - Del Corso M, Del Corso M, et al. Choukroun's platelet-rich fibrin (PRF) stimulates *in vitro* proliferation and differentiation of human oral bone mesenchymal stem cell in a dose-dependent way. *Arch Oral Biol* (2010) 55(3):185–94. doi: 10.1016/j.archoralbio.2010.01.004

43. Strauss FJ, Nasirzade J, Kargarpoor Z, Stahli A, Gruber R. Effect of platelet-rich fibrin on cell proliferation, migration, differentiation, inflammation, and osteoclastogenesis: A systematic review of *in vitro* studies. *Clin Oral Investig* (2020) 24(2):569–84. doi: 10.1007/s00784-019-03156-9

44. Goričan L, Gole B, Potočnik U. Head and neck cancer stem cell-enriched spheroid model for anticancer compound screening. *Cells* (2020) 9(7):1–18. doi: 10.3390/cells9071707

45. Naipal KA, Verkaik NS, Sánchez H, van Deurzen CH, den Bakker MA, Hoeijmakers JH, et al. Tumor slice culture system to assess drug response of primary breast cancer. *BMC Cancer* (2016) 16:78. doi: 10.1186/s12885-016-2119-2

frontiers | Frontiers in Oncology

TYPE Review
PUBLISHED 11 April 2023
DOI 10.3389/fonc.2023.1135401

OPEN ACCESS

EDITED BY
Giulia Adriani,
Singapore Immunology Network (A*STAR), Singapore

REVIEWED BY
Ioannis Zervantonakis,
University of Pittsburgh, United States
Manuela Santarosa,
CRO Aviano (IRCCS), Italy
Michele Zanoni,
Scientific Institute of Romagna for the Study and Treatment of Tumors (IRCCS), Italy

*CORRESPONDENCE
Simone Bersini
simone.bersini@eoc.ch
Matteo Moretti
matteo.moretti@eoc.ch

†These authors have contributed equally to this work and share last authorship

SPECIALTY SECTION
This article was submitted to Molecular and Cellular Oncology, a section of the journal Frontiers in Oncology

RECEIVED 31 December 2022
ACCEPTED 27 March 2023
PUBLISHED 11 April 2023

CITATION
Lamouline A, Bersini S and Moretti M (2023) *In vitro* models of breast cancer bone metastasis: analyzing drug resistance through the lens of the microenvironment. *Front. Oncol.* 13:1135401. doi: 10.3389/fonc.2023.1135401

In vitro models of breast cancer bone metastasis: analyzing drug resistance through the lens of the microenvironment

Anaïs Lamouline[1,2,3], Simone Bersini[1,2,4*†] and Matteo Moretti[1,2,4,5*†]

[1]Regenerative Medicine Technologies Laboratory, Laboratories for Translational Research (LRT), Ente Ospedaliero Cantonale (EOC), Bellinzona, Switzerland, [2]Service of Orthopaedics and Traumatology, Department of Surgery, EOC, Lugano, Switzerland, [3]Department of Electronics, Information and Bioengineering, Politecnico di Milano, Milano, Italy, [4]Euler Institute, Faculty of Biomedical Sciences, Università della Svizzera italiana (USI), Lugano, Switzerland, [5]Cell and Tissue Engineering Laboratory, IRCCS Istituto Ortopedico Galeazzi, Milano, Italy

Even though breast cancers usually have a good outcome compared to other tumors, the cancer can progress and create metastases in different parts of the organism, the bone being a predilection locus. These metastases are usually the cause of death, as they are mostly resistant to treatments. This resistance can be caused by intrinsic properties of the tumor, such as its heterogeneity, but it can also be due to the protective role of the microenvironment. By activating signaling pathways protecting cancer cells when exposed to chemotherapy, contributing to their ability to reach dormancy, or even reducing the amount of drug able to reach the metastases, among other mechanisms, the specificities of the bone tissue are being investigated as important players of drug resistance. To this date, most mechanisms of this resistance are yet to be discovered, and many researchers are implementing *in vitro* models to study the interaction between the tumor cells and their microenvironment. Here, we will review what is known about breast cancer drug resistance in bone metastasis due to the microenvironment and we will use those observations to highlight which features *in vitro* models should include to properly recapitulate these biological aspects *in vitro*. We will also detail which elements advanced *in vitro* models should implement in order to better recapitulate *in vivo* physiopathology and drug resistance.

KEYWORDS

drug resistance, breast cancer, bone metastasis, organ-on-a-chip, tumor microenvironment

1 Introduction

According to the World Health Organization, breast cancer is the most common cancer worldwide as of 2020, with the number of diagnoses having nearly doubled in the last two decades. Breast cancer is the second most deadly cancer amongst women, with mortality being especially high in countries with low income and in women of color (1–3). If the cancer is caught early enough, the treatments are usually very effective. However, breast cancer frequently metastasizes to bones, especially for the more advanced cases, rendering conventional treatments ineffective as metastases poorly respond to chemotherapy (4). Around 70% of the patients with advanced cancer will develop bone metastases (5).

It is now commonly accepted that breast cancer colonizes the bone according to the "seed and soil" theory proposed by Stephen Paget in 1889. According to this hypothesis, certain secondary organs such as the bone are better "soils" than others and are more at risk of developing metastases. Moreover, the primary tumor has the capacity to prepare the secondary loci for metastatic colonization, here the bone marrow, then cancer cells migrate towards this newly remodeled microenvironment as disseminated tumor cells (DTCs) through the vascular system. Once in the bone marrow, DTCs can stay quiescent for years before invading the surrounding bone (4). Awakened cancer cells interact with different bone cell populations (e.g. osteoblasts, osteoclasts, immune cells, mesenchymal stromal cells) to hijack and enhance the bone remodeling process in order to benefit their own growth. This process, called the vicious cycle, leads to what are known as osteolytic lesions, which are skeletal-related events linked to a loss of bone that causes debilitating pain for the patient. The bone is also considered a hub for further dissemination, as cancer cells in the bone get primed to further invade other organs (6).

To this date, no treatment to cure bone metastasis exists and only palliative care is available due to the inability to block the vicious cycle, as well as to drug resistance generated by the microenvironment (7). Indeed, it is now well known that the bone and the bone marrow exert a protective effect on cancer cells by shielding them from cytotoxic drugs or even increasing their aggressiveness (7–9). However, there is still a lack of knowledge regarding the specific role that the microenvironment plays in this process. In this context, the gold standard for pre-clinical drug testing (i.e. 2D assays in mono or coculture) cannot give enough information to accurately predict the effect of a drug. For example, 2D assays cannot recapitulate the bone remodeling process, even though the vicious cycle is one of the main reasons for the aggressiveness of bone metastasis. These models are also unable to properly recapitulate drug pharmacokinetics due to their lack of 3D perfusable blood vessels and extracellular matrix (ECM). The results obtained with traditional 2D assays are then generally validated in rodents, which have a different physiology compared to humans. Hence, the impact of the human tumor microenvironment is underestimated or even neglected during the first steps of the drug development process (10). For example, mouse/rat models have a vastly different immune system compared to humans, which affects the cancer progression as well as the metabolic reaction to anti-cancer drugs (11). Rodents also rarely form spontaneous metastases to bones (12). On top of that, animal models do not allow to easily perform parametric studies in high-throughput like removing or adding specific cell types to study a particular feature of the microenvironment. 3D human models hence represent a valuable tool to complement current pre-clinical drug testing approaches in order to more efficiently identify novel therapies. Indeed, these models can include various human cell types embedded in an ECM-like environment and allow for the high-throughput study of various biological mechanisms in a controlled and customizable setting, hence effectively predicting cancer cell behavior in response to drugs (13). The reader can refer to the following reviews for more details on the various existing 3D modeling techniques focused on oncology and drug screening (14–16). Even though it is currently not possible to completely bypass the use of animal models in drug testing, screening and analysis in every field, it is likely that the prevalence of complex *in vitro* models could reduce or even replace the requirement of systematic *in vivo* experiments in the next decades. For example, a recent study on liver toxicology showed that an organ-on-a-chip model outperformed conventional models, highlighting hepatotoxic reactions that were missed in animal models (17). Therefore, having a better comprehension of the interactions occurring in human tissues would most likely benefit the research community and potentially optimize the drug discovery pipeline.

In this review, we analyze the role of the bone microenvironment in the onset of drug resistance during the progression of breast cancer with the final goal to highlight which components and specifications 3D human bone models should include to properly recapitulate clinical observations.

2 Breast cancer bone metastasis and treatment

The development of bone metastases is associated with a poor prognosis: at this date, no cure exists and only palliative treatments are available. Moreover, the symptoms associated with bone metastases are very debilitating. They include severe pain, pathological fractures, nerve compression syndrome and hypercalcemia, all of them severely impairing the patient's quality of life (18).

The process of bone metastasis formation is usually described with three steps, where the role of the microenvironment is tightly linked to the development of metastases. Firstly, the pre-metastatic niche is created. This process allows for the cancer cells to remotely influence the microenvironment of foreign tissues to facilitate future colonization by recruiting specific cancer-associated cells to remodel the ECM and create an immune-suppressive environment. Then, "educated" stromal cells facilitate the extravasation and attachment of DTCs (19). This process is driven by the interaction between cancer cell receptors with blood vessel surface ligands as well as with specific ECM proteins (e.g. laminins, fibronectin, vitronectin, osteopontin (OPN), bone sialoprotein). Indeed, these ECM proteins contain the arginylglycylaspartic acid

(RGD) tripeptide that can be recognized by cancer cell surface proteins (e.g. integrins $\alpha_v\beta_3$ and $\alpha_4\beta_1$, C-X-C chemokine receptor 4 (CXCR4), CD44) (20, 21). Cancer cells finally settle in the bone marrow niches (i.e. perivascular and endosteal), where they can remain dormant for years or even decades. During dormancy, these cells do not replicate and are able to evade the action of chemotherapy (22).

Once awakened, these metastases disrupt the bone remodeling process by enhancing bone resorption by osteoclasts and decreasing bone formation by osteoblasts. This process, called vicious cycle, is due to an increased bone resorption which releases growth factors that further stimulate metastasis growth (21, 23). Current therapies are generally initiated when overt metastases are already present and challenging to eradicate, mainly due to the onset of microenvironment-mediated drug resistance (9).

Breast cancer often becomes resistant to common therapies (24). For estrogen receptor positive (ER+) tumors, the first line treatment includes ER modulators or down-regulators. Currently, there are 6 drugs on the market targeting ER+ tumors. Most of these drugs are recommended to be used in combination with aromatase inhibitors, which are molecules that act directly on the estrogen production (24). Furthermore, 5 drugs are currently available for patients with human epidermal growth factor receptor 2 (HER2) positive tumors, all of them targeting either the extracellular or intracellular domain of this protein (24). Finally, 19 chemotherapy compounds have been approved for treatment, either as neoadjuvant or adjuvant drugs (i.e. before or after surgery resection, respectively), or for metastatic breast cancer. Though combinations of drugs are usually administered for an early-stage breast cancer, it appears that patients with metastatic cancer are usually administered the drugs one at a time, with 9 drugs most commonly prescribed (24, 25). All therapies and their effects are detailed in Table 1.

Bone metastasis can also be targeted using radiotherapy and immunotherapy. The latter treatment targets immune checkpoints such as programmed cell death protein-1 (PD-1), PD-ligand 1 (PD-L1) and cytotoxic T-lymphocyte–associated antigen 4 (CTLA-4). Immunotherapy has been approved in many cancers, sometimes at stage IV [such as metastatic bladder cancer (26)], and even as a pan-cancer treatment for the anti-PD1 antibody Pembrolizumab (as long as the cancer has microsatellite instability) (27). For more details, the reader can refer to these reviews (27–29). However, targeting bone metastases with immunotherapies has been challenging and to this date no systematic review has clearly highlighted the impact of immune checkpoint inhibitors. Indeed, despite the high number of immune cells in the bone marrow, most of them are still immature and cannot overcome cancer cell proliferation (30). Furthermore, the presence of inhibitory immune cells such as myeloid-derived suppressor cells severely impairs the eradication of metastases (30).

Multiple side effects can be observed upon treatment with both chemotherapy and immunotherapy. Regarding chemotherapy, most drugs focus on cells with a short replication time by targeting their DNA. Hence, a high number of normal cells with a high replication rate are also affected. Though the most common side effects are hair loss, soreness and digestive issues, chemotherapy can sometimes target very specific organs like the liver, kidneys, nerves and lungs, causing more debilitating symptoms such as urinary dysfunctions, pain, fatigue and dizziness, or even heart damage (31). Moreover, the higher the dose of chemotherapy, the higher the risk of side effects. For immunotherapy, the side effects commonly observed in chemotherapy (e.g. gastrointestinal diseases, mucositis or myelosuppression) are not or rarely observed. Generally, in around 10% of patients skin reactions and flu-like symptoms are noticed (32). The main side effects leading to casualties observed are colitis, pneumonitis, hepatitis and neurotoxic effects, however they tend to appear at a lower rate than with other treatments (33). Thus, having treatments that could target the microenvironment and increase the sensitivity of cancer cells to chemotherapy could not only impair cancer dissemination but also diminish the risk of side effects.

As of today, there are only two kinds of drugs specifically targeting bone metastases (i.e. Bisphosphates and Denosumab). These drugs are administered in combination with classic anti-cancer drugs. Bisphosphonates are molecules that inhibit the metabolic pathway of mevalonate, resulting in osteoclast apoptosis (34). The most effective and commonly used Bisphosphonate is Zoledronic Acid. This drug binds to hydroxyapatite and is released during bone digestion by osteoclasts. Osteoclasts then absorb it through endocytosis, where it inhibits the mevalonate pathway which is essential for post-translational prenylation of GTP-binding proteins. On the other hand, Denosumab is a monoclonal antibody that binds to RANK-L and inhibits the recruitment of osteoclasts (3). Both Bisphosphonates and Denosumab are palliative treatments that reduce pain and improve the quality of life of patients. However, their contribution to completely eradicate skeletal-related events (SREs) is limited. Moreover, these drugs are associated with side effects such as renal impairment and acute-phase reactions for Zoledronic Acid, and hypocalcaemia and osteonecrosis of the jaw for Denosumab (35).

Because anti-cancer treatments generally do not take into account the role of the bone microenvironment, with the exception of the partially effective Denosumab and Zoledronic Acid, it is emerging the concept that the next generation of therapies should combine traditional anti-cancer therapies with novel molecules targeting the other cell populations involved in the metastatic growth. In this scenario, the design of advanced *in vitro* 3D models recapitulating the metastatic bone microenvironment could significantly improve the identification of novel targets and the design of more effective combination therapies. The integration of these models with traditional animal studies could significantly increase the efficiency of the drug development pipeline and effectively identify mechanisms of drug resistance. For example, introducing 3D models as an effective high-throughput screening assay would help to determine with more efficacy which drugs or combinations have an impact on the disease progression. In

TABLE 1 Classification of currently available drugs targeting different breast cancer subtypes.

Type	Name of the drug	Name of molecule	Target	Effect	Side effects	Current use
Endocrine therapy for HR+ tumors	Novaldex (pill) Soltamox (liquid)	Tamoxifen	ER	Selective ER modulator	Blood clots, stroke, endometrial cancer	Most prescribed Early and advanced stage 5-10 year long treatment
	Faslodex	Fulverstrant	ER	Prevent oestrogen from biding to CCs -> ER down-regulators		ERBB2- No previous endocrine therapy Can be taken alone or with Ibrance
	Afinitor	Everolimus	FKBP12	mTOR inhibition -> restore sensitivity to ER treatments	Stomatitis, rash	Accepted by FDA with exemestane (aromatase inhibitor)
	Ibrance	Palbociclib	CDK4/6 inhibitors	Stop cell division	Lung, neutropenia (low count of white blood cells), blood clots	Used in combination with Faslodexinhibitor for advanced-stage or metastatic ERBB2-
	Kisqali	ribociclib			cardiotoxic, liver, lung issues, neutropenia	
	Verzenio	Abemaciclib			Blood clots & inflammation in the lungs	End of phase III for early high-risk to decrease the risk of relapse + combined with endocrine therapy
Therapy for ERBB2+ (HER2+) tumors	Herceptin	Trastuzumab	Extracellular domain of ERBB2	Slow/stop CC growth + alert immune system	cardiotoxic & lung issues	FDA approved for metastatic cancer
	Perjeta	Pertuzumab	Anti-ERBB2 Ab	Inhibits tumor growth	Cardiac dysfunction	Can be used in combination with trastuzumab
	Kadcyla	T-DM1 = herceptin + emtansine	chemo + ERBB2 target	action of emtansine without the extremely harmful side effects	cardiotoxic, lung and liver issues	FDA approved for advanced or metastatic
	Nerlynx	Neratinib	irreversible pan-HER chemical inhibitor	Inhibits tumor growth	renal impairement	FDA approved with capecitabine advanced or metastatic
	Tykerb	Lapatinib	small-molecule tyrosine kinase inhibitor	blocks ERBB2 inside the cell	small cardiotoxic issues	FDA approved with capecitabine or aromatase inhibitor Femara for advanced or metastatic
Chemotherapy	Adrucil	5-fluorouracil	DNA	antimetabolite - kills cancer cell during division	Neutropenia	Used with other chemotherapies Early or advanced
	Abraxane	Albumin-bound Taxane	Microtubules	Prevent cell division	Neutropenia, neuropathy	Used with other chemotherapies Advanced
	Adriamycin & Doxil	Doxorubicin Anthracycline	DNA	Block transcription + ROS production	cardiotoxic & leukemogenic	Early and advanced BC
	Cerubidine & DaunoXome	Daunorubicin Anthracycline	DNA	Block transcription + ROS production	cardiotoxic & leukemogenic	Early and advanced BC
	Cytoxan	Cyclophosphamide	DNA	Alkylating agent	Neutropenia	Advanced BC
	Ellence	epirubicin Anthracycline	DNA	Block transcription + ROS production	cardiotoxic & leukemogenic	Advanced or early BC
	Gemzar	Gemcitabine	DNA	antimetabolite	Neuropenia, anemia	Metastatic Used with other treatments

(Continued)

TABLE 1 Continued

Type	Name of the drug	Name of molecule	Target	Effect	Side effects	Current use
	Halaven	Eribulin	microtubules	Prevent cell division	Neutropenia, neuropathy, anemia	Metastatic BC that stopped responding to other treatments
	Ixempra	Ixabepilone	Tubulin	Prevent cell division		Metastatic Alone or with Xeloda
	Lynparza	Olaparib	PARP enzyme inhibitor	prevent PARP from reparing DNA damages	BM failure, leukemia, anemia, neutropenia	ERBB2-, BRCA1 or BRCA2+ Already treated with chemotherapy molecules
	Mexate, Folex, Rheumatrex	Methotrexate = amethopterin	DNA	antimetabolite		Advanced Used with other chemotherapy molecules
	Navelbine	Vinorelbine	microtubules	Vinca alkaloid blocks beta-tubulin	Neutropenia	Advanced
	Novantrone	Mitoxantrone Anthracycline	DNA	Block transcription + ROS production	cardiotoxic & leukemogenic	Advanced BC
	Talzenna	Talazoparib	Inhibitor of PARP, PARP1 & PARP2 (that repair DNA)	prevent PARP from reparing DNA damages	BM failure, leukemia, anemia, netropenia, thrombocytopenia	ERBB2-, BRCA1 or BRCA2+ metastatic
	Taxol	Paclitaxel Taxane	antimitotic drug	Prevent cell division	Neutropenia	Most widely used anticancer drug
	Taxotere	Docetaxel Taxane	microtubules	Prevent cell division	Neutropenia, neuropathy	Advanced metastatic BC after other treatments
	Tecentriq	Atezolizumab	PD-L1 inhibitor	Allow T cells to kill the cancer cells by blockig the PD-1/PD-L1 interaction	Lung, liver, colon, hormone glands, cardiotoxic issues Neutropenia, neuropathy	FDA approved for metastatic TN , PD-L1+ with Abraxane
	Thioplex	Thiotepa	DNA	Alkylating agent	neutropenia	Advanced BC with other chemo
	Xeloda	Capecitabine	DNA	antimetabolite Converted in cells in 5-FU		Metastatic BC that stopped responding to other treatments
Other	Avastin	Bevacizumab	VEGF	anti-angiogenic	cardiotoxic and kidney neutropenia	FDA approved with Taxol
	Paraplatin	Carboplatin	DNA	Platinum-based Damages the genetic material	kidney damage	advanced BC given in combination with chemotherapy

addition, these models could be a useful tool to tailor the correct drug concentration, also considering potential side effects on the surrounding tissues (16). This approach would also allow to reduce the number of animals tested for each experiment and to limit the risk of testing molecules that were efficient in 2D but not in a 3D organ-specific context.

3 Role of the microenvironment in cancer cell proliferation and drug resistance

Multiple cell types are implicated in the bone metastasis process. Apart from osteoblasts and osteoclasts, additional stromal, vascular, immune and stem/progenitor cells appear to be essential for cancer cell homing, colonization, proliferation, quiescence and drug resistance. Here, we will describe how the bone microenvironment can influence cancer cell proliferation and drug resistance by detailing the role of cancer–associated fibroblasts (CAFs), macrophages, mesenchymal stromal cells, hematopoietic stem cells (HSCs) and adipocytes. Furthermore, we will analyze the contribution that the ECM and its remodeling have in boosting the growth of bone metastases. A graphical abstract of the role of the bone microenvironment in drug resistance is available in Figure 1. A summary of the main mechanisms, pathways and potential therapies in breast cancer bone metastases is compiled in Table 2.

3.1 Osteoblasts

Together with osteoclasts, osteoblasts are known to play a role in the proliferation of bone metastasis since they are involved in the vicious cycle. Osteoblasts tend to show decreased activity and send signals for the recruitment of osteoclasts, leading to enhanced bone

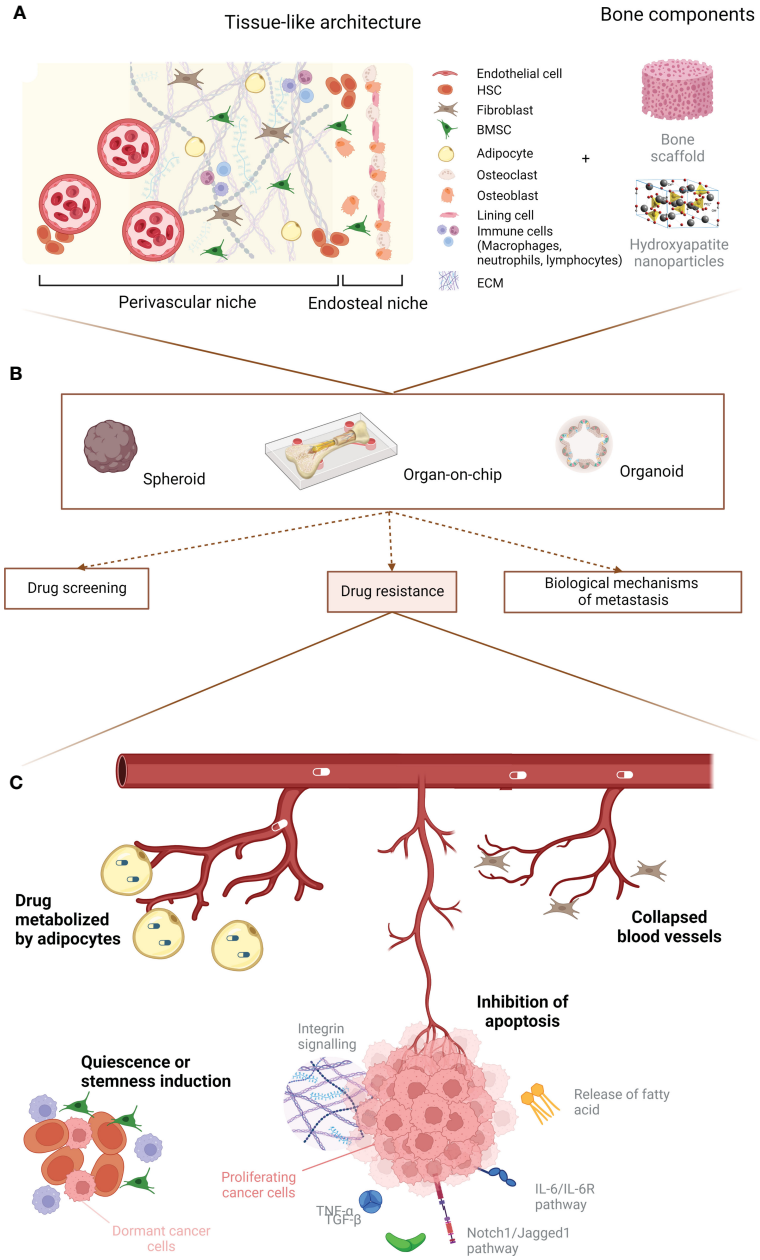

FIGURE 1
Graphical abstract. **(A)** Principal cellular players of the bone microenvironment. **(B)** Main uses for 3D *in vitro* models. **(C)** Summary of the predominant events leading to breast cancer drug resistance due to the microenvironment. Created with BioRender.com.

loss (58). Osteoblasts can also contribute to the survival of cancer cells in the bone, as regulation of calcium intake by cancer cells cannot be done without the presence of osteogenic cells. Indeed, cancer cells cannot efficiently absorb calcium from the microenvironment and a direct cell-cell connection using Connexin 43 is used to transfer calcium ions from osteoblasts to cancer cells (59). In this context, gap junction inhibitors like MEFL or CBX do present a positive outcome in inhibiting this interaction, although as a side effect they are known to increase the vertebral curvature. On the other hand, two already approved drugs (i.e. Danusertib and Arsenic Trioxide) were shown to effectively block this survival mechanism.

Osteoblasts also have a role in breast cancer drug resistance. For example, osteoblasts are known to produce high levels of interleukin (IL)-6 (60), which correlates to Tamoxifen resistance. Inhibition of IL-6Rα with the FDA-approved antibody Tocilizumab was able to sensitize resistant ER+ breast cancer cells to Tamoxifen both *in vitro* and *in vivo* (36). Moreover, direct (through gap junction and calcium signaling) and indirect (through fibroblast growth factor 2 (FGF2) and platelet-derived growth factor-DD (PDGF-DD) secretion) interactions between cancer cells and osteogenic cells leads to a reduction in estrogen receptors. This process translates into a decreased sensitivity of ER+ breast cancer cells to endocrine therapy, which involves an enhancer of zeste homolog 2

TABLE 2 Biological mechanisms and pathways involved in metastatic breast cancer drug resistance.

Cell	General mechanism	Involved pathways (if known)	Potential therapies	Reference number
Osteoblasts	Decreased sensitivity to endocrine therapy due to loss of ER expression	IL-6/STAT3 direct cell-cell contact: gap junctions and Ca2+ signalling FGF2 & PDGF-DD induces EZH2-mediated reprogramming impacting Wnt and Notch TNFα/TNR1 MCP1/CCR2 (PI3K/Akt/mTor cascade)	Tocilizumab (anti-IL-R6 Ab) Sunitinib (PDGFR inhibitor) EPZ011989 (EZH2 inhibitor)	(36)
	Induction of stemness			(37)
	Inhibition of apoptosis	Jagged1/Notch1/p-53	15D11 (anti-Jagged1 Ab)	(38)
	Induction of dormancy	TNFα/TNR1 MCP1/CCR2 (PI3K/Akt/mTor cascade)	anti-TNR1 or anti-CCR2 antibody	(39)
MAFs	Supression of T cell function	Prostaglandin E2, TGF-β, VEGF		(22, 40)
	Collapse of blood vessels -> decreased drug delivery	Increased collagen and hyaluronan production	Losartan (TSP-1 inhibitor) Angiostin signalling blockade	(41)
	Induction of stemness	IL-6	See above	(42, 43)
TAMs	Decrease endocrine therapy sensitivity	secretion of CCL2 activating the PI3K/Akt/mTor signalling pathway		(44)
	Induction dormancy	GJIC		(45)
MDSCs	Supression of T cell function	Arginase expression	See paper from Chesney et al	(46)
Neutrophils	Inhibition of apoptosis	TNF-α/CXCR2 S100A8/9	TNF-α antibody CXCR2 blockers	(47)
MSCs	Supression of T cell proliferation	Secretion of TGF-β, hepatocyte growth factors, IDO, PGE2, nitric acid suppression of Stat5 phosphorylation	antibodies against TGF-β or hepatocyte growth factor inhibitors of IDO, prostaglandin or NOS	(48)
	Induction of dormancy	GJIC and transfer of miNRA targeting CXCL12	target of miRNA target of GJIC (ex: H89)	(49, 50)
	Inhibition of apoptosis	polyunsaturated fatty acid (PIFA) released upon platinium-based treatment	blockade of PIFA-producing enzymes	(51)
		TGF-β		(52)
Adipocytes	metabolizes and deactivates chemotherapy molecules			(53, 54)
Microvascular endothelium	Inhibition of cytostatic effect	Secretion of integrins (β1 and αvβ3) Von Willebrand Factor VCAM1	Antibodies against integrins β1 and αvβ3	(55)
ECM	Inhibition of apoptosis	β1 and αvβ3 integrins PI3K/Akt pathway	Antibodies against integrins β1 and αvβ3	(56, 57)

Mechanisms and pathways are divided based on specific cell populations of the bone microenvironment.

(EZH2)-mediated reprogramming that also seems to induce stemness in breast cancer bone metastasis (37). Osteoblast lineage cells also tend to protect cancer cells against chemotherapy in the bone through the overexpression of Jagged1, which interacts with the Notch1 receptor on cancer cells and circumvents apoptosis by affecting the p53-regulated apoptotic pathway. Injection of a Jagged1 inhibitor (such as an anti-Jagged1 monoclonal antibody, here 15D11) in mice improved the chemosensitivity of cancer cells, making it a promising candidate for targeting the bone microenvironment (38). Osteoblasts can also protect breast cancer cells from chemotherapy by inducing a dormancy state, notably due to the secretion of cytokines such as tumor necrosis factor α (TNFα) and monocyte chemoattractant protein-1 (MCP1). The first one modulates the Fas-associated death domain protein (FADD)/tumor necrosis factor receptor type 1-associated death domain protein (TRADD) by biding to the TNF receptor 1 (TNFR1), while MCP1 binds to C-C chemokine receptor type 2 (CCR2) and induces the phosphatidylinositol 3-kinases/protein kinase B/mammalian target of rapamycin (PI3K/Akt/mTOR) cascade (39).

Osteoclasts represent the counterpart of osteoblasts in the bone remodeling process, since they play a very important role in the

vicious cycle and thereby in the aggressiveness of the tumor (58). However, their role in drug resistance has not yet been studied.

3.2 Metastasis-associated fibroblasts

Metastasis-associated fibroblasts (MAFs) (also called CAFs for cancer-associated fibroblasts when talking about cancer in general) also seem to have an important role on the metastatic proliferation of breast cancer cells into bone. MAFs can derive from multiple cell lines including mesenchymal stromal cells (MSCs) in the bone marrow (61), adipocytes, pericytes and even endothelial cells (62). Furthermore, inflammatory modulators such as interleukins, direct contact with cancer cells and physical changes in the ECM architecture contribute to the differentiation of MAFs (62). These activated cells produce growth factors (e.g. hepatocyte growth factor (HGF), transforming growth factor β (TGF-β), stromal derived factor 1/C-X-C motif chemokine ligand 12 (SDF-1/CXCL12), vascular endothelial growth factor (VEGF), insulin-like growth factor 1 (IGF-1)), interleukins, matrix metalloproteinases (MMPs) and exosomes which promote primary tumor and metastatic growth (63).

The presence of MAFs in the tumor microenvironment has been shown to cause chemoresistance through mechanisms that are so far poorly understood. A study showed that a few key players (e.g. retinoic acid receptor β (RARβ), peroxisome proliferator-activated receptor β and δ (PPARβ/δ), vitamin D receptor (VDR), glucocorticoid receptor (GR) and androgen receptor (AR) in the context of skin cancer) seem to be involved in both cancer aggressiveness and drug resistance. Moreover, targeting nuclear receptors that modulate the expression of those proteins led to a decreased drug resistance to cisplatin (64).

MAFs also tend to suppress the normal function of immune T cells in the microenvironment through immunosuppressive factors (e.g. prostaglandin E2, TGF-β, VEGF). Moreover, MAFs secrete pro-inflammatory cytokines including IL-6 that help to recruit tumor-associated macrophages (TAMs) and promote their transition from M0 to immune-suppressive M2 (22, 40).

MAFs are also known for stimulating angiogenesis, mostly through secretion of VEGF, platelet-derived growth factor C (PDGF-C) and IL-6 (22, 65). At the same time, MAFs can induce the collapse of existing blood vessels due to increased matrix stiffness, leading to hypoxia and to the proliferation of more aggressive metastatic clones. This effect can be reduced by a blood-pressure medication, Losartan, that decreases both the amount of collagen and hyaluronan causing vessel compression, and MAF activation (41). Importantly, this lack of blood vessels also leads to a decrease in drug delivery, enhancing the appearance of drug resistance (41, 66). Importantly, multiple studies also place MAFs as important protagonists in drug resistance, although not focused specifically on breast cancer. These studies highlight the role of MAFs in the secretion of IL-6 which enhances drug resistance by increasing the endothelial to mesenchymal transition (Endo-MT) and the generation of cancer stem cells (42, 43). Finally, upon chemotherapy administration it was shown that normal stromal fibroblasts tend to switch from an aerobic to glycolytic metabolism, correlating with a transformation of stromal fibroblasts into MAFs (67). Although not directly related to drug resistance, this study highlights how conventional therapies can alter the microenvironment and paradoxically enhance the metastatic dissemination.

Even though no treatment options have been tested in the specific context of breast cancer, a few therapeutic strategies have been evaluated to specifically target these aberrant fibroblasts. For example, in pancreatic adenocarcinoma, administering both Nab-paclitaxel and Gemcitabine helped in reducing the amount of CAFs in patients. In non-small-cell lung cancer, combining Paclitaxel with a tyrosine kinase inhibitor (i.e. Nindetanib, targeting VEGF, FGF and PDGF) impaired the interactions between cancer cells and CAFs. Finally, targeting TGF-β with monoclonal antibodies like Fresolimumab or Galunisertib seems to be a promising treatment strategy in various cancers (68).

3.3 Immune cells

3.3.1 Macrophages

Macrophages can be polarized by cancer cells towards an M2, anti-inflammatory phenotype. These M2 macrophages make up the majority of the so-called tumor associated macrophages (TAMs). These cells can constitute up to 30-50% of the tumor mass in skeletal metastases and are associated with a poor prognosis as they promote an immunosuppressive environment (69). This polarization towards an M2 phenotype tends to be enhanced by a positive feedback loop where TAMs secrete C-C motif chemokine ligand 2 (CCL2) that activates the PI3K/Akt/mTOR signaling pathway in cancer cell. This pathway tends to increase the resistance to ER modulators. Resistant cells then secrete TNF-α that activates TAMs and induces their M2 polarization (44).

TAMs seems to have a role in treatment resistance, as macrophage inhibitors (e.g. colony stimulating factor 1 (CSF-1) inhibitor) prior to chemotherapy have been shown to enhance the response to treatment in mammary and cervical cancer (70, 71). Similarly, treatment of mice with Cyclophosphamide (i.e. chemotherapy with immune-suppressive properties) combined with CSF-1 inhibitor reduced macrophage recruitment to the tumor and reversed chemotherapy resistance (44).

Finally, although not many studies consider the specific role of TAMs in the bone or bone marrow microenvironment, it seems that TAMs in the bone marrow are able to induce breast cancer cell dormancy by using GJIC, a mechanism used to evade chemotherapy which only targets rapidly-proliferating cells (45).

3.3.2 Myeloid-derived suppressor cells

Myeloid-derived suppressor cells (MDSCs) are immature myeloid cells that later differentiate into macrophages, dendritic cells or granulocytes. However, in presence of cancer cells there can be an accumulation of immunosuppressive MDSCs, leading to a suppression of both innate and adaptive immune response (46). In bone metastasis, MDSCs are shown to contribute to immunotherapeutic resistance by inhibiting antitumor T cell proliferation and cytotoxic activity. They also promote the expansion of protumorigenic T regulatory cells, thus dampening

the host immune response against the tumor, which in turns promotes angiogenesis, tumor invasion and metastasis (46). The many preclinical and clinical MDSC inhibitors are detailed elsewhere (46).

One study highlighted the role of MDSCs in drug (i.e. 5-FU) resistance in the case of hepatocellular cancer. This effect was mediated by the secretion of IL-6 (72), which is also known to increase drug resistance in metastatic breast cancer (36, 42, 43, 73). Moreover, in multiple myeloma (i.e. a bone marrow cancer) it has been shown that MDSCs had a direct influence on resistance to Doxorubicin and Melphalan due to the release of soluble factors (74). However, as these soluble factors have not been identified, it would be interesting to determine if they would induce the same effect on other cancer cell types.

3.3.3 Neutrophils

Neutrophils are cells that tend to be cytotoxic towards cancer cells during the first stages of the metastatic process, but that effect appears to be lost as tumor progresses. Indeed, neutrophils create an immunosuppressive action at the late stages of the cancer (75). Neutrophils are also known to help with the generation of the pre-metastatic niche by enabling circulating tumor cell (CTC) lodging at the metastatic sites. Mature neutrophils are shown to accumulate in the metastatic site even before the arrival of cancer cells, thereby helping to create the pre-metastatic niche by inducing an *in-situ* vascular remodeling and stimulating metastasis initiation (76).

As described with MAFs, neutrophils can also have a pro-tumorigenic effect post-chemotherapy treatment. Indeed, release of TNF-α by bone marrow derived cells in response to chemotherapy treatment has been observed, which leads to the activation of Nuclear factor kappa B (NFκB) and secretion of CXCL1/2 by cancer cells. These signals attract neutrophils to the tumor site where they produce S100A8/9 enhancing cancer cell survival. The hypothesis of anti TNF-α antibodies or CXCR2 blockers as a treatment option is currently being investigated (47).

3.3.4 T-cells

T cells are a group of immune cells critical to the adaptive response to pathogens and aberrant cell proliferation. They are divided in two main categories, CD4+ (or Th, for T helper cells) which modulate the activity of other immune cells, and CD8+ (or CTLs, for cytotoxic T lymphocytes) which can induce cell death (77). In cancer, immunosuppressive mechanisms are put in place, both by cancer cells and the tumor microenvironment to hinder the effectiveness of T cells (78). It has been shown that the presence of T cells in the tumor site increases the chance of immunotherapy response (79). However, a subcategory of T cells called regulatory T cells (T_{regs}), known to suppress the immune response (80), seems to have an impact on cancer cell proliferation. Indeed, tumor growth is promoted by the infiltration of leukocytes towards the stromal compartment of the bone marrow. This process seems to be partially mediated by the recruitment of T_{regs} (81). One of the treatments currently in place to reduce T cell dysfunction and exhaustion, two mechanisms that contribute to the immunosuppressive environment of the tumor, is PD-1/PD-L1 blockade. Indeed, cancer cells overexpress PD-L1, leading to an imbalance of the ratio of PD-1high CTLs and PD-1low CTLs, with a higher number of PD-1high CTLs in cancer patients compared to healthy ones that causes dysregulation and exhaustion of CTLs. However, this blockade might stimulate the expression of PD-1 in T_{regs}, which causes further immune resistance (79).

In prostate cancer, a study showed that the presence of CD4+ T cells in the tumor site promotes chemotherapy resistance (specifically to Enzalutamide and Doxorubicin) through the C-C motif chemokine ligand 5 (CCL5) signaling pathway (82), known to activate the Signal transducer and activator of transcription 3 (STAT3). This pathway could also be involved in breast cancer chemoresistance (83).

3.4 Mesenchymal stomal cells

Mesenchymal stromal cells (MSCs) are known to have an important role in bone metastasis development. By being the progenitors for osteoblasts, MSCs play a critical role in osteoblast proliferation, bus also in osteoclastogenesis, angiogenesis and immunosuppression (84–86). MSCs are also essential for HSC maintenance and thus contribute to the survival of the bone marrow niche. When it comes to bone metastases, multiple studies point towards a pro-tumorigenic role of MSCs, mainly *via* activation of MMPs which promote angiogenesis, stimulate epithelial-mesenchymal transition (EMT) and suppress the immune response, notably T-cell proliferation through secreted molecules or free radicals (48, 87). Moreover, MSCs may play a role in preserving the self-renewal ability of cancer cells as they do with HSCs, thus favoring the establishment of a tumor niche with long-term proliferative potential (20). This ability is believed to be effective on a small subset of breast cancer cells that show high expression of the pluripotency marker *OCT4*. This subset has been shown to create gap junctional intercellular communications (GJICs) with bone marrow stromal cells, a process that allows the transfer of quiescence-promoting miRNA, thus inducing dormancy and subsequently chemotherapy evasion and cancer relapse even after high doses of chemotherapy (88). This effect seems to be due to miRNA targeting CXCL12 in cancer cells, leading to decreased levels of CXCL12 and lower proliferation. These miRNAs could be a therapeutic target (49). In order to more accurately define and target these GJICs, a study showed that these connections were mediated by the protein kinase A (PKA) enzyme, whose activation could be induced or inhibited (i.e. using LY294002/LY303511 and H89, respectively) (50).

DTCs also use chemokine gradients in the bone marrow and adhesion molecules expressed by the HSC niche (e.g. CXCL12) that are believed to be crucial for HSC homing and survival (89). It is believed that cancer cells can acquire chemotherapy resistance by using an HSC-like state of dormancy to avoid drugs targeting rapidly-proliferating cells. Both cancer cells and HSCs use similar pathways to induce dormancy, such as the CXCL12/CXCR4 axis. The implication of CXCL12 in dormancy is controversial: on one hand, it is known to promote HSC self-renewal and pool

maintenance, either by supporting their self-division or potentially by inhibiting their cycling status (90). On the other hand, CXCL12 is mostly known to activate key survival signaling pathways upon biding to CXCR4, such as the PI3K/Akt, the mitogen-activated protein/extracellular-signal-regulated kinases (MAPK/ERK) and the Janus kinase/signal transducer and activator of transcription (JAK/STAT). Contradicting studies have shown either an overexpression and a dowregulation or CXCR4 in breast cancer bone metastasis, both pointing to a proliferative role of the CXCL12/CXCR4 axis (91–93). The mechanism leading to an avoidance of cancer cells rapid proliferation by CXCL12 and, thus chemotherapy treatment (94) is, so far, poorly understood. It has also been found that this dormancy is related to the Notch2 pathway, as blocking this signal resulted in a mobilization of previously dormant breast cancer cells (95).

The role of MSCs in breast cancer drug resistance can be induced by chemotherapy itself. For example, platinum-based chemotherapy, commonly used in triple negative breast cancer (TNBC) (96), can induce resistance mechanisms due to the reaction of MSCs to platinum. Indeed, upon platinum stimulation MSCs can release poly-unsaturated fatty acids, which induce broad-spectrum resistance to chemotherapeutic agents (51). In other cancers, such as leukemia, MSCs can protect cancer cells from further chemotherapy-induced apoptosis through the activation of the TGF-β pathway (52).

3.5 Adipocytes

Although previously underestimated, increasing interest is growing around the contribution of the adipogenic niche in bone metastasis. Indeed, elderly patients are characterized by an increase of bone marrow adipogenic niche when aging (97). Furthermore, direct cellular interactions occur between cancer cells and adipocytes, for instance through adipose-derived leptin and IL-1β (65). More importantly, bone marrow adipocytes alter the metabolism of cancer cells, stimulate cell adhesion, colonization and proliferation, and promote resistance to chemotherapy through various adipokines (98). For example, it has been shown that metastatic breast cancer cells tend to migrate more towards a medium enriched with leptin, a protein released by adipocytes (99). Moreover, lipids arising from adipocytes have been demonstrated to increase tumor growth and invasiveness by increasing the expression of fatty acid binding protein 4 (FABP4, i.e. fatty acid chaperone that is involved in glucose and lipid metabolism), heme oxygenase 1 (HMOX) and IL-1β (100). It has also been shown that cancer cells can hijack adipocytes and transform them into cancer-associated adipocytes (CAAs), that overexpress IL-6 and other pro-tumor cytokines (101). Regarding anti-cancer treatments, a major concern around adipocytes is that the adipose tissue is known for metabolizing and thus deactivating chemotherapy drugs (53). Co-culture of adipocytes and cancer cells in presence of Doxorubicin enhances the capacity of cancer cells to store the drug in vesicles instead of in the nucleus, which further increased the resistance of cancer cells (54). Moreover, in specific cases of ovarian cancer metastases, adipocytes were reprogrammed towards a more catabolic state and secreted free fatty acids that were used by cancer cell to generate ATP, hence conferring chemoresistance (102). Currently, it is still unknown if these mechanisms also happen in bone metastases from breast cancer.

3.6 Microvascular endothelium

DTCs mostly reside in the perivascular niche, which is a region in close proximity to blood vessels. A specificity of the bone marrow is indeed the capacity of its blood vessels to express adhesive molecules (e.g. P-selectin, E-selectin, intracellular adhesion molecule 1 and vascular cell adhesion molecule 1) without the requirement of stimulation by inflammatory cytokines, contrary to other tissues. These molecules interact with cancer cells and facilitate their adhesion (103). Within this niche, the distance between a cancer cell and a blood vessel is almost 30 times smaller than the average distance between an osteoblast and a blood vessel. Following chemotherapy treatment, the distance between cancer cells and blood vessels is even reduced suggesting that cells located closer to blood vessels are resistant to the treatment. This resistance seems to be directly linked with the expression of integrin β_1 and integrin $\alpha_v\beta_3$ on cancer cells, since inhibiting these integrins with specific antibodies induced an increased sensitivity to Doxorubicin (55). In this scenario, it seems that integrin $\alpha_v\beta_3$ protects DTCs from chemotherapy through signaling triggered by endothelial Von Willebrand Factor (VWF). In addition, DTC chemoresistance is driven by vascular cell adhesion molecule 1 (VCAM1). This endothelial surface molecule is an integrin $\alpha_4\beta_1$ ligand along with other endothelial-derived integrin $\alpha_4\beta_1$ ligands. Combined treatment with antibodies targeting both integrins β_1 and $\alpha_v\beta_3$ leads to a higher percentage of DTC cells sensitized to Doxorubicin both *in vitro* and in mice (55).

In lymphomas, which frequently metastasize to the bone marrow, a vicious cycle between B cells and endothelial cells occurs. FGF-4 is secreted by lymphoma cells, leading to an activation of fibroblast growth factor receptor FGFR-1 on endothelial cells and to an upregulation of Notch ligand Jagged1. As a consequence, lymphoma cells increase their aggressiveness, invasiveness and chemoresistance (104). It is important to note that breast cancer cells also use the Jagged1/Notch pathway to promote bone metastases (105), thus a focus on FGFR-1 expression in breast cancer bone metastases could unveil new answers in drug resistance mechanisms.

3.7 Tissue non-specific chemotherapy-induced resistance

Chemotherapy itself can act as a metastasis-inducer. For example, a chemotherapy treatment on the initial primary breast tumor can select chemoresistant clones that could form metastases, leading to secondary tumors already resistant to the first line of chemotherapy (106). Moreover, a few *in vitro* studies demonstrated

that preoperative/neoadjuvant as well as post-operative/adjuvant chemotherapy can induce metastases. This phenomenon could be due to the induction of tissue damage that the body repairs through the secretion of cytokines that also promote the generation of resistant clones (107). For example, Paclitaxel activates the toll-like receptor 4 (TLR4), which is present on macrophages to recognize polysaccharides and it is also expressed by breast cancer cells. This activation tends to exacerbate a pro-inflammatory microenvironment, leading to angiogenesis and cancer cell invasion. Paclitaxel can also promote an EMT-like phenotype in cancer cells (i.e. decreased E-cadherin expression and increased formation of invadopodia), thus enhancing the likelihood of metastases. Chemotherapy can also increase the risk of CTCs invading secondary tissues by inducing the release of platelet-derived microvesicles that bind to the CTC surface and facilitate their attachment to the endothelium. These "coated" CTCs are also more protected against immunological destruction by natural killer (NK) cells (107).

3.8 ECM

Cancer cells expressing $\alpha_v\beta_3$ integrin, which is often upregulated in breast cancer, bind to the ECM components fibronectin and osteopontin, which along with vitronectin are highly expressed in bone marrow. In epithelial cancers it has been shown that adhesion through $\alpha_v\beta_3$ integrins leads to chemotherapy resistance. A similar effect has been reported with β_1 integrins, most likely due to a protective effect of the nuclear response to DNA-targeting agents (56). Moreover, expression of β_1 integrins also showed a drug resistance effect on Paclitaxel and Vincristine, two molecules targeting the microtubules. The signaling pathways activated through β_1 integrin ligation induce an inhibition of cytochrome c release and activation of the PI3K/Akt pathway, reducing the expected apoptosis effect of the chemotherapeutic agents (57). Even though the specific role of the ECM in resistance is still yet to be fully understood, it seems that targeting elements of the cell-matrix interaction (e.g. integrins) through novel mechanobiological therapies could help to increase the sensitivity of cancer cells to chemotherapy treatment.

4 *In vitro* models of bone metastasis to analyze drug resistance

It is now becoming evident that the microenvironment plays a non-negligible role in the homing, survival, proliferation and drug resistance of cancer cells. In the bone, multiple cell types induce various pathways that help the cells to avoid or resist chemotherapy treatment. For instance, osteoblasts, MSCs or even ECM proteins can directly influence the apoptosis pathway in cancer cells, while TAMs, MSCs or HSCs allow cancer cells to adopt a dormancy behavior. Furthermore, MAFs, MDSCs or MSCs can decrease the efficacy of immunotherapy by suppressing T cell function. Other cell populations can have a more direct impact on drug distribution: adipocytes metabolize and eliminate chemotherapy molecules from the tissue, while MAFs induce the collapse of blood vessels, hence decreasing the availability of the drug. Overall, it is clear that drug screening without the presence of a microenvironment significantly decreases the likelihood of recapitulating the actual action of the drug in humans.

However, so far drug screening assays have traditionally been performed on simplified 2D cultures of cancer cell lines. Animal and clinical studies have highlighted that the local microenvironment is a key mediator of the drug resistance observed in patients. Hence, the next generation of pre-clinical models should focus on the successful integration of organ-specific, physiological-like microenvironments to overcome limitations of conventional systems (108–111). Indeed, *in vitro* models represent a useful tool to identify earlier potential drug resistance mechanisms during the drug development pipeline or clarify basic mechanisms that cannot be quickly identified with animal studies.

In this scenario, introducing a 3D microenvironment without a complex cellular composition has already proved to be effective in modeling biological processes or drug response. Kim et al. proposed a microfluidic device where MCF-7 breast cancer cells were able to aggregate into spheroids and showed that the drug sensitivity of the cancer cells in the spheroids was decreased compared to 2D monolayers (112). Increasing the level of complexity, some models included a very basic 3D microenvironment. For instance, co-cultures of cancer-associated fibroblasts with breast cancer cells showed higher drug resistance compared to a 3D monoculture of cancer cells (113). The authors hypothesize that this drug resistance might be due to both reduced drug penetration in spheroids (compared to a monolayer) and to intercellular contacts activating cell survival pathways such as PI3K/Akt, NF-κB and STAT3. However, the specific pathways involved were not investigated. These results confirm that 3D models populated with a simplified microenvironment can help to decipher differences in drug sensitivities due the presence of both the 3D matrix (i.e. the interactions with the ECM and the decreased drug diffusion compared to 2D), as well as the surrounding cells.

A few biofabricated 3D models specifically focused on studying the drug resistance of breast cancer due to the bone microenvironment compared to a simplified control (often 2D). Zhu et al. created a bone model using a biomimetic bone matrix seeded with human bone marrow MSCs and MDA-MB-231 or MCF-7 breast cancer cell lines (114). The study highlighted a higher drug resistance when the 3D microenvironment was subject to an anti-cancer treatment with 5-FU compared to 2D culture. However, the authors did not propose an analysis of the pathways involved in the observed resistance, even though they hypothesize that reduced drug diffusion and altered transporter expression due to cell-matrix interactions could play a role. Similarly, Kar and co-authors created a co-culture model on a 3D polycaprolactone/hydroxyapatite PCL/HAP clay scaffold with MSCs and either MDA-MB-231 or MCF7 breast cancer cell lines (115). The authors compared the sensitivity to Paclitaxel of these cell lines in their 3D co-culture and 2D monoculture showing a higher resistance in 3D. This resistance was correlated with an up-regulation of STAT3, leading to the overexpression of B-cell lymphoma 2 [Bcl-2, known to have an increased expression in chemoresistant cells (116)] or multidrug

resistant protein 1 (MRP1) and ATP Binding Cassette Subfamily G Member 2 (ABCG2) [known to be upregulated in multiresistant cells, meaning cancer cells resistant to multiple chemotherapeutic drugs with different structures and mechanisms of action (117, 118)]. Likewise, Langer and co-authors assessed the effect of the microenvironment on drug sensitivity (119). The proposed model included fibroblasts, endothelial cells, adipocytes and bone marrow MSCs, which have been shown to have a detrimental effect on drug treatment. Using MCF-7 breast cancer cell line, the authors showed that the microenvironment not only contributed to the aggressiveness of the metastatic process, but also to drug resistance. Indeed, the concentrations of Doxorubicin and Paclitaxel were respectively 20 times and 5,000 times higher in the 3D model than in the 2D control to achieve the same level of cancer cell mortality. The study also showed that part of this effect was due to a paracrine influence of fibroblasts by using a fibroblast-conditioned medium in a 3D cancer cell monoculture, where the authors still observed a lack of therapeutic response. The authors concluded that secreted factors from fibroblasts were able to induce resistance to mTOR inhibition. The device proposed in this study is a great example of the usefulness of 3D models, both for the field of drug screening but also for deciphering the molecular pathways involved in drug resistance. Finally, another bone model composed by bone marrow MSCs and endothelial cells on a decellularized bone matrix (120) showed a higher drug resistance of breast cancer cells when the whole system was subject to an interstitial flow compared to static conditions. This phenomenon is explained by the better maturation of the vasculature (compared to the static condition), leading to less proliferative cancer cells. This particular feature makes this model a great tool to study dormancy in the bone niche. This finding highlights the importance of recapitulating both the cellular complexity and the biophysical stimuli characterizing the bone microenvironment in order to fully reproduce *in vivo* mechanisms. These models are summarized in Figure 2.

To date, very few models are focusing on the effect of the bone microenvironment on drug resistance, especially considering breast cancer. Even though the field of drug testing in 3D models is still at its infancy, many researchers are starting to highlight the benefits of including complexity in the drug screening process. Since the immune system plays a significant role in terms of metastatic proliferation and drug resistance, a few models included immune cells when studying breast cancer bone metastases. However, these models are not yet considering drug resistance mechanisms. For example, Crippa et al. designed a breast cancer bone metastasis model embedding endothelial cells, bone marrow MSCs, osteoblasts, fibroblasts and neutrophils in two separate chambers connected by perfusable vessels (122). This study showed a higher recruitment of neutrophils when breast cancer cells were present in the device, as well as a higher cancer cell mortality due to neutrophil attack. However, the authors did not perform any drug treatment through the model. It would have been interesting to use that model to test the influence of the immune system on drug sensitivity, especially with neutrophils which are known to have both an anti- and pro-tumorigenic effect. In another study, the immune system was introduced as bone-resident macrophages (123), which were co-cultured with breast cancer cells, endothelial cells, osteoblasts and osteoclasts. The model was then challenged with Doxorubicin or Rapamycin. The authors showed that the bone microenvironment protected cancer cells from both treatments, hence more closely mimicking what is observed *in vivo* compared to conventional 2D *in vitro* cultures, both regarding the arrangement of the cancer cells (e.g. cluster formation *in vivo* and in the 3D model) and their localization (e.g. close proximity to endothelial cells and osteoclasts). Focusing on the design of a bone marrow model, Glaser and co-authors included bone marrow MSCs, osteoblasts, hematopoietic stem/progenitor cells (HSPCs) as well as endothelial cells in a fibrin gel (121). In addition to a different proliferative and invasive behavior of breast cancer cells in their 3D coculture model compared to a fibrin-only control, the authors also observed an altered reaction of the microenvironment to Doxorubicin (i.e. mimicking the neutropenic effect of chemotherapy and increasing neutrophil production, both usually observed *in vivo* upon chemotherapy treatment). This effect was not observed in 2D culture. Unfortunately, the authors did not study the effect of chemotherapy on breast cancer cells in their model. 3D models can also be a great tool to study the molecular pathways leading to drug resistance. For example, understanding how dormancy is induced in breast cancer cells would be of great help to explore therapeutic solutions to avoid breast cancer relapse and late recurrence. With that goal in mind, Pradhan et al. designed a 3D *in vitro* model composed of breast cancer cells, human MSCs and fetal osteoblasts, and demonstrated that cytokines secreted by osteoblasts (e.g. TNFα, MCP1) were able to induce dormancy in the cancer cells (39). This mechanism could be reversed by blocking the receptors of these cytokines with monoclonal antibodies.

Other models have been built to replicate the bone or the bone marrow without a specific focus on breast cancer. For example, Ma et al. created a bone model including endothelial cells, MSCs and osteoblasts embedded in a hydrogel to test the resistance of leukemia cells. The study showed that drug resistance of cancer cells was higher in presence of the bone niche (124). A similar model embedding endothelial cells, MSCs and osteoblasts also focused on leukemia analyzing the differences in drug sensitivity in 2D, 3D static and 3D dynamic conditions (125). The authors demonstrated the protective role of the microenvironment by comparing cancer cell response to a chemotherapeutic agent (i.e. the antimetabolite chemotherapeutic drug Ara-C) and showed increased drug resistance due to the presence of the cells and ECM. The authors hypothesize that this observed chemoresistance can mostly be attributed to CXCL12/CXCR4 signaling, but also to direct cell-cell interactions involving vascular cell adhesion molecule 1/very late antigen-4 (VCAM-1/VLA-4). These two pathways lead to the activation of the prosurvival signaling NF-κB. Finally, several 3D models of bone or bone marrow have been created to test the effect of a surrounding niche on the drug sensitivity of multiple myeloma (126, 127), prostate cancer (128), osteosarcoma (129) and Ewing sarcoma (130, 131). All these models highlighted the requirement of a higher dose of anti-cancer drug to reach the mortality achieved in 2D controls. This effect is mainly due to the microenvironment, either physically preventing the drug to reach cancer cells or by

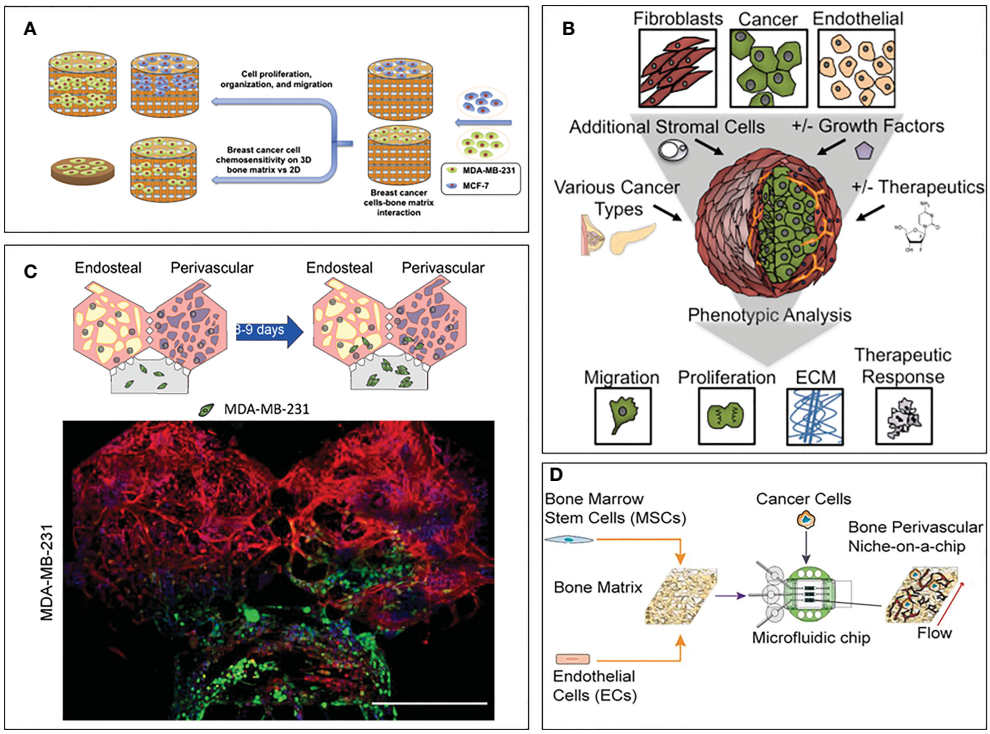

FIGURE 2
3D models focusing on drug sensitivity in breast cancer bone metastasis. **(A)** Model by Zhu et al. (114). Breast cancer cells and bone marrow MSCs were seeded on a bone matrix and showed drug resistance in presence of the microenvironment compared to the 2D culture. **(B)** Model by Langer et al. (119). Breast cancer cells were seeded with fibroblasts, endothelial cells, adipocytes and bone marrow MSCs. Increased cancer cell aggressiveness and drug resistance were observed compared to the 2D control. **(C)** Model by Glaser et al. (121). Breast cancer cells were seeded with bone marrow MSCs, osteoblasts, HSCs and endothelial cells. Differences in cell behavior were observed when breast cancer cells were co-cultured with bone and stromal cells compared to fibrin only hydrogels. **(D)** Model by Marturano-Kruik et al., (120). Cancer cells showed drug resistance when exposed to interstitial flow.

diminishing drug efficacy. These models could be easily adapted to study breast cancer metastases.

Taken together, these examples clearly show that a 2D assay of chemotherapy alone cannot accurately predict the efficacy of the drug in *in vivo* setting, leading to potential drug failure in clinical trial or increased side effects. 3D models with complex microenvironments thus seem to be a better alternative in order to properly replicate the mechanisms involved in cancer proliferation and drug resistance, and would benefit from being developed further. Indeed, multiple cell types such as immune cells, that are now known to have an effect on cancer aggressiveness and drug resistance, have never been tested in a drug screening scenario in a 3D setting. It is likely that introducing them within the biofabricated microenvironment could yield results regarding drug effectiveness better mimicking what is observed in patients.

However, it is important to remember that current *in vitro* 3D models do not have the ability to fully replace rodent models, as their complexity is highly limited by the amount of different cell types able to co-exist in the same matrix, as well as by their simplified architecture that can only partially mimic a real tissue unit. Moreover, off target cytotoxicity cannot be easily tested with 3D models as it would require the development of bodies-on-a-chip [the reader can refer to these reviews for more information about these systems (132, 133)] that are extremely challenging to develop and run. At the same time, even though this and other reviews describe in length the advantages of testing drug compounds in 3D systems, it is worth noting that these models are still thought to be complicated and costly, making them less attractive than 2D monocultures in a high-throughput context (134). However, as technological advances progress and commercially available tests are developed, their cost is expected to become more competitive. Cost reduction and superior performances are expected to outperform conventional 2D screening technologies, especially in cancer research (135, 136).

5 Conclusion and perspectives

As highlighted in this review, the microenvironment is a key driver for the establishment of drug resistance in cancer metastases. Unfortunately, the complexity of this microenvironment implies that the combined action of many cell types on drug sensitivity cannot be studied using conventional assays. Advanced *in vitro* 3D models could be a great tool to better understand the mechanisms and pathways involved in the onset of drug resistance and to develop more effective therapeutic options.

Considering the bone microenvironment, multiple cell types influence the behavior of cancer cells when subject to a drug

treatment. By protecting cancer cells from apoptosis, guiding them towards dormancy, or even metabolizing the drug themselves, cells from the bone microenvironment put in place a plethora of different mechanisms to help cancer cells to survive chemo-, immune-, radio- or endocrine therapy. Combined with the very high failure rate of anti-cancer drugs during clinical trials, it is becoming clear that the current gold-standards of preclinical testing (i.e. 2D cultures and animal models) are lacking critical information to accurately predict how the drug will behave in the patient. The emergence of more complex 3D models which more accurately mimic cell-ECM and cell-cell interactions thus seems to be a promising alternative (10). However, to this date most bone or bone marrow models are still focusing on the biofabrication of the scaffold and the microenvironment and very few have tried to add cancer cells to their model (137). Noteworthy, only a small fraction of them is focusing on drug resistance. These models have demonstrated that adding a chemotherapy treatment against cancer cells clearly show the establishment of drug resistance induced by the microenvironment (114, 115, 119, 120). This effect is not observed in 2D or monoculture assays.

Regarding breast cancer metastases to bone, it would be extremely helpful to create a comprehensive summary of which cells in the bone microenvironment have an influence on cancer cell proliferation and drug sensitivity. Compiling this summary would require the setup of large parametric studies combining statistical approaches of design of experiment with artificial intelligence-driven data analysis. Having such information would allow to create physiological-like *in vitro* 3D bone models that have the best chance of mimicking accurate cell-cell interactions and identify molecular pathways involved in drug resistance, ultimately helping life-changing treatments to arrive quicker on the market. In particular, these advanced models could help to observe how the bone microenvironment is gradually skewed by cancer cells to shield them from the effect of a given drug.

These models could also be used to test already approved drugs, either for a different bone pathology or as a combination to tackle breast cancer drug resistance. For instance, second line treatments are administered when the first line has failed causing the tumor to start its growth again due to the presence of cells fully resistant to the first treatment (106). With this in mind, administering different chemotherapies as a sequence or a combo before the tumor has time to start growing back could be the future to prevent drug resistance. Studying the onset of unknown drug resistance by testing different treatments in a row could also be a useful technique to find ways to counteract it. Human *in vitro* 3D bone models reproducing the metastatic microenvironment would be an effective tool to perform these studies, potentially employing patient-derived cells in the context of personalized medicine. These models could be easily employed for large-scale drug screenings that cannot be easily performed with *in vivo* models like rodents due to higher costs, raising ethical issues and longer experimental times. Within the drug-discovery pipeline, using 3D *in vitro* bone models as a tool for accurate large-scale drug screening before testing them in animals could help identifying which drugs are expected to yield better results, thus leading to a reduction of animals needed in agreement with the 3Rs principle [replace, reduce, refine (138)]. We thus envision that the integration of the 3D human bone microenvironment with high-throughput drug screening methods would allow for a more efficient pre-clinical testing and improve the success rate of clinical trials.

It is worth mentioning that, while 2D models can only be ameliorated by adding additional cell types to the culture, 3D models present a greater ability to get improved in order to more closely resemble the organ they are mimicking. For example, while cellular complexity seems to be essential to accurately represent mechanisms happening between the cells of interest (e.g. cancer cells) and their microenvironment, there can be many other ways to improve the accuracy of the model. Incorporating a scaffold, inorganic components present in the tissue, flow or even mechanical or electrical simulation will make the model more relevant. This additional level of complexity cannot be included in conventional 2D assays. Regarding the bone, a tissue that is highly vascularized and experiences constant compression forces, introducing flow in a microfluidic device as well as mechanical stimulation would be a great way to better mimic physiological conditions. Indeed, the presence of a flow influences the behavior of bone cells, notably by inducing the release of osteogenic factors which influence the bone remodeling process (i.e. matrix mineralization and collagen deposition, as well as osteoblast proliferation) (139). A similar observation can be made when adding a scaffold whose geometry closely mimics the one found in human tissue units. For instance, the pattern of the scaffold can influence the distribution of shear stress forces as well as bone cell behavior (140). The rest of the microenvironment can also benefit from being cultured in 3D compared to 2D monolayers. For example, bone marrow adipocytes tend to adopt a more *in vivo* like morphology and biochemical behavior in 3D compared to a 2D control. Indeed, cells in a monolayer tend to be forced into a restrictive demeanor with a forced polarity due to the presence of altered focal adhesions. In addition, cells grown on plastic surfaces are subject to an increased stiffness that usually leads to an improper gene expression (141, 142), while cells cultivated on a 3D scaffold show higher survival, differentiation as well as drug sensitivity (141).

Concluding, the field of pre-clinical assays is starting to shift towards more accurate *in vitro* 3D models to predict the efficiency of a drug. Human 3D models of the bone microenvironment have the potential to help understanding in more depth the biological mechanisms underlying drug resistance due to the possibility to selectively introduce specific components (e.g. cells, matrix proteins, growth factors) in the biofabricated model. By balancing complexity and throughput, these systems could be designed to perform large experimental campaigns of drug screening. On a longer time scale, introducing patient-derived cells from biopsies of the metastatic bone tissue would allow to create personalized treatments based on the genetic background of the tumor and on the response of the microenvironment. Finally, designing a tunable microenvironment to fit the specificities of the patient (e.g. introducing pre-existing comorbidities) could further improve the design of patient-specific treatments.

Author contributions

AL conceptualized and wrote the manuscript. SB and MM reviewed the manuscript. All authors contributed to the article and approved the submitted version.

Funding

This project has received funding from the European Union's Horizon 2020 research and innovation programme under the Marie Skłodowska-Curie grant agreement No 860715. This work was supported by the Swiss State Secretariat for Education, Research and Innovation (SERI) under contract number MB22.00085. Open access funding by Università Della Svizzera Italiana.

Conflict of interest

The authors declare that the research was conducted in the absence of any commercial or financial relationships that could be construed as a potential conflict of interest.

Publisher's note

References

1. Martei YM, Pace LE, Brock JE, Shulman LN. Breast cancer in low- and middle-income countries. *Clin Lab Med* (2018) 38(1):161–73. doi: 10.1016/j.cll.2017.10.013

2. Yedjou CG, Sims JN, Miele L, Noubissi F, Lowe L, Fonseca DD, et al. Health and racial disparity in breast cancer. *Adv Exp Med Biol* (2019) 1152:31–49. doi: 10.1007/978-3-030-20301-6_3

3. Yoo GJ, Levine EG, Pasick R. Breast cancer and coping among women of color: a systematic review of the literature. *Support Care Cancer* (2014) 22(3):811–24. doi: 10.1007/s00520-013-2057-3

4. Salvador F, Llorente A, Gomis RR. From latency to overt bone metastasis in breast cancer: potential for treatment and prevention. *J Pathol* (2019) 249(1):6–18. doi: 10.1002/path.5292

5. Huang JF, Shen J, Li X, Rengan R, Silvestris N, Wang M, et al. Incidence of patients with bone metastases at diagnosis of solid tumors in adults: a large population-based study. *Ann Transl Med* (2020) 8(7):482. doi: 10.21037/atm.2020.03.55

6. Zhang W, Bado IL, Hu J, Wan YW, Wu L, Wang H, et al. The bone microenvironment invigorates metastatic seeds for further dissemination. *Cell* (2021) 184(9):2471–2486.e20. doi: 10.1016/j.cell.2021.03.011

7. Venetis K, Piciotti R, Sajjadi E, Invernizzi M, Morganti S, Criscitiello C, et al. Breast cancer with bone metastasis: Molecular insights and clinical management. *Cells* (2021) 10(6):1377. doi: 10.3390/cells10061377

8. Brook N, Brook E, Dharmarajan A, Dass CR, Chan A. Breast cancer bone metastases: pathogenesis and therapeutic targets. *Int J Biochem Cell Biol* (2018) 96:63–78. doi: 10.1016/j.biocel.2018.01.003

9. Massagué J, Obenauf AC. Metastatic colonization. *Nature* (2016) 529(7586):298–306. doi: 10.1038/nature17038

10. Moffat JG, Vincent F, Lee JA, Eder J, Prunotto M. Opportunities and challenges in phenotypic drug discovery: an industry perspective. *Nat Rev Drug Discovery* (2017) 16(8):531–43. doi: 10.1038/nrd.2017.111

11. Mestas J, Hughes CCW. Of mice and not men: Differences between mouse and human immunology. *J Immunol* (2004) 172(5):2731–8. doi: 10.4049/jimmunol.172.5.2731

12. Rosol TJ, Tannehill-Gregg SH, LeRoy BE, Mandl S, Contag CH. Animal models of bone metastasis. *Cancer Treat Res* (2004) 118:47–81. doi: 10.1007/978-1-4419-9129-4_3

13. Mittal R, Woo FW, Castro CS, Cohen MA, Karanxha J, Mittal J, et al. Organ-on-chip models: Implications in drug discovery and clinical applications. *J Cell Physiol* (2019) 234(6):8352–80. doi: 10.1002/jcp.27729

14. Jubelin C, Muñoz-Garcia J, Griscom L, Cochonneau D, Ollivier E, Heymann MF, et al. Three-dimensional *in vitro* culture models in oncology research. *Cell Biosci* (2022) 12(1):155. doi: 10.1186/s13578-022-00887-3

15. Hoarau-Véchot J, Rafii A, Touboul C, Pasquier J. Halfway between 2D and animal models: Are 3D cultures the ideal tool to study cancer-microenvironment interactions? *Int J Mol Sci* (2018) 19(1):181. doi: 10.3390/ijms19010181

16. Langhans SA. Three-dimensional in vitro cell culture models in drug discovery and drug repositioning. *Front Pharmacol* (2018) 9:6. doi: 10.3389/fphar.2018.00006

17. Ewart L, Apostolou A, Briggs SA, Carman CV, Chaff JT, Heng AR, et al. Performance assessment and economic analysis of a human liver-chip for predictive toxicology. *Commun Med* (2022) 2(1):1–16. doi: 10.1038/s43856-022-00209-1

18. Akhtari M, Mansuri J, Newman KA, Guise TM, Seth P. Biology of breast cancer bone metastasis. *Cancer Biol Ther* (2008) 7(1):3–9. doi: 10.4161/cbt.7.1.5163

19. Liu Y, Cao X. Characteristics and significance of the pre-metastatic niche. *Cancer Cell* (2016) 30(5):668–81. doi: 10.1016/j.ccell.2016.09.011

20. Sanmartin MC, Borzone FR, Giorello MB, Pacienza N, Yannarelli G, Chasseing NA. Bone marrow/bone pre-metastatic niche for breast cancer cells colonization: The role of mesenchymal stromal cells. *Crit Rev Oncol Hematol* (2021) 164:103416. doi: 10.1016/j.critrevonc.2021.103416

21. Zhang Y, Ma B, Fan Q. Mechanisms of breast cancer bone metastasis. *Cancer Lett* (2010) 292(1):1–7. doi: 10.1016/j.canlet.2009.11.003

22. Mukaida N, Zhang D, Sasaki SI. Emergence of cancer-associated fibroblasts as an indispensable cellular player in bone metastasis process. *Cancers (Basel)* (2020) 12(10):E2896. doi: 10.3390/cancers12102896

23. Le Pape F, Vargas G, Clézardin P. The role of osteoclasts in breast cancer bone metastasis. *J Bone Oncol* (2016) 5(3):93–5. doi: 10.1016/j.jbo.2016.02.008

24. *Treatment options*. Available at: https://www.breastcancer.org/treatment.

25. *Chemotherapy for breast cancer | breast cancer treatment*. Available at: https://www.cancer.org/cancer/breast-cancer/treatment/chemotherapy-for-breast-cancer.html.

26. Goswami S, Chen Y, Anandhan S, Szabo PM, Basu S, Blando JM, et al. ARID1A mutation plus CXCL13 expression act as combinatorial biomarkers to predict responses to immune checkpoint therapy in mUCC. *Sci Trans Med* (2020) 12(548):eabc4220. doi: 10.1126/scitranslmed.abc4220

27. Twomey JD, Zhang B. Cancer immunotherapy update: FDA-approved checkpoint inhibitors and companion diagnostics. *AAPS J* (2021) 23(2):39. doi: 10.1208/s12248-021-00574-0

28. Darvin P, Toor SM, Sasidharan Nair V, Elkord E. Immune checkpoint inhibitors: recent progress and potential biomarkers. *Exp Mol Med* (2018) 50(12):1–11. doi: 10.1038/s12276-018-0191-1

29. Mellman I, Coukos G, Dranoff G. Cancer immunotherapy comes of age. *Nature* (2011) 480(7378):480–9. doi: 10.1038/nature10673

30. Liu C, Wang M, Xu C, Li B, Chen J, Chen J, et al. Immune checkpoint inhibitor therapy for bone metastases: Specific microenvironment and current situation. *J Immunol Res* (2021) 2021:e8970173. doi: 10.1155/2021/8970173

31. *Chemotherapy's effects on organ and body systems - health encyclopedia - university of Rochester medical center*. Available at: https://www.urmc.rochester.edu/encyclopedia/content.aspx?ContentID=P07155&ContentTypeID=85.

32. *Side effects of immunotherapy - NCI*. Available at: https://www.cancer.gov/about-cancer/treatment/types/immunotherapy/side-effects.

33. Martins F, Sofiya L, Sykiotis GP, Lamine F, Maillard M, Fraga M, et al. Adverse effects of immune-checkpoint inhibitors: epidemiology, management and surveillance. *Nat Rev Clin Oncol* (2019) 16(9):563–80. doi: 10.1038/s41571-019-0218-0

34. Rizzoli R, Ferrari S. Bisphosphonates and combined treatments osteoporosis. *Rev Med Suisse* (2005) 1(35):2269–71.

35. Chen J, Zhou L, Liu X, Wen X, Li H, Li W. Meta-analysis of clinical trials to assess denosumab over zoledronic acid in bone metastasis. *Int J Clin Pharm* (2021) 43(1):2–10. doi: 10.1007/s11096-020-01105-1

36. Tsoi H, Man EPS, Chau KM, Khoo US. Targeting the IL-6/STAT3 signalling cascade to reverse tamoxifen resistance in estrogen receptor positive breast cancer. *Cancers (Basel)* (2021) 13(7):1511. doi: 10.3390/cancers13071511

37. Bado IL, Zhang W, Hu J, Xu Z, Wang H, Sarkar P, et al. The bone microenvironment increases phenotypic plasticity of ER+ breast cancer cells. *Dev Cell* (2021) 56(8):1100–1117.e9. doi: 10.1016/j.devcel.2021.03.008

38. Zheng H, Bae Y, Kasimir-Bauer S, Tang R, Chen J, Ren G, et al. Therapeutic antibody targeting tumor- and osteoblastic niche-derived Jagged1 sensitizes bone metastasis to chemotherapy. *Cancer Cell* (2017) 32(6):731–747.e6. doi: 10.1016/j.ccell.2017.11.002

39. Pradhan L, Moore D, Ovadia EM, Swedzinski SL, Cossette T, Sikes RA, et al. Dynamic bioinspired coculture model for probing ER+ breast cancer dormancy in the bone marrow niche. *Sci Adv* (2023) 9(10):eade3186. doi: 10.1126/sciadv.ade3186

40. Portillo-Lara R, Annabi N. Microengineered cancer-on-a-chip platforms to study the metastatic microenvironment. *Lab Chip* (2016) 16(21):4063–81. doi: 10.1039/C6LC00718J

41. Chauhan VP, Martin JD, Liu H, Lacorre DA, Jain SR, Kozin SV, et al. Angiotensin inhibition enhances drug delivery and potentiates chemotherapy by decompressing tumour blood vessels. *Nat Commun* (2013) 4:2516. doi: 10.1038/ncomms3516

42. Shintani Y, Fujiwara A, Kimura T, Kawamura T, Funaki S, Minami M, et al. IL-6 secreted from cancer-associated fibroblasts mediates chemoresistance in NSCLC by increasing epithelial-mesenchymal transition signaling. *J Thorac Oncol* (2016) 11(9):1482–92. doi: 10.1016/j.jtho.2016.05.025

43. Bussard KM, Mutkus L, Stumpf K, Gomez-Manzano C, Marini FC. Tumor-associated stromal cells as key contributors to the tumor microenvironment. *Breast Cancer Res* (2016) 18(1):84. doi: 10.1186/s13058-016-0740-2

44. Xiao M, He J, Yin L, Chen X, Zu X, Shen Y. Tumor-associated macrophages: Critical players in drug resistance of breast cancer. *Front Immunol* (2021) 12:799428. doi: 10.3389/fimmu.2021.799428

45. Walker ND, Elias M, Guiro K, Bhatia R, Greco SJ, Bryan M, et al. Exosomes from differentially activated macrophages influence dormancy or resurgence of breast cancer cells within bone marrow stroma. *Cell Death Dis* (2019) 10(2):1–16. doi: 10.1038/s41419-019-1304-z

46. Chesney JA, Mitchell RA, Yaddanapudi K. Myeloid-derived suppressor cells-a new therapeutic target to overcome resistance to cancer immunotherapy. *J Leukoc Biol* (2017) 102(3):727–40. doi: 10.1189/jlb.5VMR1116-458RRR

47. Acharyya S, Oskarsson T, Vanharanta S, Malladi S, Kim J, Morris PG, et al. A CXCL1 paracrine network links cancer chemoresistance and metastasis. *Cell* (2012) 150(1):165–78. doi: 10.1016/j.cell.2012.04.042

48. Sato K, Ozaki K, Oh I, Meguro A, Hatanaka K, Nagai T, et al. Nitric oxide plays a critical role in suppression of T-cell proliferation by mesenchymal stem cells. *Blood* (2006) 109(1):228–34. doi: 10.1182/blood-2006-02-002246

49. Lim PK, Bliss SA, Patel SA, Taborga M, Dave MA, Gregory LA, et al. Gap junction–mediated import of MicroRNA from bone marrow stromal cells can elicit cell cycle quiescence in breast cancer cells. *Cancer Res* (2011) 71(5):1550–60. doi: 10.1158/0008-5472.CAN-10-2372

50. Bodenstine TM, Vaidya KS, Ismail A, Beck BH, Cook LM, Diers AR, et al. Homotypic gap junctional communication associated with metastasis suppression increases with PKA activity and is unaffected by PI3K inhibition. *Cancer Res* (2010) 70(23):10002–11. doi: 10.1158/0008-5472.CAN-10-2606

51. Roodhart JML, Daenen LGM, Stigter ECA, Prins HJ, Gerrits J, Houthuijzen JM, et al. Mesenchymal stem cells induce resistance to chemotherapy through the release of platinum-induced fatty acids. *Cancer Cell* (2011) 20(3):370–83. doi: 10.1016/j.ccr.2011.08.010

52. Zheng H, Li W, Kang Y. Tumor-stroma interactions in bone metastasis: Molecular mechanisms and therapeutic implications. *Cold Spring Harb Symp Quant Biol* (2016) 81:151–61. doi: 10.1101/sqb.2016.81.030775

53. Samimi A, Ghanavat M, Shahrabi S, Azizidoost S, Saki N. Role of bone marrow adipocytes in leukemia and chemotherapy challenges. *Cell Mol Life Sci* (2019) 76(13):2489–97. doi: 10.1007/s00018-019-03031-6

54. Lehuédé C, Li X, Dauvillier S, Vaysse C, Franchet C, Clement E, et al. Adipocytes promote breast cancer resistance to chemotherapy, a process amplified by obesity: role of the major vault protein (MVP). *Breast Cancer Res* (2019) 21(1):7. doi: 10.1186/s13058-018-1088-6

55. Carlson P, Dasgupta A, Grzelak CA, Kim J, Barrett A, Coleman IM, et al. Targeting the perivascular niche sensitizes disseminated tumour cells to chemotherapy. *Nat Cell Biol* (2019) 21(2):238–50. doi: 10.1038/s41556-018-0267-0

56. Hoyt DG, Rusnak JM, Mannix RJ, Modzelewski RA, Johnson CS, Lazo JS. Integrin activation suppresses etoposide-induced DNA strand breakage in cultured murine tumor-derived endothelial cells. *Cancer Res* (1996) 56(18):4146–9.

57. Aoudjit F, Vuori K. Integrin signaling inhibits paclitaxel-induced apoptosis in breast cancer cells. *Oncogene* (2001) 20(36):4995–5004. doi: 10.1038/sj.onc.1204554

58. Yin JJ, Pollock CB, Kelly K. Mechanisms of cancer metastasis to the bone. *Cell Res* (2005) 15(1):57–62. doi: 10.1038/sj.cr.7290266

59. Wang H, Tian L, Liu J, Goldstein A, Bado I, Zhang W, et al. The osteogenic niche is a calcium reservoir of bone micrometastases and confers unexpected therapeutic vulnerability. *Cancer Cell* (2018) 34(5):823–839.e7. doi: 10.1016/j.ccell.2018.10.002

60. Lu Y, Zhang J, Dai J, Dehne LA, Mizokami A, Yao Z, et al. Osteoblasts induce prostate cancer proliferation and PSA expression through interleukin-6-mediated activation of the androgen receptor. *Clin Exp Metastasis* (2004) 21(5):399–408. doi: 10.1007/s10585-005-0056-6

61. Ping Q, Yan R, Cheng X, Wang W, Zhong Y, Hou Z, et al. Cancer-associated fibroblasts: overview, progress, challenges, and directions. *Cancer Gene Ther* (2021) 28(9):984–99. doi: 10.1038/s41417-021-00318-4

62. Sahai E, Astsaturov I, Cukierman E, DeNardo DG, Egeblad M, Evans RM, et al. A framework for advancing our understanding of cancer-associated fibroblasts. *Nat Rev Cancer* (2020) 20(3):174–86. doi: 10.1038/s41568-019-0238-1

63. Mao X, Xu J, Wang W, Liang C, Hua J, Liu J, et al. Crosstalk between cancer-associated fibroblasts and immune cells in the tumor microenvironment: new findings and future perspectives. *Mol Cancer* (2021) 20:131. doi: 10.1186/s12943-021-01428-1

64. Chan JSK, Sng MK, Teo ZQ, Chong HC, Twang JS, Tan NS. Targeting nuclear receptors in cancer-associated fibroblasts as concurrent therapy to inhibit development of chemoresistant tumors. *Oncogene* (2018) 37(2):160–73. doi: 10.1038/onc.2017.319

65. Haider MT, Smit DJ, Taipaleenmäki H. The endosteal niche in breast cancer bone metastasis. *Front Oncol* (2020) 10:335. doi: 10.3389/fonc.2020.00335

66. Jain RK, Martin JD, Stylianopoulos T. The role of mechanical forces in tumor growth and therapy. *Annu Rev BioMed Eng* (2014) 16:321–46. doi: 10.1146/annurev-bioeng-071813-105259

67. Peiris-Pagès M, Sotgia F, Lisanti MP. Chemotherapy induces the cancer-associated fibroblast phenotype, activating paracrine hedgehog-GLI signalling in breast cancer cells. *Oncotarget* (2015) 6(13):10728–45. doi: 10.18632/oncotarget.3828

68. Belli C, Trapani D, Viale G, D'Amico P, Duso BA, Della Vigna P, et al. Targeting the microenvironment in solid tumors. *Cancer Treat Rev* (2018) 65:22–32. doi: 10.1016/j.ctrv.2018.02.004

69. Mendoza-Reinoso V, McCauley LK, Fournier PGJ. Contribution of macrophages and T cells in skeletal metastasis. *Cancers (Basel)* (2020) 12(4):E1014. doi: 10.3390/cancers12041014

70. Strachan DC, Ruffell B, Oei Y, Bissell MJ, Coussens LM, Pryer N, et al. CSF1R inhibition delays cervical and mammary tumor growth in murine models by attenuating the turnover of tumor-associated macrophages and enhancing infiltration by CD8+ T cells. *Oncoimmunology* (2013) 2(12):e26968. doi: 10.4161/onci.26968

71. Ruffell B, Chang-Strachan D, Chan V, Rosenbusch A, Ho CMT, Pryer N, et al. Macrophage IL-10 blocks CD8+ T cell-dependent responses to chemotherapy by suppressing IL-12 expression in intratumoral dendritic cells. *Cancer Cell* (2014) 26(5):623–37. doi: 10.1016/j.ccell.2014.09.006

72. Xu M, Zhao Z, Song J, Lan X, Lu S, Chen M, et al. Interactions between interleukin-6 and myeloid-derived suppressor cells drive the chemoresistant phenotype of hepatocellular cancer. *Exp Cell Res* (2017) 351(2):142–9. doi: 10.1016/j.yexcr.2017.01.008

73. Felcher CM, Bogni ES, Kordon EC. IL-6 cytokine family: A putative target for breast cancer prevention and treatment. *Int J Mol Sci* (2022) 23(3):1809. doi: 10.3390/ijms23031809

74. Ramachandran IR, Condamine T, Lin C, Herlihy SE, Garfall A, Vogl DT, et al. Bone marrow PMN-MDSCs and neutrophils are functionally similar in protection of multiple myeloma from chemotherapy. *Cancer Lett* (2016) 371(1):117–24. doi: 10.1016/j.canlet.2015.10.040

75. Patel S, Fu S, Mastio J, Dominguez GA, Purohit A, Kossenkov A, et al. Unique pattern of neutrophil migration and function during tumor progression. *Nat Immunol* (2018) 19(11):1236–47. doi: 10.1038/s41590-018-0229-5

76. Saini M, Szczerba BM, Aceto N. Circulating tumor cell-neutrophil tango along the metastatic process. *Cancer Res* (2019) 79(24):6067–73. doi: 10.1158/0008-5472.CAN-19-1972

77. Wik JA, Skålhegg BS. T Cell metabolism in infection. *Front Immunol* (2022) 13:840610. doi: 10.3389/fimmu.2022.840610

78. Thommen DS, Schumacher TN. T Cell dysfunction in cancer. *Cancer Cell* (2018) 33(4):547–62. doi: 10.1016/j.ccell.2018.03.012

79. Farhood B, Najafi M, Mortezaee K. CD8+ cytotoxic T lymphocytes in cancer immunotherapy: A review. *J Cell Physiol* (2019) 234(6):8509–21. doi: 10.1002/jcp.27782

80. Kond˙lková K, Vokurková D, Krejsek J, Borská L, Fiala Z, Ctirad A. Regulatory T cells (TREG) and their roles in immune system with respect to immunopathological disorders. *Acta Med (Hradec Kralove)* (2010) 53(2):73–7. doi: 10.14712/18059694.2016.63

81. Whiteside TL. The tumor microenvironment and its role in promoting tumor growth. *Oncogene* (2008) 27(45):5904–12. doi: 10.1038/onc.2008.271

82. Xiang P, Jin S, Yang Y, Sheng J, He Q, Song Y, et al. Infiltrating CD4+ T cells attenuate chemotherapy sensitivity in prostate cancer *via* CCL5 signaling. *Prostate* (2019) 79(9):1018–31. doi: 10.1002/pros.23810

83. Manore SG, Doheny DL, Wong GL, Lo HW. IL-6/JAK/STAT3 signaling in breast cancer metastasis: Biology and treatment. *Front Oncol* (2022) 12:866014. doi: 10.3389/fonc.2022.866014

84. Zhao P, Xiao L, Peng J, Qian YQ, Huang CC. Exosomes derived from bone marrow mesenchymal stem cells improve osteoporosis through promoting osteoblast proliferation *via* MAPK pathway. *Eur Rev Med Pharmacol Sci* (2018) 22(12):3962–70. doi: 10.26355/eurrev_201806_15280

85. Liu S, Liu F, Zhou Y, Jin B, Sun Q, Guo S. Immunosuppressive property of MSCs mediated by cell surface receptors. *Front Immunol* (2020) 11:1076. doi: 10.3389/fimmu.2020.01076

86. Pacini S, Petrini I. Are MSCs angiogenic cells? new insights on human nestin-positive bone marrow-derived multipotent cells. *Front Cell Dev Biol* (2014) 2:20. doi: 10.3389/fcell.2014.00020

87. Ahn SY. The role of MSCs in the tumor microenvironment and tumor progression. *Anticancer Res* (2020) 40(6):3039–47. doi: 10.21873/anticanres.14284

88. Patel SA, Ramkissoon SH, Bryan M, Pliner LF, Dontu G, Patel PS, et al. Delineation of breast cancer cell hierarchy identifies the subset responsible for dormancy. *Sci Rep* (2012) 2:906. doi: 10.1038/srep00906

89. Pinho S, Frenette PS. Haematopoietic stem cell activity and interactions with the niche. *Nat Rev Mol Cell Biol* (2019) 20(5):303–20. doi: 10.1038/s41580-019-0103-9

90. Sugiyama T, Kohara H, Noda M, Nagasawa T. Maintenance of the hematopoietic stem cell pool by CXCL12-CXCR4 chemokine signaling in bone marrow stromal cell niches. *Immunity* (2006) 25(6):977–88. doi: 10.1016/j.immuni.2006.10.016

91. Dubrovska A, Hartung A, Bouchez LC, Walker JR, Reddy VA, Cho CY, et al. CXCR4 activation maintains a stem cell population in tamoxifen-resistant breast cancer cells through AhR signalling. *Br J Cancer* (2012) 107(1):43–52. doi: 10.1038/bjc.2012.105

92. Mukherjee D, Zhao J. The role of chemokine receptor CXCR4 in breast cancer metastasis. *Am J Cancer Res* (2013) 3(1):46–57.

93. Nobutani K, Shimono Y, Mizutani K, Ueda Y, Suzuki T, Kitayama M, et al. Downregulation of CXCR4 in metastasized breast cancer cells and implication in their dormancy. *PloS One* (2015) 10(6):e0130032. doi: 10.1371/journal.pone.0130032

94. Shiozawa Y, Pienta KJ, Taichman RS. Hematopoietic stem cell niche is a potential therapeutic target for bone metastatic tumors. *Clin Cancer Res* (2011) 17 (17):5553–8. doi: 10.1158/1078-0432.CCR-10-2505

95. Capulli M, Hristova D, Valbret Z, Carys K, Arjan R, Maurizi A, et al. Notch2 pathway mediates breast cancer cellular dormancy and mobilisation in bone and contributes to haematopoietic stem cell mimicry. *Br J Cancer* (2019) 121(2):157–71. doi: 10.1038/s41416-019-0501-y

96. Liu M, Mo QG, Wei CY, Qin QH, Huang Z, He J. Platinum-based chemotherapy in triple-negative breast cancer: A meta-analysis. *Oncol Lett* (2013) 5 (3):983–91. doi: 10.3892/ol.2012.1093

97. Aaron N, Costa S, Rosen CJ, Qiang L. The implications of bone marrow adipose tissue on inflammaging. *Front Endocrinol* (2022) 13:853765. doi: 10.3389/fendo.2022.853765

98. Shin E, Koo JS. The role of adipokines and bone marrow adipocytes in breast cancer bone metastasis. *Int J Mol Sci* (2020) 21(14):4967. doi: 10.3390/ijms21144967

99. *The effect of marrow secretome and culture environment on the rate of metastatic breast cancer cell migration in two and three dimensions - PubMed*. Available at: https://pubmed.ncbi.nlm.nih.gov/33689396/.

100. Zarrer J, Haider MT, Smit DJ, Taipaleenmäki H. Pathological crosstalk between metastatic breast cancer cells and the bone microenvironment. *Biomolecules* (2020) 10(2):E337. doi: 10.3390/biom10020337

101. Reagan MR, Fairfield H, Rosen CJ. Bone marrow adipocytes: A link between obesity and bone cancer. *Cancers (Basel)* (2021) 13(3):364. doi: 10.3390/cancers13030364

102. Hanahan D, Coussens LM. Accessories to the crime: functions of cells recruited to the tumor microenvironment. *Cancer Cell* (2012) 21(3):309–22. doi: 10.1016/j.ccr.2012.02.022

103. Raymaekers K, Stegen S, van Gastel N, Carmeliet G. The vasculature: a vessel for bone metastasis. *Bonekey Rep* (2015) 4:742. doi: 10.1038/bonekey.2015.111

104. Cao Z, Ding BS, Guo P, Lee SB, Butler JM, Casey SC, et al. Angiocrine factors deployed by tumor vascular niche induce b cell lymphoma invasiveness and chemoresistance. *Cancer Cell* (2014) 25(3):350–65. doi: 10.1016/j.ccr.2014.02.005

105. Zhang Y, Xie ZY, Guo XT, Xiao XH, Xiong LX. Notch and breast cancer metastasis: Current knowledge, new sights and targeted therapy. *Oncol Lett* (2019) 18 (3):2743. doi: 10.3892/ol.2019.10653

106. Gatenby RA, Brown JS. Integrating evolutionary dynamics into cancer therapy. *Nat Rev Clin Oncol* (2020) 17(11):675–86. doi: 10.1038/s41571-020-0411-1

107. Karagiannis GS, Condeelis JS, Oktay MH. Chemotherapy-induced metastasis: mechanisms and translational opportunities. *Clin Exp Metastasis* (2018) 35(4):269–84. doi: 10.1007/s10585-017-9870-x

108. Subia B, Dahiya UR, Mishra S, Ayache J, Casquillas GV, Caballero D, et al. Breast tumor-on-chip models: From disease modeling to personalized drug screening. *J Control Release* (2021) 331:103–20. doi: 10.1016/j.jconrel.2020.12.057

109. Gonçalves IM, Carvalho V, Rodrigues RO, Pinho D, Teixeira SFCF, Moita A, et al. Organ-on-a-Chip platforms for drug screening and delivery in tumor cells: A systematic review. *Cancers (Basel)* (2022) 14(4):935. doi: 10.3390/cancers14040935

110. Sun W, Luo Z, Lee J, Kim HJ, Lee K, Tebon P, et al. Organ-on-a-Chip for cancer and immune organs modeling. *Adv Healthc Mater* (2019) 8(4):e1801363. doi: 10.1002/adhm.201801363

111. Bersini S, Arrigoni C, Lopa S, Bongio M, Martin I, Moretti M. Engineered miniaturized models of musculoskeletal diseases. *Drug Discovery Today* (2016) 21 (9):1429–36. doi: 10.1016/j.drudis.2016.04.015

112. Kim C, Bang JH, Kim YE, Lee SH, Kang JY. On-chip anticancer drug test of regular tumor spheroids formed in microwells by a distributive microchannel network. *Lab Chip* (2012) 12(20):4135–42. doi: 10.1039/c2lc40570a

113. Brancato V, Gioiella F, Imparato G, Guarnieri D, Urciuolo F, Netti PA. 3D breast cancer microtissue reveals the role of tumor microenvironment on the transport and efficacy of free-doxorubicin in vitro. *Acta Biomater* (2018) 75:200–12. doi: 10.1016/j.actbio.2018.05.055

114. Zhu W, Holmes B, Glazer RI, Zhang LG. 3D printed nanocomposite matrix for the study of breast cancer bone metastasis. *Nanomed: Nanotechnol Biol Med* (2016) 12 (1):69–79. doi: 10.1016/j.nano.2015.09.010

115. Kar S, Katti DR, Katti KS. Bone interface modulates drug resistance in breast cancer bone metastasis. *Colloids Surfaces B: Biointerfaces* (2020) 195:111224. doi: 10.1016/j.colsurfb.2020.111224

116. Sharifi S, Barar J, Hejazi MS, Samadi N. Roles of the bcl-2/Bax ratio, caspase-8 and 9 in resistance of breast cancer cells to paclitaxel. *Asian Pac J Cancer Prev* (2014) 15 (20):8617–22. doi: 10.7314/APJCP.2014.15.20.8617

117. Litviakov NV, Cherdyntseva NV, Tsyganov MM, Denisov EV, Garbukov EY, Merzliakova MK, et al. Changing the expression vector of multidrug resistance genes is related to neoadjuvant chemotherapy response. *Cancer Chemother Pharmacol* (2013) 71(1):153–63. doi: 10.1007/s00280-012-1992-x

118. Li YJ, Lei YH, Yao N, Wang CR, Hu N, Ye WC, et al. Autophagy and multidrug resistance in cancer. *Chin J Cancer* (2017) 36(1):52. doi: 10.1186/s40880-017-0219-2

119. Langer EM, Allen-Petersen BL, King SM, Kendsersky ND, Turnidge MA, Kuziel GM, et al. Modeling tumor phenotypes in vitro with three-dimensional bioprinting. *Cell Rep* (2019) 26(3):608–623.e6. doi: 10.1016/j.celrep.2018.12.090

120. Marturano-Kruik A, Nava MM, Yeager K, Chramiec A, Hao L, Robinson S, et al. Human bone perivascular niche-on-a-chip for studying metastatic colonization. *Proc Natl Acad Sci* (2018) 115(6):1256–61. doi: 10.1073/pnas.1714282115

121. Glaser DE, Curtis MB, Sariano PA, Rollins ZA, Shergill BS, Anand A, et al. Organ-on-a-chip model of vascularized human bone marrow niches. *Biomaterials* (2022) 280:121245. doi: 10.1016/j.biomaterials.2021.121245

122. Crippa M, Talò G, Lamouline A, Bolis S, Arrigoni C, Bersini S, et al. A microfluidic model of human vascularized breast cancer metastasis to bone for the study of neutrophil-cancer cell interactions. *Mater Today Bio* (2022) 17:100460. doi: 10.1016/j.mtbio.2022.100460

123. Colombo MV, Bersini S, Arrigoni C, Gilardi M, Sansoni V, Ragni E, et al. Engineering the early bone metastatic niche through human vascularized immuno bone minitissues. *Biofabrication* (2021) 13(3):035036. doi: 10.1088/1758-5090/abefea

124. Ma C, Witkowski MT, Harris J, Dolgalev I, Sreeram S, Qian W, et al. Leukemia-on-a-chip: Dissecting the chemoresistance mechanisms in b cell acute lymphoblastic leukemia bone marrow niche. *Sci Adv* (2020) 6(44):eaba5536. doi: 10.1126/sciadv.aba5536

125. Bruce A, Evans R, Mezan R, Shi L, Moses BS, Martin KH, et al. Three-dimensional microfluidic tri-culture model of the bone marrow microenvironment for study of acute lymphoblastic leukemia. *PloS One* (2015) 10(10):e0140506. doi: 10.1371/journal.pone.0140506

126. Khin ZP, Ribeiro MLC, Jacobson T, Hazlehurst L, Perez L, Baz R, et al. A preclinical assay for chemosensitivity in multiple myeloma. *Cancer Res* (2014) 74 (1):56–67. doi: 10.1158/0008-5472.CAN-13-2397

127. Pak C, Callander NS, Young EWK, Titz B, Kim K, Saha S, et al. MicroC3: an ex vivo microfluidic cis-coculture assay to test chemosensitivity and resistance of patient multiple myeloma cells. *Integr Biol (Camb)* (2015) 7(6):643–54. doi: 10.1039/C5IB00071H

128. Fitzgerald KA, Guo J, Tierney EG, Curtin CM, Malhotra M, Darcy R, et al. The use of collagen-based scaffolds to simulate prostate cancer bone metastases with potential for evaluating delivery of nanoparticulate gene therapeutics. *Biomaterials* (2015) 66:53–66. doi: 10.1016/j.biomaterials.2015.07.019

129. Rimann M, Laternser S, Gvozdenovic A, Muff R, Fuchs B, Kelm JM, et al. An *in vitro* osteosarcoma 3D microtissue model for drug development. *J Biotechnol* (2014) 189:129–35. doi: 10.1016/j.jbiotec.2014.09.005

130. Fong ELS, Lamhamedi-Cherradi SE, Burdett E, Ramamoorthy V, Lazar AJ, Kasper FK, et al. Modeling Ewing sarcoma tumors *in vitro* with 3D scaffolds. *Proc Natl Acad Sci U S A* (2013) 110(16):6500–5. doi: 10.1073/pnas.1221403110

131. Santoro M, Menegaz BA, Lamhamedi-Cherradi SE, Molina ER, Wu D, Priebe W, et al. Modeling stroma-induced drug resistance in a tissue-engineered tumor model of Ewing sarcoma. *Tissue Eng Part A* (2017) 23(1–2):80–9. doi: 10.1089/ten.tea.2016.0369

132. Picollet-D'hahan N, Zuchowska A, Lemeunier I, Le Gac S. Multiorgan-on-a-Chip: A systemic approach to model and decipher inter-organ communication. *Trends Biotechnol* (2021) 39(8):788–810. doi: 10.1016/j.tibtech.2020.11.014

133. Sung JH, Wang YI, Sriram NN, Jackson M, Long C, Hickman JJ, et al. Recent advances in body-on-a-chip systems. *Anal Chem* (2019) 91(1):330–51. doi: 10.1021/acs.analchem.8b05293

134. *2D vs 3D - creative biolabs*. Available at: https://www.creative-biolabs.com/adc/2d-vs-3d.htm.

135. Jensen C, Teng Y. Is it time to start transitioning from 2D to 3D cell culture? *Front Mol Biosci* (2020) 7:33. doi: 10.3389/fmolb.2020.00033

136. Fontoura JC, Viezzer C, dos Santos FG, Ligabue RA, Weinlich R, Puga RD, et al. Comparison of 2D and 3D cell culture models for cell growth, gene expression and drug resistance. *Mater Sci Engineering: C* (2020) 107:110264. doi: 10.1016/j.msec.2019.110264

137. Fischetti T, Di Pompo G, Baldini N, Avnet S, Graziani G. 3D printing and bioprinting to model bone cancer: The role of materials and nanoscale cues in directing cell behavior. *Cancers (Basel)* (2021) 13(16):4065. doi: 10.3390/cancers13164065

138. Hampshire VA, Gilbert SH. Refinement, reduction, and replacement (3R) strategies in preclinical testing of medical devices. *Toxicol Pathol* (2019) 47(3):329–38. doi: 10.1177/0192623318797289

139. Wittkowske C, Reilly GC, Lacroix D, Perrault CM. *In vitro* bone cell models: Impact of fluid shear stress on bone formation. *Front Bioengineering Biotechnol* (2016) 4:87. doi: 10.3389/fbioe.2016.00087

140. Mainardi VL, Arrigoni C, Bianchi E, Talò G, Delcogliano M, Candrian C, et al. Improving cell seeding efficiency through modification of fiber geometry in 3D printed scaffolds. *Biofabrication* (2021) 13(3):035025. doi: 10.1088/1758-5090/abe5b4

141. Lewis KT, MacDougald OA. Bone: Bone marrow adipocytes in 3D. *Nat Rev Endocrinol* (2018) 14(5):254–5. doi: 10.1038/nrendo.2018.31

142. Yi B, Xu Q, Liu W. An overview of substrate stiffness guided cellular response and its applications in tissue regeneration. *Bioactive Mater* (2022), 15: 82–102. doi: 10.1016/j.bioactmat.2021.12.005

frontiers | Frontiers in Oncology

TYPE Review
PUBLISHED 28 April 2023
DOI 10.3389/fonc.2023.1164535

OPEN ACCESS

EDITED BY
Giulia Adriani,
Singapore Immunology Network (A*STAR), Singapore

REVIEWED BY
Anirban Roy,
University of Houston, United States
Jozsef Dudas,
Innsbruck Medical University, Austria
Zhuoyang Fan,
Fudan University, China

*CORRESPONDENCE
Marco Vanoni
marco.vanoni@unimib.it
Mara Gilardi
mara.gilardi@gmail.com

RECEIVED 13 February 2023
ACCEPTED 11 April 2023
PUBLISHED 28 April 2023

CITATION
Proietto M, Crippa M, Damiani C, Pasquale V, Sacco E, Vanoni M and Gilardi M (2023) Tumor heterogeneity: preclinical models, emerging technologies, and future applications.
Front. Oncol. 13:1164535.
doi: 10.3389/fonc.2023.1164535

Tumor heterogeneity: preclinical models, emerging technologies, and future applications

Marco Proietto[1,2,3], Martina Crippa[4,5], Chiara Damiani[6,7], Valentina Pasquale[6,7], Elena Sacco[6,7], Marco Vanoni[6,7]* and Mara Gilardi[3,8]*

[1]Next Generation Sequencing Core, The Salk Institute for Biological Studies, La Jolla, CA, United States, [2]Gene Expression Laboratory, The Salk Institute for Biological Studies, La Jolla, CA, United States, [3]NOMIS Center for Immunobiology and Microbial Pathogenesis, The Salk Institute for Biological Studies, La Jolla, CA, United States, [4]Vita-Salute San Raffaele University, Milan, Italy, [5]Experimental Imaging Center, Istituti di Ricovero e Cura a Carattere Scientifico (IRCCS) Ospedale San Raffaele, Milan, Italy, [6]Infrastructure Systems Biology Europe /Centre of Systems Biology (ISBE/SYSBIO) Centre of Systems Biology, Milan, Italy, [7]Department of Biotechnology and Biosciences, School of Sciences, University of Milano-Bicocca, Milan, Italy, [8]Salk Cancer Center, The Salk Institute for Biological Studies, La Jolla, CA, United States

Heterogeneity describes the differences among cancer cells within and between tumors. It refers to cancer cells describing variations in morphology, transcriptional profiles, metabolism, and metastatic potential. More recently, the field has included the characterization of the tumor immune microenvironment and the depiction of the dynamics underlying the cellular interactions promoting the tumor ecosystem evolution. Heterogeneity has been found in most tumors representing one of the most challenging behaviors in cancer ecosystems. As one of the critical factors impairing the long-term efficacy of solid tumor therapy, heterogeneity leads to tumor resistance, more aggressive metastasizing, and recurrence. We review the role of the main models and the emerging single-cell and spatial genomic technologies in our understanding of tumor heterogeneity, its contribution to lethal cancer outcomes, and the physiological challenges to consider in designing cancer therapies. We highlight how tumor cells dynamically evolve because of the interactions within the tumor immune microenvironment and how to leverage this to unleash immune recognition through immunotherapy. A multidisciplinary approach grounded in novel bioinformatic and computational tools will allow reaching the integrated, multilayered knowledge of tumor heterogeneity required to implement personalized, more efficient therapies urgently required for cancer patients.

KEYWORDS

tumor microenvironment (TME), tumor heterogeneity, tumor immune microenvironment, heterogeneity models, human *in vitro* models

1 Tumor heterogeneity: a multifaceted phenomenon

The NCI Dictionary of Cancer describes cancer heterogeneity as "the differences between tumors of the same type in different patients, the differences between cancer cells within a single tumor, or the differences between a primary (original) tumor and a secondary tumor" ((NCI), n.d.). Tumor heterogeneity first originates from the clonal expansion of individually mutated cells that, interacting with the evolution of the tumor microenvironment, provide the genetic and epigenetic material upon which Darwinian and non-Darwinian evolutionary trajectories drive cancer evolution (1). The cancer phenotypic properties are modulated at the epigenetic, transcriptional, protein, and environmental levels, where different cell types contribute to the heterogeneity of the cancer tissue in both time (as the tumor evolves) and space, where the evolving composition of the tumor microenvironment—that includes dynamically interacting cancer, immune, or stromal cells—originates the ability of the cancer tissue to respond to environmental cues and access nutrients, growth factors, and oxygen. In turn, this molecular and cellular heterogeneity translates to intra- and interpatient spatiotemporal variability in the global properties of the tumor, deeply affecting drug response and disease outcome (2).

Intertumoral heterogeneity describes the tumor-by-tumor differences among different patients and is dependent on environmental factors impacting patients' phenotypes.

On the other hand, intratumor heterogeneity (ITH) is the cellular diversity within the same tumor or between primary and metastatic lesions. It includes copy number variations (3), epigenetic alterations, coding and non-coding somatic alterations, and transcriptome, proteome, and metabolome differences (4) (Figure 1).

In tumor sites, the accumulation of genetic and epigenetic alterations and chromosomal aberrations is strongly accelerated for various reasons. It can be fostered by: i) the expression of oncogenes or the loss of tumor suppressor genes that compromise the DNA repair mechanisms or the spindle assembly checkpoint, causing genomic instability; ii) exposure to endogenous or exogenous toxic factors including therapeutic agents; iii) the tumor microenvironment (TME) (nutrient limitation/hypoxia/immune system); iv) other genetic and non-genetic factors.

Among the several genes whose deregulation contributes to tumor heterogeneity, the tumor suppressor *TP53* stands out. The loss of function of the *TP53* gene determines the deregulation of the cell cycle arrest checkpoint allowing cell proliferation despite the presence of stress signals and DNA damages or skipping apoptosis also in the presence of severe DNA damages (5). Also, the deregulation of genes involved in the DNA repair system (mismatch repair or proofreading machinery) drives genome instability and subclonal heterogeneity in the tumor sites (6, 7). Large-scale chromosomal alteration events causing the loss of genetic material in the order of hundreds of genes greatly accelerate subclonal evolution and increase the tumor mutational burden (the total number of mutations per coding area of a tumor genome) which can positively or negatively correlate with prognosis and pharmacological response (8).

Exogenous factors contributing to tumor heterogeneity include physical factors, such as ionizing and non-ionizing electromagnetic radiation (UV); chemical factors such as heavy metals and toxic chemicals including drugs used in anticancer treatments; and biological factors, such as viruses, bacteria, and reactive oxygen species (ROS) arising as a by-product of the mitochondrial energy metabolism (9). In this context, it has been shown that some types of tumors such as melanoma and lung cancer have a high clonal "homogeneous coding" mutational burden due to the continuous exposure of stem cell niches to carcinogens, such as UV for skin and tobacco for lungs.

Nutrient shortage and hypoxia experienced by the cells within the core of a newly formed and non-vascularized tumor mass impose profound metabolic rearrangements, selecting clones preferring fermentative anaerobic metabolism (10–12). The TME can also affect tumor heterogeneity in terms of quantity and phenotypic characteristics of immune and stromal cells recruited at the tumor site (13–15).

The stroma and immune system's role in tumor heterogeneity will be extensively described in Section 6.

In this manuscript, we will review established and emerging models used to study tumor heterogeneity and how the integrated use of these models and technologies can improve our knowledge of tumor heterogeneity, with a special focus on the increasing role of immune cells.

2 Non-human models to study heterogeneity

Animal models and cellular *in vitro* models have long been exploited to better understand the complex biological processes characterizing normal human physiology and disease (Figure 2).

In particular, the mouse is the most used animal model for biomedical research, discovery, and validation. More recently, novel approaches leveraging bioengineering and complex culture methods have become more present in the field. Since TME is such a complex and dynamic microenvironment, different models and more comprehensive ways to dissect the mechanism underlying heterogeneity and response to treatment have been developed. Remarkably, for every single research application and biological question, there is a right model and strategy to apply.

2.1 Murine models used to uncover tumor heterogeneity

The most used animal models for cancer research are genetically engineered mice (GEMMs). GEMMs are immunocompetent transgenic mice that spontaneously develop malignancies (16). GEMMs allowed the fundamental discovery that tumor development is driven by the gene loss of a tumor suppressor gene and/or an oncogene overexpression (17, 18).

10.3389/fonc.2023.1164535

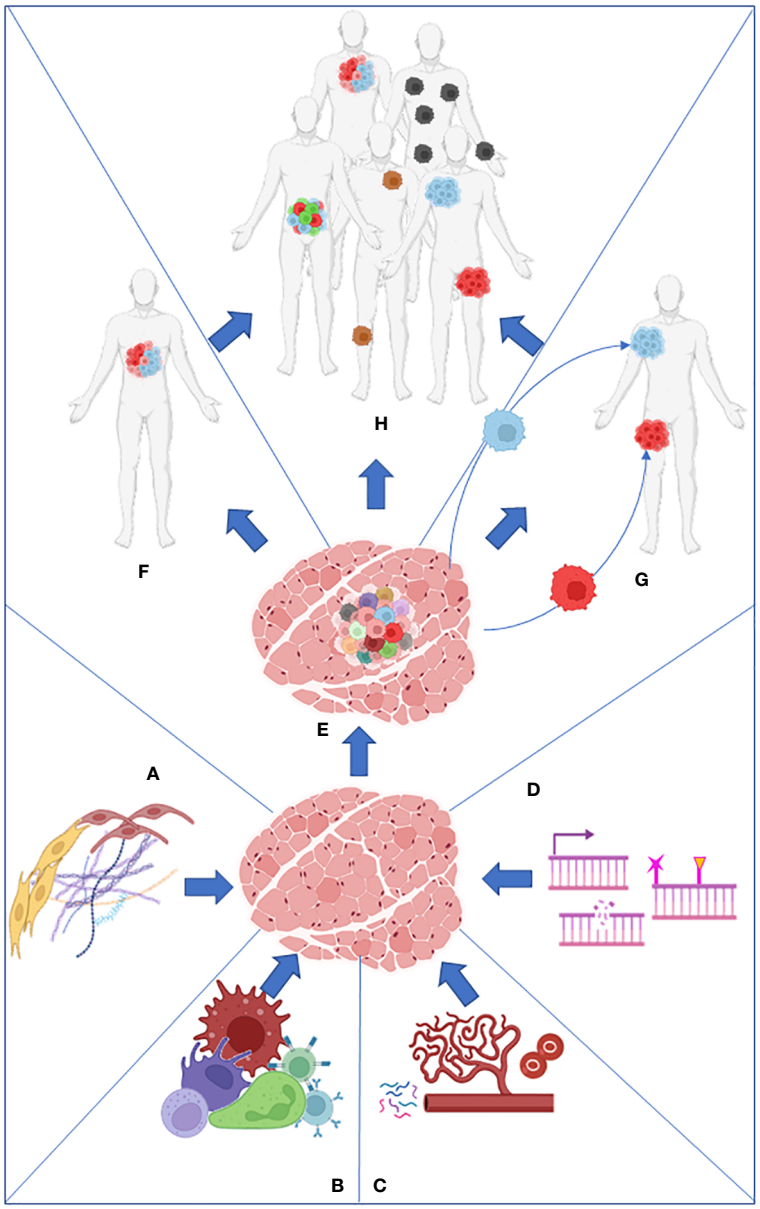

FIGURE 1
Stroma **(A)**, immune cells **(B)**, nutrients present in the microenvironment **(C)**, and intrinsic factors such as DNA damage and epigenome **(D)** work together to produce the primary tumor heterogeneity **(E)**. Intratumor heterogeneity can arise from the primary tumor **(F)** or from its metastasis **(G)**. Both processes collaborate in the establishment of intertumoral heterogeneity in the population **(H)**.

While the field has relied extensively in the past 20 years on Cre/Lox models, the more recent development of CRISPR/Cas9 approaches has further accelerated the development of mouse models of human cancers.

Because the mice used in these experiments live in controlled environments and are genetically similar, tumor development and associated phenotypes are highly reproducible, allowing longitudinal studies that are more difficult in humans. Nevertheless, even in the most controlled environment, mouse tumors arising from defined genetic events do evolve to be genetically different and unique, like human tumors (19). However, mouse tumors may evolve with a lower level of genetic heterogeneity due to the absence of environmental mutagens in most cases leading to limited translational value.

A great strategy to study heterogeneity in murine models is lineage tracing allowing for the definition of the mode of tumor growth by clonal analysis. This technique has been extensively used in differentiation studies, and it has also been exploited in cancer. For example, leveraging this, Schepers et al. identified Lgr5+ stem cell activity in mouse intestinal adenomas (20).

Another simple way to mimic the human situation is to treat mice with the same carcinogens that are known to cause cancer in humans (21). For example, the 4NQO carcinogen present in tobacco has been used to induce head and neck cancer development in mice mimicking up to 94% tobacco mutational

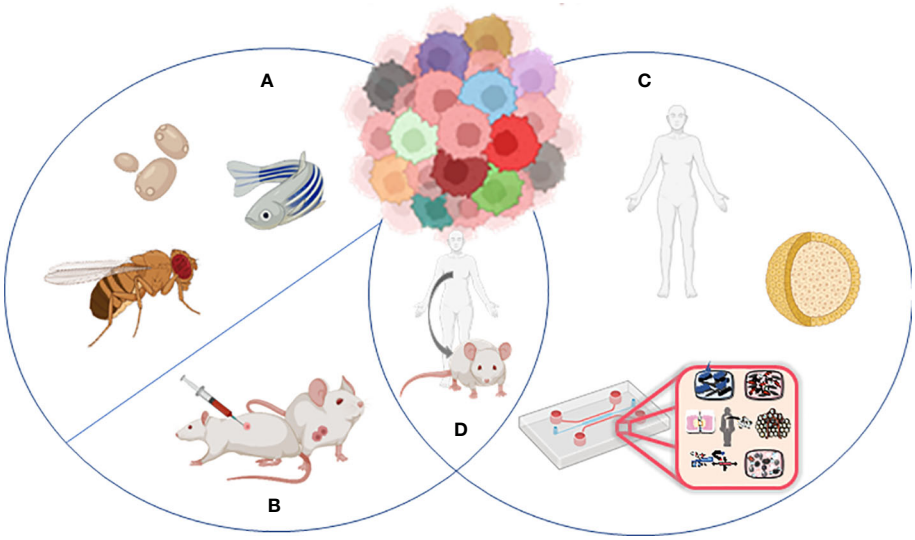

FIGURE 2
Models to study tumor heterogeneity: **(A)** non-murine models (*Drosophila melanogaster, Danio renio, Saccharomyces cerevisiae*), **(B)** murine models (syngeneic models, GEMMs), **(C)** human *in vitro* models (organoids, organ-on-chip), and **(D)** humanized murine models.

signatures (22). The importance of these types of models is supported by their extremely extensive use (23–25).

The use of GEMMs is limited by intrinsic problems, including reduced viability if the mutations occur in the germline, early death in case of simultaneous development of multiple tumors, and non-synchronous tumor development in different mice due to incomplete mutation penetrance (26). Some of these limitations can be overcome with the application of novel technologies (17, 27, 28), but mostly reliable heterogeneity studies rely on patient-derived xenograft (PDX) models (29, 30). Human tumor cells are transplanted into an immune-deficient mouse to obtain a PDX, maintaining the heterogeneity of the primary tumor (31). A greater success rate can be achieved with major immunosuppression in the animal host, and the exploitation of mice lacking B and T lymphocytes and NK cells shows a better success rate (32). An advantage of using PDXs is that aggressive tumors such as colorectal and gastric cancer have more possibilities to engraft in the host, making PDX an extremely valuable resource to study aggressive pathologies. Human hormonal treatment of transplanted mice can improve the engraftment rate of hormone-driven tumors (30).

The biological differences between mice and humans are limiting factors in the direct translation of many discoveries to the clinical setting. Thus, a growing need for a mouse model that better recapitulates the important features of human biology and immunity became more urgent. With the advent of immunotherapeutic drugs leveraging the immune system and since the mouse immune system does not always replicate the human one, new humanized mouse models providing the immune components required to test new therapies have been generated. These humanized models represent a tremendous advantage in providing a platform resembling the human response. Humanized mice with a partial or fully reconstituted immune system have been developed through stem cell transplant, and they are a promising platform to assess the efficacy of immune checkpoint inhibitors. However, since the human immune system engraftment process necessitates multiple donors, this generates a high variability in the results requiring both an increased number of donors and mice. As an alternative, knock-in mice have been developed. These models express human genes such as immune checkpoint inhibitors, PD-1, allowing efficacy studies in immune-competent systems (33).

2.2 Non-murine models exploited in the understanding of tumor heterogeneity

Although most of the research that focused on cancer heterogeneity has relied on primary patient samples, murine xenograft, and murine models, there are more evolutionarily distant model organisms that are genetically, histologically, and behaviorally similar to the human cancer disease, and they can have a potential key role in our understanding of cancer heterogeneity.

2.2.1 Yeast

The yeast *Saccharomyces cerevisiae*—a eukaryotic unicellular organism that has long been successfully used as a model organism for human biology (34)—can grow both in liquid and solid media using different sugars to support its growth. Approximately half of the yeast genes exhibit periodic expression patterns when grown under continuous, nutrient-limited conditions. The cell cycle stage significantly exacerbates the natural variability present in the population (35). Similarly, tumor cells could respond differently to the TME according to their cell cycle stage.

Individual yeast cells respond differently to sugar sources, and variability in the expression of sugar-metabolizing genes is observed. For example, single-cell sequencing data showed that only 1.5% of cells express genes required for galactose metabolism without this sugar (36).

The group of Teusink showed that metabolic heterogeneity within a yeast population could be established and maintained without any genetic difference (37).

This metabolic variability is observable and even amplified in yeast colonies growing on solid media. The cells within a yeast colony are all the progeny from a single founder and share the same genome. Nevertheless, individual cells in a colony have different access to resources. Cells in the colony's lower part—i.e., closer to the solid medium—have easier access to nutritional resources, expressing genes related to respiratory metabolism, while in the upper part, the cells which cannot directly access the nutrients rely on fermentation (38). As a result, in a single colony, a small number of cells survive using gluconeogenesis, releasing metabolites consumed by another subpopulation with a different metabolic phenotype (39).

2.2.2 Zebrafish

Zebrafish and humans share 70% of protein-coding genes (40), and their cancers are genetically and histologically similar (41), also sharing some important drivers in the onset (42). In the field of heterogeneity studies, zebrafish optical clarity has been combined with tumor labeling and new imaging techniques by White et al., who transplanted single-cell tumors into zebrafish and studied the clonal evolution in response to drug delivery, also taking advantage of the possibility of using thousands of fish simultaneously, generating a massive amount of data (41).

Stemness is another characteristic of cancer involved in the heterogeneity process and a mechanism that needs to be uncovered. Ignatius et al. selectively labeled differentiated and non-differentiated cells with different fluorophores, being able to sort through FACS the two different populations, revealing divergent expression profiles and behaviors (with the more differentiated cells being highly migratory) after microarray analysis (43). FACS sorting has been also exploited to isolate zebrafish leukemia cells and transplant them into syngeneic recipients allowing the production of monoclonal antibodies and paving the way to new zebrafish cancer models for drug development (44).

It is also possible to prepare libraries of single tumors and transplant them into recipient fish to recapitulate the ITH and to study the effects of drugs (43, 45). The Zebrabow technology based on the multispectral cell labeling for cell tracing and lineage analysis in zebrafish allows the labeling of different tumor clones with different colors and *in vivo* following their migrations and competition in the heterogeneous tissue, also assessing the effects of drug treatments (46, 47).

The optically clear immune-compromised zebrafish "casper" allows the direct visualization of fluorescently labeled transplanted cancer cells and supports the neovascularization and the tumor propagation of heterogeneous clones (48). The "Modeling Approach in Zebrafish for Rapid Tumor Initiation" (MAZERATI) allows to express oncogenes and inactivate candidate tumor suppressor genes using two particular CRISPR vectors, spatially controlling the tumor spreading (49).

2.2.3 Drosophila

Sixty percent of the *Drosophila melanogaster* genome is homologous to humans, with 90% of genes involved in human cancer development having an ortholog in the fly (50, 51). Together with a fast generation time and low maintenance costs, these features contributed to the development of genetic tools to use the fly as a model organism for cancer research (52). The "genetic mosaic technique" lately perfectioned into the "mosaic analysis with a repressible cell marker (MARCM)" creates individually labeled homozygous cells in a heterozygous population, generating cells with a different genotype in a single organism, allowing the researchers to follow the labeled subpopulation destiny (53). MARCM revealed how a single mutated cell in a healthy tissue does not simply overgrow but mostly stimulates the overgrowth and metastasis in the neighbor cells, contributing to cancer progression and probably recurrence (54). The same technique also showed that heterogeneity induces cancer and metastasis by signal propagation (55), molecule exocytosis (56), amino acid release (57), or ROS production (58). Other studies highlighted how different cell populations cooperate in generating tumors: cells mutated in the spindle assembly checkpoints extrude from the epithelium, losing epithelial morphology and adhesion. These mesenchymal-like cells are unable to proliferate but establish a tumor environment by secreting molecules which promote the growth of epithelial cells. So, in this case, epithelial and mesenchymal/mutant cells, which at the beginning are genetically identical, cooperate in the tumor establishment, with the mutant cells unable to proliferate but still activating the others (59–61).

3 Human *in vitro* models to study heterogeneity

The biological similarity between animal models and humans has been the basis of the extensive use of these approaches in the study of cancer. However, the failure of many clinical trials and the undeniable evidence of discrepancies in the fidelity of the different models in replicating human physiology generated the necessity of human-derived models.

3.1 Organoids

Organoids can be described as microscopic self-organizing, three-dimensional structures, recapitulating many structural and functional aspects of their *in vivo* counterpart organs (62). Biological material such as primary tissues (single cells or tissue chunks), stem cells like adult stem cells (ASCs), induced pluripotent stem cells (iPSCs), and embryonic stem cells (ESCs) can be employed as starting material for organoid production (63). The cells are embedded in an extracellular matrix structure resembling the tissue scaffold and mirroring the physiological milieu to contemplate both matrix influence on cell growth and spatial organization (64); the final result is a heterotypic three-dimensional structure that replicates the multilineage composition

of the tissue of origin as well as its molecular, metabolic, and spatial heterogeneity.

It is possible to derive lineage heterogeneity through organogenesis using stem cells (65), while unfortunately, the different cell lineages are not easily preserved in patient-derived organoids (PDOs) obtained from tumor sampling due to the selection of epithelial cells during tissue processing (66, 67). To work around this issue, the introduction of further cell lineages has been applied to organoid models to depict a more complex microenvironment. For example, the desmoplastic reaction represents a neoplastic feature influencing inflammatory response and drug distribution, especially in pancreatic cancer, one of the deadliest cancers worldwide (67); to better investigate tumor–fibroblast interactions in pancreatic ductal adenocarcinoma (68), Biffi et al. (69) developed a co-culture system combining naive pancreatic stellate cells, a precursor of cancer-associated fibroblast (CAF), to organoids generated from pancreatic cancer cells arising from a GEMM spontaneously developing pancreatic cancer. This model was able to reproduce the functional differentiation of pancreatic stellate cells to inflammatory CAF and myofibroblastic CAF elicited by the tumor milieu.

Organoids are also applied to a wide range of tissues and pathologies, e.g., breast cancer (70), liver cancer (71, 72), gastric cancer (73), colorectal cancer (74), prostate cancer (75), and pancreatic cancer (76–78).

In the immune context, Neal et al. (79) were able to establish a patient-derived organoid culture from samples coming from 100 individual patients, covering 19 different tissue sites and 28 pathology subtypes using an air–liquid interface method; however, they encountered major difficulties in preserving the stromal population. The generated organoids mostly recapitulated the parental tumor histology and maintained a complex tissue architecture, but in 70% of the tumors, the stromal myofibroblast population progressively decreased. On the other hand, they observed that PDO-retained tumor-infiltrating lymphocytes ($CD3^+$) were integrally embedded in close proximity to the tumor epithelium, macrophages, cytotoxic T cells ($CD8^+$), helper T cells ($CD4^+$), natural killer (NK) cells, and natural killer T (NKT) cells, which they were able to support using IL-2 supplementation until 60 days of culture. Instead of evaluating resident and tumor-infiltrating immune cells, Dijkstra et al. (80) successfully produced colon-rectal and non-small cell lung cancer PDOs, and later, to study immune response toward cancer and delineate a strategy to develop tailored immunotherapy, they used T-cell populations from peripheral blood to generate a co-culture with organoids; in such a manner, they were able to elicit a specific antitumor immune response mediated by $CD8^+$ T cells toward the PDOs. Extensive genetic heterogeneity within cancer cell populations is also documented beyond lineage heterogeneity. ITH, as already presented, provides a substrate for tumor development promoting drug resistance and metastasis. Therefore, it is necessary to model the mutational diversity associated with the branched evolution of clonogenicity, which can be an innate characteristic of PDOs coming from the genetic diversity in the tumor of origin (81) or can be promoted in stem cell-derived organoids through genetic engineering (74, 82, 83). Bolhaqueiro et al. (84) employed colorectal cancer PDOs to investigate the prevalence of chromosomal instability. Single-cell analysis through three-dimensional live-cell imaging and karyotype sequencing highlighted a high frequency of chromosomal instability, which results in aneuploidy and genomic heterogeneity and promotes drug resistance in colorectal cancer.

The highlighted attention to intratumor diversity in molecular studies is promoting an overrunning of personalized medicine and individual clinical plan toward a precision medicine approach that targets heterogeneity itself embracing intracellular modification as well.

In the field of metabolism, three-dimensional organization and multicellular diversification drive the development of differentiated areas and layers resulting in the impaired distribution of nutrients and oxygen with an impact on cell proliferation and metabolism (85); indeed, metabolic heterogeneity affects drug response as well as carcinogenesis (86). Several methodological approaches have been developed for real-time and spatial-resolved metabolism analysis in organoids such as extracellular flux analysis (Seahorse XF analyzer) which allows measuring at the same time and in real time on living cells the oxygen consumption rate (OCR) and the extracellular acidification rate (ECAR) on both cells, spheroids, and organoids in a microplate (87–89). Advanced metabolic flow cytometry analysis such as SCENITH (90) monitors the metabolism through protein synthesis, while MET-FLOW detects rate-limiting enzymes (91). FLIM and PLIM are live-cell microscopy techniques (70, 92–98) that provide unique sensitivity in detecting the metabolic changes occurring during carcinogenesis and anticancer drug response.

While PLIM requires the use of dedicated cell-penetrating phosphorescent O_2-sensitive probes to perform live-cell microscopy of oxygen, FILM is a non-invasive, label-free, cell-specific direct analysis of metabolism which takes advantage of the intrinsic fluorescence properties of NADH and FAD; an increment in the NADH/FAD ratio observed through metabolic imaging enabled the identification of malignant cells exploiting the Warburg effect (70). These technologies also brought the discovery of metabolic differences between epithelial and fibroblast cells inside an organoid (96) or the detection of intratumor differential response to paclitaxel mediated by the heterogeneous metabolic shift among cancer cell populations (94, 95).

The presence of intratumor multiple stemness niches could be generated as a response to metabolic rewiring due to limited access to nutrients or metabolic changes, which are required to adapt to proliferation rate modifications. Sundar et al. (99) studying cancer stem cell populations (CSCs) in glioblastoma PDO noted that therapeutic resistance is driven by altered biological mechanisms rather than physical limitations of therapeutic access due to the presence of a highly heterogeneous population of CSCs and cycling/senescent cells. Another study shows that tumor organoids displayed spatial heterogeneity with highly proliferating outer region cells surrounding a hypoxic core of mainly non-stem senescent cells, sensitive to radiotherapy, and diffuse, quiescent CSCs which on the contrary were radioresistant (100).

Ultimately, multiple approaches for the unraveling of tumor heterogeneity have been converged in the recent study of Dekkers

et al. With the aim to study tumor infiltration and targeting by engineered immune cells (e.g., CAR T cells), the authors developed BEHAV3D, an organoid-based 3D imaging transcriptomic platform (101). This approach integrates multiple techniques to allow functional single-cell behavior analysis of multilineage organoids with spatial resolution (3D imaging) and integrated transcriptomic profiling.

3.2 Microfluidic on-chip models, macro models, and advanced co-culture systems

Although the so-far described strategies provide a valuable complement to traditional preclinical models in the study of tumor invasiveness or drug effects concerning specific DNA aberrations, they lack the representation of the stromal compartment which plays a crucial role in cell spatial distribution, growth, invasiveness, and drug sensitivity (102, 103).

Basically, in the models mentioned above, the environmental context, which could both contribute to the development of tumor heterogeneity or be affected by it, is missed.

A step forward in this direction is represented by bioprinted models (104). Indeed, combining organoids with bioprinting technology could be a promising strategy to mimic the genetic, histological, and functional aspects of cancer heterogeneity, proposing it as a useful platform for personalized therapies (102). The introduction into the system of the extracellular matrix (ECM) with the control of its mechanical properties (e.g., matrix stiffness, architecture, density, protein crosslinking, and fiber network configuration) mimics cell growth, cell proliferation, and differentiation reproducing the surrounding physiological environment for cancer heterogeneity development. This approach allows not only to reproduce the background behind the tumor and tumor microenvironment heterogeneity but also to identify the elements involved in this process, controlling and targeting them.

A crucial element that is still missed also by the bioprinted model is the vasculature which could significantly affect and interact with tumor cell differentiation. In trying to overcome this limitation and to resemble the conditions that surround the development of tumor heterogeneity, many efforts have been done in the field of tissue engineering (103–107). Magdeldin et al. developed biomimetic tumoroids which recreate the spatially different exposition to nutrients and oxygen, allowing to test how the induced cancer cell heterogeneity affects the formation of the vascular network and cancer-invasive capability (108). Gilardi et al. developed a variety of *in vitro* assays and readouts to dissect different extravasation steps involved in the metastatic cascade. The authors highlighted a key role of FAK phosphorylation in trans-endothelial migration validating the results in a metastatic *in vivo* model (109). These results drag a parallel between *in vitro* and *in vivo* fostering the employment of *in vitro* models in the development of new effective antimetastatic treatments.

Another attempt aimed to include the stromal compartment within the study of cancer heterogeneity correlates the development of different morphological phenotypes of tumor cells with the heterogeneity of collagen organization confirming the key role played by the tumor microenvironment (110).

A fundamental component of the tumor microenvironment that develops heterogeneous phenotypes is represented by immune cells, particularly T effector cells, T helper, NK cells, B cells, and dendritic cells (24, 111–113). In the context of immune regulation, many cells are involved such as T and B regulatory cells and medullary thymic epithelial cells (mTECs); however, the most studied are the macrophages and neutrophils (112, 114, 115), known to be able to polarize toward both the anti- and protumor phenotypes. Specific protocols have been developed to recreate *in vitro* the polarization of immune cells, paving the way for the possibility of better mimicking the heterogeneity of the tumor microenvironment (116).

A promising future development is represented by on-a-chip models, which allow complex and dynamic culture systems to mimic the heterogeneity of the tumor microenvironment. Indeed, these models potentially include 3D structures, such as the microvasculature, and chemical or physical stimuli (117). Despite their potential, these platforms have not yet been really exploited for cancer heterogeneity studies, but they could hopefully be coupled with patient-derived models to increase the complexity and the reliability of preclinical studies.

Another aspect of tumor heterogeneity is represented by the tumor surrounding environment including the cell–cell and cell–matrix interactions and their role in the tumor fate.

The most suitable model to elucidate this is represented by microfluidic devices which recreate a controlled 3D structure in terms of matrix composition and stiffness, including patient-derived materials (118) and the addition of chemical and physical stimuli, stromal cells such as fibroblast (109) and mesenchymal cells (119), and vascular compartments (120–123). Through microfluidic models, it is possible to reproduce the recruitment of immune cells (124–127) and their heterogeneous behavior able to develop both pro- and antitumor phenotypes (127, 128).

Aside from the improvement brought by the 3D microfluidic models, there are still some important limitations that need to be overcome. Since the complete recreation of all cellular and structural elements of a physiological environment is still unreachable, it is important to carefully focus on the elements principally involved in the pathway of study (119), trying to include at least the most relevant ones. Indeed, the next challenges consist of increasing the complexity of these models, extending the range of analysis techniques applicable, and promoting the validation through clinical studies to obtain evermore reliable platforms.

The works presented in paragraphs 2 and 3 showed the huge ongoing effort in developing preclinical models including the heterogeneity of the tumor itself and of the tumor microenvironment. We showed that there are different approaches to face this peculiar characteristic of the tumor, from the collection of data from patients to the attempt to recreate the heterogeneity through genetic manipulation or the stimuli and the composition of the surrounding microenvironment. All of them have the same goal of identifying and targeting the drug-resistant tumor subphenotypes responsible for therapy failure.

4 Emerging technologies to study heterogeneity: single-cell sequencing and spatial genomic analysis

As it will be better described later, heterogeneity depends on cellular interactions and knowing the rules orchestrating the TME and how different cellular subtypes correlate to the clinical relevance would make a huge difference in improving current therapeutic strategies.

In the past, proteomics and transcriptomics in cancer have been studied at the macroscopic level leveraging techniques that are still very important including bulk DNA/RNA sequencing and flow cytometry. For studies regarding rare cellular populations within the TME, such as immune cells, it was difficult to extensively study the impact of the different immune populations.

In the past, bulk RNA-seq has been incredibly helpful in identifying different tumor mechanisms. The gene expression profiles of deconvolution methods estimating the abundance of cells in a mixed population such as the CIBERSORTx algorithm (129) and xCell (130) have been fundamental in understanding the contribution of each cellular population.

More recently, with the increased awareness of the role played by TME and the underlying complex cellular interactions, more complex technologies providing single-cell data have been developed. Emerging single-cell technologies and spatial transcriptomics provide new tools to give insights at the single-cell level within tumors and dissect the roles each cell plays in tumor progression (Figure 3).

4.1 scRNA-seq and spatial analysis

In the last 10 years, the most used technologies to uncover heterogeneity are represented by single-cell RNA (scRNA) and DNA sequencing methods. scRNA sequencing allows the identification of tumor subtypes, definition of cancer cell states, lineage tracing and phenotyping of cellular subpopulation, and differential expression analysis (131).

The new technology applied to cancer heterogeneity allows to detect rare cell subpopulations within the tumor mass, which are very important when it comes to defining the probability of relapse leading to better precision medicine (132). Single-cell data define divergent survival probability improving the clinical prognostic evaluation of each case and therapeutic regimens.

Single-cell profiling of tumor heterogeneity and the microenvironment has been done in many cancer types and metastasis (133) including advanced non-small cell lung cancer, triple-negative breast cancer (TNBC) primary tumor, and paired lymph nodes (134).

Leveraging scRNA, Xue et al. stratified patients into five separate subtypes spatially organized and associated with chemokine networks and genomic features. Remarkably, the authors found that tumor-associated neutrophil (TAN) enriched in the myeloid-cell-enriched subtype was associated with a negative prognosis (135).

Moreover, single-cell transcriptome analysis revealed tumor immune microenvironment heterogenicity and granulocyte enrichment in colorectal cancer liver metastases (131), the role of M2 macrophages in TNBC aggressiveness (136), and the role of TLR4 and TLR8 in TNBC (137). Furthermore, single-cell sequencing coupled with TCR and BCR sequencing allows not only the transcriptomic analysis at the single-cell level but also the possibility to study immune cell clonal expansion. The single-cell level information regarding the immune populations is fundamental to understanding how the diverse immune players will react to different drugs boosting immunotherapy efficacy and the complexity of researchers' approaches to design novel and more effective combinatorial treatments.

Huipeng Li et al. were able to exploit the single-cell approach to discriminate into subgroups presenting divergent survival probability tumors that were previously assigned to single subtypes through bulk RNA-seq (138). The single-cell technology allowed Wai-Hung Ho et al. to explore the interrelationship between liver cancer stem cell markers reporting new subpopulations of cells and novel stemness-related genes (132).

Single-cell sequencing revolutionized the cancer field providing detailed information at the cellular level. However, given the procedure used to prepare the single cells, the spatial data and all the information regarding the hierarchical structure and how the cells are distributed in the TME are not included in the output.

Digestion of solid tumors characterizes the single-cell RNA sequencing (scRNA-seq) protocol eliminating spatial information and the organization of individual cells in the neighborhood. Tissues are characterized by hierarchical structure organizing how the cells composing the tissue are localized reciprocally. Spatial localization is fundamental in defining cellular interactions and tumor progression. In fact, clones, subclones, immune cells, endothelial cells, and stroma localize in different districts within a tumor tissue, and the spatial information can be used as predictive of therapy response.

Spatial phenotyping allows the combination of various markers within the same tissue slide underlying novel patterns and correlations that would not be evident with non-spatial technologies. A comprehensive overview describing the differences in spatial technologies has been extensively reported (139).

PhenoCycler CODEX, NanoString GeoMx Digital Spatial Profiler (DSP), CosMx, 10X Visium, and MERFISH are among the most used technologies which allow a spatial analysis.

Meyer et al. used the highly multiplexed immunofluorescence imaging technology CODEX to generate a tissue atlas of inflammation in the context of ulcerative colitis compared with healthy tissues. The authors characterized the cell types, cell–cell contacts, and cellular neighborhoods highlighting that cellular neighborhood dictates the functional states of the cells composing the tissue. In addition, this analysis was able to identify different inflammatory cell subsets and spatial neighborhoods peculiar to patients treated with TNF inhibitors, paving the way for targeting specific cellular niches responsible for resistance (51). Spatially resolved data provided insights into ITH allowing phenotype tracking and clonal evolution within tumors.

10.3389/fonc.2023.1164535

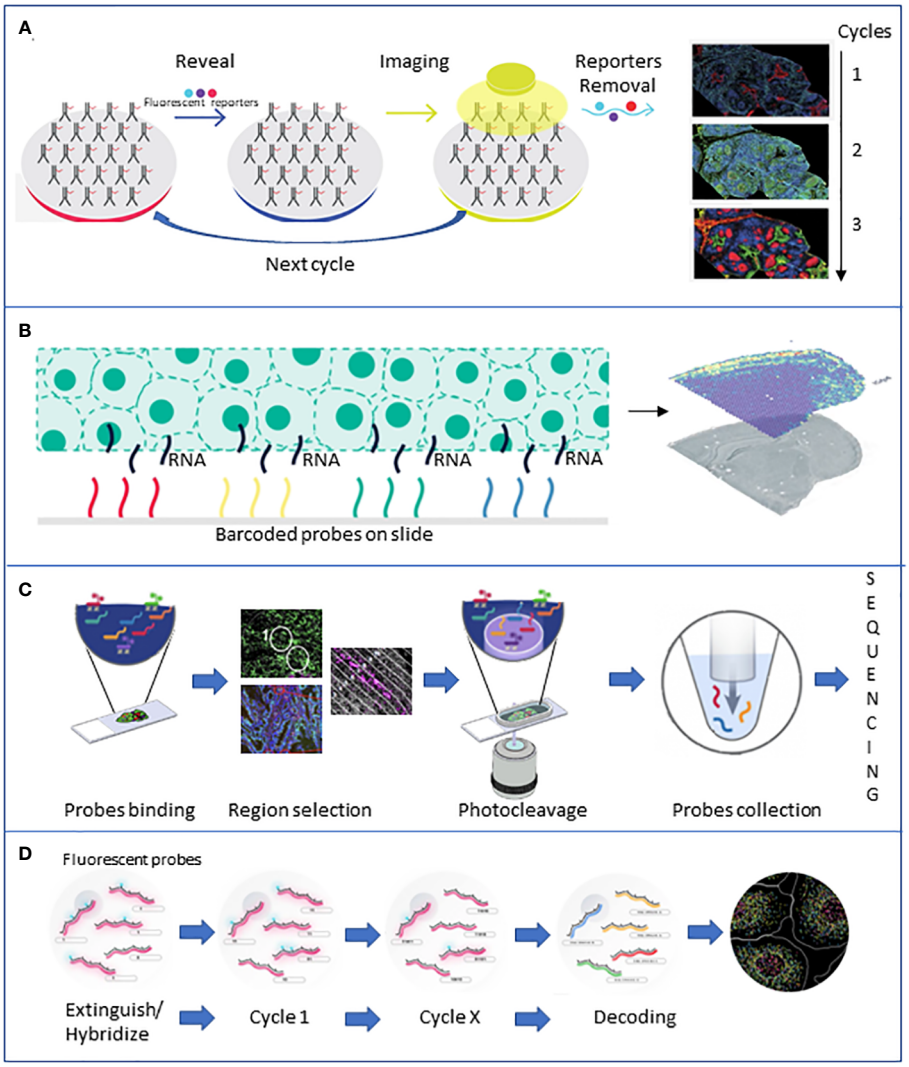

FIGURE 3
Brief description of the major spatial technologies. **(A)** CODEX is based on a panel of antibodies that binds to specific fluorescent reporters that reveal their position during the imaging phase. At the end of the first cycle of image acquisition, the reporters are detached, and another cycle with new reporters starts. **(B)** 10X Visium is based on slides of barcoded capture probes that bind to the polyA tail of RNAs released from the tissue. RNA is retrotranscribed into cDNA and sequenced. **(C)** GeoMX DSP is based on panels of antibodies or photocleavable barcoded probes. Once an area of interest is selected, a stream of light releases the probes that are lately sequenced. **(D)** MERFISH is based on fluorescently tagged probes that label RNA of interest. Sequential rounds of imaging enable spatial resolution. All the pictures have been adapted from the providers' web pages.

In this context, Rovira-Clave et al. realized the *in situ* tracking of barcodes in small cell lung cancer tumor microenvironment coupling epitopes for imaging (EpicTags) and multiplexed ion beam imaging (EpicMIBI) (140). This approach promoted the ITH spatial investigation interrogating both cell-intrinsic and cell-extrinsic events leading to therapeutic resistance. Hajiran et al. compared survival outcomes to patterns of immune cell distributions defined by spatial analysis in metastatic clear cell renal cell carcinoma (ccRCC). In this study, augmented macrophages together with the decrease in Th1 presence within the tissues correlated with both poor overall survival and worse patient outcome (141). These pieces of evidence support the importance of spatial analysis of immune cells in the tumor microenvironment for the future assessment of clinically relevant associations for improved patient treatments.

Another use of spatial technology is the study of the tumor microenvironment profile to identify potential biomarkers to predict clinical outcomes. Within the new technologies for spatial analysis, 10X Visium and NanoString GeoMX DSP are the most used and often combined (139). The first is based on fixed tissues permeabilized to allow the RNA capture through oligo-dT overhangs, which will be later reverse-transcribed and sequenced, while the second is based on regions-of-interest selection guided by fluorescence methods. Bullman's group exploited the Visium to study the tumor microenvironment in OSCC and colorectal cancer, showing a spatial heterogeneity in the microbiota with bacterial communities populating the less vascularized and highly immunosuppressed area. Also, they showed that cancer cells infected with bacteria can recruit myeloid cells into the bacterial regions (142).

On the other hand, the GeoMX DSP approach allowed Toki et al. to associate different series of expression patterns to immunotherapy response. Remarkably, this study highlights that PD-L1 expression on macrophages correlates with a positive response to immunotherapy that could potentially be used to predict clinical response to immune therapy in melanoma patients (143). In the context of NSCLC, the treatment with immune checkpoint inhibitors does not provide complete benefit in the clinic, and one of the reasons is that there is still a lack of effective biomarkers to stratify the patient for αPD-1 treatments. The exploitation of the DSP technology showed that the correlation of CD44 levels exclusively in the tumor compartment was associated with a positive response to immunotherapy excluding the immune cells from the analysis. This type of compartmentalized analysis on only the tumor's immune compartment is peculiar to the DSP workflow and very useful for immunotherapy response biomarker discovery. Leveraging this, Moutafi et al. identified a novel promising biomarker to predict NSCLC sensitivity to αPD-1 therapy (143), while Rimm's group quantified 39 immune parameters simultaneously in four tissue compartments, correlating overall survival with a high count of $CD56^+$ immune cells (143). Remarkably, Hwang et al. recently applied the power of DSP in the context of pancreatic cancer, identifying a new neural-like malignant progenitor enriched after chemo- and radiotherapy, associating it with poor prognosis (144). Nirmal et al. took advantage of the possibility of studying boundaries between different cell populations, identifying a spatially restricted suppressive microenvironment along the tumor stroma boundary in cutaneous melanoma (145).

A recent upgrade of the GeoMX DSP which provides cellular-level data is the CosMx, which brings the spatial analysis to the next level, allowing the localization of RNAs at the subcellular level. Despite being a very novel and recent technology, CosMx has been exploited already by Beechem's group who analyzed 980 RNAs in non-small cell lung and breast cancer, identifying 10 unique tumor microenvironments inside the cell, proving the presence of spatial heterogeneity inside a single cell (146). A similar output has been obtained by Xia et al. using a different technology called MERFISH, based on a combination of imaging and *in situ* hybridization. The authors determined the subcellular compartmentalization of RNAs and identified populations that are cell cycle-dependent and independent inside the same cell (147).

One major challenge in spatial transcriptomics is the resolution of the data, as the number of cells within a single spatial location (also known as a "spot") can range from a few to several hundred. This variability can make it difficult to accurately assign cell types and identify spatial patterns of gene expression. Various approaches have been developed to overcome these limitations, such as the use of supervised learning approaches and leveraging cell type profiles learned from scRNA-seq data (148).

The huge amount of data generated by spatial transcriptomic technologies requires new computational methods for the storage and annotation of spatially resolved single-cell data. Another challenge is the integration of gene expression and spatial information. Traditional scRNA-seq techniques do not capture spatial information, so methods have been developed to integrate scRNA-seq data with spatial transcriptomics data (149, 150), as recently reviewed by Longo et al. (151). However, these methods can be complex and may not always produce reliable results (151).

There is also a need for robust downstream analysis tools that can extract biological signals from raw spatial transcriptomics data and identify the spatial organization and cell–cell communications. Some of the existing tools may be limited by technology-specific biases or may not be suitable for all types of spatial transcriptomics data. Computational methods are emerging (152). Recently, new efforts in the field promoted the generation of new methods of analysis of spatially resolved single-cell data allowing a more accurate cell-type annotation and phenotyping such as Seurat, stellaR, SpatialDecon, and tangram, summarized elsewhere (153). These types of tools favor the discovery of new types of cells in spatially resolved datasets at a single-cell level, a fundamental step in the definition of tissue hierarchy and underlying biological processes. The reader is referred to Dries et al. for a review of the art of spatial transcriptomic data downstream analysis methods and pipelines (154).

This recent progress is just an anticipation of how single-cell RNA sequencing and spatial transcriptomics techniques will play an essential role in the next future in incorporating tissue architecture with transcriptomics data. The ability to see what is going on at the reface of a tumor-infiltrated tissue and its healthy neighbors at the RNA and protein levels or the possibility of visualizing what a particular group of immune cells express when they are interacting will greatly impact our prognostic abilities and our knowledge on heterogeneity.

Being able to combine the data coming from different techniques will require interdisciplinary teams composed of molecular biologists, pathologists, and wet lab and data scientists. Yet, the information implemented in the clinical system will unlock enormous achievements in the field of targeted therapies to overcome resistance to treatment and prevent metastasis.

4.2 Bioinformatics and computational modeling

The computational approaches that are fundamental to tackle ITH can be grouped into three families: 1) approaches that try to infer the tree of clonal evolution from sequencing data, 2) approaches that aim to identify the different cell types in a cancer cell mixture from single-cell and/or spatial transcriptomics and epigenomics data, and 3) knowledge-based models that aim at simulating the dynamics of cancer cell populations (Figure 4).

4.2.1 Inference of cancer progression models from sequencing data

Genomic alterations [i.e., single-nucleotide variants (SNVs); structural variants, such as insertions and deletions; and copy number alterations (CNVs)], which can be identified by opportunely processing next-generation sequencing (NGS) data (e.g., DNA-seq, RNA-seq, or ATAC-seq) of tumor samples, can

10.3389/fonc.2023.1164535

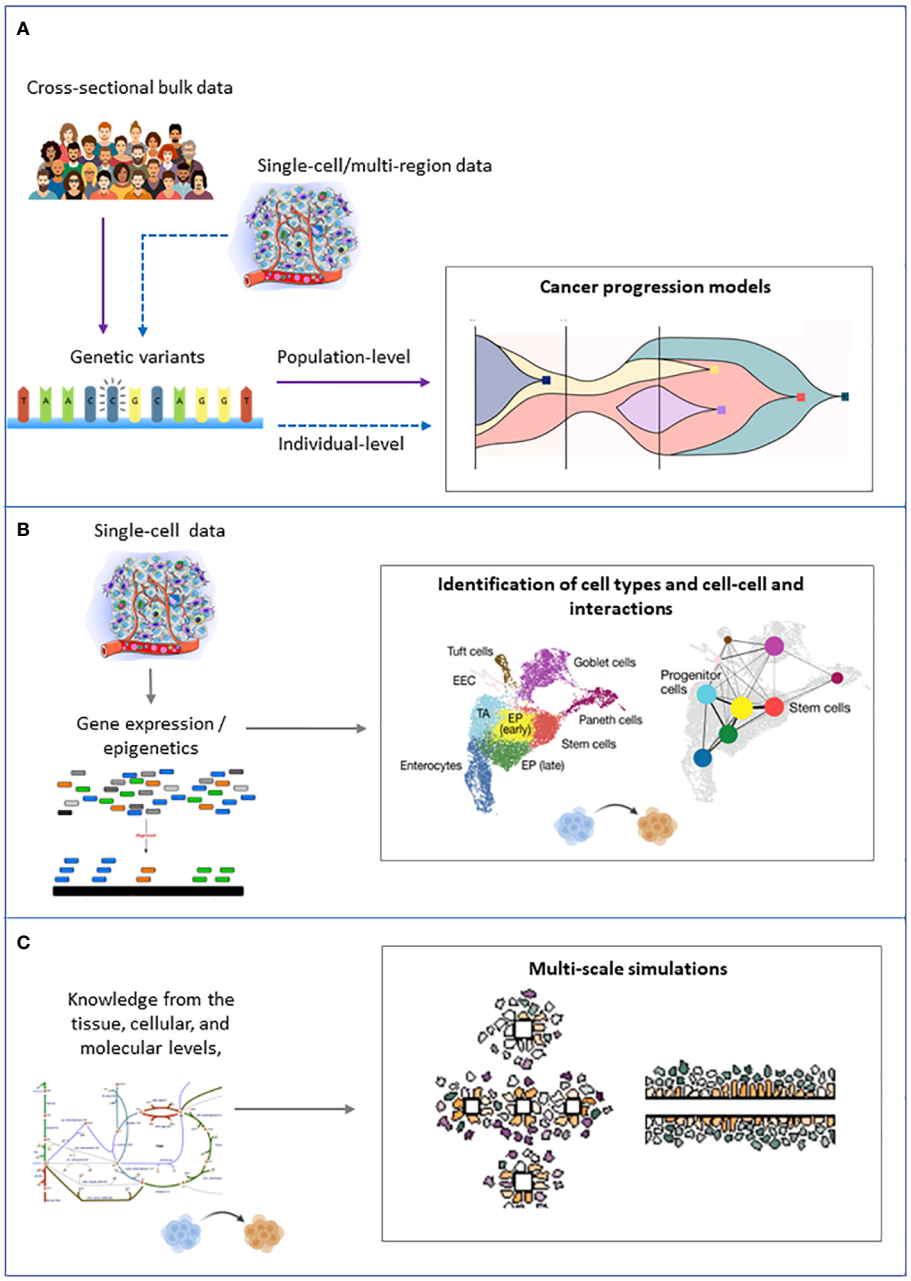

FIGURE 4
Schematic representation of the inputs (left) and outputs (right) of the main families of computational approaches to tackle intratumor heterogeneity. **(A)** Cancer progression models. **(B)** Clustering of single cells. **(C)** Multiscale modeling and simulation.

be used to track tumor progression. The philosophy and clinical implications of this approach are reviewed elsewhere (3).

The basic idea is that the positively selected (i.e., functionally advantageous) genomic alterations (i.e., drivers) identified in every cancer cell represent the clonal trunk, whereas those identified in a subset of cancer cells defined the coexisting (sub)clones.

In the last years, a plethora of bioinformatics tools have been developed to exploit mutational profiles of cancer samples to reconstruct a model of cancer evolution, either at the population or at the individual level. Genomic alterations can be used to characterize and track down tumor progression through NGS (3).

Population-level models are typically inferred from cross-sectional bulk sequencing data, in which one sample is available for each patient. The objective is to infer a unique progression model for the patient cohort under study, which usually represents a specific tumor (sub)type (155). In the final model (which can either be trees or direct acyclic graphs), edges represent the most likely trends of accumulation of genomic alteration for that specific tumor (sub)type and can be used to both predict the next evolutionary steps and to stratify patients in risk groups.

Individual-level models aim to reconstruct a personalized progression model for each individual. These models ideally

require multiple measurements for the same tumor, which can either be:

- single-cell sequencing data, collected either at single (156) or multiple time points (longitudinal), e.g., from patient-derived cell cultures, xenografts, or organoids.
- multiregion bulk sequencing data (156).

In this case, the output model (a mutational/clonal tree) depicts the evolutionary history of a single tumor and, in the case of longitudinal experiments, allows one to assess the impact of external interventions, such as therapies.

The methodology at the core of these tools is generally based on traditional sequence-based phylogenetics (157, 158) or on Bayesian/maximum-likelihood statistical frameworks (159–161). The main differences between the two approaches are illustrated here (162).

Fundamental data preprocessing steps are needed upstream of all aforementioned methodologies and differ according to the specific experiment type (single cell or bulk) and data type (DNA, RNA, ATAC, and related technology/protocol). A non-exhaustive list includes the correction of sequencing reads; the correction for purity, ploidy, absolute copy number, and mutation multiplicity; variant calling; and estimation of variant allele frequency (VAF), which must be converted into a cancer cell fraction (CCF) taking into account gene copy numbers. To maximize the sensitivity and specificity of calling clonal and subclonal mutations, the PCAWG Evolution and Heterogeneity Working Group and the PCAWG Consortium used an ensemble approach integrating the output of alternative algorithms (163). However, the number of tumor regions sequenced and the depth and purity of what is sequenced largely affect the ability to distinguish truly clonal from pseudoclonal mutation. Strong tumor sampling bias, high levels of technical noise, and biological variability also hinder the robust inference of cancer progression models. To mitigate this problem, a recent work has proposed to use a transfer learning approach to infer from multiregion data multiple patient evolutionary models simultaneously, seeking to maximize their structural correlation (164).

It remains an open question whether cancer progression models can truly predict the likely course of tumor progression or whether the occurrence of neutral evolution and drift may limit the ability to predict a tumor's next step. To address this question, Diaz-Uriarte and Vasallo (165) analyzed four different approaches and concluded that these methods can predict only with moderate success and only under representable fitness landscapes and with very large sample sizes, but even perfect algorithms might not work if intrinsic evolutionary unpredictability is large.

4.2.2 Clustering and lineage inference from single-cell transcriptomics and epigenomics data

Phenotypic data at the single-cell level allow variability due to the environment and interactions among cancer subclones as well as with the other player in the TME to be considered. In this regard, unsupervised machine learning methods (clustering) on single-cell RNA-sequencing data were successful in unraveling the composition in terms of cell phenotypes of a cancer mixture (166, 167). RNA velocity and cell lineage reconstruction might also be employed to investigate the similarity and dynamics of cancer cell types (168). Computational methods to infer cell–cell communication events from scRNA-seq data have also been proposed (169), even focused on the identification of metabolic cooperation phenomena (170).

The noisy nature of single-cell RNA-sequencing data requires *ad hoc* preprocessing steps. To this aim, the best practices (171) and tools implementing them such as Seurat (148) and Scanpy (172) are now well established. A preprocessing stage that requires special care and that is largely debated is denoising of scRNA-seq data, as reviewed by Patruno et al. (173) This step becomes fundamental when the aim is to identify metabolic subpopulations from scRNA-seq, as demonstrated by Galuzzi et al. (174).

Approaches to integrate scRNA-seq data with other -omics have recently emerged. For example, CONGAS integrates bulk DNA and single-cell RNA measurements from independent assays to jointly identify clusters of single cells with subclonal CNAs and differences in RNA expression. The opportunity provided by the latest technologies to simultaneously profile intranuclear proteins, chromatin accessibility, and gene expression in single cells is pushing forward the need for single-cell multiomics data integration (175, 176). In particular, methodologies for handling sequencing data that simultaneously measure gene expression and chromatin accessibility in the same cell are increasingly being proposed (177–179); for instance, statistical and machine learning methods for spatially resolved transcriptomics data analysis are currently being developed and have been previously reviewed (179).

4.2.3 Multiscale modeling and simulation

The data science approaches described above cannot identify mechanisms nor probe whether the correlation is causal. On the contrary, multiscale modeling in systems biology allows the behavior at the larger scale to emerge naturally from the collective action at smaller scales.

Multiscale models integrate a priori knowledge from the tissue, cellular, and molecular levels and can simulate complex cell–cell interactions and emerging population-level dynamics. These models are generally based on ordinary differential equations that can simulate the integral response of the tumor to pharmaceutical interventions (180) but fail in capturing spatial phenomena. For the study of invasion and metastasis, models based on partial differential equations or agent-based models are applied (181). In particular, agent-based modeling is the most suitable framework to model ITH because it can describe the dynamics of a large number of heterogeneous and interacting agents (i.e., cells or clones) that act autonomously in an environment according to certain rules. Agent-based models have been used to study the differentiation of cancer stem cells (182), clonal evolution (183, 184), and interaction between different cell types (185) and different metabolic phenotypes (186).

While multiscale models can provide unprecedented insight into mechanistic detail, they are computationally expensive and

require a large number of unknown parameters to be defined. Real-world data are generally used only to fit the model parameters, for example *via* approximate Bayesian computation (ABC), whereas attempts to include omics data directly as parameters of the multiscale model are still in their infancy (187, 188).

The definition of new computational frameworks that bridge the gap between top-down approaches (close to the data but far from the mechanisms) and bottom-up approaches (close to the mechanisms but far from the data) is a key objective to enable the reconstruction of digital twins that integrate biological knowledge and population data with personalized data. In this regard, machine learning and multiscale modeling can naturally complement each other to create robust predictive models that include physicochemical constraints (189). Data generated by mechanism-based simulations can also supplement training data for machine learning models.

5 Tumor heterogeneity, drug resistance, and clinical outcomes

It is well established that tumors with high levels of ITH may predispose patients to worse clinical outcomes (189). The main reason is that ITH implies the coexistence of subclones with different genetic, epigenetic, and metabolic endowments.

On the one hand, this can expose to a greater probability of achieving in at least one tumor cell population, with subsequent genetic and epigenetic alterations, a molecular combination that leads to the acquisition of a physiological alteration determining a clonal expansion *in situ* or dissemination, thus contributing to tumor progression.

On the other hand, it guarantees the tumor greater adaptability to environmental changes, possibly induced by exogenous factors such as pharmacological treatment, and therefore, increases the fitness and survival of cancer cells and intrinsic resistance to therapeutic treatments that determine tumor relapse.

Resistance is considered intrinsic when conditions for escape from the drug response are already inherent in the treated tumor. It is considered acquired when the treatment itself activates adaptive mechanisms that lead to resistance.

An example of intrinsic and acquired resistance is found in tumors associated with hyperactivation of the epidermal growth factor receptor, EGFR, which transduces the mitogenic signal in response to the growth factor by activating Ras proteins and their cellular effectors. The oncogenic activation of this receptor may be due to gene amplification (copy number variation) increasing its expression level, deletions (truncations of regulatory regions as in EGFvII and EGFR carboxyl-terminal deletions), or point mutations (substitutions of residues critical for the function) that make the receptor constitutionally activated (190, 191).

Although many effective treatments are available (192, 193), there is also a very high percentage of patients who after a few months of treatment manifest resistance and tumor relapse (194) due to on-target mechanisms dependent on the coexistence of cell populations with different sensitivities to the drug (present before the treatment or acquired by selective pressure) (195) and/or off-target mechanisms depending on the oncogenic activation of other genes and proteins (196, 197). Other examples of drug resistance due to heterogeneity can be found in the study of Blaquier et al. (198) and in other studies (192, 194, 199).

Another example of ITH leading to drug resistance concerns the presence of cancer stem cell niches in the tumors, with a small population of cells endowed with stemness properties, including enhanced capacity for self-renewal cloning, the undifferentiated state combined with differentiating potential, long cell cycling, genome repair abilities, peculiar energy metabolism, ability to educate the neighboring cells to provide nutrients although highly resistant to lack of nutrients and hypoxia, and ability to collaborate in the elusion from the immune system (200). Cancer stem cells confer high plasticity to the tumor and contribute to drug resistance with multiple mechanisms, for instance by remaining quiescent during chemotherapeutic treatment specifically targeting proliferating cells and then regrowing for repopulation or efficiently repairing DNA damage induced by some chemotherapeutic agents, such as platinum drugs and alkylating agents.

In summary, ITH and the response to drug treatment are interdependent phenomena. On the one hand, pretreatment tumor heterogeneity is mainly responsible for intrinsic drug resistance and relies on multiple mechanisms including the presence of cells in the tumor site expressing elements that bypass target inhibition because they promote aberrant downstream signaling (i.e., Ras oncoproteins in EGFR-hyperactivated tumors), or cells expressing MDR pumps, or cells endowed with potentiated DNA repair system, or cancer stem cell niches. On the other hand, the adaptation to pharmacological treatment, particularly if directed against a specific target as in the context of precision medicine, feeds the ITH and predisposes it to drug resistance negatively affecting clinical outcomes.

Historically, heterogeneity has been mostly associated with mutations, and only recently, heterogeneity has acquired an enlarged origin including selective stimuli from targeted therapy and the tumor immune microenvironment. All these factors have been known to be responsible for the heterogeneity mechanisms, yet the emergence of new features peculiar to cancer cells only has been associated with the generation of neoantigens correlated with a positive outcome, especially in immunotherapy. Thus, understanding how to modulate the immune response by controlling heterogeneity should be further investigated to better develop targeted therapies.

6 The role of the tumor microenvironment in heterogeneity

Selective death in the TME can lead to heterogeneity. To explain this concept, we will leverage a conservation biology theory by Martin and Sapsis. The "pyrodiversity promotes biodiversity" theory first proposed that fire promotes biodiversity by generating

heterogeneous ecological niches and inducing species to adapt to environmental changes (201, 202).

We can look at the cancer ecosystem in the same way. Usually, selective pressure such as therapy (fire) eliminates all the cells. However, in rare special niches, the conditions for clonal evolution instead of death are presently leading to adaptation through mutation, evolution, and in the end, cancer progression (203).

Many other different things can happen to a tumor cell exposed to the challenges peculiar to the microenvironment. Stromal cell interaction and immune recognition can be some of the key heterogeneity driving factors which a cancer cell should adapt to survive (204) (Figure 5).

6.1 Immune recognition and cancer heterogeneity

In the past, heterogeneity has been seen as a negative factor present in tumors correlated to an increased mutational burden, cancer progression, and acquired resistance. In the context of heterogeneity-involved diseases, it is dutiful to mention metastases. Metastases are responsible for more than 90% of cancer-related mortality, and one of the triggering processes is the selective pressure in the TME (205–207). Thus, a deep understanding of heterogeneity underlying these mechanisms will provide the required insight for primary tumor and metastasis eradication.

The advent of improved experimental technologies, such as RNA sequencing, single cells, and spatial analysis of tissues, together with better bioinformatic tools boosted correlative studies between immune profiling, mutational burden, and patient outcomes which will be discussed later in this review.

Neoantigens derived from cancer mutations are one of the keys to unleash an effective and lasting immune response, yet they are derived from mutations that are known to lead to heterogeneity and resistance. A consistent portion of research has been done in the neoantigens field in the last 20 years (3, 163, 208, 209). Yet, the argument is still controversial.

Clinical studies reported a tight association between high tumor mutational burden (TMB) and improved outcomes during immune checkpoint inhibitor regimens. TMB is also reported as a biomarker to predict immunotherapy and chemotherapy efficacy (210).

Ke-Yue Ma et al. (211) characterized in lung adenocarcinoma the ITH of immune response-related genes. They showed that the decrease in the number of neoantigens was correlated with an acquired resistance phenotype. Moreover, the authors reported that MHC-II genes were the common genes shared by the top favorable prognostic pathways supporting that neoantigen presentation by MHC-II may be a positive factor triggering cancer eradication by immune cells.

The improved response to therapy observed in high TMB tumors is also probably due to a broader repertoire of tumor-specific mutant epitopes presented by antigen-presenting cells (APCs) (212) and to enhanced epitope-spreading mechanisms diversifying the ability of the immune cells to recognize multiple targets (113).

Epitope spreading is a mechanism enhancing and diversifying endogenous lymphocyte recognition to new antigens beyond the original one which was the initial target antigen. This mechanism can involve intramolecular antigens (recognition of epitopes within the same protein) or intermolecular ones (involving other proteins) and can lead to enhanced cytotoxic T-cell activity and anticancer antibody production by B cells (213). Although epitope spreading positively correlates with patients' responses representing an important predictive marker (214), it correlates also with side

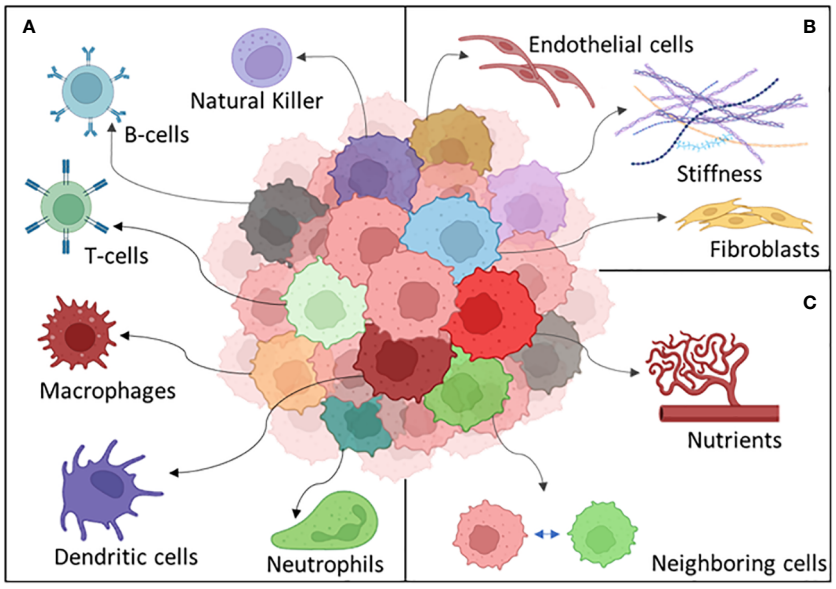

FIGURE 5
The different components of the tumor microenvironment: **(A)** the immune system, **(B)** stroma, and **(C)** external factors.

effects due to T-cell recognition of autoantigens and to the expansion of the autoantibody repertoire (215, 216).

Epitope spreading is an incredibly powerful mechanism triggering parallel immune recognition and also autoimmunity. Its fine regulation makes the process very complex; thus, more efforts need to be made to be able to leverage it therapeutically to overcome autoimmunity.

Reuben et al. (217) studying lung adenocarcinoma showed that although an increasing variety of neoantigens promote a wider heterogeneity in the T-cell receptor repertoire, it also correlates with impaired survival and tumor relapse. There can be many reasons why more neoantigens lead to negative outcomes. One of the hypotheses can be designed by dragging a parallel between cancer cells and pathogens. The mechanism underlying cancer immune escape leveraging heterogeneity can be associated with the ability of some pathogens, such as *Borrelia burgdoferii*, to escape immune recognition by overwhelming the immune system with antigens that are not determinants of pathogen eradication (218).

Other immune cells beyond lymphocytes are involved in reshaping the heterogeneity of the TME. Clinical cancer stage and metastatic tumor burden are linked to ineffective immune response and increased immune suppression due to myeloid cell infiltration in different tumor types including pancreatic cancer (219) and breast cancer (220). In line with these findings, Zhang et al. (131) revealed tumor immune microenvironment heterogenicity and granulocyte enrichment in colorectal cancer liver metastases.

A common model for cancer heterogeneity is the "cancer stem cell" in which tumor-propagating cells have the same genetic mutations as the differentiated cells but are blocked in a different maturation stage. This is known to correlate with poor patient outcomes, resistance, metastasis, and immune suppression (221, 222).

Cancer cells can leverage epigenetic reprogramming to increase stemness and escape the immune system (223). Consistent with this, Miranda et al. (224) described a negative parallel correlating decreased survival, impaired T cells, natural killer cells, B-cell immune infiltration, and increased stemness. Barker et al. (225) identified cancer stem cells in the small intestine and colon using Lgr5 as a marker opening the door to targeted therapy directly tackling stem cells. This type of antigen could be exploited for targeted immunotherapy. Another way to see stemness is that cancer cells do not upregulate stemness on purpose. Instead, it could be that the cells with stemness characteristics are those that can escape the immune system recognition being the resistant ones. Supporting this, it has been discovered in animal models that NK recognition of metastatic cells in the liver is responsible for dormancy (226) (a quiescent cell state often associated with stemness), highlighting how cancer cells' interaction within the TME regulates cancer cell survival to modulate their behaviors to escape (227). In another study, it has been highlighted how the macrophage-secreted factor supports pancreatic cancer metastasis by inducing fibrosis (228). Thus, impaired immune recognition by the immune system due to other circumstances can lead to metastatic overt colonization.

The so-called epithelial-to-mesenchymal transition (EMT) is involved in cancer evolution concurring with the development of more aggressive subclones (229). Different studies leveraging RNA-sequencing data correlated EMT-related gene expression profiles with increased aggressiveness. Although these data are very important to reveal the mechanisms involved in the TME, it is unknown if EMT signatures were from cancer or stromal cells given the bulk nature of the analysis. McCorry et al. (230) highlighted EMT signatures in the stromal fibroblast within the tumor microenvironment instead of a change in the cancer cells. Fibroblasts within the TME are not only involved in EMT; Chen et al. (231) showed that tumor-associated macrophages promote EMT and cancer stem cell properties in TNBC. Altogether, these lines of evidence show how important stromal and immune cell heterogeneity is in tumor progression.

In clinical and preclinical work, huge efforts are currently active toward combinatorial therapies leveraging both chemotherapy and immune checkpoint inhibitors targeting the TME (232–235). In this setting, while chemotherapy mediates tumor destruction which leads to the release of tumor neoantigens, immunotherapy keeps the immune system active, targeting exhaustion and suppression. These combinatorial strategies tackle cancer from both angles leveraging neoantigens (generated by mutations) as weapons to train the immune soldiers to fight more efficiently. In solid tumors, high quality and quantity of neoantigens correlate with improved survival and response to immunotherapies (236, 237). In a deeper analysis, a decrease in expressed clonal neoantigens correlates with increased immune infiltration (238) indicating the impact of the immune activity regulating tumor heterogeneity. Altogether, these data show that modulating heterogeneity will be an effective way to have controlled and targeted immunotherapy increasing efficacy while overcoming unwanted side effects.

6.2 Stroma heterogeneity in the TME

Other cells within the tumor immune microenvironment can be responsible for selective pressure on cancer cells since they are able to modulate environmental conditions such as cytokines, nutrients, metabolites, matrix stiffness, pH, and redox status.

One of the main populations involved in shaping the TME is the fibroblast. This population of cells is heterogeneous and responsive to different stimuli. CAFs turned out to be responsible for the immunosuppressive microenvironment linked to therapy resistance (239, 240) and metastatic progression (239, 241, 242). Furthermore, fibroblasts are responsible for fibrosis leading to hypoxia, reduced immune infiltration and vascularization, and nutrient deprivation in pre-HCC conditions, leading to HCC cancer progression (243–245).

The heterogeneity of CAFs has been associated with organ-specific metastasis in pancreatic ductal adenocarcinoma (241). Furthermore, in another study, the promotion of cholangiocarcinoma growth by diverse cancer-associated fibroblast subpopulations has been reported (246).

Cancer cells are also able to reprogram CAF gene expression and metabolism (247). More recently, it has been reported that $CD10^{+}GPR77^{+}$ CAFs promote cancer formation and chemoresistance by supporting cancer cell stemness (242). In the

context of metabolism, cancer-derived exosomal HSPC111 promotes colorectal cancer liver metastasis by reprogramming lipid metabolism in CAFs (248).

Mentioning the interaction between CAFs and immune cells, Krishnamurty et al. (249) reported that LRRC15$^+$ myofibroblasts dictate the stromal setpoint to suppress tumor immunity.

Endothelial cells are fundamental players in the TME being involved in angiogenesis and adhesion molecule expression on the vasculature regulating immune cells and nutrient trafficking. The endothelium is a heterogeneous tissue, and different expression profiles have been reported characterizing endothelial cells from different organs. Ultimately, in order to generate more effective targeted approaches against cancer progression and metastasis, we need to take into account the different endothelial barrier properties contributing to organotropism metastatic behaviors of different tumors (250).

The cellular component is not only involved in the control of tumor heterogeneity. The sensing compartment composed of the matrix is important as well in regulating how the cells sense the surrounding environment. The tumor matrix stiffness plays a role in the mechanotransduction of tumor cells involving integrins signaling to modulate how cancer cells can feel the microenvironment.

It has been demonstrated that different stiffness leads to modified gene expression (251–255). Stiffness reduction has been proven to improve bevacizumab response in metastatic colorectal cancer (256). Changes in other parameters such as pH have also been reported to improve immunotherapy efficacy (257).

This plethora of parameters present in the TME modulates in turn the immune system leading to inflammation (14) or immunosuppression (114, 115, 258). These two types of TME determine the fate of cancer cells (229) selectively pressuring them to evolve or perish. Learning how to control the mechanisms underlying heterogeneity will provide knowledge to leverage this information therapeutically. The final aim will be modulating heterogeneity to make cancer cells seen by the immune system to unlock immune recognition.

7 Discussion and conclusions

The recent awareness of the importance of heterogeneity in the development and establishment of tumors opens up new possibilities for understanding tumor development and—in perspective—improving and personalizing therapeutic approaches to tumors. Different technologies, some of which are discussed in this review, open hitherto unexplored windows to the understanding of tumor biology at the single-cell and spatial levels.

In particular, single-cell techniques enabled the discovery of cellular differences that usually get lost during bulk RNA-sequencing sampling methods, helping the scientific community to understand how different cellular populations express different sets of genes. The spatially resolved transcriptional analysis revolutionized the study of heterogeneity allowing transcriptome analysis without losing the spatial organization of tissue architecture.

Both single-cell and spatial transcriptomics can generate heavy databases of data, challenging the scientific community in developing new ways to analyze, store, and integrate the data. Multiomics technologies with the promise to deliver high-throughput genomic and epigenetic molecular data in parallel will combine RNA, DNA, and ATAC sequencing technologies for more comprehensive studies. For instance, scATAC-seq allows epigenetic studies, lineage tracing, and genomic regulation, providing insights on chromatin accessibility, and the full-length mRNA profiling in single cells exploited to study the alternative splicing (259). The processing of millions of cells is required to detect a rare subpopulation of cells, and this can be achieved by single-cell sequencing (combinatorial indexing). Accordingly, integrating data of a widely diverse nature in terms of dimensionality of data (a few proteins, hundreds of biochemical or imaging features, the whole transcriptome) and experimental approach (targeted, hypothesis-driven *vs.* exploratory genome-wide) is probably the primary challenge. Therefore, it is necessary to use computer and computational techniques for an in-depth analysis of individual data (i.e., transcriptomic, proteomic, or any -omics data) and also to integrate and structure data related to different layers of biological complexity: the final aim is to describe the emergent properties derived from the interaction of the system components and those that cannot be derived by the mere knowledge of the properties of the individual components (260). For instance, because of the special role played by metabolism in orchestrating cellular activities (261), the simulation of computational models of metabolism acts as an integrator able to explain at the system level the phenotypic properties of cellular systems and even their interaction (262). The modeling approach is somehow complementary to the artificial intelligence/machine learning approach, which excels in differentiating and stratifying patient populations but so far has proven less suitable for identifying the laws governing complex biological phenomena (261, 263). Wiring together the analytical and correlative ability of machine learning with the ability of mathematical models of metabolism and other cellular functions to structure biological information could allow a quantum leap in our understanding of tumor heterogeneity.

The generation of enhanced computational models to prioritize and predict therapeutic efficacy leveraging cancer molecular profiles has been recently developed.

An example of successful integration of multiomics data together with phenotypic and therapeutic response profiles falls into the computational strategy called pharmaco-pheno-multiomic (PPMO).

This model allowed the establishment of novel complex biomarker profiles to predict prospective therapeutic regimen response in acute myeloid leukemia and ovarian tumor cohorts (264). These strategies already demonstrated their extraordinary potential in predicting therapeutic response in human tumors and need to be further exploited on different cancer types and broader cohorts in the future.

The availability of different non-human models of tumor heterogeneity is of great value since it will allow us to experimentally test in an iterative cycle the computer-generated predictions (265). Figure 6 graphically summarizes some of the key

10.3389/fonc.2023.1164535

properties of different models highlighted in this review. Despite lacking some aspects of the complexity present in mammalian systems, non-murine models can be exploited for preliminary screening to answer precise biological questions. Zebrafish, *Drosophila*, and yeast, among others, have already proven their efficacy in recapitulating basic and conserved biological mechanisms, coupling this with the possibility of collecting thousands of data points in a quick and cheap way. Although the way of life of yeast is unicellular, yeast cells demonstrate the ability to coordinate to form multicellular communities with specialized subpopulations, as what happens in a tumor mass where, from a single progenitor, many cells arise and specialize to survive. An extra layer of complexity concerns the signaling between different colonies, which induces metabolic reprogramming (38) to maintain the identity of the single colony. The study of this intra-and intercolony crosstalk could uncover evolutionarily conserved mechanisms that can be targeted to prevent the establishment of a colony/tumor mass in a new environment. With 90% of genes involved in human cancer development, fast generation time, and low maintenance costs, *Drosophila* is perfectly suited to study the basic mechanisms of cancer heterogeneity. Zebrafish is a unique model that allows extensive characterization of the mechanism of clonal evolution, also allowing the identification of dominant drivers. Transgenesis, transplantation, single-cell functional assays, and live imaging can provide an economical and large-scale *in vivo* screening tool which provides statistically relevant data to complement focused studies done in mice or humans, as published by Smith et al. (44), where a zebrafish study revealed that one in 100 leukemia transplanted cells was able to drive tumor growth, a higher number than expected if compared to mouse studies.

Models such as yeast and 2D cultures excel in their ability to perform genetic and environmental modulation of growth conditions and in their ability to run omics analyses, including single-cell transcriptomics. Although the clonal nature of cell lines grown as monolayer offers high reproducibility and low intrinsic heterogeneity, their high intrinsic plasticity allows fostering of different phenotypes within the same cell line, for instance by using inflammatory cytokines and growth factors (266).

Murine models, on the other hand, provide a complex systemic platform to evaluate biological mechanisms and both drug efficacy and toxicity.

Since their development, mouse models have become more sophisticated and accurate in replicating human tumors including *ad hoc* models to study heterogeneity.

Among these, GEMMs and syngeneic models are exploited for their high reproducibility and flexibility, yet mouse tumors have different evolution routes if compared to human ones. This results in decreased genetic heterogeneity which penalizes the clinical translational relevance of these models. To overcome the species-specific issues, human cell line-derived xenografts (CDXs) are largely leveraged due to their fast and standardized growth.

Although CDXs are composed of clonal populations, their level of genetic heterogeneity does not compare with human tumors. Immortalization and *in vitro* clonal selection can be the cause of genetic drift. In addition, the lack of cell–cell interactions within a 3D human microenvironment limits the clinical predictivity of the findings obtained by exploiting human cell lines.

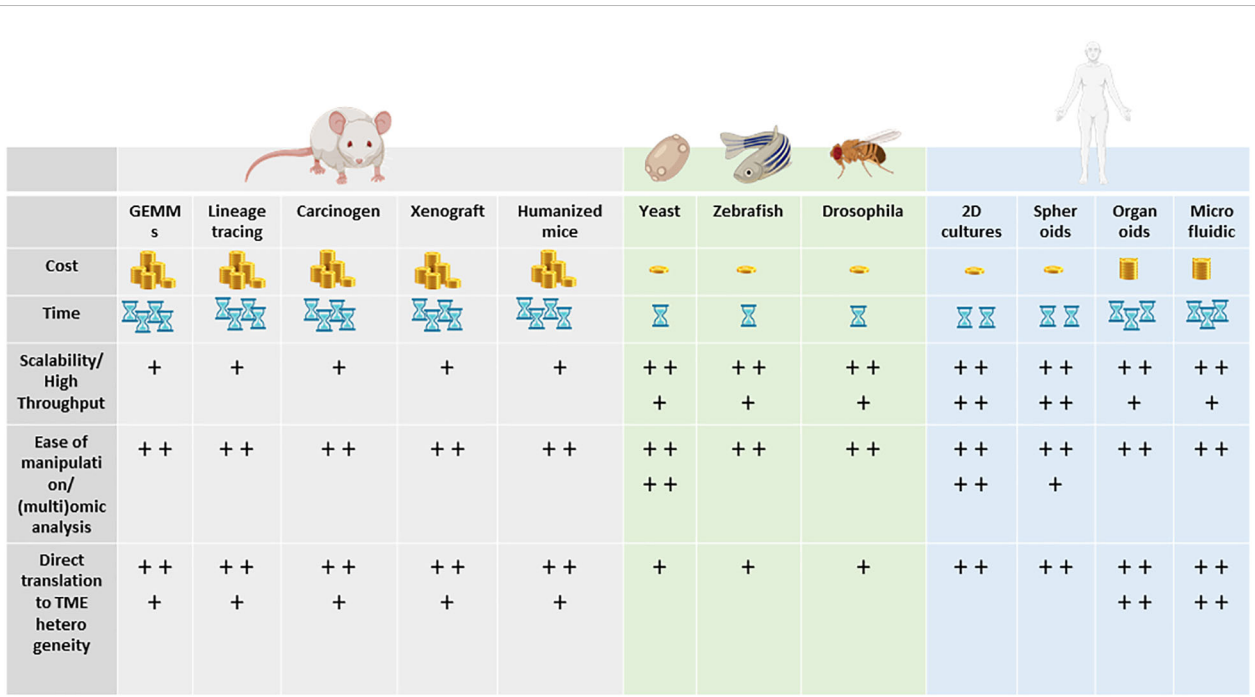

FIGURE 6
Key properties (cost, time, scalability, ease of manipulation, direct translation to TME heterogeneity) of the different models highlighted in this review. From left to right: murine models, non-murine models, and human models. + = low, ++ = medium, +++ = good / high, ++++ = excellent / very high.

The type of mouse model that mostly translates the results of the experiments to clinical response is the PDX which maintains the heterogeneity of the patient's primary tumor especially when used at low passages (less than 10). PDXs have been successfully used in the context of personalized cancer treatment as an investigational platform for therapeutic decision-making (267).

Given the predictive capacity of PDXs in clinical translational studies, the urgent need to leverage them to predict immunotherapy outcomes emerged quickly. In fact, to study immune therapeutic regimens with PDXs, the animal host requires a functional immune system of human origin. The implementation of humanized mice together with low-passage PDXs in the same study allows for both the clonal heterogeneity of the human tumor and the immune microenvironment to be reconstituted. One of the limitations is the graft-*versus*-host disease (GVHD) happening when the engrafted human immune cells are from a different donor with respect to the PDX one. To avoid unwanted GVHD which will impair the validity of the study results, human leukocyte antigen (HLA) matching strategies between the donors should be done. Ideally, autologous models can be proposed. However, this option is still very limited given the lack of primary matched tumor and immune material from the same patient.

In basic science and preclinical settings in the attempt to replicate tumor heterogeneity, animal models have been extremely powerful and extensively used. Searching for faster, cheaper, and more ethical models to evaluate in high-throughput entire libraries of drugs and the divergence of these models in mimicking some aspects of human biology paved the way for the establishment of human-derived advanced *in vitro* models.

Organoids and on-chip microfluidic models using human-derived cells are great tools for retaining tumor heterogeneity, especially when employing low-passage primary human cells. These *in vitro* models are suitable for high-throughput screening of multiple therapeutic combinations or as a platform to investigate human key molecular pathways allowing the analysis of complex cell–cell and cell–matrix interactions in biochemically and biophysically controlled conditions. In addition, the reduced time in providing the results makes the *in vitro* humanized models ideal for preclinical studies adding value to the animal models, which, on the other hand, are still essential for systemic and toxicological studies. Despite the tremendous advances in modeling, when the preclinical use of these models is required, researchers need to consider that different models display variable fidelity to human tumor biology. Organoids represent the best option to preserve tissue heterogeneity using *in vitro* culture. By carefully choosing the protocol of production, it is possible to retain molecular, spatial, and metabolic heterogeneity of the tissue of origin. However, there are limitations regarding the cell lineage that can survive inside the organoids during culture (e.g., immune cells), and the sampling of the tissue of origin can affect the heterogeneity of the cell population itself. If there is a need to keep the model simple and preserve reproducibility and feasibility, simplified organoids (spheroids) can be produced starting from a single cell line. Spheroid heterogeneity can be improved stepwise either by co-culturing different cell lines and/or by providing a cocktail of different extracellular matrices. Microfluidic devices are tunable platforms in which cell lines as well as organoids can be cultured. The flexibility of the system allows to compartmentalize and add different components of the tumor including vasculature immune cells and stroma in highly controlled experimental conditions. Given the unique interchangeable geometry of the system, physical stimuli such as stiffness or shear stress can be modulated in the system adding to the level of environmental heterogeneity, known to play a key role in tumor progression. High resolution and live imaging are still the main readouts; thus, good image analysis expertise is required to extract data and succeed in quantifying different parameters including tumor growth and migration. Unfortunately, omics analyses are not always easy to perform given the low number of cells.

Thus, the use of each model should be carefully evaluated in terms of its faithfulness in replicating a given human biological feature or mechanism. In an attempt to define the transcriptional fidelity, the Cancer Genome Atlas dataset has been compared with cell lines, 3D cultures, GEMMs, and PDXs leveraging the CancerCellNet (CNN) tool. Unfortunately, this effort is limited to a small number of tumor-derived models making the validity of this effort very limited.

Recently, immunotherapies have revolutionized the entire cancer treatment field. Immuno-oncology studies and the development of immune checkpoint inhibitors able to boost cancer cell immune recognition have led to recognizing the fundamental role of the immune system in tumor progression. On top of this, increased awareness has been reserved regarding the importance of stromal cells including the ones composing the vasculature and CAFs.

Taking together all this information about the complex hierarchy within the tumor immune microenvironment, it is clear why, despite the different models already available, there is an urgent need to further improve the complexity and fidelity of the platforms replicating humanized settings.

Extending the efforts beyond generating complex models, the need for new technologies to analyze the TME promoted the emergence of single-cell genomics and spatial approaches as powerful strategies in delineating the complex molecular landscapes of cancers.

The acquired knowledge will ultimately be implemented in a digital twin (i.e., "a virtual model" of a physical entity, with dynamic, bi-directional links between the physical entity and its corresponding twin in the digital domain) (268). A digital twin can then be personalized using biological data (269). Personalized digital twins can then be used to test treatment protocols, in the development and identification of new pharmacological targets, and in the rational identification of more effective combined pharmacological protocols that will maximize the therapeutic efficacy for each individual, minimizing the side effects.

In conclusion, understanding tumor heterogeneity and its exploitation in the clinical field will require quantitative determination of multiple features and their integrated analysis by combined machine learning and simulation approaches. Only the combined effort of an interdisciplinary team of scientists with expertise in different fields, such as pathology, molecular biology, bioengineering, clinic, and computation, able to communicate and

work in synergy will provide new integration and interrogation modality to predict therapy response and to implement more efficient targeted and combinatorial therapies which are urgently required for cancer patients.

Author contributions

MG, MV, and MP conceived and designed the review. MG, MV, MP, MC, CD, VP, and ES wrote sections of the manuscript. MG, MP, MC, and CD prepared the figures. MG, MV, and MP reviewed and edited the manuscript. All authors contributed to the article and approved the submitted version.

Funding

MV received funds from Ministero dell'Università e della Ricerca (MIUR)–grant 2021-NAZ-0057/A-JRUISBE-IT-BTBS, grant CHRONOS (``Dipartimenti di Eccellenza 2017"), from EU Seventh Framework Programme, grant EraNET-ITFOC and H2020 grants EpiPredict n.642691 and Amplitude n.871277 and Next Generation EU, (ElixirxNextGenIT, Proposta Progettuale IR0000010). ES received funds from European Union - NextGenerationEU through the Italian Ministry of University and Research under PNRR - M4C2-I1.3 Project PE_00000019 "HEAL ITALIA". MC was supported by Fondazione Umberto Veronesi.

Conflict of interest

The authors declare that the research was conducted in the absence of any commercial or financial relationships that could be construed as a potential conflict of interest.

Publisher's note

References

1. Vendramin R, Litchfield K, Swanton C. Cancer evolution: Darwin and beyond. *EMBO J* (2021) 40(18). doi: 10.15252/embj.2021108389

2. Kashyap A, Rapsomaniki MA, Barros V, Fomitcheva-Khartchenko A, Martinelli AL, Rodriguez AF, et al. Quantification of tumor heterogeneity: from data acquisition to metric generation. *Trends Biotechnol* (2022) 40(6):647–76. http://www.cell.com/article/S0167799921002675/fulltext. doi: 10.1016/j.tibtech.2021.11.006

3. McGranahan N, Swanton C. Clonal heterogeneity and tumor evolution: past, present, and the future. *Cell* (2017) 168(4):613–28. doi: 10.1016/j.cell.2017.01.018

4. Gascoigne KE, Taylor SS. Cancer cells display profound intra- and interline variation following prolonged exposure to antimitotic drugs. *Cancer Cell* (2008) 14 (2):111–22. doi: 10.1016/j.ccr.2008.07.002

5. Jänicke RU, Sohn D, Schulze-Osthoff K. The dark side of a tumor suppressor: anti-apoptotic p53. *Cell Death Differ* (2008) 15(6):959–76. doi: 10.1038/cdd.2008.33

6. Salk JJ, Fox EJ, Loeb LA. Mutational heterogeneity in human cancers: origin and consequences. *Annu Rev Pathol* (2010) 5:51–75. doi: 10.1146/annurev-pathol-121808-102113

7. Kumar A, Coleman I, Morrissey C, Zhang X, True LD, Gulati R, et al. Substantial interindividual and limited intraindividual genomic diversity among tumors from men with metastatic prostate cancer. *Nat Med* 22(4):369–78. doi: 10.1038/nm.4053

8. Lalonde E, Ishkanian AS, Sykes J, Fraser M, Ross-Adams H, Erho N, et al. Tumour genomic and microenvironmental heterogeneity for integrated prediction of 5-year biochemical recurrence of prostate cancer: a retrospective cohort study. *Lancet Oncol* (2014) 15(13):1521–32. doi: 10.1016/S1470-2045(14)71021-6

9. Newlands ES, Stevens MFG, Wedge SR, Wheelhouse RT, Brock C. Temozolomide: a review of its discovery, chemical properties, pre-clinical development and clinical trials. *Cancer Treat Rev* (1997) 23(1):35–61. doi: 10.1016/S0305-7372(97)90019-0

10. Pezzuto A, Carico E. Role of HIF-1 in cancer progression: novel insights. a review. *Curr Mol Med* (2018) 18(6):343–51.

11. Chiaradonna F, Sacco E, Manzoni R, Giorgio M, Vanoni M, Alberghina L. Ras-dependent carbon metabolism and transformation in mouse fibroblasts. *Oncogene* (2006) 25(39):5391–404. doi: 10.1038/sj.onc.1209528

12. Damiani C, Colombo R, Gaglio D, Mastroianni F, Pescini D, Westerhoff HV, et al. A metabolic core model elucidates how enhanced utilization of glucose and glutamine, with enhanced glutamine-dependent lactate production, promotes cancer cell growth: the WarburQ effect. *PloS Comput Biol* (2017) 13(9):e1005758. doi: 10.1371/journal.pcbi.1005758

13. Yang L, Lin PC. Mechanisms that drive inflammatory tumor microenvironment, tumor heterogeneity, and metastatic progression. *Semin Cancer Biol* (2017) 47:185–95. doi: 10.1016/j.semcancer.2017.08.001

14. Greten FR, Grivennikov SI. Inflammation and cancer: triggers, mechanisms, and consequences. *Immunity* (2019) 51(1):27–41. doi: 10.1016/j.immuni.2019.06.025

15. Meng X, Riordan NH. Cancer is a functional repair tissue. *Med Hypotheses* (2006) 66(3):486–90. doi: 10.1016/j.mehy.2005.09.041

16. Kersten K, de Visser KE, van Miltenburg MH, Jonkers J. Genetically engineered mouse models in oncology research and cancer medicine. *EMBO Mol Med* (2017) 9 (2):137–53. doi: 10.15252/emmm.201606857

17. Heyer J, Kwong LN, Lowe SW, Chin L. Non-germline genetically engineered mouse models for translational cancer research. *Nat Rev Cancer* (2010) 10(7):470–80. doi: 10.1038/nrc2877

18. Sinn E, Muller W, Pattengale P, Tepler I, Wallace R, Leder P. Coexpression of MMTV/v-ha-ras and MMTV/c-myc genes in transgenic mice: synergistic action of oncogenes *in vivo*. *Cell* (1987) 49(4):465–75. doi: 10.1016/0092-8674(87)90449-1

19. McFadden DG, Papagiannakopoulos T, Taylor-Weiner A, Stewart C, Carter SL, Cibulskis K, et al. Genetic and clonal dissection of murine small cell lung carcinoma progression by genome sequencing. *Cell* (2014) 156(6):1298–311. doi: 10.1016/j.cell.2014.02.031

20. Schepers AG, Snippert HJ, Stange DE, Van Den Born M, Van Es JH, Van De Wetering M, et al. Lineage tracing reveals Lgr5+ stem cell activity in mouse intestinal adenomas. *Science* (2012) 337(6095):730–5. doi: 10.1126/science.1224676

21. Akbay EA, Kim J. Autochthonous murine models for the study of smoker and never-smoker associated lung cancers. *Transl Lung Cancer Res* (2018) 7(4):464–86. doi: 10.21037/tlcr.2018.06.04

22. Wang Z, Wu VH, Allevato MM, Gilardi M, He Y, Luis Callejas-Valera J, et al. Syngeneic animal models of tobacco-associated oral cancer reveal the activity of *in situ* anti-CTLA-4. *Nat Commun* (2019) 10(1):1–13. doi: 10.1038/s41467-019-13471-0

23. Kono M, Saito S, Egloff AM, Allen CT, Uppaluri R. The mouse oral carcinoma (MOC) model: a 10-year retrospective on model development and head and neck cancer investigations. *Oral Oncol* (2022) 132:106012. doi: 10.1016/j.oraloncology.2022.106012

24. Gilardi M, Saddawi-Konefka R, Wu VH, Lopez-Ramirez MA, Wang Z, Soto F, et al. Microneedle-mediated intratumoral delivery of anti-CTLA-4 promotes cDC1-dependent eradication of oral squamous cell carcinoma with limited irAEs. *Mol Cancer Ther* (2022) 21(4):616–24. doi: 10.1158/1535-7163.MCT-21-0234

25. Hingorani DV, Crisp JL, Doan MK, Camargo MF, Quraishi MA, Aguilera J, et al. Redirecting extracellular proteases to molecularly guide radiosensitizing drugs to tumors. *Biomaterials* (2020) 248:120032. doi: 10.1016/j.biomaterials.2020.120032

26. Day CP, Merlino G, Van Dyke T. Preclinical mouse cancer models: a maze of opportunities and challenges. *Cell* (2015) 163(1):39–53. doi: 10.1016/j.cell.2015.08.068

27. Zitvogel L, Pitt JM, Daillère R, Smyth MJ, Kroemer G. Mouse models in oncoimmunology. *Nat Rev Cancer* (2016) 16(12)759–73. doi: 10.1038/nrc.2016.91

28. Gargiulo G. Next-generation in vivo modeling of human cancers. *Front Oncol* (2018) 8(OCT). doi: 10.3389/fonc.2018.00429

29. Gilardi M, Wang Z, Proietto M, Chilla A, Calleja-Valera JL, Goto Y, et al. Tipifarnib as a precision therapy for HRAS-mutant head and neck squamous cell carcinomas. *Mol Cancer Ther* (2020) 19(9):1784–96. doi: 10.1158/1535-7163.MCT-19-0958

30. Hoffman RM. Patient-derived orthotopic xenografts: better mimic of metastasis than subcutaneous xenografts. *Nat Rev Cancer* (2015) 15(8):451–2. doi: 10.1038/nrc3972

31. Hidalgo M, Amant F, Biankin AV, Budinská E, Byrne AT, Caldas C, et al. Patient-derived xenograft models: an emerging platform for translational cancer research. *Cancer Discov* (2014) 4(9):998–1013. doi: 10.1158/2159-8290.CD-14-0001

32. Okada S, Vaeteewoottacharn K, Kariya R. Application of highly immunocompromised mice for the establishment of patient-derived xenograft (PDX) models. *Cells* (2019) 8(8):889. doi: 10.3390/cells8080889

33. DeAngelis N, Ferrante C, Powers G, Sendecki J, Mattson B, Pizutti D, et al. Discovery and pharmacological characterization of cetrelimab (JNJ-63723283), an anti-programmed cell death protein-1 (PD-1) antibody, in human cancer models. *Cancer Chemother Pharmacol* (2022) 89(4):515–27. doi: 10.1007/s00280-022-04415-5

34. Nielsen J. Yeast systems biology: model organism and cell factory. *Biotechnol J* (2019) 14(9):1800421. doi: 10.1002/biot.201800421

35. Rao AR, Pellegrini M. Regulation of the yeast metabolic cycle by transcription factors with periodic activities. *BMC Syst Biol* (2011) 5:160. doi: 10.1186/1752-0509-5-160

36. Nadal-Ribelles M, Islam S, Wei W, Latorre P, Nguyen M, de Nadal E, et al. Sensitive high-throughput single-cell RNA-seq reveals within-clonal transcript-correlations in yeast populations. *Nat Microbiol* (2019) 4(4):683. doi: 10.1038/s41564-018-0346-9

37. Van Heerden JH, Wortel MT, Bruggeman FJ, Heijnen JJ, Bollen YJM, Planqué R, et al. Lost in transition: start-up of glycolysis yields subpopulations of nongrowing cells. *Science* (1979) 343(6174):1245114. doi: 10.1126/science.1245114

38. Čáp M, Štěpánek L, Harant K, Váchová L, Palková Z. Cell differentiation within a yeast colony: metabolic and regulatory parallels with a tumor-affected organism. *Mol Cell* (2012) 46(4):436–48. doi: 10.1016/j.molcel.2012.04.001

39. Varahan S, Walvekar A, Sinha V, Krishna S, Laxman S. Metabolic constraints drive self-organization of specialized cell groups. *Elife* (2019) 8:e46735. doi: 10.7554/eLife.46735

40. Howe K, Clark MD, Torroja CF, Torrance J, Berthelot C, Muffato M, et al. The zebrafish reference genome sequence and its relationship to the human genome. *Nature* (2013) 496(7446):498–503. doi: 10.1038/nature12111

41. White R, Rose K, Zon L. Zebrafish cancer: the state of the art and the path forward. *Nat Rev Cancer* (2013) 13(9):624–36. doi: 10.1038/nrc3589

42. Pinkel D, Albertson DG. Array comparative genomic hybridization and its applications in cancer. *Nat Genet* (2005) 37(Suppl 6S):S11–7. doi: 10.1038/ng1569

43. Ignatius MS, Chen E, Elpek NM, Fuller AZ, Tenente IM, Clagg R, et al. *In vivo* Imaging of tumor-propagating cells, regional tumor heterogeneity, and dynamic cell movements in embryonal rhabdomyosarcoma. *Cancer Cell* (2012) 21(5):680–93. doi: 10.1016/j.ccr.2012.03.043

44. Smith ACH, Raimondi AR, Salthouse CD, Ignatius MS, Blackburn JS, Mizgirev IV, et al. High-throughput cell transplantation establishes that tumor-initiating cells are abundant in zebrafish T-cell acute lymphoblastic leukemia. *Blood* (2010) 115(16):3296–303. doi: 10.1182/blood-2009-10-246488

45. Blackburn JS, Langenau DM. Zebrafish as a model to assess cancer heterogeneity, progression and relapse. *Dis Model Mech* (2014) 7(7):755–62. doi: 10.1242/dmm.015842

46. Livet J, Weissman TA, Kang H, Draft RW, Lu J, Bennis RA, et al. Transgenic strategies for combinatorial expression of fluorescent proteins in the nervous system. *Nature* (2007) 450(7166):56–62. doi: 10.1038/nature06293

47. Albert Pan Y, Freundlich T, Weissman TA, Schoppik D, Cindy Wang X, Zimmerman S, et al. Zebrabow: multispectral cell labeling for cell tracing and lineage analysis in zebrafish. *Development* (2013) 140(13):2835–46. doi: 10.1242/dev.094631

48. Tang Q, Moore JC, Ignatius MS, Tenente IM, Hayes MN, Garcia EG, et al. Imaging tumour cell heterogeneity following cell transplantation into optically clear immune-deficient zebrafish. *Nat Commun* (2016) 7:10358. doi: 10.1038/ncomms10358

49. Ablain J, Xu M, Rothschild H, Jordan RC, Mito JK, Daniels BH, et al. Human tumor genomics and zebrafish modeling identify SPRED1 loss as a driver of mucosal melanoma. *Science* (2018) 362(6418):1055–60. doi: 10.1126/science.aau6509

50. Hu Y, Flockhart I, Vinayagam A, Bergwitz C, Berger B, Perrimon N, et al. An integrative approach to ortholog prediction for disease-focused and other functional studies. *BMC Bioinf* (2011) 12:357. doi: 10.1186/1471-2105-12-357

51. Bailey MH, Tokheim C, Porta-Pardo E, Sengupta S, Bertrand D, Weerasinghe A, et al. Comprehensive characterization of cancer driver genes and mutations. *Cell* (2018) 173(2):371–385.e18. doi: 10.1016/j.cell.2018.02.060

52. Mirzoyan Z, Sollazzo M, Allocca M, Valenza AM, Grifoni D, Bellosta P. Drosophila melanogaster: a model organism to study cancer. *Front Genet* (2019) 10. doi: 10.3389/fgene.2019.00051

53. Lee T, Luo L. Mosaic analysis with a repressible cell marker for studies of gene function in neuronal morphogenesis. *Neuron* (1999) 22(3):451–61. doi: 10.1016/S0896-6273(00)80701-1

54. Enomoto M, Vaughen J, Igaki T. Non-autonomous overgrowth by oncogenic niche cells: cellular cooperation and competition in tumorigenesis. *Cancer Sci* (2015) 106(12):1651–8. doi: 10.1111/cas.12816

55. Wu M, Pastor-Pareja JC, Xu T. Interaction between Ras(V12) and scribbled clones induces tumour growth and invasion. *Nature* (2010) 463(7280):545–8. doi: 10.1038/nature08702

56. Chabu C, Xu T. Oncogenic ras stimulates Eiger/TNF exocytosis to promote growth. *Development* (2014) 141(24):4729–39. doi: 10.1242/dev.108092

57. Katheder NS, Khezri R, O'Farrell F, Schultz SW, Jain A, Schink MKO, et al. Microenvironmental autophagy promotes tumour growth. *Nature* (2017) 541(7637):417–20. doi: 10.1038/nature20815

58. Ohsawa S, Sato Y, Enomoto M, Nakamura M, Betsumiya A, Igaki T. Mitochondrial defect drives non-autonomous tumour progression through hippo signalling in drosophila. *Nature* (2012) 490(7421):547–51. doi: 10.1038/nature11452

59. Muzzopappa M, Murcia L, Milán M. Feedback amplification loop drives malignant growth in epithelial tissues. *Proc Natl Acad Sci USA* (2017) 114(35):E7291–300. doi: 10.1073/pnas.1701791114

60. Clemente-Ruiz M, Murillo-Maldonado JM, Benhra N, Barrio L, Pérez L, Quiroga G, et al. Gene dosage imbalance contributes to chromosomal instability-induced tumorigenesis. *Dev Cell* (2016) 36(3):290–302. doi: 10.1016/j.devcel.2016.01.008

61. Dekanty A, Barrio L, Muzzopappa M, Auer H, Milán M. Aneuploidy-induced delaminating cells drive tumorigenesis in drosophila epithelia. *Proc Natl Acad Sci USA* (2012) 109(50):20549–54. doi: 10.1073/pnas.1206675109

62. Tuveson D, Clevers H. Cancer modeling meets human organoid technology. *Science* (2019) 364(6444):952–5. doi: 10.1126/science.aaw6985

63. Clevers H. Modeling development and disease with organoids. *Cell* (2016) 165(7):1586–97. doi: 10.1016/j.cell.2016.05.082

64. LeSavage BL, Suhar RA, Broguiere N, Lutolf MP, Heilshorn SC. Next-generation cancer organoids. *Nat Mater* (2022) 21(2):143–59. doi: 10.1038/s41563-021-01057-5

65. Tang XY, Wu S, Wang D, Chu C, Hong Y, Tao M, et al. Human organoids in basic research and clinical applications. *Signal Transduct Target Ther* (2022) 7(1):168. doi: 10.1038/s41392-022-01024-9

66. Kondo J, Inoue M. Application of cancer organoid model for drug screening and personalized therapy. *Cells* (2019) 8(5):470. doi: 10.3390/cells8050470

67. Siegel RL, Miller KD, Fuchs HE, Jemal A. Cancer statistics, 2021. *CA Cancer J Clin* (2021) 71(1):7–33. doi: 10.3322/caac.21654

68. Öhlund D, Handly-Santana A, Biffi G, Elyada E, Almeida AS, Ponz-Sarvise M, et al. Distinct populations of inflammatory fibroblasts and myofibroblasts in pancreatic cancer. *J Exp Med* (2017) 214(3):579–96. doi: 10.1084/jem.20162024

69. Biffi G, Oni TE, Spielman B, Hao Y, Elyada E, Park Y, et al. IL1-induced JAK/STAT signaling is antagonized by TGFβ to shape CAF heterogeneity in pancreatic ductal adenocarcinoma. *Cancer Discov* (2019) 9(2):282–301. doi: 10.1158/2159-8290.CD-18-0710

70. Walsh AJ, Cook RS, Sanders ME, Aurisicchio L, Ciliberto G, Arteaga CL, et al. Quantitative optical imaging of primary tumor organoid metabolism predicts drug response in breast cancer. *Cancer Res* (2014) 74(18):5184–94. doi: 10.1158/0008-5472.CAN-14-0663

71. Broutier L, Mastrogiovanni G, Verstegen MMA, Francies HE, Gavarró LM, Bradshaw CR, et al. Human primary liver cancer-derived organoid cultures for disease modeling and drug screening. *Nat Med* (2017) 23(12):1424–35. doi: 10.1038/nm.4438

72. Nuciforo S, Fofana I, Matter MS, Blumer T, Calabrese D, Boldanova T, et al. Organoid models of human liver cancers derived from tumor needle biopsies. *Cell Rep* (2018) 24(5):1363–76. doi: 10.1016/j.celrep.2018.07.001

73. Wang K, Yuen ST, Xu J, Lee SP, Yan HHN, Shi ST, et al. Whole-genome sequencing and comprehensive molecular profiling identify new driver mutations in gastric cancer. *Nat Genet* (2014) 46(6):573–82. doi: 10.1038/ng.2983

74. Drost J, van Boxtel R, Blokzijl F, Mizutani T, Sasaki N, Sasselli V, et al. Use of CRISPR-modified human stem cell organoids to study the origin of mutational signatures in cancer. *Science* (2017) 358(6360):234–8. doi: 10.1126/science.aao3130

75. Gao D, Vela I, Sboner A, Iaquinta PJ, Karthaus WR, Gopalan A, et al. Organoid cultures derived from patients with advanced prostate cancer. *Cell* (2014) 159(1):176–87. doi: 10.1016/j.cell.2014.08.016

76. Boj SF, Hwang C, Baker LA, Chio IIC, Engle DD, Corbo V, et al. Organoid models of human and mouse ductal pancreatic cancer. *Cell* (2015) 160(1–2):324–38. doi: 10.1016/j.cell.2014.12.021

77. Tsai S, McOlash L, Palen K, Johnson B, Duris C, Yang Q, et al. Development of primary human pancreatic cancer organoids, matched stromal and immune cells and 3D tumor microenvironment models. *BMC Cancer* (2018) 18(1):335. doi: 10.1186/s12885-018-4238-4

78. Tiriac H, Belleau P, Engle DD, Plenker D, Deschênes A, Somerville TDD, et al. Organoid profiling identifies common responders to chemotherapy in pancreatic cancer. *Cancer Discov* (2018) 8(9):1112–29.

79. Neal JT, Li X, Zhu J, Giangarra V, Grzeskowiak CL, Ju J, et al. Organoid modeling of the tumor immune microenvironment. *Cell* (2018) 175(7):1972–1988.e16.

80. Dijkstra KK, Cattaneo CM, Weeber F, Chalabi M, van de Haar J, Fanchi LF, et al. Generation of tumor-reactive T cells by Co-culture of peripheral blood lymphocytes and tumor organoids. *Cell* (2018) 174(6):1586–1598.e12.

81. Schumacher D, Andrieux G, Boehnke K, Keil M, Silvestri A, Silvestrov M, et al. Heterogeneous pathway activation and drug response modelled in colorectal-tumor-derived 3D cultures. *PloS Genet* (2019) 15(3):e1008076

82. Bian S, Repic M, Guo Z, Kavirayani A, Burkard T, Bagley JA, et al. Genetically engineered cerebral organoids model brain tumor formation. *Nat Methods* (2018) 15 (8):631–9. doi: 10.1038/s41592-018-0070-7

83. Lu Z, Nie B, Zhai W, Hu Z. Delineating the longitudinal tumor evolution using organoid models. *J Genet Genomics* (2021) 48(7):560–70. doi: 10.1016/j.jgg.2021.06.010

84. Bolhaqueiro ACF, Ponsioen B, Bakker B, Klaasen SJ, Kucukkose E, van Jaarsveld RH, et al. Ongoing chromosomal instability and karyotype evolution in human colorectal cancer organoids. *Nat Genet* (2019) 51(5):824–34. doi: 10.1038/s41588-019-0399-6

85. Benien P, Swami A. 3D tumor models: history, advances and future perspectives. *Future Oncol* (2014) 10(7):1311–27. doi: 10.2217/fon.13.274

86. Liebau S, Parvin B, Ergün S, Richiardone E, Van Den Bossche V, Corbet C. Metabolic studies in organoids: current applications, opportunities and challenges. *Organoids* (2022) 1(1):85–105. doi: 10.3390/organoids1010008

87. Campioni G, Pasquale V, Busti S, Ducci G, Sacco E, Vanoni M. An optimized workflow for the analysis of metabolic fluxes in cancer spheroids using seahorse technology. *Cells* (2022) 11(5):866. doi: 10.3390/cells11050866

88. Ludikhuize MC, Meerlo M, Burgering BMT, Rodríguez Colman MJ. Protocol to profile the bioenergetics of organoids using seahorse. *STAR Protoc* (2021) 2(1):100386. doi: 10.1016/j.xpro.2021.100386

89. Rodríguez-Colman MJ, Schewe M, Meerlo M, Stigter E, Gerrits J, Pras-Raves M, et al. Interplay between metabolic identities in the intestinal crypt supports stem cell function. *Nature* (2017) 543(7645):424–7. doi: 10.1038/nature21673

90. Argüello RJ, Combes AJ, Char R, Gigan JP, Baaziz AI, Bousiquot E, et al. SCENITH: a flow cytometry-based method to functionally profile energy metabolism with single-cell resolution. *Cell Metab* (2020) 32(6):1063–1075.e7. doi: 10.1016/j.cmet.2020.11.007

91. Ahl PJ, Hopkins RA, Xiang WW, Au B, Kaliaperumal N, Fairhurst AM, et al. Met-flow, a strategy for single-cell metabolic analysis highlights dynamic changes in immune subpopulations. *Commun Biol* (2020) 3(1):98. doi: 10.1038/s42003-020-1027-9

92. Okkelman IA, Papkovsky DB, Dmitriev RI. Estimation of the mitochondrial membrane potential using fluorescence lifetime imaging microscopy. *Cytomet A* (2020) 97(5):471–82. doi: 10.1002/cyto.a.23886

93. Okkelman IA, Foley T, Papkovsky DB, Dmitriev RI. Multi-parametric imaging of hypoxia and cell cycle in intestinal organoid culture. *Adv Exp Med Biol* (2017) 1035:85–103. doi: 10.1007/978-3-319-67358-5_6

94. Sharick JT, Jeffery JJ, Karim MR, Walsh CM, Esbona K, Cook RS, et al. Cellular metabolic heterogeneity *In Vivo* is recapitulated in tumor organoids. *Neoplasia* (2019) 21(6):615–26. doi: 10.1016/j.neo.2019.04.004

95. Sharick JT, Walsh CM, Sprackling CM, Pasch CA, Pham DL, Esbona K, et al. Metabolic heterogeneity in patient tumor-derived organoids by primary site and drug treatment. *Front Oncol* (2020) 10. doi: 10.3389/fonc.2020.00553

96. Walsh AJ, Castellanos JA, Nagathihalli NS, Merchant NB, Skala MC. Optical imaging of drug-induced metabolism changes in murine and human pancreatic cancer organoids reveals heterogeneous drug response. *Pancreas* (2016) 45(6):863–9. doi: 10.1097/MPA.0000000000000543

97. Okkelman IA, Foley T, Papkovsky DB, Dmitriev RI. Live cell imaging of mouse intestinal organoids reveals heterogeneity in their oxygenation. *Biomaterials* (2017) 146:86–96. doi: 10.1016/j.biomaterials.2017.08.043

98. Okkelman IA, Neto N, Papkovsky DB, Monaghan MG, Dmitriev RI. A deeper understanding of intestinal organoid metabolism revealed by combining fluorescence lifetime imaging microscopy (FLIM) and extracellular flux analyses. *Redox Biol* (2020) 30:101420. doi: doi: 10.1016/j.redox.2019.101420

99. Sundar SJ, Shakya S, Barnett A, Wallace LC, Jeon H, Sloan A, et al. Three-dimensional organoid culture unveils resistance to clinical therapies in adult and pediatric glioblastoma. *Transl Oncol* (2022) 15(1):101251. doi: 10.1016/j.tranon.2021.101251

100. Hubert CG, Rivera M, Spangler LC, Wu Q, Mack SC, Prager BC, et al. A three-dimensional organoid culture system derived from human glioblastomas recapitulates the hypoxic gradients and cancer stem cell heterogeneity of tumors found *In Vivo*. *Cancer Res* (2016) 76(8):2465–77. doi: 10.1158/0008-5472.CAN-15-2402

101. Dekkers JF, Alieva M, Cleven A, Keramati F, Wezenaar AKL, van Vliet EJ, et al. Uncovering the mode of action of engineered T cells in patient cancer organoids. *Nat Biotechnol* (2023) 41(1):60–9. doi: 10.1038/s41587-022-01397-w

102. Almela T, Tayebi L, Moharamzadeh K. 3D bioprinting for in vitro models of oral cancer: toward development and validation. *Bioprinting* (2021) 22:e00132. doi: 10.1016/j.bprint.2021.e00132

103. Arrigoni C, Gilardi M, Bersini S, Candrian C, Moretti M. Bioprinting and organ-on-Chip applications towards personalized medicine for bone diseases. *Stem Cell Rev Rep* (2017) 13(3):407–17. doi: 10.1007/s12015-017-9741-5

104. Sun W, Starly B, Daly AC, Burdick JA, Groll J, Skeldon G, et al. The bioprinting roadmap. *Biofabrication* (2020) 12(2). doi: 10.1088/1758-5090/ab5158

105. Visone R, Gilardi M, Marsano A, Rasponi M, Bersini S, Moretti M. Cardiac meets skeletal: what's new in microfluidic models for muscle tissue engineering. *Molecules* (2016) 21(9):1128. doi: 10.3390/molecules21091128

106. Bersini S, Gilardi M, Arrigoni C, Talò G, Zamai M, Zagra L, et al. Human *in vitro* 3D co-culture model to engineer vascularized bone-mimicking tissues combining computational tools and statistical experimental approach. *Biomaterials* (2016) 76:157–72. doi: 10.1016/j.biomaterials.2015.10.057

107. Khademhosseini A, Langer R. A decade of progress in tissue engineering. *Nat Protoc* (2016) 11(10):1775–81. doi: 10.1038/nprot.2016.123

108. Magdeldin T, López-Dávila V, Pape J, Cameron GWW, Emberton M, Loizidou M, et al. Engineering a vascularised 3D in vitro model of cancer progression. *Sci Rep* (2017) 7:44045. doi: 10.1038/srep44045

109. Gilardi M, Bersini S, Valtorta S, Proietto M, Crippa M, Boussommier-Calleja A, et al. The driving role of the Cdk5/Tln1/FAKS732 axis in cancer cell extravasation dissected by human vascularized microfluidic models. *Biomaterials* (2021) 276:120975. doi: 10.1016/j.biomaterials.2021.120975

110. Mazio C, Casale C, Imparato G, Urciuolo F, Netti PA. Recapitulating spatiotemporal tumor heterogeneity in vitro through engineered breast cancer microtissues. *Acta Biomater* (2018) 73:236–49. doi: 10.1016/j.actbio.2018.04.028

111. Kinders R, Rubinstein L, Parchment RE, Murgo AJ, Collins J, Pickeral O, et al. The tumour microenvironment as a target for chemoprevention. *Nat Rev Cancer* (2007) 7(2):139–47. doi: 10.1038/nrc2067

112. Cassetta L, Fragkogianni S, Sims AH, Swierczak A, Forrester LM, Zhang H, et al. Human tumor-associated macrophage and monocyte transcriptional landscapes reveal cancer-specific reprogramming, biomarkers, and therapeutic targets. *Cancer Cell* (2019) 35(4):588–602.e10. doi: 10.1016/j.ccell.2019.02.009

113. Laumont CM, Banville AC, Gilardi M, Hollern DP, Nelson BH. Tumour-infiltrating b cells: immunological mechanisms, clinical impact and therapeutic opportunities. *Nat Rev Cancer* (2022) 22(7):414–30. doi: 10.1038/s41568-022-00466-1

114. Zhang B, Vogelzang A, Miyajima M, Sugiura Y, Wu Y, Chamoto K, et al. B cell-derived GABA elicits IL-10+ macrophages to limit anti-tumour immunity. *Nature* (2021) 599(7885):471–6. doi: 10.1038/s41586-021-04082-1

115. Gilardi M, Ramos M, Hollern D. B cells secrete GABA, which provokes a pro-tumor immune microenvironment. *Cancer Cell* (2022) 40(1):17–9. doi: 10.1016/j.ccell.2021.12.007

116. Erbel C, Rupp G, Helmes CM, Tyka M, Linden F, Doesch AO, et al. An in vitro model to study heterogeneity of human macrophage differentiation and polarization. *J Vis Exp* (2013) 76:e50332. doi: 10.3791/50332

117. Bhatia SN, Ingber DE. Microfluidic organs-on-chips. *Nat Biotechnol* (2014) 32 (8):760–72. doi: 10.1038/nbt.2989

118. Aref AR, Campisi M, Ivanova E, Portell A, Larios D, Piel BP, et al. 3D microfluidic ex vivo culture of organotypic tumor spheroids to model immune checkpoint blockade. *Lab Chip* (2018) 18(20):3129–43. doi: 10.1039/c8lc00322j

119. Chung M, Ahn J, Son K, Kim S, Jeon NL. Biomimetic model of tumor microenvironment on microfluidic platform. *Adv Healthc Mater* (2017) 6(15). doi: 10.1002/adhm.201700196

120. Arrigoni C, Ostano P, Bersini S, Crippa M, Colombo MV, Gilardi M, et al. Differential angiogenesis of bone and muscle endothelium in aging and inflammatory processes. *Commun Biol* (2023) 6(1):126. doi: 10.1038/s42003-023-04515-9

121. Haase K, Kamm RD. Advances in on-chip vascularization. *Regenerative Med* (2017) 12(3):285–302. doi: 10.2217/rme-2016-0152

122. Crippa M, Talò G, Lamouline A, Bolis S, Arrigoni C, Bersini S, et al. A microfluidic model of human vascularized breast cancer metastasis to bone for the study of neutrophil-cancer cell interactions. *Mater Today Bio*. (2022) 17:100460. doi: 10.1016/j.mtbio.2022.100460

123. Crippa M, Bersini S, Gilardi M, Arrigoni C, Gamba S, Falanga A, et al. A microphysiological early metastatic niche on a chip reveals how heterotypic cell interactions and inhibition of integrin subunit β3 impact breast cancer cell extravasation. *Lab Chip* (2021) 21(6):1061–72. doi: 10.1039/D0LC01011A

124. Adriani G, Pavesi A, Kamm RD. Studying TCR T cell anti-tumor activity in a microfluidic intrahepatic tumor model. *Methods Cell Biol* (2018) 146:199–214. doi: 10.1016/bs.mcb.2018.05.009

125. Pavesi A, Tan AT, Chen MB, Adriani G, Bertoletti A, Kamm RD. Using microfluidics to investigate tumor cell extravasation and T-cell immunotherapies, in: *Proceedings of the Annual International Conference of the IEEE Engineering in Medicine and Biology Society. Annu Int Conf IEEE Eng Med Biol Soc*. (2015) 2015:1853–6.

126. Adriani G, Pavesi A, Tan AT, Bertoletti A, Thiery JP, Kamm RD. Microfluidic models for adoptive cell-mediated cancer immunotherapies. *Drug Discov Today* (2016) 21(9):1472–8. doi: 10.1016/j.drudis.2016.05.006

127. Surendran V, Rutledge D, Colmon R, Chandrasekaran A. A novel tumor-immune microenvironment (TIME)-on-Chip mimics three dimensional neutrophil-tumor dynamics and neutrophil extracellular traps (NETs)-mediated collective tumor invasion. *Biofabrication* (2021) 13(3):10. doi: 10.1088/1758-5090/abe1cf

128. Lin L, He Z, Jie M, Lin JM, Zhang J. 3D microfluidic tumor models for biomimetic engineering of glioma niche and detection of cell morphology, migration and phenotype change. *Talanta* (2021) 234:122702. doi: 10.1016/j.talanta.2021.122702

129. Steen CB, Liu CL, Alizadeh AA, Newman AM. Profiling cell type abundance and expression in bulk tissues with CIBERSORTx. *Methods Mol Biol* (2020) 2117:135–57. doi: 10.1007/978-1-0716-0301-7_7

130. Aran D, Hu Z, Butte AJ. xCell: digitally portraying the tissue cellular heterogeneity landscape. *Genome Biol* (2017) 18(1):220. doi: 10.1186/s13059-017-1349-1

131. Zhang Y, Song J, Zhao Z, Yang M, Chen M, Liu C, et al. Single-cell transcriptome analysis reveals tumor immune microenvironment heterogenicity and granulocytes enrichment in colorectal cancer liver metastases. *Cancer* (2020) 470:84–94. doi: 10.1016/j.canlet.2019.10.016

132. Ho DWH, Tsui YM, Sze KMF, Chan LK, Cheung TT, Lee E, et al. Single-cell transcriptomics reveals the landscape of intra-tumoral heterogeneity and stemness-related subpopulations in liver cancer. *Cancer Lett* (2019) 459:176–85. doi: 10.1016/j.canlet.2019.06.002

133. Yuan X, Ma S, Fa B, Wei T, Ma Y, Wang Y, et al. A high-efficiency differential expression method for cancer heterogeneity using large-scale single-cell RNA-sequencing data. *Front Genet* (2022) 13:1063130. doi: 10.3389/fgene.2022.1063130

134. Liu T, Liu C, Yan M, Zhang L, Zhang J, Xiao M, et al. Single cell profiling of primary and paired metastatic lymph node tumors in breast cancer patients. *Nat Commun* (2022) 13(1):6823. doi: 10.1038/s41467-022-34581-2

135. Xue R, Zhang Q, Cao Q, Kong R, Xiang X, Liu H, et al. Liver tumour immune microenvironment subtypes and neutrophil heterogeneity. *Nature* (2022) 612 (7938):141–7. doi: 10.1038/s41586-022-05400-x

136. Bao X, Shi R, Zhao T, Wang Y, Anastasov N, Rosemann M, et al. Integrated analysis of single-cell RNA-seq and bulk RNA-seq unravels tumour heterogeneity plus M2-like tumour-associated macrophage infiltration and aggressiveness in TNBC. *Cancer Immunol Immunother* (2021) 70(1):189–202. doi: 10.1007/s00262-020-02669-7.

137. Roychowdhury A, Jondhale M, Saldanha E, Ghosh D, Kumar Panda C, Chandrani P, et al. Landscape of toll-like receptors expression in tumor microenvironment of triple negative breast cancer (TNBC): distinct roles of TLR4 and TLR8. *Gene* (2021) 792:145728. doi: 10.1016/j.gene.2021.145728

138. Li H, Courtois ET, Sengupta D, Tan Y, Chen KH, Goh JJL, et al. Reference component analysis of single-cell transcriptomes elucidates cellular heterogeneity in human colorectal tumors. *Nat Genet* (2017) 49(5):708–18. doi: 10.1038/ng.3818

139. Wang N, Li X, Wang R, Ding Z. Spatial transcriptomics and proteomics technologies for deconvoluting the tumor microenvironment. *Biotechnol J* (2021) 6(9): e2100041. doi: 10.1002/biot.202100041

140. Rovira-Clavé X, Drainas AP, Jiang S, Bai Y, Baron M, Zhu B, et al. Spatial epitope barcoding reveals clonal tumor patch behaviors. *Cancer Cell* (2022) 40 (11):1423. doi: 10.1016/j.ccell.2022.09.014

141. Hajiran A, Chakiryan N, Aydin AM, Zemp L, Nguyen J, Laborde JM, et al. Reconnaissance of tumor immune microenvironment spatial heterogeneity in metastatic renal cell carcinoma and correlation with immunotherapy response. *Clin Exp Immunol* (2021) 204(1):96–106. doi: 10.1111/cei.13567

142. Galeano Niño JL, Wu H, LaCourse KD, Kempchinsky AG, Baryiames A, Barber B, et al. Effect of the intratumoral microbiota on spatial and cellular heterogeneity in cancer. *Nature* (2022) 611(7937):810–7. doi: 10.1038/s41586-022-05435-0

143. Toki MI, Merritt CR, Wong PF, Smithy JW, Kluger HM, Syrigos KN, et al. High-plex predictive marker discovery for melanoma immunotherapy treated patients using digital spatial profiling. *Clin Cancer Res* (2019) 25(18):5503. doi: 10.1158/1078-0432.CCR-19-0104

144. Hwang WL, Jagadeesh KA, Guo JA, Hoffman HI, Yadollahpour P, Reeves JW, et al. Single-nucleus and spatial transcriptome profiling of pancreatic cancer identifies multicellular dynamics associated with neoadjuvant treatment. *Nat Genet* (2022) 54 (8):1178–91. doi: 10.1038/s41588-022-01134-8

145. Nirmal AJ, Maliga Z, Vallius T, Quattrochi B, Chen AA, Jacobson CA, et al. The spatial landscape of progression and immunoediting in primary melanoma at single-cell resolution. *Cancer Discov* (2022) 12(6):1518–41. doi: 10.1158/2159-8290.CD-21-1357

146. He S, Bhatt R, Brown C, Brown EA, Buhr DL, Chantranuvatana K, et al. High-plex imaging of RNA and proteins at subcellular resolution in fixed tissue by spatial molecular imaging. *Nat Biotechnol* (2022) 40(12):1794–806. doi: 10.1038/s41587-022-01483-z

147. Xia C, Fan J, Emanuel G, Hao J, Zhuang X. Spatial transcriptome profiling by MERFISH reveals subcellular RNA compartmentalization and cell cycle-dependent gene expression. *Proc Natl Acad Sci U.S.A.* (2019) 116(39):19490–9. doi: 10.1073/pnas.1912459116

148. Hao Y, Hao S, Andersen-Nissen E, Mauck WM, Zheng S, Butler A, et al. Integrated analysis of multimodal single-cell data. *Cell* (2021) 184(13):3573–3587.e29. doi: 10.1016/j.cell.2021.04.048

149. Elosua-Bayes M, Nieto P, Mereu E, Gut I, Heyn H. SPOTlight: seeded NMF regression to deconvolute spatial transcriptomics spots with single-cell transcriptomes. *Nucleic Acids Res* (2021) 49(9):e50–0. doi: 10.1093/nar/gkab043

150. Zeira R, Land M, Strzalkowski A, Raphael BJ. Alignment and integration of spatial transcriptomics data. *Nat Methods* (2022) 19(5):567–75. doi: 10.1038/s41592-022-01459-6

151. Longo SK, Guo MG, Ji AL, Khavari PA. Integrating single-cell and spatial transcriptomics to elucidate intercellular tissue dynamics. *Nat Rev Genet* (2021) 22 (10):627–44. doi: 10.1038/s41576-021-00370-8

152. Li J, Chen S, Pan X, Yuan Y, Bin SH. Cell clustering for spatial transcriptomics data with graph neural networks. *Nat Comput Sci* (2022) 2(6):399–408. doi: 10.1038/s43588-022-00266-5

153. Kleino I, Frolovaitė P, Suomi T, Elo LL. Computational solutions for spatial transcriptomics. *Comput Struct Biotechnol J* (2022) 20:4870–84. doi: 10.1016/j.csbj.2022.08.043

154. Dries R, Chen J, Del Rossi N, Khan MM, Sistig A, Yuan GC. Advances in spatial transcriptomic data analysis. *Genome Res* (2021) 31(10):1706–18. doi: 10.1101/gr.275224.121

155. Ramazzotti D, Caravagna G, Olde Loohuis L, Graudenzi A, Korsunsky I, Mauri G, et al. CAPRI: efficient inference of cancer progression models from cross-sectional data. *Bioinformatics* (2015) 31(18):3016–26. doi: 10.1093/bioinformatics/btv296

156. Ramazzotti D, Angaroni F, Maspero D, Ascolani G, Castiglioni I, Piazza R, et al. LACE: inference of cancer evolution models from longitudinal single-cell sequencing data. *J Comput Sci* (2022) 58:101523. doi: 10.1016/j.jocs.2021.101523

157. Bouckaert R, Heled J, Kühnert D, Vaughan T, Wu CH, Xie D, et al. BEAST 2: a software platform for Bayesian evolutionary analysis. *PloS Comput Biol* (2014) 10(4): e1003537. doi: 10.1371/journal.pcbi.1003537

158. Ronquist F, Teslenko M, van der Mark P, Ayres DL, Darling A, Höhna S, et al. MrBayes 3.2: efficient Bayesian phylogenetic inference and model choice across a large model space. *Syst Biol* (2012) 61(3):539–42. doi: 10.1093/sysbio/sys029

159. Jahn K, Kuipers J, Beerenwinkel N. Tree inference for single-cell data. *Genome Biol* (2016) 17(1):17–86. doi: 10.1186/s13059-016-0936-x

160. Kuipers J, Jahn K, Raphael BJ, Beerenwinkel N. Single-cell sequencing data reveal widespread recurrence and loss of mutational hits in the life histories of tumors. *Genome Res* (2017) 27(11):1885–94. doi: 10.1101/gr.220707.117

161. Caravagna G, Graudenzi A, Ramazzotti D, Sanz-Pamplona R, De Sano L, Mauri G, et al. Algorithmic methods to infer the evolutionary trajectories in cancer progression. *Proc Natl Acad Sci U.S.A.* (2016) 113(28):E4025–34. doi: 10.1073/pnas.1520213113

162. Holder M, Lewis PO. Phylogeny estimation: traditional and Bayesian approaches. *Nat Rev Genet* (2003) 4(4):275–84. doi: 10.1038/nrg1044

163. Dentro SC, Leshchiner I, Haase K, Tarabichi M, Wintersinger J, Deshwar AG, et al. Characterizing genetic intra-tumor heterogeneity across 2,658 human cancer genomes. *Cell* (2021) 184(8):2239–2254.e39. doi: 10.1016/j.cell.2021.03.009

164. Caravagna G, Giarratano Y, Ramazzotti D, Tomlinson I, Graham TA, Sanguinetti G, et al. Detecting repeated cancer evolution from multi-region tumor sequencing data. *Nat Methods* (2018) 15(9):707–14. doi: 10.1038/s41592-018-0108-x

165. Diaz-Uriarte R, Vasallo C. Every which way? on predicting tumor evolution using cancer progression models. *PloS Comput Biol* (2019) 15(8):e1007246. doi: 10.1371/journal.pcbi.1007246

166. Jiang G, Tu J, Zhou L, Dong M, Fan J, Chang Z, et al. Single-cell transcriptomics reveal the heterogeneity and dynamic of cancer stem-like cells during breast tumor progression. *Cell Death Dis* (2021) 12(11).

167. Eyler CE, Matsunaga H, Hovestadt V, Vantine SJ, Van Galen P, Bernstein BE. Single-cell lineage analysis reveals genetic and epigenetic interplay in glioblastoma drug resistance. *Genome Biol* (2020) 21(1):174. doi: 10.1186/s13059-020-02085-1

168. Qiu X, Zhang Y, Martin-Rufino JD, Weng C, Hosseinzadeh S, Yang D, et al. Mapping transcriptomic vector fields of single cells. *Cell* (2022) 185(4):690–711.e45. doi: 10.1016/j.cell.2021.12.045

169. Baruzzo G, Cesaro G, Di Camillo B. Identify, quantify and characterize cellular communication from single-cell RNA sequencing data with scSeqComm. *Bioinformatics* (2022) 38(7):1920–9. doi: 10.1093/bioinformatics/btac036.

170. Efremova M, Vento-Tormo M, Teichmann SA, Vento-Tormo R. CellPhoneDB: inferring cell-cell communication from combined expression of multi-subunit ligand-receptor complexes. *Nat Protoc* (2020) 15(4):1484–506. doi: 10.1038/s41596-020-0292-x

171. Luecken MD, Theis FJ. Current best practices in single-cell RNA-seq analysis: a tutorial. *Mol Syst Biol* (2019) 15(6):e8746. doi: 10.15252/msb.20188746

172. Wolf FA, Angerer P, Theis FJ. SCANPY: large-scale single-cell gene expression data analysis. *Genome Biol* (2018) 19(1):15. doi: 10.1186/s13059-017-1382-0

173. Patruno L, Craighero F, Maspero D, Graudenzi A, Damiani C. Combining multi-target regression deep neural networks and kinetic modeling to predict relative fluxes in reaction systems. *Inf Comput* (2021) 281. doi: 10.1016/j.ic.2021.104798

174. Galuzzi BG, Vanoni M, Damiani C. Combining denoising of RNA-seq data and flux balance analysis for cluster analysis of single cells. *BMC Bioinf* (2022) 23(Suppl 6):445. doi: 10.1186/s12859-022-04967-6

175. Chen AF, Parks B, Kathiria AS, Ober-Reynolds B, Goronzy JJ, Greenleaf WJ. NEAT-seq: simultaneous profiling of intra-nuclear proteins, chromatin accessibility and gene expression in single cells. *Nat Methods* (2022) 19(5):547–53. doi: 10.1038/s41592-022-01461-y

176. De Sanctis G, Colombo R, Damiani C, Sacco E, Vanoni M. Omics and clinical data integration. *Integration Omics Approaches Syst Biol Clin Appl* (2017), 248–73. doi: 10.1002/9781119183952.ch15

177. Ranzoni AM, Tangherloni A, Berest I, Riva SG, Myers B, Strzelecka PM, et al. Integrative single-cell RNA-seq and ATAC-seq analysis of human developmental hematopoiesis. *Cell Stem Cell* (2021) 28(3):472–487.e7. doi: 10.1016/j.stem.2020.11.015

178. Cao ZJ, Gao G. Multi-omics single-cell data integration and regulatory inference with graph-linked embedding. *Nat Biotechnol* (2022) 40(10):1458–66. doi: 10.1038/s41587-022-01284-4

179. Li G, Fu S, Wang S, Zhu C, Duan B, Tang C, et al. A deep generative model for multi-view profiling of single-cell RNA-seq and ATAC-seq data. *Genome Biol* (2022) 23(1):20. doi: 10.1186/s13059-021-02595-6

180. Watanabe Y, Dahlman EL, Leder KZ, Hui SK. A mathematical model of tumor growth and its response to single irradiation. *Theor Biol Med Model* (2016) 13(1):6. doi: 10.1186/s12976-016-0032-7

181. Hartung N, Mollard S, Barbolosi D, Benabdallah A, Chapuisat G, Henry G, et al. Mathematical modeling of tumor growth and metastatic spreading: validation in tumor-bearing mice. *Cancer Res* (2014) 74(22):6397–407. doi: 10.1158/0008-5472.CAN-14-0721

182. De Matteis G, Graudenzi A, Antoniotti M. A review of spatial computational models for multi-cellular systems, with regard to intestinal crypts and colorectal cancer development. *J Math Biol* (2013) 66(7):1409–62. doi: 10.1007/s00285-012-0539-4

183. Angaroni F, Guidi A, Ascolani G, d'Onofrio A, Antoniotti M, Graudenzi A. J-SPACE: a Julia package for the simulation of spatial models of cancer evolution and of sequencing experiments. *BMC Bioinf* (2022) 23(1):269. doi: 10.1186/s12859-022-04779-8

184. Aubert M, Badoual M, Christov C, Grammaticos B. A model for glioma cell migration on collagen and astrocytes. *J R Soc Interface* (2008) 5(18):75–83. doi: 10.1098/rsif.2007.1070

185. Nivlouei SJ, Soltani M, Carvalho J, Travasso R, Salimpour MR, Shirani E. Multiscale modeling of tumor growth and angiogenesis: evaluation of tumor-targeted therapy. *PloS Comput Biol* (2021) 17(6):e1009081. doi: 10.1371/journal.pcbi.1009081

186. Graudenzi A, Maspero D, Damiani C. A multiscale modeling framework combining cellular automata and flux balance analysis. *J OF Cell AUTOMATA* (2021) 15(1–2):75–95.

187. Zangooei MH, Margolis R, Hoyt K. Multiscale computational modeling of cancer growth using features derived from microCT images. *Sci Rep* (2021) 11 (1):18524. doi: 10.1038/s41598-021-97966-1

188. Damiani C, Maspero D, Di Filippo M, Colombo R, Pescini D, Graudenzi A, et al. Integration of single-cell RNA-seq data into population models to characterize cancer metabolism. *PloS Comput Biol* (2019) 15(2):e1006733. doi: 10.1371/journal.pcbi.1006733

189. Dagogo-Jack I, Shaw AT. Tumour heterogeneity and resistance to cancer therapies. *Nat Rev Clin Oncol* (2018) 15(2):81–94. doi: 10.1038/nrclinonc.2017.166

190. Santarius T, Shipley J, Brewer D, Stratton MR, Cooper CS. A census of amplified and overexpressed human cancer genes. *Nat Rev Cancer* (2010) 10(1):59–64. doi: 10.1038/nrc2771

191. Yarden Y, Pines G. The ERBB network: at last, cancer therapy meets systems biology. *Nat Rev Cancer* (2012) 12(8):553–63. doi: 10.1038/nrc3309

192. Capdevila J, Elez E, Macarulla T, Ramos FJ, Ruiz-Echarri M, Tabernero J. Anti-epidermal growth factor receptor monoclonal antibodies in cancer treatment. *Cancer Treat Rev* (2009) 35(4):354–63. doi: 10.1016/j.ctrv.2009.02.001

193. Thomas R, Weihua Z. Rethink of EGFR in cancer with its kinase independent function on board. *Front Oncol* (2019) 9(AUG):800. doi: 10.3389/fonc.2019.00800

194. Bertotti A, Sassi F. Molecular pathways: sensitivity and resistance to anti-EGFR antibodies. *Clin Cancer Res* (2015) 21(15):3377–83. doi: 10.1158/1078-0432.CCR-14-0848

195. Andor N, Graham TA, Jansen M, Xia LC, Aktipis CA, Petritsch C, et al. Pan-cancer analysis of the extent and consequences of intratumor heterogeneity. *Nat Med* (2016) 22(1):105–13. doi: 10.1038/nm.3984

196. Tisi R, Spinelli M, Palmioli A, Airoldi C, Cazzaniga P, Besozzi D, et al. The multi-level mechanism of action of a pan-ras inhibitor explains its antiproliferative activity on cetuximab-resistant cancer cells. *Front Mol Biosci* (2021) 8. doi: 10.3389/fmolb.2021.625979

197. Johnson CW, Lin YJ, Reid D, Parker J, Pavlopoulos S, Dischinger P, et al. Isoform-specific destabilization of the active site reveals a molecular mechanism of intrinsic activation of KRas G13D. *Cell Rep* (2019) 28(6):1538–1550.e7. doi: 10.1016/j.celrep.2019.07.026

198. Blaquier JB, Cardona AF, Recondo G. Resistance to KRASG12C inhibitors in non-small cell lung cancer. *Front Oncol* (2021) 11. doi: 10.3389/fonc.2021.787585

199. Chaudhary PM, Roninson IB. Induction of multidrug resistance in human cells by transient exposure to different chemotherapeutic drugs. *JNCI: J Natl Cancer Institute*. (1993) 85(8):632–9. doi: 10.1093/jnci/85.8.632

200. Aponte PM, Caicedo A. Stemness in cancer: stem cells, cancer stem cells, and their microenvironment. *Stem Cells Int* (2017) 2017:5619472. doi: 10.1155/2017/5619472

201. Prichard SJ, Hessburg PF, Hagmann RK, Povak NA, Dobrowski SZ, Hurteau MD, et al. Adapting western north American forests to climate change and wildfires: 10 common questions. *Ecol Appl* (2021) 31(8):2433. doi: 10.1002/eap.2433

202. Fox S, Sikes BA, Brown SP, Cripps CL, Glassman SI, Hughes K, et al. Fire as a driver of fungal diversity - a synthesis of current knowledge. *Mycologia* (2022) 114 (2):215–41. doi: 10.1080/00275514.2021.2024422

203. Martinez-Outschoorn UE, Bartrons M, Bartrons R. Editorial: cancer ecosystems. *Front Oncol* (2019) 9:718. doi: 10.3389/fonc.2019.00718

204. Laplane L, Duluc D, Bikfalvi A, Larmonier N, Pradeu T. Beyond the tumour microenvironment. *Int J Cancer* (2019) 145(10):2611–8. doi: 10.1002/ijc.32343

205. Sun L, Kees T, Almeida AS, Liu B, He XY, Ng D, et al. Activating a collaborative innate-adaptive immune response to control metastasis. *Cancer Cell* (2021) 39 (10):1361–1374.e9. doi: 10.1016/j.ccell.2021.08.005

206. Ruffell B, Coussens LM. Macrophages and therapeutic resistance in cancer. *Cancer Cell* (2015) 27(4):462–72. doi: 10.1016/j.ccell.2015.02.015

207. López-Soto A, Gonzalez S, Smyth MJ, Galluzzi L. Control of metastasis by NK cells. *Cancer Cell* (2017) 32(2):135–54. doi: 10.1016/j.ccell.2017.06.009

208. Schumacher TN, Schreiber RD. Neoantigens in cancer immunotherapy. *Science* (2015) 348(6230):69–74. doi: 10.1126/science.aaa4971

209. Damo M, Fitzgerald B, Lu Y, Nader M, William I, Cheung JF, et al. Inducible de novo expression of neoantigens in tumor cells and mice. *Nat Biotechnol* (2021) 39 (1):64–73. doi: 10.1126/science.aaa4971

210. Ricciuti B, Wang X, Alessi JV, Rizvi H, Mahadevan NR, Li YY, et al. Association of high tumor mutation burden in non-small cell lung cancers with increased immune infiltration and improved clinical outcomes of PD-L1 blockade across PD-L1 expression levels. *JAMA Oncol* (2022) 8(8):1160–8. doi: 10.1001/jamaoncol.2022.1981.

211. Ma KY, Schonnesen AA, Brock A, Van Den Berg C, Eckhardt SG, Liu Z, et al. Single-cell RNA sequencing of lung adenocarcinoma reveals heterogeneity of immune response-related genes. *JCI Insight* (2019) 4(4):e121387. doi: 10.1172/jci.insight.121387

212. Chalmers ZR, Connelly CF, Fabrizio D, Gay L, Ali SM, Ennis R, et al. Analysis of 100,000 human cancer genomes reveals the landscape of tumor mutational burden. *Genome Med* (2017) 9(1):34. doi: 10.1186/s13073-017-0424-2

213. Vanderlugt CL, Miller SD. Epitope spreading in immune-mediated diseases: implications for immunotherapy. *Nat Rev Immunol* (2002) 2(2):85–95. doi: 10.1038/nri724

214. Hu Z, Leet DE, Allesøe RL, Oliveira G, Li S, Luoma AM, et al. Personal neoantigen vaccines induce persistent memory T cell responses and epitope spreading in patients with melanoma. *Nat Med* (2021) 27(3):515–25. doi: 10.1038/s41591-020-01206-4

215. Shinohara S, Takahashi Y, Demachi-Okamura A, Matsushita H. Identification of neoantigens and development of antigen-specific immunotherapy. *Rinsho Ketsueki* (2020) 61(9):1433–9. doi: 10.11406/rinketsu.61.1433

216. Hutchison S, Pritchard AL. Identifying neoantigens for use in immunotherapy. *Mamm Genome* (2018) 29(11–12):714–30. doi: 10.1007/s00335-018-9771-6

217. Reuben A, Gittelman R, Gao J, Zhang J, Yusko EC, Wu CJ, et al. TCR repertoire intratumor heterogeneity in localized lung adenocarcinomas: an association with predicted neoantigen heterogeneity and postsurgical recurrence. *Cancer Discov* (2017) 7(10):1088–97. doi: 10.1158/2159-8290.CD-17-0256

218. Anderson C, Brissette CA. The brilliance of borrelia: mechanisms of host immune evasion by Lyme disease-causing spirochetes. *Pathogens* (2021) 10(3):281. doi: 10.3390/pathogens10030281

219. Xu XD, Hu J, Wang M, Peng F, Tian R, Guo XJ, et al. Circulating myeloid-derived suppressor cells in patients with pancreatic cancer. *Hepatobiliary Pancreat Dis Int* (2016) 15(1):099–105. doi: 10.1016/S1499-3872(15)60413-1

220. Diaz-Montero CM, Salem ML, Nishimura MI, Garrett-Mayer E, Cole DJ, Montero AJ. Increased circulating myeloid-derived suppressor cells correlate with clinical cancer stage, metastatic tumor burden, and doxorubicin-cyclophosphamide chemotherapy. *Cancer Immunol Immunother* (2009) 58(1):49–59. doi: 10.1007/s00262-008-0523-4

221. Kirk R. Tumour evolution: evidence points to the existence of cancer stem cells. *Nat Rev Clin Oncol* (2012) 9(10):552. doi: 10.1038/nrclinonc.2012.149

222. McCarthy N. Cancer stem cells: tracing clones. *Nat Rev Cancer* (2012) 12 (9):579. doi: 10.1038/nrc3354

223. Costoya JA, Arce VM. Cancer cells escape the immune system by increasing stemness through epigenetic reprogramming. *Cell Mol Immunol* (2022) 20(1):6–7. doi: 10.1038/s41423-022-00953-3

224. Miranda A, Hamilton PT, Zhang AW, Pattnaik S, Becht E, Mezheyeuski A, et al. Cancer stemness, intratumoral heterogeneity, and immune response across cancers. *Proc Natl Acad Sci U.S.A.* (2019) 116(18):9020–9. doi: 10.1073/pnas.1818210116

225. Barker N, Van Es JH, Kuipers J, Kujala P, Van Den Born M, Cozijnsen M, et al. Identification of stem cells in small intestine and colon by marker gene Lgr5. *Nature* (2007) 449(7165):1003–7. doi: 10.1038/nature06196

226. Weidenfeld K, Barkan D. EMT and stemness in tumor dormancy and outgrowth: are they intertwined processes? *Front Oncol* (2018) 8(SEP). doi: 10.3389/fonc.2018.00381

227. Malladi S, MacAlinao DG, Jin X, He L, Basnet H, Zou Y, et al. Metastatic latency and immune evasion through autocrine inhibition of WNT. *Cell* (2016) 165 (1):45–60. doi: 10.1016/j.cell.2016.02.025

228. Nielsen SR, Quaranta V, Linford A, Emeagi P, Rainer C, Santos A, et al. Macrophage-secreted granulin supports pancreatic cancer metastasis by inducing liver fibrosis. *Nat Cell Biol* (2016) 18(5):549–60. doi: 10.1038/ncb3340

229. Hanahan D, Weinberg RA. Hallmarks of cancer: the next generation. *Cell* (2011) 144(5):646–74. doi: 10.1016/j.cell.2011.02.013

230. McCorry AMB, Loughrey MB, Longley DB, Lawler M, Dunne PD. Epithelial-to-mesenchymal transition signature assessment in colorectal cancer quantifies tumour stromal content rather than true transition. *J Pathol* (2018) 246(4):422–6. doi: 10.1002/path.5155

231. Chen X, Yang M, Yin J, Li P, Zeng S, Zheng G, et al. Tumor-associated macrophages promote epithelial-mesenchymal transition and the cancer stem cell properties in triple-negative breast cancer through CCL2/AKT/β-catenin signaling. *Cell Commun Signal* (2022) 20(1):92. doi: 10.1186/s12964-022-00888-2

232. Cohen EEW, Soulières D, le Tourneau C, Dinis J, Licitra L, Ahn MJ, et al. Pembrolizumab versus methotrexate, docetaxel, or cetuximab for recurrent or metastatic head-and-neck squamous cell carcinoma (KEYNOTE-040): a randomised, open-label, phase 3 study. *Lancet* (2019) 393(10167):156–67. doi: 10.1016/S0140-6736(18)31999-8

233. Bauman JE, Cohen E, Ferris RL, Adelstein DJ, Brizel DM, Ridge JA, et al. Immunotherapy of head and neck cancer: emerging clinical trials from a national cancer institute head and neck cancer steering committee planning meeting. *Cancer* (2017) 123(7):1259. doi: 10.1002/cncr.30449

234. Lee JB, Ha SJ, Kim HR. Clinical insights into novel immune checkpoint inhibitors. *Front Pharmacol* (2021) 12:1074. doi: 10.3389/fphar.2021.681320

235. Robert C. A decade of immune-checkpoint inhibitors in cancer therapy. *Nat Commun* (2020) 11(1):1–3. doi: 10.1038/s41467-020-17670-y

236. Angelova M, Mlecnik B, Vasaturo A, Bindea G, Fredriksen T, Lafontaine L, et al. Evolution of metastases in space and time under immune selection. *Cell* (2018) 175(3):751–765.e16. doi: 10.1016/j.cell.2018.09.018

237. Davidson G, Coassolo S, Kieny A, Ennen M, Pencreach E, Malouf GG, et al. Dynamic evolution of clonal composition and neoantigen landscape in recurrent metastatic melanoma with a rare combination of driver mutations. *J Invest Dermatol* (2019) 139(8):1769–1778.e2. doi: 10.1016/j.jid.2019.01.027

238. Jiang T, Shi T, Zhang H, Hu J, Song Y, Wei J, et al. Tumor neoantigens: from basic research to clinical applications. *J Hematol Oncol* (2019) 12(1):1–13. doi: 10.1186/s13045-019-0787-5

239. Kieffer Y, Hocine HR, Gentric G, Pelon F, Bernard C, Bourachot B, et al. Single-cell analysis reveals fibroblast clusters linked to immunotherapy resistance in cancer. *Cancer Discov* (2020) 10(9):1330–51. doi: 10.1158/2159-8290.CD-19-1384

240. Dominguez CX, Müller S, Keerthivasan S, Koeppen H, Hung J, Gierke S, et al. Single-cell RNA sequencing reveals stromal evolution into LRRC15+ myofibroblasts as a determinant of patient response to cancer immunotherapy. *Cancer Discov* (2020) 10(2):232–53. doi: 10.1158/2159-8290.CD-19-0644

241. Pan X, Zhou J, Xiao Q, Fujiwara K, Zhang M, Mo G, et al. Cancer-associated fibroblast heterogeneity is associated with organ-specific metastasis in pancreatic ductal adenocarcinoma. *J Hematol Oncol* (2021) 14(1):184. doi: 10.1186/s13045-021-01203-1

242. Su S, Chen J, Yao H, Liu J, Yu S, Lao L, et al. CD10+GPR77+ cancer-associated fibroblasts promote cancer formation and chemoresistance by sustaining cancer stemness. *Cell* (2018) 172(4):841–856.e16. doi: 10.1016/j.cell.2018.01.009

243. Quintavalle C, Meyer-Schaller N, Roessler S, Calabrese D, Marone R, Riedl T, et al. miR-579-3p controls hepatocellular carcinoma formation by regulating the phosphoinositide 3-Kinase-Protein kinase b pathway in chronically inflamed liver. *Hepatol Commun* (2022) 6(6):1467–81. doi: 10.1002/hep4.1894

244. Rey S, Quintavalle C, Burmeister K, Calabrese D, Schlageter M, Quagliata L, et al. Liver damage and senescence increases in patients developing hepatocellular carcinoma. *J Gastroenterol Hepatol* (2017) 32(8):1480–6. doi: 10.1111/jgh.13717

245. Omar JM, Hai Y, Jin S. Hypoxia-induced factor and its role in liver fibrosis. *PeerJ* (2022) 10:e14299. doi: 10.7717/peerj.14299

246. Affo S, Nair A, Brundu F, Ravichandra A, Bhattacharjee S, Matsuda M, et al. Erratum: promotion of cholangiocarcinoma growth by diverse cancer-associated fibroblast subpopulations. *Cancer Cell* (2021) 39(6):883. doi: 10.1016/j.ccell.2021.03.012

247. Hu JL, Wang W, Lan XL, Zeng ZC, Liang YS, Yan YR, et al. CAFs secreted exosomes promote metastasis and chemotherapy resistance by enhancing cell stemness and epithelial-mesenchymal transition in colorectal cancer. *Mol Cancer* (2019) 18(1):91. doi: 10.1186/s12943-019-1019-x

248. Zhang C, Wang XY, Zhang P, He TC, Han JH, Zhang R, et al. Cancer-derived exosomal HSPC111 promotes colorectal cancer liver metastasis by reprogramming lipid metabolism in cancer-associated fibroblasts. *Cell Death Dis* (2022) 13(1):57. doi: 10.1038/s41419-022-04506-4

249. Krishnamurty AT, Shyer JA, Thai M, Gandham V, Buechler MB, Yang YA, et al. LRRC15+ myofibroblasts dictate the stromal setpoint to suppress tumour immunity. *Nature* (2022) 611(7934):148–54:7934. doi: 10.1038/s41586-022-05272-1

250. McCarthy SA, Kuzu I, Gatter KC, Bicknell R. Heterogeneity of the endothelial cell and its role in organ preference of tumour metastasis. *Trends Pharmacol Sci* (1991) 12(C):462–7. doi: 10.1016/0165-6147(91)90637-8

251. Wu S, Zheng Q, Xing X, Dong Y, Wang Y, You Y, et al. Matrix stiffness-upregulated LOXL2 promotes fibronectin production, MMP9 and CXCL12 expression and BMDCs recruitment to assist pre-metastatic niche formation. *J Exp Clin Cancer Res* (2018) 37(1):99. doi: 10.1186/s13046-018-0761-z

252. Xing X, Wang Y, Zhang X, Gao X, Li M, Wu S, et al. Matrix stiffness-mediated effects on macrophages polarization and their LOXL2 expression. *FEBS J* (2021) 288(11):3465–77. doi: 10.1111/febs.15566

253. Swift J, Ivanovska IL, Buxboim A, Harada T, Dingal PCDP, Pinter J, et al. Nuclear lamin-a scales with tissue stiffness and enhances matrix-directed differentiation. *Science* (2013) 341(6149):1240104. doi: 10.1126/science.1240104

254. Dong Y, Zheng Q, Wang Z, Lin X, You Y, Wu S, et al. Higher matrix stiffness as an independent initiator triggers epithelial-mesenchymal transition and facilitates HCC metastasis. *J Hematol Oncol* (2019) 12(1):112. doi: 10.1186/s13045-019-0795-5

255. Rømer AMA, Thorseth ML, Madsen DH. Immune modulatory properties of collagen in cancer. *Front Immunol* (2021) 12. doi: 10.3389/fimmu.2021.791453

256. Shen Y, Wang X, Lu J, Salfenmoser M, Wirsik NM, Schleussner N, et al. Reduction of liver metastasis stiffness improves response to bevacizumab in metastatic colorectal cancer. *Cancer Cell* (2020) 37(6):800–817.e7. doi: 10.1016/j.ccell.2020.05.005

257. Ando H, Emam SE, Kawaguchi Y, Shimizu T, Ishima Y, Eshima K, et al. Increasing tumor extracellular pH by an oral alkalinizing agent improves antitumor responses of anti-PD-1 antibody: implication of relationships between serum bicarbonate concentrations, urinary pH, and therapeutic outcomes. *Biol Pharm Bull* (2021) 44(6):844–52. doi: 10.1248/bpb.b21-00076

258. Noy R, Pollard JW. Tumor-associated macrophages: from mechanisms to therapy. *Immunity* (2014) 41(1):49. doi: 10.1016/j.immuni.2014.06.010

259. Ramsköld D, Luo S, Wang YC, Li R, Deng Q, Faridani OR, et al. Full-length mRNA-seq from single-cell levels of RNA and individual circulating tumor cells. *Nat Biotechnol* (2012) 30(8):777–82. doi: 10.1038/nbt.2282

260. Bhalla US, Iyengar R. Emergent properties of networks of biological signaling pathways. *Science* (1999) 283(5400):381–7. doi: 10.1126/science.283.5400.381

261. Nielsen J. Systems biology of metabolism: a driver for developing personalized and precision medicine. *Cell Metab* (2017) 25(3):572–9. doi: 10.1016/j.cmet.2017.02.002

262. Damiani C, Gaglio D, Sacco E, Alberghina L, Vanoni M. Systems metabolomics: from metabolomic snapshots to design principles. *Curr Opin Biotechnol* (2020) 63:190–9. doi: 10.1016/j.copbio.2020.02.013

263. Lecca P. Machine learning for causal inference in biological networks: perspectives of this challenge. *Front Bioinf* (2021) 1:45. doi: 10.3389/fbinf.2021.746712

264. Silberberg G. Pharmaco-Pheno-Multiomic integration reveals biomarker profiles and therapeutic response prediction models in leukemia and ovarian cancer. *Arch Clin Biomed Res* (2023). doi: 10.1101/2022.06.14.495846

265. Kitano H. Looking beyond the details: a rise in system-oriented approaches in genetics and molecular biology. *Curr Genet* (2002) 41(1):1–10. doi: 10.1007/s00294-002-0285-z

266. Bhat-Nakshatri P, Appaiah H, Ballas C, Pick-Franke P, Goulet R, Badve S, et al. SLUG/SNAI2 and tumor necrosis factor generate breast cells with CD44+/CD24- phenotype. *BMC Cancer* (2010) 10:411. doi: 10.1186/1471-2407-10-411

267. Garralda E, Paz K, López-Casas PP, Jones S, Katz A, Kann LM, et al. Integrated next-generation sequencing and avatar mouse models for personalized cancer treatment. *Clin Cancer Res* (2014) 20(9):2476–84. doi: 10.1158/1078-0432.CCR-13-3047

268. Kamel Boulos MN, Zhang P. Digital twins: from personalised medicine to precision public health. *J Pers Med* (2021) 11(8):745. doi: 10.3390/jpm11080745

269. Di Filippo M, Damiani C, Vanoni M, Maspero D, Mauri G, Alberghina L, et al. Single-cell digital twins for cancer preclinical investigation. *Methods Mol Biol* (2020) 2088:331–43. doi: 10.1007/978-1-0716-0159-4_15

frontiers | Frontiers in Oncology

TYPE Review
PUBLISHED 01 May 2023
DOI 10.3389/fonc.2023.1172314

OPEN ACCESS

EDITED BY
Sara Lovisa,
Humanitas University, Italy

REVIEWED BY
Paola Trono,
National Research Council (CNR), Italy
Yuzhou Chang,
The Ohio State University, United States

*CORRESPONDENCE
Joe Poh Sheng Yeong
joe.yeong.p.s@sgh.com.sg
Mai Chan Lau
lau_mai_chan@bii.a-star.edu.sg

†These authors have contributed equally to this work

RECEIVED 23 February 2023
ACCEPTED 18 April 2023
PUBLISHED 01 May 2023

CITATION
Lee RY, Ng CW, Rajapakse MP, Ang N, Yeong JPS and Lau MC (2023) The promise and challenge of spatial omics in dissecting tumour microenvironment and the role of AI.
Front. Oncol. 13:1172314.
doi: 10.3389/fonc.2023.1172314

The promise and challenge of spatial omics in dissecting tumour microenvironment and the role of AI

Ren Yuan Lee[1,2†], Chan Way Ng[3†], Menaka Priyadharsani Rajapakse[3], Nicholas Ang[3], Joe Poh Sheng Yeong[4,5*] and Mai Chan Lau[3,6*]

[1]Singapore Thong Chai Medical Institution, Singapore, Singapore, [2]Yong Loo Lin School of Medicine, National University of Singapore, Singapore, Singapore, [3]Singapore Immunology Network (SIgN), Agency for Science, Technology and Research (A*STAR), Singapore, Singapore, [4]Department of Anatomical Pathology, Singapore General Hospital, Singapore, Singapore, [5]Cancer Science Institute of Singapore, National University of Singapore, Singapore, Singapore, [6]Bioinformatics Institute (BII), Agency for Science, Technology and Research (A*STAR), Singapore, Singapore

Growing evidence supports the critical role of tumour microenvironment (TME) in tumour progression, metastases, and treatment response. However, the *in-situ* interplay among various TME components, particularly between immune and tumour cells, are largely unknown, hindering our understanding of how tumour progresses and responds to treatment. While mainstream single-cell omics techniques allow deep, single-cell phenotyping, they lack crucial spatial information for *in-situ* cell-cell interaction analysis. On the other hand, tissue-based approaches such as hematoxylin and eosin and chromogenic immunohistochemistry staining can preserve the spatial information of TME components but are limited by their low-content staining. High-content spatial profiling technologies, termed spatial omics, have greatly advanced in the past decades to overcome these limitations. These technologies continue to emerge to include more molecular features (RNAs and/or proteins) and to enhance spatial resolution, opening new opportunities for discovering novel biological knowledge, biomarkers, and therapeutic targets. These advancements also spur the need for novel computational methods to mine useful TME insights from the increasing data complexity confounded by high molecular features and spatial resolution. In this review, we present state-of-the-art spatial omics technologies, their applications, major strengths, and limitations as well as the role of artificial intelligence (AI) in TME studies.

KEYWORDS

spatial omics, tumour microenvironment, artificial intelligence, machine learning, deep learning, spatial proteomics, spatial transcriptomics, digital pathology

Introduction

Tumour microenvironment (TME) plays an important role in disease progression and clinical outcomes. TME is made up of multiple components including fibroblasts, immunosuppressive cells, immune effector cells, and cytokines (1). Specific T-cell subsets, including $CD4^+$ helper and $CD8^+$ T-cells offer protective immunity (2). On the other hand, tumour-associated macrophages (TAM) which is the most prevalent infiltrating immune cells in the TME can promote tumour growth when accompanied by the activation of fibroblasts. Localization of TAM near invasive borders correlates with unfavorable prognoses in tumors such as colorectal cancer (CRC) (3). Similarly, tumour-associated neutrophils (TANs) can transition from anticancer to pro-tumorigenic phenotypes due to unclear mechanisms (4, 5). TME influences treatment outcomes through multiple mechanisms. In ovarian and lung malignancies, TAM-associated exosomes, which are small membrane-bound vesicles that contain proteins, lipids, and nucleic acids which can be transferred to neighboring cells to influence their physiological behavior, thereby increasing tumour proliferation, apoptosis inhibition and drug resistance (6, 7). TANs were found to have tumour-promoting effects in the lung TME, leading to unfavorable immunotherapy (IO) outcomes (8). Higher mast cell levels in TME were associated with higher PD-L1 expression (9) indicating potential impact on immune checkpoint inhibitor (ICI) efficacy. Increased $CD4^+$ helper T-cells have been postulated to improve IO outcomes through enhancing cytotoxic T-cell response (10). A previous study has shown that phenotypically defined T-cell subsets, rather than overall T-cells, may be useful in predicting therapy outcomes (11).

While traditional immunohistochemistry (IHC) and hematoxylin and eosin (H&E) tissue staining have been used routinely for tumour diagnosis, their low-content limits usefulness in TME analysis. On the other hand, high-throughput technologies such as single-cell RNA-sequencing (scRNAseq) and flow cytometry, despite allowing for high-content molecular profiling, they lose spatial information during tissue dissociation. Additionally, experimental tissue dissociation may result in unexpected cell phenotypic alterations unrepresentative of the actual TME. To address these issues, novel tissue-based spatial omics approaches have recently been developed (12). These advanced spatial techniques enable deep phenotyping, such as distinguishing M1- from M2-polarized macrophages (13) and mature from immature myeloid cells (14), which cannot be achieved with IHC and H&E alone. Additionally, by conserving the spatial information, these techniques allows identification of unique spatial patterns of immune cells in TME with novel biological significance, such as TAM-associated cellular neighborhoods with different antitumor characteristics (15), TMEs with various TAN subtypes linked to prognosis and survival (16), differing states of T cell dysfunction contributing to tumour propagation (17), and ligand-receptor cell interactions (18) associated with various prognoses and treatment outcomes (19). In this review, we will introduce and discuss how state-of-the-art spatial proteomics (SP), spatial transcriptomics (ST) and the utilization of artificial intelligence (AI) approaches that can benefit TME analysis (Figure 1). We will also provide our perspectives on the challenges and future development needed to advance the field of spatial omics.

SP techniques

In this section, we discuss the two major groups of SP techniques, namely fluorescent-labelling and metal isotope-labelling assays (Table 1), which differ in the number of plexing, throughput, resolution, and cost (39).

Fluorescence-labelling techniques

OPAL-based multiplex IHC (mIHC)/immunofluorescence (IF) technique allows staining up to 9 markers on a single formalin-fixed, paraffin-embedded (FFPE) tissue section through tyramide signal amplification (TSA). It represents one of the most popular SP techniques for (i) its widely validated consistency against conventional IHC (40, 41); (ii) autostainer availability, particularly BondMax (Leica Biosystems, Germany) for staining consistency (39, 42–45); and (iii) clinical feasibility and usefulness (46–48). The technique has been widely applied for investigating the complex TME through enabling accurate and deep cell phenotyping (e.g., macrophage polarization states, myeloid cell maturity and immunosuppressivity, and T cell phenotypes) (13), revealing the spatial heterogeneity of immune cells (49–51), and characterizing immune localization patterns associated with patient survivals or treatment outcomes (20). Using proximity analysis, Feng et al. showed that hampered survival outcomes of oral squamous cell cancers (SCC) was associated with $CD8^+$ T-cells surrounded by immunosuppressive $FoxP3^+$ or $PD\text{-}L1^+$ cells (52); Väyrynen et al. showed that CRC patients with mature monocytic cell ($CD14^+HLADR^+$) closer to tumour cells harbored better survival (14). One disadvantage of OPAL-based mIHC/IF technique is the possibility of physical steric hindrance caused by multiple antibodies at a single site, resulting in noisy signals (53).

To enable comprehensive immune profiling, hyper-plex cyclic mIHC/IF techniques have been developed, including COMET (Lunaphore, Switzerland) and PhenoCycler (Akoya Biosciences, USA). COMET provides an automated workflow cycling through staining, imaging, and elution of 3 markers each time, up to 40 markers in the same tissue section, whereby fluorophores are directly attached to secondary antibodies without TSA. This approach not only reduces steric hindrance with lesser markers per cycle, but also enhances signal stability through reducing incubation time (i.e., tissue exposure time to harsh reagents). Using a 40-plex COMET assay, Almeida et al. found that myeloid and T regulatory cells were spatially restricted in primary lung cancers (21). Using machine learning (ML), the authors also identified distinct subsets of myeloid cells within the same TME.

To further reduce the steric hindrance effect, PhenoCylcer (formerly CODEX) replaces the large molecular secondary antibodies in the OPAL approach with DNA-conjugated antibodies tagged to fluorescent reporters, allowing staining of up

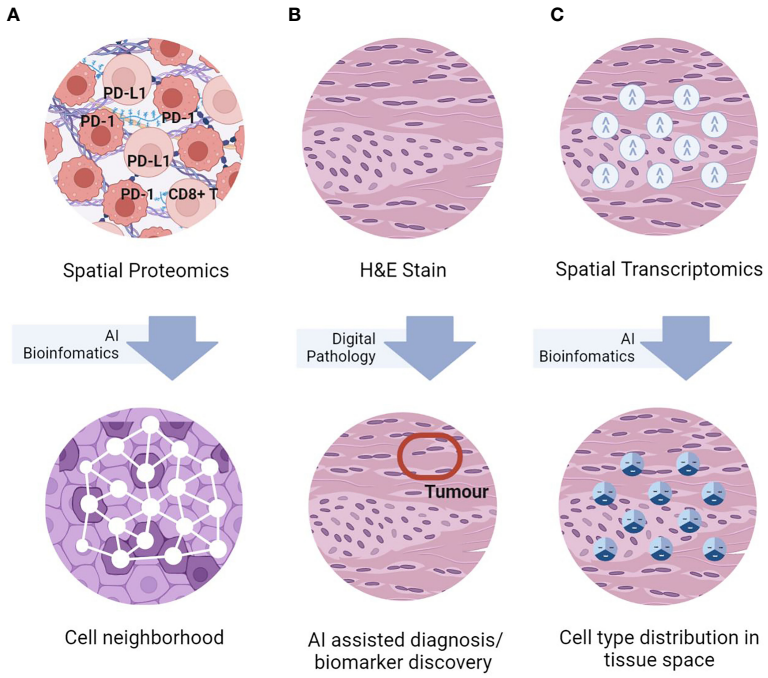

FIGURE 1
Simplified graphical representations of the three key spatial omics technologies, namely **(A)** spatial proteomics assays for *in-situ* single-cell phenotyping using surface marker; **(B)** H&E staining for histomorphological assessment, and **(C)** spatial transcriptomics for *in-situ* transcriptomics characterization, and representative TME analyses enabled by AI bioinformatics.

to 50 markers (3 per cycle). Applying tensor decomposition, cell-type differential enrichment and canonical correlation analysis on PhenoCycler data, Schürch et al. found 9 distinct cellular neighborhoods associated with survival outcomes which were conserved across 35 CRC samples (22).

Metal isotope-labelling techniques

Metal-based methods employ stable metal isotopes to replace the fluorophores (54), where protein expression is measured by detecting isotope signals using laser scanning or ion beams. Autofluorescence and background noise can be considerably reduced with endogenous metals (55). Imaging mass cytometry (IMC) (Standard BioTools, USA) uses high-resolution scanning laser ablation (a fixed lateral resolution of 1,000nm) followed by mass cytometry to quantify up to 50 markers at subcellular resolution using fresh frozen (FF)/FFPE tissues (56–58). Using 37-plex IMC, Ali et al. identified heterotypic neighborhoods of a specific myofibroblast phenotype which was associated with poor outcomes in breast cancer (BC) (23).

Another metal-based method, multiplexed ion beam imaging (MIBI) (Ionpath, USA) uses a tuneable ion beam voltage and mass spectrometry to detect molecules of interest (24), analyzing up to 100 markers at subcellular resolution using FF/FFPE tissues (25, 59, 60). Ptacek et al. validated the robustness, sensitivity, and reproducibility of MIBI against individual IHC stains (24), while Angelo et al. and Rost et al. tested the consistency of MIBI against IHC procedures for estrogen receptor alpha, progesterone receptor and human epidermal growth factor receptor 2 using FFPE BC samples (60, 61). ML techniques have been extensively used in these MIBI studies for rapid exploration and analysis of data for novel discoveries. For examples, Keren et al. developed a computational pipeline to chart the immune landscape in triple-negative breast cancer. In their pipeline, they employed multiple ML techniques such as DeepCell for cell segmentation, *k*-nearest neighbor algorithm for noise filtering, quantile normalization for batch effects correction, and hierarchical clustering to identify unique and shared spatial interactions among patients (25). Padmanabhan et al. built multiple DL models for segmentation of cells and regions, and for cell classification. A containerized cluster platform that can run a workflow comprising of pre-trained DL models as directed acyclic graph has been used to accelerate the discovery of associations and spatial patters in TME (26). Authors in (23, 60) used CellProfiler, an image analysis tool encompassing number of ML algorithms such as random forest, principal component analysis, and neural networks (NN) to understand phenotypic impact of genomic alterations and to gain new insights from the combination of tissue microarchitecture with multiplexed protein expression patterns, respectively.

ST techniques

ST methods can be broadly categorized into next-generation sequencing (NGS)-based and imaging-based methods, measuring either near whole-transcriptome at multi-cell (10s to hundreds) resolution or selected genes at subcellular spatial resolution. NGS-

TABLE 1 Summary of SP and ST techniques as well as their associated applications in TME analysis.

Technique	Detection	Vendor	Profiling technology	Plexing	Tissue Type	Companion analytical software	Key TME applications
Opal-based multiplex IHC	Proteins	Akoya Biosciences	Fluorescence-labelling reagent kits	9	FFPE	InForm	Deep phenotyping of macrophage polarization state, myeloids, T-cell subsets (15) in CRC (14) and pancreatic cancers (20).
COMET	Proteins	Lunaphore	Cyclic fluorescence labelling platform	40	FF/ FFPE	Phenoplex	Identification of spatially restricted myeloid and T regulatory cells in primary lung cancers (21)
PhenoCylcer	Proteins	Akoya Biosciences	Cyclic fluorescence labelling platform	50	FF/ FFPE	PhenoCycler MAV software	Identification of distinct cellular neighbourhoods with survival association in CRC (22)
IMC	Proteins	Standard BioTools	Metal-based labelling	50	FF/ FFPE	Phenoplex	Study of heterotypic neighbourhoods of a specific myofibroblast phenotype in breast cancer (23)
MIBI	Proteins	Ionpath	Metal isotope-labelling	100	FF/ FFPE	MIBItracker Software	Study of the spatial organization and immuno profile of 15 tumor types, revealing infiltration of $CD8^+$ cytotoxic T cells and $CD68^+$ macrophages in ovarian serous carcinoma TME (24); spatial enrichment analysis revealed that tumors were immune mixed and compartmentalized with varying expression of PD1, PD-L1, and IDO on a cell-type and location-specific basis, where highly ordered structures with PD-L1 and IDO along the tumor-immune border served as a hallmark of tumor compartmentalization in a triple-negative breast cancer patients (25).
Visium	RNA	10X Genomics	NGS	18000	FF/ FFPE	Spaceranger, Loupe browser	Identification of enrichment of B-cell maturation and anti-tumorigenic antibody production within TLS+ compartment and positive association with clinical outcomes of renal cell carcinoma (26); study of long-term effects of SARS-CoV-2 in hepatocellular carcinoma and CRC, revealing persistent B-cell immune responses and improved in-silico IO-response scores in SARS-CoV-2-rich tissue regions (27).
GeoMx DSP	Proteins/ RNA	nanoString	NGS	100+ (proteins)/ 18000+ (RNA)	FF/ FFPE	GeoMx DSP online suite, GeoMx tools (R package)	Study of the association between CD66b expression within the CD45+CD68 compartment and ICI resistance, which however, not observed in ICI-untreated lung cancer patients (28); characterization of 4 molecularly unique compartments: tumor, leukocyte, macrophage, and immune stroma where different biomarkers in specific compartments show improved survivals in heck and neck SCC (29)
Slide-Seq/ Seeker	RNA	Curio Bioscience	NGS	whole-transcriptome	FF	–	Identification of cellular neighbourhood archetypes associated with tumour progression and malignancy (30); spatial TCR clonotypic effect of IO treatment in metastatic lung cancer (31)
Stereo-seq	RNA	Beijing Genomic Institute	NGS	whole transcriptome	FF/ FFPE	Stereo-seq Analysis Workflow (SAW) software suite	Study of hepatocellular carcinoma shows that elevated expressions of Serum Amyloid A observed in hepatocytes located near invasive fronts of the tumor were linked to increased macrophage recruitment, and were associated with a negative prognosis in intrahepatic cholangiocarcinoma (32); study of CRC tissue identified locoregional “warmed-up” immune response in predefined “cold” tumor where the "warmed-up" signature genes were found to be indicative of improved overall survival in patients with CRC (33).

(Continued)

TABLE 1 Continued

Technique	Detection	Vendor	Profiling technology	Plexing	Tissue Type	Companion analytical software	Key TME applications
MERFISH/ MERSCOPE	RNA	Vizgen	Imaging	~10,000	FF/ FFPE	–	Identification of a shift in immune spatial organization between tumour subtypes, namely human mismatch repair deficient and proficient tumours (34)
CosMx	Proteins/ RNA	nanoString	Imaging	100/ 1000+	FF/ FFPE	AtoMx Spatial Informatics Platform	Quantification of proteins in NSCLC and BC tissues down to subcellular resolution for the identification of different cell types, unique TMEs, and ligand-receptor pairs (35); Study of relationships between high-dimensional cellular heterogeneity and spatial organization of cells within renal cell carcinoma tissues (36)
Xenium	RNA	10X Genomics	Imaging	280 and 100 more customizable targets; the non-destructive nature allows post-Xenium H&E and IF staining on the same section rendering additional SP and histological information	FF/ FFPE	Xenium Explorer	Identification of novel markers at subcellular level responsible for the transition between ductal carcinoma in situ (DCIS) and invasive cancer of human breast tissues where the myoepthelial layer is broken (37); identification and interrogation of the cellular composition and differentially expressed genes among the 3 molecular subtypes of BC (low, high-grade DCIS, and invasive cancer) through integrating Xenium with H&E and IF data (38).

based methods acquire spatial transcriptomic data by attaching and sequencing unique barcodes to cell subsets in designated tissue areas such as a lattice of evenly spaced spots, user-marked regions, or marker-stained regions. This untargeted nature of NGS based methods make them suitable for exploratory studies (62). Imaging-based methods quantify transcripts *in-situ* through direct imaging of fluorescence dyes of the nucleic acid bases (termed *in-situ* sequencing) or the target-specific/bound fluorophore (termed *in-situ* hybridization (ISH)).

NGS-based ST techniques

Visium Spatial Gene Expression (10x Genomics, USA) enables genome-wide ST profiling of FF/FFPE tissues. The slide capture area (6.5mm^2) contains ~5,000 spots, each with a 55 µm diameter. Using Visium, Meylan et al. examined the B-cell response within intratumoral tertiary lymphoid structures (TLS) in renal cell carcinoma, and found positive clinical outcomes associated with intratumoral TLS+ regions enriched with B-cell maturation and anti-tumorigenic antibody production (26); Lau et al. examined the long-term effects of SARS-CoV-2 in hepatocellular carcinoma and CRC, revealing persistent B-cell immune responses and improved in-silico IO-response scores in SARS-CoV-2-rich tissue regions (27). Another genome-wide ST method, Slide-seq (Applied Biotechnology Laboratory, UK), offers higher resolution (10 µm) read-outs with a comparable capture area (in mm-range), but is limited to FF tissues (30, 63, 64). Using Slide-seq, Avraham-Davidi et al. revealed three distinct cellular neighborhood archetypes associated with tumour progression and malignancy (30). Liu et al. further developed Slide-T cell receptor (TCR)-seq and identified 1,132 unique clonotypes, some localized in restricted tissue compartments in metastatic lung cancer post anti-PD-1 therapy, revealing spatial clonotypic effect of IO treatment (31).

GeoMx digital spatial profiler (DSP) (Nanostring, USA) is capable of simultaneous ST (thousands to tens of thousands of genes) and SP (1 nuclear and 3 surface markers) profiling of FF/FFPE tissues of up to 36.2mm x 14.6mm in size (65). RNAs and proteins are quantified through oligonucleotide tagging (with RNA probes or antibodies, respectively), photocleaving, and sequencing. DSP studies showed that higher lymphoid infiltrates and T-cell clonality in the TME were associated with improved IC efficacy (66, 67); CD66b expression in the CD45$^+$CD68 molecular compartment was linked to IO therapy resistance in lung cancers (28); B2M and CD25 levels in tumour and CD11c in stroma were correlated with prolonged survival in head and neck SCC (29).

To address key shortfalls of the abovementioned ST methods (i.e., the lack of single-cell resolution read-outs), Stereo-seq (BGI, China) offers unbiased whole-transcriptomic profiling at subcellular resolution with a maximum 1 cm^2 capture area on FF/FFPE tissues. Using Stereo-seq, Wu et al. showed that poorer prognoses of intrahepatic cholangiocarcinoma and hepatocellular carcinoma were associated with tumour boundaries enriched with damaged hepatocytes, or serum amyloid A overexpression in invasive fronts (32); Zhang et al. found a locoregional immune "warmed-up" phenotype with enhanced cytokine secretion and upregulated MHC-II expression in a predefined "cold" tumour of colorectal

adenocarcinoma (33). A major challenge with Stereo-seq analysis lies with assigning pixel-level signals to individual cells (32).

Imaging-based techniques

Multiplex error robust fluorescence *in situ* hybridization (MERFISH) (Vizgen, UK) uses a combinatorial barcoding approach and sequential rounds of imaging to decode the barcode and its associated gene expression. The barcoding system confers error robustness through assigning the erroneous readout to the nearest correct barcode. MERFISH allows profiling of up to tens of thousands of RNA species at subcellular resolution, with a maximum 1 cm^2 capture area of FF/FFPE tissues. Using a 450-gene MERFISH panel, Price et al. reported a shift in immune spatial organization between the two tumour subtypes i.e., human mismatch repair deficient and proficient tumors, opening new avenues for tumour subtype-specific treatment strategies (34).

Two other multi-spatial omics methods, namely CosMx spatial molecular imaging (SMI) technique and Xenium (higher-resolution advancement from DSP and Visium, respectively), enable simultaneous ST and SP profiling of FF/FFPE tissues at subcellular resolution. CosMx SMI allows up to 1000-plex and offers 64 validated protein analytes (35, 36). Using CosMx, He et al. (35) evaluated 980 RNAs and 108 proteins in lung cancer and BC tissues, identifying over 18 different cell-types, 10 unique TMEs, and 100 ligand-receptor pairs. While Xenium offers a 280-plex human breast panel and 248-plex mouse brain panel, with additional 100 customizable targets. Due to its non-destructive nature, Xenium allows post-ST H&E staining and IF on the same section, offering additional SP and histological data. Using Xenium, Henley et at. revealed that invasive fronts of ductal carcinoma *in situ* (DCIS) BC were characterized by disrupted myoepithelial layers, and low KRT14 expression which were also positive for progesterone receptor (37); Janesick et al. predicted the hormone receptor status of three BC subtypes (low-grade and high-grade DCIS, and invasive carcinoma) whose molecular signatures were also characterized using whole-transcriptomics Visium on adjacent tissue sections (38).

AI-enabled TME analysis

Digital pathology

With recent advancements in imaging techniques and computer vision, DP has greatly emerged as a useful diagnosis assisting and prediction tool (68), alleviating the high labor cost and interobserver variability issues faced by conventional microscope-based approach (69–73). While H&E-stained histomorphology images remain the main imaging modality in DP, the use of mIHC/IF to enable subcellular molecular profiling has become popular (74).

Numerous studies use deep learning (DL) models to augment DP, greatly advancing TME analysis. DL-based cell segmentation algorithms, such as Cellpose (75) and Stardist (76), enable identification of individual nuclei, facilitating downstream cell phenotyping. Supervised DL algorithms have been developed to differentiate benign from malignant cells, and immune from stromal cells (71, 77–79). These approaches are limited by the availability of training labels, resulting in the development of unsupervised approaches (80). Novel AI approaches, such as Ronteix (81), for investigating cell-to-cell interaction have also attracted increasing attention. Besides, as image quality and stain consistency impact the performance of DP studies, several AI algorithms have been developed for stain normalization through color deconvolution (82), clustering in the hue-saturation-value color space for color separation (72) or DL-empowered stain-to-stain translation (83).

SP analytic methods

SP analysis involves image pre-processing to remove background or technical noise, cell segmentation, feature extraction (such as signal intensity, cellular area, and shape), cell phenotyping and spatial analysis (Supplementary Table 1). While image pre-processing steps differ across fluorescence-based and metal-based assays, downstream spatial analysis using extracted cell-level data are largely similar.

Composite multi-spectral images generated with fluorescence-based techniques are firstly unmixed whereby the pixel values are decomposed into the constituent pure spectrum (i.e., protein markers). Spectral unmixing can be done using software like inForm (Akoya Biosciences). Similarly, background subtraction and noise removal are critical steps in pre-processing the multi-channel images acquired from metal-based techniques; each channel portraying the abundance of a protein. Moreover, technique-specific filtering may also be needed – specifically, aggregate removal in MIBI data to eliminate unwanted effects from antibody aggregation, and hot pixels filtering to remove IMC-specific noise (25, 84)

Various cell (or object) segmentation algorithms are deployed in different image analysis tools. To this end, CellProfiler (85) offers several classical image processing approaches; whilst Ilastik (86) offers pixel-based random forest and NN approaches accounting for texture and context that can better identify cells, where both methods require user-input labels such as nuclei and background. Segmentation masks generated by Illastik can serve as the training labels in CellProfiler. These cell segmentation algorithms have been integrated into end-to-end SP analysis pipelines, including IMC Segmentation (87) and its dockerized counterpart, Steinbock (84), adding on to the built-in DL-based Mesmer method (88). More generic image analysis tools including QuPath (89) and ImageJ (90) provides built-in cell segmentation algorithm and allows customized algorithms such as Stardist (91, 92).

There are currently two main cell phenotyping approaches, namely user-input thresholding or rule-based approach, and ML-based supervised approach which require cell label training (93). Using Halo (Indica Labs), Ozbek et al. (94) built a T-cell classifier and computed the densities of 8 different T-cell phenotypes in the tumour epithelial and stromal regions in prostate cancer.

Furthermore, dedicated tools for proximity analysis, such as SPIAT (95), HistoCAT (56), imcRtools (84) and Cytomapper (96), have also been developed. These tools enable inter-cellular distance computation, touching-cell counts, cell neighborhood identification, cell-type mixing score, spatial point pattern measures (such as K-cross function), spatial heterogeneity (such as entropy), and immune gradients across tumour margins. Like many methodology studies, these works largely focused on demonstrating evident spatial immunological scenarios in individual cases. For instance, in the SPIAT work, it showed that tumour cells were closely interacting with $CD3^+CD4^+$ and $CD3^+CD8^+$ cells in one prostate cancer sample, while showing the high levels of $SOX10^+$ tumour cells did not co-exist with the $CD4^+$ immune cells in another prostate cancer sample. Nonetheless, HistoCAT study demonstrated a real oncology case wherein it revealed the enrichment and depletion of cell-cell interactions was associated with breast cancer development.

ST analytic methods

Several open-source R tools, such as Seurat (97), standR (98), GeoMxTools (99) and Giotto (100), enable end-to-end ST analysis, from data preprocessing (read mapping and quality checking), spatial clustering, spatially variable gene (SVG) identification, cell-type deconvolution to cell-cell communication. Besides these tools, various algorithms to enhance the performance of individual steps have emerged (Supplementary Table 2).

Spatial clustering groups spots (neighboring cells) with similar transcriptional profile and characterizes unique transcriptomics niche of the TME (101). These include autoencoder-based methods [such as STAGATE (102), SEDR (103), MAPLE (104), and conST (105)], deep convolution neural network (CNN) methods [such as coSTA (106), RESEPT (107), spaGCN (108), stLearn (109) and spaCell (110), and probabilistic methods (BayesSpace (111) and PRECAST (112)]. SVGs are genes with expression patterns significantly dependent on their spatial locations in the tissues. These include a neural network (NN) method called SOMDE (113); regression modelling methods such as SPARK (114) that uses a generalized linear regression to model the mean-variance relation of NGS-based or imaging-based ST data; SpatialDE (115) uses Gaussian process regression model to decompose gene expression variability into spatial and non-spatial components, tested on SeqFISH and MERFISH data; scGCO (116) addresses the key challenge in SVG analysis, i.e., scalability, by employing a hidden markov random field-based probabilistic graph model, tested on SeqFISH, MERFISH and, 3D ST data (STARmap) (117).

Cell-type deconvolution infers cell composition of the multi-cell ST data, facilitating cell-type specific analysis. These include a Bayesian modelling method called DestVI (118); methods that infer spatial cell composition from scRNAseq data such as CellDART (119) and Tangram (120); a graph-based CNN method called DSTG (121) which was used to uncover cell states of pancreatic tumor tissues. On the other hand, the ability of ST to localize gene expression to specific cell phenotypes in the TME allows effective characterization of cellular communication, which is either through cell-cell direct contact or cell signaling of neighboring cells (122). Analytic tools developed for cellular communication include a scalable random forest-based method called MISTy (123), tested on human BC Visium data; a graph NN method called NCEM (124), tested on MERFISH, PhenoCylcer, and MIBI; a graph CNN model based on a curated list of interacting ligands and receptors, called GCNG (125), tested on SeqFISH and MERFISH.

Aforementioned methods have been mainly focused on showcasing specific ST analytic methods. Studies that involve real oncology use cases are given in (103, 111, 112). In the work of SEDR, the authors analyzed the role of immune microenvironments on tumor invasiveness by clustering the TME into pro-inflammatory and anti-inflammatory regions (103); the authors of PRECAST revealed distinguished tumor/normal epithelial regions in hepatocellular cancers that associated with different signaling pathways, providing higher resolution analysis of the dynamics of tumorigenesis (112); using BayesSpace, Zhao et al. found that a higher level of chemokine activity at the tumor border and an elevated level of metastatic activities at the tumor center that could aid in clinical analysis of cancer metastasis (111).

Discussion and future perspectives

Significant advancements in spatial omics and computational techniques have unraveled many previously underappreciated roles of immune contexture in cancer progression, immune evasion, and treatment effect, enhancing our understanding of cancer immunology and helping to pave the way towards precision medicine through developing novel therapeutic targets and spatial biomarkers. Increasing evidence show that the phenotypic and functional states of cells, and thus their anti-tumorigenicity, are determined collectively by the DNA, RNA, and protein expression (126–129). Nonetheless, alternative computational solutions for integrating multiple single-spatial omics data represent a valuable resource given tremendous data have been generated separately and available in the public domain. It is also worth to note that recent development of computational methods for cohort analysis reveals important clinical implications by associating immune spatial patterns with treatment response (130, 131).

In our perspective, several challenges in spatial omics need to be addressed. Firstly, advancement in antibody development, automated workflow, image scanning quality and speed, and multi-omics integrative algorithms are needed to enhance robustness, dimensionality, and spatial resolution. Secondly, consistent and quality data is a prerequisite for clinical translation. Several taskforces, such as the Society for Immunotherapy of Cancer (132) and the Joint Effort to Develop Multiplex Immunofluorescence Standards (133), gather international efforts to standardize the workflow of OPAL-based assays, with similar efforts needed for other spatial omics techniques. Thirdly, existing computational tools often require extensive user inputs, such as number of clusters or neighbors, and distance threshold, which hinders adoption. Finally, effective

cross-spatial-modality data integration and results interpretation for comprehensive understanding of the biological system remains challenging, largely due to the variations in image format, scanning techniques, sample handling as well as the demanding requirement of computing power and data storage. When these challenges are addressed, robust, affordable, and insightful spatial TME studies may then be possible in helping advancing precision cancer immunology.

Author contributions

RL and CN contributed equally. All authors contributed to the article and approved the submitted version.

Funding

This work was supported by the Bioinformatics Institute and Singapore Immunology Network, Agency for Science, Technology and Research (A*STAR), and A*STAR Industry Alignment Fund-Pre-positioning (IAF-PP H19/01/a0/024).

Conflict of interest

The authors declare that the research was conducted in the absence of any commercial or financial relationships that could be construed as a potential conflict of interest.

Publisher's note

Supplementary material

The Supplementary Material for this article can be found online at: https://www.frontiersin.org/articles/10.3389/fonc.2023.1172314/full#supplementary-material

References

1. Hinshaw DC, Shevde LA. The tumor microenvironment innately modulates cancer progression. *Cancer Res* (2019) 79(18):4557–66. doi: 10.1158/0008-5472.CAN-18-3962

2. Martin-Orozco N, Muranski P, Chung Y, Yang XO, Yamazaki T, Lu S, et al. T Helper 17 cells promote cytotoxic T cell activation in tumor immunity. *Immunity* (2009) 31(5):787–98. doi: 10.1016/j.immuni.2009.09.014

3. Wei C, Yang C, Wang S, Shi D, Zhang C, Lin X, et al. Crosstalk between cancer cells and tumor associated macrophages is required for mesenchymal circulating tumor cell-mediated colorectal cancer metastasis. *Mol Cancer* (2019) 18(1):64. doi: 10.1186/s12943-019-0976-4

4. Granot Z, Fridlender ZG. Plasticity beyond cancer cells and the "Immunosuppressive switch". *Cancer Res* (2015) 75(21):4441–5. doi: 10.1158/0008-5472.CAN-15-1502

5. Powell DR, Huttenlocher A. Neutrophils in the tumor microenvironment. *Trends Immunol* (2016) 37(1):41–52. doi: 10.1016/j.it.2015.11.008

6. Zhu X, Shen H, Yin X, Yang M, Wei H, Chen Q, et al. Macrophages derived exosomes deliver miR-223 to epithelial ovarian cancer cells to elicit a chemoresistant phenotype. *J Exp Clin Cancer Res* (2019) 38(1):81. doi: 10.1186/s13046-019-1095-1

7. Dong C, Liu X, Wang H, Li J, Dai L, Li J, et al. Hypoxic non-small-cell lung cancer cell-derived exosomal miR-21 promotes resistance of normoxic cell to cisplatin. *Onco Targets Ther* (2019) 12:1947–56. doi: 10.2147/OTT.S186922

8. Wculek SK, Malanchi I. Neutrophils support lung colonization of metastasis-initiating breast cancer cells. *Nature* (2015) 528(7582):413–7. doi: 10.1038/nature16140

9. Lv Y, Zhao Y, Wang X, Chen N, Mao F, Teng Y, et al. Increased intratumoral mast cells foster immune suppression and gastric cancer progression through TNF-α-PD-L1 pathway. *J Immunother Cancer* (2019) 7(1):54. doi: 10.1186/s40425-019-0530-3

10. Borst J, Ahrends T, Bąbała N, Melief CJM, Kastenmüller W. CD4(+) T cell help in cancer immunology and immunotherapy. *Nat Rev Immunol* (2018) 18(10):635–47. doi: 10.1038/s41577-018-0044-0

11. Wei SC, Levine JH, Cogdill AP, Zhao Y, Anang NAS, Andrews MC, et al. Distinct cellular mechanisms underlie anti-CTLA-4 and anti-PD-1 checkpoint blockade. *Cell* (2017) 170(6):1120–33.e17. doi: 10.1016/j.cell.2017.07.024

12. Millian DE, Saldarriaga OA, Wanninger T, Burks JK, Rafati YN, Gosnell J, et al. Cutting-edge platforms for analysis of immune cells in the hepatic Microenvironment—Focus on tumor-associated macrophages in hepatocellular carcinoma. *Cancers* (2022) 14(8):1861. doi: 10.3390/cancers14081861

13. Väyrynen JP, Haruki K, Lau MC, Väyrynen SA, Zhong R, Dias Costa A, et al. The prognostic role of macrophage polarization in the colorectal cancer microenvironment. *Cancer Immunol Res* (2021) 9(1):8–19. doi: 10.1158/2326-6066.CIR-20-0527

14. Väyrynen JP, Haruki K, Väyrynen SA, Lau MC, Dias Costa A, Borowsky J, et al. Prognostic significance of myeloid immune cells and their spatial distribution in the colorectal cancer microenvironment. *J Immunother Cancer* (2021) 9(4). doi: 10.1136/jitc-2020-002297

15. Sheng J, Zhang J, Wang L, Tano V, Tang J, Wang X, et al. Topological analysis of hepatocellular carcinoma tumour microenvironment based on imaging mass cytometry reveals cellular neighbourhood regulated reversely by macrophages with different ontogeny. *Gut* (2022) 71(6):1176–91. doi: 10.1136/gutjnl-2021-324339

16. Xue R, Zhang Q, Cao Q, Kong R, Xiang X, Liu H, et al. Liver tumour immune microenvironment subtypes and neutrophil heterogeneity. *Nature* (2022) 612 (7938):141–7. doi: 10.1038/s41586-022-05400-x

17. Thommen DS. Schumacher TN. T cell dysfunction in cancer. *Cancer Cell* (2018) 33(4):547–62. doi: 10.1016/j.ccell.2018.03.012

18. Tran M, Yoon S, Min S, Andersen S, Devitt K, Lam P, et al. Spatial analysis of ligand-receptor interactions in skin cancer at genome-wide and single-cell resolution. *bioRxiv* (2020). 2020.09.10.290833. doi: 10.1101/2020.09.10.290833

19. Yu Q, Jiang M, Wu L. Spatial transcriptomics technology in cancer research. *Front Oncol* (2022) 12:1019111. doi: 10.3389/fonc.2022.1019111

20. Väyrynen SA, Zhang J, Yuan C, Väyrynen JP, Dias Costa A, Williams H, et al. Composition, spatial characteristics, and prognostic significance of myeloid cell infiltration in pancreatic cancer. *Clin Cancer Res* (2021) 27(4):1069–81. doi: 10.1158/1078-0432.CCR-20-3141

21. Almeida PM, Rivest F, Juppet Q, Kowal J, Pelz B, Cassano M, et al. Abstract 1716: mapping the cellular architecture of the tumor microenvironment by integrating hyperplex immunofluorescence and automated image analysis. *Cancer Res* (2022) 82 (12_Supplement):1716. doi: 10.1158/1538-7445.AM2022-1716

22. Schürch CM, Bhate SS, Barlow GL, Phillips DJ, Noti L, Zlobec I, et al. Coordinated cellular neighborhoods orchestrate antitumoral immunity at the colorectal cancer invasive front. *Cell* (2020) 182(5):1341–59.e19. doi: 10.1016/j.cell.2020.07.005

23. Ali HR, Jackson HW, Zanotelli VRT, Danenberg E, Fischer JR, Bardwell H, et al. Imaging mass cytometry and multiplatform genomics define the phenogenomic landscape of breast cancer. *Nat Cancer* (2020) 1(2):163–75. doi: 10.1038/s43018-020-0026-6

24. Ptacek J, Locke D, Finck R, Cvijic ME, Li Z, Tarolli JG, et al. Multiplexed ion beam imaging (MIBI) for characterization of the tumor microenvironment across tumor types. *Lab Invest* (2020) 100(8):1111–23. doi: 10.1038/s41374-020-0417-4

25. Keren L, Bosse M, Marquez D, Angoshtari R, Jain S, Varma S, et al. A structured tumor-immune microenvironment in triple negative breast cancer revealed by multiplexed ion beam imaging. *Cell* (2018) 174(6):1373–87.e19. doi: 10.1016/j.cell.2018.08.039

26. Meylan M, Petitprez F, Becht E, Bougoüin A, Pupier G, Calvez A, et al. Tertiary lymphoid structures generate and propagate anti-tumor antibody-producing plasma cells in renal cell cancer. *Immunity* (2022) 55(3):527–41.e5. doi: 10.1016/j.immuni.2022.02.001

27. Lau MC, Yi Y, Goh D, Cheung CCL, Tan B, Lim JCT, et al. Case report: understanding the impact of persistent tissue-localization of SARS-CoV-2 on immune response activity *via* spatial transcriptomic analysis of two cancer patients with COVID-19 co-morbidity. *Front Immunol* (2022) 13:978760. doi: 10.3389/fimmu.2022.978760

28. Moutafi M, Martinez-Morilla S, Divakar P, Vathiotis I, Gavrielatou N, Aung TN, et al. Discovery of biomarkers of resistance to immune checkpoint blockade in NSCLC using high-plex digital spatial profiling. *J Thorac Oncol* (2022) 17(8):991–1001. doi: 10.1016/j.jtho.2022.04.009

29. Gavrielatou N, Vathiotis I, Aung TN, Shafi S, Burela S, Fernandez A, et al. Digital spatial profiling to uncover biomarkers of immunotherapy outcomes in head and neck squamous cell carcinoma. *J Clin Oncol* (2022) 40(16_suppl):6050. doi: 10.1200/JCO.2022.40.16_suppl.6050

30. Avraham-Davidi I, Mages S, Klughammer J, Moriel N, Imada S, Hofree M, et al. Integrative single cell and spatial transcriptomics of colorectal cancer reveals multicellular functional units that support tumor progression. *bioRxiv* (2022). 2022.10.02.508492. doi: 10.1101/2022.10.02.508492

31. Liu S, Iorgulescu B, Li S, Morriss J, Borji M, Murray E, et al. 76 spatial mapping of T cell receptors and transcriptomes in renal cell carcinoma following immune checkpoint inhibitor therapy. *J ImmunoTher Cancer* (2021) 9(Suppl 2):A84–A5. doi: 10.1136/jitc-2021-SITC2021.076

32. Wu L, Yan J, Bai Y, Chen F, Xu J, Zou X, et al. Spatially-resolved transcriptomics analyses of invasive fronts in solid tumors. *bioRxiv* (2021). 2021.10.21.465135. doi: 10.1101/2021.10.21.465135

33. Zhang R, Feng Y, Ma W, Guo Y, Luo M, Li Y, et al. Spatial transcriptome unveils a discontinuous inflammatory pattern in proficient mismatch repair colorectal adenocarcinoma. *Fundam Res* (2022). doi: 10.1016/j.fmre.2022.01.036

34. Price C, Chen JH, Pelka K, Chao S, Therrien M, Wiggin T, et al. Abstract 2030: a single-cell spatially resolved map of colorectal cancer identifies novel spatial relationships between cancer cells and the microenvironment. *Cancer Res* (2022) 82 (12_Supplement):2030. doi: 10.1158/1538-7445.AM2022-2030

35. He S, Bhatt R, Brown C, Brown EA, Buhr DL, Chantranuvatana K, et al. High-plex multiomic analysis in FFPE at subcellular level by spatial molecular imaging. *bioRxiv* (2022). 2021.11.03.467020. doi: 10.1101/2021.11.03.467020

36. Newell E, Kim Y, Ryu H, Li S, Leon M, Kim S, et al. 50 *In-situ* visualization and measurement of tumor-infiltrating lymphocytes (TILs) on intact FFPE renal cell carcinoma (RCC) tissue using the spatial molecular imager (SMI). *J ImmunoTher Cancer* (2021) 9(Suppl 2):A57–A. doi: 10.1136/jitc-2021-SITC2021.050

37. Henley R, Rapicavoli N, Janesick A, Shelansky R, Kim A, Hensel J, et al. 95 characterization of human breast cancer tissue with the xenium *In Situ* platform reveals a novel marker for invasiveness. *J ImmunoTher Cancer* (2022) 10(Suppl 2):A104–A. doi: 10.1136/jitc-2022-SITC2022.0095

38. Janesick A, Shelansky R, Gottscho AD, Wagner F, Rouault M, Beliakoff G, et al. High resolution mapping of the breast cancer tumor microenvironment using integrated single cell, spatial and *in situ* analysis of FFPE tissue. *bioRxiv* (2022). 2022.10.06.510405. doi: 10.1101/2022.10.06.510405

39. Tan WCC, Nerurkar SN, Cai HY, Ng HHM, Wu D, Wee YTF, et al. Overview of multiplex immunohistochemistry/immunofluorescence techniques in the era of cancer immunotherapy. *Cancer Commun* (2020) 40(4):135–53. doi: 10.1002/cac2.12023

40. Lu S, Stein JE, Rimm DL, Wang DW, Bell JM, Johnson DB, et al. Comparison of biomarker modalities for predicting response to PD-1/PD-L1 checkpoint blockade: a systematic review and meta-analysis. *JAMA Oncol* (2019) 5(8):1195–204. doi: 10.1001/jamaoncol.2019.1549

41. Bosisio FM, Van Herck Y, Messiaen J, Bolognesi MM, Marcelis L, Van Haele M, et al. Next-generation pathology using multiplexed immunohistochemistry: mapping tissue architecture at single-cell level. *Front Oncol* (2022) 12. doi: 10.3389/fonc.2022.918900

42. Surace M, DaCosta K, Huntley A, Zhao W, Bagnall C, Brown C, et al. Automated multiplex immunofluorescence panel for immuno-oncology studies on formalin-fixed carcinoma tissue specimens. *J Vis Exp* (2019) (143). doi: 10.3791/58390

43. Wee YTF, Alkaff SMF, Lim JCT, Loh JJH, Hilmy MH, Ong C, et al. An integrated automated multispectral imaging technique that simultaneously detects and quantitates viral RNA and immune cell protein markers in fixed sections from Epstein-Barr virus-related tumours. *Ann Diagn Pathol* (2018) 37:12–9. doi: 10.1016/j.anndiagpath.2018.09.002

44. Lim JCT, Yeong JPS, Lim CJ, Ong CCH, Wong SC, Chew VSP, et al. An automated staining protocol for seven-colour immunofluorescence of human tissue sections for diagnostic and prognostic use. *Pathology* (2018) 50(3):333–41. doi: 10.1016/j.pathol.2017.11.087

45. Humphries MP, Bingham V, Abdullahi Sidi F, Craig SG, McQuaid S, James J, et al. Improving the diagnostic accuracy of the PD-L1 test with image analysis and multiplex hybridization. *Cancers (Basel)* (2020) 12(5). doi: 10.3390/cancers12051114

46. Yeong J, Tan T, Chow ZL, Cheng Q, Lee B, Seet A, et al. Multiplex immunohistochemistry/immunofluorescence (mIHC/IF) for PD-L1 testing in triple-negative breast cancer: a translational assay compared with conventional IHC. *J Clin Pathol* (2020) 73(9):557–62. doi: 10.1136/jclinpath-2019-206252

47. Van Herck Y, Antoranz A, Andhari MD, Milli G, Bechter O, De Smet F, et al. Multiplexed immunohistochemistry and digital pathology as the foundation for next-generation pathology in melanoma: methodological comparison and future clinical applications. *Front Oncol* (2021) 11. doi: 10.3389/fonc.2021.636681

48. Halse H, Colebatch AJ, Petrone P, Henderson MA, Mills JK, Snow H, et al. Multiplex immunohistochemistry accurately defines the immune context of metastatic melanoma. *Sci Rep* (2018) 8(1):11158. doi: 10.1038/s41598-018-28944-3

49. Dias Costa A, Väyrynen SA, Chawla A, Zhang J, Väyrynen JP, Lau MC, et al. Neoadjuvant chemotherapy is associated with altered immune cell infiltration and an anti-tumorigenic microenvironment in resected pancreatic cancer. *Clin Cancer Res* (2022) 28(23):5167–79. doi: 10.1158/1078-0432.CCR-22-1125

50. Masugi Y, Abe T, Ueno A, Fujii-Nishimura Y, Ojima H, Endo Y, et al. Characterization of spatial distribution of tumor-infiltrating CD8(+) T cells refines their prognostic utility for pancreatic cancer survival. *Mod Pathol* (2019) 32(10):1495–507. doi: 10.1038/s41379-019-0291-z

51. Moncada R, Barkley D, Wagner F, Chiodin M, Devlin JC, Baron M, et al. Integrating microarray-based spatial transcriptomics and single-cell RNA-seq reveals tissue architecture in pancreatic ductal adenocarcinomas. *Nat Biotechnol* (2020) 38 (3):333–42. doi: 10.1038/s41587-019-0392-8

52. Feng Z, Bethmann D, Kappler M, Ballesteros-Merino C, Eckert A, Bell RB, et al. Multiparametric immune profiling in HPV- oral squamous cell cancer. *JCI Insight* (2017) 2(14). doi: 10.1172/jci.insight.93652

53. Boisson A, Noël G, Saiselet M, Rodrigues-Vitória J, Thomas N, Fontsa ML, et al. Fluorescent multiplex immunohistochemistry coupled with other state-Of-The-Art techniques to systematically characterize the tumor immune microenvironment. *Front Mol Biosci* (2021) 8. doi: 10.3389/fmolb.2021.673042

54. Schlecht A, Boneva S, Salie H, Killmer S, Wolf J, Hajdu RI, et al. Imaging mass cytometry for high-dimensional tissue profiling in the eye. *BMC Ophthalmol* (2021) 21 (1):338. doi: 10.1186/s12886-021-02099-8

55. *Imaging mass cytometry services: visikol*. Available at: https://visikol.com/services/digipath/imaging-mass-cytometry-services/.

56. Schapiro D, Jackson HW, Raghuraman S, Fischer JR, Zanotelli VRT, Schulz D, et al. histoCAT: analysis of cell phenotypes and interactions in multiplex image cytometry data. *Nat Methods* (2017) 14(9):873–6. doi: 10.1038/nmeth.4391

57. Bouzekri A, Esch A, Ornatsky O. Multidimensional profiling of drug-treated cells by imaging mass cytometry. *FEBS Open Bio* (2019) 9(9):1652–69. doi: 10.1002/2211-5463.12692

58. Jackson HW, Fischer JR, Zanotelli VRT, Ali HR, Mechera R, Soysal SD, et al. The single-cell pathology landscape of breast cancer. *Nature* (2020) 578(7796):615–20. doi: 10.1038/s41586-019-1876-x

59. Baharlou H, Canete NP, Cunningham AL, Harman AN, Patrick E. Mass cytometry imaging for the study of human diseases-applications and data analysis strategies. *Front Immunol* (2019) 10:2657. doi: 10.3389/fimmu.2019.02657

60. Angelo M, Bendall SC, Finck R, Hale MB, Hitzman C, Borowsky AD, et al. Multiplexed ion beam imaging of human breast tumors. *Nat Med* (2014) 20(4):436–42. doi: 10.1038/nm.3488

61. Rost S, Giltnane J, Bordeaux JM, Hitzman C, Koeppen H, Liu SD. Multiplexed ion beam imaging analysis for quantitation of protein expresssion in cancer tissue sections. *Lab Invest* (2017) 97(8):992–1003. doi: 10.1038/labinvest.2017.50

62. Rao A, Barkley D, França GS, Yanai I. Exploring tissue architecture using spatial transcriptomics. *Nature* (2021) 596(7871):211–20. doi: 10.1038/s41586-021-03634-9

63. Rodriques SG, Stickels RR, Goeva A, Martin CA, Murray E, Vanderburg CR, et al. Slide-seq: a scalable technology for measuring genome-wide expression at high spatial resolution. *Science* (2019) 363(6434):1463–7. doi: 10.1126/science.aaw1219

64. Asp M, Bergenstråhle J, Lundeberg J. Spatially resolved transcriptomes–next generation tools for tissue exploration. *BioEssays* (2020) 42(10):1900221. doi: 10.1002/bies.201900221

65. Bergholtz H, Carter J, Cesano A, Cheang M, Church S, Divakar P, et al. Best practices for spatial profiling for breast cancer research with the GeoMx® digital spatial profiler. *Cancers* (2021) 13:4456. doi: 10.3390/cancers13174456

66. Amaria RN, Reddy SM, Tawbi HA, Davies MA, Ross MI, Glitza IC, et al. Neoadjuvant immune checkpoint blockade in high-risk resectable melanoma. *Nat Med* (2018) 24(11):1649–54. doi: 10.1038/s41591-018-0197-1

67. Blank CU, Rozeman EA, Fanchi LF, Sikorska K, van de Wiel B, Kvistborg P, et al. Neoadjuvant versus adjuvant ipilimumab plus nivolumab in macroscopic stage III melanoma. *Nat Med* (2018) 24(11):1655–61. doi: 10.1038/s41591-018-0198-0

68. Saito A, Kuroda M. [AI application on the pathology-from diagnosis assisting tool to prediction tool]. *Gan to kagaku ryoho Cancer Chemother* (2019) 46(3):427–31.

69. Martin B, Schäfer E, Jakubowicz E, Mayr P, Ihringer R, Anthuber M, et al. Interobserver variability in the H&E-based assessment of tumor budding in pT3/4 colon cancer: does it affect the prognostic relevance? *Virchows Archiv* (2018) 473 (2):189–97. doi: 10.1007/s00428-018-2341-1

70. Lidbury JA, Rodrigues Hoffmann A, Ivanek R, Cullen JM, Porter BF, Oliveira F, et al. Interobserver agreement using histological scoring of the canine liver. *J Vet Internal Med* (2017) 31(3):778–83. doi: 10.1111/jvim.14684

71. Gomez-Brouchet A, Gilhodes J, Van Acker N, Brion R, Bouvier C, Assemat P, et al. Characterization of macrophages and osteoclasts in the osteosarcoma tumor microenvironment at diagnosis: new perspective for osteosarcoma treatment? *Cancers* (2021) 13(3):423. doi: 10.3390/cancers13030423

72. Zarella MD, Breen DE, Plagov A, Garcia FU. An optimized color transformation for the analysis of digital images of hematoxylin & eosin stained slides. *J Pathol Inform* (2015) 6(1):33. doi: 10.4103/2153-3539.158910

73. Azevedo Tosta TA, de Faria PR, Neves LA, do Nascimento MZ. Computational normalization of H&E-stained histological images: progress, challenges and future potential. *Artif Intell Med* (2019) 95:118–32. doi: 10.1016/j.artmed.2018.10.004

74. Liu Y, Li X, Zheng A, Zhu X, Liu S, Hu M, et al. Predict ki-67 positive cells in H&E-stained images using deep learning independently from IHC-stained images. *Front Mol Biosci* (2020) 7. doi: 10.3389/fmolb.2020.00183

75. Stringer C, Wang T, Michaelos M, Pachitariu M. Cellpose: a generalist algorithm for cellular segmentation. *Nat Methods* (2021) 18(1):100–6. doi: 10.1038/s41592-020-01018-x

76. Schmidt U, Weigert M, Broaddus C, Myers G eds. *Cell detection with star-convex polygons. medical image computing and computer assisted intervention – MICCAI 2018*. Cham: Springer International Publishing (2018).

77. Väyrynen JP, Lau MC, Haruki K, Väyrynen SA, Dias Costa A, Borowsky J, et al. Prognostic significance of immune cell populations identified by machine learning in colorectal cancer using routine hematoxylin and eosin–stained sections. *Clin Cancer Res* (2020) 26(16):4326–38. doi: 10.1158/1078-0432.CCR-20-0071

78. Rączkowski Ł, Paśnik I, Kukiełka M, Nicoś M, Budzinska MA, Kucharczyk T, et al. Deep learning-based tumor microenvironment segmentation is predictive of tumor mutations and patient survival in non-small-cell lung cancer. *BMC Cancer* (2022) 22(1):1001. doi: 10.1186/s12885-022-10081-w

79. Jiao Y, Li J, Qian C, Fei S. Deep learning-based tumor microenvironment analysis in colon adenocarcinoma histopathological whole-slide images. *Comput Methods Prog Biomed* (2021) 204:106047. doi: 10.1016/j.cmpb.2021.106047

80. Bulten W, Litjens G. *Unsupervised prostate cancer detection on H&E using convolutional adversarial autoencoders*. Ithaca, NY: Cornell University (2018). Available at: https://arxiv.org/abs/1804.07098.

81. Ronteix G, Aristov A, Bonnet V, Sart S, Sobel J, Esposito E, et al. Griottes: a generalist tool for network generation from segmented tissue images. *BMC Biol* (2022) 20(1):178. doi: 10.1186/s12915-022-01376-2

82. Macenko M, Niethammer M, Marron JS, Borland D, Woosley JT, Xiaojun G, et al. eds. (2009). A method for normalizing histology slides for quantitative analysis, in: *2009 IEEE International Symposium on Biomedical Imaging: From Nano to Macro*. Available at: https://biag.cs.unc.edu/publication/dblp-confisbi-macenko-nmbwgst-09/.

83. Salehi P, Chalechale A eds. (2020). Pix2Pix-based stain-to-Stain translation: a solution for robust stain normalization in histopathology images analysis, in: *2020 International Conference on Machine Vision and Image Processing (MVIP)*. Available at: https://arxiv.org/abs/2002.00647.

84. Windhager J, Bodenmiller B, Eling N. An end-to-end workflow for multiplexed image processing and analysis. *bioRxiv* (2021). 2021.11.12.468357. doi: 10.1101/2021.11.12.468357

85. Stirling DR, Swain-Bowden MJ, Lucas AM, Carpenter AE, Cimini BA, Goodman A. CellProfiler 4: improvements in speed, utility and usability. *BMC Bioinf* (2021) 22(1):433. doi: 10.1186/s12859-021-04344-9

86. Berg S, Kutra D, Kroeger T, Straehle CN, Kausler BX, Haubold C, et al. Ilastik: interactive machine learning for (bio)image analysis. *Nat Methods* (2019) 16(12):1226–32. doi: 10.1038/s41592-019-0582-9

87. Zanotelli VRT, Bodenmiller B. ImcSegmentationPipeline: a pixelclassification based multiplexed image segmentation pipeline. *Zenodo* (2017). doi: 10.5281/zenodo.3841961

88. Greenwald NF, Miller G, Moen E, Kong A, Kagel A, Dougherty T, et al. Whole-cell segmentation of tissue images with human-level performance using large-scale data annotation and deep learning. *Nat Biotechnol* (2022) 40(4):555–65. doi: 10.1038/s41587-021-01094-0

89. Bankhead P, Loughrey MB, Fernández JA, Dombrowski Y, McArt DG, Dunne PD, et al. QuPath: open source software for digital pathology image analysis. *Sci Rep* (2017) 7(1):16878. doi: 10.1038/s41598-017-17204-5

90. Rasband WS. *ImageJ*. USA: National Institutes of Health (1997). Available at: https://imagej.net/ij/.

91. Stevens M, Nanou A, Terstappen LWMM, Driemel C, Stoecklein NH, Coumans FAW. StarDist image segmentation improves circulating tumor cell detection. *Cancers* (2022) 14(12):2916. doi: 10.3390/cancers14122916

92. Mi H, Bivalacqua TJ, Kates M, Seiler R, Black PC, Popel AS, et al. Predictive models of response to neoadjuvant chemotherapy in muscle-invasive bladder cancer using nuclear morphology and tissue architecture. *Cell Rep Med* (2021) 2(9):100382. doi: 10.1016/j.xcrm.2021.100382

93. Mori H, Bolen J, Schuetter L, Massion P, Hoyt CC, VandenBerg S, et al. Characterizing the tumor immune microenvironment with tyramide-based multiplex immunofluorescence. *J Mammary Gland Biol Neoplasia* (2020) 25(4):417–32. doi: 10.1007/s10911-021-09479-2

94. Ozbek B, Ertunc O, Erickson A, Vidal ID, Gomes-Alexandre C, Guner G, et al. Multiplex immunohistochemical phenotyping of T cells in primary prostate cancer. *Prostate* (2022) 82(6):706–22. doi: 10.1002/pros.24315

95. Yang T, Ozcoban V, Pasam A, Kocovski N, Pizzolla A, Huang Y-K, et al. SPIAT: an r package for the spatial image analysis of cells in tissues. *bioRxiv* (2020). 2020.05.28.122614. doi: 10.1101/2020.05.28.122614

96. Eling N, Damond N, Hoch T, Bodenmiller B. Cytomapper: an R/Bioconductor package for visualization of highly multiplexed imaging data. *Bioinformatics* (2020) 36 (24):5706–8. doi: 10.1101/2020.09.08.287516

97. Hao Y, Hao S, Andersen-Nissen E, Mauck WMIII, Zheng S, Butler A, et al. Integrated analysis of multimodal single-cell data. *Cell* (2021) 184(13):3573–87.e29. doi: 10.1016/j.cell.2021.04.048

98. Liu N, Bhuva D, Mohamed A, Tan CW, Davis M. *standR package* (2022). Available at: https://bioconductor.org/packages/devel/bioc/vignettes/standR/inst/doc/standR_introduction.html.

99. Ortogero N, Yang Z, Vitancol R, Griswold M, Henderson D. *GeomxTools: NanoString GeoMx tools. r package version 3.2.0* 2022.

100. Dries R, Zhu Q, Dong R, Eng C-HL, Li H, Liu K, et al. Giotto: a toolbox for integrative analysis and visualization of spatial expression data. *Genome Biol* (2021) 22 (1):78. doi: 10.1186/s13059-021-02286-2

101. Li Y, Stanojevic S, Garmire LX. Emerging artificial intelligence applications in spatial transcriptomics analysis. *Comput Struct Biotechnol J* (2022) 20:2895–908. doi: 10.1016/j.csbj.2022.05.056

102. Dong K, Zhang S. Deciphering spatial domains from spatially resolved transcriptomics with an adaptive graph attention auto-encoder. *Nat Commun* (2022) 13(1):1739. doi: 10.1038/s41467-022-29439-6

103. Fu H, Xu H, Chong K, Li M, Ang KS, Lee HK, et al. Unsupervised spatially embedded deep representation of spatial transcriptomics. *bioRxiv* (2021). 2021.06.15.448542. doi: 10.1101/2021.06.15.448542

104. Allen C, Chang Y, Ma Q, Chung D. MAPLE: a hybrid framework for multi-sample spatial transcriptomics data. *bioRxiv* (2022). 2022.02.28.482296. doi: 10.1101/2022.02.28.482296

105. Zong Y, Yu T, Wang X, Wang Y, Hu Z, Li Y. conST: an interpretable multi-modal contrastive learning framework for spatial transcriptomics. *bioRxiv* (2022). 2022.01.14.476408. doi: 10.1101/2022.01.14.476408

106. Xu Y, McCord RP. CoSTA: unsupervised convolutional neural network learning for spatial transcriptomics analysis. *BMC Bioinf* (2021) 22(1):397. doi: 10.1186/s12859-021-04314-1

107. Chang Y, He F, Wang J, Chen S, Li J, Liu J, et al. Define and visualize pathological architectures of human tissues from spatially resolved transcriptomics using deep learning. *Comput Struct Biotechnol J* (2022) 20:4600–17. doi: 10.1016/j.csbj.2022.08.029

108. Hu J, Li X, Coleman K, Schroeder A, Ma N, Irwin DJ, et al. SpaGCN: integrating gene expression, spatial location and histology to identify spatial domains and spatially variable genes by graph convolutional network. *Nat Methods* (2021) 18 (11):1342–51. doi: 10.1038/s41592-021-01255-8

109. Pham D, Tan X, Xu J, Grice LF, Lam PY, Raghubar A, et al. stLearn: integrating spatial location, tissue morphology and gene expression to find cell types, cell-cell interactions and spatial trajectories within undissociated tissues. *bioRxiv* (2020). 2020.05.31.125658. doi: 10.1101/2020.05.31.125658

110. Tan X, Su A, Tran M, Nguyen Q. SpaCell: integrating tissue morphology and spatial gene expression to predict disease cells. *Bioinformatics* (2020) 36(7):2293–4. doi: 10.1093/bioinformatics/btz914

111. Zhao E, Stone MR, Ren X, Guenthoer J, Smythe KS, Pulliam T, et al. Spatial transcriptomics at subspot resolution with BayesSpace. *Nat Biotechnol* (2021) 39 (11):1375–84. doi: 10.1038/s41587-021-00935-2

112. Liu W, Liao X, Luo Z, Yang Y, Lau MC, Jiao Y, et al. Probabilistic embedding, clustering, and alignment for integrating spatial transcriptomics data with PRECAST. *Nat Commun* (2023) 14(1):296. doi: 10.1038/s41467-023-35947-w

113. Hao M, Hua K, Zhang X. SOMDE: a scalable method for identifying spatially variable genes with self-organizing map. *bioRxiv* (2021). 2020.12.10.419549. doi: 10.1093/bioinformatics/btab471

114. Sun S, Zhu J, Zhou X. Statistical analysis of spatial expression patterns for spatially resolved transcriptomic studies. *Nat Methods* (2020) 17(2):193–200. doi: 10.1038/s41592-019-0701-7

115. Svensson V, Teichmann SA, Stegle O. SpatialDE: identification of spatially variable genes. *Nat Methods* (2018) 15(5):343–6. doi: 10.1038/nmeth.4636

116. Zhang K, Feng W, Wang P. Identification of spatially variable genes with graph cuts. *Nat Commun* (2022) 13(1):5488. doi: 10.1038/s41467-022-33182-3

117. Wang X, Allen WE, Wright MA, Sylwestrak EL, Samusik N, Vesuna S, et al. Three-dimensional intact-tissue sequencing of single-cell transcriptional states. *Science* (2018) 361(6400). doi: 10.1126/science.aat5691

118. Lopez R, Li B, Keren-Shaul H, Boyeau P, Kedmi M, Pilzer D, et al. DestVI identifies continuums of cell types in spatial transcriptomics data. *Nat Biotechnol* (2022) 40(9):1360–9. doi: 10.1038/s41587-022-01272-8

119. Bae S, Na KJ, Koh J, Lee DS, Choi H, Kim YT. CellDART: cell type inference by domain adaptation of single-cell and spatial transcriptomic data. *Nucleic Acids Res* (2022) 50(10):e57. doi: 10.1093/nar/gkac084

120. Biancalani T, Scalia G, Buffoni L, Avasthi R, Lu Z, Sanger A, et al. Deep learning and alignment of spatially resolved single-cell transcriptomes with tangram. *Nat Methods* (2021) 18(11):1352–62. doi: 10.1038/s41592-021-01264-7

121. Song Q, Su J. DSTG: deconvoluting spatial transcriptomics data through graph-based artificial intelligence. *Briefings Bioinf* (2021) 22(5). doi: 10.1093/bib/bbaa414

122. Jin S, Ramos R. Computational exploration of cellular communication in skin from emerging single-cell and spatial transcriptomic data. *Biochem Soc Trans* (2022) 50 (1):297–308. doi: 10.1042/BST20210863

123. Tanevski J, Flores ROR, Gabor A, Schapiro D, Saez-Rodriguez J. Explainable multiview framework for dissecting spatial relationships from highly multiplexed data. *Genome Biol* (2022) 23(1):97. doi: 10.1186/s13059-022-02663-5

124. Fischer DS, Schaar AC, Theis FJ. Modeling intercellular communication in tissues using spatial graphs of cells. *Nat Biotechnol* (2023) 41:332–6. doi: 10.1038/s41587-022-01467-z

125. Yuan Y, Bar-Joseph Z. GCNG: graph convolutional networks for inferring gene interaction from spatial transcriptomics data. *Genome Biol* (2020) 21(1):300. doi: 10.1186/s13059-020-02214-w

126. Feder ME, Walser JC. The biological limitations of transcriptomics in elucidating stress and stress responses. *J Evol Biol* (2005) 18(4):901–10. doi: 10.1111/j.1420-9101.2005.00921.x

127. Alfaro JA, Sinha A, Kislinger T, Boutros PC. Onco-proteogenomics: cancer proteomics joins forces with genomics. *Nat Methods* (2014) 11(11):1107–13. doi: 10.1038/nmeth.3138

128. Cieślik M, Chinnaiyan AM. Cancer transcriptome profiling at the juncture of clinical translation. *Nat Rev Genet* (2018) 19(2):93–109. doi: 10.1038/nrg.2017.96

129. de Vries NL, Mahfouz A, Koning F, de Miranda NFCC. Unraveling the complexity of the cancer microenvironment with multidimensional genomic and cytometric technologies. *Front Oncol* (2020) 10. doi: 10.3389/fonc.2020.01254

130. Blise KE, Sivagnanam S, Banik GL, Coussens LM, Goecks J. Single-cell spatial architectures associated with clinical outcome in head and neck squamous cell carcinoma. *NPJ Precis Oncol* (2022) 6(1):10. doi: 10.1038/s41698-022-00253-z

131. Wu Z, Trevino AE, Wu E, Swanson K, Kim HJ, D'Angio HB, et al. Graph deep learning for the characterization of tumour microenvironments from spatial protein profiles in tissue specimens. *Nat Biomed Engineering* (2022) 6(12):1435–48. doi: 10.1038/s41551-022-00951-w

132. Taube JM, Akturk G, Angelo M, Engle EL, Gnjatic S, Greenbaum S, et al. The society for immunotherapy of cancer statement on best practices for multiplex immunohistochemistry (IHC) and immunofluorescence (IF) staining and validation. *J Immunother Cancer* (2020) 8(1). doi: 10.1136/jitc-2019-000155corr1

133. Fincham REA, Bashiri H, Lau MC, Yeong J. Editorial: multiplex Immunohistochemistry/Immunofluorescence technique: the potential and promise for clinical application. *Front Mol Biosci* (2022) 9:831383. doi: 10.3389/fmolb.2022.831383

frontiers | Frontiers in Oncology

TYPE Review
PUBLISHED 17 May 2023
DOI 10.3389/fonc.2023.1170264

OPEN ACCESS

EDITED BY
Giulia Adriani,
Singapore Immunology Network (A*STAR), Singapore

REVIEWED BY
Manzoor A. Mir,
University of Kashmir, India
Kishore Hari,
Indian Institute of Science (IISc), India

*CORRESPONDENCE
Paola Defilippi
paola.defilippi@unito.it

†These authors have contributed equally to this work and share first authorship

RECEIVED 20 February 2023
ACCEPTED 28 April 2023
PUBLISHED 17 May 2023

CITATION
Salemme V, Centonze G, Avalle L, Natalini D, Piccolantonio A, Arina P, Morellato A, Ala U, Taverna D, Turco E and Defilippi P (2023) The role of tumor microenvironment in drug resistance: emerging technologies to unravel breast cancer heterogeneity.
Front. Oncol. 13:1170264.
doi: 10.3389/fonc.2023.1170264

The role of tumor microenvironment in drug resistance: emerging technologies to unravel breast cancer heterogeneity

Vincenzo Salemme[1,2†], Giorgia Centonze[1,2†], Lidia Avalle[1,2†], Dora Natalini[1,2†], Alessio Piccolantonio[1,2†], Pietro Arina[3†], Alessandro Morellato[1,2], Ugo Ala[4], Daniela Taverna[1,2], Emilia Turco[1] and Paola Defilippi[1,2*]

[1]Department of Molecular Biotechnology and Health Sciences, University of Turin, Turin, Italy, [2]Molecular Biotechnology Center (MBC) "Guido Tarone", Turin, Italy, [3]UCL, Bloomsbury Institute of Intensive Care Medicine, Division of Medicine, University College London, London, United Kingdom, [4]Department of Veterinary Sciences, University of Turin, Grugliasco, TO, Italy

Breast cancer is a highly heterogeneous disease, at both inter- and intra-tumor levels, and this heterogeneity is a crucial determinant of malignant progression and response to treatments. In addition to genetic diversity and plasticity of cancer cells, the tumor microenvironment contributes to tumor heterogeneity shaping the physical and biological surroundings of the tumor. The activity of certain types of immune, endothelial or mesenchymal cells in the microenvironment can change the effectiveness of cancer therapies via a plethora of different mechanisms. Therefore, deciphering the interactions between the distinct cell types, their spatial organization and their specific contribution to tumor growth and drug sensitivity is still a major challenge. Dissecting intra-tumor heterogeneity is currently an urgent need to better define breast cancer biology and to develop therapeutic strategies targeting the microenvironment as helpful tools for combined and personalized treatment. In this review, we analyze the mechanisms by which the tumor microenvironment affects the characteristics of tumor heterogeneity that ultimately result in drug resistance, and we outline state of the art preclinical models and emerging technologies that will be instrumental in unraveling the impact of the tumor microenvironment on resistance to therapies.

KEYWORDS

tumor microenvironment, cancer heterogenicity, drug resistance, molecular mechanisms, breast cancer

1 Introduction

Breast cancer (BC) is the second leading cause of cancer death in women. Data from WHO (World Health Organization) reported about 2.3 million new cases and about 685,000 deaths from BC globally (1). Similarly, American Cancer Society's projections for BC incidence in the United States in 2023 (https://www.cancer.org/cancer/breast-cancer/about/how-common-is-breast-cancer.html), estimate about 297,790 new cases of invasive BC in women, about 55,720 new diagnosis of ductal carcinoma *in situ* (DCIS), and about 43,700 death from this disease. The same statistics indicate for 2023 more than 3.8 million BC survivors in the United States, and 7.8 million worldwide, including both patients currently being treated and making this type of cancer the most prevalent worldwide. The median age at the time of diagnosis is 62 years and a woman's lifetime risk of acquiring breast cancer in the United States is around 13%, with incidence rates rising by 0.5% annually in recent years. Currently, a woman's chance of dying from BC is around 2.5%, death rates have been decreased due to improved therapeutic regimens, as well as earlier BC detection through screening programs and increased awareness. However, in recent years, the trend has marginally halted.

The breast cancer mass is composed not only by epithelial cancer cells, but also by a plethora of heterogeneous populations coming from the host, including endothelial cells, stromal fibroblasts, and a variety of immune cells that form the so-called tumor microenvironment (TME) (2, 3). The TME is a highly complex biological community embedded in a composite matrix of structural proteins constituting the extracellular matrix (ECM), in which immune cells (including macrophages, polymorphonuclear cells, mast cells, natural killer cells, dendritic cells (DCs), and T and B lymphocytes) and non-immune cells (such as endothelial cells and stromal cells) establish subtle interactions with cancer cells. This cellular cross-talk is based on the production of specific soluble (growth factors and cytokines) and insoluble (ECM proteins) molecules, and it determines the tumor's natural history.

BC comprises numerous subtypes that differ genetically, pathologically, and clinically. Indeed, it is currently considered a group of neoplasms originating from mammary gland epithelial cells caused by a variety of genetic alterations, with different disease courses, responses to treatments, and clinical outcomes. This was best exemplified by next-generation sequencing studies depicting comprehensive molecular BC portraits in Cancer Genome Atlas (4, 5) and identifying more than 1600 likely driver mutations in 93 BC genes (6). BC can have distinct molecular profiles from one another, leading to a complex heterogeneity of tumor cell subpopulations within single tumors, between primary tumors and their metastasis, or between independent metastasis, as a consequence of tumor clonal evolution (7, 8). In addition to clonal evolution, tumor heterogeneity can occur also at the level of cancer cell plasticity. The capability of BC cells to reprogram their gene expression and change their behavior when triggered by internal or external stimuli coming from surrounding cells and secreted factors, provides dynamic and context-dependent features to tumor heterogeneity (9, 10). Moreover, heterogeneity is also modulated by the different composition of the TME, with different ratio between tumor-infiltrating lymphocytes, myeloid cells, macrophages (3), with the increased presence of cancer-associated fibroblasts (CAFs) (11) and endothelial cells that controls cancer cell properties. The heterogeneity in components of the BC mass can be either observed between the different BC subtypes, known as inter-tumor heterogeneity, or within the same tumors, known as intra-tumor heterogeneity (12).

Therapeutic approaches are still currently largely based on clinical and pathological BC features, mostly on the presence or absence of targets like the hormone receptors or the Human Epidermal growth factor Receptor 2 (HER2) (13), and they are not yet tailored to individual patients. In particular, endocrine therapy is expected for hormone-dependent BC patients, targeted therapy with monoclonal antibodies for HER2-positive patients, and chemotherapy for TNBC patients. However, the different mechanisms that contribute to the inter- and intra-tumor heterogeneity are responsible for tumor escape from therapeutic interventions.

Drug resistance is among the major obstacles to reach a long-term cure, and overcoming this problem is the biggest challenge in BC research today. Indeed, the heterogeneous pattern of molecular aberrations found in each cancer plays a crucial role in the resistance to anticancer treatment (14–16). The goal of cancer therapy is to target a population of cancer cells within a particular host environment. The pharmacological properties of the therapy, together with intrinsic and acquired molecular features of cancer cells, controlled also by the TME components, dictate the therapy's efficacy. Unfortunately, despite the clinical management of BC improving every day, the number of patients developing drug-resistant tumors is still high (17). The resistance can be already present before the treatment (innate) or appear after the treatment administration (acquired) (18–20). The innate resistance is mainly due to intrinsic tumor heterogeneity: in primary cancer one or more subpopulations (e.g., Cancer Stem Cells) are resistant to the treatments from the beginning; on the contrary, the acquired resistance becomes evident after the therapy. In the clinical setting, innate and acquired resistance may coexist, making the long-term fight against cancer more complex.

In BC, standard chemotherapies and targeted therapies have both been extensively correlated to the escape of tumor cells that shape the clonal evolution of tumors, giving rise to drug-resistant subclones (21–23). Moreover, a comparison of the genetic diversity between pre- and post-treatment in tumor specimens indicates the role of therapy in selectively expanding resistant cancer clones that were initially present but at low frequency (14). In this context, TME cells play an important role in mediating the drug response and educating the cancer cells to become resistant to the therapy through extensive molecular crosstalk that we will discuss below (24–26).

We will first describe here what is currently known regarding inter-tumor and intra-tumor heterogeneity and the impact of TME on cancer progression and drug resistance. Moreover we will discuss the up-to-date tools for studying these complex interactions in preclinical models and in patient derived samples in cancer progression and drug resistance. We will present

emerging technologies, such as the spatial location of tumor subclones and TME cells within their native spatial context. We will show how the rapid growth of these techniques together with the multi-omics conjoint analysis mode and deep learning network architecture, promise to provide a more comprehensive understanding of cell-to-cell variation within and between individual tumors.

2 Heterogeneity in breast cancer

2.1 Inter-tumor heterogeneity

Surgeons and pathologists have long reported BC heterogeneity, and its classification system has been continuously updated as knowledge of cancer cell biology increases (27–29). To be exploited as a prognostic factor (to estimate disease outcome of newly diagnosed patients) and predictive factor (to predict response to specific treatment), the classification system has been integrated with information on patient treatments and survival. Classical histopathologic evaluation distinguished preinvasive (*in situ*) and invasive BC based on their morphology and structural organization, classifying the vast majority of tumors as invasive ductal carcinoma not otherwise specified (IDC NOS, 75%), invasive lobular carcinoma (ILC, 15%) and other special subtypes of BC, rare and significantly different in terms of prognosis and response to treatment (30).

Immunohistopathologic classification, based on the expression/absence of Estrogen Receptor (ER), Progesterone Receptor (PR), or receptor tyrosine kinase HER2, allowed the definition of the major BC subtypes (Figure 1). This classification has strong prognostic and predictive significance, and it is critical together with grade and stage in the selection of targeted therapeutic options for every patient (31). The expression of these biomarkers is highly variable between tumors, with ER/PR positive cells ranging from 1 to 100 percent, where a frequency of stained cells higher than 1% in tumor biopsy is considered a cutoff for ER/PR positivity. In addition, HER2 expression is heterogeneous, and its positivity is accompanied by a score that integrates the percentage of positive cells, staining intensity, and membrane distribution (31). The concomitant lack of ER, PR, and HER2 defines Triple- Negative Breast Cancer (TNBC), a subtype that comprises 15-20% of all BC, highly prevalent in women younger than 40, Black, or with *BRCA1* gene mutation, and represents the most challenging BC to be treated. Molecular characterization of BC, based on gene expression profiling (32) and the definition of distinct transcriptional signatures, provided intrinsic molecular subtypes that partially recapitulated the histological classification (33): 1. luminal A (ER-positive/PR-positive, enriched in genes regulated by ER signaling pathway), 2. luminal B (ER-positive/PR-negative, HER2-positive or negative, enriched in genes regulated by ER signaling pathway and proliferation-associated genes), 3. HER2 enriched (HER2-positive, HER2-related gene expression, ER and PR-positive, and ER and PR-negative), 4. Basal-like (enrichment for genes expressed in basal epithelial cells, 70% of them are TNBC), 5. Claudin low (stem-like and Epithelial-to-Mesenchymal Transition-like signatures, mainly TNBC) (34). Contributing to heterogeneity, several genes are mutated, amplified, or deleted in various subtypes of BC and can be considered as drivers, the top 10 most frequent being: *TP53, PIK3CA, MYC, CCND1, PTEN, ERBB2, ZNF703/FGFR1* locus, *GATA3, RB1* and *MAP3K1* (6). *BRCA1* and *BRCA2* germline or somatic inactivating mutations, as well as methylation of the *BRCA1* promoter, also represent driver mutations for BC, usually associated with many genomic rearrangements. These different

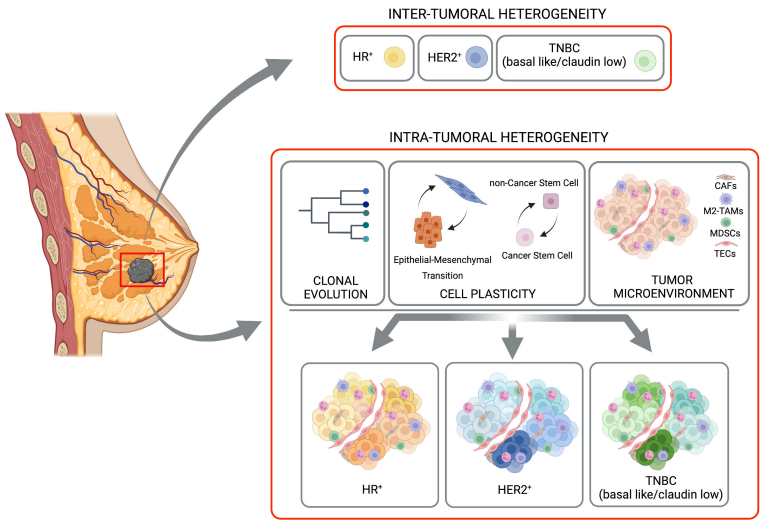

FIGURE 1
Inter-tumoral and intra-tumoral heterogeneity. BC is subdivided in three major subtypes based with inter-tumoral heterogeneity, on the expression of hormone receptor (HR-positive, HR+), HER2 receptor (HER2-positive, HER2+) or their complete absence (TNBC, basal like/claudin low). A strong heterogeneity inside each of these subtypes (the Intra-Tumoral Heterogeneity) is caused mainly by clonal evolution, cell plasticity (in terms of transition between Epithelial and Mesenchimal and/or Cancer Stem Cells and non-Cancer Stem Cells), and tumor microenvironment. Created with BioRender.com.

transforming events can originate in different cells of the mammary gland, and the differentiation state of these cells-of-origin plays a role in the determination of the tumor phenotype (31, 35, 36). Moreover, alterations in the expression of BC key genes have been reported as associated with epigenetic changes in DNA methylation and histone modifications, providing a further source of heterogeneity (30).

The metastatic progression of BC reflects its heterogeneous nature, with metastases to regional lymph nodes and in different distant organs such as bone, liver, lung, and brain. Association of molecular BC subtypes and metastatic sites has been reported with an increased frequency of brain metastases in the basal-like subtype, while showing bone metastases in luminal A and B subtypes and soft tissue metastases in the ER-negative subtype. It is well accepted that metastases originate from subsets of cells within the primary lesion, and the "seed and soil" model suggests that metastasizing cells may find in different organs the local microenvironment (the so-called niche) that favors their growth, generating secondary lesions that are the results of complex context-dependent interactions (30, 37).

2.2 Intra-tumor heterogeneity

Beside the differences found between tumors in different patients, distinct tumor cell populations, with different molecular and phenotypic profiles have been clearly described within the same tumor specimen, adding a further level of complexity to BC biology. Here we will focus on clonal evolution and cell plasticity as sources of intra-tumor heterogeneity (Figure 1).

2.2.1 Genetic diversity of cell subpopulations: clonal evolution

Tumor initiation and progression rely on stochastic mutational events that ultimately lead mutated cells to acquire advantageous properties in terms of cell proliferation, resistance to cell death, and resistance to therapy. Tumors are generally thought to originate from a single cell, in which genetic driver alterations are followed by the acquisition of genomic instability, generating spontaneous mutations that can confer competitive advantages and driving the evolution of subclones with different functional features (6, 38). As described in (8, 10, 39), tumor subclones can derive from the selective pressure of therapy and can acquire drug resistance through i) the selection of rare pre-existing subclones that are able to expand or ii) the presence of new genomic/transcriptomic/epigenetic aberrations contributing to the drug-resistant phenotype (40). However, the resistance can be pre-existing in a large majority of the cells, and therefore the therapy does not impact the frequency of subclones (10). Relapsed or metastatic BC largely share the vast majority of their genomic alterations with the corresponding primary disease indicating pre-existing resistant clones. However, many metastatic cancers also harbor additional mutations that were previously undetected or are subclonal in the primary disease (8, 41).

From clonal evolution emerges the concept of temporal heterogeneity that indicates that tumor composition constantly changes over time. Tumors are the result of constantly ongoing competition between subclones under the selective pressure exerted by other clones, TME interactions, and therapies (42–44). The spatial distribution of the different clones is an additional source of heterogeneity; indeed, multiple biopsies from primary BC showed a locally constrained expansion of subclones, implicating their clonal evolutionary outgrowth and suggesting that sampling of a particular tumor's area can be misleading in its molecular characterization (9).

2.2.2 Cell plasticity: cancer stem cells and EMT

The genetic information encoded in cells' nuclei is far from representing the only determinant of their complex behaviors; indeed, regulation of gene expression in response to intrinsic signaling pathways and extracellular stimuli from the TME strongly dictate tumor cells' phenotype.

For a long time, mammary tumors have been considered a hierarchical model, with some rare cells capable of self-renewing, the Cancer Stem Cells (CSCs), relatively quiescent and resistant to treatments at the top of the hierarchy, and a vast majority rapidly dividing non-CSCs (45). According to this model, only CSCs, due to their intrinsic properties, can give origin to new tumors, including metastasis and relapse, and by asymmetric division to all the heterogeneous cell types found in a tumor. These non-CSCs are rapidly proliferating but poorly tumorigenic, incapable of self-renewal, and intended to differentiate (46). As in many other cancer types, lineage tracing experiments revealed cell plasticity in BC, showing that in the mouse mammary tumor virus-polyoma middle tumor-antigen (MMTV-PyMT) mouse model of mammary tumor (see below), some CSCs can disappear and new CSCs can form, demonstrating that stem cell state is plastic and cells can dynamically transit between CSCs and non-CSCs (47). Tumor cells of different phenotypic states coexist and evolve within the same tumor leading to cell subpopulations with different functional properties. Indeed, cell subpopulations showing stem cell-, basal- or luminal-like features isolated from BC cell lines are capable of generating functionally competent cells of all three phenotypes in a stochastic manner. Interestingly, under specific environmental stimuli, all three subpopulations efficiently seeded tumors in xenografts models, showing the tumorigenic phenotype classically ascribed to CSCs (48). In BC, a CSC-like phenotype can be acquired by cancer cells upon the activation of the so-called Epithelial-to-Mesenchymal Transition (EMT), a transient developmental program that leads to the de-differentiation of tumor cells with the acquisition of mesenchymal features. During EMT, cell-cell contacts between epithelial cells are lost, and cancer cells acquire a migratory and invasive phenotype, which can be reverted to more epithelial states via Mesenchymal-to-Epithelial Transition (MET). EMT is emerging as a heterogeneous range of differentiation states rather than a binary process; indeed, distinct intermediate states have been described in BC, with similar tumor-initiating capabilities but different plasticity and invasive potential (49, 50). The plasticity described between various differentiation states is not exclusively intrinsic to cancer cells but is also sustained by signaling from the TME surrounding CSCs and is defined as the CSC niche. Interestingly, CSC themselves

can reprogram stromal cells to further sustain their activity, not only in the primary tumors but also in distant organs, eventually priming them for metastatic colonization. Indeed, it has been shown that BC circulating cells can reach nearly every organ, but tissue-specific microenvironments play a differential role in their engraftment and generation of metastases (51).

3 Cellular components of the tumor microenvironment

We will briefly introduce the main cellular components of TME cells, such as Type 2 Tumor-Associated Macrophages (M2-TAMs), Myeloid-Derived Suppressor Cells (MDSCs), Cancer-associated Fibroblasts (CAFs) and Tumor Endothelial Cells (TECs) ((Figures 1, 2) (3, 11, 52–54).

3.1 Type 2-tumor associated macrophages M2-TAM

Tumor Associated Macrophages (TAMs) are an important and abundant immune component in the BC microenvironment. They mainly derive from circulating monocytes that reach the primary site, influencing several aspects of the tumor progression (53). Generally, TAMs have been classified as M1, with anti-tumor activity, or M2, with tumor sustaining roles.

3.2 Myeloid-derived suppressor cells

MDSCs are immature heterogeneous cells belonging to the myeloid family. Generally, they are subdivided into two main groups: polymorphonuclear (PMN) and monocytic (Mo) MDSC. The first population is characterized by the $CD11b^{+}Ly\text{-}6G^{+}Ly\text{-}6C^{low}$ phenotype and the expression of high levels of arginase-1 (Arg-1). The second one is identified by the expression of $CD11b^{+}Ly\text{-}6G^{low}Ly\text{-}6C^{hi}$ surface markers (55). As underlined by their name, the main feature of MDSCs is immunosuppression. In cancer, several soluble molecules, such as such as for example granulocytic-colony stimulating factor (G-CSF), C-X-C chemokine ligand (CXCL)2, CC-chemokine ligand (CCL)2, CCL5, CXCL5, and CXCL12 secreted by the tumor cause the block of myeloid differentiation, affecting their mobilization from the bone marrow and infiltration into the primary and secondary tumors (3). G-CSFAs underlined by their name, the main feature of MDSCs is immunosuppression. We recently described the ability of the adaptor protein p140Cap to counteract the mobilization and intratumor accumulation of polymorphonuclear myeloid-derived suppressive cells (PMN-MDSC), to prevent the establishment of a tumor conducive immune environment (56). (Salemme et al., 2023 in press).

3.3 Cancer-associated fibroblasts

Within BC TME, CAFs are a highly abundant and heterogeneous cell population belonging to the mesenchymal lineage. CAFs actively contribute to cancer progression via the production and remodeling of extracellular matrix components, secreted factors, and exosomes, influencing tumor growth and progression, angiogenesis, immune responses, and drug resistance (57) both in primary and metastatic lesions. Several hypotheses co-exist regarding CAFs' origin, ranging from recruitment of bone marrow or adipose tissue-derived mesenchymal stem cells, EMT of tumor cells, activation of tissue-resident fibroblasts, to the trans-

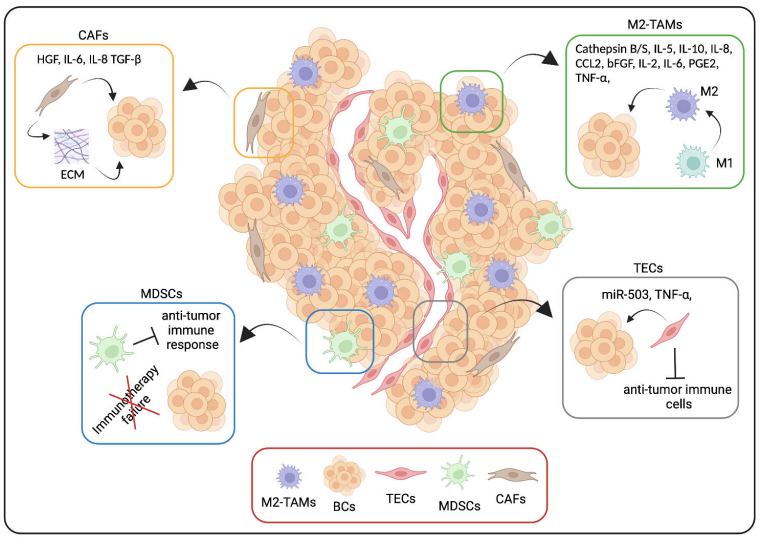

FIGURE 2
TME cellular components and drug resistance. We summarize here some molecular mechanisms through which TME cells, in particular Type 2 Tumor-Associated Macrophages (M2-TAMs), Myeloid-Derived Suppressor Cells (MDSCs), Cancer-associated Fibroblasts (CAFs) and Tumor Endothelial Cells (TECs) are able to induce drug resistance. Created with BioRender.com.

differentiation of endothelial cells. CAFs are also heterogeneous from the functional point of view, with a plethora of evidence showing their pro-tumorigenic effects (58) and some suggesting their tumor-constraining role in the early phases of tumorigenesis (59, 60). Limitation to our understanding of CAFs' biology in BC derives from the lack of specific surface markers to identify and functionally characterize this heterogeneous cell type. Morphology is still the most consistent manner to distinguish CAFs within the TME, as commonly used biomarkers, such as α-smooth muscle actin (SMA), fibroblast-specific protein 1 (FSP-1/S100A4), or fibroblast activation protein (FAP), are neither all-encompassing nor completely specific, suggesting that CAFs include several subtypes of cells.

3.4 Tumor endothelial cells

The endothelium is a key component of the TME. Endothelial cells (ECs) play a role in regulating the exchanges between the bloodstream and the tissues. In pathological conditions, such as cancer, the TECs show a distinct phenotype at the molecular, structural, and functional levels. In particular, the vasculature becomes irregular, excessively fenestrated, and loose intercellular junctions, contributing in this way also to tumor growth, proliferation, dissemination, and metastasis (54).

4 TME mediated drug resistance

Overall, the cellular components of the TME engage in dynamic and extensive cross-talks based on both cell-cell interactions and paracrine signaling between each other and with the cancer cells, ultimately contributing to drug resistance with many mechanisms, some of which will be underlined below.

4.1 Type 2-tumor associated macrophages

TAMs protect cancer cells from drug attacks through the secretion into TME of numerous soluble factors, including enzymes, exosomes, interleukins, and chemokines. Shree et al. found that macrophages expressing cathepsin B and S protected BC cells against paclitaxel-induced cell death. Indeed, the combined administration of paclitaxel and cathepsin inhibitors can effectively enhance the therapeutic response (61).

Moreover, in BC, the treatment with cyclopamine, a known Hedgehog pathway inhibitor, increases the infiltration of M2-TAMs that, in turn, can limit the efficacy of chemotherapy by secreting Interleukin-6 (IL-6) (62). Interestingly, neutralizing antibodies directed against TAMs-derived Interleukin-10 (IL-10) significantly enhance the sensitivity of BC cells due to the reported relationship between the IL-10/STAT3/Bcl-2 signaling pathway and the BC cell resistance to paclitaxel treatment (63).

As a positive feedback loop between M2-TAMs and BC cells, the TAM-mediated secretion of the chemokine CCL2 contributes to the activation of the PI3K/Akt/mTOR pathway in BC cells, increasing their resistance to the anti-estrogen tamoxifen treatment. In contrast, tamoxifen-resistant BC cells secrete Tumor Necrosis Factor alpha (TNF-α), activate mTORC1-FOXK1, and promote TAMs M2 polarization that, in turn, secrete a high amount of CCL2 (64).

Another example of how TAMs are able to induce drug resistance is provided by Niu X. et al., reporting that the M2-TAMs activate the EGFR/PI3K/Akt pathway and, consequently, the sodium/glucose cotransporter 1 (SGLT1) expression to promote tamoxifen resistance in ER-positive BC cells (65).

Moreover, M2-TAMs, by secreting a variety of cytokines such as basic Fibroblast Growth Factor (bFGF), Interleukin-2 (IL-2), IL-6, TNF-α, prostaglandin 2 (PGE2) can trigger increased aromatase activity and estrogen production (66–68). TAMs could mediate doxorubicin and paclitaxel chemotherapy resistance through the secretion of high levels of IL-10 and activation of IL-10/IL-10 receptor/STAT3/Bcl-2 signaling pathway in TNBC cells (63, 69). In addition, in BC, resistance to carboplatin chemotherapy is related to M2-TAMs. Interestingly, in the study, the authors described that macrophages in the bone marrow stroma contribute to BC cell dormancy, leading to a CSC behavior. M2-TAMs and CSCs form intercellular gap junction communication, which is responsible for carboplatin resistance (70).

Several articles identify the M2-TAMs' involvement also in resistance against targeted therapy. Ahmed S. et al. showed that, by secreting Interleukin-8 (IL-8), the TAMs activate Src/STAT3/ERK1/2-mediated EGFR signaling in BC cells, contributing to the resistance of HER2-positive BC to the small drug HER2 inhibitor lapatinib (71). Hu et al. described another interesting mechanism in which TAMs, after neoadjuvant treatment with the anti-HER2 humanized antibody trastuzumab, develop an immunosuppressive phenotype, upregulating B7-H4, a member of the B7 family of T cell costimulatory molecules, and causing the immune escape of HER2-positive BC cells (72). This TAMs' "evolution" leads to a poor response after trastuzumab treatment.

The immunotherapy efficacy is also affected by the M2-TAMs infiltration into the primary tumor, as reported by Ekiz HA. et al. In particular, the expression of the receptor tyrosine kinase RON on macrophages inhibits the anti-tumor immune response enhancing the PDL-1 expression on TAMs as well as the Macrophage stimulating protein (MSP)-Macrophage Stimulating-1 Receptor (RON) signaling up-regulates the binding of CD80 and CTLA-4 to inhibit T cell activation, reducing the effectiveness of immune checkpoint inhibitors in the BC treatment (73).

Overall, the interactions between tumor cells and TAMs that promote TAMs to differentiate into immunosuppressive M2-polarized macrophages under treatment pressure play a role in drug resistance because M2-TAMs through the mechanisms above reported (and not only) are able to reduce the treatment efficacy.

4.2 Myeloid-derived suppressor cells

As underlined by their name, the main feature of MDSCs is immunosuppression; indeed, both PMN- and Mo-MDSCs are able to inhibit different types of immune cells, negatively impacting the

ability of the host immune system to counteract the tumor progression and affecting the efficacy of the immunotherapy (3, 52, 74).

Thus, the MDSCs are the main obstacle to cancer immunotherapies, and the inhibition of their expansion/recruitment into the primary/secondary tumor sites may be a beneficial strategy for improving the efficiency of immunotherapeutic interventions.

4.3 Cancer-associated fibroblasts

In BC, different subsets of CAFs have been reported to accumulate differently in distinct subtypes and exhibit specific spatial distribution, with myofibroblastic subtypes accumulating in TNBC able to confer a tumor-suppressive TME (75). In particular, CAF secrete the C-X-C Motif Chemokine Ligand 12 CXCL12 attracting and retaining both myeloid (76) and CD4 +/CD25+ T cells in the tumor, ultimately promoting their differentiation to Tregs immune cells and their survival via the expression of T cell interacting proteins (58, 75). BC CAFs have been characterized at the molecular level (77). Recent single-cell analysis of 768 CAFs isolated from the genetically engineered MMTV-PyMT preclinical model of BC reported three transcriptionally diverse subpopulations of CAFs, with a spatial separation of the CAF subclasses attributable to different origins, including the perivascular niche, the mammary fat pad, and the transformed epithelium. Notably, gene expression profiles of the three distinct CAFs classes correlate to different functional programs. Moreover, these profiles had independent prognostic values as biomarkers for metastatic disease and biomarker-driven development of drugs for precision targeting of CAFs.

The involvement of tumor stroma in BC prognosis is so evident that stromal gene expression can predict disease progression and clinical outcome independently of standard prognostic factors and published molecular signatures (11, 78–81). Moreover, in ER-negative BC, a stromal gene signature has been identified as associated with resistance to anthracycline-based neoadjuvant chemotherapy (82), with a predictive value for therapy response. CAFs' role in conferring drug resistance has been observed in different tumors (83–86) and can occur via the release of paracrine survival factors or by activating pathways in tumor cells that ultimately lead to decreased chemosensitivity, such as the expansion of therapy-resistant tumor-initiating cells (87) and the enhanced expression of multidrug transporters (88). However, reflecting the heterogeneity of CAFs subpopulations and phenotypes, a few pieces of evidence indicating a role for tumor stroma in sensitizing BC to treatment have been reported (89).

A mechanism through which CAFs confer resistance to therapy is mediated by their role in the deposition and remodeling of extracellular matrix components. In particular, the integrins' ligands collagens and fibronectin have been shown to be responsible for the decreased drug sensitivity of different BC cell lines to several treatments (i.e., paclitaxel, vincristine chemotherapy, tamoxifen, ionizing radiation, lapatinib, trastuzumab) through the activation of PI3K/AKT and Ras/Raf/MEK/ERK1-2 pathways (89). Tumor cells themselves can reprogram CAFs to increase the production of collagen, leading to the generation of a niche favoring the acquisition of CSC phenotype, resistance to chemotherapy (90), and driving tumor progression (91, 92). Moreover, CAFs release various soluble factors which contribute to the evasion of cancer cells from the cytotoxic effects of chemotherapy. CAF-secreted HGF and its receptor c-Met have been linked to increased resistance to EGFR and HER2 inhibitors in BC cells from different subtypes (89). An emerging technology based on microenvironment microarray (MEMA, consisting of printed ECM protein supplemented with soluble ligands) allowed to monitor of the growth of tyrosine-kinase inhibitors treated BC cells in more than 2500 different combinations of 56 soluble components and 46 matrix proteins of the TME (86). This study showed that specific soluble factors, highly expressed in BC CAFs, conferred lapatinib resistance to different BC cell types: in basal-like HER2-positive cells, HGF-mediated MET activation, while in luminal-like HER2-positive cells, neuregulin 1 beta (NRG1β), a ligand for the tyrosine kinase HER3, favored HER2-HER3 heterodimerization (86).

CAFs play a crucial role in sustaining tumor inflammation, engaging in intense cross-talk based on cytokines signaling with both TME components and tumor cells (11, 93, 94). As extensively reviewed by Dittmer and Leyh, cytokines such as the Tumor Growth Factor beta (TGF-β) and IL-6 are secreted by CAFs and contribute to drug resistance through both maintenances of CSCs and induction of EMT, whose key transcription factors (i.e., Snail, Twist) mediate the upregulation of transporters genes responsible for multidrug resistance. IL-6, IL-8, and complement cascade have been recently linked to CAF-mediated BC resistance to treatment. Indeed, a new subset of CAF defined as CD10+/GPR77+ (a C5a receptor) has been described as functionally relevant for stem cell maintenance. Niches formed by these CAFs foster the survival of CSCs, providing constant IL-6 and IL-8 secretion, which leads to persistent NF-kB signaling in BC cells and protects them from chemotherapy-induced cell death (88), regulating ABCG2 transporter expression.

A recent work exploited 3D co-cultures and microfluidic to unravel the dynamics of four TME cell populations (cancer, immune, endothelial cells, and fibroblasts) in the presence of the antibody-based HER2 targeting therapy Trastuzumab. Cell interactions have been visualized and quantified *ex vivo*, showing that Trastuzumab promotes longer interactions between cancer and immune cells that result in an anti-tumor ADCC (antibody-dependent cell-mediated cytotoxicity) immune response, while CAFs antagonized this effect (95) (see below). In line with this, recent evidence obtained analyzing 2 cohorts of Trastuzumab treated patients and a fully humanized immunocompetent *ex vivo* model of HER2-positive BC identified a population of TGF-β-activated CAFs specific of tumors resistant to Trastuzumab therapy (96). This CAF population has immunosuppressive functions associated with low IL-2 activity of functional relevance since antibody-based FAP-mediated stromal delivery of IL-2 in non-responsive tumors restored Trastuzumab efficacy (96). Another explanation for CAF-mediated Trastuzumab resistance resides in the newly identified subset of BC CAFs that express CD16 (also

known as FcγRII, a cluster of differentiation molecule found on the surface of natural killer cells, neutrophils, monocytes, macrophages, and certain T cells) and which abundance in HER2-positive patients is associated with poor prognosis and resistance to Trastuzumab. The peculiar pro-tumor effect of CD16 in this CAF subpopulation has been explained by the ability of Trastuzumab-CD16 interaction to activate intracellular signaling involving the SYK-VAV2-RhoA-ROCK-MLC2-MRTF-A pathway, that ultimately leads to elevated contractile force, enhanced matrix production, and stiffness. Targeting of a Rho family guanine nucleotide exchange factor, VAV2, which is indispensable for the function of CD16 in fibroblasts rather than leukocytes, reverses desmoplasia provoked by CD16+ fibroblasts, revealing a role for the fibroblast FcγR in drug resistance, and suggesting that VAV2 is a promising target to enhance the effects of Trastuzumab treatment (97).

4.4 Tumor endothelial cells

Some evidence indicates an involvement of TECs in BC drug resistance. Bovy N. et al. reported that BC patients receiving neoadjuvant chemotherapy showed increased miR-503 production. Interestingly, the origin of this increased production is ascribed to the exosome released by TECs, mediating an acquired resistance (98). Moreover, the product of the NF-κB signaling cascade TNF-α was upregulated in BC ECs after doxorubicin chemotherapy treatment. In turn, TNF-α induces the overexpression of CXCL1/2 in BC cells that, through its receptor CXCCR-2, stimulates the CD11b+Gr1+ myeloid cells to secrete S100A8/9. The activation of the TNF-α-CXCL1/2-S100A8/9 paracrine network mediates the pro-survival effect in BC cells and drives chemoresistance by activating ERK1/2, p38 MAPK, and p70S6K (99). In addition, as an alternative pathway, TEC cells, through Notch signals, are able to promote BC stemness mediating the acquisition of resistance to therapy (100). An important role of TECs in drug resistance against immunotherapy has been described. In particular, TECs are able to favor the recruitment of immunosuppressive cells as well as to inhibit primary tumor infiltration by anti-tumor immune cells. The downregulation of the endothelial E-selectin/P-selectin, ICAM-1, and VCAM-1 proteins results in the inhibition of T cell adhesion as well as the altered chemokine expression such as the nitrosylation of CCL2 by reactive nitrogen species blocks CD8+ T cell recruitment while improving MDSCs recruitment. Moreover, the increased expression on TECs of both PD-L1/2 and FasL expression induces T cell exhaustion and apoptosis, respectively (101).

5 *In vivo* models to mimic BC complexity

Nowadays, preclinical mouse models are widely used to recapitulate the tumor complexity and how this complexity affects drug response. Accurately choosing the best model is crucial to translate the *in vivo* preclinical findings to patients (Figure 3).

5.1 Orthotopic injection in syngeneic mouse models

In syngeneic mouse models, mouse-derived BC cells are implanted orthotopically into immune-intact mice of the same genetic background. These immune-competent models allow the investigation of different aspects of the tumor-immune system crosstalk. The high engraftment rate and the rapid tumor growth make this model an attractive approach to studying BC biology and drug response. Nevertheless, a recent study by Zhong et al. revealed significant differences in the genomic, proteomic, and immunohistochemistry profile of a panel of ten commonly used syngeneic mouse models, including the most widely used BC syngeneic models EMT-6 and 4T1, compared to the subtype-matched human tumors (102). It is crucial to carefully consider that syngeneic mouse models of BC do not form these cancers spontaneously. Therefore, they do not recapitulate the complex

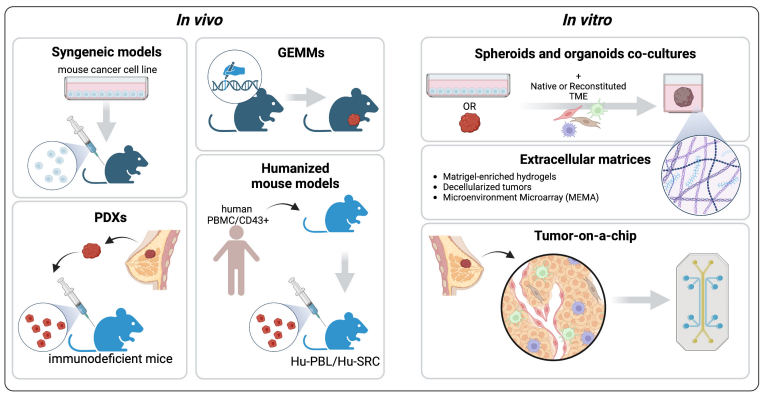

FIGURE 3
Pre-clinical models to recapitulate the TME. The common *in vivo* platforms that mimic different aspects of the BC TME are syngeneic Genetically Engineered Mouse Models (GEMMs), Patient-Derived Xenografts, and Humanized mouse models. Among the *in vitro* models we describe spheroids and organoids co-cultures with native or reconstituted TME components, engineered extracellular matrices (ECMs), and tumor-on-a-chip platforms. Created with BioRender.com.

interactions between tumor cells and the TME that characterize the slow evolution of human neoplasms (103). Indeed, most cell lines used for syngeneic BC models are derived from advanced tumors that have already undergone immune selection *in vivo*. Another aspect that should be thoughtfully evaluated when trying to recapitulate the human TME is optimizing the experimental design for the *in vivo* tumor growth of transplantable cell lines. In particular, injection of different numbers of cancer cells could detrimentally affect infiltrating leukocyte populations and response to immune checkpoint blockade (104).

5.2 Genetically-engineered mouse models

Genetically-engineered mouse models (GEMMs) develop cancer in an autochthonous manner upon overexpression of oncogenes or deletion of tumor suppressor genes (often combined) in a tissue-specific and temporally controlled manner (105). Compared to syngeneic models, GEMMs better recapitulate the multistep pathogenesis of BC and the crosstalk between neoplastic cells and the TME. Moreover, the competent immune system of GEMMs makes them uniquely suited for investigating cancer immunotherapy approaches. The Mammary-specific Polyomavirus Middle T antigen overexpression mouse model (MMTV-PyMT) is the most commonly used GEMM. Although the Middle T oncogene is not present in human tumors, its expression in the mammary epithelia induces transformation and generation of multifocal tumors that readily metastasize to the lungs without the need for additional mutations in metastasizing cells (42, 106). Interestingly, this murine model was used to demonstrate, via intercrossing with 27 different mouse strains, that the genetic background determines the age of tumor onset and the development of metastases, providing the first evidence that genetic heterogeneity plays an important role in tumor progression (42, 107).

According to a gene expression profile analysis, the PyMT tumor closely resembles the aggressive forms of the luminal B subtype of human BC, exhibiting loss of ER and PR expression and overexpression of HER2 and cyclin D1 with the progression of the disease (108). PyMT-derived BC tumors have provided significant genetic and mechanistic insights into breast tumorigenesis, as well as for preclinical testing of potential therapies (82). The K14cre BRCA1f/f Tp53f/f mouse model spontaneously develops tumors mimicking the human clinical features and genetics of basal-like/TNBC. This model has recently helped to provide new understandings into the crosstalk between cancer cells-intrinsic redox mechanisms and the formation of protumorigenic TME (110, 111). Specifically, activation of the transcription factor aryl hydrocarbon receptor by ROS promotes the production of chemokines to attract monocytes and activate the proangiogenic activity of macrophages (110).

5.3 Patient-derived and humanized mouse models

Preclinical mouse models that more likely recapitulate the intra-tumor and inter-tumor heterogeneity of human cancer are the patient-derived mouse models (PDXs). These models are becoming the standard platforms used for preclinical drug testing since they preserve the tumor architecture and the relative proportion of cancer cells and stromal cells. In PDXs, cancer tissue is implanted subcutaneously, orthotopically, or under kidney capsules in immunodeficient mice and can be serially transplanted. The ability to preserve the TMEs' structure, the clonal genomic landscape, transcriptomic, epigenomic and signaling pathway signatures of the original parental tumors makes PDXs a valuable tool for precision medicine, enabling drug testing and resistance studies, assessment of tumor heterogeneity and evolution during disease progression (112–114). Indeed, they are currently used for co-clinical trials, whereby preclinical studies are conducted in parallel with human trials. Using an animal "avatar" allows the integration of valuable data in a real-time manner for each patient, thus enabling a more precise stratification and treatment customization. Many research centers and pharmaceutical companies have successfully developed and characterized PDXs as models for the different clinical and molecular subtypes of BC (115–119). More recently, an extensive collection of PDXs recapitulating the deadliest forms of BC has been generated (120). This platform includes drug-resistant, metastatic, endocrine-resistant estrogen ER+ and HER2-positive tumors, many of which are primary-metastatic pairs or longitudinal collections from an individual patient over time. Importantly, these PDXs reflect the intrinsic heterogeneity of the subtypes in terms of mutational signatures, paving the way for new therapeutic opportunities for these aggressive tumors (120). The significant disadvantage of PDXs in faithfully representing the TME is the lack of human immune system components, such as circulating T and B cells.

5.4 Humanized mouse models for cancer

Humanized mouse models have been developed to overcome species-specific differences in the genetics and immune system between mice and humans (121). Humanized mouse models of cancer are immunodeficient mice reconstituted with representative subsets of human immune cells and engrafted with human tumors (122). The engraftment of specific cell populations in mice will influence the relative abundance of different human immune cell types. Therefore, it is crucial to select the most appropriate humanized mouse platform to specifically address the experimental question and gain translational potential. Injection of human Peripheral Blood Mononuclear Cells (PBMCs) into immunodeficient SCID mice is the most straightforward method for developing humanized models, namely the Human Peripheral Blood Leukocyte (Hu-PBL) SCID mice. Hu-PBL-SCID mice are characterized by limited numbers of engrafted human myeloid cells and B cells. Conversely, CD4+ and CD8+ subsets of CD3+ T cells are abundant, and their expansion eventually develops an acute immune response against mouse MHC molecules, leading to xenogeneic Graft-Versus-Host Disease (GVHD) and restricting

the experimental window for these animals to a few weeks (123). To overcome GVHD, genes encoding mouse MHC class I and II molecules have been inactivated, enabling a more extended time window for conducting experiments. Iizuka and coworkers took advantage of a human PBMC-transplanted MHC class I- and class II–deficient NOG mice engrafted with BC cell lines to test the cytotoxic activity of a bispecific antibody targeting human CD3 and B7-H4, considered to be a negative regulator of immune responses. B7-H4 is overexpressed in many human cancers, suggesting its potential role as a cancer therapy target. This therapeutic strategy resulted in enhanced tumor infiltration of activated CD8+ T cells and reduced tumor growth. Of note, because B7-H4 is highly expressed independently of HER2 or PD-L1 expression in breast cancers, they propose the use of this therapeutic agent for PD-L1–B7-H4-expressing tumors or anti-HER2 antibody nonresponsive breast tumors (124). An adequate immune reconstitution is achieved with the human Stem Repopulating Cell (Hu-SRC) mouse model, which results from the engraftment of immunodeficient mice with human CD34+ Hematopoietic Stem and Progenitor Cells (HSPCs). Hu-SRC engrafted with PDX or Cell line-Derived Xenografts (CDX) have been used to study the human immune system–tumor crosstalk, evaluate biomarkers, and the preclinical activity of immuno-oncology agents (125–127). For instance, Scherer and coworkers recently developed and characterized an immune-humanized PDX model of estrogen-independent endocrine-resistant ER-positive metastatic BC that harbors a naturally occurring ESR1 mutation (126). Mutant ESR1 promotes endocrine resistance since it renders the ER protein constitutively active and less dependent on estrogen for its function, limiting treatment options. Importantly, ESR1 mutant tumors gain basal-like features associated with increased immune activation, implicating potential immune therapeutic vulnerabilities that should be deeply investigated using immune humanized preclinical models (128). The limitations of this model are mainly the requirement of pre-experimental sub-lethal γ-irradiation to enable engraftment and the limited maturation of human T cells in the murine thymus (121). To promote the development of T cells in a human thymus-like environment, researchers have co-implanted human CD34+ HSPCs and autologous fetal thymus tissue into SCID mice, generating a mouse model named BLT (bone marrow - liver - thymus) (129).

6 *In vitro* models to mimic BC complexity

In vitro systems have a major advantage over mouse models: the ability to precisely control the experimental settings (Figure 3). Indeed, *in vitro* platforms can recapitulate different aspects of the TME, including the cellular compartments, physical properties, and chemical cues (130). Compared to cell lines grown in conventional 2D culture, 3D systems enable the integration of these elements, capturing more faithfully the intra-tumor heterogeneity and allowing the study of tumor-stromal interactions and drug responses. Here, the commonly used and emerging platforms to study the BC TME are presented (Figure 3).

6.1 Spheroids

To investigate the role of the TME in 3D conditions, researchers have developed a variety of protocols for the generation of spheroids, cellular entities cultured as free-floating aggregates, with or without the addition of extracellular matrix and growth factors (131). Mammospheres are BC spheroid cultures enriched in progenitor cells that differentiate along multiple lineages. To this concern, mammospheres derived from freshly isolated BC samples exhibit CSC-like properties and multiple drug resistances (132). L. Hamm and coworkers established a high throughput tumor spheroid microprinting technology to produce homogeneously-sized spheroids to model the interaction of CAFs and TNBC cells and examine drug resistance (133). In another work, the 3D bioprint technology was leveraged to manufacture a 3D structure containing BC cells in the core and adipose-derived mesenchymal stem/stromal cells (ADMSCs) in the edges. The authors proposed the use of this 3D model for chemoresistance studies (134).

6.2 Patient-derived organoids

Tumor organoids are complex 3D structures that originate from dissociated tumor tissues or circulating tumor cells that are embedded into the bio-mimetic matrices with growth factor supplements to encourage a self-organizing process (135). Compared to spheroids, they better resemble the original tissue both histologically and genetically Patient-derived organoids (PDOs) largely retain the parental tumor heterogeneity, therefore providing the enormous potential to understand resistance mechanisms and predict response to treatment in individual patients (136, 137). Organoids can be cryopreserved and expanded for long-term culture. Of note, banks of human BC organoids are currently available (120, 138). In particular, the collection of nine sets of matched human BC tumors, PDXs, and PDOs generated by Guillen and coworkers represent a promising platform for drug screening treatment-resistant tumors (120). Primary PDOs contain subsets of stromal cells, including fibroblast and immune cells; however, these cells are gradually lost during the long-term culture (139). Nevertheless, researchers have grown organoids with native or reconstituted TME elements (140). Recently, Rivas and coworkers developed an *ex vivo* 3D model of HER2-positive BC that recapitulates patients' response to treatment, consisting of fluorescent human HER2-positive BC cells co-cultured with patient-derived fibroblasts and naïve primary immune cells collected from the peripheral blood of healthy donors (96).

6.3 Mimicking the ECM

Organoids are commonly cultured in hydrogels enriched in extracts of ECM proteins. Among these, the basement membrane extract Matrigel is considered the gold standard for supporting tumor organoids' growth. However, Matrigel typically suffers from inherent compositional variation and lot-to-lot variability, which can confound analysis and affect the model's reproducibility (141). As an alternative biomaterial, decellularized breast tumors or Patient-Derived Scaffolds (PDSs) have been used to better recapitulate the native tumor ecosystem. In recent work, BC PDSs were recellularized with cancer cell lines as platforms for drug testing, revealing that MCF7 cells enhanced their resistance against the conventional chemotherapy drugs 5-fluorouracil, doxorubicin, and paclitaxel in comparison to 2D cultures (142). These data suggest that PDSs could be exploited to examine the effects of the ECM on cancer drug responses in the clinical setting and may represent a significant step forward in the field of personalized medicine (143). The MEMA platform is used to interrogate the impact of thousands of microenvironmental proteins on the phenotype of different cancer cells, including primary cells and cell lines (144). By printing specific and defined combinations of functional proteins into well plates, it was possible to study microenvironment effects on anti-HER2 tyrosine-kinase inhibitors response (86).

6.4 Tumor-on-a-chip

Recent advances in tissue engineering technology allow the development of organ-on-a-chip devices in which cancer cells are grown in a dynamic environment consisting of microchannels that can be perfused at tailorable flow rates. The ability to finely control mechanical stress, shear flow, and concentration gradients makes the organ-on-a-chip technology particularly useful for studying angiogenesis, metastasis, mechanotransduction pathways, and cancer cell behavior under shear stress (145). However, several on-chip models were designed to mimic tumor-stromal cell interactions. For example, Aung and coworkers, taking advantage of a BC-on-a-chip model consisting of a heterogeneous mix of cells and noncellular elements, investigated the role of tumor-associated hypoxia and the BC-immune cell interaction on T lymphocyte recruitment (146). BC-on-a-chip platforms could represent powerful *ex vivo* platforms to study, within immunocompetent settings, drug responses that depend on the TME (95). Moreover, it is possible to integrate these platforms with advanced live cell microscopy technologies and automated image analysis to capture the behavior of single cells in the tumor ecosystem and the cell-cell interactions (95).

7 Emerging technologies to study BC complexity

Tumor profiling is a powerful tool to dissect key molecular signatures of cancer cells and deeply investigate the sources of diseases. The role of large landmark projects, such as The Cancer Genome Atlas Program (TCGA (4)) and Molecular Taxonomy of Breast Cancer International Consortium (METABRIC (147)), and of specific analysis strategies, such as GSEA (148, 149), have allowed scientists to begin to approach the complexity of the tumor system in question, enabling accurate and precise stratification of patients. Subsequent meta-analyses based on separate BC and TME data showed that very different results emerge from the bulk transcriptomic data (150).

Single-cell analysis refers to the investigation of individual cells to obtain genomic, transcriptomic, or multi-omics information at the single-cell level. The data obtained with these technologies have a much higher resolution than conventional bulk sequencing methods in terms of the number of cells. Taking advantage of these emerging technologies, including spatial analysis and artificial intelligence, it is possible to identify comprehensive biomarkers allowing more precise patient stratification, signal resistance identification as it begins, and relapse prediction (151, 152) (Figure 4) A brief description of emerging technologies for unravelling breast cancer complexity is included in Table 1.

7.1 Single-cell RNA sequencing

The important next step in data generation and subsequent analysis occurred with single-cell experiments, leading to the opportunity of analyzing the transcriptome at the single-cell level for millions of cells in a single study. Single-cell RNA sequencing enables scientists to characterize, discriminate, and identify each cell at the transcriptome level, leading to the finding of rare but functionally significant cell sub-populations (153).

Today, a growing number of modified and enhanced single-cell RNA sequencing technologies have been designed to bring important adjustments and improvements in sample collection, single-cell capture, barcoded reverse transcription, complementary DNA (cDNA) amplification, library preparation, sequencing, and refined bioinformatics analysis. Most importantly, the cost has been drastically decreased, while throughput and automation have both been greatly boosted (153).

In single-cell RNA sequencing, single cells are isolated from tissue samples, captured, and then combined with a bead inside a nanoscale droplet (each bead contains unique molecular identifiers). Barcoding, cDNA amplification, and the library preparation steps follow this stage. In order to present and categorize the landscape of gene expression in cells of a heterogeneous population, snapshot data from single-cell RNA sequencing can be examined (153, 154).

Single-cell sequencing technologies' most recent technical and computational advancements have greatly expanded researchers' toolkits for studying TME directly from patient tissues. BC is just one of the many tumor types for which single-cell RNA sequencing has been extensively employed to depict the intra-tumoral immune landscape (155).

For instance, despite the immune checkpoint blockade (ICB) therapy having produced impressive and long-lasting clinical responses in a limited number of cancer patients, its overall response rate has been low, and many patients with initial

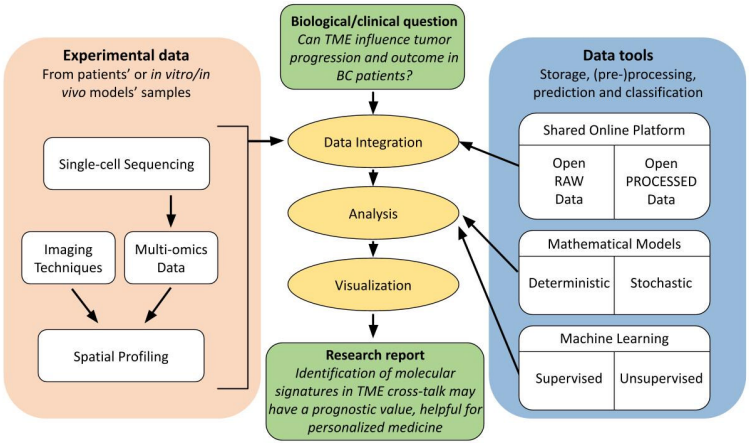

FIGURE 4
Flow diagram of good practice guidelines for spatial analysis users. Schematic representation of complexity and interconnectivity of single-cell multi-omics data in spatial analysis, from experimental data to scientific report to address a biological/clinical investigation. These techniques benefit from an integration with relative online available data and from an extensive computational analysis in order to increase the accuracy, reproducibility and reliability of the obtained results in a specific research field.

TABLE 1 Brief description of emerging technologies for unravelling breast cancer complexity.

Technologies	Description	Advantages	Limits	References
Single-cell sequencing	Genomic, transcriptomic, or other-omics information at the single-cell level.	•Higher resolution compared to conventional bulk sequencing methods in terms of the number of cells. •Heterogeneity dissected at single-cell resolution. •Analysis of gene expression changes upon drug. treatment. •Relatively low cost. •Can be integrated with other omics approaches.	•Useful as starting point for the other emerging techniques, taken alone is not much informative.	(153, 154)
Single -omic	Large-scale studies which refer to the systematic identification and quantification of the overall components of a specific cell domain (such as transcriptome, proteome, metabolome, lipidome…).	•Quite a complete overview on a single aspect of a sample of cells. •Well-assessed and validated methods. •At the level of Transcriptome is feasible also in patients but expensive, while for proteomic, metabolomic and lipidomic is still far from patients.	•Single-omics data offer only a limited amount of information on biological mechanisms restricted to a single field.	(155–157)
Multi -omics	Combination and integration of several methods and data sets of different -omic groups during the biological analysis.	•A potent integrative approach, which provides a high amount of information, allowing to connect a genotype to a phenotype for a full cellular readout. •Depending on the type of analysis and data sets employed it can lead to the direct measure of causes and consequences of biological phenotypes.	•Highly expensive.	(158, 159)
Spatial biology	Combination of different techniques of sequencing and imaging (such as MERFISH/SeqFISH, CyCIF,IMC…) in order to examine the types of cells, their distribution throughout the tissue, the patterns of biomarker co-expression, and the organization and cross-talk in their microenvironment.	•Learn new biological insights by analyzing cells in their environment.	•Highly expensive. •Need of specialized facilities. •Complexity of data analysis.	(160–171)

responses have refractory disease or have developed acquired resistance. The observed variability in ICB efficacy has been associated with a number of TME-related factors, through single-cell analysis, specifically with markers of the intra-tumoral T cell states, such as overall T cell infiltration, activation, and exhaustion. In fact, the enhancement of single-cell transcriptomic tools applied to TME studies improved our knowledge of tumor complexity, adaptability, and its intricate cross-interaction between various cell types within the TME (20, 155, 156).

With a similar approach, Gambardella et al. studied tumor heterogeneity and drug response, providing a transcriptional analysis of several BC lines. They demonstrated that the expression of clinically important markers could be detected through single-cell transcriptomics. Furthermore, they showed that different cells within the same BC cell line express heterogeneously relevant well-known BC receptors, including PR and HER2. Additionally, they observed dynamic plasticity as a consequence of drug responsiveness (157). In particular, they developed a bioinformatics tool that, starting from single-cell profiles, leads to drug response prediction at the single-cell level, firstly detecting expression-based biomarkers of drug sensitivity for several drugs, then correlating them with drug potency in different cellular lines. To experimentally validate their bioinformatic tool, they applied it to a BC cell line, the MDA-MB-361, identifying and sorting two cell subpopulations for HER2 receptor expression. Based on their computational prediction, they tested in both cell types representative drugs, obtaining results in line with the expected outcome (157).

Moreover, in line with these findings, the massive parallel sequencing and other omics technologies have demonstrated the level of heterogeneity in TNBCs, underling the potential impact of TME in therapeutic responses (152).

7.2 Multi-omics

Researchers can now study and define the TME at single-cell resolution thanks to the advent of multimodal omics technologies, which presents an unprecedented opportunity to comprehend the heterogeneous complexity of the TME (158). In fact, an efficient way to connect the patients' genetic background with a condition or trait is through genome-wide association studies, which connect genotype to phenotype, and multi-omics provides a potent integrative approach, as it consists of the combination of data sets of different omic groups during the biological analysis. Indeed, multi-omics data must be integrated to increase the accuracy of predicting the biological relationship between genotype and phenotype because single-omics data only offer a limited amount of information on biological mechanisms (132, 172). Moreover, a good practice is to further integrate the obtained multi-omics data with online available raw and processed data in the same field in order to generate reproducible and reliable results through different open datasets (173) (Figure 4).

There is an emerging need to construct integrated multi-omics data databases, such as the Multi-Omics Breast Cancer Database (MOBCdb) proposed by Xie and colleagues (174). It is an available library that incorporates clinical, genomic, transcriptomic, epigenomic, and treatment response data of many BC subtypes. By using several search methods, users of MOBCdb can receive information on single nucleotide variation, gene expression, microRNA expression, DNA methylation, and particular pharmacological responses. With this online resource, users have access to integrated multi-omics data of various BC subtypes, allowing the identification of possible new biomarkers for personalized medicine (174). Another example comes from the work by Fan et al., which provides insights into the molecular pathways behind BC prognosis, building a dataset of gene-interaction networks in BC and describing genes linked to long-term BC survival (132). Indeed, emerging evidence attributes multi-omics data integration to a prognostic value; for instance, Nguyen and colleagues identified two therapeutically relevant molecular subgroups of BC with subgroup-specific characteristics employing multi-omics datasets. These approaches hold the promise for the creation of specific diagnostic tests and personalized medicine (175).

As TME components have been shown to play a crucial role in the occurrence, growth, and metastasis of BC, the development of single-cell omics largely addressed the limitations of purely biological assays and allowed us to comprehend the changes in cell populations, metabolic profiles, and immunological state of the TME throughout tumor progression. Now there is a better understanding of tumor complexity thanks to the ongoing development of integrated tools for single-cell omics that not only detect cell heterogeneity but also expand analysis for transcription-based cell cloning aberration (176), cell traceability (177), cell-to-cell interaction (178, 179), rare cell resolution (180), and disease process simulation (181). The recent single-cell omics results have mapped out breast TME with fairly high accuracy, sorting stromal cells and immune cells into functional populations and significantly employing the TME components for clinical diagnosis and targeted treatment intervention (182).

In particular, TNBC heterogeneity is characterized by genomic instability and elevated mutation rates, with an impact on immune surveillance (183). Therefore, to pinpoint the therapeutic approach for TNBC, specific driver genes, and pathways should be determined for better patient subtyping and target therapy (184). The most frequently altered genes, the genetic profile most likely contributing to the malignancies' development, and the genes associated with metastatic TNBC can all be identified through recent advancements in whole genome sequencing. Emerging targeted therapies may enhance therapeutic effects by overcoming drug resistance and promoting patients' survival (183, 184). For instance, Xiao et al. performed an extensive immunogenomic analysis to investigate the heterogeneity and prognostic importance of the TNBC microenvironment using a big original multi-omics dataset of TNBC. They also investigated TNBC's potential immunological escape pathways. This trial is a step in the direction of individualized immunotherapy for TNBC patients, as TME phenotypes were classified in different clusters and validated with a significant prognostic efficacy (185).

Furthermore, Xie et al. focused their study on FOXO family genes and their correlation with TME in several cancers, including

breast. As they examined the relationship between the FOXOs score and a variety of drugs, they showed that the FOXOs score might reflect patients' responses to different therapies. They discovered that the majority of drugs' IC50 values in pan-cancer, but particularly in BC, were negatively linked with the FOXOs score, corroborating the theory that a high FOXOs score would make a patient more susceptible to chemotherapy and targeted medications. Collectively, their data show that the FOXOs score has a substantial correlation with the TME and may be used as a biomarker to predict the effectiveness of various treatments, including immunotherapy (159).

7.3 Spatial biology and phenotyping

The study of a variety of cellular landscapes across different dimensions is known as spatial biology. Studies of spatial biology examine the types of cells, their distribution throughout the tissue, the patterns of biomarker co-expression, and the organization and interactions that compose the TME, allowing to learn new biological insights by analyzing cells in their environment (Figure 5) (160–162).

Methods for spatial molecular profiling have dramatically increased recently and differ in resolution, scale, and molecular multiplexing, with an improvement of spatial methods, in particular for transcriptomic, proteomic, and metabolomic (160). Different length scales are used by methods to capture a variety of data: from averages across cells spanning thousands of micrometers in spot-based procedures like spatial transcriptomics to single-molecule resolution in methods like MERFISH or SeqFISH. Consequently, a variety of questions can be addressed using the most suitable technique. The number of molecular features acquired varies between methods as well, ranging from tens in Fluorescence *In Situ* Hybridization (FISH), Cyclic Immunofluorescence (CyCIF), and Imaging Mass Cytometry (IMC) to hundreds or thousands in specialized probe-based spatial transcriptomics methods (MERFISH or SeqFISH), imaging mass spectrometry, and tens of thousands in spot-based spatial transcriptomics, including Slide-Seq, Visium and High-Definition Spatial Transcriptomics (HDST) (160, 161, 163). To detect and quantify biomarkers expression as well as to visualize how cells interact and organize throughout the entire tissue landscape, true spatial biology investigations exploit whole-slide imaging at single-cell resolution. This method is also known as spatial phenotyping.

An interesting use of this new technological branch is the one applied to the study of TME. Studies utilizing spatial multi-omics methods have demonstrated the complexity of the TME heterogeneity and showed that, in addition to the cellular composition, the relative localizations and interactions with different cell types in the TME significantly impact tumor formation. In fact, a better understanding of spatial interactions led to the redefinition of tumor subtypes and the shifting of research attention to tumor-immune interaction units, to the discovery of additional cell types, and of the changes in the TME compartment throughout cancer progression (160, 164). For example, in BC, the different subclones that contribute to the heterogeneity of the cancer mass were found to map in distinct regions (165, 166), with a specific architecture suggestive of a deep role of the TME, where CAFs show great heterogeneity and spatial separation (167). Liu et al. provide a novel insight into the cellular architecture of BC and potential therapeutic strategies, revealing differential association with patient survival and therapeutic response through single-cell and spatially resolved analysis (165). The analysis of two BC samples showed that malignant subclones map to regions of stromal cell enrichment, indicating that, even if only two BC were analyzed in detail, the diverse abundance of genetically

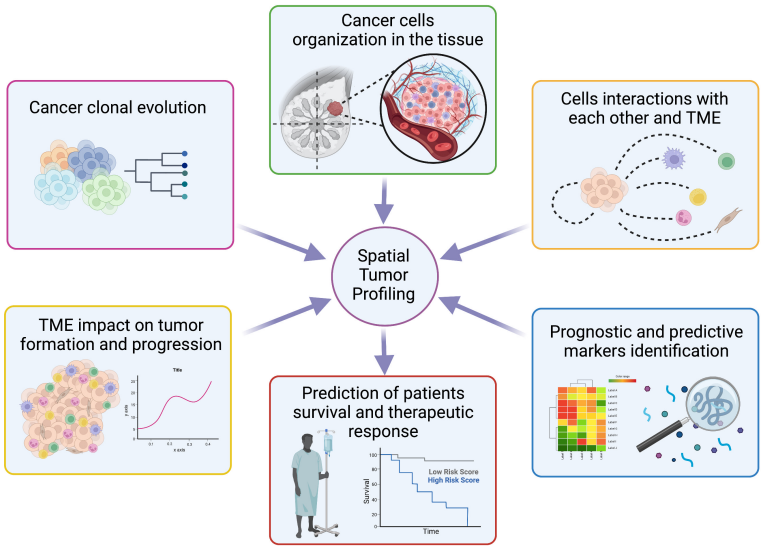

FIGURE 5
Overview of spatial tumor profiling applications. Schematic representation of the main opportunity offered by spatial techniques in the molecular biology field with possible applications to personalized medicine. Created with BioRender.com.

and spatially distinct subclones is differently associated with patient survival and therapeutic response (165). This evidence suggests that it might be worth investigating how the heterogeneous architecture of cancer cells impact therapy response.

Moreover, the treatment of several cancers has been transformed by ICB. However, unfortunately, most patients only have minimal benefit from ICB, even after an initial response. Multi-omics TME assessment is indeed required for precision immune oncology in order to discover distinctive prognostic features and proactively personalize combinatorial treatments. Through accurate epitope colocalization, multiplexed single-cell spatially resolved tissue analysis enables the discernment of cellular functional states from their spatial organization, and emerging markers evaluated in multiplexed spatial protein analysis may help determine prognostic and predictive patterns in BC (168).

In particular, the work from Tietscher and colleagues suggests that single-cell data used for a comprehensive, spatially resolved, immune-focused analysis of TME could be useful for patient stratification to select them for ICB therapy. Indeed, they have defined two unique immunological microenvironments in breast tumors; each one may influence the response to immunotherapy, considering tumor antigen presentation, T cell phenotypes, cytotoxic potential, cellular interaction, and spatial organization. As the primary marker currently utilized to stratify patients for immune checkpoint treatment in BC is PD-L1, their findings imply that PD-1, CXCL13, and MHC-I, possibly in combination with previously identified T cell exhaustion markers like LAG-3 and TIM-329, are more effective at differentiating immunological TME that may show to be differentially receptive to this treatment. Therefore, these variables may be helpful in selecting individuals for prospective clinical trials of ICB, along with other patient stratification techniques (169).

Further work by Kulasinghe et al. provides new insights into the TNBC TME and its association with chemotherapeutic response and patient survival (170). In particular, spatial studies on TNBC samples revealed differentially expressed proteins and protein signatures within tumors and stroma compartments that associate with prognosis (overall survival) and treatment response. Following this approach, they were effectively able to stratify patients by their response to therapy (170).

Overall, recent evidence indicates that cancer study in a spatial context will improve the current knowledge of how the complex cross-talk between tumor and surrounding microenvironment results in the malignant subclones' growth and progression, with an impact on survival and resistance to therapies (Figure 5) (171).

8 Mathematical modelling and artificial intelligence in unraveling BC complexity

8.1 Mathematical modelling

As well known, the origins of BC heterogeneity lie in both the stochastic nature of biological phenomena and their nonlinear dynamics. In these contexts, small changes in the complex interactions among different genetic, epigenetic, and environmental factors can have dramatically different effects on the evolution of the biological system. This strong dependence on probabilistic mechanisms and initial conditions makes it extremely difficult to fully understand the mechanisms and implications of heterogeneity in breast cancer.

To address this challenge, mathematical models have been developed and widely used to study and understand the complex processes underlying breast cancer heterogeneity. These models are based on mathematical equations, both deterministic or probabilistic, and simulations that allow researchers to investigate how different factors interact with one another and how they contribute to the development of the disease.

Examples of such models date back to at least a decade ago (48), with studies connecting different axes of phenotypic plasticity to explain the emergence of heterogeneity and drug resistance (186). These models have shown how genetic and epigenetic changes can lead to the development of different breast cancer subtypes, and how these subtypes can respond differently to different treatments.

Additionally, mathematical models have shown how a single axis of plasticity can give rise to extensive diversity upon mutations (187). This has important implications for the development of new treatments, as it suggests that targeting specific mutations may not be sufficient to treat breast cancer effectively. Instead, a more comprehensive understanding of the underlying mechanisms and interactions is needed to develop targeted and effective treatments.

In particular (48), and (187) highlight how the heterogeneity of breast cancer rests on a stochastic and combinatorial nature of the genetic and epigenetic elements that could interact together.

Finally, an additional dimension of non-linearity was highlighted in two different types of epithelial-mesenchymal transition (EMT) dynamics: one hysteretic and one non-hysteretic (188). In particular, specific gene patterns characterized by significant clinical prognosis value were highlighted in the EMT hysteretic dynamics.

These modeling efforts have been demonstrated to be useful for implementing therapeutic targets *in vivo*, allowing researchers refine their understanding of the mechanisms underlying breast cancer, to test the efficacy of new treatments and improve the effectiveness of therapies (189).

In summary, mathematical models have proven to be valuable tools for understanding the complexity of breast cancer heterogeneity while providing predictive tools on how biological systems may respond to specific perturbations.

Integration with increasingly precise and specific data, derived, for example, from scRNA_Seq techniques, will allow these models to help shed light on the mechanisms underlying the disease and develop more effective treatments for patients. The availability of increasingly rich and detailed databases has enabled the application of powerful and versatile Machine Learning/Artificial Intelligence systems to model and attempt to decipher additional levels of non-linear characters of this heterogeneity as discussed in the next paragraph.

8.2 Artificial intelligence in BC and TME

The use of Artificial Intelligence (AI) and Machine Learning (ML) is becoming widespread in the field of biology and life sciences (190). The existence of large databases, such as the one derived from the omics study in TME, necessitates the use of advanced tools and techniques. These new AI tools are rapidly becoming important for researchers (Figure 4) by leveraging the connection of large amounts of data and their elaboration, simplify the discovery of non-linear correlation in complex datasets. ML can be classified into three main categories: supervised learning, unsupervised learning, and reinforcement learning, where supervised learning involves learning from labelled data to make predictions, unsupervised learning involves finding patterns in unlabeled data, and reinforcement learning involve learning from interactions with an environment to maximize a reward signal (191).

Clustering is a popular omics analysis method that is used to find regularity and patterns in the data to help differentiate cancer molecular subtypes. One example of clustering is the assessment of immune cell infiltration levels using neural network techniques. This method can be used to classify patients based on the degree of immune cell infiltration in lung cancer (192).

Another important method is feature selection with Principal Component Analysis (PCA). This technique helps to reduce the dimensionality of the dataset, thus reducing the number of features. This can be done using different machine learning algorithms, such as Random Forest, that can be very useful in identifying genes that present a correlation with different types of cancer (193).

Feature transformation is another emerging approach that is still under development. This method aims to merge and modify existing features to create new ones. This can be helpful in merging different types of data, such as *in vitro* and clinical data. Feature transformation is an important approach to consider as it can uncover new insights and relationships in the data that are not immediately apparent.

A practical application of advanced machine learning to the study of TME in BC is DeepSpaCE (Deep learning model for Spatial gene Clusters and Expression), where advanced deep learning techniques have been applied in the context of spatial transcriptomics. In the paper (194), the authors applied a Convolutional Neural Network (CNN) to obtain a system able to reproduce with super-resolution the spatial gene expression from TME samples and then predict gene-expression levels in tissue sections within consecutive sections. This method enables users to derive hidden histological characters via spatial transcriptome and gene annotations, leading to accelerated biological discoveries without additional experiments. Indeed, they confirmed its performance using the spatial-transcriptome profiles and immunohistochemistry images of consecutive human breast cancer tissue sections. For example, the predicted expression patterns of SPARC, an invasion marker, highlighted a small tumor-invasion region that was difficult to identify using raw spatial transcriptome data alone because of a lack of measurements. They further developed semi-supervised DeepSpaCE using unlabeled histology images and increased the imputation accuracy of consecutive sections, enhancing applicability for a small sample size.

In particular, recent developments in ML algorithms have shown that deep learning (DL)-based models can recognize non-linear relationships in the data, along with linear relationships, from highly dimensional data derived from different -omics (195). In the context of omics and data analysis, ML, such as DL, can be used to identify patterns and correlations in the data that would be difficult or impossible to detect by humans (196, 197).

Finally, ML algorithms can also be applied to a well-curated scRNA-seq dataset of breast cancer patients. In this study (198), the authors developed an advanced ML model to identify cell lineage and subtypes and to automatically obtain the lowest unique molecular identifiers (UMI) threshold, reducing the time required for these analyses and simplifying the entire procedure.

9 Conclusions and perspectives

The complexity of BC, mainly due to the intra- and inter-tumor heterogeneity present in both primary tumors and metastatic lesions, represents a great obstacle in unraveling drug resistance mechanisms. In this Review, we have addressed the various determinants that contribute to BC heterogeneity, highlighting the primary role of the tumor microenvironment. We have deeply discussed the recent advances in uncovering BC heterogeneity, thanks to the ability to dissect the genetic diversity of cell subpopulations, the cancer cell plasticity, and the complexity of TME. We have also discussed the impact of tumor heterogeneity and TME on tumor progression and drug resistance, with the idea that the new molecular insights that are emerging need to be translated into improved therapeutics (Figure 4).

How to overcome cancer heterogeneity to improve cancer therapy remains a major challenge. Actually, mortality in BC is generally due to resistance to successfully treating metastatic disease. Metastases spawned via dissemination in different organs evolve in entities that are distinct from each other and from the primary tumor. Therefore, they need to be handled as independent tumors, with ongoing epigenetic evolution combined with the contribution of the specific TME in the metastatic site. Recent results also strongly put forward that dissimilar TME can affect the metastatic sites, leading to selection for survival and outgrowth of genetically different metastatic variants.

We describe the developments in single-cell RNA sequencing and in multi-omics technology on clinical samples, which are already providing insights into the phylogenetic correlation of primary tumors and metastases at the level of somatic tumor genetics, and that can reveal fundamental mechanisms of the metastatic process. However, deeper insights are needed to study variations that occur at the epigenetic level of matched primary and metastatic tumors of larger numbers of patient and experimental tissue samples. An emerging field to take into account is also the importance of the personal genetic landscape of each patient, which can strongly modify tumor and metastasis biology, their response to TME, and their drug responsiveness.

The *in vivo* preclinical models remain fundamental to study processes that cannot be readily inquired in humans and also to allow the study of the natural history of disease progression in the untreated state. However, since these studies are costly and labor-intensive, the bright use of mouse models should take into account the features that differ from human BC. Preclinical models, therefore, offer an important vehicle for generating and testing hypotheses that can then be validated across the broader human population. Where possible, models should include an intact immune system, the humanized mice being important platforms to overcome species-specific differences in the genetics and immune system between mice and humans. Moreover, attempts should be made to incorporate genetic heterogeneity in study designs by using several diverse models on different genetic backgrounds. On the other hand, *in vitro* organoid models derived from GEMMs or human clinical material could offer new perspectives in terms of rapid functional screening of genes and pathways that can influence tumor progression and of availability of material to analyze epigenomics and chromatin landscape evolution that is currently difficult to do using only human biopsies.

In conclusion, overcoming cancer heterogeneity to date remains a difficult task. In terms of TME, a better understanding of its complex organization, spatial heterogeneity, and changes in metastatic progression under the pressure of therapy is crucial for patient survival. The available targets are few and this field still needs further research. In the meantime, it's worth mentioning that using a combination of drugs can increase therapy response, likely due to the synergistic effect of the drugs in selectively killing cancer cells and creating a more restrictive environment. In addition, high-resolution sequencing techniques prior to therapy and longitudinal sampling can provide a good source of information to delineate the optimal therapeutic strategy.

As shown by Navarro Ocon et al., new nanomedicine-based therapies have been proposed to alleviate immunosuppression in tumors and reduce the emergence of tumor heterogeneity in BC patients. Indeed, nanomedicine can improve the delivery, retention, and release of immunostimulatory agents in targeted cells and tumor tissues in numerous malignancies, including breast cancer (199). Moreover, the goal of finding new ways to revert a hostile TME by immune-activating cytokines is frequently hampered by the severe toxicity associated with their systemic administration. Very recent works in mouse models of glioblastoma (GBM) (200), melanoma, and mammary tumors (201) demonstrated a TME reprogramming toward anti-tumor activity upon targeted delivery of IL-12 via different approaches. In particular, Birocchi et al. describe a lentiviral vector-based platform that can engineer hematopoietic stem cells *ex vivo* with the aim of releasing, via their tumor-infiltrating monocyte/macrophage progeny, Interferon alpha (IFN-α) or IL-12 at the tumor site with spatial and temporal selectivity. In a preclinical syngeneic GBM mouse model, the inducible release of IFN-α within the TME achieved strong tumor inhibition up to eradication and outperformed systemic treatment with the recombinant protein in terms of efficacy, tolerability, and specificity. Single-cell RNA sequencing of the tumor immune infiltrates revealed reprogramming of the immune microenvironment toward a proinflammatory and antitumoral state, demonstrating a potential therapeutic approach for GBM (200) and paving the way to treat with locally delivered IL-12 other solid tumors, including melanoma and BC.

Author contributions

VS, GC, LA, DN, AP, and PA designed the structure of the review and analyzed the state of the art in the field UA, DT, ET, and PD supervised data collection. All authors wrote the review. All authors contributed to the article and approved the submitted version.

Funding

The research leading to these results has received funding from AIRC under IG 2017 – ID. 20107 project and IG 2022 - ID. 27353 project – P.I. PD. This work was also supported by: Fondazione CRT 2020.1798, RILO University of Torino (IG 11904, IG 15538), Ministero della Salute (RF-2021-12371961) to PD, and PNRR M4C2-Investimento 1.4-CN00000041 "Finanziato dall'Unione Europea-NextGenerationEU" to PD and DT.

Conflict of interest

The authors declare that the research was conducted in the absence of any commercial or financial relationships that could be construed as a potential conflict of interest.

Publisher's note

References

1. Siegel RL, Miller KD, Fuchs HE, Jemal A. Cancer statistics, 2022. *CA Cancer J Clin* (2022) 72(1):7–33. doi: 10.3322/caac.21708

2. Giraldo NA, Sanchez-Salas R, Peske JD, Vano Y, Becht E, Petitprez F, et al. The clinical role of the TME in solid cancer. *Br J Cancer* (2019) 120(1):45–53. doi: 10.1038/s41416-018-0327-z

3. Salemme V, Centonze G, Cavallo F, Defilippi P, Conti L. The crosstalk between tumor cells and the immune microenvironment in breast cancer: implications for immunotherapy. *Front Oncol* (2021) 11:610303. doi: 10.3389/fonc.2021.610303

4. Cancer Genome Atlas N. Comprehensive molecular portraits of human breast tumours. *Nature* (2012) 490(7418):61–70. doi: 10.1038/nature11412

5. Ciriello G, Gatza ML, Beck AH, Wilkerson MD, Rhie SK, Pastore A, et al. Comprehensive molecular portraits of invasive lobular breast cancer. *Cell* (2015) 163(2):506–19. doi: 10.1016/j.cell.2015.09.033

6. Nik-Zainal S, Davies H, Staaf J, Ramakrishna M, Glodzik D, Zou X, et al. Landscape of somatic mutations in 560 breast cancer whole-genome sequences. *Nature* (2016) 534(7605):47–54. doi: 10.1038/nature17676

7. Banerji S, Cibulskis K, Rangel-Escareno C, Brown KK, Carter SL, Frederick AM, et al. Sequence analysis of mutations and translocations across breast cancer subtypes. *Nature* (2012) 486(7403):405–9. doi: 10.1038/nature11154

8. Mavrommati I, Johnson F, Echeverria GV, Natrajan R. Subclonal heterogeneity and evolution in breast cancer. *NPJ Breast Cancer* (2021) 7(1):155. doi: 10.1038/s41523-021-00363-0

9. Luond F, Tiede S, Christofori G. Breast cancer as an example of tumour heterogeneity and tumour cell plasticity during malignant progression. *Br J Cancer* (2021) 125(2):164–75. doi: 10.1038/s41416-021-01328-7

10. Marusyk A, Janiszewska M, Polyak K. Intratumor heterogeneity: the Rosetta stone of therapy resistance. *Cancer Cell* (2020) 37(4):471–84. doi: 10.1016/j.ccell.2020.03.007

11. Avalle L, Raggi L, Monteleone E, Savino A, Viavattene D, Statello L, et al. STAT3 induces breast cancer growth via ANGPTL4, MMP13 and STC1 secretion by cancer associated fibroblasts. *Oncogene* (2022) 41(10):1456–67. doi: 10.1038/s41388-021-02172-y

12. Koren S, Bentires-Alj M. Breast tumor heterogeneity: source of fitness, hurdle for therapy. *Mol Cell* (2015) 60(4):537–46. doi: 10.1016/j.molcel.2015.10.031

13. Stephens PJ, Tarpey PS, Davies H, Van Loo P, Greenman C, Wedge DC, et al. The landscape of cancer genes and mutational processes in breast cancer. *Nature* (2012) 486(7403):400–4. doi: 10.1038/nature11017

14. Dagogo-Jack I, Shaw AT. Tumour heterogeneity and resistance to cancer therapies. *Nat Rev Clin Oncol* (2018) 15(2):81–94. doi: 10.1038/nrclinonc.2017.166

15. McGranahan N, Swanton C. Clonal heterogeneity and tumor evolution: past, present, and the future. *Cell* (2017) 168(4):613–28. doi: 10.1016/j.cell.2017.01.018

16. Vasan N, Baselga J, Hyman DM. A view on drug resistance in cancer. *Nature* (2019) 575(7782):299–309. doi: 10.1038/s41586-019-1730-1

17. Cosentino G, Plantamura I, Tagliabue E, Iorio MV, Cataldo A. Breast cancer drug resistance: overcoming the challenge by capitalizing on MicroRNA and tumor microenvironment interplay. *Cancers (Basel)* (2021) 13(15). doi: 10.3390/cancers13153691

18. Emran TB, Shahriar A, Mahmud AR, Rahman T, Abir MH, Siddiquee MF, et al. Multidrug resistance in cancer: understanding molecular mechanisms, immunoprevention and therapeutic approaches. *Front Oncol* (2022) 12:891652. doi: 10.3389/fonc.2022.891652

19. Marine JC, Dawson SJ, Dawson MA. Non-genetic mechanisms of therapeutic resistance in cancer. *Nat Rev Cancer* (2020) 20(12):743–56. doi: 10.1038/s41568-020-00302-4

20. Sharma P, Hu-Lieskovan S, Wargo JA, Ribas A. Primary, adaptive, and acquired resistance to cancer immunotherapy. *Cell* (2017) 168(4):707–23. doi: 10.1016/j.cell.2017.01.017

21. O'Leary B, Cutts RJ, Liu Y, Hrebien S, Huang X, Fenwick K, et al. The genetic landscape and clonal evolution of breast cancer resistance to palbociclib plus fulvestrant in the PALOMA-3 trial. *Cancer Discovery* (2018) 8(11):1390–403. doi: 10.1158/2159-8290.CD-18-0264

22. Sivakumar S, Jin DX, Tukachinsky H, Murugesan K, McGregor K, Danziger N, et al. Tissue and liquid biopsy profiling reveal convergent tumor evolution and therapy evasion in breast cancer. *Nat Commun* (2022) 13(1):7495. doi: 10.1038/s41467-022-35245-x

23. Venizelos A, Engebrethsen C, Deng W, Geisler J, Geisler S, Iversen GT, et al. Clonal evolution in primary breast cancers under sequential epirubicin and docetaxel monotherapy. *Genome Med* (2022) 14(1):86. doi: 10.1186/s13073-022-01090-2

24. Mehraj U, Dar AH, Wani NA, Mir MA. Tumor microenvironment promotes breast cancer chemoresistance. *Cancer Chemother Pharmacol* (2021) 87(2):147–58. doi: 10.1007/s00280-020-04222-w

25. Ni Y, Zhou X, Yang J, Shi H, Li H, Zhao X, et al. The role of tumor-stroma interactions in drug resistance within tumor microenvironment. *Front Cell Dev Biol* (2021) 9:637675. doi: 10.3389/fcell.2021.637675

26. Xiao M, He J, Yin L, Chen X, Zu X, Shen Y. Tumor-associated macrophages: critical players in drug resistance of breast cancer. *Front Immunol* (2021) 12:799428. doi: 10.3389/fimmu.2021.799428

27. Rakha EA, Reis-Filho JS, Baehner F, Dabbs DJ, Decker T, Eusebi V, et al. Breast cancer prognostic classification in the molecular era: the role of histological grade. *Breast Cancer Res* (2010) 12(4):207. doi: 10.1186/bcr2607

28. Muller K, Jorns JM, Tozbikian G. What's new in breast pathology 2022: WHO 5th edition and biomarker updates. *J Pathol Transl Med* (2022) 56(3):170–1. doi: 10.4132/jptm.2022.04.25

29. Tan PH, Ellis I, Allison K, Brogi E, Fox SB, Lakhani S, et al. The 2019 world health organization classification of tumours of the breast. *Histopathology* (2020) 77(2):181–5. doi: 10.1111/his.14091

30. Bertos NR, Park M. Breast cancer - one term, many entities? *J Clin Invest* (2011) 121(10):3789–96. doi: 10.1172/JCI57100

31. Turashvili G, Brogi E. Tumor heterogeneity in breast cancer. *Front Med (Lausanne)* (2017) 4:227. doi: 10.3389/fmed.2017.00227

32. Perou CM, Sorlie T, Eisen MB, van de Rijn M, Jeffrey SS, Rees CA, et al. Molecular portraits of human breast tumours. *Nature* (2000) 406(6797):747–52. doi: 10.1038/35021093

33. Kim HK, Park KH, Kim Y, Park SE, Lee HS, Lim SW, et al. Discordance of the PAM50 intrinsic subtypes compared with immunohistochemistry-based surrogate in breast cancer patients: potential implication of genomic alterations of discordance. *Cancer Res Treat* (2019) 51(2):737–47. doi: 10.4143/crt.2018.342

34. Gote V, Nookala AR, Bolla PK, Pal D. Drug resistance in metastatic breast cancer: tumor targeted nanomedicine to the rescue. *Int J Mol Sci* (2021) 22(9). doi: 10.3390/ijms22094673

35. Koren S, Reavie L, Couto JP, De Silva D, Stadler MB, Roloff T, et al. PIK3CA(H1047R) induces multipotency and multi-lineage mammary tumours. *Nature* (2015) 525(7567):114–8. doi: 10.1038/nature14669

36. Liu S, Ginestier C, Charafe-Jauffret E, Foco H, Kleer CG, Merajver SD, et al. BRCA1 regulates human mammary stem/progenitor cell fate. *Proc Natl Acad Sci U S A.* (2008) 105(5):1680–5. doi: 10.1073/pnas.0711613105

37. Langley RR, Fidler IJ. The seed and soil hypothesis revisited–the role of tumor-stroma interactions in metastasis to different organs. *Int J Cancer* (2011) 128(11):2527–35. doi: 10.1002/ijc.26031

38. Polyak K. Heterogeneity in breast cancer. *J Clin Invest* (2011) 121(10):3786–8. doi: 10.1172/JCI60534

39. Shah SP, Roth A, Goya R, Oloumi A, Ha G, Zhao Y, et al. The clonal and mutational evolution spectrum of primary triple-negative breast cancers. *Nature* (2012) 486(7403):395–9. doi: 10.1038/nature10933

40. Yates LR, Gerstung M, Knappskog S, Desmedt C, Gundem G, Van Loo P, et al. Subclonal diversification of primary breast cancer revealed by multiregion sequencing. *Nat Med* (2015) 21(7):751–9. doi: 10.1038/nm.3886

41. Schiavon G, Hrebien S, Garcia-Murillas I, Cutts RJ, Pearson A, Tarazona N, et al. Analysis of ESR1 mutation in circulating tumor DNA demonstrates evolution during therapy for metastatic breast cancer. *Sci Transl Med* (2015) 7(313):313ra182. doi: 10.1126/scitranslmed.aac7551

42. Hunter KW, Amin R, Deasy S, Ha NH, Wakefield L. Genetic insights into the morass of metastatic heterogeneity. *Nat Rev Cancer* (2018) 18(4):211–23. doi: 10.1038/nrc.2017.126

43. Klein CA. Selection and adaptation during metastatic cancer progression. *Nature* (2013) 501(7467):365–72. doi: 10.1038/nature12628

44. Yates LR, Knappskog S, Wedge D, Farmery JHR, Gonzalez S, Martincorena I, et al. Genomic evolution of breast cancer metastasis and relapse. *Cancer Cell* (2017) 32(2):169–84 e7. doi: 10.1016/j.ccell.2017.07.005

45. Nguyen LV, Vanner R, Dirks P, Eaves CJ. Cancer stem cells: an evolving concept. *Nat Rev Cancer* (2012) 12(2):133–43. doi: 10.1038/nrc3184

46. Batlle E, Clevers H. Cancer stem cells revisited. *Nat Med* (2017) 23(10):1124–34. doi: 10.1038/nm.4409

47. Zomer A, Ellenbroek SI, Ritsma L, Beerling E, Vrisekoop N, Van Rheenen J. Intravital imaging of cancer stem cell plasticity in mammary tumors. *Stem Cells* (2013) 31(3):602–6. doi: 10.1002/stem.1296

48. Gupta PB, Fillmore CM, Jiang G, Shapira SD, Tao K, Kuperwasser C, et al. Stochastic state transitions give rise to phenotypic equilibrium in populations of cancer cells. *Cell* (2011) 146(4):633–44. doi: 10.1016/j.cell.2011.07.026

49. Luond F, Sugiyama N, Bill R, Bornes L, Hager C, Tang F, et al. Distinct contributions of partial and full EMT to breast cancer malignancy. *Dev Cell* (2021) 56(23):3203–21 e11. doi: 10.1016/j.devcel.2021.11.006

50. Pastushenko I, Brisebarre A, Sifrim A, Fioramonti M, Revenco T, Boumahdi S, et al. Identification of the tumour transition states occurring during EMT. *Nature* (2018) 556(7702):463–8. doi: 10.1038/s41586-018-0040-3

51. Fessler E, Dijkgraaf FE, De Sousa EMF, Medema JP. Cancer stem cell dynamics in tumor progression and metastasis: is the microenvironment to blame? *Cancer Lett* (2013) 341(1):97–104. doi: 10.1016/j.canlet.2012.10.015

52. Veglia F, Sanseviero E, Gabrilovich DI. Myeloid-derived suppressor cells in the era of increasing myeloid cell diversity. *Nat Rev Immunol* (2021) 21(8):485–98. doi: 10.1038/s41577-020-00490-y

53. DeNardo DG, Ruffell B. Macrophages as regulators of tumour immunity and immunotherapy. *Nat Rev Immunol* (2019) 19(6):369–82. doi: 10.1038/s41577-019-0127-6

54. Nagl L, Horvath L, Pircher A, Wolf D. Tumor endothelial cells (TECs) as potential immune directors of the tumor microenvironment - new findings and future perspectives. *Front Cell Dev Biol* (2020) 8:766. doi: 10.3389/fcell.2020.00766

55. Talmadge JE, Gabrilovich DI. History of myeloid-derived suppressor cells. *Nat Rev Cancer* (2013) 13(10):739–52. doi: 10.1038/nrc3581

56. Salemme V, Vedelago M, Sarcinella A, Moietta F, Piccolantonio A, Moiso E, et al. p140Cap inhibits b-catenin in the breast cancer stem cell compartment instructing a protective anti-tumor immune response. *Nat Commun* (2023).

57. Kalluri R. The biology and function of fibroblasts in cancer. *Nat Rev Cancer* (2016) 16(9):582–98. doi: 10.1038/nrc.2016.73

58. Sahai E, Astsaturov I, Cukierman E, DeNardo DG, Egeblad M, Evans RM, et al. A framework for advancing our understanding of cancer-associated fibroblasts. *Nat Rev Cancer* (2020) 20(3):174–86. doi: 10.1038/s41568-019-0238-1

59. Ozdemir BC, Pentcheva-Hoang T, Carstens JL, Zheng X, Wu CC, Simpson TR, et al. Depletion of carcinoma-associated fibroblasts and fibrosis induces immunosuppression and accelerates pancreas cancer with reduced survival. *Cancer Cell* (2014) 25(6):719–34. doi: 10.1016/j.ccr.2014.04.005

60. Rhim AD, Oberstein PE, Thomas DH, Mirek ET, Palermo CF, Sastra SA, et al. Stromal elements act to restrain, rather than support, pancreatic ductal adenocarcinoma. *Cancer Cell* (2014) 25(6):735–47. doi: 10.1016/j.ccr.2014.04.021

61. Shree T, Olson OC, Elie BT, Kester JC, Garfall AL, Simpson K, et al. Macrophages and cathepsin proteases blunt chemotherapeutic response in breast cancer. *Genes Dev* (2011) 25(23):2465–79. doi: 10.1101/gad.180331.111

62. Xu X, Ye J, Huang C, Yan Y, Li J. M2 macrophage-derived IL6 mediates resistance of breast cancer cells to hedgehog inhibition. *Toxicol Appl Pharmacol* (2019) 364:77–82. doi: 10.1016/j.taap.2018.12.013

63. Yang C, He L, He P, Liu Y, Wang W, He Y, et al. Increased drug resistance in breast cancer by tumor-associated macrophages through IL-10/STAT3/bcl-2 signaling pathway. *Med Oncol* (2015) 32(2):352. doi: 10.1007/s12032-014-0352-6

64. Li D, Ji H, Niu X, Yin L, Wang Y, Gu Y, et al. Tumor-associated macrophages secrete CC-chemokine ligand 2 and induce tamoxifen resistance by activating PI3K/Akt/mTOR in breast cancer. *Cancer Sci* (2020) 111(1):47–58. doi: 10.1111/cas.14230

65. Niu X, Ma J, Li J, Gu Y, Yin L, Wang Y, et al. Sodium/glucose cotransporter 1-dependent metabolic alterations induce tamoxifen resistance in breast cancer by promoting macrophage M2 polarization. *Cell Death Dis* (2021) 12(6):509. doi: 10.1038/s41419-021-03781-x

66. Gingras S, Moriggl R, Groner B, Simard J. Induction of 3beta-hydroxysteroid dehydrogenase/delta5-delta4 isomerase type 1 gene transcription in human breast cancer cell lines and in normal mammary epithelial cells by interleukin-4 and interleukin-13. *Mol Endocrinol* (1999) 13(1):66–81. doi: 10.1210/mend.13.1.0221

67. Purohit A, Singh A, Ghilchik MW, Reed MJ. Inhibition of tumor necrosis factor alpha-stimulated aromatase activity by microtubule-stabilizing agents, paclitaxel and 2-methoxyestradiol. *Biochem Biophys Res Commun* (1999) 261(1):214–7. doi: 10.1006/bbrc.1999.1010

68. Purohit A, Singh A, Ghilchik MW, Serlupi-Crescenzi O, Reed MJ. Inhibition of IL-6+IL-6 soluble receptor-stimulated aromatase activity by the IL-6 antagonist, sant 7, in breast tissue-derived fibroblasts. *Br J Cancer* (2003) 88(4):630–5. doi: 10.1038/sj.bjc.6600785

69. Emami F, Pathak S, Nguyen TT, Shrestha P, Maharjan S, Kim JO, et al. Photoimmunotherapy with cetuximab-conjugated gold nanorods reduces drug resistance in triple negative breast cancer spheroids with enhanced infiltration of tumor-associated macrophages. *J Control Release* (2021) 329:645–64. doi: 10.1016/j.jconrel.2020.10.001

70. Walker ND, Elias M, Guiro K, Bhatia R, Greco SJ, Bryan M, et al. Exosomes from differentially activated macrophages influence dormancy or resurgence of breast cancer cells within bone marrow stroma. *Cell Death Dis* (2019) 10(2):59. doi: 10.1038/s41419-019-1304-z

71. Ahmed S, Mohamed HT, El-Husseiny N, El Mahdy MM, Safwat G, Diab AA, et al. IL-8 secreted by tumor associated macrophages contribute to lapatinib resistance in HER2-positive locally advanced breast cancer via activation of Src/STAT3/ERK1/2-mediated EGFR signaling. *Biochim Biophys Acta Mol Cell Res* (2021) 1868(6):118995. doi: 10.1016/j.bbamcr.2021.118995

72. Hu X, Liu Y, Zhang X, Kong D, Kong J, Zhao D, et al. The anti-B7-H4 checkpoint synergizes trastuzumab treatment to promote phagocytosis and eradicate breast cancer. *Neoplasia* (2020) 22(11):539–53. doi: 10.1016/j.neo.2020.08.007

73. Ekiz HA, Lai SA, Gundlapalli H, Haroun F, Williams MA, Welm AL. Inhibition of RON kinase potentiates anti-CTLA-4 immunotherapy to shrink breast tumors and prevent metastatic outgrowth. *Oncoimmunology* (2018) 7(9):e1480286. doi: 10.1080/2162402X.2018.1480286

74. Veglia F, Perego M, Gabrilovich D. Myeloid-derived suppressor cells coming of age. *Nat Immunol* (2018) 19(2):108–19. doi: 10.1038/s41590-017-0022-x

75. Costa A, Kieffer Y, Scholer-Dahirel A, Pelon F, Bourachot B, Cardon M, et al. Fibroblast heterogeneity and immunosuppressive environment in human breast cancer. *Cancer Cell* (2018) 33(3):463–79 e10. doi: 10.1016/j.ccell.2018.01.011

76. Houthuijzen JM, de Bruijn R, van der Burg E, Drenth AP, Wientjens E, Filipovic T, et al. CD26-negative and CD26-positive tissue-resident fibroblasts contribute to functionally distinct CAF subpopulations in breast cancer. *Nat Commun* (2023) 14(1):183. doi: 10.1038/s41467-023-35793-w

77. Bauer M, Su G, Casper C, He R, Rehrauer W, Friedl A. Heterogeneity of gene expression in stromal fibroblasts of human breast carcinomas and normal breast. *Oncogene* (2010) 29(12):1732–40. doi: 10.1038/onc.2009.463

78. Finak G, Bertos N, Pepin F, Sadekova S, Souleimanova M, Zhao H, et al. Stromal gene expression predicts clinical outcome in breast cancer. *Nat Med* (2008) 14(5):518–27. doi: 10.1038/nm1764

79. Liu L, Liu L, Yao HH, Zhu ZQ, Ning ZL, Huang Q. Stromal myofibroblasts are associated with poor prognosis in solid cancers: a meta-analysis of published studies. *PloS One* (2016) 11(7):e0159947. doi: 10.1371/journal.pone.0159947

80. Yamashita M, Ogawa T, Zhang X, Hanamura N, Kashikura Y, Takamura M, et al. Role of stromal myofibroblasts in invasive breast cancer: stromal expression of alpha-smooth muscle actin correlates with worse clinical outcome. *Breast Cancer* (2012) 19(2):170–6. doi: 10.1007/s12282-010-0234-5

81. Gomez-Cuadrado L, Bullock E, Mabruk Z, Zhao H, Souleimanova M, Noer PR, et al. Characterisation of the stromal microenvironment in lobular breast cancer. *Cancers (Basel)* (2022) 14(4). doi: 10.3390/cancers14040904

82. Farmer P, Bonnefoi H, Anderle P, Cameron D, Wirapati P, Becette V, et al. A stroma-related gene signature predicts resistance to neoadjuvant chemotherapy in breast cancer.. *Nature medicine* (2009) 15(1):68–74. doi: 10.1038/nm.1908

83. Bhattacharya S, Mohanty A, Achuthan S, Kotnala S, Jolly MK, Kulkarni P, et al. Group behavior and emergence of cancer drug resistance. *Trends Cancer* (2021) 7(4):323–34. doi: 10.1016/j.trecan.2021.01.009

84. Hirata E, Girotti MR, Viros A, Hooper S, Spencer-Dene B, Matsuda M, et al. Intravital imaging reveals how BRAF inhibition generates drug-tolerant microenvironments with high integrin beta1/FAK signaling. *Cancer Cell* (2015) 27(4):574–88. doi: 10.1016/j.ccell.2015.03.008

85. Marusyk A, Tabassum DP, Janiszewska M, Place AE, Trinh A, Rozhok AI, et al. Spatial proximity to fibroblasts impacts molecular features and therapeutic sensitivity of breast cancer cells influencing clinical outcomes. *Cancer Res* (2016) 76(22):6495–506. doi: 10.1158/0008-5472.CAN-16-1457

86. Watson SS, Dane M, Chin K, Tatarova Z, Liu M, Liby T, et al. Microenvironment-mediated mechanisms of resistance to HER2 inhibitors differ between HER2+ breast cancer subtypes. *Cell Syst* (2018) 6(3):329–42 e6. doi: 10.1016/j.cels.2018.02.001

87. Boelens MC, Wu TJ, Nabet BY, Xu B, Qiu Y, Yoon T, et al. Exosome transfer from stromal to breast cancer cells regulates therapy resistance pathways. *Cell* (2014) 159(3):499–513. doi: 10.1016/j.cell.2014.09.051

88. Su S, Chen J, Yao H, Liu J, Yu S, Lao L, et al. CD10(+)GPR77(+) cancer-associated fibroblasts promote cancer formation and chemoresistance by sustaining cancer stemness. *Cell* (2018) 172(4):841–56 e16. doi: 10.1016/j.cell.2018.01.009

89. Dittmer J, Leyh B. The impact of tumor stroma on drug response in breast cancer. *Semin Cancer Biol* (2015) 31:3–15. doi: 10.1016/j.semcancer.2014.05.006

90. Cazet AS, Hui MN, Elsworth BL, Wu SZ, Roden D, Chan CL, et al. Targeting stromal remodeling and cancer stem cell plasticity overcomes chemoresistance in triple negative breast cancer. *Nat Commun* (2018) 9(1):2897. doi: 10.1038/s41467-018-05220-6

91. Barcus CE, O'Leary KA, Brockman JL, Rugowski DE, Liu Y, Garcia N, et al. Elevated collagen-I augments tumor progressive signals, intravasation and metastasis of prolactin-induced estrogen receptor alpha positive mammary tumor cells. *Breast Cancer Res* (2017) 19(1):9. doi: 10.1186/s13058-017-0801-1

92. Boyle ST, Poltavets V, Kular J, Pyne NT, Sandow JJ, Lewis AC, et al. Publisher correction: ROCK-mediated selective activation of PERK signalling causes fibroblast reprogramming and tumour progression through a CRELD2-dependent mechanism. *Nat Cell Biol* (2020) 22(7):908. doi: 10.1038/s41556-020-0539-3

93. Araujo AM, Abaurrea A, Azcoaga P, Lopez-Velazco JI, Manzano S, Rodriguez J, et al. Stromal oncostatin m cytokine promotes breast cancer progression by reprogramming the tumor microenvironment. *J Clin Invest* (2022) 132(7):320-322. doi: 10.1172/JCI148667

94. Wen S, Hou Y, Fu L, Xi L, Yang D, Zhao M, et al. Cancer-associated fibroblast (CAF)-derived IL32 promotes breast cancer cell invasion and metastasis via integrin beta3-p38 MAPK signalling. *Cancer Lett* (2019) 442:320–32. doi: 10.1016/j.canlet.2018.10.015

95. Nguyen M, De Ninno A, Mencattini A, Mermet-Meillon F, Fornabaio G, Evans SS, et al. Dissecting effects of anti-cancer drugs and cancer-associated fibroblasts by on-chip reconstitution of immunocompetent tumor microenvironments. *Cell Rep* (2018) 25(13):3884–93 e3. doi: 10.1016/j.celrep.2018.12.015

96. Rivas EI, Linares J, Zwick M, Gomez-Llonin A, Guiu M, Labernadie A, et al. Targeted immunotherapy against distinct cancer-associated fibroblasts overcomes treatment resistance in refractory HER2+ breast tumors. *Nat Commun* (2022) 13(1):5310. doi: 10.1038/s41467-022-32782-3

97. Liu X, Lu Y, Huang J, Xing Y, Dai H, Zhu L, et al. CD16(+) fibroblasts foster a trastuzumab-refractory microenvironment that is reversed by VAV2 inhibition. *Cancer Cell* (2022) 40(11):1341–57 e13. doi: 10.1016/j.ccell.2022.10.015

98. Bovy N, Blomme B, Freres P, Dederen S, Nivelles O, Lion M, et al. Endothelial exosomes contribute to the antitumor response during breast cancer neoadjuvant chemotherapy via microRNA transfer. *Oncotarget* (2015) 6(12):10253–66. doi: 10.18632/oncotarget.3520

99. Acharyya S, Oskarsson T, Vanharanta S, Malladi S, Kim J, Morris PG, et al. A CXCL1 paracrine network links cancer chemoresistance and metastasis. *Cell* (2012) 150 (1):165–78. doi: 10.1016/j.cell.2012.04.042

100. Ghiabi P, Jiang J, Pasquier J, Maleki M, Abu-Kaoud N, Rafii S, et al. Endothelial cells provide a notch-dependent pro-tumoral niche for enhancing breast cancer survival, stemness and pro-metastatic properties. *PloS One* (2014) 9(11):e112424. doi: 10.1371/journal.pone.0112424

101. Duru G, van Egmond M, Heemskerk N. A window of opportunity: targeting cancer endothelium to enhance immunotherapy. *Front Immunol* (2020) 11:584723. doi: 10.3389/fimmu.2020.584723

102. Zhong W, Myers JS, Wang F, Wang K, Lucas J, Rosfjord E, et al. Comparison of the molecular and cellular phenotypes of common mouse syngeneic models with human tumors. *BMC Genomics* (2020) 21(1):2. doi: 10.1186/s12864-019-6344-3

103. Lipinski KA, Barber LJ, Davies MN, Ashenden M, Sottoriva A, Gerlinger M. Cancer evolution and the limits of predictability in precision cancer medicine. *Trends Cancer* (2016) 2(1):49–63. doi: 10.1016/j.trecan.2015.11.003

104. Lal JC, Townsend MG, Mehta AK, Oliwa M, Miller E, Sotayo A, et al. Comparing syngeneic and autochthonous models of breast cancer to identify tumor immune components that correlate with response to immunotherapy in breast cancer. *Breast Cancer Res* (2021) 23(1):83. doi: 10.1186/s13058-021-01448-1

105. Holen I, Speirs V, Morrissey B, Blyth K. *In vivo* models in breast cancer research: progress, challenges and future directions. *Dis Model Mech* (2017) 10(4):359–71. doi: 10.1242/dmm.028274

106. Guy CT, Cardiff RD, Muller WJ. Induction of mammary tumors by expression of polyomavirus middle T oncogene: a transgenic mouse model for metastatic disease. *Mol Cell Biol* (1992) 12(3):954–61. doi: 10.1128/mcb.12.3.954-961.1992

107. Lifsted T, Le Voyer T, Williams M, Muller W, Klein-Szanto A, Buetow KH, et al. Identification of inbred mouse strains harboring genetic modifiers of mammary tumor age of onset and metastatic progression. *Int J Cancer* (1998) 77(4):640–4. doi: 10.1002/(SICI)1097-0215(19980812)77:4<640::AID-IJC26>3.0.CO;2-8

108. Pfefferle AD, Herschkowitz JI, Usary J, Harrell JC, Spike BT, Adams JR, et al. Transcriptomic classification of genetically engineered mouse models of breast cancer identifies human subtype counterparts. *Genome Biol* (2013) 14(11):R125. doi: 10.1186/gb-2013-14-11-r125

109. Attalla S, Taifour T, Bui T, Muller W. Insights from transgenic mouse models of PyMT-induced breast cancer: recapitulating human breast cancer progression in vivo.. *Oncogene* (2021) 40(3):475–91. doi: 10.1038/s41388-020-01560-0

110. Kubli SP, Bassi C, Roux C, Wakeham A, Gobl C, Zhou W, et al. AhR controls redox homeostasis and shapes the tumor microenvironment in BRCA1-associated breast cancer. *Proc Natl Acad Sci U S A.* (2019) 116(9):3604–13. doi: 10.1073/pnas.1815126116

111. Roux C, Jafari SM, Shinde R, Duncan G, Cescon DW, Silvester J, et al. Reactive oxygen species modulate macrophage immunosuppressive phenotype through the up-regulation of PD-L1. *Proc Natl Acad Sci U S A.* (2019) 116(10):4326–35. doi: 10.1073/pnas.1819473116

112. Cassidy JW, Caldas C, Bruna A. Maintaining tumor heterogeneity in patient-derived tumor xenografts. *Cancer Res* (2015) 75(15):2963–8. doi: 10.1158/0008-5472.CAN-15-0727

113. Izumchenko E, Paz K, Ciznadija D, Sloma I, Katz A, Vasquez-Dunddel D, et al. Patient-derived xenografts effectively capture responses to oncology therapy in a heterogeneous cohort of patients with solid tumors. *Ann Oncol* (2017) 28(10):2595–605. doi: 10.1093/annonc/mdx416

114. Woo XY, Giordano J, Srivastava A, Zhao ZM, Lloyd MW, de Bruijn R, et al. Conservation of copy number profiles during engraftment and passaging of patient-derived cancer xenografts. *Nat Genet* (2021) 53(1):86–99. doi: 10.1038/s41588-020-00750-6

115. Dobrolecki LE, Airhart SD, Alferez DG, Aparicio S, Behbod F, Bentires-Alj M, et al. Patient-derived xenograft (PDX) models in basic and translational breast cancer research. *Cancer Metastasis Rev* (2016) 35(4):547–73. doi: 10.1007/s10555-016-9653-x

116. Kabos P, Finlay-Schultz J, Li C, Kline E, Finlayson C, Wisell J, et al. Patient-derived luminal breast cancer xenografts retain hormone receptor heterogeneity and help define unique estrogen-dependent gene signatures. *Breast Cancer Res Treat* (2012) 135(2):415–32. doi: 10.1007/s10549-012-2164-8

117. Li S, Shen D, Shao J, Crowder R, Liu W, Prat A, et al. Endocrine-therapy-resistant ESR1 variants revealed by genomic characterization of breast-cancer-derived xenografts. *Cell Rep* (2013) 4(6):1116–30. doi: 10.1016/j.celrep.2013.08.022

118. Veyssiere H, Passildas J, Ginzac A, Lusho S, Bidet Y, Molnar I, et al. XENOBREAST trial: a prospective study of xenografts establishment from surgical specimens of patients with triple negative or luminal b breast cancer. *F1000Res* (2020) 9:1219. doi: 10.12688/f1000research.26873.1

119. Zhang X, Claerhout S, Prat A, Dobrolecki LE, Petrovic I, Lai Q, et al. A renewable tissue resource of phenotypically stable, biologically and ethnically diverse, patient-derived human breast cancer xenograft models. *Cancer Res* (2013) 73 (15):4885–97. doi: 10.1158/0008-5472.CAN-12-4081

120. Guillen KP, Fujita M, Butterfield AJ, Scherer SD, Bailey MH, Chu Z, et al. A human breast cancer-derived xenograft and organoid platform for drug discovery and precision oncology. *Nat Cancer* (2022) 3(2):232–50. doi: 10.1038/s43018-022-00337-6

121. Yin L, Wang XJ, Chen DX, Liu XN, Wang XJ. Humanized mouse model: a review on preclinical applications for cancer immunotherapy. *Am J Cancer Res* (2020) 10(12):4568–84.

122. Jin KT, Du WL, Lan HR, Liu YY, Mao CS, Du JL, et al. Development of humanized mouse with patient-derived xenografts for cancer immunotherapy studies: a comprehensive review. *Cancer Sci* (2021) 112(7):2592–606. doi: 10.1111/cas.14934

123. Tary-Lehmann M, Lehmann PV, Schols D, Roncarolo MG, Saxon A. Anti-SCID mouse reactivity shapes the human CD4+ T cell repertoire in hu-PBL-SCID chimeras. *J Exp Med* (1994) 180(5):1817–27. doi: 10.1084/jem.180.5.1817

124. Iizuka A, Nonomura C, Ashizawa T, Kondou R, Ohshima K, Sugino T, et al. A T-cell-engaging B7-H4/CD3-bispecific fab-scFv antibody targets human breast cancer. *Clin Cancer Res* (2019) 25(9):2925–34. doi: 10.1158/1078-0432.CCR-17-3123

125. Park N, Pandey K, Chang SK, Kwon AY, Cho YB, Hur J, et al. Preclinical platform for long-term evaluation of immuno-oncology drugs using hCD34+ humanized mouse model. (2020) 8(2):e001513. doi: 10.1136/jitc-2020-001513

126. Scherer SD, Riggio AI, Haroun F, DeRose YS, Ekiz HA, Fujita M, et al. An immune-humanized patient-derived xenograft model of estrogen-independent, hormone receptor positive metastatic breast cancer. *Breast Cancer Res* (2021) 23 (1):100. doi: 10.1186/s13058-021-01476-x

127. Wang M, Yao LC, Cheng M, Cai D, Martinek J, Pan CX, et al. Humanized mice in studying efficacy and mechanisms of PD-1-targeted cancer immunotherapy. *FASEB J* (2018) 32(3):1537–49. doi: 10.1096/fj.201700740R

128. Li Z, McGinn O, Wu Y, Bahreini A, Priedigkeit NM, Ding K, et al. ESR1 mutant breast cancers show elevated basal cytokeratins and immune activation. *Nat Commun* (2022) 13(1):2011. doi: 10.1038/s41467-022-29498-9

129. Moquin-Beaudry G, Benabdallah B, Maggiorani D, Le O, Li Y, Colas C, et al. Autologous humanized mouse models of iPSC-derived tumors enable characterization and modulation of cancer-immune cell interactions. *Cell Rep Methods* (2022) 2 (1):100153. doi: 10.1016/j.crmeth.2021.100153

130. Devarasetty M, Forsythe SD, Shelkey E, Soker S. *In vitro* modeling of the tumor microenvironment in tumor organoids. *Tissue Eng Regener Med* (2020) 17(6):759–71. doi: 10.1007/s13770-020-00258-4

131. Froehlich K, Haeger JD, Heger J, Pastuschek J, Photini SM, Yan Y, et al. Generation of multicellular breast cancer tumor spheroids: comparison of different protocols. *J Mammary Gland Biol Neoplasia* (2016) 21(3-4):89–98. doi: 10.1007/s10911-016-9359-2

132. Fan Y, Kao C, Yang F, Wang F, Yin G, Wang Y, et al. Integrated multi-omics analysis model to identify biomarkers associated with prognosis of breast cancer. *Front Oncol* (2022) 12:899900. doi: 10.3389/fonc.2022.899900

133. Ham SL, Thakuri PS, Plaster M, Li J, Luker KE, Luker GD, et al. Three-dimensional tumor model mimics stromal - breast cancer cells signaling. *Oncotarget* (2018) 9(1):249–67. doi: 10.18632/oncotarget.22922

134. Wang Y, Shi W, Kuss M, Mirza S, Qi D, Krasnoslobodtsev A, et al. 3D bioprinting of breast cancer models for drug resistance study. *ACS Biomater Sci Eng* (2018) 4(12):4401–11. doi: 10.1021/acsbiomaterials.8b01277

135. Drost J, Clevers H. Organoids in cancer research. *Nat Rev Cancer* (2018) 18 (7):407–18. doi: 10.1038/s41568-018-0007-6

136. Bleijs M, van de Wetering M, Clevers H, Drost J. Xenograft and organoid model systems in cancer research. *EMBO J* (2019) 38(15):e101654. doi: 10.15252/embj.2019101654

137. Campaner E, Zannini A, Santorsola M, Bonazza D, Bottin C, Cancila V, et al. Breast cancer organoids model patient-specific response to drug treatment *(Basel)* (2020) 12(12). doi: 10.3390/cancers12123869

138. Sachs N, de Ligt J, Kopper O, Gogola E, Bounova G, Weeber F, et al. A living biobank of breast cancer organoids captures disease heterogeneity. *Cell* (2018) 172(1-2):373–86:e10. doi: 10.1016/j.cell.2017.11.010

139. Clinton J, McWilliams-Koeppen P. Initiation, expansion, and cryopreservation of human primary tissue-derived normal and diseased organoids in embedded three-dimensional culture. *Curr Protoc Cell Biol* (2019) 82(1):e66. doi: 10.1002/cpcb.66

140. Yuki K, Cheng N, Nakano M, Kuo CJ. Organoid models of tumor immunology. *Trends Immunol* (2020) 41(8):652–64. doi: 10.1016/j.it.2020.06.010

141. Langhans SA. Three-dimensional in vitro cell culture models in drug discovery and drug repositioning. *Front Pharmacol* (2018) 9:6. doi: 10.3389/fphar.2018.00006

142. Leiva MC, Garre E, Gustafsson A, Svanstrom A, Bogestal Y, Hakansson J, et al. Breast cancer patient-derived scaffolds as a tool to monitor chemotherapy responses in human tumor microenvironments. *J Cell Physiol* (2021) 236(6):4709–24. doi: 10.1002/jcp.30191

143. Landberg G, Fitzpatrick P, Isakson P, Jonasson E, Karlsson J, Larsson E, et al. Patient-derived scaffolds uncover breast cancer promoting properties of the microenvironment. *Biomaterials* (2020) 235:119705. doi: 10.1016/j.biomaterials.2019.119705

144. Smith R, Devlin K, Kilburn D, Gross S, Sudar D, Bucher E, et al. Using microarrays to interrogate microenvironmental impact on cellular phenotypes in cancer. *J Vis Exp* (2019) 147). doi: 10.3791/58957

145. Frankman ZD, Jiang L, Schroeder JA, Zohar Y. Application of microfluidic systems for breast cancer research. *Micromachines (Basel)* (2022) 13(2). doi: 10.3390/mi13020152

146. Aung A, Kumar V, Theprungsirikul J, Davey SK, Varghese S. An engineered tumor-on-a-Chip device with breast cancer-immune cell interactions for assessing T-cell recruitment. *Cancer Res* (2020) 80(2):263–75. doi: 10.1158/0008-5472.CAN-19-0342

147. Curtis C, Shah SP, Chin SF, Turashvili G, Rueda OM, Dunning MJ, et al. The genomic and transcriptomic architecture of 2,000 breast tumours reveals novel subgroups. *Nature* (2012) 486(7403):346–52. doi: 10.1038/nature10983

148. Mootha VK, Lindgren CM, Eriksson KF, Subramanian A, Sihag S, Lehar J, et al. PGC-1alpha-responsive genes involved in oxidative phosphorylation are coordinately downregulated in human diabetes. *Nat Genet* (2003) 34(3):267–73. doi: 10.1038/ng1180

149. Subramanian A, Tamayo P, Mootha VK, Mukherjee S, Ebert BL, Gillette MA, et al. Gene set enrichment analysis: a knowledge-based approach for interpreting genome-wide expression profiles. *Proc Natl Acad Sci U S A.* (2005) 102(43):15545–50. doi: 10.1073/pnas.0506580102

150. Savino A, De Marzo N, Provero P, Poli V. Meta-analysis of microdissected breast tumors reveals genes regulated in the stroma but hidden in bulk analysis. *Cancers (Basel)* (2021) 13(13). doi: 10.3390/cancers13133371

151. Danenberg E, Bardwell H, Zanotelli VRT, Provenzano E, Chin SF, Rueda OM, et al. Breast tumor microenvironment structures are associated with genomic features and clinical outcome. *Nat Genet* (2022) 54(5):660–9. doi: 10.1038/s41588-022-01041-y

152. Derakhshan F, Reis-Filho JS. Pathogenesis of triple-negative breast cancer. *Annu Rev Pathol* (2022) 17:181–204. doi: 10.1146/annurev-pathol-042420-093238

153. Jovic D, Liang X, Zeng H, Lin L, Xu F, Luo Y. Single-cell RNA sequencing technologies and applications: a brief overview. *Clin Transl Med* (2022) 12(3):e694. doi: 10.1002/ctm2.694

154. Ziegenhain C, Vieth B, Parekh S, Reinius B, Guillaumet-Adkins A, Smets M, et al. Comparative analysis of single-cell RNA sequencing methods. *Mol Cell* (2017) 65(4):631–43 e4. doi: 10.1016/j.molcel.2017.01.023

155. Guo T, Li W, Cai X. Applications of single-cell omics to dissect tumor microenvironment. *Front Genet* (2020) 11:548719. doi: 10.3389/fgene.2020.548719

156. Binnewies M, Roberts EW, Kersten K, Chan V, Fearon DF, Merad M, et al. Understanding the tumor immune microenvironment (TIME) for effective therapy. *Nat Med* (2018) 24(5):541–50. doi: 10.1038/s41591-018-0014-x

157. Gambardella G, Viscido G, Tumaini B, Isacchi A, Bosotti R, di Bernardo D. A single-cell analysis of breast cancer cell lines to study tumour heterogeneity and drug response. *Nat Commun* (2022) 13(1):1714. doi: 10.1038/s41467-022-29358-6

158. Van Oekelen O, Lagana A. Multi-omics profiling of the tumor microenvironment. *Adv Exp Med Biol* (2022) 1361:283–326. doi: 10.1007/978-3-030-91836-1_16

159. Xie J, Zhang J, Tian W, Zou Y, Tang Y, Zheng S, et al. The pan-cancer multi-omics landscape of FOXO family relevant to clinical outcome and drug resistance. *Int J Mol Sci* (2022) 23(24). doi: 10.3390/ijms232415647

160. Hsieh WC, Budiarto BR, Wang YF, Lin CY, Gwo MC, So DK, et al. Spatial multi-omics analyses of the tumor immune microenvironment. *J BioMed Sci* (2022) 29(1):96. doi: 10.1186/s12929-022-00879-y

161. Wang N, Li X, Wang R, Ding Z. Spatial transcriptomics and proteomics technologies for deconvoluting the tumor microenvironment. *Biotechnol J* (2021) 16(9):e2100041. doi: 10.1002/biot.202100041

162. Zheng B, Fang L. Spatially resolved transcriptomics provide a new method for cancer research. *J Exp Clin Cancer Res* (2022) 41(1):179. doi: 10.1186/s13046-022-02385-3

163. Hill TG. Mohs' technique for recurrent basal cell cancers of the face. *Plast Reconstr Surg* (1986) 77(3):501–2. doi: 10.1097/00006534-198603000-00046

164. Tzoras E, Zerdes I, Tsiknakis N, Manikis GC, Mezheyeuski A, Bergh J, et al. Dissecting tumor-immune microenvironment in breast cancer at a spatial and multiplex resolution. *Cancers (Basel)* (2022) 14(8). doi: 10.3390/cancers14081999

165. Liu SQ, Gao ZJ, Wu J, Zheng HM, Li B, Sun S, et al. Single-cell and spatially resolved analysis uncovers cell heterogeneity of breast cancer. *J Hematol Oncol* (2022) 15(1):19. doi: 10.1186/s13045-022-01236-0

166. Wu SZ, Al-Eryani G, Roden DL, Junankar S, Harvey K, Andersson A, et al. A single-cell and spatially resolved atlas of human breast cancers. *Nat Genet* (2021) 53(9):1334–47. doi: 10.1038/s41588-021-00911-1

167. Bartoschek M, Oskolkov N, Bocci M, Lovrot J, Larsson C, Sommarin M, et al. Spatially and functionally distinct subclasses of breast cancer-associated fibroblasts revealed by single cell RNA sequencing. *Nat Commun* (2018) 9(1):5150. doi: 10.1038/s41467-018-07582-3

168. Massa D, Tosi A, Rosato A, Guarneri V, Dieci MV. Multiplexed in situ spatial protein profiling in the pursuit of precision immuno-oncology for patients with breast cancer. *Cancers (Basel)* (2022) 14(19). doi: 10.3390/cancers14194885

169. Tietscher S, Wagner J, Anzeneder T, Langwieder C, Rees M, Sobottka B, et al. A comprehensive single-cell map of T cell exhaustion-associated immune environments in human breast cancer. *Nat Commun* (2023) 14(1):98. doi: 10.1038/s41467-022-35238-w

170. Kulasinghe A, Monkman J, Shah ET, Matigian N, Adams MN, O'Byrne K. Spatial profiling identifies prognostic features of response to adjuvant therapy in triple negative breast cancer (TNBC). *Front Oncol* (2021) 11:798296. doi: 10.3389/fonc.2021.798296

171. Lewis SM, Asselin-Labat ML, Nguyen Q, Berthelet J, Tan X, Wimmer VC, et al. Spatial omics and multiplexed imaging to explore cancer biology. *Nat Methods* (2021) 18(9):997–1012. doi: 10.1038/s41592-021-01203-6

172. Guo X, Song Y, Liu S, Gao M, Qi Y, Shang X. Linking genotype to phenotype in multi-omics data of small sample. *BMC Genomics* (2021) 22(1):537. doi: 10.1186/s12864-021-07867-w

173. Krassowski M, Das V, Sahu SK, Misra BB. State of the field in multi-omics research: from computational needs to data mining and sharing. *Front Genet* (2020) 11:610798. doi: 10.3389/fgene.2020.610798

174. Xie B, Yuan Z, Yang Y, Sun Z, Zhou S, Fang X. MOBCdb: a comprehensive database integrating multi-omics data on breast cancer for precision medicine. *Breast Cancer Res Treat* (2018) 169(3):625–32. doi: 10.1007/s10549-018-4708-z

175. Nguyen QH, Nguyen H, Nguyen T, Le DH. Multi-omics analysis detects novel prognostic subgroups of breast cancer. *Front Genet* (2020) 11:574661. doi: 10.3389/fgene.2020.574661

176. Gao R, Bai S, Henderson YC, Lin Y, Schalck A, Yan Y, et al. Delineating copy number and clonal substructure in human tumors from single-cell transcriptomes. *Nat Biotechnol* (2021) 39(5):599–608. doi: 10.1038/s41587-020-00795-2

177. Buenrostro JD, Corces MR, Lareau CA, Wu B, Schep AN, Aryee MJ, et al. Integrated single-cell analysis maps the continuous regulatory landscape of human hematopoietic differentiation. *Cell* (2018) 173(6):1535–48 e16. doi: 10.1016/j.cell.2018.03.074

178. Giladi A, Cohen M, Medaglia C, Baran Y, Li B, Zada M, et al. Dissecting cellular crosstalk by sequencing physically interacting cells. *Nat Biotechnol* (2020) 38(5):629–37. doi: 10.1038/s41587-020-0442-2

179. Kumar MP, Du J, Lagoudas G, Jiao Y, Sawyer A, Drummond DC, et al. Analysis of single-cell RNA-seq identifies cell-cell communication associated with tumor characteristics. *Cell Rep* (2018) 25(6):1458–68 e4. doi: 10.1016/j.celrep.2018.10.047

180. Ebinger S, Ozdemir EZ, Ziegenhain C, Tiedt S, Castro Alves C, Grunert M, et al. Characterization of rare, dormant, and therapy-resistant cells in acute lymphoblastic leukemia. *Cancer Cell* (2016) 30(6):849–62. doi: 10.1016/j.ccell.2016.11.002

181. Van Egeren D, Escabi J, Nguyen M, Liu S, Reilly CR, Patel S, et al. Reconstructing the lineage histories and differentiation trajectories of individual cancer cells in myeloproliferative neoplasms. *Cell Stem Cell* (2021) 28(3):514–23 e9. doi: 10.1016/j.stem.2021.02.001

182. Tan Z, Kan C, Sun M, Yang F, Wong M, Wang S, et al. Mapping breast cancer microenvironment through single-cell omics. *Front Immunol* (2022) 13:868813. doi: 10.3389/fimmu.2022.868813

183. Kudelova E, Smolar M, Holubekova V, Hornakova A, Dvorska D, Lucansky V, et al. Genetic heterogeneity, tumor microenvironment and immunotherapy in triple-negative breast cancer. . *Int J Mol Sci* (2022) 23(23). doi: 10.3390/ijms232314937

184. Asleh K, Riaz N, Nielsen TO. Heterogeneity of triple negative breast cancer: current advances in subtyping and treatment implications. *J Exp Clin Cancer Res* (2022) 41(1):265. doi: 10.1186/s13046-022-02476-1

185. Xiao Y, Ma D, Zhao S, Suo C, Shi J, Xue MZ, et al. Multi-omics profiling reveals distinct microenvironment characterization and suggests immune escape mechanisms of triple-negative breast cancer. *Clin Cancer Res* (2019) 25(16):5002–14. doi: 10.1158/1078-0432.CCR-18-3524

186. Sahoo S, Mishra A, Kaur H, Hari K, Muralidharan S, Mandal S, et al. A mechanistic model captures the emergence and implications of non-genetic heterogeneity and reversible drug resistance in ER+ breast cancer cells. *NAR Cancer* (2021) 3(3):zcab027. doi: 10.1093/narcan/zcab027

187. Watanabe K, Panchy N, Noguchi S, Suzuki H, Hong T. Combinatorial perturbation analysis reveals divergent regulations of mesenchymal genes during epithelial-to-mesenchymal transition. *NPJ Syst Biol Appl* (2019) 5:21. doi: 10.1038/s41540-019-0097-0

188. Celia-Terrassa T, Bastian C, Liu DD, Ell B, Aiello NM, Wei Y, et al. Hysteresis control of epithelial-mesenchymal transition dynamics conveys a distinct program with enhanced metastatic ability. *Nat Commun* (2018) 9(1):5005. doi: 10.1038/s41467-018-07538-7

189. Li X, Thirumalai D. A mathematical model for phenotypic heterogeneity in breast cancer with implications for therapeutic strategies. *J R Soc Interface* (2022) 19(186):20210803. doi: 10.1098/rsif.2021.0803

190. Kourou K, Exarchos KP, Papaloukas C, Sakaloglou P, Exarchos T, Fotiadis DI. Applied machine learning in cancer research: a systematic review for patient diagnosis, classification and prognosis. *Comput Struct Biotechnol J* (2021) 19:5546–55. doi: 10.1016/j.csbj.2021.10.006

191. Sarker IH. Machine learning: algorithms, real-world applications and research directions. *SN Comput Sci* (2021) 2(3):160. doi: 10.1007/s42979-021-00592-x

192. Wilkerson MD, Hayes DN. ConsensusClusterPlus: a class discovery tool with confidence assessments and item tracking. *Bioinformatics* (2010) 26(12):1572–3. doi: 10.1093/bioinformatics/btq170

193. Liu Z, He J, Han J, Yang J, Liao W, Chen N. m6A regulators mediated methylation modification patterns and tumor microenvironment infiltration characterization in nasopharyngeal carcinoma. *Front Immunol* (2021) 12:762243. doi: 10.3389/fimmu.2021.762243

194. Monjo T, Koido M, Nagasawa S, Suzuki Y, Kamatani Y. Efficient prediction of a spatial transcriptomics profile better characterizes breast cancer tissue sections without costly experimentation. *Sci Rep* (2022) 12(1):4133. doi: 10.1038/s41598-022-07685-4

195. Mohaiminul Islam M, Huang S, Ajwad R, Chi C, Wang Y, Hu P. An integrative deep learning framework for classifying molecular subtypes of breast cancer. *Comput Struct Biotechnol J* (2020) 18:2185–99. doi: 10.1016/j.csbj.2020.08.005

196. Arjmand B, Hamidpour SK, Tayanloo-Beik A, Goodarzi P, Aghayan HR, Adibi H, et al. Machine learning: a new prospect in multi-omics data analysis of cancer. *Front Genet* (2022) 13:824451. doi: 10.3389/fgene.2022.824451

197. Nicora G, Vitali F, Dagliati A, Geifman N, Bellazzi R. Integrated multi-omics analyses in oncology: a review of machine learning methods and tools. *Front Oncol* (2020) 10:1030. doi: 10.3389/fonc.2020.01030

198. Bishara I, Chen J, Griffiths JI, Bild AH, Nath A. A machine learning framework for scRNA-seq UMI threshold optimization and accurate classification of cell types. *Front Genet* (2022) 13:982019. doi: 10.3389/fgene.2022.982019

199. Navarro-Ocon A, Blaya-Canovas JL, Lopez-Tejada A, Blancas I, Sanchez-Martin RM, Garrido MJ, et al. Nanomedicine as a promising tool to overcome immune escape in breast cancer. *Pharmaceutics* (2022) 14(3). doi: 10.3390/pharmaceutics 14030505

200. Birocchi F, Cusimano M, Rossari F, Beretta S, Rancoita PMV, Ranghetti A, et al. Targeted inducible delivery of immunoactivating cytokines reprograms glioblastoma microenvironment and inhibits growth in mouse models. *Sci Transl Med* (2022) 14(653):eabl4106. doi: 10.1126/scitranslmed.abl4106

201. Kirchhammer N, Trefny MP, Natoli M, Brucher D, Smith SN, Werner F, et al. NK cells with tissue-resident traits shape response to immunotherapy by inducing adaptive antitumor immunity. *Sci Transl Med* (2022) 14(653):eabm9043. doi: 10.1126/scitranslmed.abm9043

frontiers | Frontiers in Oncology

TYPE Mini Review
PUBLISHED 04 July 2023
DOI 10.3389/fonc.2023.1148930

OPEN ACCESS

EDITED BY
Francesca Caccuri,
University of Brescia, Italy

REVIEWED BY
Kristina Koop,
University Hospital Erlangen, Germany

*CORRESPONDENCE
Jia Ning Nicolette Yau
e0005862@u.nus.edu
Giulia Adriani
giulia_adriani@immunol.a-star.edu.sg

RECEIVED 20 January 2023
ACCEPTED 15 May 2023
PUBLISHED 04 July 2023

CITATION
Yau JNN and Adriani G (2023) Three-dimensional heterotypic colorectal cancer spheroid models for evaluation of drug response. *Front. Oncol.* 13:1148930. doi: 10.3389/fonc.2023.1148930

Three-dimensional heterotypic colorectal cancer spheroid models for evaluation of drug response

Jia Ning Nicolette Yau[1]* and Giulia Adriani[2,3]*

[1]Department of Pharmacy, Faculty of Science, National University of Singapore, Singapore, Singapore, [2]Singapore Immunology Network (SIgN), Agency for Science, Technology and Research (A*STAR), Singapore, Singapore, [3]Department of Biomedical Engineering, Faculty of Engineering, National University of Singapore, Singapore, Singapore

Colorectal cancer (CRC) is a leading cause of death worldwide. Improved preclinical tumor models are needed to make treatment screening clinically relevant and address disease mortality. Advancements in 3D cell culture have enabled a greater recapitulation of the architecture and heterogeneity of the tumor microenvironment (TME). This has enhanced their pathophysiological relevance and enabled more accurate predictions of tumor progression and drug response in patients. An increasing number of 3D CRC spheroid models include cell populations such as cancer-associated fibroblasts (CAFs), endothelial cells (ECs), immune cells, and gut bacteria to better mimic the *in vivo* regulation of signaling pathways. Furthermore, cell heterogeneity within the 3D spheroid models enables the identification of new therapeutic targets to develop alternative treatments and test TME-target therapies. In this mini review, we present the advances in mimicking tumor heterogeneity in 3D CRC spheroid models by incorporating CAFs, ECs, immune cells, and gut bacteria. We introduce how, in these models, the diverse cells influence chemoresistance and tumor progression of the CRC spheroids. We also highlight important parameters evaluated during drug screening in the CRC heterocellular spheroids.

KEYWORDS

spheroid, heterotypic 3D model, colorectal cancer, cancer associated fibroblast (CAF), endothelial cell, gut microbiota, drug screening, tumor associated macrophages (TAMs)

Introduction

Colorectal cancer (CRC) is the third most common cancer in males and the second most common cancer in females worldwide and continues to be a leading cause of death (1, 2). Reliable cancer models are imperative to advance cancer research and treatment (3). The traditional two-dimensional (2D) cell culture models have been critical in developing many first-line chemotherapeutics, such as cisplatin (4, 5). However, the limitations of 2D culture models prevent them from effectively recapitulating the physiological

characteristics of native tumors. A key limitation of 2D cultures is the change in cell morphology, signaling, and functions compared to *in vivo* conditions in response to different external stimuli from the culture substrate and the neighboring cells (5–7). Consequently, 2D tumor models often overscore the effectiveness of potential drug candidates, resulting in lower efficacy and greater toxicity than predicted when translated into *in vivo* animal models or clinical trials (8). Patient-derived tumor xenograft and *in vivo* tumor models have been important for rational drug design and predicting response and side effects of chemotherapeutic regimens (9, 10). However, animal models often show a low success rate of engraftment (11), are expensive, require a cross-species comparison, and raise ethical controversies, challenging their utilization.

The TME is a complex and dynamic environment around the tumor composed of blood vessels, fibroblasts, immune cells, mesenchymal stromal cells, extracellular matrix, and cell-secreted factors (12). The TME is now recognized as a leading player in tumor development and response to chemo and immunotherapeutic strategies (12, 13). Therefore, recapitulating *in vitro* the heterogeneous human TME by introducing its main constituents in a three-dimensional (3D) format is essential for developing preclinical models with greater clinical relevance than 2D systems.

In this scenario, 3D tumor spheroid cultures that utilize hydrogels made of natural biomaterials (e.g. collagens, fibrin, hyaluronic acid) or synthetic polymers have been gaining increasing attention to better recapitulate the structure of tissues and native tumors compared to 2D cultures (3, 7, 14, 15). The development of 3D tumor spheroid cultures has prompted a paradigm shift in cancer research toward more clinically-relevant models, further fueled by advancements in biotechnologies. For instance, improvements in sampling and storage techniques allow clinicians to culture patient-derived 3D spheroids to identify genetic markers to predict disease progression and chemoresistance (16, 17). Tissue engineering techniques, such as the synthesis of scaffolds mimicking the extracellular matrix (ECM), and advances in microfluidic devices have improved the culture of spheroids in 3D settings to take into consideration cell-ECM and cell-cell interactions leading to a greater correspondence with native tumors compared to 2D cultures (18–24).

Specifically for CRC, recent reviews of 3D spheroid models highlight the utility of spheroids for drug screening (25), nanomedicine screening (26), and biomarker discovery (27). These reviews discuss strategies for adapting spheroids of various complexities for drug screening and developing better treatment strategies. However, these reviews only partially address the significance of recapitulating the heterogeneity of the CRC TME for drug screening.

Various 3D CRC spheroid models were derived from cancer cell lines only (monoculture) and used for drug screening (28–32) with success in modeling hypoxia and necrosis associated with tumor resistance to drugs (33).

CRC patient-derived xenografts (34) and patient-derived cells (35, 36) have also been used for drug screening predicting the efficacies of chemotherapy regimens in personalized medicine, as extensively discussed in another review (37). Patient-derived spheroids enable the recapitulation of essential tumor tissue characteristics, such as the integrity of the genomic profile (38). A critical limitation of the patient-derived spheroid model remains the accessibility of the tissue and the success rate of spheroid formation. Unlike commercially available cell lines, *in vitro* cultures of patient-derived cells require skilled technical personnel for consistent cell isolation and culture conditions. Cell dissociation methods, either mechanical or enzymatic, can dramatically affect the yield and quality of the isolated cells (39). Conversely, commercially available cancer cell lines are ideal for reproducible high-yield production of 3D CRC spheroids for drug testing. 3D tumor spheroid models with an increased cellular complexity have been developed by culturing heterogeneous cell types within the spheroid, such as fibroblasts (40, 41), immune cells (42, 43), and endothelial cells (44, 45). These models aim to emulate the heterogeneity of the TME better to achieve a more significant physiological association with native tissue (Figure 1). Broadening the heterogeneity of 3D cultures is essential to drug development as cytokines released from immune cells and fibroblasts are known to modulate chemoresistance (41, 46). However, the validation of cell-line-derived heterotypic spheroids in recapitulating tumor heterogeneity as observed in patients remains challenging given the lack of a systematic comparison with patient tissues, which are not always available for research purposes.

The integration of a microfluidic device to host the 3D CRC spheroid culture in hydrogel has enabled greater control over the cellular environment during therapeutic screening for monoculture (47–49) as well as heterocellular spheroids (50, 51), including critical molecular gradients to resemble *in vivo* conditions more closely (52). CRC spheroid models are increasing their heterogeneity by incorporating elements of the gut microbiome, a unique component of the TME of CRC, which heavily influences disease progression and response to anti-tumor therapies (53, 54). Therefore, in this mini-review, we report the recent research progress towards incorporating different cell populations in 3D CRC spheroid models, namely CAFs, tumor-associated macrophages (TAMs), ECs, and gut bacterial cells to mimic the TME heterogeneity. Differently from existing reviews, we focus on the significance of the heterogeneous cell populations during drug screening to improve the prediction of tumor response to therapy.

3D CRC spheroid models with fibroblasts

Fibroblasts are the major constituents of the CRC stroma and play an essential role in tumor cell invasion and progression (55, 56). CAFs are generally characterized by an increased expression of fibroblast activation protein (FAP) and smooth muscle alpha-actin (α-SMA) (57) triggered by secreted factors from surrounding cancer cells (58). CAFs secrete soluble factors, which include cytokines, chemokines, and growth factors such as interleukin 6 (IL-6), C-type lectin domain family 3 member B (CLEC3B), C-X-C motif chemokine 12 (CXCL12), and epidermal growth factor (EGF) to transform the TME to support tumor growth (59–62). Elevated serum levels of CAF-derived soluble factors stimulate signaling

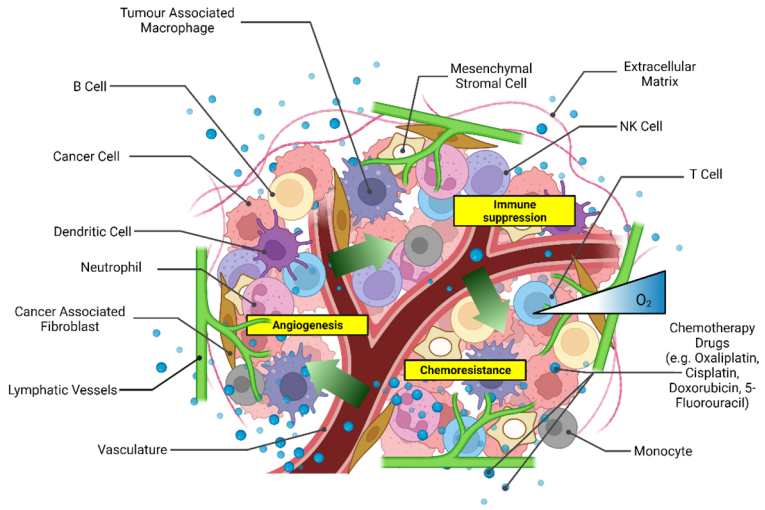

FIGURE 1
Scheme of the main components of the tumor microenvironment that could be recapitulated in heterotypic 3D CRC spheroid models for drug screening. Created with Biorender.com.

pathways that actively transform the TME to promote tumor metastasis and survival (63). For instance, the Wnt2 secreted from patient-derived CAFs has been shown to stimulate the Wnt signaling pathway, enhancing colon cancer cell proliferation and migration *in vitro* (64).

Recent evidence has revealed subpopulations of CAFs with different roles and prognostic significance in CRC (65, 66). Mosa et al., for instance, distinguished inflammatory-like CAFs (iCAFs) from contractile cancer-associated myofibroblasts (myCAFs) by reduced endogenous Wnt activity. Heterogeneous tumor organoids with iCAFs observed upregulated endothelial mesenchymal transition (EMT) markers, promoting tumor metastasis, whereas those with myCAFs did not (67). The heterogeneity of CAFs has been attributed to different origins and differences in secreted factors from cancer cells at each stage of tumor development (58, 65). Besides representing potential therapeutic targets within the TME, CAFs in heterotypic CRC spheroids contribute to angiogenic, invasiveness, and chemoresistance mechanisms, modulating and regulating inflammation and immunosuppression (68, 69). Therefore, CAFs heterogeneity should also be included in 3D CRC models, especially when screening for immunotherapeutic therapies.

To study the impact of fibroblasts during drug screening, Zoetemelk et al. developed a multi-cellular CRC spheroid model grown from various CRC cell lines (DLD1, HCT116, SW620) in the absence (monoculture) and presence (co-culture) of normal human fibroblasts (CCD18co) within the spheroids (45). CRC spheroids were cultured within 96 u-bottom well plates with a 0.2% gelatin-coated surface with up to 70% fibroblast population in a mixture of cell culture media (DMEM, RPMI and EMEM) supplemented with 2.5% Matrigel®. The co-culture spheroids also included a 5% immortalized human EC population to mimic the tumor stroma better (Figure 2A). Some of the co-culture spheroids displayed a higher metabolic activity and survival compared to monoculture CRC spheroids after 72 h of treatment with chemotherapeutic drugs regorafenib, erlotinib, and 5-fluorouracil (5-FU). The co-culture spheroids also displayed striking morphological differences compared to the monoculture spheroids, whereby the co-culture spheroids were characterized as irregularly shaped and with multi-directional outgrowth. The decreased sphericity potentially contributed to the enhanced survival of the co-culture spheroids by increasing the surface area for improved exchange of oxygen and nutrients. The co-culture spheroids exclusively produced fibronectin, an extracellular matrix component that assists tumor growth, progression, and invasion (72). Notably, this heterotypic 3D culture was maintained for up to 10 days, wherein the spheroids observed sustained continuous proliferation measured by their increasing diameter, making it ideal for studies on drug testing lasting up to 10 days. Zoetemelk et al. simulated a multi-dose regimen in patients through an additional 48 h treatment of their co-culture spheroids after the initial 72 h incubation, which improved the treatment efficacy in comparison to the single high-dose drug administration. Zoetemelk et al. demonstrated that the contribution of fibroblasts to tumor survival during chemotherapy was successfully recapitulated in the co-culture spheroids and the possibility for heterotypic spheroids to test multi-dose regimens *in vitro*.

Dolznig et al. generated co-culture CRC spheroids in collagen matrix containing 10x PBS, fibroblast growth medium (FGM)/20% methylcellulose and collagen in 1:4:5 volumetric ratio at neutral pH (41). They considered various colon adenocarcinoma cell lines (LS174T, HCT116, SW480, SW620, Colo205, and HT29), colon fibroblast cell lines (CCD18Co, Caco-2, and BJ-1), and CAFs isolated from patients. The tumor model containing CAFs and LS174T cells presented an enhanced invasive potential of the cancer cells and a higher percentage of the nuclear β-catenin positive cells, indicating the Wnt pathway activation as observed in patients (41). This co-culture CRC spheroid model was applied to evaluate the therapeutic efficacy of PI3K inhibitor LY294002 in FGM supplemented with 2.5% serum, observing up to a 3-fold suppression of spheroid growth over 7 days of incubation (41).

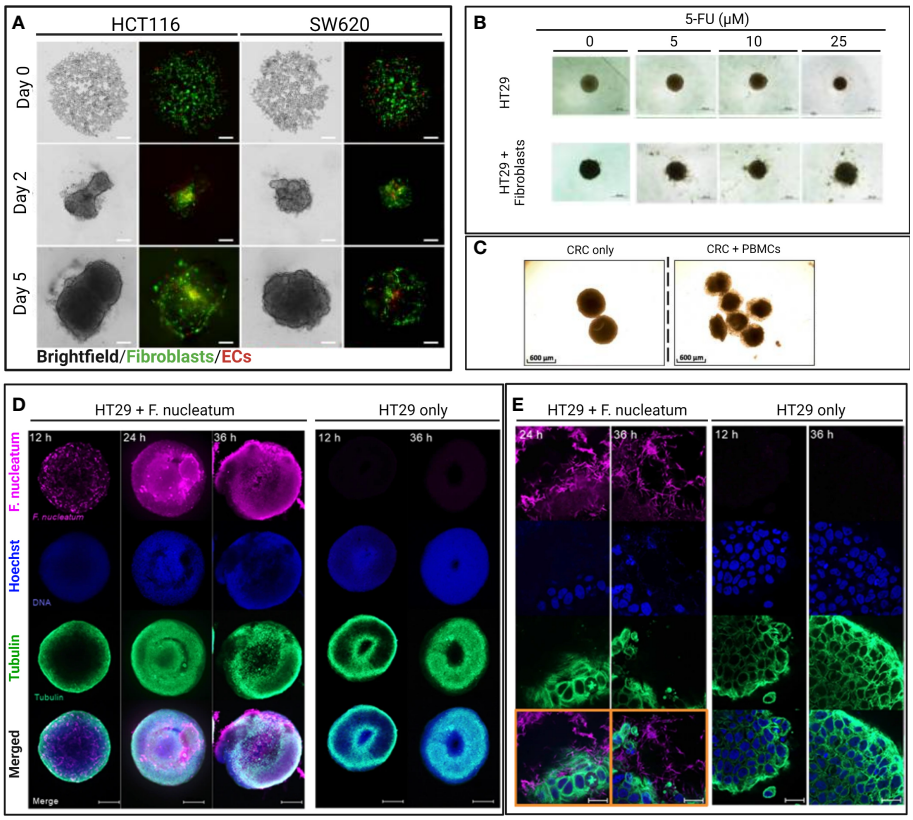

FIGURE 2
Selected images of representative heterotypic 3D CRC models from original figures of published scientific articles. **(A)** Brightfield and confocal images of intra-spheroid localization of CRC cells (HCT116 and SW620), fibroblast, and endothelial cells over time. Spheroids were formed with a 1:1 ratio of cancer cells (HCT116, SSW620) and normal human colon fibroblasts (CCD18co) with 5% of human immortalized ECs (ECRF24) and used to study drug sensitivity (45). Scale bar = 200 μm. **(B)** Brightfield images of monoculture and heterotypic HT29 spheroids treated with different concentrations of 5-FU for 48 h. Heterotypic spheroids consisted of HT29 spheroids co-cultured with (2 x 10^5) activated MRC-5 fibroblasts (70). Scale bar = 500 μm. **(C)** Brightfield images of 3D CRC models cultured for 48 h and consisting of cancer cells (HT29) and $CD19^-CD14^-$ peripheral blood mononuclear cells (PBMC) from healthy donors to study immunomodulatory antibodies (43). Scale bar = 600 μm. **(D)** Confocal images of bacteria-spheroid co-culture consisting of HT29 cancer cells and Fusobacterium nucleatum (labeled in pink), and HT29 only spheroid at 12, 24, and 36 h. Scale bar = 200 μm. **(E)** High magnification (63 x) confocal images of 3D CRC spheroids at 12 and 36 h with and without F. nucleatum (in pink) (71). Scale bar = 20 μm.

The enhanced fibroblast-associated cancer cell proliferation and migration in patients makes CAFs potential therapeutic targets. Consequently, researchers can use 3D CRC spheroid models to test therapeutic strategies modulating CAFs (alone or in combination) as done by Dana et al. (70) (Figure 2B). They demonstrated resveratrol-loaded liposomes (L-RES) therapeutic efficacy in reducing fibroblast activation and increasing drug sensitivity of co-culture spheroid during 5-FU treatment. The co-culture spheroids were formed with HT29 colorectal adenocarcinoma cell line and human lung fibroblasts MRC-5 cultured for 3 days in 96 well round bottom ultra-low attachment plates. For the drug sensitivity assay, the co-culture CRC spheroids were treated with 25 μM of L-RES in combination with 5-FU at concentrations of 5–25 μM for 2 more days (70).

All the described 3D CRC spheroid models well mimicked the fibroblast-associated chemoresistance and cancer progression observed in patients (64), supporting the importance of recapitulating the cell heterogeneity within the TME in heterotypic 3D CRC spheroid models for drug testing. In addition to cell viability, proliferation, and migration previously mentioned as quantifiable parameters, several metastatic biomarkers (e.g., AGR2, CacyBP, and EphA2) could be measured in these 3D models to further assess changes in the tumor metastatic potential. As observed in Zoetemelk et al. (45), CRC spheroid culture can be designed to accommodate multi-dose drug testing, although 3D *in vitro* tumor models are mostly conceived to achieve a fast prediction of the drug efficacy to speed up the drug development rather than establish long-term cultures.

3D CRC spheroid models with fibroblasts and immune cells

Colorectal tumors often observe a robust population of infiltrating immune cells and an increased expression of pro-inflammatory cytokines (73). Immune cells, specifically TAMs, and their secreted cytokines are essential components of the TME, significantly influencing tumor progression, immunosuppression, and, indirectly, chemoresistance (74, 75). In particular, TAMs in CRC, as in many solid tumors, consist of pro-inflammatory M1-like

and anti-inflammatory M2-like macrophages, with a dynamic population ratio that varies with tumor progression (76). Väyrynen et al., for instance, observed that higher cancer survival was associated with higher density of M1-like macrophages than M2-like macrophages (77), in agreement with the evidence of M1-like macrophages having anti-tumor properties (e.g., inhibiting angiogenesis and tumor cell infiltration) whereas M2-like macrophages promoting tumor progression (78). This suggests that the roles and functions of TAMs must be considered during drug screening in 3D CRC spheroid models. However, we found only a few examples in the literature of 3D CRC spheroid models including immune cells that were applied for testing therapeutics.

To the best of our knowledge, the only 3D CRC spheroid model including both fibroblasts and macrophages within the tumor spheroid used for chemotherapeutic screening was presented by Bauleth-Ramos et al. (42). A heterogeneous CRC spheroid model was formed in 7 days, consisting of (90.8 ± 2.4%) CRC cancer cells (HCT116), (5.6 ± 1.6%) human intestinal fibroblasts, and (7.5 ± 1.2%) macrophages matured from blood derived monocytes from human donors. The spheroids were developed in agarose micro-molds produced with 3D Petri Dish® and cultured in 12 well plates with RPMI medium for the evaluation of a combined chemo-immune treatment for 48 h. The macrophages, identified by flow cytometry as mixed M1/M2 population with a major proportion of M2-like macrophages, promoted continuous tumor cell proliferation in spheroids through days 1 to 7, whereas spheroids lacking the macrophages demonstrated stagnant growth. The metastatic potential of the CRC spheroids was observed as cell dispersion from the spheroids but not quantified to compare monoculture and triculture (42). However, the consistent increase in diameter over time of the triculture CRC spheroids suggested a tumor-promoting role of M2-like macrophages in line with previous literature (79). The spheroids with increasing heterogeneity were treated with the chemotherapeutic Nutlin-3a (Nut3a) and granulocyte-macrophage colony-stimulating factor (GM-CSF) loaded in spermine-modified acetylated dextran nanoparticles (NPs). The Nut3a-loaded NPs showed a dose-dependent anti-proliferative effect in triculture and promoted the M1 over M2 polarization in spheroids as measured by the ratio of CD163 (M2 marker) to CD86 (M1 marker) expression (42).

Aside from macrophages, other immune cells are found in the TME and play important roles in regulating tumor growth, metastasis, and drug sensitivity, including dendritic cells (80), T cells, and NK cells (81). Courau et al. demonstrated that T cells and NK cells, enriched from human donor peripheral blood mononuclear cells (PBMC) and co-cultured with CRC spheroid in RPMI medium in 96 well plates after spheroid formation, successfully infiltrated the spheroids to initiate tumor cell apoptosis after 48 h (Figure 2C) (43). T and NK cells' contribution to the CRC TME is important, especially for screening immunotherapies that have yet to achieve satisfying clinical efficacy as CRC treatment (82). For instance, Herter et al. developed a CRC spheroid model with cancer cells (LoVo and LS174T) and fibroblasts (CCD18Co) in an FGM-2 medium to evaluate an interleukin-2 variant, IgG-IL2v, as novel immunotherapeutic. They measured the IgG-IL2v influence on the infiltration of human peripheral blood monocytes into the CRC spheroids after 72 h (40), highlighting the possibility of studying the influence of various immune cells infiltrated within 3D CRC spheroid models.

Triculture 3D CRC spheroid models with fibroblasts and TAMs may be considered more suited for evaluating immunotherapy strategies compared to 3D CRC spheroid models with only cancer cells or co-culture of cancer cells and fibroblasts. Further, as the crosstalk among cancer, stromal and immune cells modulate the release of immunosuppressive cytokines within the TME, impacting cell metabolisms, cell differentiation and functions (83–85), the stromal and immune components should be taken into consideration for a more comprehensive evaluation when testing not only immunotherapies (86) but any anti-tumor therapeutic, providing insights into drug mechanisms and influence over critical parameters in the TME.

3D CRC spheroid models with ECs

The secretion by tumor cells of pro-angiogenic growth factors, such as vascular endothelial growth factor (VEGF) and vascular endothelial growth factor receptor 2 (VEGFR2), promotes the development of new irregular blood vessels that supply tumors with nutrients and oxygen (87). The ECs contribute to a disordered TME, influencing tumor progression (88) and chemoresistance (89). The ECs associated with tumor angiogenesis have demonstrated phenotypic and genetic differences from normal ECs and are, at times, specifically referred to as tumor-associated endothelial cells (TECs) (90, 91). Consequently, TECs may influence the TME and the tumor sensitivity to drugs differently from normal ECs (92). Therefore, it is advisable to determine the nature of ECs (as "normal" or "tumor-associated") when integrated into spheroid models to rationalize the contribution of incorporating the EC population in mimicking the TME. This determination could be performed by genomic profiling (91) or by comparing the relative expressions of key markers of TECs such as biglycan (93).

As anticipated, Zoetemelk et al. introduced a 5% cell population of human immortalized vascular endothelial cells, ECRF24, in their heterogeneous human 3D CRC spheroid model containing cancer cells and fibroblasts (45). The authors discussed the spatial localization of ECs close to fibroblasts in the center of the spheroids for those formed with DLD1, SW620, and HCT116 cells. However, since the drugs were screened on either monoculture or triculture condition, no specific association between the spheroid sensitivity and EC presence was possible.

More recently, Carvalho et al. published a quadruple multi-cellular human CRC spheroid model by co-culturing HCT116 with human intestinal fibroblasts (HIFs), human pulmonary microvascular endothelial cells (HPMECs) and human monocytes to mimic a pro-angiogenic TME and test anti-angiogenic nanoparticles (NPs) containing bevacizumab (BVZ) (94). Three different ratios of HCT116:HPMECs:HIFs:monocytes (1:1:1:1, 1:4:4:4 and 1:4:1:4) were tested to form spheroids on agarose

micro-molds and cultured in RPMI medium over 7 days. The 1:1:1:1 model contained the highest expression of angiogenic CD31 marker and was selected to best recapitulate the pro-angiogenic TME. The NPs-based treatment resulted in the reduction of the endothelial cell marker CD31 and consequently reduced the angiogenic potential of the CRC spheroids, demonstrating the efficiency of the CRC model in screening anti-angiogenic drugs and nanoparticles. Furthermore, while not discussed, the high heterogeneity of the model by inclusion of stromal, endothelial and immune cells also enables the evaluation of chemo-immunotherapy strategies and multi-action drugs, although a different cell ratio may be optimal.

While vascularized heterotypic CRC spheroids will indeed represent a pathophysiologically relevant TME for drug screening (95) and studying the permeation of drugs through vasculature (96), few vascularized CRC models (97, 98) have been presented.

3D CRC spheroid models with gut bacteria

The gut microbiome is among the most important environmental factors contributing to CRC development (53, 99, 100). The gut microbiome consists of several micro-organisms, including bacteria, viruses, and fungi (54, 99, 101). Over 1000 species and 7000 strains of bacteria may be found in an adult gut (53). Disturbances to the gut microbiome balance, such as an individual's psychosocial stress or consuming antibiotics, can contribute to CRC (53, 54, 99, 100). For example, Clostridium butyicum helps to generate butyrate, folate, and biotin, which are important for regulating epithelial proliferation, thereby mitigating the risks of specific diets for developing CRC (53). Other biotas may have the opposite effect, secreting epigenetic factors that promote CRC (102). For example, a high-fat diet can cause excessive accumulation of lipopolysaccharides, a bacteria side product, that can enter the intestinal circulation and cause inflammation which may develop into CRC (103). Apart from carcinogenesis, the gut microbiome has implications for the development of chemoresistance, and it contains potential therapeutic targets (100). For instance, Fusobacterium nucleatum (F. nucleatum) has been linked to the chemoresistance of CRC to 5-FU through two separate mechanisms (104). However, few 3D models have been developed to consider the gut microbiome's role in CRC.

Kasper et al. developed a 3D model of a spheroid derived from CRC cell lines (HCT116 and HT29) capable of housing and promoting the growth of two strains of the anaerobic bacteria F. nucleatum (Figures 2D, E) after spheroid formation in McCoy's 5 A medium (supplemented with serum) to observe bacteria-tumor cell interactions and metabolic crosstalk within the TME (71). Interestingly, the tumor-bacteria spheroids shown an enriched IL-8 metastatic signaling, mirroring the increased IL-8 expression in CRC patients with high F. nucleatum. IL-8 has been shown to promote proliferation and survival of cancer cells (105, 106). However, the model has a limited culture time because the F. nucleatum induced tumor cytotoxicity after 24 h (71). Therefore, this human tumor-bacteria co-culture in a 3D setting should be further optimized for evaluating potential drug candidates or therapeutic regimens for treating CRC while considering the potential chemoresistance induced by F. nucleatum.

Lee et al. evaluated the potential anti-cancer activity of another component of the gut microbiome, the probiotic bacterium Lactobacillus fermentum (grown and expanded in Lactobacilli De Man, Rogosa, Sharpe broth), in their 3D CRC spheroid model cultured in RPMI medium (supplemented with serum) in 96 well round bottom plate (107). The effect of Lactobacillus fermentum was observed through increased apoptosis of HCT116 cells after 72 h, which was observed solely in the 3D CRC model and not in 2D monolayer cultures (107). Rubert et al. instead demonstrated that the native (poly)phenols and gut microbial metabolites inhibited the propagation and viability of HCT116 spheroids cultured in RPMI medium (supplemented with serum) in 96 well round bottom plate after 72 h incubation (108).

Indeed, the gut microbiome's influence on CRC progression, survival, and chemoresistance warrants research work to determine their potential as therapeutic targets. However, 2D cultures are insufficient to assess the gut microbiota's activity in CRC (107). In this resepct, 3D CRC spheroid models provide an attractive *in vitro* strategy for exploring the specific role of gut microbiota in influencing chemoresistance, tumor progression, and survival. Drug evaluations in human 3D CRC spheroid models should, therefore, include a systematic evaluation of the activity of the gut microbiota to better appreciate their role in the TME during treatment.

Conclusions

There needs to be more standardization and validation of the methodologies for applying human 3D CRC spheroid models to preclinically assess the efficacy of drugs or other therapeutic strategies. This limitation has challenged the reproducible implementation of 3D spheroid models in drug development and confidence in the drug efficacies observed (109). Monoculture spheroids are simple and quick to optimize, justifying their use for high-throughput screening of drugs until the processes for heterogeneous spheroid formation, treatment, and assessment are better validated and automated. Indeed, heterogeneous spheroids have been demonstrated to have pathophysiological similarities and relevance to native tumor tissue. By incorporating fibroblasts, ECs, TAMs, and gut microbiota, human CRC spheroid models enable more in-depth investigations into the role of specific cell populations on tumor progression, survival, and chemoresistance unfeasible in traditional 2D cultures and spheroid monoculture. Diverse cell populations within the 3D models also represent attractive therapeutic targets that cannot be identified and validated in monoculture. Heterotypic 3D CRC spheroids thereby offer great potential for more precise predictions of the efficacy of chemotherapies to aid the discovery and development of new drug candidates, representing a promising preclinical tool for overcoming some of the limitations of previous *in vitro* and *in vivo* models.

Author contributions

JY manuscript writing, GA review and editing. All authors have read and agreed to the published version of the manuscript. All authors contributed to the article and approved the submitted version.

Funding

This work was supported by the Singapore Immunology Network, Agency for Science, Technology and Research (A*STAR).

Acknowledgments

We gratefully acknowledge Prof. Giorgia Pastorin for her exceptional support and guidance.

Conflict of interest

The authors declare that the research was conducted in the absence of any commercial or financial relationships that could be construed as a potential conflict of interest.

Publisher's note

References

1. Rawla P, Sunkara T, Barsouk A. Epidemiology of colorectal cancer: incidence, mortality, survival, and risk factors. *Prz Gastroenterol* (2019) 14(2):89–103. doi: 10.5114/pg.2018.81072

2. Sung H, Ferlay J, Siegel RL, Laversanne M, Soerjomataram I, Jemal A, et al. Global cancer statistics 2020: GLOBOCAN estimates of incidence and mortality worldwide for 36 cancers in 185 countries. *CA Cancer J Clin* (2021) 71(3):209–49. doi: 10.3322/caac.21660

3. Nunes AS, Barros AS, Costa EC, Moreira AF, Correia IJ. 3D tumor spheroids as *in vitro* models to mimic *in vivo* human solid tumors resistance to therapeutic drugs. *Biotechnol Bioeng* (2019) 116(1):206–26. doi: 10.1002/bit.26845

4. Takebe T, Imai R, Ono S. The current status of drug discovery and development as originated in united states academia: the influence of industrial and academic collaboration on drug discovery and development. *Clin Trans Sci* (2018) 11(6):597–606. doi: 10.1111/cts.12577

5. Alderden RA, Hall MD, Hambley TW. The discovery and development of cisplatin. *J Chem Educ* (2006) 83(5):728. doi: 10.1021/ed083p728

6. Baker BM, Chen CS. Deconstructing the third dimension–how 3D culture microenvironments alter cellular cues. *J Cell Sci* (2012) 125(13):3015–24. doi: 10.1242/jcs.079509

7. Jensen C, Teng Y. Is it time to start transitioning from 2D to 3D cell culture? *Front Mol Biosci* (2020) 7:33. doi: 10.3389/fmolb.2020.00033

8. Kapałczyńska M, Kolenda T, Przybyła W, Zajączkowska M, Teresiak A, Filas V, et al. 2D and 3D cell cultures–a comparison of different types of cancer cell cultures. *Arch Med Sci* (2018) 14(4):910–9. doi: 10.5114/aoms.2016.63743

9. Rubio-Viqueira B, Hidalgo M. Direct *in vivo* xenograft tumor model for predicting chemotherapeutic drug response in cancer patients. *Clin Pharmacol Ther* (2009) 85(2):217–21. doi: 10.1038/clpt.2008.200

10. Williams CH, Hong CC. Multi-step usage of *in vivo* models during rational drug design and discovery. *Int J Mol Sci* (2011) 12(4):2262–74. doi: 10.3390/ijms12042262

11. Byrne AT, Alférez DG, Amant F, Annibali D, Arribas J, Biankin AV, et al. Interrogating open issues in cancer precision medicine with patient-derived xenografts. *Nat Rev Cancer* (2017) 17(4):254–68. doi: 10.1038/nrc.2016.140

12. Wei Y, Au JLS. Role of tumour microenvironment in chemoresistance. In: Meadows G. G., editor. *Integration/Interaction of Oncologic Growth*. (Dordrecht: Springer) (2005) 285–321. doi: 10.1007/1-4020-3414-8_17

13. Han Y, Cho U, Kim S, Park IS, Cho JH, Dhanasekaran DN, et al. Tumour microenvironment on mitochondrial dynamics and chemoresistance in cancer. *Free Radical Res* (2018) 52(11-12):1271–87. doi: 10.1080/10715762.2018.1459594

14. Jubelin C, Muñoz-Garcia J, Griscom L, Cochonneau D, Ollivier E, Heymann M-F, et al. Three-dimensional *in vitro* culture models in oncology research. *Cell Biosci* (2022) 12(1):155. doi: 10.1186/s13578-022-00887-3

15. Rodrigues J, Heinrich MA, Teixeira LM, Prakash J. 3D *in vitro* model (R) evolution: unveiling tumor–stroma interactions. *Trends Cancer* (2021) 7(3):249–64. doi: 10.1016/j.trecan.2020.10.009

16. Mulholland T, McAllister M, Patek S, Flint D, Underwood M, Sim A, et al. Drug screening of biopsy-derived spheroids using a self-generated microfluidic concentration gradient. *Sci Rep* (2018) 8(1):14672. doi: 10.1038/s41598-018-33055-0

17. Spoerri L, Gunasingh G, Haass NK. Fluorescence-based quantitative and spatial analysis of tumour spheroids: a proposed tool to predict patient-specific therapy response. *Front Digit Health* (2021) 3:668390. doi: 10.3389/fdgth.2021.668390

18. Lam M, Reales-Calderon J, Ow JR, Joey A, Damien T, Ceccarello E, et al. G9a/GLP inhibition during ex vivo lymphocyte expansion increases in vivo cytotoxicity of engineered TCR-T cells against hepatocellular carcinoma. (2021) 14:563. doi: 10.1038/s41467-023-36160-5

19. Lee SWL, Adriani G, Ceccarello E, Pavesi A, Tan AT, Bertoletti A, et al. Characterizing the role of monocytes in T cell cancer immunotherapy using a 3D microfluidic model. *Front Immunol* (2018) 9:416. doi: 10.3389/fimmu.2018.00416

20. Bai J, Adriani G, Dang T-M, Tu T-Y, Penny H-XL, Wong S-C, et al. Contact-dependent carcinoma aggregate dispersion by M2a macrophages via ICAM-1 and β2 integrin interactions. *Oncotarget* (2015) 6(28):25295. doi: 10.18632/oncotarget.4716

21. Sabhachandani P, Sarkar S, Mckenney S, Ravi D, Evens AM, Konry T. Microfluidic assembly of hydrogel-based immunogenic tumor spheroids for evaluation of anticancer therapies and biomarker release. *J Control Release* (2019) 295:21–30. doi: 10.1016/j.jconrel.2018.12.010

22. Ding L, Liu C, Yin S, Zhou Z, Chen J, Chen X, et al. Engineering a dynamic three-dimensional cell culturing microenvironment using a 'sandwich'structure-liked microfluidic device with 3D printing scaffold. *Biofabrication* (2022) 14(4):045014. doi: 10.1088/1758-5090/ac8a19

23. Antunes J, Gaspar VM, Ferreira L, Monteiro M, Henrique R, Jeronimo C, et al. In-air production of 3D co-culture tumor spheroid hydrogels for expedited drug screening. *Acta Biomater* (2019) 94:392–409. doi: 10.1016/j.actbio.2019.06.012

24. Aref AR, Campisi M, Ivanova E, Portell A, Larios D, Piel BP, et al. 3D microfluidic ex vivo culture of organotypic tumor spheroids to model immune checkpoint blockade. *Lab Chip* (2018) 18(20):3129–43. doi: 10.1039/C8LC00322J

25. Reidy E, Leonard NA, Treacy O, Ryan AE. A 3D view of colorectal cancer models in predicting therapeutic responses and resistance. *Cancers (Basel)* (2021) 13 (2):227. doi: 10.3390/cancers13020227

26. Castro F, Leite Pereira C, Helena Macedo M, Almeida A, Jose Silveira M, Dias S, et al. Advances on colorectal cancer 3D models: the needed translational technology for nanomedicine screening. *Adv Drug Deliv Rev* (2021) 175:113824. doi: 10.1016/j.addr.2021.06.001

27. de Wit M, Fijneman RJ, Verheul HM, Meijer GA, Jimenez CR. Proteomics in colorectal cancer translational research: biomarker discovery for clinical applications. *Clin Biochem* (2013) 46(6):466–79. doi: 10.1016/j.clinbiochem.2012.10.039

28. Wan X, Li Z, Ye H, Cui Z. Three-dimensional perfused tumour spheroid model for anti-cancer drug screening. *Biotechnol Lett* (2016) 38(8):1389–95. doi: 10.1007/s10529-016-2035-1

29. Ek F, Blom K, Selvin T, Rudfeldt J, Andersson C, Senkowski W, et al. Sorafenib and nitazoxanide disrupt mitochondrial function and inhibit regrowth capacity in three-dimensional models of hepatocellular and colorectal carcinoma. *Sci Rep* (2022) 12(1):8943. doi: 10.1038/s41598-022-12519-4

30. Nittayaboon K, Leetanaporn K, Sangkhathat S, Roytrakul S, Navakanitworakul R. Cytotoxic effect of metformin on butyrate-resistant PMF-K014 colorectal cancer spheroid cells. *BioMed Pharmacother* (2022) 151:113214. doi: 10.1016/j.biopha.2022.113214

31. Sogawa C, Eguchi T, Namba Y, Okusha Y, Aoyama E, Ohyama K, et al. Gel-free 3D tumoroids with stem cell properties modeling drug resistance to cisplatin and

imatinib in metastatic colorectal cancer. *Cells* (2021) 10(2):344. doi: 10.3390/cells10020344

32. Virgone-Carlotta A, Lemasson M, Mertani HC, Diaz J-J, Monnier S, Dehoux T, et al. In-depth phenotypic characterization of multicellular tumor spheroids: effects of 5-fluorouracil. *PloS One* (2017) 12(11):e0188100. doi: 10.1371/journal.pone.0188100

33. Däster S, Amatruda N, Calabrese D, Ivanek R, Turrini E, Droeser RA, et al. Induction of hypoxia and necrosis in multicellular tumor spheroids is associated with resistance to chemotherapy treatment. *Oncotarget* (2017) 8(1):1725. doi: 10.18632/oncotarget.13857

34. Ong LJY, Chia S, Wong SQR, Zhang X, Chua H, Loo JM, et al. A comparative study of tumour-on-chip models with patient-derived xenografts for predicting chemotherapy efficacy in colorectal cancer patients. *Front Bioeng Biotechnol* (2022) 10. doi: 10.3389/fbioe.2022.952726

35. Jeppesen M, Hagel G, Glenthoj A, Vainer B, Ibsen P, Harling H, et al. Short-term spheroid culture of primary colorectal cancer cells as an *in vitro* model for personalizing cancer medicine. *PloS One* (2017) 12(9):e0183074. doi: 10.1371/journal.pone.0183074

36. Manfredonia C, Muraro MG, Hirt C, Mele V, Governa V, Papadimitropoulos A, et al. Maintenance of primary human colorectal cancer microenvironment using a perfusion bioreactor-based 3D culture system. *Adv Biosyst* (2019) 3(4):1800300. doi: 10.1002/adbi.201800300

37. Pyo DH, Hong HK, Lee WY, Cho YB. Patient-derived cancer modeling for precision medicine in colorectal cancer: beyond the cancer cell line. *Cancer Biol Ther* (2020) 21(6):495–502. doi: 10.1080/15384047.2020.1738907

38. De Witt Hamer P, Van Tilborg A, Eijk P, Sminia P, Troost D, Van Noorden C, et al. The genomic profile of human malignant glioma is altered early in primary cell culture and preserved in spheroids. *Oncogene* (2008) 27(14):2091–6. doi: 10.1038/sj.onc.1210850

39. Failli A, Consolini R, Legitimo A, Spisni R, Castagna M, Romanini A, et al. The challenge of culturing human colorectal tumor cells: establishment of a cell culture model by the comparison of different methodological approaches. *Tumori J* (2009) 95 (3):343–7. doi: 10.1177/030089160909500312

40. Herter S, Morra L, Schlenker R, Sulcova J, Fahrni L, Waldhauer I, et al. A novel three-dimensional heterotypic spheroid model for the assessment of the activity of cancer immunotherapy agents. *Cancer Immunol Immunother* (2017) 66(1):129–40. doi: 10.1007/s00262-016-1927-1

41. Dolznig H, Rupp C, Puri C, Haslinger C, Schweifer N, Wieser E, et al. Modeling colon adenocarcinomas *in vitro* a 3D co-culture system induces cancer-relevant pathways upon tumor cell and stromal fibroblast interaction. *Am J Pathol* (2011) 179(1):487–501. doi: 10.1016/j.ajpath.2011.03.015

42. Bauleth-Ramos T, Feijão T, Gonçalves A, Shahbazi M-A, Liu Z, Barrias C, et al. Colorectal cancer triple co-culture spheroid model to assess the biocompatibility and anticancer properties of polymeric nanoparticles. *J Control Release* (2020) 323:398–411. doi: 10.1016/j.jconrel.2020.04.025

43. Courau T, Bonnereau J, Chicoteau J, Bottois H, Remark R, Assante Miranda L, et al. Cocultures of human colorectal tumor spheroids with immune cells reveal the therapeutic potential of MICA/B and NKG2A targeting for cancer treatment. *J Immunother Cancer* (2019) 7(1):1–14. doi: 10.1186/s40425-019-0553-9

44. Cattin S, Ramont L, Rüegg C. Characterization and *in vivo* validation of a three-dimensional multi-cellular culture model to study heterotypic interactions in colorectal cancer cell growth, invasion and metastasis. *Front Bioeng Biotechnol* (2018) 6:97. doi: 10.3389/fbioe.2018.00097

45. Zoetemelk M, Rausch M, Colin DJ, Dormond O, Nowak-Sliwinska P. Short-term 3D culture systems of various complexity for treatment optimization of colorectal carcinoma. *Sci Rep* (2019) 9(1):7103. doi: 10.1038/s41598-019-42836-0

46. Yin Y, Yao S, Hu Y, Feng Y, Li M, Bian Z, et al. The immune-microenvironment confers chemoresistance of colorectal cancer through macrophage-derived IL6. *Clin Cancer Res* (2017) 23(23):7375–87. doi: 10.1158/1078-0432.CCR-17-1283

47. Petreus T, Cadogan E, Hughes G, Smith A, Pilla Reddy V, Lau A, et al. Tumour-on-chip microfluidic platform for assessment of drug pharmacokinetics and treatment response. *Commun Biol* (2021) 4(1):1001. doi: 10.1038/s42003-021-02526-y

48. Wang T, Green R, Howell M, Martinez T, Dutta R, Mohapatra S, et al. The design and characterization of a gravitational microfluidic platform for drug sensitivity assay in colorectal perfused tumoroid cultures. *Nanomedicine* (2020) 30:102294. doi: 10.1016/j.nano.2020.102294

49. Chen Y, Gao D, Liu H, Lin S, Jiang Y. Drug cytotoxicity and signaling pathway analysis with three-dimensional tumor spheroids in a microwell-based microfluidic chip for drug screening. *Anal Chim Acta* (2015) 898:85–92. doi: 10.1016/j.aca.2015.10.006

50. Jeong S-Y, Lee J-H, Shin Y, Chung S, Kuh H-J. Co-Culture of tumor spheroids and fibroblasts in a collagen matrix-incorporated microfluidic chip mimics reciprocal activation in solid tumor microenvironment. *PloS One* (2016) 11(7):e0159013. doi: 10.1371/journal.pone.0159013

51. Bourn MD, Batchelor DVB, Ingram N, McLaughlan JR, Coletta PL, Evans SD, et al. High-throughput microfluidics for evaluating microbubble enhanced delivery of cancer therapeutics in spheroid cultures. *J Control Release* (2020) 326:13–24. doi: 10.1016/j.jconrel.2020.06.011

52. Sung KE, Beebe DJ. Microfluidic 3D models of cancer. *Adv Drug Deliv Rev* (2014) 79-80:68–78. doi: 10.1016/j.addr.2014.07.002

53. Rebersek M. Gut microbiome and its role in colorectal cancer. *BMC Cancer* (2021) 21(1):1325. doi: 10.1186/s12885-021-09054-2

54. Wong SH, Yu J. Gut microbiota in colorectal cancer: mechanisms of action and clinical applications. *Nat Rev Gastroenterol Hepatol* (2019) 16(11):690–704. doi: 10.1038/s41575-019-0209-8

55. Drev D, Harpain F, Beer A, Stift A, Gruber ES, Klimpfinger M, et al. Impact of fibroblast-derived SPARC on invasiveness of colorectal cancer cells. *Cancers (Basel)* (2019) 11(10):1421. doi: 10.3390/cancers11101421

56. Tommelein J, Verset L, Boterberg T, Demetter P, Bracke M, De Wever O. Cancer-associated fibroblasts connect metastasis-promoting communication in colorectal cancer. *Front Oncol* (2015) 5:63. doi: 10.3389/fonc.2015.00063

57. Xing F, Saidou J, Watabe K. Cancer associated fibroblasts (CAFs) in tumor microenvironment. *Front biosci: J virtual library* (2010) 15:166. doi: 10.2741/3613

58. Rai A, Greening DW, Chen M, Xu R, Ji H, Simpson RJ. Exosomes derived from human primary and metastatic colorectal cancer cells contribute to functional heterogeneity of activated fibroblasts by reprogramming their proteome. *Proteomics* (2019) 19(8):1800148. doi: 10.1002/pmic.201800148

59. De Boeck A, Hendrix A, Maynard D, Van Bockstal M, Daniëls A, Pauwels P, et al. Differential secretome analysis of cancer-associated fibroblasts and bone marrow-derived precursors to identify microenvironmental regulators of colon cancer progression. *Proteomics* (2013) 13(2):379–88. doi: 10.1002/pmic.201200179

60. Zhu H-F, Zhang X-H, Gu C-S, Zhong Y, Long T, Ma Y-D, et al. Cancer-associated fibroblasts promote colorectal cancer progression by secreting CLEC3B. *Cancer Biol Ther* (2019) 20(7):967–78. doi: 10.1080/15384047.2019.1591122

61. Mishra P, Banerjee D, Ben-Baruch A. Chemokines at the crossroads of tumor-fibroblast interactions that promote malignancy. *J Leukocyte Biol* (2011) 89(1):31–9. doi: 10.1189/jlb.0310182

62. Torres S, Bartolomé RA, Mendes M, Barderas R, Fernandez-Aceñero MJ, Peláez-García A, et al. Proteome profiling of cancer-associated fibroblasts identifies novel proinflammatory signatures and prognostic markers for colorectal CancerMolecular signatures of colon cancer–associated fibroblasts. *Clin Cancer Res* (2013) 19(21):6006–19. doi: 10.1158/1078-0432.CCR-13-1130

63. Hanahan D, Weinberg RA. Hallmarks of cancer: the next generation. *Cell* (2011) 144(5):646–74. doi: 10.1016/j.cell.2011.02.013

64. Aizawa T, Karasawa H, Funayama R, Shirota M, Suzuki T, Maeda S, et al. Cancer-associated fibroblasts secrete Wnt2 to promote cancer progression in colorectal cancer. *Cancer Med* (2019) 8(14):6370–82. doi: 10.1002/cam4.2523

65. Simon T, Salhia B. Cancer-associated fibroblast subpopulations with diverse and dynamic roles in the tumor microenvironment. *Mol Cancer Res* (2022) 20(2):183–92. doi: 10.1158/1541-7786.MCR-21-0282

66. Zhao Z, Li W, Zhu L, Xu B, Qiu J, Ma N, et al. Construction and verification of a fibroblast-related prognostic signature model for colon cancer. *Front Genet* (2022) 1821. doi: 10.3389/fgene.2022.908957

67. Mosa MH, Michels BE, Menche C, Nicolas AM, Darvishi T, Greten FR, et al. A wnt-induced phenotypic switch in cancer-associated fibroblasts inhibits EMT in colorectal CancerWnt-induced fibroblast plasticity in colorectal cancer. *Cancer Res* (2020) 80(24):5569–82. doi: 10.1158/0008-5472.CAN-20-0263

68. Stadler M, Pudelko K, Biermeier A, Walterskirchen N, Gaigneaux A, Weindorfer C, et al. Stromal fibroblasts shape the myeloid phenotype in normal colon and colorectal cancer and induce CD163 and CCL2 expression in macrophages. *Cancer Lett* (2021) 520:184–200. doi: 10.1016/j.canlet.2021.07.006

69. Kinugasa Y, Matsui T, Takakura N. CD44 expressed on cancer-associated fibroblasts is a functional molecule supporting the stemness and drug resistance of malignant cancer cells in the tumor microenvironment. *Stem Cells* (2014) 32(1):145–56. doi: 10.1002/stem.1556

70. Dana P, Thumrongsiri N, Tanyapanyachon P, Chonniyom W, Punnakitikashem P, Saengkrit N. Resveratrol loaded liposomes disrupt cancer associated fibroblast communications within the tumor microenvironment to inhibit colorectal cancer aggressiveness. *Nanomaterials* (2022) 13(1):107. doi: 10.3390/nano13010107

71. Kasper SH, Morell-Perez C, Wyche TP, Sana TR, Lieberman LA, Hett EC. Colorectal cancer-associated anaerobic bacteria proliferate in tumor spheroids and alter the microenvironment. *Sci Rep* (2020) 10(1):1–13. doi: 10.1038/s41598-020-62139-z

72. Han Z, Lu Z-R. Targeting fibronectin for cancer imaging and therapy. *J Mater Chem B* (2017) 5(4):639–54. doi: 10.1039/C6TB02008A

73. Atreya I, Neurath MF. Immune cells in colorectal cancer: prognostic relevance and therapeutic strategies. *Expert Rev Anticancer Ther* (2008) 8(4):561–72. doi: 10.1586/14737140.8.4.561

74. Chanmee T, Ontong P, Konno K, Itano N. Tumor-associated macrophages as major players in the tumor microenvironment. *Cancers* (2014) 6(3):1670–90. doi: 10.3390/cancers6031670

75. Zhong X, Chen B, Yang Z. The role of tumor-associated macrophages in colorectal carcinoma progression. *Cell Physiol Biochem* (2018) 45(1):356–65. doi: 10.1159/000486816

76. Sica A, Schioppa T, Mantovani A, Allavena P. Tumour-associated macrophages are a distinct M2 polarised population promoting tumour progression: potential targets of anti-cancer therapy. *Eur J Cancer* (2006) 42(6):717–27. doi: 10.1016/j.ejca.2006.01.003

77. Väyrynen JP, Haruki K, Lau MC, Väyrynen SA, Zhong R, Dias Costa A, et al. The prognostic role of macrophage polarization in the colorectal cancer microenvironment. *Cancer Immunol Res* (2021) 9(1):8–19. doi: 10.1158/2326-6066.CIR-20-0527

78. Bi Y, Shirure VS, Liu R, Cunningham C, Ding L, Meacham JM, et al. Tumor-on-a-chip platform to interrogate the role of macrophages in tumor progression. *Integr Biol* (2020) 12(9):221–32. doi: 10.1093/intbio/zyaa017

79. Lan J, Sun L, Xu F, Liu L, Hu F, Song D, et al. M2 macrophage-derived exosomes promote cell migration and invasion in colon cancer. *Cancer Res* (2019) 79(1):146–58. doi: 10.1158/0008-5472.CAN-18-0014

80. Michielsen AJ, O'Sullivan JN, Ryan EJ. Tumor conditioned media from colorectal cancer patients inhibits dendritic cell maturation. *Oncoimmunology* (2012) 1(5):751–3. doi: 10.4161/onci.19570

81. Xing Y, Ruan G, Ni H, Qin H, Chen S, Gu X, et al. Tumor immune microenvironment and its related miRNAs in tumor progression. *Front Immunol* (2021) 12:624725. doi: 10.3389/fimmu.2021.624725

82. Puzzoni M, Silvestris N, Leone F, Giampieri R, Faloppi L, Demurtas L, et al. The immune revolution in gastrointestinal tumours: leading the way or just following? *Target Oncol* (2016) 11(5):593–603. doi: 10.1007/s11523-016-0437-6

83. Kitamura T, Qian B-Z, Pollard JW. Immune cell promotion of metastasis. *Nat Rev Immunol* (2015) 15(2):73–86. doi: 10.1038/nri3789

84. Blomberg OS, Spagnuolo L, de Visser KE. Immune regulation of metastasis: mechanistic insights and therapeutic opportunities. *Dis Models Mech* (2018) 11(10): dmm036236. doi: 10.1242/dmm.036236

85. Binnewies M, Roberts EW, Kersten K, Chan V, Fearon DF, Merad M, et al. Understanding the tumor immune microenvironment (TIME) for effective therapy. *Nat Med* (2018) 24(5):541–50. doi: 10.1038/s41591-018-0014-x

86. Kamal Y, Schmit SL, Frost HR, Amos CI. The tumor microenvironment of colorectal cancer metastases: opportunities in cancer immunotherapy. *Immunotherapy* (2020) 12(14):1083–100. doi: 10.2217/imt-2020-0026

87. Carmeliet P, Jain RK. Angiogenesis in cancer and other diseases. *Nature* (2000) 407(6801):249–57. doi: 10.1038/35025220

88. Madden E, Logue SE, Healy SJ, Manie S, Samali A. The role of the unfolded protein response in cancer progression: from oncogenesis to chemoresistance. *Biol Cell* (2019) 111(1):1–17. doi: 10.1111/boc.201800050

89. Weis SM, Cheresh DA. Tumor angiogenesis: molecular pathways and therapeutic targets. *Nat Med* (2011) 17(11):1359–70. doi: 10.1038/nm.2537

90. Xiong Y-Q, Sun H-C, Zhang W, Zhu X-D, Zhuang P-Y, Zhang J-B, et al. Human hepatocellular carcinoma tumor–derived endothelial cells manifest increased angiogenesis capability and drug resistance compared with normal endothelial CellsTEC cells increase drug resistance. *Clin Cancer Res* (2009) 15(15):4838–46. doi: 10.1158/1078-0432.CCR-08-2780

91. Croix BS, Rago C, Velculescu V, Traverso G, Romans KE, Montgomery E, et al. Genes expressed in human tumor endothelium. *Science* (2000) 289(5482):1197–202. doi: 10.1126/science.289.5482.1197

92. Chen WZ, Jiang JX, Yu XY, Xia WJ, Yu PX, Wang K, et al. Endothelial cells in colorectal cancer. *World J Gastrointest Oncol* (2019) 11(11):946. doi: 10.4251/wjgo.v11.i11.946

93. Yamamoto K, Ohga N, Hida Y, Maishi N, Kawamoto T, Kitayama K, et al. Biglycan is a specific marker and an autocrine angiogenic factor of tumour endothelial cells. *Br J Cancer* (2012) 106(6):1214–23. doi: 10.1038/bjc.2012.59

94. Carvalho S, Silveira MJ, Domingues M, Ferreira B, Pereira CL, PalmiraGremião M, et al. Multicellular quadruple colorectal cancer spheroids as an *In vitro* tool for anti-angiogenic potential evaluation of nanoparticles. *Adv Ther* (2023) 6(4):2200282. doi: 10.1002/adtp.202200282

95. Ko J, Ahn J, Kim S, Lee Y, Lee J, Park D, et al. Tumor spheroid-on-a-chip: a standardized microfluidic culture platform for investigating tumor angiogenesis. *Lab Chip* (2019) 19(17):2822–33. doi: 10.1039/C9LC00140A

96. Ahn J, Kim D-H, Koo D-J, Lim J, Park T-E, Lee J, et al. 3D microengineered vascularized tumor spheroids for drug delivery and efficacy testing. *Acta Biomater* (2022) 165:153–167. doi: 10.1016/j.actbio.2022.10.009

97. Hachey SJ, Movsesyan S, Nguyen QH, Burton-Sojo G, Tankazyan A, et al. An *in vitro* vascularized micro-tumor model of human colorectal cancer recapitulates *in vivo* responses to standard-of-care therapy. *Lab on a Chip* (2021) 21(7):1333–51. doi: 10.1039/D0LC01216E

98. Ehsan SM, Welch-Reardon KM, Waterman ML, Hughes CC, George SC. A three-dimensional *in vitro* model of tumor cell intravasation. *Integr Biol* (2014) 6 (6):603–10. doi: 10.1039/c3ib40170g

99. Gopalakrishnan V, Helmink BA, Spencer CN, Reuben A, Wargo JA. The influence of the gut microbiome on cancer, immunity, and cancer immunotherapy. *Cancer Cell* (2018) 33(4):570–80. doi: 10.1016/j.ccell.2018.03.015

100. Koyande N, Gangopadhyay M, Thatikonda S, Rengan AK. The role of gut microbiota in the development of colorectal cancer: a review. *Int J Colorectal Dis* (2022) 37:1–15. doi: 10.1007/s00384-022-04192-w

101. Hofseth LJ, Hebert JR, Chanda A, Chen H, Love BL, Pena MM, et al. Early-onset colorectal cancer: initial clues and current views. *Nat Rev Gastroenterol Hepatol* (2020) 17(6):352–64. doi: 10.1038/s41575-019-0253-4

102. Huang P, Liu Y. A reasonable diet promotes balance of intestinal microbiota: prevention of precolorectal cancer. *BioMed Res Int* (2019) 2019:3405278. doi: 10.1155/2019/3405278

103. Zhang S, Yang Y, Weng W, Guo B, Cai G, Ma Y, et al. Fusobacterium nucleatum promotes chemoresistance to 5-fluorouracil by upregulation of BIRC3 expression in colorectal cancer. *J Exp Clin Cancer Res* (2019) 38(1):1–13. doi: 10.1186/s13046-018-0985-y

104. Ternes D, Karta J, Tsenkova M, Wilmes P, Haan S, Letellier E. Microbiome in colorectal cancer: how to get from meta-omics to mechanism? *Trends Microbiol* (2020) 28(5):401–23. doi: 10.1016/j.tim.2020.01.001

105. Kostic AD, Chun E, Robertson L, Glickman JN, Gallini CA, Michaud M, et al. Fusobacterium nucleatum potentiates intestinal tumorigenesis and modulates the tumor-immune microenvironment. *Cell Host Microbe* (2013) 14(2):207–15. doi: 10.1016/j.chom.2013.07.007

106. Ning Y, Manegold PC, Hong YK, Zhang W, Pohl A, Lurje G, et al. Interleukin-8 is associated with proliferation, migration, angiogenesis and chemosensitivity *in vitro* and in vivo in colon cancer cell line models. *Int J Cancer* (2011) 128:2038–2049. doi: 10.1002/ijc.25562

107. Lee J-E, Lee J, Kim JH, Cho N, Lee SH, Park SB, et al. Characterization of the anti-cancer activity of the probiotic bacterium lactobacillus fermentum using 2D vs 3D culture in colorectal cancer cells. *Biomolecules* (2019) 9(10):557. doi: 10.3390/biom9100557

108. Rubert J, Gatto P, Pancher M, Sidarovich V, Curti C, Mena P, et al. A screening of native (Poly) phenols and gut-related metabolites on 3D HCT116 spheroids reveals gut health benefits of a flavan-3-ol metabolite. *Mol Nutr Food Res* (2022) 66 (21):2101043. doi: 10.1002/mnfr.202101043

109. Begley CG, Ioannidis JP. Reproducibility in science: improving the standard for basic and preclinical research. *Circ Res* (2015) 116(1):116–26. doi: 10.1161/CIRCRESAHA.114.303819

frontiers | Frontiers in Oncology

TYPE Original Research
PUBLISHED 14 July 2023
DOI 10.3389/fonc.2023.1156769

OPEN ACCESS

EDITED BY
Manuela Viola,
University of Insubria, Italy

REVIEWED BY
Ting-Yuan Tu,
National Cheng Kung University, Taiwan
Rainer Heuchel,
Karolinska Instutet, CLINTEC, Sweden

*CORRESPONDENCE
Giulio Giustarini
Giulio_giustarini@immunol.a-star.edu.sg
Giulia Adriani
Giulia_adriani@immunol.a-star.edu.sg

RECEIVED 01 February 2023
ACCEPTED 27 June 2023
PUBLISHED 14 July 2023

CITATION
Giustarini G, Teng G, Pavesi A and Adriani G (2023) Characterization of 3D heterocellular spheroids of pancreatic ductal adenocarcinoma for the study of cell interactions in the tumor immune microenvironment.
Front. Oncol. 13:1156769.
doi: 10.3389/fonc.2023.1156769

Characterization of 3D heterocellular spheroids of pancreatic ductal adenocarcinoma for the study of cell interactions in the tumor immune microenvironment

Giulio Giustarini[1]*, Germaine Teng[1], Andrea Pavesi[2,3] and Giulia Adriani[1,4]*

[1]Singapore Immunology Network (SIgN), Agency for Science, Technology and Research (ASTAR), Singapore, Singapore, [2]Institute of Molecular and Cell Biology (IMCB), Agency for Science, Technology and Research (ASTAR), Singapore, Singapore, [3]Mechanobiology Institute, National University of Singapore, Singapore, Singapore, [4]Department of Biomedical Engineering, National University of Singapore, Singapore, Singapore

Pancreatic ductal adenocarcinoma (PDAC) is one of the deadliest malignancies nowadays. The available chemo- and immunotherapies are often ineffective in treating PDAC due to its immunosuppressive and highly desmoplastic tumor immune microenvironment (TIME), which is hardly reproduced in the existing preclinical models. The PDAC TIME results from a peculiar spatial organization between different cell types. For this reason, developing new human models recapitulating the tissue organization and cell heterogeneity of PDAC is highly desirable. We developed human 3D heterocellular tumor spheroids of PDAC formed by cancer cells, endothelial cells, pancreatic stellate cells (PSC), and monocytes. As a control, we formed spheroids using immortalized epithelial pancreatic ductal cells (non-cancerous spheroids) with cellular heterogeneity similar to the tumor spheroids. Normal spheroids containing endothelial cells formed a complex 3D endothelial network significantly compromised in tumor spheroids. Monocyte/macrophages within the 4-culture tumor spheroids were characterized by a higher expression of CD163, CD206, PD-L1, and CD40 than those in the non-cancerous spheroids suggesting their differentiation towards an immunosuppressive phenotype. The heterocellular tumor spheroids presented a hypoxic core populated with PSC and monocytes/macrophages. The 4-culture tumor spheroids were characterized by spatial proximity of PSC and monocytes to the endothelial cells and a cytokine signature with increased concentrations of CXCL10, CCL2, and IL-6, which have been observed in PDAC patients and associated with poor survival. Further, 4-culture tumor spheroids decreased the concentrations of T-cell chemoattracting cytokines, i.e., CCL4, CCL5, and CXCL9, when compared with the non-cancerous spheroids, revealing a critical immunosuppressive feature of the different types of cells forming the tumor spheroids. Our results showed that the 4-culture tumor spheroids better

resembled some critical features of patients' PDAC TIME than monoculture tumor spheroids. Using the proposed human 3D spheroid model for therapy testing at the preclinical stage may reveal pitfalls of chemo- and immuno-therapies to help the development of better anti-tumor therapies.

KEYWORDS

pancreatic ductal adenocarcinoma, cancer, spheroids, *in vitro* model, heterocellular, tumor immune microenvironment, macrophages, cytokines

Introduction

Pancreatic Ductal Adeno-Carcinoma (PDAC) represents 2.6% of the incidence of cancer worldwide, nonetheless, 4.7% of the mortality (1). Available therapies, namely chemotherapies, immunotherapies, and radiotherapies for treating PDAC are characterized by a poor response associated with minimal survival (2, 3). The lack of effective therapies undoubtfully contributes to the 10.8% 5-year relative survival of PDAC patients (4). Within the tumor immune microenvironment (TIME), cells, extracellular matrix, and soluble factors play a pivotal role in the resistance to therapies (5). The available preclinical models for PDAC, including both *in vivo* and *in vitro* models, suffer limitations in identifying clinically effective therapies due to their inability to fully recapitulate the complex and heterogeneous TIME observed in patients. The development of 3D heterocellular PDAC spheroids represents a step forward in predicting chemoresistance, better simulating key features of PDAC pathophysiology compared to 2D *in vitro* tests (6). Pancreatic stellate cells (PSC) are the main source of extracellular matrix (ECM) in PDAC (7) and have been shown to play a key role in tumor vascularization and in establishing an immunosuppressed environment in PDAC (8, 9). PSC have similar functions to the hepatic stellate cells and their transcriptional profile in response to inflammation is unique among the other fibroblastic populations in pancreatic cancer (10), dramatically expanding during carcinogenesis in an orthotopic murine model (11). Recently, Helms et al. demonstrated that PSC-derived myofibroblasts, rather than other fibroblasts of different origins, have a non-redundant capability to shape the desmoplastic PDAC TIME (10), although representing only 10 to 15% of the cancer-associated fibroblasts in an orthotopic murine model (8, 9). In two different models, PSC showed their capability to increase proliferation and expression of vimentin (mesenchymal marker) whereas decreasing the expression of E-cadherin (epithelial marker) in the pancreatic cancer cell line PANC-1 when co-cultured in a 3D spheroid (12, 13). Adding MRC-5 immortalized fibroblastic cells of fetal lung origin to 3D PDAC spheroid models have shown to implement certain features observed in patients' TIME, such as the differentiation of monocyte to M2-like macrophages (14). However, is still unclear whether PSC influences cancer cells and primary human monocytes/macrophages in 3D co-culture systems. This uncertainty arises because human PSC-derived fibroblasts exhibit protective effects on pancreatic cancer cells, which are not observed in co-cultures with MRC-5 fibroblastic cells, (15).

Macrophages of both fetal and hematopoietic stem cell ontogeny have been observed within the PDAC TIME. Embryonically- and hematopoietic stem cell-derived macrophages exert different functions, such as shaping the fibrotic processes and regulating the immune responses, respectively, as demonstrated in an orthotopic murine model of PDAC (16). In line with these findings, clinical trials have shown that the dual inhibition of chemotactic receptors (CCR2 and CCR5) for the recruitment of monocytes has a beneficial effect on the anti-tumor immunity and chemotherapeutic response in PDAC compared to either strategy alone. This evidence tailored a fundamental immunosuppressive and drug-resistance role for monocytes within the PDAC TIME, underlining their involvement in response to therapies (Tomás-Bort et al., 2020).

An abundant cell type within the PDAC TIME is represented by endothelial cells, even though tumor vascularization is often heavily compromised (17). To include endothelial cells (EC), a previous study has combined human umbilical vein EC (HUVEC) with lung fibroblasts and different pancreatic cancer cell lines to form 3D PDAC spheroids. The heterogeneous spheroids containing the three cell types showed stronger chemoresistance of cancer cells to standard therapies (i.e., doxorubicin and gemcitabine) when compared with spheroids formed by only cancer cells, underlining important synergisms between endothelial cells and other cells in the spheroids to reproduce drug resistance as observed in patients (18).

However, none of the 3D heterocellular PDAC spheroids mentioned above or similar models (6, 15, 19) included immune cells within the PDAC heterocellular spheroids.

We hypothesized that *in vitro* co-culture of monocytes/macrophages with cancer, endothelial, and stellate cells in 3D spheroids could reproduce a microenvironment similar to what was observed in the immune niche of different tissues (20, 21), in which cells establish a partnership promoting mutual changes in transcription and survival, shaping their differentiation and activation within the spheroids.

Therefore, here we present the first 3D heterocellular human spheroid model of PDAC formed using PANC-1 cancer cells, pancreatic stellate cells (PSC), endothelial cells (EC) and peripheral blood mononuclear cell (PBMC)-derived monocytes. Combining immunofluorescence, flow cytometry, and cytokine analysis, we characterize the viability, proliferation, cytokine concentrations, and

monocyte differentiation within the spheroids. We observed that the 4-culture spheroids were characterized by spatial proximity of PSC, monocytes, and EC, which formed a 3D endothelial network and were characterized by a cytokine signature resembling the one observed in PDAC patients with poor survival. The model included control spheroids formed using h-TERT-human pancreatic epithelial nestin-expressing cells (HPNE), which served and will serve to validate differences with cancer spheroids. Ultimately, we envision that the cellular interactions within the heterocellular PDAC spheroids containing the four cell types (cancer, stellate, endothelial cells, and monocytes) will better simulate key features of PDAC and our heterocellular spheroids will represent a better tool for more complex microfluidic models studying T cell interaction with the patient's TIME.

Material and methods

Cell culture

PANC-1 (American Type Culture Collection, ATCC), h-TERT-HPNE (human pancreatic epithelial nestin-expressing cells immortalized by transducing with a h-TERT cDNA) (ATCC, Manassas, VA, USA) (22) were maintained in Iscove Modified Dulbecco Media (IMDM) supplemented with 10% fetal bovine serum (FBS, ThermoScientific Cat#10082147) and penicillin/streptomycin (100 U/mL, Invitrogen/Gibco Cat#15140122). Human Pancreatic Stellate Cells (HPaSteC, here referred as PSC) (Gene Etichs Cat#3830, Lot#14358) were maintained in Stellate Cell Medium (SteCM, ScienCell Research Laboratories, Cat#5301) supplemented with 2% FBS (ScienCell Research Laboratories, Cat#0010), 1% stellate cell growth supplement (ScienCell Research Laboratories, SteCGS, Cat#5352) and 1% antibiotic solution (ScienCell Research Laboratories, Cat#0503). Human umbilical vein endothelial cells (HUVEC, Lonza, C2519AS, Lot#633426) and RFP-HUVEC (Angioproteomie cAP-001RFP, Lot#2021122802) were cultured in EGM-2™ SingleQuot™ containing 0.5 ng/ml VEGF, 5 ng/ml EGF, 10 ng/ml bFGF, 20 ng/ml long R3-IGF-1, 22.5 µg/ml heparin, 1 µg/ml ascorbic acid, 0.2 µg/ml hydrocortisone, gentamicin (1/1000 dilution) and 2% FBS. All cells were cultured in 75 and 175 cm^2 tissue culture treated flasks in a humidified atmosphere composed of 95% air and 5% CO_2 and a temperature of 37°C. Cells were passaged every 72 h using 0.25% (PANC-1 and HPNE) or 0.05% (HUVEC and PSC) Trypsin-EDTA (Gibco, Thermo Fisher Scientific, Cat# 25300054).

Generation of GFP-PANC-1 cells

The generation of GFP-tagged PANC-1 cells was achieved using lipofectamine 2000-mediated transfection following manufacturer's instruction. Briefly, PANC-1 cells were cultured and maintained in appropriate growth media before transfection with an enhanced green fluorescent protein (eGFP) encoding plasmid (pEGFP-C1 EGFP-3XNLS, cat. N. #58468, Addgene) encapsulated in Lipofectamine 2000. The lipofectamine-GFP plasmid complex was added to the PANC-1 cells and allowed to incubate for 48 h. Following the transfection, the GFP-tagged PANC-1 cells were monitored under a fluorescence microscope to confirm successful GFP expression and subsequently FACS sorted to enrich the positive population.

Human blood cells

Ethical approval for obtaining healthy human volunteer blood cones was obtained by the institutional ethical review board under the Project No.: 201306-04 and all subjects provided written informed consent.

Monocyte isolation

Peripheral blood mononuclear cells (PBMC) were isolated from blood cones using a density gradient of Ficoll/Paque PLUS (GE Healthcare, Marlborough, MA, USA). The content of the blood cones was diluted 40x in phosphate buffer saline (PBS) and placed onto a layer of Ficoll/Pacque (density 1.077 g/L) before centrifuging at 900 x g, at room temperature (RT) for 20 min. The obtained PBMC layer was collected using a sterile pipette and washed with Ca^-Mg^- PBS before incubation with red blood cell lysis (155 mM NH_4Cl, 10 mM $KHCO_3$, 0.1 mM EDTA) for 5 min at RT. Cells were washed in Ca^-Mg^- PBS and prepared for cryopreservation using Bambanker™ (Fujifilm Wako Chemicals U.S.A. Corporation, Richmond, VA, USA). On the day of the experiment, cryopreserved PBMC suspension was used for the isolation of untouched monocytes using Pan Monocyte Isolation kit (Miltenyi Biotec, Bergisch Gladbach, Germany). The isolated cells were characterized by the expression of CD14 and CD16 in a $CD45^+/CD3^-$ gate. Monocytes represented more than 95% of the total $CD45^+$ cells.

Cell labeling

Cells were collected in tubes and counted before washing them once in PBS. Cells were spun down at 300 x g for 5 min and the supernatant discarded. PBS containing CellTrace™ Violet (cat. n. C34557, Thermo Fisher, dilution 1/1000), CellTracker™ Deep Red (cat. n. C34565, Thermo Fisher, dilution 1/1000) and CellTracker™ Green CMFDA (cat. n. C2925, Thermo Fisher, dilution 1/500) was used to stain the different cell types according to the requirements of the experiment. The cell pellet was resuspended in PBS containing the dyes and incubated at 37°C. After 30 min, 5 ml of medium containing FBS was used to stop the staining reaction. Other 5 ml of medium containing FBS was used to wash the cells before resuspending them in EGM-2 for spheroid formation.

Hanging-drop spheroid formation

Heterogeneous cell suspensions for the spheroid formation were obtained by mixing either PANC-1 or HPNE with PSC, HUVEC and PBMC-derived monocytes following the ratios shown in Table 1. The

seeding number of PANC-1 cells was determined to achieve a minimum radius of approximately 250 μm and a viability above 90% of the spheroids at day 7. EGM-2 was adopted as medium for the spheroid formation after we assessed no significant changes in the cell number of PANC-1, HPNE, HPaSteC and monocytes in 2D culture using EGM-2 compared to the respective recommended media (Supplementary Figure 1). The PANC-1 cell number was kept constant to better assess the contribution of each cell type on cancer cells. The cell ratio to PANC-1 cell was tuned to observe the arrangement of endothelial cells into a three-dimensional (3D) network. With this aim, several preliminary ratios were investigated for EC, PSC and monocytes. We selected the ratios supporting the formation of the 3D EC network. The seeding number of HPNE cells was determined by their ability to form spheroids with a radius similar to the PANC-1 spheroids, while ensuring their viability remains above 90%. The other cell types in the HPNE spheroids were kept in the same number as for the PANC-1 spheroids. Cells were resuspended in EGM-2 and seeded using a custom-made polydimethylsiloxane (PDMS) support for the formation of spheroids with the hanging drop technique. Spheroids were formed in 4 or 7 days depending on the experiment.

Immunofluorescence

At day 4 or 7, spheroids were spun down at 300 x g for 1 min and each drop was assessed for the formation of the spheroid by an inverted microscope. All the formed spheroids were collected in 1.5 mL microcentrifuge tubes and spun down for 1 min at 300 x g. Supernatant was removed, and spheroids were incubated with new medium containing a dilution of the membrane impermeable DNA-staining DRAQ7 (Thermo-Fisher Scientific, Waltham, MA, USA) for 30 min at 37°C. Spheroids were washed in PBS before adding PBS containing 4% paraformaldehyde. After 20 min at RT spheroids were washed 3 times with PBS + 1% bovine serum albumin (BSA) before proceeding with the staining. For intracellular staining, spheroids were permeabilized using PBS $Ca^{-}Mg^{-}$ + 0.5% Triton-X-100. After 30 min, spheroids were washed two times with PBS $Ca^{-}Mg^{-}$ + 1% BSA before incubating them with PBS $Ca^{-}Mg^{-}$ + 0.5% Triton-X-100 0.5% + 5% BSA for 3 h. After washing with PBS $Ca^{-}Mg^{-}$ + 1% BSA, spheroids were incubated overnight with PBS $Ca^{-}Mg^{-}$ + 1% BSA containing one of the following antibodies: rat AlexaFluor594-conjugated anti-human Ki67 antibody (1:100, cat. n. 11-5698-82, EBioscience, Thermo-Fisher Scientific), recombinant anti-human eFluor650-conjugated HIF-1α antibody (1:50, cat. n. 190569, Abcam, Cambridge, UK) and rabbit anti-human purified collagen I antibody (1:50, cat. n. 34710, Abcam, Cambridge, UK). For collagen I immunofluorescent staining, overnight incubation at 4°C with goat anti-rabbit AlexaFluor546 anti-IgG secondary antibody (Fisher Scientific, Carlsbad, CA, USA) in PBS $Ca^{-}Mg^{-}$ + 1% BSA. Spheroids were washed 3 times with PBS $Ca^{-}Mg^{-}$ + 1% BSA. The spheroids stained for Ki67 were incubated with Hoechst 33342 (1 μg/ml) in PBS + 1% BSA. After 1 h, spheroids were washed with PBS $Ca^{-}Mg^{-}$ + 1% BSA before proceeding with image acquisition using an inverted confocal microscope Olympus FV1000 (Olympus, Tokyo, Japan).

Flow cytometry

Spheroids were collected in 1.5 mL Eppendorf tubes and washed with PBS $Ca^{-}Mg^{-}$ + 1% BSA before proceeding with cell dissociation. Dissociation was performed in 2 steps: 1) incubation with RPMI containing 1 mg/ml Collagenase type IV (Worthington Biochemical Corporation, USA) for 20 min at 37°C; 2) addition of 0.25% trypsin + EDTA (0.53 mM) and further incubation for 20 min. Enzymatic activity was stopped by addition of RPMI containing 10% FBS. Cells were washed with fluorescence-activated cell sorting buffer (PBS containing 0.5% BSA, 0.05% NaN_3, 0.5 mM EDTA) and prepared for flow cytometry staining. Cells were first stained with LIVE/DEAD® Fixable Dead Cell Stain (Molecular Probes, Invitrogen, Carlsbad, CA, USA) followed by incubation with fragment crystallizable region receptor (FcR)-blocking antibody to block the FcR. The following antibodies were used for the extracellular staining of cells obtained from the spheroids: mouse PerCP-cy5.5-conjugated anti-human CD86 (clone: 2331) (cat. n. 561129, BD Bioscience, Franklin Lakes, NJ, USA), mouse PE-conjugate anti-human CD68 (clone: Y1/82A) (cat.

TABLE 1 Composition of PANC-1 spheroids (ratios).

Condition	PANC-1		HPaSteC		HUVEC		Monocytes	
	Ratio	Cell number	Ratio	Cell number	Ratio	Cell number	Ratio	Cell number
PANC-1	1	(1500)	–	(-)	–	(-)	–	(-)
PANC-1+PSC	1	(1500)	2	(3000)	–	(-)	–	(-)
PANC-1+EC	1	(1500)	–	(-)	2	(3000)	–	(-)
PANC-1+Mono	1	(1500)	–	(-)	–	(-)	4	(6000)
PANC-1+PSC+EC	1	(1500)	2	(3000)	2	(3000)	–	(-)
PANC-1+PSC+Mono	1	(1500)	2	(3000)	–	(-)	4	(6000)
PANC-1+EC+Mono	1	(1500)	–	(-)	2	(3000)	4	(6000)
PANC-1+PSC+EC+Mono	1	(1500)	2	(3000)	2	(3000)	4	(6000)

-, Cell type not included in the spheroid.

n. 333808, BioLegend, San Diego, CA, USA), mouse Pacific Orange-conjugated anti-human CD14 (clone: TuK4) (cat. n. MHCD1430, Invitrogen), mouse anti-human eFluor-450 CD206 (clone: 19.2) (cat. n. 48-2069-41, eBioscience), mouse BUV395-conjugated CD45 anti-human (clone: HI30) (cat. n. 563791, BD Bioscience), mouse BUV737-conjugated anti-human CD40 (clone: 5C3)(cat. n. 741847, BD Bioscience), mouse PE-CF594-conjugated anti-human CD163 (clone: GHI/61) (cat. n. 562670, BD Bioscience), mouse PE-cy7-conjugated anti-human CD274 (PD-L1, clone: MH3) (cat. n. 329718, BioLegend), mouse BV605-conjugated anti-human HLA-DR (clone: L243) (cat. n. 307640, BioLegend). For those analysis requiring the intracellular staining, after the cells were stained for the extracellular staining, they were fixed using intracellular fixation buffer (eBioscience). Following procedures reported in the manufacturer's instructions, the permeabilization buffer was used to incubate the antibodies recognizing α-SMA and HIF-1α. The antibodies used to recognize these proteins are the following: mouse AlexaFluor 488-conjugated anti-human α-SMA (cat. n. 53-9760-82, Invitrogen), recombinant eFluor650-conjugated anti-human HIF-1α (cat. n. 190569, Abcam). After the intracellular staining cells were resuspended in FACS buffer and prepared for acquisition at BD FACS Symphony A3. Data were analyzed using FlowJo analysis software (Tree Star, Inc., Ashland, OR, USA).

Microscopy

Images of the spheroids were acquired using the inverted confocal microscope Olympus FV1000. Images were processed using IMARIS software (v. 9.7.1, Bitplane). We identified Ki67 positive nuclei using the functions "spots". PANC-1 nuclei were identified selecting mean intensity of Hoechst 33342 and GFP using background subtraction and considering the fluorescent signal elongation due to the acquisition. Ki67 foci positive cells were considered positive using the intensity sum of the signal emitted by the AlexaFluor594-conjugated anti-human Ki67 antibody within the identified nuclei. Dead cells were excluded based on their mean intensity for DRAQ7.

Analogously, for HIF quantification nuclei were identified using Hoechst 33342 signal using the function "spots" and HIF-AlexaFluor647 signal was identified using a cobalt chloride treated spheroid (positive control). HIF-1α positive control was obtained exposing the formed spheroid to 200 μM cobalt chloride in EGM-2 for 24 h.

Cell composition of the spheroids was identified using the fluorescence of different CellTrackers/CellTracers, GFP-PANC-1 and RFP-HUVEC. Cells were identified using both "spots" and "surface" functions selecting a diameter of cells and a threshold for the mean/median fluorescence intensities after automatic background subtraction and considering the fluorescent signal elongation due to the acquisition. Object to object distance was used to plot distance between different cell types using "Vantage". Normal spatial distributions of the identified spots were provided by the software. ImageJ software was used to determine the spatial distribution of the different cell types within the HPNE/PANC-1 spheroid. Mean fluorescence of the cells was assessed using the function "plot profile" selecting a region of interest containing the spheroids. Diameter of the spheroids was used to identify an outer and inner region as depicted in Supplementary Figure 2. Area under the curve of mean fluorescence was calculated for each region (inner, outer) and the inner/outer ratio of the areas (distribution ratio) plotted as arbitrary unit (A.U.).

Human cytokine multiplex bead-based assay

The analysis of multiple cytokines in the spheroid formation medium at day 7 was performed using the Luminex technology. For each condition at day 7 after seeding, the spheroid formation medium of 18 spheroids was pooled in a single Eppendorf tube. Spheroids were centrifuged 1 min at 300 x g and supernatant transferred in a new Eppendorf tube. First, the supernatant was centrifuged 5 min at 400 x g. The supernatant was collected and further centrifuged for 10 min at 2000 x g. Supernatant was transferred in a 96 well plate and stored at -80°C until analysis. Supernatant was thawed the day of the assay and prepared for the use of Bio-Plex Pro Human Cytokine Screening Panel 48-Plex (Biorad). Samples were incubated with fluorescent-coded magnetic beads pre-coated with respective antibodies in a black 96 well clear-bottom plate overnight at 4°C. After incubation, plates were washed 5 times with wash buffer (PBS with 1% BSA (Capricorn Scientific) and 0.05% Tween-20 (Promega)). Sample-antibody-bead complexes were incubated with Biotinylated detection antibodies for 1 h and washed 5 times with wash buffer. Subsequently, Streptavidin-PE was added and incubated for another 30 min. Plates were washed 5 times again, before sample-antibody-bead complexes were re-suspended in sheath fluid for acquisition on the FLEXMAP® 3D (Luminex) using xPONENT® 4.0 (Luminex) software. Data analysis was done on Bio-Plex ManagerTM 6.1.1 (Bio-Rad). Standard curves were generated with a 5-PL (5-parameter logistic) algorithm, reporting values for both mean florescence intensity (MFI) and concentration data.

Statistics

Data are presented as means ± standard error of the mean (SEM) if not differently stated in the figure caption. Statistical significance for comparisons was determined by one- or two-way ANOVA with different *post-hoc* tests. Proper *post-hoc* test is indicated in the figure legend. A p-value less than 0.05 was considered statistically significant. All data are analyzed using GraphPad Prism (version 6.07) software (San Diego, CA, USA).

Results

HPNE and PANC-1 cells form viable heterocellular spheroids

Heterogenous cell suspensions with the composition indicated in Table 1 were cultured using a custom-made PDMS layer for the spheroid formation by hanging drop technique (Figure 1A). On day

7, the spheroids were collected and prepared for imaging to assess size and viability (Figure 1B; Supplementary Figures 4, 5). PANC-1 spheroids with lower cell heterogeneity, namely the monoculture PANC-1 spheroids and the bi-culture (2-culture) PANC-1+PSC spheroids, showed a significantly smaller size when compared with the other spheroids containing more cell types with mean radii ranging between 248 µm for monoculture and 318 µm for quadri-culture (4-culture) (Supplementary Figure 3A). Among the different conditions, spheroid containing PANC-1+EC showed the highest mean radius of 380 µm. DRAQ7+ cells, representing the non-viable cells with a compromised cell membrane, did not exceed 10% of the total number of cells (Supplementary Figure 3B) for all the spheroid compositions, suggesting good viability of the spheroids at the time point assessed. Spheroids obtained using h-TERT HPNE only slightly increased their size accordingly with their heterogeneity without a statistically significant difference among different spheroid compositions (Figure 1C). The radii of the HPNE spheroids were shorter than the PANC-1 spheroids with the same heterogeneity.

Different cell types co-exist and interact in the heterocellular HPNE and PANC-1 spheroids

The cell composition analysis of the spheroids was performed using flow cytometry after spheroid dissociation on day 7 (Figure 1C). The cell composition was determined as percentage of each cell type over the total cell number in the spheroid. For PANC-1 spheroids, EC (in red in Figure 1C) were detected only in spheroids containing PSC and were averagely of 0.5 and 1% in PANC-1+PSC+EC+Mono and PANC-1+PSC+EC conditions respectively (Figure 1C). By contrast for HPNE, EC were detected in all the spheroids (Figure 1C). For

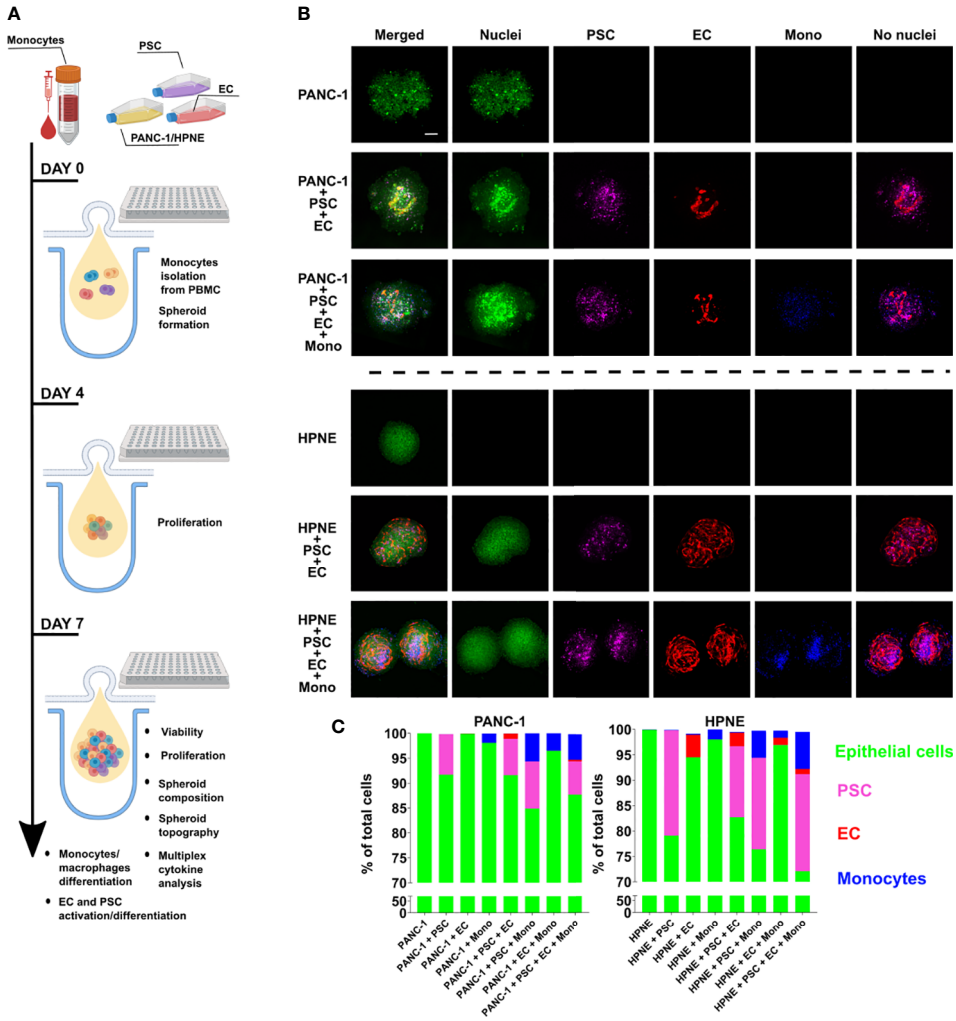

FIGURE 1
Characterization of size, viability and composition of HPNE and PANC-1 spheroids with different cellular heterogeneity. PANC-1 and HPNE cells were combined with PSC, EC and monocytes following the ratio shown in Table 1. **(A)** Schematic illustration of the workflow of spheroid formation and assays performed. **(B)** Representative images of monoculture, 3-culture and 4-culture of PANC-1 and HPNE spheroids at day 7 using confocal imaging (green: nuclei, purple: PSC, red: EC, blue: monocytes); scale bar: 100 µm. **(C)** Parts of whole graph showing the spheroid composition as % of each cell type on the total number of live cells, determined by flow cytometry analysis at day 7.

PANC-1 spheroids, PSC (in purple in Figure 1C) were present in all the spheroids. The percentage of PSC in the spheroids was ranging from 6.7 to 9% without significant differences among the spheroid conditions (Figure 1C). Similarly, for HPNE spheroids, PSC were ranging between 14 to 20% without significant differences among conditions (Figure 1C). For PANC-1 spheroids, monocytes (in blue in Figure 1C) at day 7 were increasing their percentages accordingly with the increase in heterogeneity of the PANC-1 spheroids. In particular, we observed that monocytes were ~1% when cultured alone with PANC-1 but their percentage increased to 3% in PANC-1 +EC+Mono, and 5% in PANC-1+PSC+Mono and PANC-1+PSC +EC+Mono spheroids (Figure 1C). Although a similar percentage increase of monocytes was observed within HPNE spheroids with a higher heterogeneity, monocyte percentage in HPNE+EC+Mono spheroids was not statistically different from the percentage detected in HPNE+Mono spheroids (Figure 1C).

PSC and monocytes distribute in proximity of a disrupted endothelial cell network within the PANC-1 tumor spheroids

Spatial cell organization and cellular functions are interconnected parameters as demonstrated by recent transcriptional and proteomic studies (23). The spatial organization of individual cells into aggregates has been shown to be dependent on self-assembly occurring *via* ligand-receptor interactions (24).

It has been demonstrated that vasculature in PDAC TIME has compromised functions due to the highly desmoplastic TIME. The molecules contained in the ECM take part in the physical stress causing the vessels within the tumor to collapse (25). The structures of the 3D endothelial network did not exhibit a lumen and, for this reason, they were not defined as vessels. However, we assessed the formation of endothelial networks within our spheroids and whether the presence of other cell types influences the EC organization using RFP-labeled EC (Figure 2). The RFP-EC were imaged within the spheroids by confocal microscopy (Figures 2A, C) and the complexity of the endothelial cell network was quantified by measuring the volume of the RFP fluorescence signal as percentage of the RFP-EC volume in HPNE +PSC+EC (Figure 2B) or PANC-1+PSC+EC (Figure 2D) for HPNE and PANC1 spheroids, respectively. We observed that HPNE spheroids collected at day 7 showed a complex 3D endothelial network with similar volumes in all the spheroids (Figures 2A, B). By contrast, PANC-1 spheroids collected at day 7 had no endothelial network formation when cultured without PSC (Figures 2C, D). The representative images of the RFP fluorescence signal showed a distinct reduction of the 3D endothelial network complexity in PANC-1 spheroids when compared to HPNE spheroids (Figures 2A, C). Indeed, a disrupted endothelial network was observed at day 7 in PANC-1 spheroids containing PSC (Figure 2C) compared to the HPNE spheroids with the same cell composition (Figure 2A). In addition, PANC-1+PSC+EC+Mono spheroids showed a significant decrease of ~28% in the RFP fluorescence volume compared to the PANC-1+PSC+EC spheroids not containing monocytes (Figures 2C, D).

By utilizing the 3D endothelial cell network as a reference, we evaluated the spatial cellular organization of PANC-1 4-culture spheroids that emerged from cell-cell interactions during the formation of the spheroids.

Distances between different cell types were calculated using the function "object-to-object" statistics and plotted using "Vantage" with IMARIS software. EC were identified as "surfaces" whereas the other cell types were identified as "spots" and the software quantified the distance of each spot from the EC surface.

The distribution of the distances between the different cell types showed that PSC and monocytes were at a median distance of respectively 15.80 and 22.00 µm from the EC surface, whereas PANC-1 cells showed a significantly greater median distance of 72.05 µm from the EC surface (Figure 3A). The cumulative distribution function of PSC showed that 50% of the identified PSC were located within a 26.95 µm mean distance from the EC surface (Figure 3B) and this was not significantly affected by the presence of monocytes within the aggregates (data not shown). The cumulative distribution function of monocytes showed that 50% of these cells were located within a 36.25 µm mean distance from the EC surface. By contrast, the distribution of PANC-1 cells revealed that 50% of the cells were located at a significant greater mean distance of 72.40 µm from the EC surface compared to PSC and monocytes (Figure 3B).

PSC and monocytes are located in the core of PANC-1 tumor spheroids

We assessed the spatial cell distribution within the spheroids by dividing the spheroid in two concentric areas: an outer (OUT) and an inner (IN) area. We defined the inner area as the circle having half of the total spheroid radius and having the same center of the spheroid. The remain area of the spheroid was considered the outer area (Supplementary Figure 2). In these areas we calculated the area under the curve (AUC) of the fluorescent signal of each cell type. The AUC IN/OUT ratio of the fluorescent signal of each cell type provides an understanding of the preferred location of the cells within the spheroid.

Independently of the other cells in the PANC-1 spheroids, the integrated fluorescence intensity signal of PSC in the inner region of the spheroids was greater than the one detected in the outer region with an average AUC IN/OUT distribution ratio above 1.2 (Figures 4A, B) suggesting that PSC are preferentially located in the inner area for all spheroid conditions. A statistically significant 25% decrease of the AUC IN/OUT ratio was observed in the 4-culture when compared to the PANC-1+PSC spheroids which presented the greatest mean ratio among the tested conditions (Figure 4B) suggesting that the PSC tend to distribute more homogeneously within the spheroids when in 4-culture.

Monocyte distribution within the PANC-1 spheroids was characterized by a statistically significant higher AUC IN/OUT distribution ratio when co-cultured with PSC in 3-culture and 4-culture spheroids with an average AUC IN/OUT distribution ratio above 1.1, whereas PANC-1 spheroids not containing PSC had a distribution ratio approximately equal to 1 (Figures 4C, D), suggesting that the monocytes were preferentially distributed within the inner area of the spheroids only when in co-culture with the PSC.

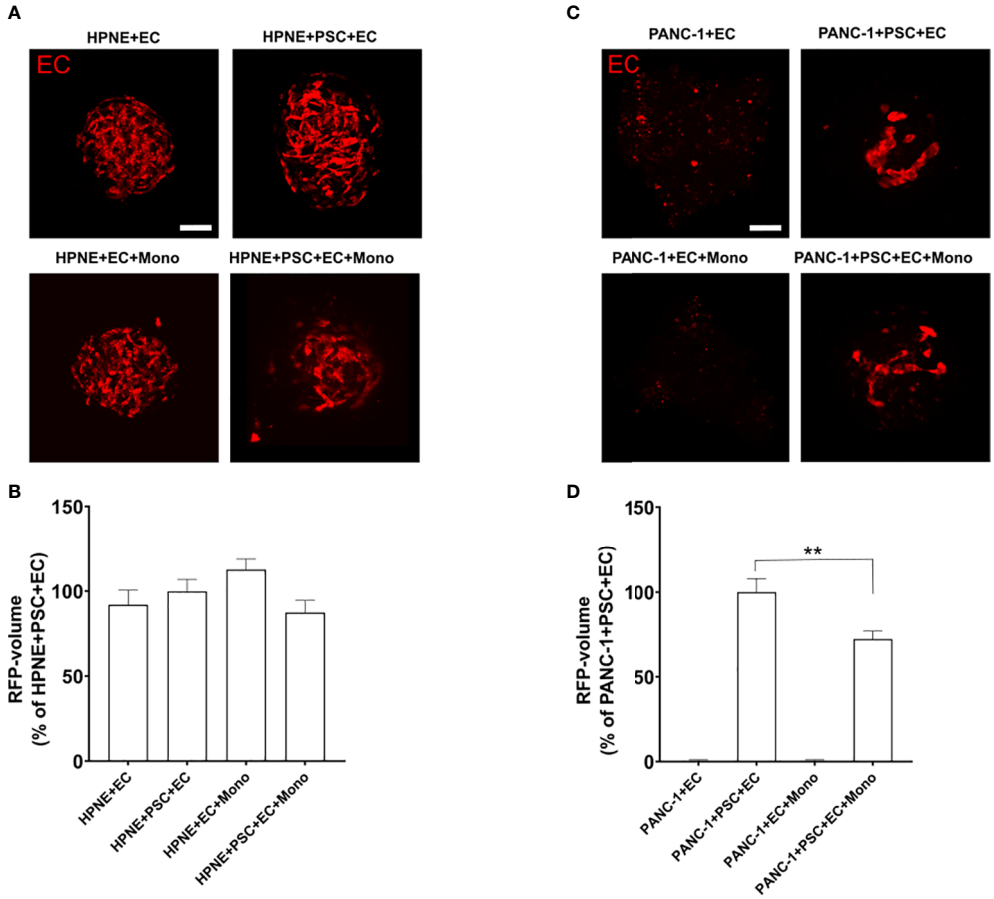

FIGURE 2
PANC-1 spheroids show a disrupted 3D endothelial network compared to HPNE spheroids. Spheroids were formed using RFP-EC in order to assess by confocal microscopy the EC organization within the spheroids with different cellular composition. **(A)** Representative confocal images of the different PANC-1 spheroids containing RFP-EC at day 7. **(B)** Bar plot of the volume of the EC network quantified as percentage of the RFP volume of PANC-1+PSC+EC spheroids. Data shows mean ± SEM. Statistical significance for comparisons was determined by one-way ANOVA with Dunnett's *post-hoc* test **p<0.01 when compared to the volume of PANC-1+PSC+EC. **(C)** Representative confocal images of the HPNE spheroids containing RFP-EC at day 7. **(D)** Bar plot of the volume of the EC network quantified as percentage of the RFP volume of HPNE+PSC+EC spheroids. Data shows mean ± SEM. Statistical significance for comparisons was determined by one-way ANOVA with Dunnett's *post-hoc* test.

PANC-1 4-culture spheroids produce peripheral collagen I and express HIF-1α in the spheroid's core

Collagen I represents one of the most abundant molecules in the ECM of PDAC and it is often identified as the molecule responsible of the desmoplastic reaction associated with a reduced survival in patients (26). Hypoxic responses are often observed in collagen-rich conditions in PDAC mostly due to the cross-linked molecules of collagen which exert a compression on the vasculature (27). Hypoxia-related gene transcription is regulated by a class of transcription factors called the hypoxic inducible factors (HIFs), and in particular, the ubiquitous HIF-1α. The activation of the hypoxic responses has a role in shaping the TIME by mediating the transcription of genes involved in cancer cell metabolism and modulating the release of cytokines and growth factors (28). Thus, we characterized the expression of collagen I and HIF-1α in our spheroids with different cellular heterogeneity.

The immunofluorescent staining revealed that 4-culture spheroids have a significantly greater expression of collagen I when compared to any other tested PANC-1 spheroid (Figure 5A). The collagen I was mainly observed at the periphery of the spheroids, especially in the PANC-1 4-culture spheroids (Figure 5B).

In order to quantify the activation of HIF-1α we assessed the percentage of HIF-1α positive nuclei on the total number of nuclei (Figure 5C). We observed that PANC-1 monoculture spheroids had a limited percentage of positive nuclei (Figure 5D) as well as 2-culture PANC-1 spheroids. By contrast, spheroids containing monocytes had very bright positive nuclei (Figure 5D). Interestingly, the combination of PSC and monocytes in the 3- and 4-culture PANC-1 spheroids resulted in a significant increase of the percentage of HIF-1α positive nuclei when compared to the other tested spheroids (Figure 5C). Moreover, the HIF-1α positive nuclei of 3- and 4-culture PANC-1 spheroids were mainly located in the core of the spheroids rather than in the outer region (Figure 5D).

Using flow-cytometry we investigated the expression of HIF-1α on the cells used to form the PANC-1 4-culture spheroids. As showed in the histogram plot in Figure 5E, monocytes had the greater median expression of HIF-1α among the cells within the

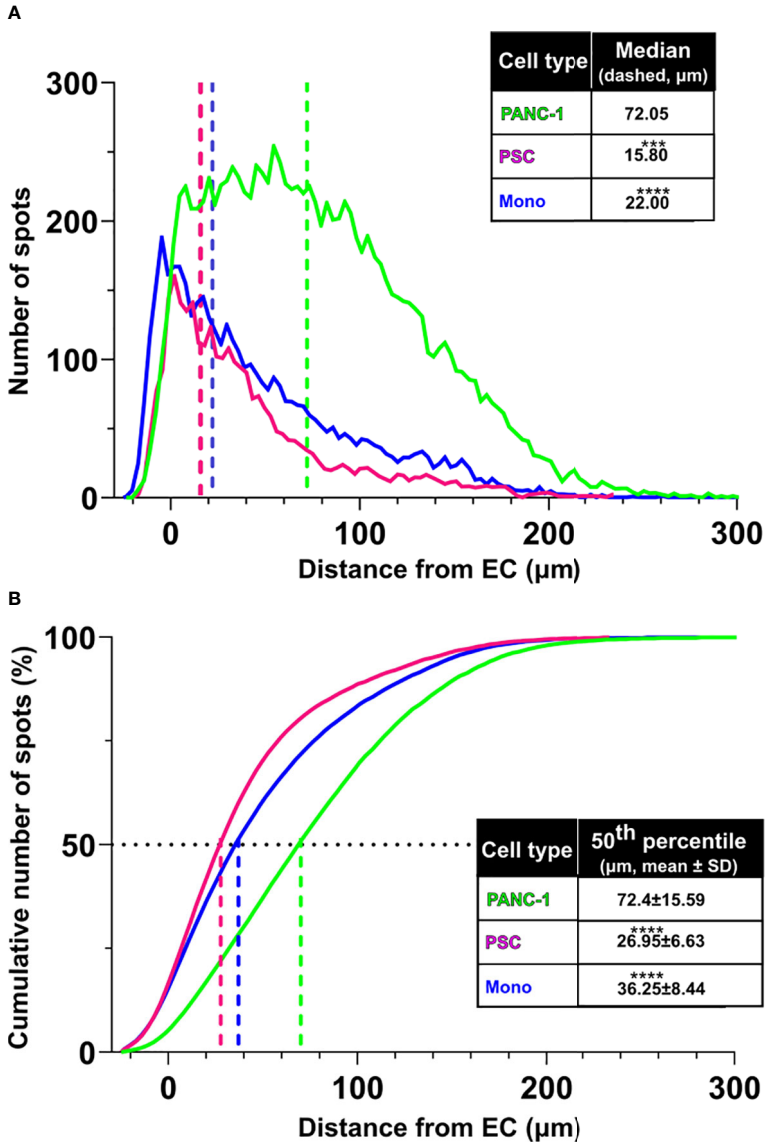

FIGURE 3
PSC and monocytes distribute in proximity of the EC network. **(A)** Distribution of cell distance from the EC surface by cell type (green: PANC-1, purple: PSC, blue: monocytes. Statistical significance for comparisons was determined by one-way ANOVA with Kruskal-Wallis' *post-hoc* test. **(B)** Plot of the cumulative distribution of the distance of PANC-1, PSC and monocytes from the EC network. The plot shows also the distance from EC at which 50% of the total number of each cell type is detected. Mean values of the 50th percentile distance was used for statistical significance using one-way ANOVA with Dunnett's *post-hoc* test. ****p<0.0001, ***p<0.001 when compared to distance from EC of the PANC-1 cells.

PANC-1 4-culture spheroids, suggesting the monocytes greatly contributed to the high HIF-1α nuclear expression observed in the PANC-1 3- and 4-culture spheroids.

To assess the size-dependency of the HIF-1α expression, we further formed monoculture spheroids with the same diameter of the 4-culture spheroids by increasing the number of initial PANC-1 cells seeded for spheroid formation. Monocyte embedded in these spheroids were stained with Cell Tracker Violet (CTV). Our results were confirmed because also the bigger PANC-1 monoculture spheroids presented fewer positive nuclei for HIF-1α compared to the PANC-1 4-culture spheroids that presented an evident HIF-1α expression in the core. Among the positive nuclei in the 4-culture we could detect several monocytes although positivity was also detected into PANC-1-GFP cells (Figure 5F).

PSC increase PANC-1 cell proliferation

Although we seeded the same number of PANC-1 cells for spheroid formation across the different conditions, we measured an increased number of GFP-PANC-1 cells when they were co-cultured for 7 days in 2-culture, 3-culture and 4-culture with the different combinations of PSC, EC or monocytes (Figure 6A). To assess the proliferation of the GFP-PANC-1 cells we measured the Ki67 expression during the spheroid formation at day 4 and day 7. We quantified the proliferating cells by selecting GFP^{+} cells (only PANC-1) expressing nuclear Ki67 and plotted the values as percentage of the total number of GFP-PANC-1 cells at day 4 and day 7 (Figure 6B). At day 4, PANC-1 spheroids containing PSC showed an increased percentage of proliferating PANC-1 cells which was

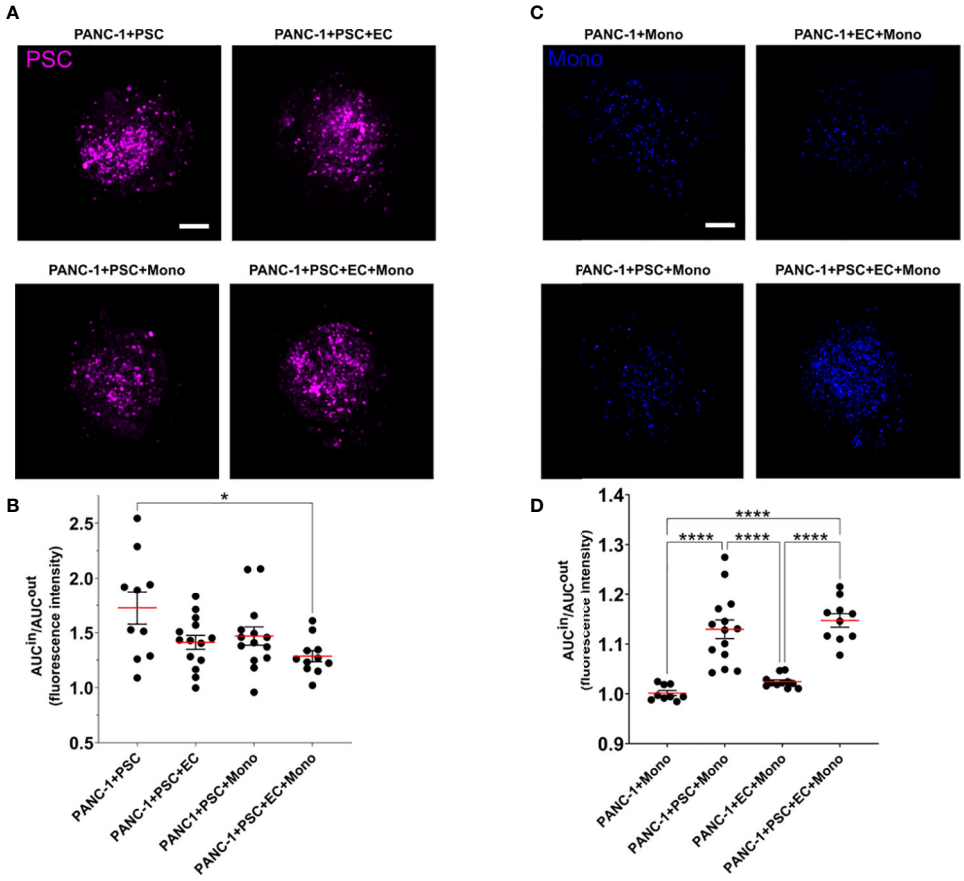

FIGURE 4
PSC and monocytes spatial distribution within the PANC-1 spheroids. **(A)** Representative images of PANC-1 spheroids at day 7 with different compositions acquired using confocal imaging showing only the fluorescent signal of PSC (purple). Scale bar: 100 µm. **(B)** Dot plot of the ratio between the area under the curve (AUC) of the PSC fluorescent signal in the outside or inside regions of the spheroids. Data are shown as mean ± SEM. Statistical significance for comparisons was determined by one-way ANOVA with Tukey's *post-hoc* test. *p<0.05 when compared to PANC1 +PSC spheroids. **(C)** Representative images of PANC-1 spheroids at day 7 with different compositions acquired using confocal imaging showing only the fluorescent signal of monocytes (blue). Scale bar: 100 µm. **(D)** Dot plot of the ratio between the area under the curve (AUC) of the monocyte fluorescent signal in the outside or inside regions of the spheroids. Data are shown as mean ± SEM. Statistical significance for comparisons was determined by one-way ANOVA with Tukey's *post-hoc* test. ****p<0.0001.

averagely double the percentage of proliferating cells observed in PANC-1 only spheroids (Figures 6B, C). In contrast, PANC-1 spheroids containing EC or monocyte without PSC did not show any increased Ki67 expression at day 4 (Figures 6B, C). At day 7, only PANC-1+PSC showed an increased percentage of Ki67+ positive nuclei when compared to the monoculture spheroids (Figure 6B).

Monocytes increased expression of CD68, CD206, CD163, PD-L1 and CD40 in 4-culture tumor spheroids

Dual ontogeny of macrophages in PDAC TIME has been described by recent studies (16). Both macrophages of fetal and bone marrow origin can be found within the PDAC TIME. To partly reproduce the bone marrow-derived myeloid component of the tumor, we decided to add monocytes to the PANC-1 spheroids. To understand the effect of the TIME on the expression of key markers of differentiation/polarization on monocytes we performed flow-cytometry on cells dissociated from the PANC-1 and HPNE spheroids at day 7 (Figure 7). The flow cytometry analysis confirmed our previous observations on PSC supporting role for monocytes survival and embedding within the tumor spheroids (Figure 4). The percentage of $CD45^+/CD14^+$ events among the live cells, in fact, increased when monocytes were in co-culture with PSC compared to the monoculture condition, either in PANC-1 or HPNE spheroids. However, the increment of $CD45^+/CD14^+$ monocytes when in co-culture with PSC was statistically significant in PANC-1 spheroids but not in HPNE spheroids.

At day 7 monocyte-derived cells ($CD45/CD14^+$ cells) obtained from the 4-culture PANC-1 spheroids showed an increased expression of CD163, CD206, CD40, CD68, and PD-L1 when compared with the same cells obtained from the dissociation of 4-culture HPNE spheroids (Supplementary Figure 6). The percentage of monocytes/macrophages expressing CD68, CD163, CD206, PD-L1, CD40 in PANC-1 4-culture spheroids was significantly greater than the one observed in the PANC-1 +PSC+Mono spheroids (3-culture) and the HPNE 4-culture spheroids (Figures 7C–G). The higher expression of CD68, CD163, CD206 on $CD45/CD14^+$ cells in the 4-culture PANC-1 spheroids suggest a

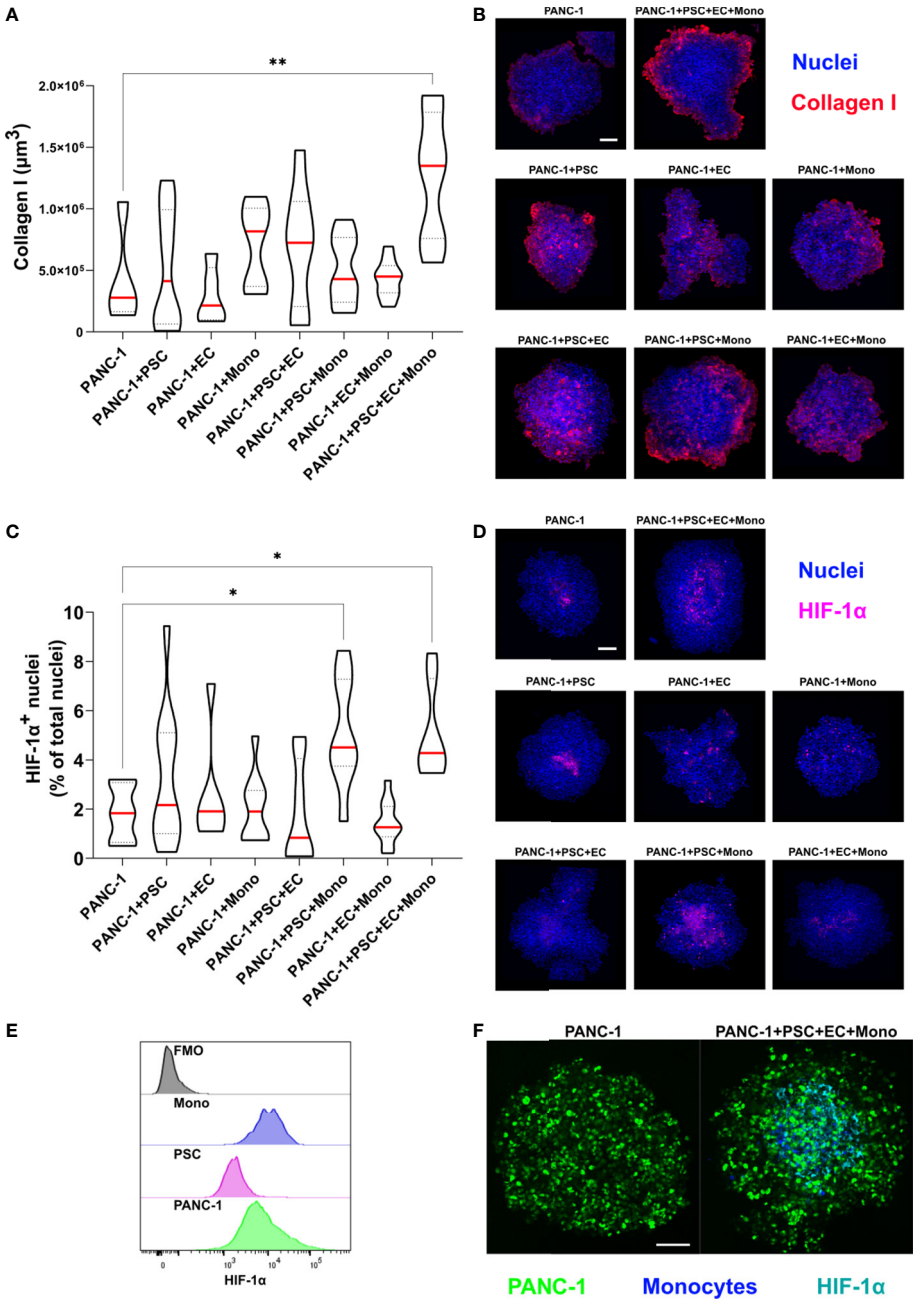

FIGURE 5
PANC-1 4-culture spheroids are characterized by peripheral collagen I deposition and a hypoxic core. PANC-1 spheroids were collected at day 7 and prepared for immunofluorescent staining with collagen I and HIF-1α antibodies. **(A)** Truncated violin plot showing the volume of collagen I fluorescent signal which was quantified as volume using IMARIS™ (red line: median, dotted line: 25th and 75th quartiles). Statistical significance for comparisons was determined by one-way ANOVA with Dunnett's *post-hoc* test. **p<0.01 when compared to PANC-1 monoculture spheroids at day 7 **(B)** Representative pictures of PANC-1 spheroids stained with anti-collagen I antibody and Hoechst 33342. (Collagen I: red; blue: nuclei). Scale bar: 100 µm. **(C)** Truncated violin plot showing the number of HIF-1α positive nuclei in the PANC-1 spheroids. Nuclei were identified as spots using IMARIS™ and data were presented as percentage of the total nuclei (red line: median, dotted line: 25th and 75th quartiles). Statistical significance for comparisons was determined by one-way ANOVA with Dunnett's *post-hoc* test **p<0.01 when compared to PANC-1 monoculture spheroids at day 7. **(D)** Representative pictures of PANC-1 spheroids stained with anti-HIF-1α antibody (nuclei: blue, nuclear HIF-1α: purple). Scale bar: 100 µm. **(E)** Distribution of HIF-1α fluorescent intensity assessed by flowcytometry in the different cell types within PANC-1 4-culture spheroids. **(F)** Representative pictures of monoculture and 4-culture PANC-1 spheroids with similar dimensions stained with HIF-1α (PANC-1: green; HIF-1α: cyan). Scale bar: 100 µm. *p<0.05

monocytes differentiation into M2-like macrophages, known to have tumor supporting functions. The increased expression of PD-L1 on CD45/CD14$^+$ cells in the 4-culture PANC-1 spheroids also suggests that these cells may have an immunosuppressive role. The higher expression of the co-stimulatory molecule and M1 marker CD40 on CD45/CD14$^+$ cells in the 4-culture PANC-1 spheroids could explain the therapeutic effect of CD40 ligand/agonists in the treatment of PDAC, boosting an anti-tumor response (29, 30).

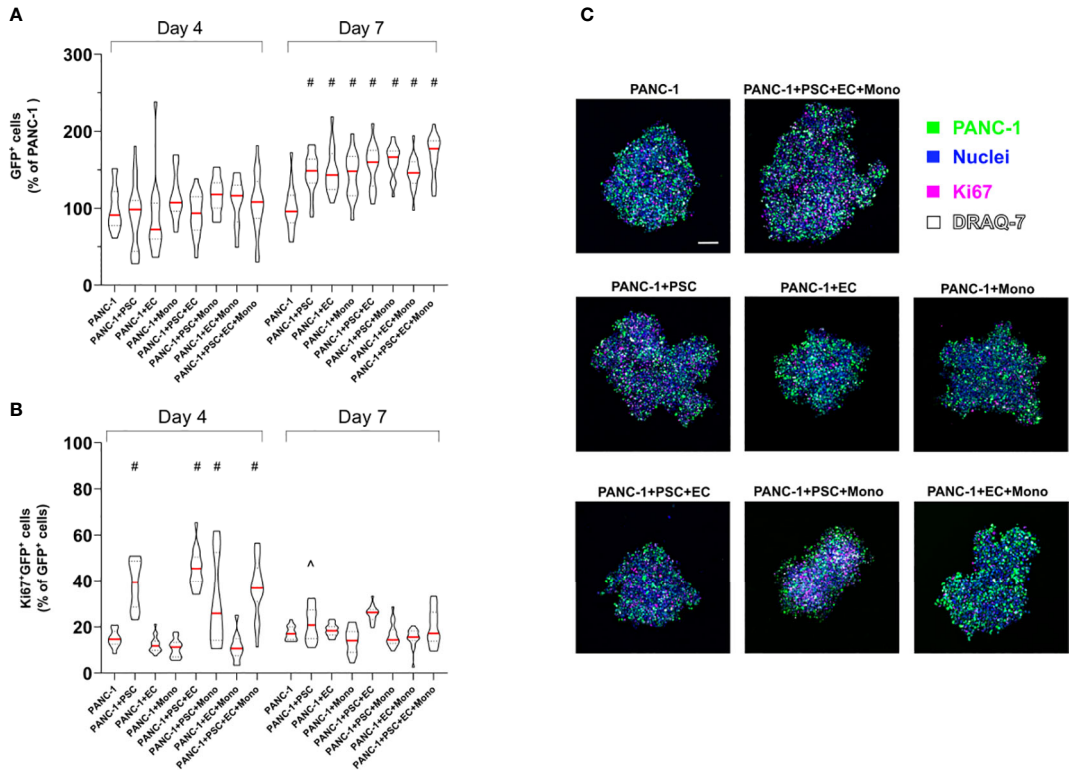

FIGURE 6
PSC increase PANC-1 proliferation. GFP-PANC-1 cells were used to form the spheroids with different cellular heterogeneity and stained for the detection of Ki67 both at day 4 and 7 and imaged with a confocal microscope **(A)** Truncated violin plot of the live GFP-PANC-1 cells were counted using IMARIS^{TM} software and identified as Hoechst 33342^{+} (blue)/GFP^{+} (green)/DRAQ7^{-} (white) spots. Number of live GFP-PANC-1 cells were plotted as percentage of the number of live GFP-PANC-1 cells in monoculture spheroids. Data are shown as median (red line), 25th and 75th quartiles (dotted lines). Statistical significance for comparisons was determined by two-way ANOVA with Sidak's *post-hoc* test. $^{\#}$p <0.0001 when compared to PANC-1 monoculture spheroids at day 7. **(B)** Violin plot of the Ki67^{+} cancer cells (purple) plotted as percentage of live GFP-PANC-1 at each condition. Data are shown as median (red line), 25th and 75th quartiles (dotted lines). Statistical significance for comparisons was determined by two-way ANOVA with Sidak's *post-hoc* test. $^{\#}$p<0.0001 when compared to PANC-1 monoculture spheroids at day 4. ^p<0.01 when compared to PANC-1 monoculture spheroids at day 7. **(C)** Representative confocal images of the heterogeneous spheroids at day 4 labeled with the different markers. Scale bar: 100 µm.

The percentage of monocyte-derived cells expressing PD-L1 or CD40 was greater in both 4-culture and 3-culture PANC-1 spheroids compared to HPNE 4-culture spheroids. By contrast, the CD45^{+}/CD14^{+} cells obtained from the HPNE and PANC-1 4-culture spheroids did not show a statistically significant increase in the expression of the CD86 co-stimulatory molecule, although the average CD86 expression was higher for the PANC-1 spheroids.

Although not statistically significant, also the monocyte-derived cells of the 3-culture PANC-1 spheroids containing PANC-1+PSC+Mono showed an increased expression of CD163 and CD68 when compared with the 4-culture HPNE spheroids. However, in the PANC-1 3-culture spheroids, the percentage of CD68^{+} or CD163^{+} cells in the CD45^{+}/CD14^{+} population was not different from the one observed the HPNE 4-culture spheroids.

PANC-1 4-culture spheroid cytokine signature mimics PDAC patient features

The cytokines released by each cell type present in the TIME affects the proximal (within the TIME) and the distal (plasma) concentrations of molecular signals that participate in the recruitment and activation of cells (31). We, therefore, conceived that a relevant spheroid model will be able to recapitulate the production of key cytokines observed in patients. Current monoculture tumor spheroid models lack the presence of specific cytokines present in the PDAC TIME, such as CCL4/MIP-1β, CCL5/RANTES, CXCL9, and CXCL10 accidentally simulating an immune silent or excluded PDAC TIME. Indeed, these monoculture tumor models are missing the key cellular and humoral interplays responsible for the modulation of cytokine signaling within the PDAC TIME, ultimately leading to immunosuppression or immunoregulation in the context of chronic inflammation (32).

Essentially, shaping PDAC TIME requires various cytokines produced by different cell types from the TIME cooperating with a mutated Ras signaling in pancreatic epithelial ductal cells (31). Established the key role of cytokines in the PDAC TIME, we assessed the levels of some principal cytokines in the supernatant of PANC-1 and HPNE spheroids with increasing cellular heterogeneity to characterize the cytokine expression in our model (Supplementary Figure 7) and compare it to PDAC patient samples. In some cases, the cytokine analysis allowed us to identify the type of cell in the spheroid responsible for the changes in the cytokine signaling and potential cellular synergisms that lead to cytokine modulation.

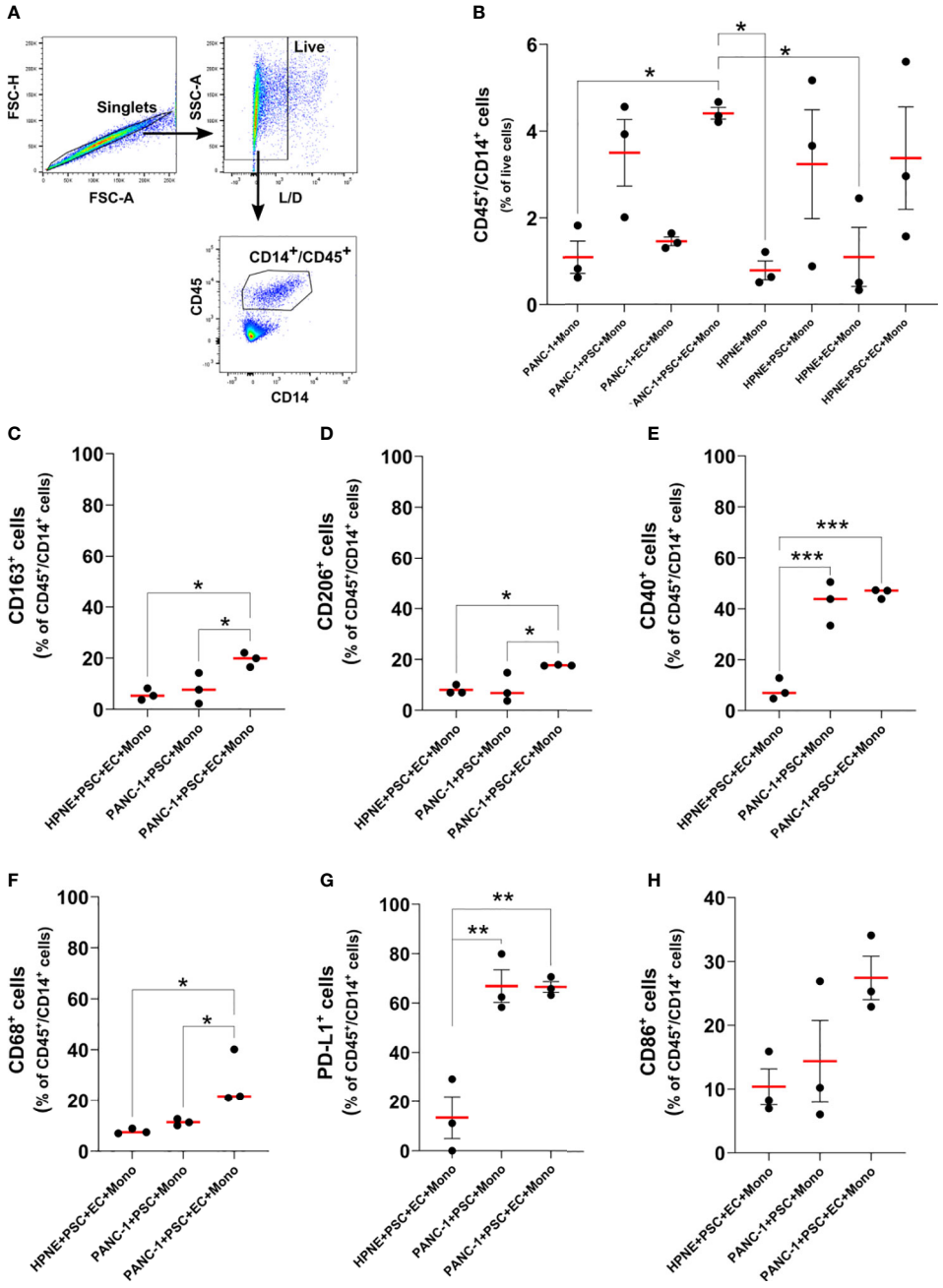

FIGURE 7
Monocytes differentiate in macrophages with increased expression of M2-like markers, CD40, and PD-L1 in PANC-1 4-culture spheroids. **(A)** Gating strategy of flow cytometry data to identify monocytes as CD45+/CD14+ live single cells. **(B)** Dot plot of the flow data showing the number of CD45+/CD14+ monocyte as percentage of live cells for each PANC-1 and HPNE spheroids. Data are shown as mean ± SEM. Statistical significance for comparisons was determined by one-way ANOVA with Dunnett's *post-hoc* test. *p <0.05. **(C–H)**. Expression of key macrophage markers for PANC-1 and HPNE 4-culture (PANC-1 4-culture and HPNE 4-culture, respectively) are presented as dot plot of the fold change from the respective FMO intensity (left plot), histograms (center plot) and as dot plot of the percentage of the total number of CD45+/CD14+ monocytes (right plot). Data are shown as mean ± SEM in the dot plots. Statistical significance for comparisons was determined by one-way ANOVA with Dunnett's *post-hoc* test. *p<0.05, **p<0.01, ***p<0.0001.

M1 macrophage-associated cytokines are less expressed in PANC-1 spheroids compared to HPNE spheroids

The enrichment of M2-like macrophages in the tumor of PDAC patients is usually described as a negative prognostic marker (33). The presence of M2-like macrophages within the TIME inhibits cytotoxic CD8 T-cell functions *via* the reduction of anti-inflammatory cytokines that promote T-cell proliferation and anti-tumor responses (33). M1-like macrophages, on the contrary, have been shown to promote anti-tumor responses mainly *via* the release of pro-inflammatory cytokines which are significantly reduced in M2-like macrophages cultures (34).

Our multiplex bead-based cytokine analysis showed that at day 7 pro-inflammatory cytokines were overall significantly decreased in the supernatant of PANC-1 4-culture spheroids when compared to those of HPNE 4-culture except CXCL10 as shown in Figures 8A, B. Among the selected cytokines the greatest and significant decreases between PANC-1 4-culture spheroids and HPNE 4-culture spheroids were observed mainly in the cytokine involved in M1 polarization (Figure 8B). In addition to pro-inflammatory cytokines, many of the other cytokines in the panel were significantly downregulated in cancer spheroids compared to HPNE spheroids.

PANC-1 4-culture spheroids showed greater concentrations of plasma-detectable cytokines associated with poor prognosis in patients

Among the different cytokines that can be detected in plasma of patients, an increase of IL-6, IL-8, IL-10, CCL2/MCP-1, IP-10/CXCL10 at diagnosis have been associated with poor prognosis of PDAC patients (35–37).

Our multiplex bead-based cytokine analysis on the supernatant of *PANC-1 spheroids* at day 7, showed that IL-6, IL-10, IP-10/CXCL10 cytokines were non-detectable (n.d. in Figures 8C, D, 9D), whereas the MCP-1/CCL2 and IL-8 presented very low concentrations (Figures 8E, F) in PANC-1 monoculture spheroids. The addition of PSC to the PANC-1 cells with or without EC made IL-6 and IL-10 detectable and increased the concentration of MCP-1/CCL2 (Figures 8C–E). The co-culture of monocytes with PSC, EC and PANC-1 cancer cells (PANC-1 4-culture) significantly increased the concentration of IL-6 when compared to any of the spheroids with a lower cellular heterogeneity (Figure 8C). By contrast, the PANC-1 4-culture spheroids did not show a significant increase in the concentration of IL-10 and MCP-1/CCL-2 when compared with any other PANC-1 3-culture condition. However, at day 7 the concentrations of MCP-1/CCL2 (Figure 8E) in the supernatant of PANC-1 3- and 4-cultures spheroids were significantly higher than the one detected in the samples obtained from PANC-1 2-culture and monoculture spheroids.

Notably, concentrations of the regulatory T cell-recruiting chemokine CXCL10 were significantly increased in PANC-1 4-culture spheroids when compared to any other tested PANC-1 and HPNE condition (Figure 9D).

4-culture spheroids chemotactic signals for T cell recruitment are modulated by PANC-1 cells and monocytes

The TIME of PDAC patients with a shorter overall survival is usually classified as “cold”. With this term the scientific community define a tumor lacking T cells infiltration as a result of a low mutation burden, low major histocompatibility complex I (MHCI) expression, and high expression of molecules with immunoregulating or immunosuppressive functions. Immune profiling on PDAC patient samples revealed that accumulation of CD3+ T cells in the tumor correlates with better survival (38). A recent study showed that the recruitment of T cells within the PDAC TIME and the associated anti-tumor response is dependent

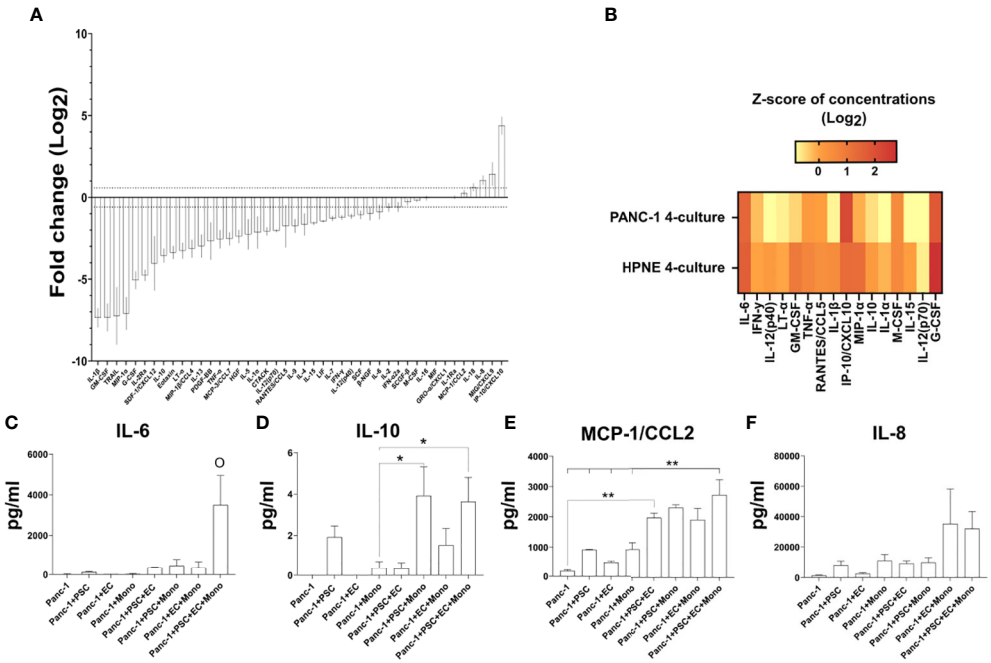

FIGURE 8
Expression of cytokines in the supernatant of PANC-1 spheroids and their comparison to non-cancerous HPNE spheroids. **(A)** Log2 fold changes of the cytokine concentrations observed in PANC-1 4-culture spheroids at day 7 using the HPNE 4-culture spheroids as control. Dotted lines indicate ± 1.5 fold change. **(B)** Heatmap the multiplex bead-based cytokine analysis of the supernatant of the spheroids at 7 days of culture presenting typical M1-like macrophage-associated cytokines as z-scores of concentrations (Log2). **(C–F)** Bar plots of the concentrations of IL-6 **(C)**, IL-10 **(D)**, MCP-1/CCL2 [**(E)** IL-8 **(F)**] cytokines that have been detected in high concentration in the plasma of patients with poor survival.

on the greater co-expression of 4 chemokines: CCL4/MIP-1β, CCL5/RANTES, CXCL9 and CXCL10 (39). In order to study cell-cell interactions within the TIME and to test immunotherapies, a relevant cancer model should simulate the secretion of chemokines involved in the infiltration of T cells (cytotoxic, helper or regulatory) within the tumor as well as mimics modulation of chemotactic and activating factors by myeloid cells, well-known to suppress cytotoxic T cell response in cancer (40).

Concentration of T cell recruiting cytokines were undetectable or very low in both PANC-1 and HPNE monoculture spheroids (Figures 9A–D). The addition of monocytes to both PANC-1 and HPNE spheroids resulted in an increase of CCL4/MIP-1β concentrations, significantly lower in PANC-1 spheroids when compared to HPNE analogues (Figure 9A). CXCL9 was also detectable in presence of monocytes for both HPNE and PANC-1 spheroids. The comparison of MIG/CXCL9 concentrations between HPNE+Mono and PANC-1+Mono showed that the expression of this cytokine is significantly more concentrated in presence of PANC-1 cells (Figure 9C). The presence of either PSC or EC to the PANC-1 spheroids containing also monocytes lowered the concentrations of MIG/CXCL9 up to 23.9% and 26.3%, respectively (Figure 9C). The PANC-1 4-culture spheroids, containing PSC, EC, and monocytes did not further decreased the expression of CXCL9 when compared with the PANC-1 3-culture spheroids containing monocytes. The concentrations of RANTES/CCL5 were significantly increased in PANC-1 spheroids containing also PSC when compared to PANC-1 monoculture spheroids. The co-culture of PSC and EC with PANC-1 cells significantly increased the concentrations of RANTES/CCL5 when compared to PANC-1+PSC spheroids (Figure 9B). By contrast, the PANC-1 4-culture spheroids containing monocytes showed a significant decrease of RANTES/CCL5 when compared to the same spheroids not containing monocytes, showing concentrations comparable to those detected in PANC-1 monoculture spheroids (Figure 9B). The HPNE 4-culture spheroids showed a non-statistically significant increase in the concentration of RANTES/CCL5 when compared with the same spheroids not containing monocytes. The concentrations of the chemokine IP-10/CXCL10 were increased in PANC-1+PSC spheroids and further increased with higher cellular heterogeneity reaching the greater concentration in PANC-1 4-culture spheroids (Figure 9D). PANC-1+EC concentration of IP-10/CXCL10 were not detectable as observed in PANC-1 monoculture spheroids whereas PANC-1+Mono spheroids had 1/3 of the concentration of IP-10/CXCL10 when compared with PANC-1+PSC. Within the PANC-1 spheroids, the combination of PSC with monocytes or EC clearly showed a synergism of IP-10/CXCL10 secretion which is not the mere sum of the concentrations observed in each 2-culture condition (PANC-1+PSC, PANC-1+EC, PANC-1+Mono) (Figure 9D). In HPNE spheroids, the detection of IP-10/CXCL10 was only associated to the presence of monocytes and was not detectable in HPNE+PSC. Overall, the analysis of the cytokine/chemokine expression shows how the PANC-1 4 culture spheroids intrinsically contains the potential of expressing crucial chemokines contained in the PDAC TIME and the interplay among the different cell types recreates an immunoregulation on those expressed cytokines.

Discussion

To increase the number of effective therapies for the treatment of PDAC reaching clinical trials, recapitulating the TIME in preclinical models is imperative. Tumor preclinical models should be designed to reproduce the composition of PDAC TIME as closely as possible, posing particular attention to mimicking the intra- and inter-cellular interplays occurring in PDAC TIME of patients who do not respond to existing therapies. Currently, the available preclinical models either do not consider interspecies differences (animal models) or do not reasonably reproduce the TIME of PDAC, lacking specific cell types and their 3D spatial organization. The PDAC TIME is densely populated with non-cancer cells like endothelial, stellate, and immune cells, which have been shown to interact with each other shaping the TIME and playing a critical role in establishing therapy resistance (16, 41, 42). Stem cell-derived organoids serve as essential *in vitro* models for investigating cancer cell mechanisms, especially because they recapitulate cell lineages often organized in functional units like organs. Regrettably, despite extensive efforts to establish heterocellular organoids, further work is necessary to comprehensively represent the cellular interactions among stromal, immune and endothelial cells within the TIME (43). Recent studies characterized 3D hetero-cellular tumor spheroids models, accounting for different PDAC stroma cell types. However, none simultaneously co-cultured the four most abundant and critical cells in PDAC TIME: cancer cells, endothelial cells, pancreatic stellate cells, and macrophages. In recent years our work focused on improving 3D *in vitro* models by incorporating complexity that is fundamental in understanding the tumor microenvironment and the immune system interaction (44–48).

In this study, we formed and characterized, for the first time, viable PANC-1 tumor spheroids containing human endothelial cells, pancreatic stellate cells, and blood-derived monocytes. The non-cancerous cell types (PSC, EC, and monocytes) were well represented on day 7, especially in the 4-culture tumor spheroids. The percentage of EC was low, although these cells demonstrated the capability to interact with each other, forming 3D endothelial networks similar to the compressed vessels observed in murine models of PDAC and histological analysis of the patient tumors (49, 50). The difference observed in the 3D endothelial network arrangement of PANC-1 and HPNE spheroids suggests that the co-culturing of EC and cancer cells significantly impacts the formation of the EC structures. Most importantly, the EC network was only observed in tumor spheroids containing the combination of PSC and EC, suggesting a critical pro-angiogenic interplay between these two cell types, but also an anti-angiogenic effect exerted by the cancer cells as previously demonstrated by Di Maggio et al. (50). Although it cannot be entirely ruled out that the

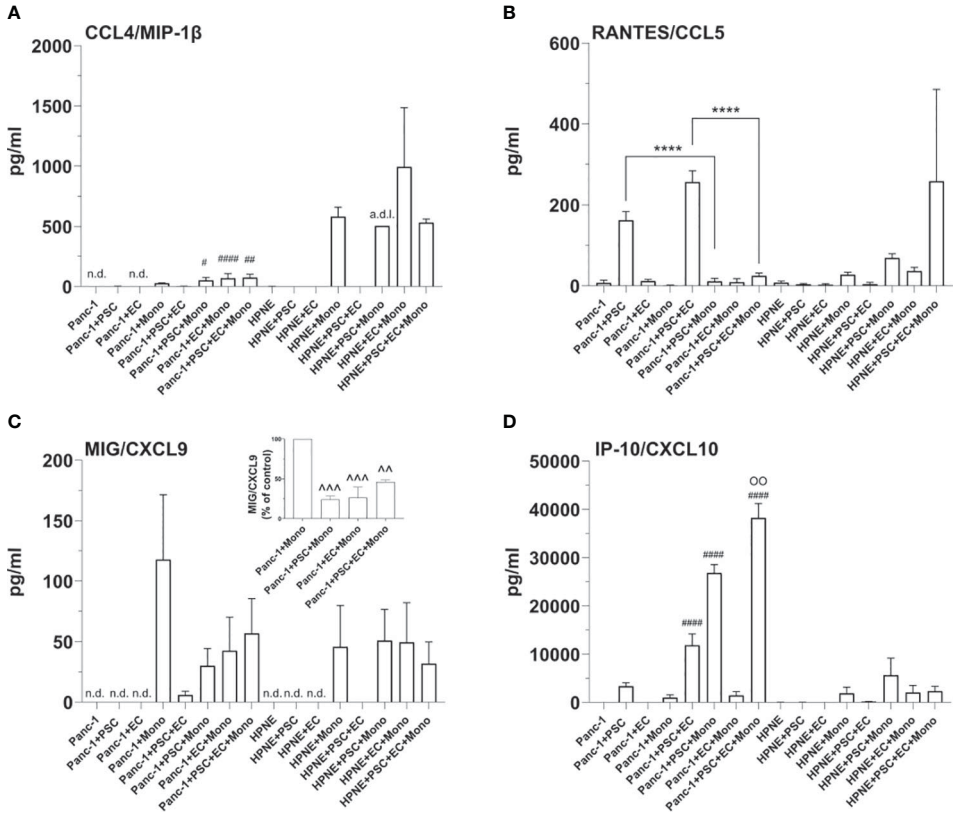

FIGURE 9
Cellular interplays within the spheroids modulate the expression of T cell recruiting cytokines. Bar plots of the concentrations of T-cell attracting cytokines, i.e. MIP-1β **(A)**, RANTES **(B)**, MIG **(C)**, IP-10 **(D)**. Statistical significance for comparisons was determined by one-way ANOVA with Dunnett's *post-hoc* test. OO p <0.01 when compared with any of the other tested conditions; ****p<0.0001; $^{\#}$p<0.05, $^{\#\#}$p<0.01, $^{\#\#\#\#}$p<0.0001 when compared to the HPNE analogue spheroid containing the same type of additional cells; ^^p<0.01, ^^^p<0.001 when compared to PANC-1+Mono spheroids; n.d., non detectable, a.d.l., above detection limit.

disrupted EC structures observed in PANC-1 spheroids are partly attributable to EC death, it is worth considering that the typical features of the TIME, such as lack of substrates and the elevated production of reactive oxygen species, might have additionally contributed to the reduced proliferation of these cells, as previously demonstrated (51–53). The volume of the 3D endothelial network observed in our tumor 4-culture spheroids was also significantly reduced compared to the same tumor spheroids lacking monocytes. We can speculate that the increased collagen I deposition observed in the tumor 4-culture spheroids physically compresses the EC network, as demonstrated by different studies performed in murine models of PDAC (27, 54, 55). In these studies, the decrease in collagen I deposition or inhibition of enzymes deputed to collagen crosslinking was associated with the decompression of the vessels. On the other hand, other physical and molecular factors due to the presence of monocytes in the tumor 4-culture spheroids may have contributed to the decreased volume of the EC network. Additional experiments reducing the deposition of collagen I or its crosslinking may clarify the cause of the reduced EC network volume in tumor 4-culture spheroids.

It has been shown that vascular structures develop in an environment in which perivascular cells, such as PSC, are present (50, 56). Therefore, we assessed the distance between EC and PSC in our tumor spheroids. Through our spatial analysis, we confirmed that PSC surrounded EC and that monocyte-derived macrophages were also localized in the proximity of the endothelial structures. Of note, macrophages have been localized in the stroma of PDAC, where PSC and EC were located in orthotopic murine tumor models (16), similar to what was observed in our tumor spheroids. The spatial localization of these three cell types (PSC, EC, and monocytes) in the core of the tumor spheroids seems to rely mainly on the presence of the PSC that localize in the core of the tumor spheroids even when co-cultured alone with cancer cells. In human and murine PDAC, activated PSC are the main cells producing the stiff fibrotic ECM leading to desmoplasia and hypoxia. Hypoxia is usually observed in the core of spheroids larger than 200 μm (57), mainly through the nuclear translocation of HIF-1α. It promotes the secretion of several cytokines involved in the recruitment of fibroblasts and immune cells (58), potentially explaining the localization of PSC and monocytes within the core of our tumor spheroids.

When we assessed the expression and nuclear translocation of the transcription factor HIF-1α as a key regulator of the hypoxic response, we noticed HIF-1α expressed with two different intensities. The high-intensity HIF-1α was mainly located in the

nuclei of cells in the core of the spheroids. From the flow cytometry analysis, it was possible to discriminate that these cells with a higher intensity were both monocytes and PANC-1 cells (Figure 5E). To rule out the possibility that the size of the spheroids rather than the cell composition was affecting the HIF-1α expression, we compared the monoculture and 4-culture tumor spheroids having about the same size. Notably, the HIF-1α expression was significantly lower in monoculture spheroids when compared with 4-culture spheroids underlining that the cell composition was critical for the increased HIF-1α expression and nuclear translocation.

Another effect of the PSC presence in the tumor spheroids was an increased size and number of cancer cells counted in our tumor spheroids, probably associated with the higher proliferation observed on day 4 and in agreement with other *in vitro* studies (15, 59). Instead, for the heterocellular tumor spheroids without PSC, the increased number of cancer cells could be attributed to an improved embedding of the cancer cells within the spheroids.

Although PSC-induced proliferation represents an interplay between cancer cells and stellate cells, other fibroblast populations in the PDAC TIME may contribute to cancer cell proliferation, as observed in a recent study of PSC depletion in an orthotropic mouse model (10). By contrast, the resistance to radiotherapy in PDAC patients (60) seems specifically induced by PSC (15). Mantoni et al. demonstrated that only human PSC and not MRC-5 confer radiotherapy resistance to pancreatic cancer cells, reinforcing the importance of developing a PDAC TIME model containing stellate cells of pancreatic origin.

In addition to affecting cancer cell functions, PSC depletion decreased the number of macrophages within the tumor (10). Accordingly, we observed that the monocyte percentage in PANC-1 spheroids increases with PSC, suggesting that PSC-monocyte interplay observed in *in vivo* models may occur in our *in vitro* model. Characterizing the monocytes embedded within the spheroids with different compositions further demonstrated that interaction with each cell type contributed to the expression of key macrophage polarization markers and the immune checkpoint PD-L1. We observed how the polarization of monocytes toward an M2-like macrophage phenotype occurs only in the PANC-1 4-culture at 7 days after seeding, as demonstrated by the increased expression of CD68, CD163, and CD206 markers in the spheroids with higher cellular heterogeneity. In line with this observation, the PANC-1 4-culture spheroids better mimic the M2 macrophage-populated PDAC TIME of patients with poorer prognoses (61). Differently, the expression of critical immune regulators, namely PD-L1 and the M1 marker CD40, on monocytes/macrophages in our tumor spheroids depended on their co-culture with PANC-1 cells and PSC. At the same time, we did not observe any significant increase in the expression of either CD40 or PD-L1 in monocytes/macrophages within HPNE spheroids. Similarly, Kung et al. elegantly showed in their *in vitro* experiments (62) that under the influence of PSC, cancer cells increased the secretion of S100A9, causing the increased expression of PD-L1 on monocytes/macrophages.

The increased percentage of M2-like macrophages in our 4-culture tumor model well reflects the decreased concentrations of typical M1 cytokines detected in the PANC-1 spheroids compared to the HPNE spheroids (Figure 8). The supernatant of HPNE spheroids showed high concentrations of several pro-inflammatory cytokines, most probably due to VEGF stimulation and cellular stress occurring during the formation of the spheroids. It has been demonstrated that VEGF promotes the release of inflammatory cytokines (such as IL-6, IL-8/CXCL-8, and GRO-α/CXCL-1) by endothelial cells through VEGF receptor 2 activation. In turn, inflammatory cytokines such as TNF-α, IL-1β, IL-6, and IL-8/CXCL-8 induce VEGF expression, reinforcing angiogenesis and inflammation (63). The HPNE spheroids served as a control of inflammation to understand how the key cellular players in the TIME modulate the secretion of key inflammatory cytokines. In the HPNE spheroids, we observed multiple cell interplays leading to positive and negative regulation of cytokines. It was clear that pro-inflammatory cytokines were concentrated in HPNE spheroids, but cancer cells contributed to reducing the concentration of typical Th1 cytokines (e.g., TNF, IFN-γ, IL-12). From the cytokine analysis, we concluded that multicellular interactions within the tumor spheroids determine significant changes in the cytokine pattern, leading to the polarization of monocytes into an M2-like phenotype. The tumor spheroids with the higher degree of cellular heterogeneity (4-culture) better resemble the cytokine signature observed in the plasma of patients with poor survival and not responding to therapies (36, 37), making this model suitable for further investigations to identify new strategies for reprogramming the PDAC TIME. Strikingly, CCL2/MCP-1, well known to mediate the recruitment of monocytes in the hypoxic areas (64), were more concentrated in 3- and 4-culture tumor spheroids, supporting our results on the spatial localization of monocytes in the hypoxic area of the spheroid.

We also assessed the expression of key cytokines involved in T-cell recruitment and activation in PDAC patients (39). These cytokines were highly affected by the presence of the different cell types. Briefly, we could observe that the concentrations of these cytokines (mainly MIP-1β/CCL4, RANTES/CCL5, MIG/CXCL9) were kept low in PANC-1 4-culture spheroids as a result of the combined cell types. In the tumor spheroids, we could establish the role of each cell type on cytokine secretion by assessing their concentrations in spheroids missing one of the cell types. T cell recruiting cytokines identified by Romero and collaborators were mainly suppressed by monocytes and PSC within the aggregate, reinforcing the importance of cellular heterogeneity in spheroid models of PDAC.

Interestingly, IP-10/CXCL10 was the only T-cell-related cytokine among the 4 suggested by Romero et al., which was increased in the PANC-1 spheroids. Notably, in more than one study, high plasma concentrations of IP-10/CXCL10 have been associated with decreased survival in PDAC patients (19, 37). Lunardi et al. showed that IP-10/CXCL10 was increased in the co-culture of the PSC with pancreatic cancer cells. IP-10/CXCL10 has been shown to be a chemoattractant for T cells, including CD4-

Th1, CD8, and Tregs (65, 66). In particular, the increased concentrations of IP-10/CXCL10 in the TIME of pancreatic cancer have been linked to the recruitment of Tregs to the tumor site (19), which, in turn, may contribute to disease progression (67). This increase was also observed in our experiments and IP-10/CXCL10 synergistically increased in the presence of EC and/or monocytes. Lunardi et al. also demonstrated that the patients' higher expression of IP-10/CXCL10 was associated with a denser stroma. Accordingly, with these clinical data, in our PANC-1 4-culture spheroids, we observed an increased expression of collagen I associated with increased secretion of IP-10/CXCL10. Although collagen I is not the only component of the dense PDAC stroma, it has been shown to play a key role in the induction of the desmoplastic response (26). Therefore, the increased collagen I deposition observed in our PANC-1 4-culture spheroids sustains another key similarity between our tumor model and the PDAC TIME of patients.

In conclusion, our PANC-1 4-culture spheroids represent a promising tool for studying cell-cell interactions in the PDAC TIME. Future studies may also address if the PANC-1 4-culture spheroids are recapitulating the increased infiltration of Treg as shown in the *in vitro* model of Lunardi et al. More broadly, PANC-1 spheroids could be helpful in functional assays of T and myeloid cell infiltration (68, 69) to observe if the tumor spheroids induce chemotaxis and immune responses similar to those observed in patients, as confinement, anergy, and immunosuppression. Although this study aims to develop a tool for studying cell interactions in the PDAC TIME, it is important to exercise caution regarding potential therapeutic testing using this system. We foresee further research studies with our PDAC spheroids with different cellular heterogeneity embedded in microfluidic devices to test their sensitivities to established treatments (chemotherapy, radiotherapy, and immunotherapies) (70), aiming to validate the model for drug screening. The PANC-1 4-culture spheroids, as described in this study, being an *in vitro* tumor model, come with intrinsic limitations when compared to a patient's tumor. Although the increased number of degrees of freedom resulting from the heterogeneity of the spheroids might represent limitations for mechanistic studies using this model, we believe that leveraging advanced spatial transcriptomics and proteomics techniques will enable the extrapolation of crucial molecular changes. This will facilitate the study of mechanisms that were previously difficult to reproduce or assess in other tumor models. Importantly, our model still lacks a poorly perfusable tumor-associated vasculature and mimicking the pathophysiological recruitment of immune cells as observed in *in vivo* models. With an opportune tuning of the culture conditions, patient-derived vascularized heterocellular PDAC spheroids could be developed to answer patient-specific questions bridging preclinical and clinical research.

Data availability statement

The original contributions presented in the study are included in the article/Supplementary Material. Further inquiries can be directed to the corresponding authors.

Author contributions

Contributions by authors in publication: GG, SIgN, conceived and designed the analysis, collected the data, contributed data or analysis tools, performed the analysis, wrote the paper. GT, SIgN, contributed to perform analysis. AP, IMCB, contributed to designing the analysis. GA, SIgN, initiated, directed and supervised the study, co-designed the experiments and contributed in writing the manuscript. All authors contributed to the article and approved the submitted version.

Funding

This work was supported by A*STAR Career Development Fund (project n. C210812050).

Acknowledgments

The authors thank the Agency for Science, Technology and Research (A*STAR)'s Singapore Immunology Network (SIgN) Multiplex Analysis of Proteins (MAP) platform and SIgN Flow Cytometry platform for enabling respectively the Luminex and the flow cytometry work for this publication. A*STAR's SIgN MAP platform and SIgN Flow Cytometry platform are supported by research grants including the Biomedical Research Council (BMRC) grant and the National Research Foundation (NRF), Immunomonitoring Service Platform (Ref: ISP: NRF2017_SISFP09) grant. The authors thank Akhila Balachander for enabling the imaging work in this paper.

Conflict of interest

The authors declare that the research was conducted in the absence of any commercial or financial relationships that could be construed as a potential conflict of interest.

Publisher's note

Supplementary material

The Supplementary Material for this article can be found online at: https://www.frontiersin.org/articles/10.3389/fonc.2023.1156769/full#supplementary-material

References

1. Sung H, Ferlay J, Siegel RL, Laversanne M, Soerjomataram I, Jemal A, et al. Global cancer statistics 2020 : GLOBOCAN estimates of incidence and mortality worldwide for 36 cancers in 185 countries. *CA: A Cancer Journal for Clinicians* (2021) 71:209–49. doi: 10.3322/caac.21660

2. Singh RR, O'Reilly EM. New treatment strategies for metastatic pancreatic ductal adenocarcinoma. *Drugs* (2020) 80:647–69. doi: 10.1007/s40265-020-01304-0

3. Brouwer TP, Vahrmeijer AL, Miranda NFCC. Immunotherapy for pancreatic cancer : chasing the light at the end of the tunnel. *Cellular Oncology* (2021) 4:261–78. doi: 10.1007/s13402-021-00587-z

4. American Cancer Society. Cancer facts & figures. *Am Cancer Soc* (2022), 1–80. doi: 10.3238/arztebl.2008.0255

5. Foucher ED, Ghigo C, Chouaib S, Galon J, Iovanna J, Olive D. Pancreatic ductal adenocarcinoma: a strong imbalance of good and bad immunological cops in the tumor microenvironment. *Front Immunol* (2018) 9:1044. doi: 10.3389/fimmu.2018.01044

6. Longati P, Jia X, Eimer J, Wagman A, Witt MR, Rehnmark S, et al. 3D pancreatic carcinoma spheroids induce a matrix-rich, chemoresistant phenotype offering a better model for drug testing. *BMC Cancer* (2013) 13:1–13. doi: 10.1186/1471-2407-13-95

7. Wu Y, Zhang C, Jiang K, Werner J, Bazhin AV, D'Haese JG. The role of stellate cells in pancreatic ductal adenocarcinoma: targeting perspectives. *Front Oncol* (2021) 10:621937/BIBTEX. doi: 10.3389/FONC.2020.621937/BIBTEX

8. Tang D, Wang D, Yuan Z, Xue X, Zhang Y, An Y, et al. Persistent activation of pancreatic stellate cells creates a microenvironment favorable for the malignant behavior of pancreatic ductal adenocarcinoma. *Int J Cancer* (2013) 132:993–1003. doi: 10.1002/ijc.27715

9. Li C, Cui L, Yang L, Wang B, Zhuo Y, Zhang L, et al. Pancreatic stellate cells promote tumor progression by promoting an immunosuppressive microenvironment in murine models of pancreatic cancer. *Pancreas* (2020) 49:120–7. doi: 10.1097/MPA.0000000000001464

10. Helms EJ, Berry MW, Chaw RC, Dufort CC, Sun D, Onate MK, et al. Mesenchymal lineage heterogeneity underlies nonredundant functions of pancreatic cancer–associated fibroblasts. *Cancer Discovery* (2022) 12:484–501. doi: 10.1158/2159-8290.CD-21-0601

11. Garcia PE, Adoumie M, Kim EC, Zhang Y, Scales MK, El-Tawil YS, et al. Differential contribution of pancreatic fibroblast subsets to the pancreatic cancer stroma. *Cmgh* (2020) 10(3):581–99. doi: 10.1016/j.jcmgh.2020.05.004

12. Norberg KJ, Liu X, Fernández Moro C, Strell C, Nania S, Blümel M, et al. A novel pancreatic tumour and stellate cell 3D co-culture spheroid model. *BMC Cancer* (2020) 20:1–13. doi: 10.1186/s12885-020-06867-5

13. Jang SD, Song J, Kim HA, Im CN, Khawar IA, Park JK, et al. Anti-cancer activity profiling of chemotherapeutic agents in 3D co-cultures of pancreatic tumor spheroids with cancer- associated fibroblasts and macrophages. *Cancers (Basel)* (2021) 13:1-20. doi: 10.3390/cancers13235955

14. Kuen J, Darowski D, Kluge T, Majety M. Pancreatic cancer cell/fibroblast co-culture induces M2 like macrophages that influence therapeutic response in a 3D model. *PLOS ONE* (2017) 12:1–19. doi: 10.1371/journal.pone.0182039

15. Mantoni TS, Lunardi S, Al-assar O, Masamune A, Thomas B. Pancreatic stellate cells radioprotect pancreatic cancer cells through β 1-integrin signaling. *Cancer Res* (2011) 71:3453–8. doi: 10.1158/0008-5472.CAN-10-1633.Pancreatic

16. Zhu Y, Herndon JM, Sojka DK, Kim K, Knolhoff BL, Zuo C, et al. Tissue resident macrophages in pancreatic ductal adenocarcinoma originate from embryonic hematopoiesis and promote tumor progression. *Immunity* (2018) 47:323–38. doi: 10.1016/j.immuni.2017.07.014.Tissue

17. Natividad R, Phan J, Huang Y, Lin D, Taniguchi CM. Resolving the HIF paradox in pancreatic cancer natividad. *J Int Soc Burn Injuries* (2017) 43:909–32. doi: 10.1016/j.canlet.2020.05.033.Resolving

18. Lazzari G, Nicolas V, Matsusaki M, Akashi M, Couvreur P, Mura S. Multicellular spheroid based on a triple co-culture: a novel 3D model to mimic pancreatic tumor complexity. *Acta Biomater* (2018) 78:296–307. doi: 10.1016/J.ACTBIO.2018.08.008

19. Lunardi S, Jamieson NB, Lim SY, Griffiths KL, Carvalho-Gaspar M, Al-Assar O, et al. IP-10/CXCL10 induction in human pancreatic cancer stroma influences lymphocytes recruitment and correlates with poor survival. *Oncotarget* (2014) 5:11064–80. doi: 10.18632/oncotarget.2519

20. Bonnardel J, T'Jonck W, Gaublomme D, Browaeys R, Scott CL, Martens L, et al. Stellate cells, hepatocytes, and endothelial cells imprint the kupffer cell identity on monocytes colonizing the liver macrophage niche. *Immunity* (2019) 51:638–654.e9. doi: 10.1016/j.immuni.2019.08.017

21. Fu T, Dai LJ, Wu SY, Xiao Y, Ma D, Jiang YZ, et al. Spatial architecture of the immune microenvironment orchestrates tumor immunity and therapeutic response. *J Hematol Oncol* (2021) 14:1-25. doi: 10.1186/s13045-021-01103-4

22. Lee KM, Nguyen C, Ulrich AB, Pour PM, Ouellette MM. Immortalization with telomerase of the nestin-positive cells of the human pancreas. *Biochem Biophys Res Commun* (2003) 301:1038–44. doi: 10.1016/S0006-291X(03)00086-X

23. Marx V. Method of the year 2020: spatially resolved transcriptomics. *Nat Methods* (2021) 18:1. doi: 10.1038/s41592-020-01042-x

24. Toda S, Blauch LR, Tang SKY, Morsut L, Lim WA. Programming self-organizing multicellular structures with synthetic cell-cell signaling. *Sci (1979)* (2018) 361:156–62. doi: 10.1126/SCIENCE.AAT0271/SUPPL_FILE/AAT0271S7.MOV

25. Chauhan VP, Boucher Y, Ferrone CR, Roberge S, Martin JD, Stylianopoulos T, et al. Compression of pancreatic tumor blood vessels by hyaluronan is caused by solid stress and not interstitial fluid pressure. *Cancer Cell* (2014) 26:14–5. doi: 10.1016/j.ccr.2014.06.003

26. Whatcott CJ, Diep CH, Jiang P, Watanabe A, Lobello J, Sima C, et al. Desmoplasia in primary tumors and metastatic lesions of pancreatic cancer. *Clin Cancer Res* (2015) 21:3561–8. doi: 10.1158/1078-0432.CCR-14-1051

27. Nieskoski MD, Marra K, Gunn JR, Hoopes PJ, Doyley MM, Hasan T, et al. Collagen complexity spatially defines microregions of total tissue pressure in pancreatic cancer. *Sci Rep* (2017) 7:1–12. doi: 10.1038/s41598-017-10671-w

28. Tao J, Yang G, Zhou W, Qiu J, Chen G, Luo W, et al. Targeting hypoxic tumor microenvironment in pancreatic cancer. *J Hematol Oncol* (2021) 14:1–25. doi: 10.1186/s13045-020-01030-w

29. Beatty GL, Chiorean EG, Fishman MP, Saboury B, Teitelbaum R, Sun W, et al. CD40 agonists alter tumor stroma and show efficacy against pancreatic carcinoma in mice and humans. *Sci (1979)* (2012) 331:1612–6. doi: 10.1126/science.1198443.CD40

30. Lim CY, Chang JH, Lee WS, Kim J, Park IY. CD40 agonists alter the pancreatic cancer microenvironment by shifting the macrophage phenotype toward M1 and suppress human pancreatic cancer in organotypic slice cultures. *Gut Liver* (2022) 16:645–59. doi: 10.5009/gnl210311

31. Bhatia R, Bhyravbhatla N, Kisling A, Li X, Batra SK, Kumar S. Cytokines chattering in pancreatic ductal adenocarcinoma tumor microenvironment. *Semin Cancer Biol* (2022) 86:499–510. doi: 10.1016/j.semcancer.2022.03.021

32. Zhu Y-H, Zheng J-H, Jia Q-Y, Duan Z-H, Yao H-F, Yang J, et al. Immunosuppression, immune escape, and immunotherapy in pancreatic cancer: focused on the tumor microenvironment. *Cellular Oncology* (2022). doi: 10.1007/s13402-022-00741-1

33. Hu H, Hang JJ, Han T, Zhuo M, Jiao F, Wang LW. The M2 phenotype of tumor-associated macrophages in the stroma confers a poor prognosis in pancreatic cancer. *Tumor Biol* (2016) 37:8657–64. doi: 10.1007/s13277-015-4741-z

34. Smith TD, Tse MJ, Read EL, Liu WF. Regulation of macrophage polarization and plasticity by complex activation signals. *Integr Biol (Camb)* (2016) 8:946–55. doi: 10.1039/c6ib00105j.Regulation

35. Chen Y, Shi M, Yu GZ, Qin XR, Jin G, Chen P, et al. Interleukin-8, a promising predictor for prognosis of pancreatic cancer. *World J Gastroenterol* (2012) 18:1123–9. doi: 10.3748/wjg.v18.i10.1123

36. Farren MR, Mace TA, Geyer S, Mikhail S, Wu C, Ciombor K, et al. Systemic immune activity predicts overall survival in treatment naïve patients with metastatic pancreatic cancer. *Clin Cancer Res Clin Cancer Res* (2016) 22:2565–74. doi: 10.1158/1078-0432.CCR-15-1732.Systemic

37. Piro G, Simionato F, Carbone C, Frizziero M, Malleo G, Zanini S, et al. A circulating TH2 cytokines profile predicts survival in patients with resectable pancreatic adenocarcinoma. *Oncoimmunology* (2017) 6:1–7. doi: 10.1080/2162402X.2017.1322242

38. Miksch RC, Schoenberg MB, Weniger M, Bösch F, Ormanns S, Mayer B, et al. Prognostic impact of tumor-infiltrating lymphocytes and neutrophils on survival of patients with upfront resection of pancreatic cancer. *Cancers (Basel)* (2019) 11:1-19. doi: 10.3390/cancers11010039

39. Romero JM, Grünwald B, Jang GH, Bavi PP, Jhaveri A, Masoomian M, et al. A four-chemokine signature is associated with a T-cell- inflamed phenotype in primary and metastatic pancreatic cancer. *Clin Cancer Res* (2020) 26:1997–2010. doi: 10.1158/1078-0432.CCR-19-2803

40. Yang S, Liu Q, Liao Q. Tumor-associated macrophages in pancreatic ductal adenocarcinoma: origin, polarization, function, and reprogramming. *Front Cell Dev Biol* (2021) 8:607209. doi: 10.3389/fcell.2020.607209

41. Von Ahrens D, Bhagat TD, Nagrath D, Maitra A, Verma A. The role of stromal cancer-associated fibroblasts in pancreatic cancer. *J Hematol Oncol* (2017) 10:1–8. doi: 10.1186/s13045-017-0448-5

42. Peng J, Sun BF, Chen CY, Zhou JY, Chen YS, Chen H, et al. Single-cell RNA-seq highlights intra-tumoral heterogeneity and malignant progression in pancreatic ductal adenocarcinoma. *Cell Res* (2019) 29:725–38. doi: 10.1038/s41422-019-0195-y

43. Gunti S, Hoke ATK, Vu KP, London NR. Organoid and spheroid tumor models: techniques and applications. *Cancers (Basel)* (2021) 13:1–18. doi: 10.3390/cancers13040874

44. Preece R, Pavesi A, Gkazi SA, Stegmann KA, Georgiadis C, Tan ZM, et al. CRISPR-mediated base conversion allows discriminatory depletion of endogenous T cell receptors for enhanced synthetic immunity. *Mol Ther Methods Clin Dev* (2020) 19:149–61. doi: 10.1016/j.omtm.2020.09.002

45. Giustarini G, Pavesi A, Adriani G. Nanoparticle-based therapies for turning cold tumors Hot : how to treat an immunosuppressive tumor microenvironment. *Front Bioeng Biotechnol* (2021) 9:689245. doi: 10.3389/fbioe.2021.689245

46. Hafezi M, Lin M, Chia A, Chua A, Ho ZZ, Fam R, et al. Immunosuppressive drug-resistant armored T-cell receptor T cells for immune therapy of HCC in liver transplant patients. *Hepatology* (2021) 74:200–13. doi: 10.1002/HEP.31662

47. Healy K, Pavesi A, Parrot T, Sobkowiak MJ, Reinsbach SE, Davanian H, et al. Human MAIT cells endowed with HBV specificity are cytotoxic and migrate towards HBV-HCC while retaining antimicrobial functions. *JHEP Rep* (2021) 3:1-12. doi: 10.1016/j.jhepr.2021.100318

48. Lam MSY, Reales-Calderon JA, Ow JR, Aw JJY, Tan D, Vijayakumar R, et al. G9a/GLP inhibition during ex vivo lymphocyte expansion increases *in vivo* cytotoxicity of engineered T cells against hepatocellular carcinoma. *Nat Commun* (2023) 14:563. doi: 10.1038/s41467-023-36160-5

49. Provenzano PP, Cuevas C, Chang AE, Goel VK, Von Hoff DD, Hingoran SR. Enzymatic targeting of the stroma ablates physical barriers to treatment of pancreatic ductal adenocarcinoma. *Bone* (2012) 21:418–29. doi: 10.1016/j.ccr.2012.01.007.Enzymatic

50. Di Maggio F, Arumugam P, Delvecchio FR, Batista S, Lechertier T, Hodivala-Dilke K, et al. Pancreatic stellate cells regulate blood vessel density in the stroma of pancreatic ductal adenocarcinoma. *Pancreatology* (2016) 16:995–1004. doi: 10.1016/j.pan.2016.05.393

51. Bussolati B, Deambrosis I, Russo S, Deregibus MC, Camussi G. Altered angiogenesis and survival in human tumor-derived endothelial cells. *FASEB J* (2003) 17:1159–61. doi: 10.1096/fj.02-0557fje

52. Fitzgerald G, Soro-Arnaiz I, De Bock K. The warburg effect in endothelial cells and its potential as an anti-angiogenic target in cancer. *Front Cell Dev Biol* (2018) 6:100. doi: 10.3389/fcell.2018.00100

53. Jimenez Trinidad FR, Ruiz MA, Batlló NS, Badenes À.V, Gibert JB, Cañellas AV, et al. Linking *in vitro* models of endothelial dysfunction with cell senescence. *Life* (2021) 11:1-14. doi: 10.3390/life11121323

54. Miller BW, Morton JP, Pinese M, Saturno G, Jamieson NB, McGhee E, et al. Targeting the LOX/hypoxia axis reverses many of the features that make pancreatic cancer deadly: inhibition of LOX abrogates metastasis and enhances drug efficacy. *EMBO Mol Med* (2015) 7:1063–76. doi: 10.15252/emmm.201404827

55. Kuninty PR, Bansal R, De Geus SWL, Mardhian DF, Schnittert J, van Baarlen J, et al. ITGA5 inhibition in pancreatic stellate cells attenuates desmoplasia and potentiates efficacy of chemotherapy in pancreatic cancer. *Sci Adv* (2019) 5:1-15. doi: 10.1126/sciadv.aax2770

56. Pill K, Melke J, Mühleder S, Pultar M, Rohringer S, Priglinger E, et al. Microvascular networks from endothelial cells and mesenchymal stromal cells from adipose tissue and bone marrow: a comparison. *Front Bioeng Biotechnol* (2018) 6:156. doi: 10.3389/fbioe.2018.00156

57. Grimes DR, Kelly C, Bloch K, Partridge M. A method for estimating the oxygen consumption rate in multicellular tumour spheroids. *J R Soc Interface* (2014) 11. doi: 10.1098/rsif.2013.1124

58. Korbecki J, Kojder K, Barczak K, Simińska D, Gutowska I, Chlubek D, et al. Hypoxia alters the expression of CC chemokines and cc chemokine receptors in a tumor–a literature review. *Int J Mol Sci* (2020) 21:1–32. doi: 10.3390/ijms21165647

59. Lee JH, Kim SK, Khawar IA, Jeong SY, Chung S, Kuh HJ. Microfluidic co-culture of pancreatic tumor spheroids with stellate cells as a novel 3D model for investigation of stroma-mediated cell motility and drug resistance. *J Exp Clin Cancer Res* (2018) 37:1–12. doi: 10.1186/s13046-017-0654-6

60. Zhang Y, Houchen CW, Li M. Attenuating DNA damage response and immunosuppression radiosensitizes pancreatic cancer. *EBioMedicine* (2022) 76:103822. doi: 10.1016/j.ebiom.2022.103822

61. Kurahara H, Shinchi H, Mataki Y, Maemura K, Noma H, Kubo F, et al. Significance of M2-polarized tumor-associated macrophage in pancreatic cancer. *J Surg Res* (2011) 167:e211–9. doi: 10.1016/j.jss.2009.05.026

62. Kung PJ, Lai TY, Cao J, Hsu LC, Chiang TC, Ou-Yang P, et al. The role of S100A9 in the interaction between pancreatic ductal adenocarcinoma cells and stromal cells. *Cancer Immunol Immunother* (2022) 71:705–18. doi: 10.1007/s00262-021-03026-y

63. Hu T, Li L, Shen J, Zhang L, Cho C. Chronic inflammation and colorectal cancer: the role of vascular endothelial growth factor. *Curr Pharm Des* (2015) 21:2960–7. doi: 10.2174/1381612821666150514104244

64. Murdoch C, Giannoudis A, Lewis CE. Mechanisms regulating the recruitment of macrophages into hypoxic areas of tumors and other ischemic tissues. *Blood* (2004) 104:2224–34. doi: 10.1182/blood-2004-03-1109

65. Campanella GSV, Medoff BD, Manice LA, Colvin RA, Luster AD. Development of a novel chemokine-mediated *in vivo* T cell recruitment assay. *J Immunol Methods* (2008) 331:127–39. doi: 10.1016/j.jim.2007.12.002

66. Chheda ZS, Sharma RK, Jala VR, Luster AD, Haribabu B. Chemoattractant receptors BLT1 and CXCR3 regulate antitumor immunity by facilitating CD8+ T cell migration into tumors. *J Immunol* (2016) 197:2016–26. doi: 10.4049/jimmunol.1502376

67. Huang H, Zhou W, Chen R, Xiang B, Zhou S, Lan L. CXCL10 is a tumor microenvironment and immune infiltration related prognostic biomarker in pancreatic adenocarcinoma. *Front Mol Biosci* (2021) 8:611508. doi: 10.3389/fmolb.2021.611508

68. Lee SWL, Adriani G, Ceccarello E, Pavesi A, Tan AT, Bertoletti A, et al. Characterizing the role of monocytes in T cell cancer immunotherapy using a 3d microfluidic model. *Front Immunol* (2018) 9:416. doi: 10.3389/fimmu.2018.00416

69. Mollica H, Teo YJ, Tan ASM, Tan DZM, Decuzzi P, Pavesi A, et al. A 3D pancreatic tumor model to study T cell infiltration. *Biomater Sci* (2021) 9:7420–31. doi: 10.1039/d1bm00210d

70. Adriani G, Pavesi A, Tan AT, Bertoletti A, Thiery JP, Kamm RD. Microfluidic models for adoptive cell-mediated cancer immunotherapies. *Drug Discovery Today* (2016) 21:1472–8. doi: 10.1016/J.DRUDIS.2016.05.006

Frontiers in Oncology

Advances knowledge of carcinogenesis and tumor progression for better treatment and management

The third most-cited oncology journal, which highlights research in carcinogenesis and tumor progression, bridging the gap between basic research and applications to imrpove diagnosis, therapeutics and management strategies.

Discover the latest Research Topics

See more →

Frontiers

Avenue du Tribunal-Fédéral 34
1005 Lausanne, Switzerland
frontiersin.org

Contact us

+41 (0)21 510 17 00
frontiersin.org/about/contact